



ANNUAL REVIEWS **Further**

[Click here](#) for quick links to Annual Reviews content online, including:

- Other articles in this volume
- Top cited articles
- Top downloaded articles
- Our comprehensive search

Annu. Rev. Astron. Astrophys. 2011. 49:301–71

The *Annual Review of Astronomy and Astrophysics* is online at astro.annualreviews.org

This article's doi:
[10.1146/annurev-astro-083109-153241](https://doi.org/10.1146/annurev-astro-083109-153241)

Copyright © 2011 by Annual Reviews.
All rights reserved

0066-4146/11/0922-0301\$20.00

Galaxy Disks

P.C. van der Kruit¹ and K.C. Freeman²

¹Kapteyn Astronomical Institute, University of Groningen, 9700 AV Groningen, The Netherlands; email: vdkruit@astro.rug.nl

²Research School of Astronomy and Astrophysics, Australian National University, Mount Stromlo Observatory, ACT 2611, Australia; email: kcf@mso.anu.edu.au

Keywords

disks in galaxies: abundance gradients, chemical evolution, disk stability, formation, luminosity distributions, mass distributions, S0 galaxies, scaling laws, thick disks, surveys, warps and truncations

Abstract

The disks of disk galaxies contain a substantial fraction of their baryonic matter and angular momentum, and much of the evolutionary activity in these galaxies, such as the formation of stars, spiral arms, bars and rings, and the various forms of secular evolution, takes place in their disks. The formation and evolution of galactic disks are therefore particularly important for understanding how galaxies form and evolve and the cause of the variety in which they appear to us. Ongoing large surveys, made possible by new instrumentation at wavelengths from the UV (*Galaxy Evolution Explorer*), via optical (*Hubble Space Telescope* and large groundbased telescopes) and IR (*Spitzer Space Telescope*), to the radio are providing much new information about disk galaxies over a wide range of redshift. Although progress has been made, the dynamics and structure of stellar disks, including their truncations, are still not well understood. We do now have plausible estimates of disk mass-to-light ratios, and estimates of Toomre's *Q* parameter show that they are just locally stable. Disks are mostly very flat and sometimes very thin, and they have a range in surface brightness from canonical disks with a central surface brightness of about 21.5 B-mag arcsec⁻² down to very low surface brightnesses. It appears that galaxy disks are not maximal, except possibly in the largest systems. Their HI layers display warps whenever HI can be detected beyond the stellar disk, with low-level star formation going on out to large radii. Stellar disks display abundance gradients that flatten at larger radii and sometimes even reverse. The existence of a well-defined baryonic (stellar + HI) Tully-Fisher relation hints at an approximately uniform baryonic to dark matter ratio. Thick disks are common in disk galaxies, and their existence appears unrelated to the presence of a bulge component; they are old, but their formation is not yet understood. Disk formation was already advanced at redshifts of ∼2, but at that epoch disks were not yet quiescent and in full rotational equilibrium. Downsizing (the gradual reduction with time in the mass of the most actively star-forming galaxies) is now well-established. The formation and history of star formation in S0s are still not fully understood.

1. INTRODUCTION AND OVERVIEW

1.1. Historical Background

Diskes are the most prominent parts of late-type spiral galaxies. The disk of our own Milky Way Galaxy stretches as a magnificent band of light from horizon to horizon, particularly from a dark site at southern latitudes, as in the Astronomy Picture of the Day for January 27, 2009 (Pacholka 2009). Its appearance with the Galactic Center high in the sky is reminiscent of the beautiful edge-on spiral NGC 891 (Hawaiian Starlight 1999), which can be regarded as a close twin to our Galaxy (van der Kruit 1984). What might in hindsight be called the first study of the distribution of stars in a galaxy disk is William Herschel's famous cross-cut of the sidereal system based on his star gauges (*On the Construction of the Heavens*, Herschel 1785), from which he concluded that the distribution of stars in space is in the form of a flattened system with the Sun near its center. His counts, on which he based this section of the system, were performed along a great circle on the sky almost perpendicular to the Galactic equator, crossing it at longitudes 45° and 225° and missing the poles by 5° . Comparison to modern star counts shows that Herschel counted stars consistently down to magnitude $V \sim 15$ (van der Kruit 1986).

The next major step in the study of the distribution of stars in the Milky Way was that of Jacobus Kapteyn (Kapteyn & van Rhijn 1920, Kapteyn 1922). In spite of his deduction that interstellar extinction must have the effect of reddening of starlight with increasing distance, Kapteyn (1909a,b, 1914) was unable to establish the existence of interstellar absorption in a convincing way and was led to ignore it. As a result, he ended up with a model for what we now know to be the Galactic disk that erroneously had the Sun located near its center. The proceedings, *The Legacy of J.C. Kapteyn* (van der Kruit & van Berkum 2000), have a number of interesting studies of Kapteyn and astronomy in his time.

Even before galaxies were established to be island universes, spiral structure was discovered in 1845 by William Parsons, the Third Earl of Rosse. His famous drawing of M51 appears in many textbooks, popular literature, and books on the history of astronomy. The importance of the disk and the development of spiral structure were the basis for the classification scheme that John Reynolds and Edwin Hubble developed; the background and early development of galaxy classification were described by Sandage (2005). Eventually the concept of stellar populations, first proposed by Baade (1944), led to the famous Vatican Symposium of 1957 (O'Connell 1958), where a consistent picture was defined to interpret the presence of disk and halo populations in the context of the structure and formation of galaxies.

Not long after that, the collapse picture of Eggen, Lynden-Bell & Sandage (1962) provided a working picture for the formation and evolution of the Galaxy and, by implication, of galaxies in general (Sandage, Freeman & Stokes 1970). It was modified by Searle & Zinn (1978) to include extended evolution, whereby the outer globular clusters originated and underwent chemical evolution in separate fragments that fell into the Galaxy after the collapse of the central halo had been completed. The basic discrete two-component structure of the edge-on galaxy NGC 7814 led van der Kruit & Searle (1982b) to deduce that there are two discrete epochs of star formation, one before and the other after virialization of the spheroid and the formation of the disk.

Two related important developments in understanding the properties of galaxies and their formation were the discovery of dark matter halos, and the appreciation of the role of hierarchical assembly of galaxies. The concepts of hierarchical assembly were already around in the early 1970s and became widely accepted at a landmark symposium on the *Evolution of Galaxies and Stellar Populations* at Yale University in 1977 (Tinsley & Larson 1977). The discovery of dark matter halos (see below) led to the two-stage galaxy formation model of White & Rees (1978), in

which hierarchical clustering of the dark matter took place under the influence of gravity, followed by collapse and cooling of the gas in the resulting potential wells. The *Hubble Space Telescope* (HST) made possible the high-resolution imaging of galaxies at high redshift and showed directly that merging and hierarchical assembly are significant in the formation of massive galaxies.

The significance of internal secular evolution for the evolution of disks has become clear in recent years. The presence of oval distortions, bars, and spiral structure can have a profound effect on the changing structure of disks, as has been extensively reviewed by Kormendy & Kennicutt (2004) and Kormendy (2007).

The rotation of galaxies was discovered early in the twentieth century. For a historical introduction, see van der Kruit & Allen (1978), Gilmore, King & van der Kruit (1990, chapter 10), and Sofue & Rubin (2001), documenting the first derivation of rotation velocities as a function of radius using optical absorption lines (Pease 1914), emission lines (Babcock 1939), and HI (van de Hulst, Raimond & van Woerden 1957; Argyle 1965), all in the Andromeda Nebula M31. The subject developed into the extensive mapping of the velocity fields of disk galaxies in the optical and HI, which eventually led to the discovery of flat rotation curves and the existence of dark matter (see, e.g., reviews by van der Kruit & Allen 1978, Faber & Gallagher 1979, Roberts 2008).

Quantitative surface photometry of disk galaxies to study their structure and luminosity distributions began with the work of Reynolds (1913) for the bulge of M31 (for a review, see Gilmore, King & van der Kruit 1990, chapter 5). Photometry of the much fainter disks came later and revealed the exponential nature of the radial surface brightness distributions. This was first described in a Harvard thesis, using observations of M33 (Patterson 1940): the data appear as figure 10 in the review by de Vaucouleurs (1959a). He had undertaken in the late fifties a systematic survey of the light distributions in nearby spirals, particularly in M31 and M33 (de Vaucouleurs 1958, 1959b), and established the universal exponential disk description of the radial light distribution in galactic disks. At about the same time, Holmberg (1958) completed a survey of the diameters of 300 galaxies from microphotometer tracings of photographic plates in two colors. This heroic effort was the culmination of work started much earlier (Holmberg 1937).

The exponential nature of the radial surface brightness distributions of disks was discussed in detail by Freeman (1970), who noted that many of the larger spirals had a remarkably small range in the extrapolated central (face-on) surface brightness around $21.65 \text{ B-mag arcsec}^{-2}$. This result still holds for classical spiral galaxies. The exponential surface brightness distribution of starlight in disks was complemented by the observations of the vertical light distribution in edge-on spirals. The distribution could be approximated very well by an isothermal sheet (Camm 1950, but for practical purposes an exponential can be used as well) with a scaleheight that—surprisingly—is to an excellent approximation independent of galactocentric radius (van der Kruit & Searle 1981a,b, 1982a).

Freeman (1970) also noted that for a self-gravitating exponential disk the expected rotation curve peaks at 2.2 scalelengths and then declines. A decline at 2.2 scalelengths was, however, not observed in the rotation data for NGC 300 and M33 at the time. This 1970 paper appears to be the first indication from rotation curve analysis that the rotation curve is not determined by the mass distribution in the disk alone, but requires a contribution to the amplitude of the rotation curve from an extended distribution of invisible matter. Subsequent observations of rotation curves eventually led to the concept of dark halos in individual galaxies (e.g., Faber & Gallagher 1979, Roberts 2008).

An important concept in the analysis of rotation curves is that of maximum disk, introduced by Carignan & Freeman (1985) and van Albada et al. (1985). In this concept, because the M/L ratio of the disk is unknown, the contribution of the disk mass to the rotation curve is taken to be as large as permitted by the observed rotation curve. In principle, an independent measurement of the

disk mass distribution can be obtained from hydrostatic considerations, comparing the thickness and velocity dispersion of the stars, as was pioneered for the Galaxy by Kapteyn (1922) and Oort (1932), or the H_I gas (van der Kruit 1981). Sanders & McGaugh (2002) have reviewed modified Newtonian dynamics as an alternative to dark matter.

Within disks, the star-formation history was studied first in our Galaxy in the Solar Neighborhood. The stellar initial mass function (IMF; the statistical distribution of stellar masses during star formation) was derived first by Salpeter (1959). Schmidt (1959) defined the Schmidt law for the rate of star formation as a function of the density of the ISM, in which the rate of star formation is proportional to the square of the local gas density [see reviews by Kroupa (2002a) and Kennicutt (1998) for subsequent refinements]. Studies of the chemical evolution in the local disk identified the G-dwarf problem in the simple model of chemical evolution (Schmidt 1963). In this simple model, the chemical evolution is followed in a galactic disk starting as pure gas with zero metallicity and without subsequent inflow or outflow; then the result is a much higher fraction of low-metallicity, long-lived stars as G-dwarfs than is observed in the Solar Neighborhood. This can be rectified by extensions of the model (see, e.g., the review by Tinsley 1980). The basic models for chemical evolution were able to represent the radial gradients in metal abundance in the gas of disk galaxies (Searle 1973) in terms of the extent to which star formation and chemical enrichment have proceeded (e.g., Garnett & Shields 1987, for M81). The mean metal abundance of stars that formed over the lifetime of a disk approaches that of the abundance of the gas at the time of disk formation plus an effective yield (the net production of heavy elements, modified by effects of zero-metal inflow or enriched gas outflow). In this “simple model with bells and whistles” (Mould 1984), it follows that, though gas consumption is still proceeding, the abundance gradients in the stars will be, in principle, shallower than that in the gas.

Reviews of stellar populations include those by King (1971), Sandage (1986), Bahcall (1986), Freeman (1987), and Gilmore, Wyse & Kuijen (1989). An IAU Symposium in 1994 on the subject of stellar populations (van der Kruit & Gilmore 1995) includes a historical session. For a recent review on the structure and evolution of the Galaxy, see Freeman & Bland-Hawthorn (2002).

The integral properties of galaxies and the systematics of their distribution have been used as tools toward understanding galaxy formation and the origin of the variety among them. Chief among these relationships are those between the morphological type and properties of their stellar and gas content, such as H_I content and integrated color (Roberts & Hayes 1994). These latter properties were convincingly interpreted as a measure of the process of depletion of the interstellar gas in star formation and the rate of current star formation relative to that averaged over a galaxy’s lifetime (Searle & Sargent 1972; Searle, Sargent & Bagnuolo 1973; Larson & Tinsley 1978), which then correlate with galaxy type. The Tully-Fisher relation (Tully & Fisher 1977) provides a tight correlation of rotation velocity and integrated luminosity, although it still is not clear why it is so tight when the rotation velocity is determined not only by the mass in the stars that provide the luminosity but also by the dark matter halo.

We should mention here the discovery of low surface brightness (LSB) galaxies, which was anticipated by the work of Disney (1976). Disney & Phillipps (1983) showed that the observed range in central surface brightness of galaxy disks (and also of elliptical galaxies) is severely restricted by the necessity for them to stand out against the background sky; the exponential nature of disks naturally restricted samples to a small range in central surface brightness comparable to the value first noted by Freeman (1970). This selection effect had been described earlier in qualitative and more general terms by Arp (1965). Many LSB galaxies are known today, although it appears that the bright limit of the surface brightnesses seen by Freeman (1970) is not an effect of observational selection (Allen & Shu 1979, Bosma & Freeman 1993).

1.2. Setting the Scene

This brief description of the historical development of our subject already indicates that a comprehensive treatment of all aspects of galaxy disks is beyond the scope of a single Annual Reviews chapter. Topics that we do not review in detail include radio continuum studies and magnetic fields (van der Kruit & Allen 1976, Condon 1992, Beck 2008), AGNs and black holes in the centers of galaxies (Kormendy & Richstone 1995, Ferrarini & Ford 2005, Pastorini et al. 2007), spiral structure (Toomre 1977), bars (Sellwood 2011b), and secular evolution (Kormendy & Kennicutt 2004). Also we do not review issues related to physical or chemical processes in the ISM. We refer the reader to the proceedings of some recent symposia that concentrate on disks in galaxies, including *The Dynamics, Structure and History of Galaxies* (Da Costa & Jerjen 2002), *Island Universes: Structure and Evolution of Disk Galaxies* (de Jong 2007), *Formation and Evolution of Galaxy Disks* (Funes & Corsini 2008), *Unveiling the Mass: Extracting and Interpreting Galaxy Masses* (Courteau & de Jong 2009),¹ and *Galaxies and Their Masks* (Block, Freeman & Puerari 2010).

Despite the correlations between overall properties, there are galaxies with very similar properties but very different morphologies. M33 and the Large Magellanic Cloud (LMC) provide an example. Both galaxies have very similar central surface brightnesses (~ 21.2 B-mag arcsec $^{-2}$), scalelengths (~ 1.6 kpc), integrated magnitudes (~ -18.5 in B), $(B-V)$ colors (~ 0.51), Infrared Astronomical Satellite (IRAS) luminosities ($\sim 1.0 \times 10^8 L_\odot$), HI masses ($\sim 9.5 \times 10^8 M_\odot$), and rotation velocities (~ 90 – 100 km s $^{-1}$) (see Gilmore, King & van der Kruit 1990, chapter 10). The point is that these two systems differ significantly only in morphological classification and nothing else. The detailed structure of a galaxy, its morphology, and spiral structure may be determined by external properties such as environment or may even be transient, so that during the lifetime of the systems there might have been periods when M33 looked very much like the LMC and vice versa.²

In the final section, we discuss the origin of S0 galaxies. Originally introduced by Hubble as a transition class between elliptical and spirals, they were believed to be systems that had quickly used all of their remaining gas. Alternative theories were suggested, involving the stripping of gas from existing spirals by collisions (Spitzer & Baade 1951) or intergalactic gas (Gunn & Gott 1972).

2. SURVEYS

Surveys provide the basis of much of the observational studies of disk galaxies. In the past, major surveys were very time consuming. For example, the *Hubble Atlas of Galaxies* (Sandage 1961), which provided the basic source list for much of the past work on nearby galaxies, was the culmination of decades of photography of galaxies by Hubble, Sandage, and others in order to survey the variety of morphologies among galaxies. For many years, the Humason, Mayall & Sandage (1956) survey was a main source of galaxy redshifts and magnitudes; it was the result of 20 years of observations at Mount Wilson, Palomar, and Lick, and was only surpassed decades after its publication. The advent of dedicated, automated survey telescopes, multiobject spectrographs, and high-resolution imaging and spectroscopic space facilities has transformed our ability to make surveys of galaxies. In this section, we give a brief overview of surveys, currently or recently undertaken, that are relevant to studies of disks in galaxies as discussed in later sections of this review.

¹For this symposium on the occasion of Vera Rubin's 80th birthday, there will be no printed proceedings—electronic versions of presentations or posters are available through the conference website.

²Sidney van den Bergh pointed out that M33 has a central star cluster and the LMC does not. Such clusters are likely to remain visible at all times, even if their star formation is intermittent (see Section 3.9). They are common in spirals but not in irregular galaxies, which makes it less likely that an individual galaxy could sometimes be a spiral and sometimes an irregular. We thank Sidney van den Bergh for this remark.

Kinematic surveys aimed at the dynamics of (stellar) disks (see Section 3) using integral field spectrographs include DiskMass (Bershady et al. 2010a) (146 nearly face-on galaxies for which H α velocity fields have already been measured, and a subset of 46 galaxies with stellar velocities and velocity dispersions) and PINGS (*PPAK IFS Nearby Galaxies Survey*; <http://www.ast.cam.ac.uk/research/pings/html/>) (Rosales-Ortega et al. 2010), which will provide two-dimensional spectroscopy in 17 nearby galaxies. For these surveys, the data are supplemented by extensive observations at other wavelengths.

Surveys specifically designed to gather detailed information on the properties of disks in galaxies usually involve samples of nearby galaxies that are not statistically complete but are designed to cover the range of morphological types. HI surveys of individual galaxies are often complemented by optical or near-IR surface photometry to aid the analysis of their rotation curves (see Section 4). A first such survey of spiral galaxies, combining imaging (three-color photographic surface photometry) at optical wavelengths and mapping of distributions and kinematics of HI, was made by Wevers, van der Kruit & Allen (1986). This Palomar-Westerbork Survey of Northern Spiral Galaxies included only 16 galaxies, but required 64 observing periods of 12 hours with the Westerbork Synthesis Radio Telescope (WSRT) and 42 dark nights at the Palomar 48-inch Schmidt. This was extended substantially in the WHISP survey (Westerbork observations of neutral Hydrogen in Irregular and SPiral galaxies; <http://www.astro.rug.nl/~whisp>) (van der Hulst 2002, Noordermeer et al. 2005) of a sample of a few hundred galaxies. THINGS (The HI Nearby Galaxy Survey; <http://www.mpia.de/THINGS/>) (Walter et al. 2008) is the most detailed recent uniform set of high-resolution and high-sensitivity data on 34 nearby disk galaxies available at this time; data were taken with the Very Large Array (VLA). A special section, devoted to THINGS, appeared in the December 2008 issue of the *Astronomical Journal*. Another major survey of nearby galaxies is SINGS (*Spitzer Infrared Nearby Galaxies Survey*; <http://sings.stsci.edu>) (Kennicutt et al. 2003). This is a comprehensive imaging and spectroscopic study of 75 nearby galaxies in the IR.

Other surveys provide large samples of galaxy data of various kinds in different wavelength regions. Images of galaxies in two UV bands from the *Galaxy Evolution Explorer* (GALEX) (Martin et al. 2008) survey are particularly useful for estimating the recent star-formation history of galaxies. In the optical B-band, the Millennium Galaxy Catalogue (see <http://www.eso.org/~jiliske/mgc>) comes from a 37.5 deg^2 medium-deep imaging survey of galaxies in the range $13 < B < 24$, connecting the local and distant Universe. The 6dF and 2dF Galaxy Redshift Surveys (<http://www.aoe.gov.au/local/www/6df> and <http://msowww.anu.edu.au/2dFGRS>) and the SDSS (Sloan Digital Sky Survey; <http://www.sdss.org>) (York et al. 2000) provide vast samples of optical galaxy redshifts and spectroscopic properties related to their star-formation history (see Section 5). The 2MASS (Two Micron All Sky Survey; <http://www.ipac.caltech.edu/2mass>) (Skrutskie et al. 2006) gives integrated near-IR photometry for a very large sample of galaxies and also relatively shallow near-IR images for the brighter galaxies. High-resolution deep imaging in the near- and mid-IR over a wide redshift range is provided by the *Spitzer Space Telescope* mission [see Soifer, Helou & Werner (2008) for a recent summary of extragalactic studies]. Large HI surveys are of interest for studies of the HI mass function in the Universe, and also for scaling laws (see Section 6). For example, the HIPASS (HI Parkes All-Sky Survey; <http://www.atnf.csiro.au/research/multibeam/release>) survey gives integrated HI data for galaxies south of declination $+25^\circ$ out to velocities of $12,700 \text{ km s}^{-1}$.

Two major surveys are using HST to study resolved stellar populations in nearby galaxies. ANGST (ACS Nearby Galaxy Survey Treasury; <http://www.nearbygalaxies.org>) (Dalcanton et al. 2009) establishes a legacy of uniform multicolor photometry of resolved stars for a volume-limited sample of nearby galaxies. GHOSTS (Galaxy Halos, Outer disks, Substructure, Thick

disks and Star clusters; <http://www-int.stsci.edu/~dtrs/ghosts>) (de Jong et al. 2007a) is imaging several edge-on galaxies with a range in masses to study their stellar populations. These population studies are important for understanding the star-formation history in galaxies (see Sections 5 and 7). For more nearby population studies, SEGUE (Sloan Extension for Galactic Understanding and Exploration; <http://www.sdss.org/segue/>) and RAVE (RAdial Velocity Experiment; <http://www.rave-survey.aip.de/rave/>) focus on kinematic and chemical surveys of very large samples of stars in the Galactic disk and halo.

For studies of disk galaxies at high redshift, the Hubble (Ultra-)Deep Fields (Williams et al. 1996, 2000; Beckwith et al. 2006) and the GOODS (Great Observatories Origin Deep Survey; <http://www.stsci.edu/science/goods>) and COSMOS surveys have been very influential. The GOODS (Dickinson, Giavalisco & the GOODS Team 2003) survey involves two fields centered on the Hubble Deep Field North and the Chandra Deep Field South and combines deep observations from NASA's Great Observatories, *Spitzer*, *Hubble*, and *Chandra*, ESA's *Herschel* and *XMM-Newton*, and from the most powerful ground-based facilities such as Keck, VLT, Gemini, and Subaru. The *Cosmological Evolution Survey* (COSMOS; <http://cosmos.astro.caltech.edu>) covers a two-square-degree equatorial field with a similar range of facilities, aimed at probing the formation and evolution of galaxies with cosmic time (see Section 8).

Astronomy profits enormously from new facilities, and this is equally true for our subject of disk galaxies. For the future, we look forward to new insights from major facilities. In the submillimeter and radio, *Herschel* and the Atacama Large (sub-)Millimeter Array (ALMA) will revolutionize studies of star formation and the ISM in disk galaxies. The Low Frequency Array (LOFAR), its southern Murchison Widefield Array (MWA) counterpart, the Karoo Array Telescope (MeerKAT) and Australian Square Kilometer Array Pathfinder (ASKAP) arrays, and ultimately the Square Kilometer Array (SKA) itself, will have a profound impact on studies of the formation of galaxies and the structure of disk galaxies. Current deep HST surveys (see, for example, <http://candels.ucolick.org>) and surveys to come with the James Webb Space Telescope (JWST), promise to bring new insights into the properties of disk galaxies and their assembly. For studies of the stucture and evolution of the Milky Way, the *Global Astrometric Interferometer for Astrophysics* (Gaia) mission will give astrometric data of unparalleled precision. Combined with panoramic surveys like those planned with Pan-Starrs, SkyMapper, and LSST, these data will help us understand the structure and genesis of the different components of our disk galaxy.

3. STELLAR DISKS

In this section we discuss the three-dimensional distribution of stars in disks of galaxies, including warps and truncations, and the kinematics and dynamics of the stellar components. We then turn to the inferred distributions of stellar mass, the disk stability and the total mass distribution in galaxies.

3.1. Luminosity Distributions

We start by describing the luminosity distributions as inferred from surface photometry. First we concentrate on the radial distribution of flat disks and next turn to the three-dimensional one, including a description of the vertical distribution.

3.1.1. Exponential disks. The structure and general properties of stellar disks have previously been reviewed by us (e.g., van der Kruit 2002, Freeman 2007). As mentioned in the introduction,

the radial distribution of surface brightness in the disks of face-on or moderately inclined galaxies can be approximated by an exponential: $I(R) \propto \exp(-R/h)$. Fits to actual surface photometry result in two parameters, the radial scalelength h and the (extrapolated and corrected to face-on) central surface brightness μ_* , both as a function of photometric band. The determination of these parameters can in general be done in a reasonably reliable way from component separations (Kormendy 1977); Schombert & Bothun (1987) and Byun & Freeman (1995) showed from realistic simulations that one-dimensional and two-dimensional bulge-disk separations do return input values for bulge and disk parameters very well. Nevertheless, independent determinations of scalelengths of the same galaxies in the literature give results that differ with a standard deviation of 20% (Knapen & van der Kruit 1991). In his CCD study of exponential disks in a sample of bright UGC galaxies, Courteau (1996) also stresses the pitfalls and cautions that comparison of central surface brightnesses and scalelengths is complicated by the subjective nature of their measurement. We note that older fits adopt the $R^{1/4}$ law $I(R) \propto \exp R^{-1/4}$ for the bulge, whereas most researchers now use the more general Sérsic (1963) profiles $I(R) \propto \exp R^{-1/n}$, with the Sérsic index $n = 1$ for the exponential disk and $n = 4$ for the $R^{1/4}$ law. In the context of two-component decompositions of radial surface brightness distributions, we note that the flat pseudobulge structures discussed by Kormendy & Kennicutt (2004) have values for n of about 2.5.

The original publication on exponential disks by Freeman (1970) used observations in the B -band. In that paper, the distribution of the two parameters was discussed, finding an apparent constancy of μ_* for about 75% of the sample and that disk galaxies have scalelengths with a wide range of values (predominantly small in later-type galaxies). We already noted in Section 1.1 that the apparent constancy of central surface brightness is seriously affected by observational selection (Arp 1965, Disney 1976, Disney & Phillipps 1983), leading to the conclusion that there must be many lower surface brightness galaxies. However, the upper limit is believed to be real (Allen & Shu 1979, Bosma & Freeman 1993, de Jong 1996b).

With the advent of large datasets of surface photometry (such as from the SDSS), it has become possible now to study large samples of galaxies. For example, Gadotti (2009) has collected g , r , and i -band images of a representative sample of nearly 1,000 galaxies from the SDSS and decomposed them into bulges, bars, and disks. Pohlen & Trujillo (2006) and Pohlen et al. (2007) have used SDSS data to determine radial luminosity distributions and look for radial truncations (see Section 3.8). Fathi et al. (2010) determined scalelengths, using an automatic technique, for over 30,000 galaxies in five wavelength bands, together with indices for asymmetry and concentration. Comparison with the overlap with the sample of Gadotti (2009) shows, in general terms, good agreement (see figure 1 of Fathi 2010, which concerns the same sample). Fathi et al. (2010) form subsamples for which reliable morphological types or central velocity dispersions are available. As before, the average scalelength (3.8 ± 2.0 kpc) is independent of morphological type and is very similar in the optical bands (g , r , i , and z). In the u -band, they find a mean scalelength of 5 ± 3 kpc. Galaxies of smaller mass (10^9 to $10^{10} M_\odot$) have smaller scalelengths (1.5 ± 0.7 kpc) than larger mass (10^{11} to $10^{12} M_\odot$) galaxies (5.7 ± 1.9 kpc). The distributions in this study have not been corrected for sample selection.

It is possible to study the bivariate distribution function of the disk parameters. It is most important for such studies that the sample is complete with respect to well-defined selection criteria and that the distribution in the (μ_*, h) plane is corrected for the effect of these selection criteria (following the prescriptions of Disney & Phillipps 1983). This was first done by van der Kruit (1987), later at various optical and near-IR colors by de Jong & van der Kruit (1994) and de Jong (1996a–c), and more recently by Fathi (2010) using the large SDSS (Fathi et al. 2010) sample. The study of the distribution of parameters in this plane reveals important results that bear on the formation models of disks.

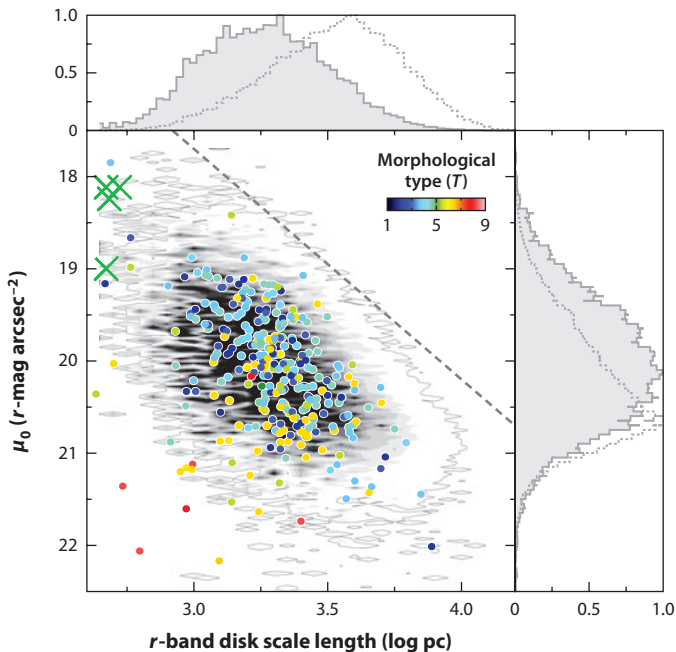


Figure 1

The bivariate distribution function of face-on central surface brightness and scalelength of galaxy disks in a sample of almost 30,000 galaxies taken from SDSS, corrected for selection effects. Superposed are the 282 most reliable data as colored points (coding for revised Hubble type) and a few disky ellipticals as green crosses. The gray diagonal dashed line shows a slope of 2.5 corresponding to a constant disk luminosity. The distributions on the right and top are as observed (*dotted*) and after correcting for sample selection (*solid with gray fill*). (From Fathi 2010).

The distribution in the $(\mu_0, \log h)$ diagram (Figure 1) shows a broad band running from bright, large disks to faint, small disks (van der Kruit 1987, de Jong 1996b, Graham & de Blok 2001, Fathi 2010). Graham & de Blok (2001) find that there is a morphological-type dependence in this plane: among LSB galaxies [central surface brightness more than 1 mag fainter than the 21.65 B -mag arcsec^{-2} mean value of Freeman (1970)], the early-type spiral galaxies have large scalelengths (larger than 8–9 kpc), whereas the late-type spirals have smaller scalelengths. Further, de Jong (1996b) finds that the scale parameters of disks and bulges are correlated at all morphological types, but are not correlated themselves with Hubble type. However, LSB galaxies are usually of late Hubble type. He also concludes that the bulge-to-disk ratio is not correlated with Hubble type, nor is the disk central surface brightness. The significant parameter that does correlate with morphological type is the effective surface brightness of the bulge. Color information shows that, within and among galaxies, LSB corresponds to bluer colors (de Jong 1996c). This results from the combined effect of mean stellar age and metallicity and not from dust reddening and implies significant mass-to-light ratio variations. Figure 2 shows the modern version of figure 5 of Freeman (1970), corrected for volume selection effects. There is still a mean value (but with a large scatter around it) that does not depend on morphological type, except for the later ones.

What properties of galaxies do correlate with h and μ_0 ? Courteau et al. (2007) collected surface photometry of 1,300 galaxies and determined the photometric parameters from either one-dimensional bulge-disk decompositions of the surface brightness profile or by using the so-called marking-the-disk method, where the extent of the exponential disk profile is judged by eye. They

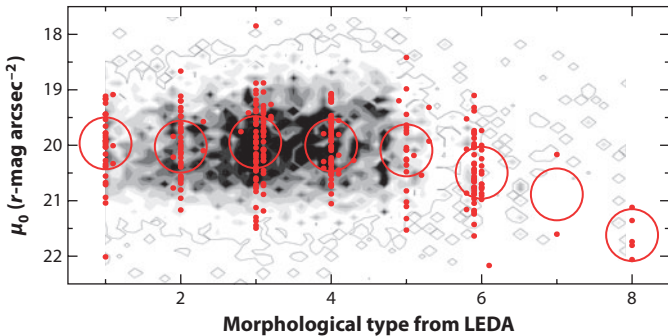


Figure 2

The distribution of face-on central surface brightness for the same sample as in **Figure 1** as a function of Hubble type, corrected for selection and again with the 282 most reliable determinations as red points. The large red open circles show the average surface brightness for each type. (From Fathi 2010).

also find some variation of central surface brightness or scalelength as a function of morphological type, with earlier types having fainter surface brightness and larger scalelengths, but the effects are marginal. In addition, they find well-defined relationships between luminosity, scalelength, and rotation velocity, but the slopes show a definite dependence on morphological type and a small but significant dependence on the wavelength band. The scalelengths in the *I*-band correlate with integrated luminosity and rotation velocity (see Equation 25 and **Figure 18** below). In summary, although *b* has no strong dependence on morphological type, it is clearly larger in the mean for more luminous and more massive galaxies.

There is some argument concerning the scalelength of the disk of our own Galaxy. If $V_{\text{rot}} = 220 \text{ km s}^{-1}$, then the expected scalelength of the Galactic disk would be 4.4 kpc with a one-sigma range between 3.6 and 6.6 kpc (see slide 19 in van der Kruit 2009). These values would be larger if $V_{\text{rot}} = 250 \text{ km s}^{-1}$ (Reid et al. 2009). The often quoted values of 2.5 to 3.0 kpc (Sackett 1997, Freudreich 1998, Hammer et al. 2007, Reylié et al. 2009, Yin et al. 2009) put the Galaxy outside the one-sigma range of scalelengths for its rotation speed. A value more like 4.5 kpc (van der Kruit 2008, 2009) (or even the probably too large 5.5 ± 1.0 kpc from the Pioneer 10 photometry alone; van der Kruit 1986) would be more typical for our Galaxy. However, Hammer et al. (2007) argue that our Galaxy is exceptional in many aspects: Their adopted low value for the scalelength of the disk is a major contributor to this conclusion.

The origin of the exponential nature of stellar disks is still uncertain. Freeman (1970, 1975) already pointed out that the distribution of angular momentum in a self-gravitating exponential disk resembles that of the uniform, uniformly rotating sphere (Mestel 1963). This is also true for an exponential density distribution with a flat rotation curve (Gunn 1982, van der Kruit 1987). A model in which the disk collapses with detailed conservation of angular momentum (Fall & Efstathiou 1980) would give a natural explanation for the exponential nature of disks and maybe even their truncations (see below). However, bars or other nonaxisymmetric structures may give rise to severe redistribution of angular momentum; nonaxisymmetric instabilities and the secular evolution of disks and their structural parameters may be important (Debattista et al. 2006).

Before leaving the subject of luminosity distributions, we briefly address the issue of LSB disks. Often these have central (face-on) surface brightnesses that are 2 magnitudes or more fainter than the canonical $21.65 B\text{-mag arcsec}^{-2}$ of Freeman (1970). Traditionally, these are thought to be galaxies with low (gas) surface densities, in which the star formation proceeded slowly. Analysis of available data (HI rotation curves, colors, and stellar velocity dispersions) led de Blok & McGaugh

(1997) to argue that LSB galaxies are not described well by models with maximum disks (see Section 3.2.4). LSB galaxies appear to be slowly evolving, low-density, dark matter-dominated systems. The star formation in LSB disks can now be studied with GALEX by directly mapping their near-UV flux. Wyder et al. (2009) combined such data with existing HI observations and optical images from the SDSS for 19 systems. Comparison with far-IR data from *Spitzer* shows that there is very little extinction in the UV, consistent with the fact that LSB galaxies appear to have little dust and molecular gas (see, e.g., de Blok & van der Hulst 1998a,b). The star-formation rate in LSB galaxies lies below the extrapolated rate as a function of gas surface density for high surface brightness galaxies, implying a lower mean star-formation efficiency in LSB systems. This may be related to the lower density of molecular gas.

3.1.2. Three-dimensional distributions. We now turn to the three-dimensional distribution. The vertical distribution of luminosity within a galactic disk can be modelled to a first approximation with an isothermal sheet (Camm 1950) with a scaleheight that is independent of galactocentric distance (van der Kruit & Searle 1981a). This is a surprising observational result. We discuss its possible origin in Section 3.2.3. In a more general form, the luminosity density distribution can be written as (van der Kruit 1988)

$$L(R, z) = L(0, 0)e^{-R/b} \operatorname{sech}^{2/n} \left(\frac{nz}{2b_z} \right). \quad (1)$$

This ranges from the isothermal distribution [$n = 1$: $L(z) \propto \operatorname{sech}^2(z/z_0)$ with $z_0 = 2b_z$] to the exponential function [$n = \infty$: $L(z) \propto \exp(-z/b_z)$], as was used by Wainscoat, Hyland & Freeman (1989, 1990) and allows for the more realistic case that the stellar distribution is not completely isothermal in the vertical direction. The uncertainty resulting from what the detailed vertical distribution of stellar mass really is in a disk can be estimated by taking a realistic range in the parameter n , as we have done, for example, in Equation 7 below. **Figure 3** shows the fits of this

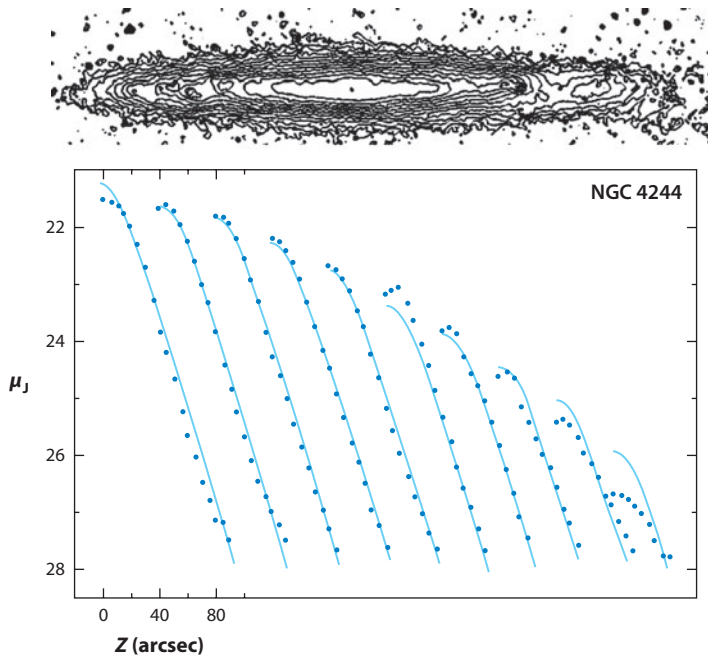


Figure 3

The surface brightness distribution in the edge-on, pure disk galaxy NGC 4244. At the top, the isophotes in blue light at 0.5 mag arcsec^{-2} intervals. At the bottom, vertical z -profiles at a range of distances from the center after averaging over the four equivalent quadrants. The lighter blue curves are those for an isothermal sheet with $n = 1$ in Equation 1. (After van der Kruit & Searle 1981a).

distribution projected in edge-on orientation to the surface brightness distribution in the pure-disk, edge-on galaxy NGC 4244, for the case of the isothermal sheet ($n = 1$). The outer profile does not fit, because the truncation (see Section 3.8) has not been taken into account. From actual fits in I and K' , de Grijs, Peletier & van der Kruit (1997) found

$$\frac{2}{n} = 0.54 \pm 0.20 \quad (2)$$

for a sample of 24 edge-on galaxies. A detailed study by de Grijs & Peletier (1997) has shown that the constancy of the vertical scaleheight b_z is accurate in disks of late-type spirals, but in early-type galaxies b_z may increase outward by as much as 50% per scalelength b .

The distribution of the scale parameters is most easily studied in edge-on galaxies. Following the work by van der Kruit & Searle (1981a,b, 1982a), an extensive sample of edge-on galaxies was studied by de Grijs (1998) and reanalyzed by Kregel, van der Kruit & de Grijs (2002). Both scalelength b and scaleheight b_z correlate well with the rotation velocity of the galaxy: for example, for the scaleheight

$$b_z = (0.45 \pm 0.05)(V_{\text{rot}}/100 \text{ km s}^{-1}) - (0.14 \pm 0.07) \text{ kpc}, \quad (3)$$

with a scatter of 0.21 kpc. This relation is important as it can be used to make a statistical estimate of the thickness of disks in galaxies that are not seen edge-on. The correlation between b and V_{rot} is comparable to that found by Courteau et al. (2007). The flattest galaxies (largest ratio of b and b_z) appear to be those with late Hubble-type, small rotation velocity, and faint (face-on) surface brightness. Among galaxies with large HI content, a large range of flattening is observed, becoming smaller with lower HI mass. The flattest disks occur among galaxies with about $10^{10} M_{\odot}$ in HI. We return to this subject in Section 3.6 when we discuss super-thin galaxies.

3.2. Stellar Kinematics, Stability, and Mass

The stellar kinematics together with the distribution of the stars can be used to study the dynamics of disks, estimate the mass distribution, and address issues like the local and global stability of stellar disks.

3.2.1. Vertical dynamics. We first turn to the dynamics of stellar disks in the vertical (z) direction. At the basis of the analysis of the vertical dynamics of a stellar disk, we have the Poisson equation for the case of axial symmetry,

$$\frac{\partial K_R}{\partial R} + \frac{K_R}{R} + \frac{\partial K_z}{\partial z} = -4\pi G\rho(R, z), \quad (4)$$

where K_R and K_z are the gravitational force components. At small z , the first two terms on the left are equal to $2(A - B)(A + B)$ (e.g., Oort 1965, Freeman 1975), and this is zero for a flat rotation curve.³ So we have

$$\frac{dK_z}{dz} = -4\pi G\rho(z). \quad (5)$$

This is the plane-parallel case, and flat rotation curves do make this an excellent approximation at low z (van der Kruit & Freeman 1986). The Jeans equation then becomes

$$\frac{d}{dz} [\rho(z)\sigma_z^2(z)] = \rho(z)K_z. \quad (6)$$

³The Oort constants are $A = 1/2(V_{\text{rot}}/R - (dV_{\text{rot}}/dR))$ and $B = -1/2(V_{\text{rot}}/R + (dV_{\text{rot}}/dR))$, so $A + B = -(dV_{\text{rot}}/dR)$.

Combining these gives (e.g., van der Kruit 1988)

$$\sigma_z(R) = \sqrt{c\pi G\Sigma(R)b_z}, \quad (7)$$

where the velocity dispersion σ_z is now the velocity dispersion integrated over all z (corresponding to the second moment of the distribution observed when the disk is seen face-on), and the constant c varies between 3/2 for an exponential [$n = \infty$ in Equation 1] to 2 for an isothermal distribution ($n = 1$). Equation 7 is the equation for hydrostatic equilibrium that relates the vertical distribution of the stars and their mean vertical velocity dispersion to the distribution of mass; this principle was used already by Kapteyn (1922) and Oort (1932) to derive the mass density in the Solar Neighborhood. If the mass-to-light ratio M/L is constant with radius, the exponential radial distribution and the constant scaleheight imply, through hydrostatic equilibrium, that the vertical velocity dispersion $\sigma_z(R)$ of the old stars in the disk should be proportional to the square root of the surface density Σ or as an exponential with galactocentric radius, but with an e-folding of twice the scalelength.

The mass-to-light ratio M/L is a crucial measure of the contribution of the disk to the rotation curve and the relative importance of disk mass and dark matter halo in a galaxy. An often used hypothesis is that of the maximum disk (see also Section 4.2), in which the disk contribution to a galaxy's rotation curve is maximized in the sense that the amplitude of the disk-alone rotation curve is made as large as the observations allow. Using hydrostatic equilibrium, we may estimate M/L and obtain information on whether or not the disk is maximal or submaximal. This can, in principle, be done from Equation 7 by measuring the velocity dispersion in a face-on galaxy and using a statistical estimate of the scaleheight.

In 1984, van der Kruit & Freeman (1984) made the first successful measurements of stellar velocity dispersion in the face-on spirals NGC 628 and 1566.⁴ This work was followed by more detailed observations by van der Kruit & Freeman (1986) for NGC 5247 (inclination about 20°), where the prediction was verified: The e-folding length of σ_z was 2.4 ± 0.6 photometric scalelengths, the predicted value of 2.0 being well within the uncertainty. Many studies have since shown that σ_z decreases with galactocentric radius (e.g., Bottema 1993; Kregel, van der Kruit & Freeman 2004, 2005; Kregel & van der Kruit 2005, and references therein). Gerssen, Kuijken & Merrifield (1997) found in NGC 488 that the kinematic gradient was comparable to the photometric gradient, which they attributed to the fact that the scalelength should really be measured in K -band to represent the stellar distribution. The same researchers (Gerssen, Kuijken & Merrifield, 2000) found, in NGC 2985, that these scalelengths were indeed as expected from a constant M/L . There is certainly support from stellar dynamics that, in general, there are no substantial gradients in mass-to-light ratios in disks.

Two recent developments are making an impact on this issue. The first is the use of integral field units that enable a more complete sampling of the disks. The DiskMass Project (Verheijen et al. 2007; Westfall et al. 2008; Bershady et al. 2010a,b) aims at mapping the stellar vertical velocity dispersion in 46 face-on or moderately inclined spiral galaxies. This will provide a kinematic measurement of the mass surface density of stellar disks. The final results have not yet appeared in the literature, but recent conference presentations show that the kinematics follows the light, i.e., the velocity dispersions drop off according to the rule described above. Also the actual values indicate relatively low mass-to-light ratios and disk masses that are well below those required for maximum disk fits.

⁴At the same time and independently, Kormendy (1984a,b) succeeded in measuring stellar velocity dispersions in the disks of two S0 galaxies with more or less the same aim; we discuss this in Section 9.

Similarly, the use of planetary nebulae (PNe) as test particles in the disks (Herrmann et al. 2008; Herrmann & Ciardullo 2009a,b) of five face-on spirals allows the velocity dispersion of these representative stars of the old disk population to be measured out to much larger radii (see also Section 9). In general, the findings are similar: Except for one system, the M/L is constant out to about three radial scalelengths of the exponential disks. Outside that radius, the velocity dispersion stops declining and becomes flat with radius. Possible explanations proposed for this behavior include an increase in the disk mass-to-light ratio, an increase in the importance of the thick disk, and heating of the thin disk by halo substructure. They also find that the disks of early-type spirals have higher values of M/L and are closer to the maximum disk than later-type spirals.

In summary, the vertical dynamics of stellar disks show that in general the velocity dispersions of the stars fall off with an e-folding length double that of the exponential light distribution, as required for a constant M/L , whereas for the majority of disks the inferred mass-to-light ratios are almost certainly lower than required in the maximum disk hypothesis.

3.2.2. Stellar velocity dispersions in the plane. The stellar velocity dispersions in the plane are more complicated to determine from observations. The radial and tangential components are not independent, but governed by the local Oort constants⁵

$$\frac{\sigma_\theta}{\sigma_R} = \sqrt{\frac{-B}{A - B}}. \quad (8)$$

For a flat rotation curve, $A = -B$ and this ratio is 0.71. In highly inclined or edge-on systems, the dispersions can be measured both from the line profiles and the asymmetric drift equation,

$$V_{\text{rot}}^2 - V_\theta^2 = \sigma_R^2 \left\{ \frac{R}{b} - R \frac{\partial}{\partial R} \ln(\sigma_R) - \left[1 - \frac{B}{B - A} \right] \right\}, \quad (9)$$

where the circular velocity V_{rot} can be measured with sufficient accuracy from the gas (optical emission lines or H I observations), which have velocity dispersions of order 10 km s $^{-1}$ or less and have therefore very little asymmetric drift.

The stability of a galactic disk to local axisymmetric disturbances depends on the (stellar) radial velocity dispersion σ_R , the epicyclic frequency κ , and the local mass surface density Σ . Toomre's (1964) criterion is

$$Q = \frac{\sigma_R \kappa}{3.36 G \Sigma}. \quad (10)$$

On small scales, local stability results from a Jeans-type stability, where tendency to collapse under gravity is balanced by the kinetic energy in random motions, but only up to a certain (Jeans) scale. On larger scales, shear as a result of galactic differential rotation provides stability. In the Toomre Q -criterion, this smallest scale is just equal to the (maximum) Jeans scale, so that local stability exists on all scales. According to Toomre (1964), local stability requires $Q > 1$. Numerical simulations suggest that galaxy disks are on the verge of instability (Hohl 1971, Sellwood & Carlberg 1984, Athanassoula & Sellwood 1986, Mihos, McGaugh & de Blok 1997, Bottema 2003), having stellar velocity dispersions that are slightly larger than Toomre's critical velocity dispersion. The simulations suggest $Q = 1.5\text{--}2.5$.

The first attempt to measure these in-plane velocity dispersion components was by van der Kruit & Freeman (1986) for the highly inclined galaxy NGC 7184. They fitted their data using two

⁵For small deviations from circular motions around the galactic center, the stellar orbit may be described by a small epicycle superposed on the circular motion around the galactic center. The frequency in the epicycle is $\kappa = 2\sqrt{-B(A - B)}$ and its axis ratio $\sqrt{-B/(A - B)}$ (Oort 1965). The ratio between the two velocity dispersions derives from the shape of the epicycle.

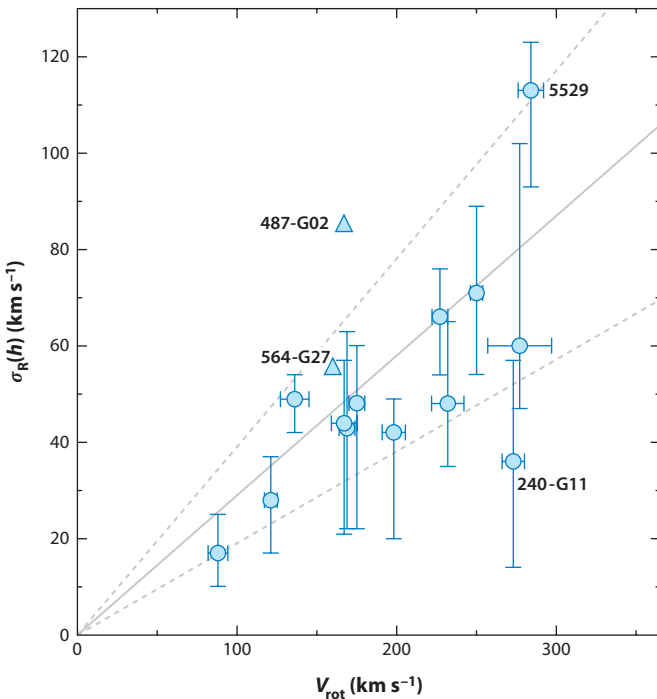


Figure 4

Stellar disk velocity dispersion, measured at one scalelength in edge-on galaxies versus the maximum rotational velocity. The gray solid and dashed lines indicate the relation and scatter $\sigma_R(b) = (0.29 \pm 0.10)V_{\text{rot}}$. (From Kregel, van der Kruit & Freeman 2005).

different assumptions for the radial dependence of the radial velocity dispersion: one that the axis ratio of the velocity ellipsoid (between the vertical and radial dispersion) is the same everywhere, and the other that the Toomre Q is constant with radius. Both assumptions worked well; over the observed range of one or two scalelengths from the center, the two assumptions correspond to similar variations (see Gilmore, King & van der Kruit 1990, p. 196).

More extensive observations by Bottema (1993) on a sample of 12 galaxies (including the Milky Way Galaxy from Lewis & Freeman 1989) resulted in the discovery of a relation between a fiducial value of the velocity dispersion (either the vertical one measured at or extrapolated to the center or the radial velocity dispersion at one scalelength) and the integrated luminosity or the rotation velocity. Luminosity and rotational velocity are equivalent through the Tully-Fisher relation. This has been confirmed by Kregel & van der Kruit (2005) and Kregel, van der Kruit & Freeman (2005) (see Figure 4). The relation⁶ is

$$\sigma_z(0) = \sigma_R(b) = (0.29 \pm 0.10)V_{\text{rot}}. \quad (11)$$

It extends to very small dwarf galaxies, e.g., UGC 4325 with a velocity dispersion of 19 km s^{-1} still falls on the relation (Swaters 1999, chapter 7). The scatter in this relation is not random but appears related to other properties. Galaxies with lower velocity dispersions have higher flattening, lower central surface brightness, or dynamical mass ($4bV_{\text{rot}}^2/G$) to disk luminosity ratio.

The linear $\sigma - V_{\text{rot}}$ relation follows from straightforward arguments, presented in Gilmore, King & van der Kruit (1990, chapter 10) (see also Bottema 1993, van der Kruit & de Grijs 1999). We evaluate properties at one radial scalelength ($R = 1b$) without using subscripts to indicate this.

⁶The formal fit to the sample in Kregel, van der Kruit, & Freeman (2005) is $\sigma_R(b) = (-2 \pm 10) + (0.33 \pm 0.05)V_{\text{rot}}$; the equation above gives the relation adopted from all available studies.

Using the definition for Toomre Q for a flat rotation curve, so that $\kappa = \sqrt{2}V_{\text{rot}}/R$, and eliminating b using a Tully-Fisher relation $L_{\text{disk}} \propto \mu_{\circ} b^2 \propto V_{\text{rot}}^4$ results in

$$\sigma_{\text{R}} \propto Q \frac{\mu_{\circ}(M/L)_{\text{disk}} b}{V_{\text{rot}}} \propto Q \left(\frac{M}{L} \right)_{\text{disk}} \mu_0^{1/2} V_{\text{rot}}. \quad (12)$$

This shows that, when Q and M/L are constant among galaxies, the Bottema relation follows, with indeed the proviso that galaxy disks with lower (face-on) central surface brightness μ_{\circ} at a given value of V_{rot} have lower stellar velocity dispersions than given by the mean $\sigma - V_{\text{rot}}$ relation.

3.2.3. Origin of the constant scaleheight. The origin of the constant scaleheight of stellar disks—or of the fall-off of stellar vertical velocity dispersion so as to precisely compensate for the decline in surface density—is not obvious. If the evolution of the stellar velocity dispersions (the heating of the disk) is similar at all radii and if it evolves to a radial velocity dispersion such that the disk is just stable everywhere, we may expect $\sigma_z/\sigma_{\text{R}}$ (the axis ratio of the velocity ellipsoid) and Toomre Q to be independent of galactocentric radius. This would, however, imply that $\sigma_z \propto (R/b) \exp(-R/b)$. Although this is not all that much different from the exponential decline $\exp(-R/2b)$ that follows from Equation 7 between say one and three scalelengths,⁷ it is significantly different at larger radii. In fact, the simple assumption would result in $b_z \propto (R/b)^2 \exp(-R/b)$, which is far from constant over the range $R = 0$ to $R = 5b$.

There are three general classes of models for the origin of the velocity dispersions of stars in galactic disks. The first, going back to Spitzer & Schwarzschild (1951), is scattering by irregularities in the gravitational field, later identified with the effects of giant molecular clouds (GMCs). The second class of models can be traced back to the work of Barbanis & Woltjer (1967), who suggested transient spiral waves as the scattering agent; this model has been extended by Carlberg & Sellwood (1985). More recently, the possibility of infall of satellite galaxies has been recognized as a third option (e.g., Velázquez & White 1999).

Almost all of the observational information about the evolution of velocity dispersion with age in galactic disks comes from the Solar Neighborhood, and we must stress that this information remains quite insecure. Although much of the earlier work invokes the results of Wielen (1977), which indicates a steady increase of stellar velocity dispersion with age, some of the more recent observational studies indicate that the velocity dispersion increases with age for only 2 to 3 Gyr and then saturates, remaining constant for disk stars of older age (see, e.g., Edvardsson et al. 1993, 1994; Freeman 1991; Soubiran et al. 2008). The observational situation regarding disk heating is far from certain, and this in turn must reflect on the various theories of disk heating.

In the Solar Neighborhood, the ratio of the radial and vertical velocity dispersion of the stars $\sigma_z/\sigma_{\text{R}}$ is usually taken as roughly 0.5 to 0.6 (Wielen 1977, Gomez et al. 1990, Dehnen & Binney 1998, Mignard 2000), although values on the order of 0.7 are also found in the literature (Woolley et al. 1977; Meusinger, Reimann & Stecklum 1991). The value of this ratio can be used to test predictions for the secular evolution in disks and perhaps distinguish between the general classes of models. Lacey (1984) and Villumsen (1985) have concluded that the Spitzer-Schwarzschild mechanism is not in agreement with observations; the predicted time dependence of the velocity dispersion of a group of stars as a function of age disagrees with the observed age–velocity dispersion relation (see also Wielen 1977), though it would not be possible for the axis ratio of the velocity ellipsoid $\sigma_z/\sigma_{\text{R}}$ to be less than about 0.7 (but see Ida, Kokuba & Makino 1993).

⁷The reason why the two analyses of the measurements of velocity dispersion in van der Kruit & Freeman (1986) and in Bottema et al. (see references in Bottema 1993) both gave good fits.

Jenkins & Binney (1990) argued that it is likely that the dynamical evolution in the directions in the plane and that perpendicular to it could have proceeded with both mechanisms contributing, but in different manners. Scattering by GMCs would then be responsible for the vertical velocity dispersion, whereas scattering from spiral irregularities would produce the velocity dispersions in the plane. The latter would be the prime source of the secular evolution; the scattering by molecular clouds is a mechanism by which some of the energy in random motions in the plane is converted into vertical random motions, hence determining the thickness of galactic disks. The effects of a possible slow, but significant accretion of gas onto the disks over their lifetimes have been studied by Jenkins (1992), who pointed out strong effects on the time dependence of the vertical velocity dispersions, in particular giving rise to enhanced velocities for the old stars. However, Hänninen & Flynn (2000, 2002) conclude that observations such as the radial dependence of stellar velocity dispersions in the Milky Way Galaxy by Lewis & Freeman (1989) can be reproduced if scattering occurs by a combination of massive halo objects (black holes) and GMCs. Dehnen & Binney (1998) conclude that spiral structure is probably a major contributor to disk heating. More recently, Minchev & Quillen (2006) suggested from 2D simulations that multiple patterns of spiral structure could cause strong variations of stellar velocity dispersions with galactocentric radius, which has not been observed. Our conclusion is that there still is much uncertainty about the process of heating of the (thin) disk. Some of this uncertainty is due to uncertainty in the observational relation between stellar ages and velocity dispersions, because stellar ages are so difficult to measure.

Theoretical arguments suggest that a constant axis ratio of the velocity ellipsoid is a fair approximation in the inner parts of galaxy disks (Cuddeford & Amendt 1992; Famaey, van Caelenberg & DeJonghe 2002). An observational argument for the approximate constancy of the velocity anisotropy is provided by the ages and kinematics of 182 F and G dwarf stars in the Solar Neighborhood (Edvardsson et al. 1993). This indicates that the anisotropy was set after an early heating phase and, although the Galaxy has probably changed much over its lifetime, has remained constant throughout the life of the old disk (Freeman 1991).

So, where does this leave us with respect to the origin of the constant scaleheight? As long as there is no detailed understanding of the evolution of the velocity dispersions as a function of galactocentric radius, we cannot even begin to address this in a meaningful way. A constant stability parameter Q and a constant axis ratio of the velocity ellipsoid σ_z/σ_R do give an approximate constant thickness over the inner few scalelengths, but this fails at larger radii.

3.2.4. Mass distributions from stellar dynamics. The stellar velocity dispersions can still be used to derive information on the disk mass distribution. For a self-gravitating disk that is exponential in both the radial and vertical direction, the vertical velocity dispersion goes as (cf. van der Kruit 1988)

$$\sigma_z(R, z) = \sqrt{\pi G b_z (2 - e^{-z/b_z}) (M/L) \mu_0} e^{-R/2b}. \quad (13)$$

Assuming a constant (but unknown) axis ratio of the velocity ellipsoid σ_z/σ_R , the radial velocity dispersion becomes

$$\sigma_R(R, z) = \sqrt{\pi G b_z (2 - e^{-z/b_z}) (M/L) \mu_0} \left(\frac{\sigma_z}{\sigma_R} \right)^{-1} e^{-R/2b}. \quad (14)$$

The distribution of the products $\sqrt{M/L_I} (\sigma_z/\sigma_R)^{-1}$, deduced from this equation in the Kregel, van der Kruit & Freeman (2005) sample, is shown in **Figure 5**. This sample of edge-on galaxies has a range of Hubble types from Sb to Scd, absolute I -magnitudes between -23.5 and -18.5 , and a range in rotation velocities from 89 to 274 km s $^{-1}$. Thirteen of the fifteen disks have $1.8 \lesssim \sqrt{M/L_I} (\sigma_z/\sigma_R)^{-1} \lesssim 3.3$. The values of the outliers may have been overestimated (see Kregel,

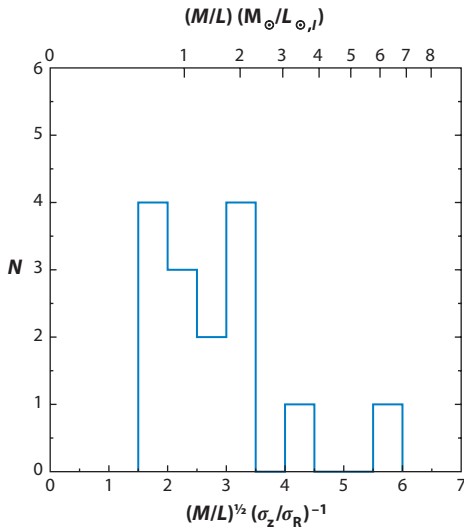


Figure 5

Histogram of the product $\sqrt{M/L_I}(\sigma_z/\sigma_R)^{-1}$ from stellar kinematics in edge-on galaxies. Except for two outliers, the distribution of $\sqrt{M/L_I}(\sigma_z/\sigma_R)^{-1}$ is rather narrow. The outliers are ESO 487-G02 and 564-G27; data for these galaxies are less complete than for the other ones. Along the top we show the values of M/L_I implied by $\sigma_z/\sigma_R = 0.6$. (From Kregel, van der Kruit & Freeman 2005).

van der Kruit & Freeman 2005). Excluding these, the average is $\langle \sqrt{M/L_I}(\sigma_z/\sigma_R)^{-1} \rangle = 2.5 \pm 0.2$ with a 1σ scatter of 0.6. The near constancy of the product can be used with mass-to-light ratios based on stellar population synthesis models to estimate the axis ratio of the velocity ellipsoid. Conversely, the upper scale of **Figure 5** indicates that a typical M/L in the I -band of a galactic stellar disk is of order unity and, for the majority of systems, lies between 0.5 and 2.

It is possible to relate the axis ratio of the velocity ellipsoid to the flattening of the stellar disk, i.e., the ratio of the radial exponential scalelength and the vertical exponential scaleheight (van der Kruit & de Grijs 1999). In the radial direction, the velocity dispersion at one scalelength can be written using the definition of Toomre Q as $\sigma_{R,h} \propto Q\Sigma(b)b/V_{\text{rot}}$, where a flat rotation curve has been assumed. At this radius of one scalelength, the hydrostatic equation gives $\sigma_z \propto \sqrt{\Sigma(b)b_z}$. Eliminating $\Sigma(b)$ between these two equations then gives

$$\left(\frac{\sigma_z}{\sigma_R} \right)_h^2 \propto \frac{1}{Q} \frac{b_z}{b}. \quad (15)$$

If Q is constant within individual disks, then the disk flattening depends directly on the axis ratio of the velocity ellipsoid.

Equation 12 shows that when Q and M/L are constant among galaxies, galaxy disks with lower (face-on) central surface brightness μ_0 have lower stellar velocity dispersions. Combining Equation 12 with the hydrostatic equilibrium of Equation 7 and using Equation 11 gives (Kregel, van der Kruit & Freeman 2005, van der Kruit & de Grijs 1999)

$$\frac{b}{b_z} \propto Q \left(\frac{\sigma_R}{\sigma_z} \right) \sigma_z^{-1} V_{\text{rot}} \propto Q \left(\frac{\sigma_R}{\sigma_z} \right). \quad (16)$$

The observed constancy of $\sqrt{M/L}(\sigma_z/\sigma_R)^{-1}$ implies that the flattening of the disk b/b_z is proportional to $Q\sqrt{M/L}$.

For a self-gravitating exponential disk, the expected rotation curve peaks at 2.2 scalelengths. The ratio of this peak of the rotation velocity of the disk to the maximum rotation velocity of the galaxy ($V_{\text{disk}}/V_{\text{rot}}$) is

$$\frac{V_{\text{disk}}}{V_{\text{rot}}} = \frac{0.880(\pi G \Sigma_0 b)^{1/2}}{V_{\text{rot}}}. \quad (17)$$

Using Equations 7 and 11, this can be rewritten as

$$\frac{V_{\text{disk}}}{V_{\text{rot}}} = (0.21 \pm 0.08) \sqrt{\frac{b}{b_z}}. \quad (18)$$

So, we can estimate the disk contribution to the rotation curve from a statistical value for the flattening (see also Bottema 1993, 1997; van der Kruit 2002). For the sample of Kregel, van der Kruit & de Grijs (2002), this then results in $V_{\text{disk}}/V_{\text{rot}} = 0.57 \pm 0.22$ (rms scatter). In the dynamical analysis of Kregel, van der Kruit & Freeman (2005), the ratio $V_{\text{disk}}/V_{\text{rot}}$ is known up to a factor σ_z/σ_R and distance-independent. The derived disk contribution to the observed maximum for the same sample rotation is, on average, $V_{\text{disk}}/V_{\text{rot}} = 0.53 \pm 0.04$, with a 1σ scatter of 0.15. Both estimates agree well.

In the maximum disk hypothesis, $V_{\text{disk}}/V_{\text{rot}}$ will be a bit lower than unity to allow a bulge contribution and let dark matter halos have a low-density core. A working definition that has been adopted generally is $V_{\text{disk}}/V_{\text{rot}} = 0.85 \pm 0.10$ (Sackett 1997). Thus, at least for this sample, the average spiral has a submaximal disk. Note that Equation 17 strictly applies to a razor-thin disk. For a disk with a flattening of $b/b_z \simeq 10$, the radial gravitational force is weaker, leading to decrease of about 5% in $V_{\text{disk}}/V_{\text{rot}}$ (van der Kruit & Searle 1982a). Taking the gravity of the gas layer and dark matter halo into account would yield a 10% effect, also in this direction. So, these effects work in the direction of making the disks more submaximal.

The values obtained from stellar dynamics are illustrated in **Figures 6** and **7**. The measurement of stellar velocity dispersions can be used to derive the disk surface density at some point (e.g., one scalelength) up to a factor $(\sigma_z/\sigma_R)^2$, but can be estimated also from the velocity dispersion for an assumed value of Q . Comparing the two then gives an estimate of the axis ratio of the velocity ellipsoid. In **Figure 7a**, Q is assumed to be 2.0 and **Figure 7b** the velocity anisotropy is assumed to be 0.6 and then a value for Q results. Most galaxies are not maximum disk. The ones that may be maximum disk have a high surface density according to **Figure 5**. From the panels, we also note that disks that are maximal appear to have more anisotropic velocity distributions or are less stable according to Toomre Q . We return to the maximum disk hypothesis below (Section 4.2).

3.3. Age Gradients and Photometric M/L Ratios

Colors contain information on the history of star formation, as can be studied in the context of integrated colors of galaxies, pioneered by Searle, Sargent & Bagnuolo (1973) and Larson & Tinsley (1978) and described in much detail by Tinsley (1980), and also as a function of radius in a galaxy disk. Observing and interpreting color gradients in galactic disks is not straightforward. Obviously one needs accurate photometry for unambiguous interpretation in terms of stellar synthesis and star-formation histories. However, the effects of age⁸ and metallicity are difficult to separate. Dust absorption is also a major factor, often making degenerate the effects of stellar age and metallicity on the one hand and extinction and reddening by dust on the other.

⁸It should be noted that in discussions of these subjects the property “stellar age” is usually the mean age of all stars derived as a luminosity-weighted average, further weighted by the star-formation rate over the lifetime of the disk, and should not be confused with the age of the oldest stars.

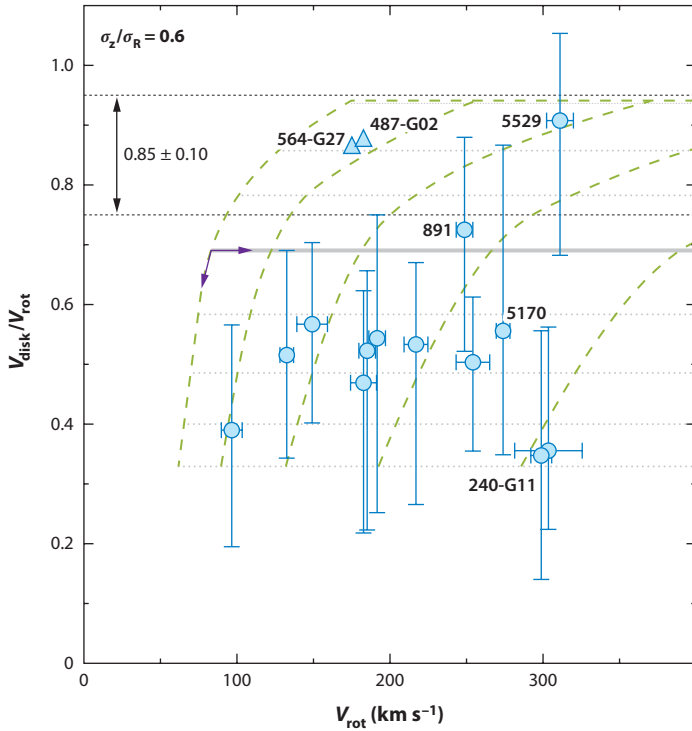


Figure 6

The contribution of the disk to the amplitude of the rotation curve $V_{\text{disk}}/V_{\text{rot}}$ for a sample of 15 edge-on galaxies as a function of the rotation velocity itself. The dotted lines at the top and arrow show the limits and interval of 0.85 ± 0.10 from Sackett (1997) for maximum disk fits. The axis ratio of the velocity ellipsoid is assumed to be 0.6. The dotted gray lines correspond to the collapse models of Dalcanton, Spergel & Summers (1997); the dashed green lines connect models of the same total mass [$\log_{10}(M_{\text{tot}}) = 10 - 13$ in steps of 0.5], and dotted lines connect models with the same spin parameter λ [see Equation (22)]. The purple arrows indicate the direction of increasing M_{tot} and λ . The two galaxies without error bars are the same ones as the outliers in Figure 5. (From Kregel, van der Kruit & Freeman 2005).

Figure 7 of Larson & Tinsley (1978) is instructive. It shows a sequence of population synthesis models in the two-color ($U-B$) versus ($B-V$) diagram, with ages of 10^{10} years and star-formation histories ranging from initial burst to constant with time. The effects of age, metallicity, and absorption, and even changes in the IMF, shift the models in very similar directions!

Wevers, van der Kruit & Allen (1986) were the first to undertake a systematic survey of the luminosity, color, and HI distributions in a well-defined set of spiral galaxies. The surface photometry was based on photographic plates and, although the data did show color gradients, Wevers (1984) was not sufficiently confident to conclude that these were significant. In hindsight, this was not justified: A detailed comparison by Begeman (1987) with later CCD photometry by Kent (1987) for three systems showed deviations of at most 0.2 mag in the radial profiles down to $26 r\text{-mag arcsec}^{-2}$. Although common wisdom holds that old photographic surface photometry is not reliable, at least some of it certainly is.

A comprehensive study of the broadband optical and near-IR colors in a sample of 86 disk galaxies was performed by de Jong & van der Kruit (1994) and de Jong (1996a–c). These studies established the existence of color gradients both within and among galaxy disks, with fainter surface brightness systematically corresponding to bluer colors. It was also found that the degeneracies

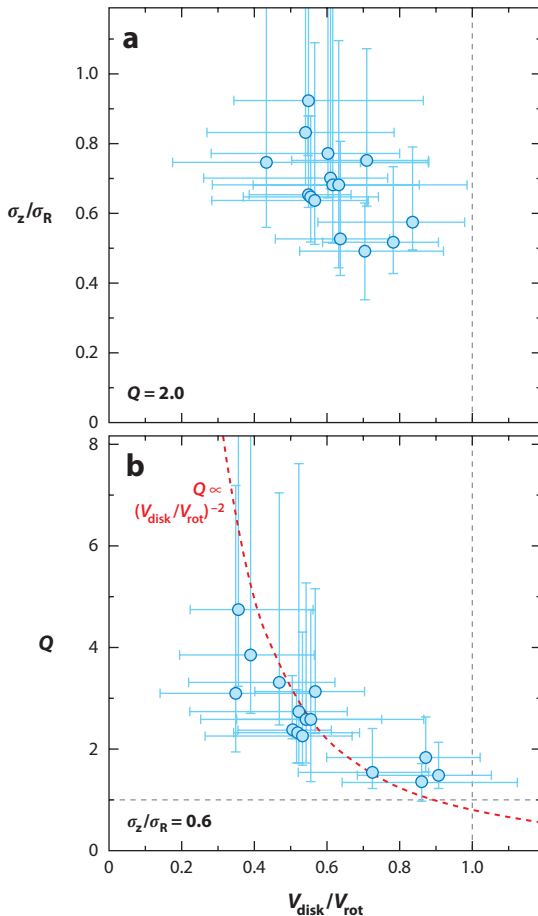


Figure 7

Stellar dynamics parameters for edge-on galaxies.
(a) The axis ratio of the velocity ellipsoid as a function of $V_{\text{disk}}/V_{\text{rot}}$ for $Q = 2.0$. (b) $V_{\text{disk}}/V_{\text{rot}}$ as a function of Q for an assumed axis ratio of the velocity ellipsoid of 0.6. (From Kregel, van der Kruit & Freeman 2005).

between dust absorption, stellar age, and metallicity can be broken to a large extent by use of a set of photometric bands from the blue (*B*-band) to the near-IR (*K*), and it was concluded from 3D radiative transfer models that dust extinction cannot be the major cause of the observed gradients. The color gradients must be the result of significant differences in star-formation history, whereby the outer regions are younger and of lower metallicity than the central parts. The lack of suitable stellar population models made it impossible to quantify the trends, although the extreme variations predicted by the models of Larson (1976) seemed outside the range of possibilities offered by the observed color gradients.

Peletier & de Grijjs (1998) used (*I*–*K*) colors in edge-on galaxies away from the central planes to derive a dust-free, near-IR, color-magnitude relation for spiral galaxies. The slope of this relation is steeper for spirals than for elliptical galaxies. This is most likely not a result of vertical abundance gradients, but of average age with height. The surprising thing is that the scatter in this relation is small, possibly even only due to observational uncertainty. Average stellar age must be an important contributor to variations in broadband colors.

Bell & de Jong (2000) made an important step forward by using maximum-likelihood methods to match observed colors with stellar population synthesis models, using simple star-formation histories. These showed that spiral galaxies almost all have significant gradients in the sense that the inner regions are older and more metal rich than the outer regions. The amplitude of these

gradients is larger in high surface brightness galaxies than in low surface brightness ones, and the progress of star formation (as evidenced by decreasing age and increasing metallicity) depends primarily on the surface brightness (most clearly in the K -band) or surface density. The local surface density seems to shape the star-formation history in a disk more strongly than the overall mass of the galaxy.

These models can also be used to derive values and gradients of the mass-to-light ratio M/L in and among disks. This was done by Bell & de Jong (2001) under the assumption of a universal IMF. They conclude that their relative trends in M/L with color are robust to uncertainties in the stellar populations and galaxy evolution models. They also find that limits on the M/L ratios derived from maximum disk fits to rotation curves [for galaxies in the Ursa Major cluster by Verheijen (2001), Verheijen & Sancisi (2001)] match their M/L ratios well, providing support for the universality of the IMF and the notion that at least some high surface brightness galaxies are close to maximum disk. The variations in M/L span a factor between 3 and 7 in the optical and about 2 in the near-IR.

The IMF provides the normalization of the M/L through the numbers of low-mass stars, but the slope of the relation between color and M/L is largely independent of what models are used or what IMF is adopted (de Jong & Bell 2009). The Salpeter IMF gives too massive a normalization (Bell & de Jong 2001), which can be remedied by using a “diet” Salpeter IMF (i.e., deficient in low-mass stars such that it has only 70% of the mass for the same color; Bell & de Jong 2001), or adopting an IMF that is itself more deficient in low-mass stars (Kennicutt 1983, Kroupa 2001, Chabrier 2003). Kroupa (2002a) has rather convincingly argued that the IMF is universal to the extent that its variations are smaller than would follow from the expected varying conditions on the basis of elementary considerations. Bastian, Covey & Meyer (2010, see abstract) have recently concluded that “there is no clear evidence that the IMF varies strongly and systematically as a function of initial conditions after the first few generations of stars.”

Default models, produced by adopting a declining star-formation rate, the population synthesis models of Bruzual & Charlot (2003), and the IMFs listed above, give consistent estimates of M/L (de Jong & Bell 2009). In fact, the M/L_I values implied in **Figure 5** on the top axis (derived for an axis ratio of the velocity ellipsoid of 0.6) are 0.2 dex lower than from Bell & de Jong (2001) but, as de Jong & Bell (2009) point out, the axis ratio of the velocity ellipsoid scales with the square of M/L . The conclusion is that the determination of mass-to-light ratios from broadband colors is reliable and robust in a relative sense, but that there are still some uncertainties in the normalization resulting from imprecise knowledge of the faint part of the IMF.

3.4. Global Stability, Bars, and Spiral Structure

Local stability of stellar disks has already been discussed in relation to local stellar velocity dispersions, Toomre’s Q , and the secular evolution (heating) of disks. We say a few words here about global stability, bars in galaxies, and spiral structure. Much of these subjects has been covered recently in the reviews, such as that on dynamics of galactic disks by Sellwood (2011a) and for the case of bars in relation to pseudobulges by Kormendy & Kennicutt (2004).

Global stability of disks has been a subject ever since numerical simulations became possible, starting about 1970 (e.g., Miller et al. 1970, Hohl 1971). Criteria for stability were formulated empirically by Ostriker & Peebles (1973) and Efstathiou et al. (1982). In the latter criterion, the halo stabilizes the disk; the criterion is in terms of observables,

$$Y = V_{\text{rot}} \left(\frac{b}{GM_{\text{disk}}} \right)^{1/2} \gtrsim 1.1, \quad (19)$$

where the disk is assumed to be exponential with scalelength b and total mass M_{disk} . Because the rotation velocity V_{rot} is related to the total mass, it is a criterion that relates to the relative mass in disk and halo. It can be rewritten to say that within the radial distance from the center corresponding to the edge of the disk, the dark matter halo contains up to 60–70% of the total mass (van der Kruit & Freeman 1986). Such galaxies are in fact submaximal. Sellwood (2011a) concludes that these criteria are only necessary for disks that have no dense centers, because central concentrations of mass in disks themselves could also provide global stability. It was shown already some decades ago (Kalnajs 1987) that halos are not very efficient in stabilizing disks as compared to bodes.

We do not discuss the formation of bars in galaxies, as this subject has been covered in detail by Kormendy & Kennicutt (2004), in relation to pseudobulges, and by Sellwood (2011a). We do want to stress the fundamental point that the incidence of bars is much larger than traditionally thought; a typical fraction that figured in previous decades—although admittedly for strongly barred galaxies as in Sandage (1961)—was of the order of a quarter to a third. Current estimates are much higher; Sheth et al. (2008) found in the COSMOS field that, in the local Universe, about 65% of luminous spiral galaxies are barred. This fraction is a strong function of redshift, dropping to 20% at a redshift of 0.8. The *Spitzer Survey of Stellar Structure in Galaxies S⁴G* (Sheth et al. 2010) aims, among other goals, at studying this in the near-IR. As an example, we show in **Figure 8a** a blue and near-IR image of the large spiral M83. Although it appears mildly barred in the optical, it is clear that in the K -band the bar is very prominent and extended.

Throughout the previous century, much attention has been paid to the matter of the formation and maintenance of spiral structure. It was extensively reviewed by Toomre (1977, 1981). Spiral structure in itself is unquestionably an important issue (see the quotation of Richard Feynman in the introduction in Toomre's review), as it is so obvious in galaxy disks and appears to play a determining role in the evolution of disks through the regulation of star formation and, therefore, the dynamical, photometric, and chemical evolution. We do not discuss theories of spiral structure itself, as progress in this area has recently been somewhat slow. We refer the reader to the contributions of Kormendy & Norman (1979), Sellwood & Carlberg (1984), Elmegreen,

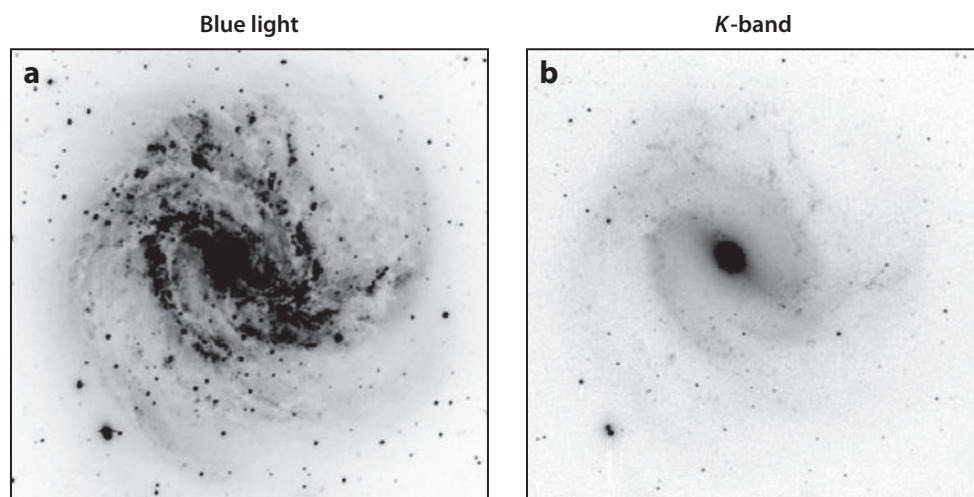


Figure 8

M83 (*a*) in blue light and (*b*) in the K -band. The bar is much more obvious in the near-IR. (Unpublished images by O.-K. Park and K.C. Freeman).

Elmegreen & Leitner (2003), and Sellwood (2008, 2011a,b). Spiral structure is often related to gravitational interaction between galaxies; for interactions and subsequent merging, see the work of Toomre & Toomre (1972), Schweizer (1986), and Barnes (1988).

3.5. The Flatness of Disks

The inner disks of galaxies are often remarkably flat. For the stellar disks, this can be studied in edge-on systems by determining the centroid in the direction perpendicular to the major axis at various galactocentric distances (e.g., Sanchez-Saavedra, Battaner & Florido 1990; Florido et al. 1991; de Grijs 1997, chapter 5). These studies were aimed at looking for warps in the outer parts of the stellar disks (see below), but it is obvious from the distributions that in the inner parts the systematic deviations are very small.

The evidence for the flatness of stellar disks is more compelling when we look at the flatness of the layers of the ISM. First, look at the dustlanes. In **Figure 9**, we collect some images of edge-on disk galaxies. In the top row are two super-thin galaxies (which we discuss further in Section 3.6); the disks are straight lines to within a few percent. The same holds for the dustlanes in NGC 4565 (*second row, left*; allow for the curvature due to its imperfectly edge-on nature) and NGC 891 (*second row, right*). Again the dustlanes indicate flat layers to a few percent. In the third row, the peculiar structure of NGC 5866 (*left*) has no measurable deviation from a straight line, whereas for the Sombrero Nebula (*right*) the outline of the dustlane fits very accurately to an ellipse. In the bottom row, NGC 7814 (*fourth row, right*) is straight again to within a few percent, but NGC 5866 (*third row, left*) is an example of a galaxy with a large warp in the dust layer.

The H α kinematics provide probably the strongest indications for flatness. In three almost completely face-on spirals (NGC 3938, 628, and 1058), van der Kruit & Shostak (1982, 1984)

Edge-on disks and dustlanes

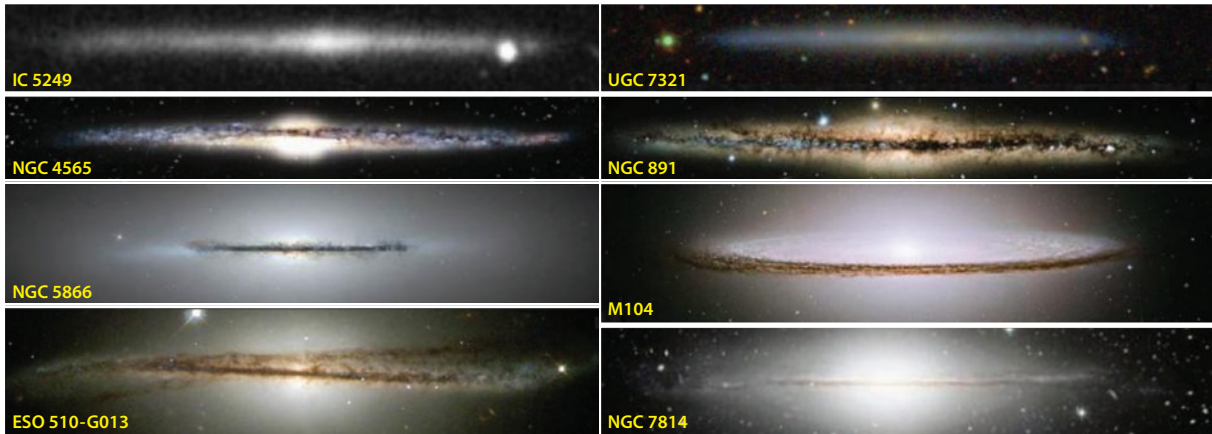


Figure 9

Selected images of edge-on disks and dustlanes from various public Web-galleries. First row: Super-thin galaxies, IC 5249 (*left*; from the Sloan Digital Sky Survey, van der Kruit et al. 2001) and UGC 7321 (*right*; http://cosmo.nyu.edu/hogg/rc3/UGC_732_irg_hard.jpg); second row: NGC 4565 (*left*; <http://www.cfht.hawaii.edu/HawaiianStarlight/AIOM/English/2004/Images/Nov-Image2003-CFHT-Coelum.jpg>) and NGC 891 (*right*; <http://www.cfht.hawaii.edu/HawaiianStarlight/Posters/NGC891-CFHT-Cuillandre-Coelum-1999.jpg>); third row: NGC 5866 (*left*; <http://heritage.stsci.edu/2006/24/big.html>) and M104 (*right*; <http://heritage.stsci.edu/2003/28/big.html>); fourth row: ESO 510-G013 (*left*; <http://heritage.stsci.edu/2001/23/big.html>) and NGC 7814 (*right*; <http://www.cfht.hawaii.edu/HawaiianStarlight/English/Poster50x70-NGC7814.html>).

and Shostak & van der Kruit (1984) found that the residual velocity field after subtraction of that of the systematic rotation shows no systematic pattern and had a root-mean-square value of only 3–4 km s⁻¹. So, vertical motions must be restricted to only a few kilometer per second (a few parsecs per million years). Then, even a vertical oscillation with a period equal to the typical time of vertical oscillation of a star in the Solar Neighborhood (10⁷ years) or of the rotation of the Sun around the Galactic Center (10⁸ years) would have an amplitude of only 10 to 100 pc. Again, this is of order a few percent or less of the diameter of a galaxy like our own. The absence of such residual patterns shows that the HI layers and, thus, because they are more massive, the stellar disks must be extraordinarily flat, except maybe in their outer regions. This obviously does not hold for galaxies that are or have recently been in interaction.

Recently, Matthews & Uson (2008a,b) found evidence for a pattern of corrugation in the disk of the edge-on galaxy IC 2233. The excursion of the plane is most pronounced in younger tracer populations, such as HI or young stars. The amplitude is up to 250 pc (compared to a radius of order 10 kpc). The older disk shows much less of an effect. IC 2233 is a relatively small galaxy (rotation velocity about 100 km s⁻¹) and has extensive star formation; it appears that the effect is related to the process of star formation.

3.6. Super-Thin Galaxies

We have indicated above that the flattening of the stellar disk b_z/b is smallest for systems that are of late Hubble type, small rotation velocity, and faint (face-on) surface brightness. It is of interest then to look more closely at systems at this extreme end of the range of flattening; such systems are referred to as superthin. Of course, the ones we can identify are seen edge-on. A prime example is the galaxy UGC 7321, studied extensively by Matthews, Gallagher & van Driel (1999), Matthews (2000), Matthews & Wood (2003), Uson & Matthews (2003), and Banerjee, Matthews & Jog (2010). This is a very LSB galaxy (its face-on B -band central surface brightness would be ~ 23.4 mag arcsec⁻²) with a scalelength of about 2 kpc, but a projected vertical scaleheight of only 150 pc. There is evidence for vertical structure: It has a color gradient (bluer near the central plane) and appears to consist of two components. Rotation curve analysis (Banerjee, Matthews & Jog 2010; O'Brien, Freeman & van der Kruit 2010c) indicates that it has a large amount of mass in its dark matter halo compared to the luminous component. Its HI is warped in the outer parts, starting at the edge of the light distribution. Extended HI emission is visible at relative high z (more than 2 kpc out of the plane). Pohlen et al. (2003) argue that the deviation in the light profile in the central regions and the shape of the isophotes point at a presence of a large bar.

Another good example of a superthin galaxy is IC 5249 (Byun 1998, Abe et al. 1999, van der Kruit et al. 2001). This also is an LSB galaxy with presumably a small fraction of the mass in the luminous disk. However, the disk scaleheight is not small (0.65 kpc). It has a very long radial scalelength (17 kpc); its faint surface brightness μ_0 then causes only the parts close to the plane to be easily visible against the background sky, while the long radial scalelength assures this to happen over a large range of R . Therefore, it appears thin on the sky. The flattening b_z/b is 0.09 (versus 0.07 for UGC 7321). The stellar velocity dispersions are similar to those in the Solar Neighborhood; disk heating must have proceeded at a pace comparable to that in the Galaxy.

The flattest galaxies appear not only very flat on the sky, but have indeed very small values of b_z/b . However, these two examples show that the detailed structure may be different. Super-thin galaxies do share the property of late-type, faint, face-on surface brightness and small amounts of luminous disk mass compared to that in the dark matter halo.

Kautsch (2009) has reviewed the observations of flat and super-thin galaxies, especially in view of the fact that these late-type, bulgeless systems present challenges to models of disk galaxy

formation within the hierarchical growth context of Λ CDM. These pure disk systems have LSB blue structures with low angular momenta, which may have formed with a lower frequency of merging events than disk galaxies with bulges and thick disks. In large and giant galaxies, the question of the frequency of the presence of a “classical” bulge has been addressed by Kormendy et al. (2010). They find that giant, pure disk galaxies are far from rare, and their existence presents a major challenge to formation pictures with histories of merging in an hierarchical clustering scenario.

3.7. Warps in Stellar Disks

In their outer parts, stellar disks have deviations from both the plane of the inner parts (warps) as well as deviations from the extrapolated exponential surface brightness distributions (truncations). We discuss these phenomena in turn.

First, we examine warps in the outer parts of stellar disks. Studies referred to above (Sanchez-Saavedra, Battaner & Florido 1990; Florido et al. 1991; de Grijs 1997; Reshetnikov et al. 2002) have indicated that most, if not all, disks display warps in their very outer parts, often up to $0.5 h_z$ or more. Recently, Saha, de Jong & Holwerda (2009) have studied edge-on galaxies observed with *Spitzer* in the $4.5\text{-}\mu$ band.⁹ Out of 24 galaxies, they found evidence for warps in 10. The radius of the onset of the warp indicates that there must also be a moderate amount of flaring, in order to match the response to the indicated mass distribution from the light distribution and rotation curve. The warp onset is asymmetric and the more so in small scalelength systems. The reason for this is not clear, but could point to asymmetries in the dark matter distribution. The warp profiles shown in their figures reinforce the point made above about the flatness of disks; in the inner parts, the deviations from a straight line are exceedingly small (only a percent or less of the radial extent). Theoretical work related to warps and dynamics in stellar disks has recently been reviewed by Sellwood (2011a), in the context of collective global instabilities, bending waves, bars, and spiral structure.

Sometimes optical warps are very pronounced, such as in the so-called Integral Sign galaxy UGC 3697 (Burbidge, Burbidge & Shelton 1967; Ann 2007). There have recently been a number of statistical studies (e.g., Schwarzkopf & Dettmar 2001, Ann & Park 2006) from large samples that contain more and less isolated systems. The conclusions are that strong warps are probably all a result of interactions, whereas at least a fraction may arise from accretion of gaseous material. An important point to note is that even isolated galaxies show signs of accretion. Beautiful examples have recently been presented in much detail, including NGC 5907 (Morrison, Boroson & Harding 1994; Martínez-Delgado et al. 2008), NGC 4736 (Trujillo et al. 2009), and NGC 4013 and NGC 5055 (Martínez-Delgado et al. 2009). In NGC 5055, the brightest part of the faint loops has been registered also in the photographic surface photometry of van der Kruit (1979) in two colors; it appeared definitely red and presumably dominated by older stars. These relatively isolated systems appear to show signs for recent accretion events, which therefore must be common. Of course, much is known now about substructure in the halo of our Galaxy (Helmi 2008) and M31 (Ferguson 2007) and the evidence for continuing accretion that this provides, but that is beyond the scope of this review.

3.8. Truncations

Truncations in stellar disks were first found in edge-on galaxies, where the remarkable feature was noted that the radial extent did not grow with deeper photographic exposures (van der Kruit

⁹This paper contains also a rather complete inventory of publications concerning warps, optical, near-IR, as well as H α .

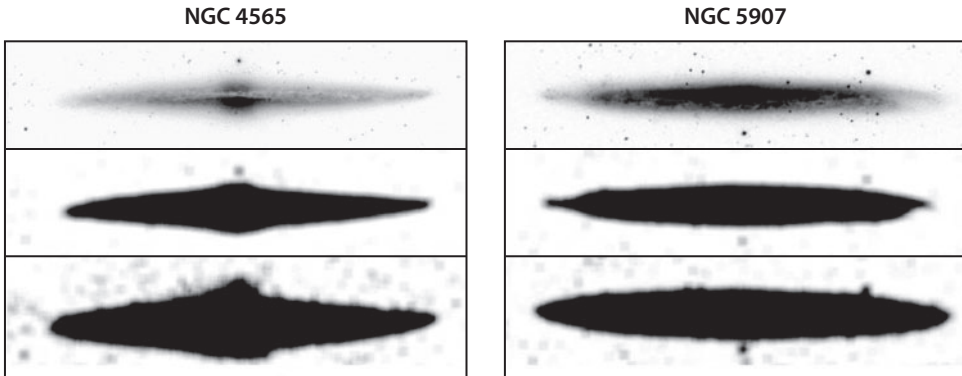


Figure 10

NGC 4565 and NGC 5907 at various light levels. These have been produced from images of the Sloan Digital Sky Survey, which were clipped at three different levels (*top to bottom*), turned into two-bit images, and subsequently smoothed (see van der Kruit 2007, for an explanation of the details). Note that the disks grow significantly along the minor axes but not in radial extent.

1979). Detailed surface photometry (van der Kruit & Searle 1981a,b) confirmed the presence of these truncations in the four brightest, edge-on, disk-dominated galaxies in the northern sky, NGC 891, 4244, 4565, and 5907. For the last two we illustrate this phenomenon of truncation in **Figure 10**. The truncations appear very sharp, although of course not infinitely.¹⁰ Sharp outer profiles are actually obtained after deprojecting near-IR observations of edge-on galaxies (e.g., Florido et al. 2006). Fry et al. (1999), using CCD surface photometry, and de Jong et al. (2007b), using HST star counts, show that the disk of NGC 4244 has a sharp truncation, occurring over only about 1 kpc.

Various models have been proposed for the origin of truncations. In the model by Larson (1976), the truncations are the current extent of the disks while they are growing from the inside out from accretion of external material. This predicts larger age gradients across disks than are observed (de Jong 1996b). Another possibility is that star formation is inhibited when the gas surface (or space?) density falls below a certain threshold for local stability (Fall & Efstathiou 1980, Kennicutt 1989, Schaye 2004). The Goldreich–Lynden–Bell criterion for stability of gas layers gives a poor prediction for the truncation radii (van der Kruit & Searle 1982a). Another problem is that the rotation curves of some galaxies, e.g., NGC 5907 and NGC 4013 (Casertano 1983, Bottema 1996), show features near the truncations that indicate that the mass distributions are also truncated.

Obviously, the truncation corresponds to the maximum in the specific angular momentum distribution of the present disk, which would correspond to that in the protogalaxy (van der Kruit 1987) if the collapse occurs with detailed conservation of specific angular momentum (Fall & Efstathiou 1980). As noted above, if the protogalaxy starts out as a Mestel (1963) sphere with uniform density and angular rotation in the force field of a dark matter halo with a flat rotation curve, a roughly exponential disk results. This disk has then a truncation at about 4.5 scalelengths, so this hypothesis provides at the same time an explanation for the exponential nature of the disk as well as for the occurrence of the truncations. However, it is possible that substantial redistribution of

¹⁰In fact, the statement in van der Kruit & Searle (1981a) reads, “This cut-off is very sharp with an e-folding of less than about 1 kpc,” based on the spacing of the outer isophotes.

angular momentum takes place, so that its distribution now is unrelated to the initial distribution in the material that formed the disks. Bars may play an important role in such redistribution, as suggested by Debattista et al. (2006) and Erwin et al. (2007). In fact, a range of possible agents in addition to bars, such as density waves, heating and stripping of stars by bombardment of dark matter subhalos, has been invoked (de Jong et al. 2007b). Roškar et al. (2008a,b) have studied the origin of truncations or breaks in the radial distributions in stellar disks as related to a rapid drop in star formation and include the effects of radial migration of stars. Observations of stellar populations and their ages in the regions near the truncation (Yoachim, Roškar & Debattista 2010) have been used to provide evidence that migration of stars is a significant phenomenon in the formation and evolution of stellar disks. Finally, there are models (Battener, Florido & Jiménez-Vicente 2002; Florido et al. 2006) in which a magnetic force breaks down as a result of star formation so that stars escape. The evidence for sufficiently strong magnetic fields needs strengthening.

Kregel & van der Kruit (2004b) derive correlations of the ratio of the cut-off radius R_{\max} to the radial scalelength b with b itself and with the face-on central surface brightness $\mu_{0,I}^{\text{fo}}$ (**Figure 11**). R_{\max}/b does not depend strongly on b , but is somewhat less than the 4.5 predicted from the collapse from a simple Mestel sphere. There is some correlation between R_{\max}/b and $\mu_{0,\text{fo}}$, indicating approximately constant disk surface density at the truncations, as possibly expected in the star-formation threshold model. But this model predicts an anticorrelation between R_{\max}/b and b (Schaye 2004), which is not observed. The maximum angular momentum hypothesis predicts that R_{\max}/b should not depend on b or $\mu_{0,\text{fo}}$ and such a model therefore requires some redistribution of angular momentum in the collapse or somewhat different initial conditions.

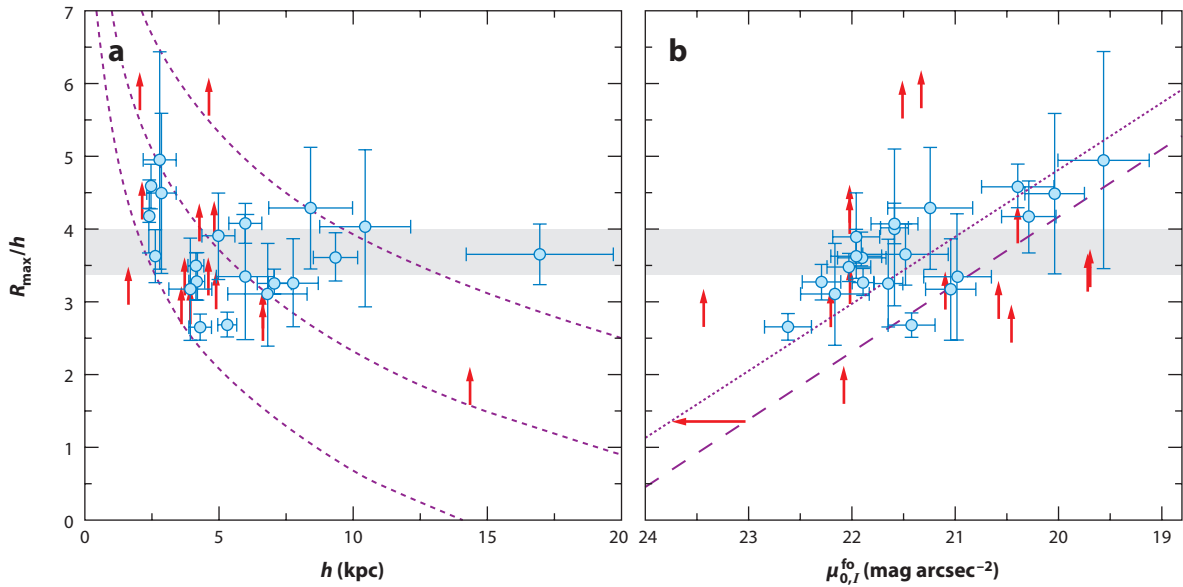


Figure 11

Correlations of R_{\max}/b with scalelength b and face-on central surface brightness $\mu_{0,I}^{\text{fo}}$ for a sample of edge-on galaxies. The gray regions show the prediction from a collapse model as in van der Kruit (1987) and Dalcanton, Spergel & Summers (1997). In panel a, the purple dotted lines show predictions from the star-formation threshold model of Schaye (2004) for three different values of the disk mass; in panel b, the dashed purple line corresponds to the Schaye (2004) prediction, whereas the dotted purple line is the same but arbitrarily shifted by 0.7 mag for an optimum fit. The red arrows are lower limits. (From Kregel & van der Kruit 2004b, and see there for details of the models).

Due to line-of-sight integration, truncations should be more difficult to detect in face-on galaxies than in edge-on ones. The expected surface brightness at 4 scalelengths is about 26 B -mag arcsec $^{-2}$, only a few percent of the dark sky.¹¹ In face-on galaxies like NGC 628 (Shostak & van der Kruit 1984, van der Kruit 1988), an isophote map shows that the outer contours have a much smaller spacing than the inner ones. In the usual analysis, one determines an azimuthally averaged radial surface brightness profile. But this will smooth out any truncation if its radius is not exactly constant with azimuthal angle. At this level, spiral disks are indeed often lopsided, as is seen from the $m = 1$ Fourier component of surface brightness maps (Rix & Zaritsky 1995, Zaritsky & Rix 1997), presumably as a result of interactions and merging. The effects are nicely illustrated in the study of NGC 5923 by Pohlen et al. (2002, their figure 9), which has isophotes in polar coordinates. The irregular outline shows that some smoothing occurs contrary to observations in edge-on systems. Unless special care is taken we will always find a (much) less sharp truncation in face-on than in edge-on systems.

Although we do not discuss oval distortions of disks here because they were reviewed by Kormendy & Kennicutt (2004), we emphasize that they are potentially important for studies of truncations and are also of intrinsic interest. Oval distortions in unbarred galaxies can have significant kinematical and dynamical effects.

Pohlen & Trujillo (2006) studied a sample of moderately inclined systems through ellipse-fitting of isophotes in SDSS data. They distinguish three types of profiles: *Type I*, no break; *Type II*, downbending break; and *Type III*, upbending break. Pohlen et al. (2007) have reported that the same profiles occur in edge-on systems; however, of their 11 systems there was only one for each of the types I and III.

Various correlations have been reviewed by van der Kruit (2009). In general, the edge-on and face-on samples agree in the distribution of R_{\max}/b ; however, the fits in moderately inclined systems result in small values of the scalelength. A prime example of a Type III profile in Pohlen & Trujillo (2006) is NGC 3310, which is a well-known case of a merging galaxy (van der Kruit 1976, Kregel & Sancisi 2001). In fact, on close examination of their images at faint levels, many of the Type III systems show signs of outer distortions, presumably due to interactions.

The truncation in the stellar disk in our Galaxy has also been identified using star counts in a number of surveys (Robin, Crézé & Mohan 1992; Ruphy et al. 1996) to occur at a galactocentric radius of 14 to 15 kpc. Typical values for the ratio between the truncation radius and the radial scalelength R_{\max}/b are 3.5 to 4 (see Figure 11), so that the Galaxy's scalelength is expected on this basis to be 3.5 to 4 kpc. There is a good correlation between the truncation radius R_{\max} and the rotation velocity (van der Kruit 2008). On average, a galaxy like our own would have an R_{\max} of 15–25 kpc. It is of interest to compare this correlation to the case of NGC 300 (Bland-Hawthorn et al. 2005), which has no truncation even at 10 scalelengths from the center ($R_{\max} > 14.4$ kpc), and therefore is an example of a type I disk in the terminology of Pohlen & Trujillo (2006). Despite showing no sign of truncation down to a very faint surface brightness level, we note that its lower limit to R_{\max} is still consistent with the observed correlation between R_{\max} and V_{rot} in edge-on systems (NGC 300 has a rotational velocity of ~ 105 km s $^{-1}$, which would give an R_{\max} of 8–15 kpc and an b of 2–4 kpc). NGC 300 could be interpreted as having an unusually small b for its V_{rot} rather than an unusually large R_{\max} for its scalelength. These examples show that at least

¹¹This surface brightness is close to that often associated with the Holmberg diameters (Holmberg 1958), which are often assumed to be diameters at 26.5 B -mag arcsec $^{-2}$ and corrected for inclination. For a discussion of the history of Holmberg radii, see the appendix in van der Kruit (2007). Contrary to common belief, they are defined in terms of photographic density (rather than a well-defined surface brightness) in two bands (photographic and photovisual rather than the B -band) and not corrected for inclination.

some of the type III galaxies could arise from the effects of interactions and merging, and type I systems could at least partly be disks with normal truncation radii, but large R_{\max}/b and small scalelengths, so that their truncations occur at much lower surface brightness.

3.9. Nuclei of Pure-Disk Galaxies

Late-type pure disk galaxies are commonly nucleated, with central nuclear star clusters (e.g., M33; Kormendy & McClure 1993). For a sample studied by Walcher et al. (2005), the dynamical masses of the nuclear clusters are in the range 8×10^5 to $6 \times 10^7 M_{\odot}$. These star clusters usually lie within a few arcsec of the isophotal centers of the galaxies (e.g., Böker et al. 2002). How are the nuclei able to locate accurately the centers of the apparently shallow central potential wells of their exponential disks? The reason may be that the center of the gravitational field of an exponential disk is actually well-defined: The radial gradient of its potential does not vanish at its center, so the force field defines the center of the disk to within a fraction of the scaleheight of the ISM of the disk, which is of order 100 pc.

Structurally the nuclear star clusters are much like Galactic globular clusters (Böker et al. 2004). Their stellar content is, however, very different. The light of the nuclear star clusters is typically dominated by a relatively young star population (Rossa et al. 2006, Kormendy et al. 2010), but the young population provides only a few percent of the stellar mass. They have an underlying older population with an extended history of episodic star formation (Walcher et al. 2006). This episodic star formation may come from gas funnelled into the center of the galaxy by local torques.

AGNs are rare or absent from these nuclei of pure disk galaxies (Satyapal et al. 2009). For the nucleus of the nearby system M33, with a total nuclear mass of about $2 \times 10^6 M_{\odot}$, Gebhardt et al. (2001) were able to derive an upper limit of $1,500 M_{\odot}$ for a supermassive black hole within the nuclear star cluster.

These nuclear star clusters, with their episodic and extended star-formation history, are interesting in their possible relation to some of the Galactic globular clusters, such as the massive cluster ω Centauri, which also shows evidence of an extended history of episodic star formation (e.g., Bellini et al. 2010) and an inhomogeneous distribution of heavy element abundances. This is unusual in globular clusters. Based on chemical evolution arguments, Searle & Zinn (1978) proposed that the Galactic globular clusters originated in small satellite galaxies that were accreted long ago by the Milky Way. The small galaxies are tidally disrupted but the globular clusters survive. Freeman (1993) and Böker (2008) argued that at least some of the globular clusters may have been the nuclei of such satellite systems.

4. HI DISKS

In this chapter we discuss the distribution and kinematics of the gas in galaxy disks, concentrating on the HI, including that at large radii and warps. We end this section with a brief discussion on dust and dustlanes in disks.

4.1. HI Distributions, Kinematics and Dynamics

The study of the distribution of HI in samples of more than a few disks in galaxies has been possible only since the advent of aperture synthesis measurements of the 21-cm line. Early observations with single disk instruments could be made only for the very nearest systems, notably the Andromeda Nebula (in particular, Roberts & Whitehurst 1975). Observations with the necessary angular resolution started with the Owens Valley Two-Element Interferometer (e.g., Rogstad & Shostak 1971), the Half-Mile Telescope at Cambridge (e.g., Baldwin et al. 1971), and the WSRT

(e.g., Allen, Goss & van Woerden 1973). This early work up to about 1977 has been reviewed in van der Kruit & Allen (1978), although mostly in the context of kinematics.

These studies revealed distributions of the HI in most cases to be much more extended than the stellar disks and often warped away from the plane of the stellar disk beyond the boundaries of the light distribution, both in edge-on (Sancisi 1976) and moderately inclined systems (Rogstad & Shostak 1971; Bosma 1981a,b). The most important finding was that the rotation curves at these radii remained flat (see Section 1.1).

Since then, many observations of disk galaxies have been taken. The first extensive survey, including comparison with optical surface photometry, was done by Wevers, van der Kruit & Allen (1986). More recently, the extensive WHISP survey (Kamphuis, Sijbring & van Albada 1996; van der Hulst, van Albada & Sancisi 2001; García-Ruiz, Sancisi & Kuijken 2002; Swaters et al. 2002; Swaters & Balcells 2002; Noordermeer et al. 2005; Noordermeer et al. 2007) was made. The most advanced survey at this stage is THINGS (de Blok et al. 2008, Walter et al. 2008), which provides very high-resolution HI maps and rotation curves and has been analyzed by comparison with 3.6- μ m data from SINGS. The details of the rotation curves correlate with the absolute magnitude of the galaxies, as was first described by Broeils (1992). Luminous galaxies have rotation curves that rise steeply, followed by a decline and an asymptotic approach to the flat outer part of the curve; low-luminosity galaxies show a more gradual increase, never quite reaching the flat part of the curve over the extent of their HI disks. Although in some curves the rotation velocity does decrease at large radii, none of the galaxies shows a decline in their rotation curves that can unambiguously be associated with a cut-off in the mass distribution so that in no case has the rotation curve been traced to the limit of the dark matter distribution (de Blok et al. 2008).

We comment on a number of properties of the surface density distribution of the neutral hydrogen first. The total content, especially relative to the amount of starlight M_{HI}/L (a property that is distance independent), is well-known to correlate with morphological type (e.g., Roberts & Hayes 1994), whereas in later types the more luminous galaxies contain relatively less HI (Verheijen & Sancisi 2001). The HI diameter compared to the optical diameter (at 25 *B*-mag arcsec⁻²) is about 1.7 with a large scatter, but does not depend on morphological type or luminosity, according to Broeils & Rhee (1997). However, there are very good correlations between HI mass and diameter, $\log M_{\text{HI}}$, and $\log D_{\text{HI}}$, both with slopes of about 2. This implies that the HI surface density averaged over the whole HI disk is constant from galaxy to galaxy, independent of luminosity or type. Also note that there is a relatively well-defined maximum surface density in disks of galaxies observed (at least with resolutions of the current synthesis telescopes), which amounts to about $10 M_{\odot} \text{ pc}^{-2}$ (Wevers, van der Kruit & Allen 1986).

Many systems have asymmetries in their HI morphologies or kinematics. Often this is in the form of lopsidedness in the surface density distributions. This can to some extent already be seen in the asymmetries in integrated profiles; studies have claimed that up to 75% of galaxies are asymmetric or lopsided (Matthews, van Driel & Gallagher 1998; Hayes et al. 1998; Swaters et al. 1999; Noordermeer et al. 2005) at some detectable level. Lopsidedness appears to be independent of whether or not the galaxy is isolated, so interactions or mergers cannot always be invoked as its origin. It is suggested that it either is an intrinsic property of the disks or is induced by asymmetries in the dark matter distribution (Noordermeer, Sparke & Levine 2001).

The extraction of kinematic data from the raw observations of moderately inclined systems has often been discussed. The basics are summarized in van der Kruit & Allen (1978), Bosma (1981a), Wevers, van der Kruit & Allen (1986), and Begeman (1987). The results are a radial distribution of HI surface brightness, a rotation curve, and a radial distribution of velocity dispersion; from these one can, in principle, make maps of residuals compared to these azimuthal averages. The

derivation of the HI velocity dispersions is easiest in face-on spirals, where there is no gradient in the systematic motions across a telescope beam (van der Kruit & Shostak 1982, 1984; Shostak & van der Kruit 1984).

For edge-on systems, the procedure is more complicated as a result of the line-of-sight integration. Various methods have been devised, initially only to derive the rotation curve and the radial distribution of HI surface brightness, later in some cases also the flaring (the increasing thickness as a function of galactocentric radius) of the HI layer (e.g., Sancisi & Allen 1979; van der Kruit 1981; Rubin et al. 1985; Sofue 1986; Mathewson, Ford & Buchhorn 1992; García-Ruiz, Sancisi & Kuijken 2002; Takamiya & Sofue 2002; Uson & Matthews 2003; Kregel & van der Kruit 2004a; Kregel, van der Kruit & de Blok 2004). Recently, Olling (1996a,b) and O'Brien and colleagues (O'Brien et al. 2010; O'Brien, Freeman & van der Kruit 2010a,b) have also fit for the HI velocity dispersion. The paper by O'Brien, Freeman & van der Kruit (2010a) provides a detailed description of the various methods and a discussion on the relative merits and pitfalls.

In general, for larger disk galaxies, the radial distributions show (sometimes in addition to a central depression) a radial surface density that falls off more slowly than that of the starlight, a rotation curve that rises to a maximum and stays at that level, and a velocity dispersion of 7–10 km s⁻¹, often near the higher end of this range in the inner regions and in spiral arms and in the lower range in the outer parts and interarm regions (Shostak & van der Kruit 1984, van der Kruit & Shostak 1984, Sicking 1997).

The velocity dispersion of the HI can be measured only in cases where there is a negligible gradient in the overall radial velocity over the beam of the radio telescope. Early determinations have been made in our Galaxy, e.g., van Woerden (1967) found 7 km s⁻¹ for the Solar Neighborhood, and Emerson (1976) found 12 ± 1 km s⁻¹ from aperture synthesis observations using the Half-Mile Telescope at Cambridge. For larger angular size galaxies, the use of face-on galaxies (as judged from the narrowness of their integrated HI profiles) is required to fulfill this condition. It was done in much detail on three galaxies that are only a few degrees from face-on (NGC 3938, 628, and 1058; van der Kruit & Shostak 1982, 1984; Shostak & van der Kruit 1984). They found that the dispersions over the optical extent of the disks were rather constant, with no significant decline with radius at 7–10 km s⁻¹. Only in NGC 628 was a systematic difference seen between the interarm region (at the lower end of the range quoted) and the spiral arms themselves (the higher end).

The most recent study of galaxies that are not very close to face-on is THINGS by Tamburro et al. (2009), where references to other earlier work can be found. They do find significant declines of velocity dispersion with radius in their sample, but there appears a characteristic value of 10 ± 2 km s⁻¹ at the outer extent of the star-forming part of the disk. Inward of this, the dispersion correlates with indicators of star formation, suggesting that the supernovae associated with this star-formation activity are driving the turbulence, although magnetorotational instabilities may add significantly to the random motions as well. In edge-on galaxies, O'Brien, Freeman & van der Kruit (2010a,b) made detailed analyses to retrieve the radial distributions of HI surface density, rotation velocity, and velocity dispersion, and found that there is significant structure, but not much systematic radial decline. This study involved HI rich, dwarf systems, quite dissimilar from the THINGS sample. Typical dispersions are 6.5 to 7.5 km s⁻¹, increasing with the amplitude of the rotation curve. In the Solar Neighborhood, the velocity dispersion of OB stars is comparable to that in the HI, so stars are born with that same amount of random motion, which then increases as a result of secular evolution. The same will happen in other spirals, but in dwarf galaxies the stellar velocity dispersions are similar to the ones reported in HI. This may suggest that no significant secular evolution of random motions occurs in dwarf systems.

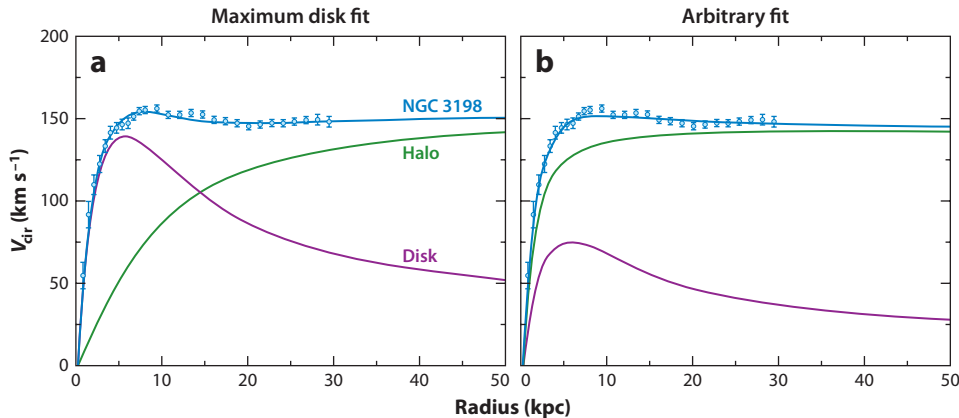


Figure 12

The rotation curve decomposition for NGC 3198. The shape of the curve for the dark matter halo is set by a core radius that determines the initial rise and tends asymptotically to that of a mass density distribution that falls off $\propto R^{-\gamma}$ with γ close to 2. The shape of the disk curve is that of the exponential disk with a scalelength from the light distribution. (a) The maximum disk fit that maximizes the amplitude of the disk rotation curve; and (b) an arbitrary fit with a disk mass 0.3 times that of the maximum disk. (From van Albada et al. 1985).

4.2. Dark Matter Halos

The discovery of dark matter halos has been described very briefly in Section 1.1, where also the concept of the maximum disk hypothesis (see Figure 12) was introduced, in which the contribution of the stellar disk to the rotation curve is taken to be as large as possible, consistent with the observations (Carignan & Freeman 1985, van Albada et al. 1985, van Albada & Sancisi 1986). As mentioned above, this contribution has, in practice, an amplitude at its maximum within the range 0.85 ± 0.10 of the observed maximum rotation, following Sackett (1997). The evidence from stellar dynamics (see Section 3.2) is that the majority of galaxies have disk masses significantly below maximum disk, except for some galaxies with the highest surface brightness.

Recent reviews of disk masses in galaxies and implications for decompositions of rotation curves into contributions from dark and baryonic matter have been presented by van der Kruit (2009) and McGaugh (2009) at the Kingston symposium. These reviewers take the view that most galaxy disks are submaximal, except possibly those with the highest surface brightness and surface density. In contrast to these studies involving mostly nonbarred galaxies, we note that Weiner, Sellwood & Williams (2001) and Pérez et al. (2004) find, from detailed fluid dynamical gas flows in some barred galaxies, that their disks are close to maximal. Debattista & Sellwood (2000) argue, from the observed rapid rotation of the bars of barred galaxies, that the stars are dominating the gravitational field in the inner regions of these galaxies.

The thickness of the gas layer in a disk galaxy can be used to measure the surface density of the disk. It has been known for a long time that this layer in our Galaxy is flaring (for a recent discussion, see Kalberla & Kerp 2009). Assume that the vertical density distribution of the exponential stellar disk is locally isothermal ($n = 1$ in Equation 1). If the HI velocity dispersion is $\langle V_z^2 \rangle_{\text{HI}}^{1/2}$ and isotropic, and if the stars dominate the gravitational field, then the HI layer has a full width at half maximum (to $\lesssim 3\%$) of

$$W_{\text{HI}} = 1.7 \langle V_z^2 \rangle_{\text{HI}}^{1/2} \left[\frac{z_0}{\pi G (M/L) \mu_0} \right]^{1/2} e^{R/2b}. \quad (20)$$

So, if the HI velocity dispersion is independent of radius, the HI layer increases exponentially in thickness with an e-folding length of $2 b$. This was first derived and applied to HI observations of NGC 891 by van der Kruit (1981) to demonstrate that the dark matter indicated by the rotation curve did indeed not reside in the disk but in a more spherical volume. Using the photometry in van der Kruit & Searle (1981b) and the observed HI flaring (Sancisi & Allen 1979) and taking a gaseous velocity dispersion of 10 km s^{-1} resulted in a rotation curve of the disk alone with a maximum of $\sim 140 \text{ km s}^{-1}$. A smaller value for $(V_z^2)_{\text{HI}}^{1/2}$ would, according to Equation 20, result in a smaller value for the inferred M/L for the same HI thickness and, therefore, to a lower value for the maximum disk-alone rotation. The observed maximum rotation velocity is $225 \pm 10 \text{ km s}^{-1}$, which indicates that NGC 891 is not maximum disk. In a similar analysis, Olling (1996b) inferred for NGC 4244 that the maximum disk-alone rotation velocity is between 40% and 80% of the observed rotational velocity.

Another important property of dark matter halos for understanding galaxy formation is their three-dimensional shape. There are various ways to address this issue, of which the use of the flaring of the HI layer is the most prominent. It was first developed by Olling (1995) and subsequently applied to the nearby edge-on dwarf galaxy NGC 4244 (Olling 1996a,b). He found the dark halo of this galaxy to be highly flattened. Observations of the kinematics in polar ring galaxies provide estimates of the potential gradients in the two orthogonal planes of the galaxies. These galaxies can potentially give useful information about the shapes of their dark halos (Sackett 1999), although it is possible that special halos are needed to host these rare polar ring systems. The resulting halo flattenings derived for polar ring galaxies and also for streams in the halo of the Galaxy (Helmi 2004) range from a few tenths to unity.

A more extensive survey of a sample of eight late-type, HI-rich dwarfs in which the dark halo appears to dominate the gravitational field even in the disk was undertaken by O'Brien et al. (2010). The basic premise of the approach is that the radial gradient of the dark matter halo force $\partial K_R / \partial R$ can be measured from the rotation curve after correction for the contribution of the stellar disk and its ISM, whereas the flaring of the HI layer together with a measurement of the velocity dispersion of the HI provides a measure of the vertical gradient $\partial K_z / \partial z$. The ratio of the two force gradients is related to the flattening of the dark halo (assumed spheroidal), as measured by the axis ratio c/a . The derivation of the necessary properties from the HI observations has been presented by O'Brien, Freeman & van der Kruit (2010a,b). The method relies on two assumptions concerning the HI velocity dispersion, that it is isotropic (because we measure in an edge-on galaxy the line-of-sight dispersion component parallel to the plane and use in the analysis the vertical component) and isothermal with z .

The first galaxy for which this analysis has been completed is UGC 7321 (O'Brien, Freeman & van der Kruit 2010c). The halo density distribution was modelled as a pseudoisothermal spheroid (Sackett et al. 1994) and the disk as a double exponential determined from R -band surface photometry. After allowing for the gravitational field of the gas layer, the hydrostatic equations give the M/L of the disk and a value for the flattening of the dark matter halo. For UGC 7321, the M/L in the disk is very low: The contribution of the stellar disk to the radial force is small and is far below maximum disk in this LSB galaxy [Banerjee, Matthews & Jog (2010) reached the same conclusion]. The best fits of the force gradients $\partial K_z / \partial z$ from the various components are shown in **Figure 13**. The vertical gradient of the total vertical force field derived from the hydrostatics of the flaring gas layer (for stars + gas + halo) is shown in purple as a function of radius. After taking off the known contribution from the gas layer, the light blue curve labeled halo + stars shows the remaining contribution from the halo + stars. This is well modelled for $R > 3 \text{ kpc}$ by the adopted contributions from the stars and the dark halo model (*dashed curve*). Note that the shape of the observed and fitted curves is remarkably similar for $R > 3 \text{ kpc}$. For this best fit, the

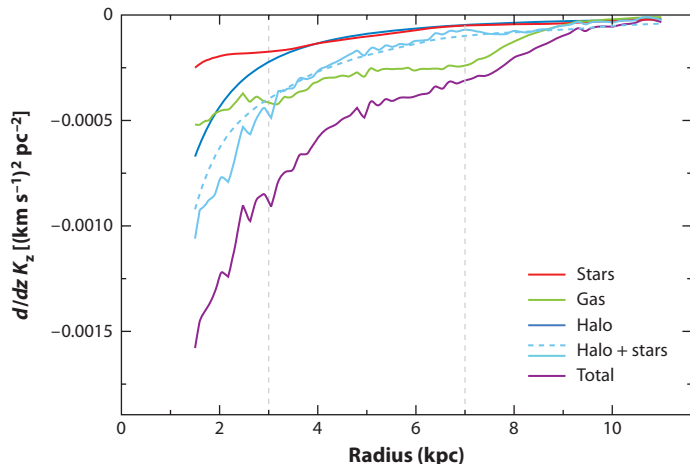


Figure 13

The vertical gradients of the force field for various components in the edge-on galaxy UGC 7321. The line “total” is inferred from the thickness of the HI layer and the HI velocity dispersion; the line “gas” is from the observed HI and corrected for helium. Subtracting these contributions gives the line “halo+stars” (*solid*). The lines “halo + stars” (*dashed*), are the best fits, where that for the stars comes from the observed luminosity distribution with the best fitting mass-to-light ratio. The measured halo flattening was $q = 1.0 \pm 0.1$. The vertical dotted gray lines show the radial regime used for the fit. (From O’Brien, Freeman & van der Kruit 2010c).

dark halo model is spherical. More analysis is required for the rest of the sample to draw firm conclusions.

In the Galaxy, the flaring of the disk can be studied in much more detail. An extensive study has been performed recently by Kalberla et al. (2007) based on the Leiden/Argentina/Bonn all-sky survey of Galactic HI (see also Kalberla & Kerp 2009). In this study, they map the Galactic HI layer and its flaring and warp in much detail and they fit the observations with models containing a dark matter disk as well as a dark matter halo. Their best fitting model has a local disk surface density of $52.5 M_{\odot} \text{ pc}^{-2}$ with a scalelength of 2.5 to 4.5 kpc. This corresponds to a maximum disk-alone rotation velocity of, respectively, 200 to 130 km sec $^{-1}$. So again, if the Galaxy has a normal scalelength (~ 4 kpc) for its rotation velocity, it is far below maximum disk, but if the scalelength is 2.5 kpc, it is close to maximum disk. A complete analysis of the flaring HI disk in terms of Galactic dark matter distribution yields evidence for a significant dark matter disk with a large scalelength of order 8 kpc and, in addition, a dark matter ring at 13 to 18 kpc. This ring could be the remnant of a merged dwarf galaxy.

The distribution of the density in the inner parts of dark halos has been a subject of much attention, as a consequence of the cold dark matter (CDM) paradigm (Blumenthal et al. 1984, 1986), in which structure grows hierarchically with small objects collapsing first and then merging into massive objects. Cosmological n -body simulations based on Λ CDM (Dubinski & Carlberg 1991; Navarro, Frenk & White 1996, 1997) have long predicted that the inner density profile of the dark matter halo ($\rho \propto r^{\alpha}$) would have an exponential slope α of about -1 (a cusp), whereas observations seemed to suggest a slope near zero (a core). The high spatial resolution of the THINGS data (de Blok et al. 2008) is well suited to investigate this matter. They find that, for massive disk-dominated galaxies, all halo models appear to fit equally well, whereas for low-mass galaxies a core-dominated halo is clearly preferred over a cusp-like halo. This cusp-core controversy (with α assuming somewhat different values) is a long-lasting hot item in the study

of HI-rich, dwarf galaxies and LSB systems, where the contribution of the dark matter to the rotation curve is large even in the inner regions. Recently, de Blok (2010) has summarized the situation in such systems, concluding that the problem is still unsolved, even with the use of current high-resolution rotation curves.

4.3. Outer HI and Warps

The warping of the outer parts of the neutral hydrogen layer of our Galaxy has been known for a long time. It was discovered independently in early surveys of the Galactic HI in the north by Burke (1957) and in the south by Kerr and Hindman (see Kerr 1957). In external spiral galaxies, the first indication came from work by Rogstad, Lockart & Wright (1974), when they obtained aperture synthesis observations of the HI in M83. The distribution and the velocity field of the HI both showed features that could be interpreted as a warping of the gaseous disk in circular motions in inclined rings. This later became known as the tilted-ring description for kinematic warps, and many more galaxies have been shown to have such deviations using this method (e.g., Bosma 1981a,b). The case that this warping occurs in many spiral galaxies was strengthened by the early observations of edge-on systems. Sancisi (1976) was the first to perform such observations and showed that the HI in four out of five observed edge-ons (including NGC 4565 and NGC 5907) displayed strong deviations from a single plane. Sancisi (1983) discussed these warps in somewhat more detail and, in particular, noted that in the radial direction the HI surface densities often display steep drop-offs followed by a shoulder or tail at larger radii.

The most extreme (prodigious) warp in an edge-on system was observed by Bottema, Shostak & van der Kruit (1987) (see also Bottema 1995, 1996) in NGC 4013. García-Ruiz and colleagues (García-Ruiz 2001; García-Ruiz, Sancisi & Kuijken 2002) presented 21-cm observations of a sample of 26 edge-on galaxies in the northern hemisphere. This showed that HI warps are ubiquitous; the researchers state in the abstract to their paper that “all galaxies that have an extended HI disk with respect to the optical are warped.” Studies of possible warps in the stellar disks have also been made (for recent results, see Section 3.7); although there is evidence for such stellar warps in most edge-on galaxies, the amplitude is very small compared to what is observed in the HI.

The origin of warps has been the subject of extensive study and has been reviewed, for example, by García-Ruiz, Sancisi & Kuijken (2002), Shen & Sellwood (2006), Binney (2007), and Sellwood (2011a). Although none of the models is completely satisfactory, most workers seem to agree that it has something to do with a constant accretion of material with an angular momentum vector misaligned to that of the main disk. In models by Jiang & Binney (1999) and Shen & Sellwood (2006), this results in an inclined outer torus in the dark matter halo that distorts the existing disk and causes it to become warped. The possibility of a misalignment in the angular momenta and, therefore, of the principal planes of the stellar disk and the dark halo (Debattista & Sellwood 1999) has recently received some observational support from the observations of Battaglia et al. (2006) of NGC 5055. The HI data suggest that the inner flat disk and the outer warped part of the HI have different kinematic centers and systemic velocities, suggesting a dark matter halo with not only a different orientation, but also an offset with respect to the disk. The detailed study of the HI in NGC 3718 by Sparke et al. (2009) shows an extensive warping, for which the observed twist can be explained as a result of differential precession in a fairly round dark halo with the same orientation as the disk. Briggs (1990) used existing observations and tilted-ring models in moderately inclined galaxies to define a set of “rules of behavior for galactic warps” (see his abstract). One was that “warps change character at a transition radius near R_{Ho} .” The latter radius is the Holmberg radius (see Section 3.8) listed for 300 bright galaxies in Holmberg (1958).

The onset of HI warps seems to occur very close to the radius of the truncation in the stellar disk (van der Kruit 2001). This can be illustrated with two archetypal examples. In an edge-on

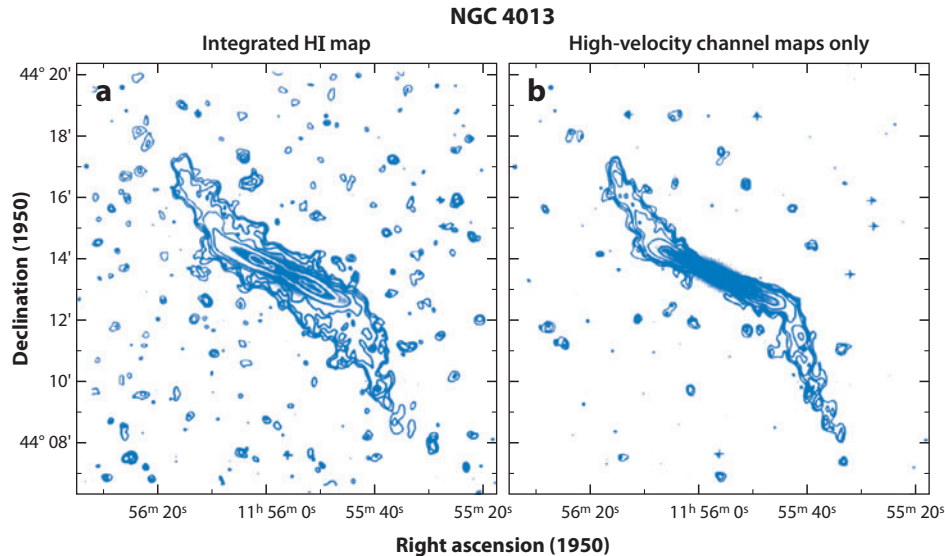


Figure 14

The HI distribution in the edge-on spiral galaxy NGC 4013 (Bottema, Shostak & van der Kruit 1987). (a) The integrated HI map, and (b) only the high-velocity channel maps. The latter selects the HI along a line perpendicular to the line of sight to the galaxy. The warp is less well defined in panel *a*, because the azimuthal angle in the plane of the galaxy, along which the deviation of the warp is largest, is not precisely perpendicular to the line of sight. The warp starts very abruptly at almost exactly the truncation radius of the stellar disk. (From Bottema 1995).

galaxy, the most pronounced warp known is in NGC 4013 (Bottema, Shostak & van der Kruit 1987; Bottema 1995, 1996). The HI warp starts very abruptly at the truncation of the stellar disk (see Figure 14) and is accompanied by a significant drop in rotational velocity. The latter suggests a truncation in the disk mass distribution as well as in the light. A face-on spiral with an HI warp is NGC 628 (Shostak & van der Kruit 1984, Kamphuis & Briggs 1996). The velocity fields suggest a warp in the HI, starting at the edge of the optical disk.

In an extended study, van der Kruit (2008) listed the following general characteristics of HI warps. Whenever a galaxy has an HI disk extended with respect to the optical disk, it has an HI warp (García-Ruiz, Sancisi & Kuijken 2002). Many galaxies, but not all, in this sample have relatively sharp truncations in their stellar disks. When an edge-on galaxy has an HI warp, the onset occurs just beyond the truncation radius. Similarly, in less inclined galaxies, the warp is seen at the boundaries of the observable optical disk (Briggs 1990). In many cases the rotation curve shows a feature at about the truncation radius (Casertano 1983, Bottema 1996), which indicates that the truncation occurs also in the mass. The onset of the warp is abrupt and discontinuous and coincides in the large majority of cases with a steep drop in the radial HI surface density distribution, after which this distribution flattens off considerably. The inner disks are extremely flat (both stellar disks as well as in gas and dust), and the onset of the warp is abrupt; beyond that, according to Briggs (1990), the warp defines a “new reference frame” (see his abstract).

These findings suggest that the inner flat disk and the outer warped disk are distinct components with different formation histories, probably involving different epochs. The inner disk forms initially, and the warped outer disk forms as a result of much later infall of gas with a higher angular momentum in a different orientation. This is also consistent with an origin of the disk truncations

that is related to the maximum specific angular momentum available during its formation, because then the truncation is also in the disk mass, giving rise to the abruptness of the onset of the warps.

The misalignment of the material in the inner disk and the outer disk and warp has been modelled by Roškar et al. (2010) as a result of the interaction between infalling cold gas and a misaligned hot gaseous halo. The gas that forms the warp is torqued and aligned with the hot gaseous halo rather than the inner disk. In this model, the outer accreted gas thus responds differently to the halo than the gas that has formed the inner disk. Although this may be consistent with the observed correlation of the onset of the warp and the truncation or break in the stellar disk, the abruptness of the onset of the warp may not follow naturally. Furthermore, this mechanism requires the existence of a hot gaseous halo, and the question is whether these are present in galaxies with smaller rotation amplitudes; the presence of warps in M33-size galaxies would then be another argument against this hypothesis.

To what extent have star formation and chemical enrichment taken place in these gaseous warps? The early work of Ferguson et al. (1998a,b) established the presence of star formation in regions beyond two R_{25} in a few galaxies through the detection of faint HII regions, whereas emission line ratios indicated very low abundances of oxygen and nitrogen in these regions. Since then, much work has been done and more is in progress, in particular in ANGST (Dalcanton et al. 2009). Early results of this project have been published for M81 (Williams et al. 2009b, Gogarten et al. 2009) and NGC 300 (Gogarten et al. 2010), but those do not yet refer to distances beyond the visible spiral structure. However, the disks do contain mostly old stars at these radii, in agreement with the view that the disk inside the truncation region and the radial onset of the HI warp forms at an early epoch in the galaxy's evolution. In NGC 2976 (Williams et al. 2010), populations of old ages are found at all radii, also beyond the break in the luminosity profile, but star formation does not appear now to extend into this outer zone. This galaxy may have been in interaction recently with the M81 group.

Shostak & van der Kruit (1984, see their figure 3) pointed out that in NGC 628 (M74) the extended, warped HI displays spiral structure that shows a smooth continuation of the prominent spiral structure in the main disk, right through the onset of the warp. Particularly interesting for studying star formation and its history in disks beyond the truncation is the comparison of outer HI with UV imaging from GALEX. Bigiel et al. (2010a) compare the HI from the THINGS (HI) survey with the far-UV data from GALEX and conclude that, although star formation does clearly take place in the outer HI, its efficiency is extremely low compared to that within the optical radius (truncation). A detailed comparison of images for M83 (Bigiel et al. 2010b; see also **Figure 15**) shows a clear correlation between star formation and HI surface density. The conclusion that star formation is proceeding in this galaxy in the very outer parts also follows from the work of Davidge (2010), comparing GALEX imaging to deep optical (Gemini) images of the outer regions of M83.

4.4. Dustlanes in Disks

We do not review in detail the distributions and properties of dust in disks of galaxies. However, we noted above that dustlanes are very straight, such as illustrated in **Figure 9**, at least in disks of massive galaxies and indicate that galaxy disks are extraordinarily flat. It has been known for a long time that dustlanes sometimes are less well defined in galaxies of later type and dwarfs. A good example is NGC 4244, which is a late-type, relatively small, pure-disk galaxy (van der Kruit & Searle 1981a), where the dustlane is not sharply outlined against the stellar disk. Dalcanton, Yoachim & Bernstein (2004) studied a sample of edge-on galaxies and found that systems with maximum rotation velocities larger than 120 km s^{-1} have well-defined dustlanes, whereas in those with smaller rotations the scaleheight of the dust is systematically larger and the distribution

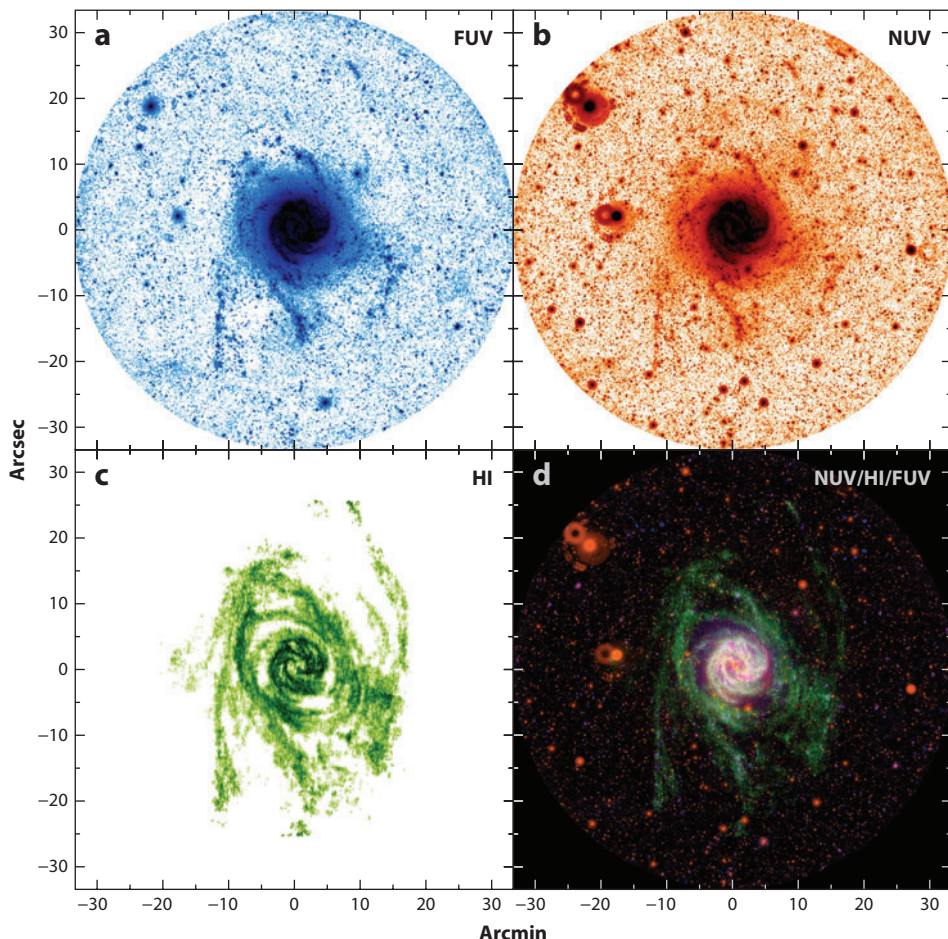


Figure 15

Images of M83,
 (a) GALEX far-UV,
 (b) near-UV, (c) HI
 map from THINGS,
 and (d) a combination
 of the three with the
 HI smoothed (From
 Bigiel et al. 2010a).

much more diffuse. Indeed, NGC 4244 has a maximum rotation velocity of about 115 km s^{-1} . This finding may have important implications for our understanding of the star-formation history and evolution of disks.

Dalcanton, Yoachim & Bernstein (2004) suggest that the transition at 120 km s^{-1} marks the rotation speed above which the disks become gravitationally unstable, whereby instabilities in the disk lead to fragmentation of the gas component with high density during a collapse that then gives rise to thin dustlanes. In a study of the vertical distributions in a number of low-mass, edge-on galaxies, Seth, Dalcanton & de Jong (2005) find that not only does the dynamical heating of the stellar population appear to occur at a much reduced rate compared to the Galactic disk in the Solar Neighborhood, but in these low-mass systems the vertical distribution of the young stellar population and of the dust layer is thicker than those in the Milky Way. This is consistent with a cold ISM in slowly rotating galaxies that has a larger scaleheight and, therefore, with an absence of well-defined dustlanes in such systems. Seth, Dalcanton & de Jong (2005) fit the distributions with an isothermal sheet ($n = 1$ in Equation 1 with $z_o = 2b_z$). In NGC 4144 (rotation velocity 67 km s^{-1}), the dust has a scaleheight z_o of about 0.5 kpc or an exponential scaleheight of half that. For comparison, in the Milky Way the three-dimensional distribution of dust has been modelled

by Drimmel & Spergel (2001): Their flaring dust disk has an exponential scaleheight at the solar radius of about 0.2 kpc.

We may examine more massive edge-on galaxies with rotation velocities well over 200 km s⁻¹ to compare with the low-rotation systems. For example, three such galaxies with obvious dustlanes are NGC 4565, 891, and 7814, for which minor axis profiles (in blue light) are available in the papers of van der Kruit & Searle (1981a,b, 1982b). When we determine the height above the symmetry plane at which the effect of the dust extinction is about one magnitude compared to the extrapolated minor axis profile of the stellar light, we get values of, respectively, 0.9, 0.7, and 0.6 kpc. These are undoubtedly overestimates when used as indications for the dust scaleheights; Kylafis & Bahcall (1987), for example, find that the dust scaleheight in NGC 891 is 0.22 kpc, compared to the stellar scaleheight of 0.5 kpc (van der Kruit & Searle 1981b). Wainscoat, Hyland & Freeman (1989) determined in IC 2531 (an NGC 891-like, edge-on galaxy) that the scaleheight of the old disk stars is about 0.5 kpc, whereas that of the dust is a quarter of that. A similar determination of the height at which the minor-axis profile indicates an absorption of one magnitude compared to the extrapolated profile yields about 0.5 kpc. On this basis, the exponential scaleheights of the dust layers in the three systems just mentioned are of the order of 3 or 4 times less than those of the old stellar disks. The important inference is that the diffuse dust layers in slow rotators have, in absolute measures, thicknesses that are not very different from those in massive galaxies with high rotation velocities.

In early-type, edge-on galaxies such as NGC 7814 and NGC 7123, where the spheroids dominate the light (and presumably stellar mass) distributions, the situation appears different. The dust distributions in these systems have scaleheights comparable to those of the stellar disks (Wainscoat, Hyland & Freeman 1989), which are of the order of 0.5 to 1 kpc. This may be the result of much longer dissipation times due to the lower gas content, so that the scaleheights of the stars (from which the dust comes) and the dust are similar.

In the sample of late-type, gas-rich, dwarf, edge-on galaxies studied by O'Brien, Freeman & van der Kruit (2010b), the mean HI velocity dispersion increases as a function of the maximum rotational velocity of the HI disk from about 5 to 8 km s⁻¹ for rotation velocities of 70 to 120 km s⁻¹. The scaleheight b of a Gaussian dust layer is related to the ISM velocity dispersion σ by

$$\frac{\sigma^2}{b^2} = -\frac{\partial K_z}{\partial z} = 4\pi G\rho_*, \quad (21)$$

where ρ_* is the mid-plane total density. The density $\rho_* = \Sigma/2b_z$, where Σ is the typical surface density of a disk. Σ and the stellar scaleheight are both approximately proportional to the maximum circular velocity V_c (Kregel, van der Kruit & de Grijs 2002; Kregel, van der Kruit & Freeman 2005; Gurovich et al. 2010), so the typical value of ρ_* is independent of V_c , and we expect the scaleheight of the dust layer to be directly proportional to the ISM velocity dispersion σ . In the O'Brien sample of galaxies, the galaxy with the largest V_c (IC2531) shows a clean, well-defined dustlane, as expected from the Dalcanton et al. observations. However, there is no evidence for a decrease in σ as V_c increases in the O'Brien et al. sample, so those data do, therefore, not support the variable turbulence explanation for the change in dustlane morphology with rotation velocity.

5. CHEMICAL EVOLUTION AND ABUNDANCE GRADIENTS

The stars and gas in galactic disks have a mean metallicity that depends on the luminosity of the galaxy (e.g., Tremonti et al. 2004) and often shows a radial gradient. In a large galaxy like the Milky Way, the typical disk metallicity [Fe/H] is near that of the Sun. For example, in the Solar Neighborhood, the metallicity of the disk stars has a mean of about -0.2 and ranges from about

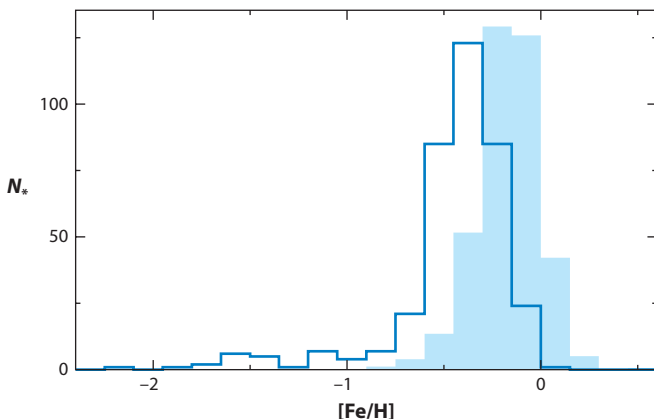


Figure 16

Metallicity distribution function for stars in the bar of the Large Magellanic Cloud, compared to the Solar Neighborhood metallicity distribution function (MDF) from McWilliam (1990) (*light blue shading*). The Solar Neighborhood MDF is about 0.2 dex more metal-rich (From Cole et al. 2005).

+0.3 to −1.0 (e.g., McWilliam 1990). **Figure 16** compares the stellar metallicity distribution functions (MDFs) of the Solar Neighborhood and the bar of the LMC. As expected from the lower luminosity of the LMC, the LMC MDF is displaced toward lower metallicities, but the shapes of the two MDFs are similar.

The MDF is believed to come from the local chemical evolution of the stars and ISM, including the effect of infall of gas from outside the Galaxy. The presence of a fairly tightly defined radial abundance gradient in the stars and in the gas in many disk galaxies suggests that the chemical evolution of the disk is determined mainly by local chemical evolution with limited radial exchange of evolution products. Much of the theory of chemical evolution of disk galaxies is based on this assumption (e.g., Chiappini, Matteucci & Gratton 1997); this view is, however, currently under challenge.

From the basic theory of chemical evolution via the continued formation and evolution of stars and enrichment of the ISM, one might expect that the metallicity of disk stars would gradually increase with time. McWilliam (1997) pointed out in his review that it was not clear observationally at the time that any age-metallicity relation (AMR) exists among the stars of the Solar Neighborhood. This is still the situation today. Edvardsson et al. (1993) found evidence for a weak decrease of [Fe/H] with age among the disk stars, but later work (e.g., Nordström et al. 2004) is less conclusive. From the white dwarf luminosity function and the directly measured ages of disk stars (e.g., Knox, Hawkins & Hambly 1999; Edvardsson et al. 1993; Sandage, Lubin & VandenBerg 2003), the age of the Galactic thin disk is about 8–10 Gyr. The open cluster NGC 6791 has an age of about 8–10 Gyr and an abundance $[Fe/H] = +0.2$, indicating that enrichment to solar level occurred very quickly in the Galactic disk, on a gigayear timescale. An early AMR figure by Sandage & Eggen (1969), based partly on open cluster ages and metallicities, shows a very rapid early evolution of the galactic abundances up to near-solar abundances and then little further change; this is still a fair representation of the current state of knowledge.

The rapidly rising and then flat AMR in the disk of the Milky Way contrasts with the situation in the LMC. Dolphin (2000) derived the star-formation history and AMR for two fields in the LMC disk. The star-formation rate shows early and late phases of star formation, with a very slow period between about 3 and 7 Gyr ago, and the AMR shows a smooth rise from below −1.5 at 10 Gyr ago to the present metallicity of $[Fe/H] = -0.4$. A smoothly rising AMR is seen also in

the outer regions of M33 (Barker et al. 2007b). This difference in the morphology of the AMR between the Milky Way and the smaller galaxies is likely to come from the different star-formation histories of larger and smaller disk systems (the downsizing phenomenon).

5.1. Gas-Phase Abundance Gradients

Many galaxies show a clear radial gradient in their gas-phase abundances. Zaritsky et al. (1994) assembled data on oxygen abundance gradients in 39 disk galaxies covering a range of luminosities. They found the now-familiar correlations between oxygen abundance and luminosity, circular velocity and morphological type. The size of the abundance gradients (in dex/isophotal radius) did not correlate with luminosity or type. The presence of a bar appears to flatten or even erase the abundance gradient (see also Alloin et al. 1981), probably due to the noncircular motions, which the bar induces in the gas of the disk.

Magrini et al. (2007) modelled the chemical evolution of M33, assuming that the galaxy is accreting gas from an external reservoir. A model with an infall rate of about $1 M_{\odot}$ year $^{-1}$ reproduces the observational constraints, including the relatively high star-formation rate and the shallow abundance gradient. The model indicates that the metallicity in the disk has increased with time at all radii, and the abundance gradient has continuously flattened over the past 8 Gyr (see also Gogarten et al. 2010 for a comparison with the evolution of the somewhat similar disk galaxy NGC 300).

For the Milky Way, Shaver et al. (1983) combined radio and optical spectroscopy to measure abundances for HII regions between about 3 and 14 kpc from the Galactic center. Fich & Silkey (1991) extended the observations to a radius of about 18 kpc. A well-defined gradient in the oxygen and nitrogen abundances of -0.07 to -0.08 dex kpc $^{-1}$ is found. Dennefeld & Kunth (1981) see a comparable gradient in nitrogen in the HII regions of the disk of M31.

5.2. Stellar Abundance Gradients

The abundance gradient for relatively young stars in the disk of the Milky Way is nicely delineated by the Cepheids (Luck, Kovtyukh & Andrievsky 2006). The gradient is about -0.06 dex kpc $^{-1}$, in good agreement with the gas-phase gradient derived by Shaver et al. (1983). The two-dimensional distribution of the Cepheid abundances over the Galactic plane shows some localized departures from axisymmetry at the level of about 0.2 dex in abundance. These departures may come from radial gas flows associated with the spiral structure.

For the older stars in the outer disk (open clusters and red giants), the abundance gradient appears to be somewhat steeper, as seen in the study by Carney, Yong & Teixera de Almeida (2005). The abundances fall to about -0.5 at 11 kpc but then stay approximately constant at this level out to radii beyond 20 kpc (**Figure 17**). The figure also compares the $[\alpha/\text{Fe}]$ ratio for the older objects and the Cepheids. It indicates that the abundance gradient in the outer disk is flatter now than it was a few gigayears ago, and also that the $[\alpha/\text{Fe}]$ ratio is nearer the solar value now than it was at the time of formation of the outer old clusters. These observations suggest that the chemical evolution of the disk gradually flattens the abundance gradient and reduces the $[\alpha/\text{Fe}]$ ratio. In the outer regions, episodic accretion of gas may trigger bursts of star formation that could erase the abundance gradient and produce the α -enriched abundances seen in the older objects. A similar bottoming out of the abundance gradient beyond about 15 kpc is seen by Worthey et al. (2005) in the outer disk of M31. We note that the environment of the outer disk in M31 has had a complex star-formation history, with much evidence for an extended period of accretion of

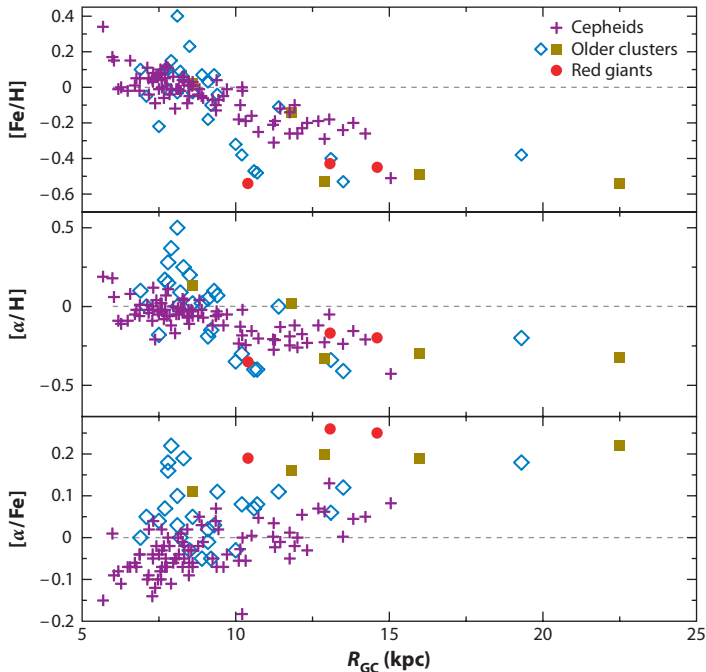


Figure 17

Upper panel: The radial abundance distribution for Cepheids (purple crosses) and older clusters (blue diamonds and dark yellow squares) and red giants (red circles) in the Galactic disk.
Lower panels: The radial $[\alpha/\text{H}]$ and $[\alpha/\text{Fe}]$ distributions for the same objects (From Carney, Yong & Teixeira de Almeida 2005).

smaller galaxies (e.g., McConnachie et al. 2009), which complicates the interpretation of radial gradients in this system.

Cioni (2009) used the radial change of the ratio of C- and M-type AGB stars in the LMC and M33 to evaluate their stellar abundance gradients. Both show a radial abundance gradient. This is particularly clearly seen in M33: The gradient in the disk persists to a radius of about 8 kpc, which is the radius at which the radial truncation of the disk occurs. At larger radii, the abundance gradient becomes much flatter. Barker et al. (2007a) also found evidence that the radial abundance gradient of M33 flattens in the outer regions.

The abundance gradients of disk galaxies may not only flatten at large radii but can also reverse. The galaxy NGC 300 is similar to M33 in appearance and absolute magnitude, and it also has a negligible bulge component. The two galaxies do, however, differ in the details of the structure of their disks. M33 shows a very well-defined truncation of its disk, at a radius of a few scalelengths (Ferguson et al. 2007), whereas the disk of NGC 300 has an unbroken exponential surface density distribution extending to a radius of at least 10 scalelengths (Bland-Hawthorn, Vlajić & Freeman 2005). The negative abundance gradient in NGC 300 persists to a radius of about 10 kpc and then appears to reverse, with the metal abundance increasing with radius. Vlajić, Bland-Hawthorn & Freeman (2009) present two possible scenarios for the reversal of the abundance gradient. One is associated with accretion and local chemical evolution. The other scenario involves radial mixing driven by resonant scattering of stars via transient spiral disturbances while preserving their near-circular orbits, as discussed by Sellwood & Binney (2002) and Roškar et al. (2008b). In this picture, the stars in the outermost disk did not form *in situ* but were scattered from the inner galaxy into the outer disk. The scattering occurs from near the corotation radius of the individual spiral disturbance. The radial extent of the scattering depends on the strength of the transient spiral wave, and the radius from which the scattering occurs depends on its pattern speed. If the inner disk of the galaxy has the usual negative abundance gradient, then the abundance distribution in

the outer disk (which is populated by stars scattered from the inner disk) would depend on the distribution of pattern speeds and pattern strengths in the inner disk. A reversal in the current abundance gradient could come from an epoch of spiral disturbances whose strength increases with their pattern speed: more metal-rich stars from smaller radii are then more strongly scattered radially. Such an epoch of spiral disturbances could also explain the difference in structure between the truncated disk of M33 and the exponential disk of NGC 300. In this scenario, the outer disk of NGC 300 is more strongly populated by radial mixing, building up the continued exponential. For an alternative view, see Gogarten et al. (2010).

The chemical evolution of disks is usually calculated assuming that each annulus in the disk evolves independently, with infall of gas from intergalactic space but with no radial exchange of processed gas or stars (e.g., Chiappini, Matteucci & Gratton 1997). In this picture, one might expect a relationship between the age of stars and their metallicity. The apparent lack of a well-defined AMR in the Solar Neighborhood has motivated alternative views of the chemical evolution of disks, involving radial flows of gas and radial mixing of stars. Schönrich & Binney (2009a) have constructed such a theory that seems to fit very well the observed stellar distribution of thin-disk stars in the $[\alpha/\text{Fe}]$ – $[\text{Fe}/\text{H}]$ plane, and also the existing AMR data. We caution, however, that the AMR data in the Solar Neighborhood are still quite uncertain.

6. SCALING LAWS FOR DISK GALAXIES

Disk galaxies demonstrate several scaling laws, i.e., relations of observable parameters to the luminosity or stellar mass of the galaxies. Some scaling laws involve parameters associated with the stellar component of the galaxies: e.g., the stellar mass–metallicity relation and the luminosity–radius relation. Others relate stellar properties to dark matter properties: e.g., the Tully–Fisher relation between the stellar luminosity L (or stellar mass or baryonic mass) and the rotation speed of the galaxy, and the scaling relations between the the luminosity of the stellar component and the central density of the dark matter halos. These scaling laws provide insight into the formation and evolution of disk galaxies.

When examining the scaling laws and other relations between observables for disk galaxies, it is useful to ask how many independent parameters there are in the ensemble of information. Principal component analysis (PCA) can provide insight, although it may be difficult to identify which of the parameters are fundamental (Brosche 1973). Recently, Disney et al. (2008) combined data from the HIPASS survey of HI in galaxies (Meyer et al. 2004) with SDSS data and derived six parameters: two optical radii (containing 50% and 90% of the light), luminosity, HI mass, dynamical mass, and $(g-r)$ color. PCA shows that the correlations are dominated by only one significant principal component. This indicates a somewhat unexpected organizational uniformity in galaxy properties.

6.1. The Tully–Fisher Law

This law, in its original form of absolute blue magnitude M_B versus the velocity width of the integrated HI profile, was discovered by Tully & Fisher (1977). For their profile width, they used W_{20} , the line width at 20% of the peak intensity, which has become widely but not universally used in Tully–Fisher relation (TFR) studies. The TFR quickly became an important tool for measuring the absolute magnitudes and distances of galaxies from their HI profile width. The magnitudes need to be corrected for Galactic and internal absorption, and the velocity widths corrected for the inclination of the disk and turbulence in the galaxy's ISM. The slope of the TFR depends on wavelength (see, for example, Sakai et al. 2000). The slope of the $\log L - \log W_{20}$ relation

goes from about 3.2 at B to about 4.4 at H , and the scatter about the TFR is smaller at longer wavelengths.

The TFR is an important and complex constraint on galaxy formation theory. Each of the variables in the TFR (luminosity and profile width) is itself the product of many complex and interacting processes involved in the formation and evolution of disk galaxies, and these processes contribute to the slope, zero-point, and scatter of the TFR. The luminosity measures the integrated star-formation history and evolution of the baryons. The HI profile width is a measure of the maximum value of $R\partial\Phi/\partial R$ in the plane of the HI disk, where R is the radius and Φ the potential. This potential comes partly from the stellar component and partly from the dark matter halo. It therefore depends on the lengthscale of the stellar component (i.e., on how much the baryons have contracted during the formation of the galaxy) and, hence, on the angular momentum of the stellar component.

The dimensionless spin parameter (Peebles 1971)

$$\lambda = \frac{J|E|^{1/2}}{GM^{5/2}}, \quad (22)$$

(where J is the system's spin angular momentum, E its binding energy, and M its mass) is relevant here. λ is a measure of how far a system is from centrifugal equilibrium. Cosmological simulations predict the distribution of λ for dark halos that form in a CDM universe (e.g., Efstathiou & Jones 1979). The distribution of λ is typically lognormal, with a mean value of about 0.06. In systems with higher values of λ , the baryons settle into disks that are more extended, more slowly rotating, and of lower surface brightness in the mean (see, e.g., Dalcanton et al. 1997) for more details). Furthermore, the parameters involved in the TFR are likely to evolve as the galaxy grows: The stellar mass will increase according to the star-formation history, the baryonic mass will be affected by feedback and accretion, and the rotational velocity is likely to change as the stellar mass increases and the dark matter halo is gradually built up. We can expect all of these changes to continue to the present time.

Although the brighter disk galaxies lie on a well-defined luminosity-velocity relation, the fainter galaxies with circular velocities less than about 100 km s^{-1} are observed to have luminosities that lie below the relation defined by the brighter galaxies. Many of these fainter disk galaxies are gas (HI) rich, so the stellar mass is only a fraction of their baryonic content. If the baryonic (stellar + HI) mass is used instead of the stellar luminosity or mass, the fainter disk systems move up to lie on the same baryonic TFR as the brighter galaxies (Freeman 1999, McGaugh et al. 2000), with a relatively small scatter of 0.33 mag. This suggests that the TFR is really a relationship between the rotational velocity and the total baryonic mass M_{bar} (see also McGaugh 2005). The change in the slope of the $L-W_{20}$ relation with wavelength is partly due to the way in which the L/M_{bar} ratio changes with M_{bar} at different wavelengths, which in turn probably reflects the different star-formation histories of disk galaxies of different masses. In the mean, the less massive galaxies are now more affected by current star formation (downsizing), and we can expect more scatter in their L/M_{bar} ratio.

There is still some disagreement about the slope of the baryonic Tully-Fisher relation (BTFR). Various researchers find slopes between $M_{bar} \propto V^3$ and $M_{bar} \propto V^4$, where V is the rotational velocity (e.g., Stark et al. 2009, Trachernach et al. 2009, Gurovich et al. 2010). CDM theory predicts a slope closer to 3, so it is important to settle this question observationally. The studies quoted estimate the stellar masses from M/L ratios based on various models. In a more direct approach, Kregel, van der Kruit & Freeman (2005) use stellar disk masses derived from stellar dynamical analysis; after adding the HI content, they find a slope for the BTFR of 3.33 ± 0.37 over 2 dex, with a scatter of 0.21 dex.

One potentially important difference in approach comes from the way in which different researchers measure the rotational velocity (see Cantinella et al. 2007 for more discussion). Some researchers use the profile width W_{20} as their velocity measure; the relationship between this quantity and the asymptotic (flat) rotational velocity of the galaxy becomes less well defined for lower mass galaxies, in which the HI often does not extend to the flat part of the rotation curve. Other researchers restrict their samples to galaxies in which the rotation curve is observed to reach the flat region and use this flat level of the rotation curve as their velocity measure. Although the flat level of the rotation curve provides a consistent estimate of the rotation, this is itself a selection effect, restricting the sample of galaxies to those in which the HI extends to the flat rotation curve region. The selected galaxies are therefore biased toward systems in which either the HI is intrinsically more extended or the dark matter halos are more centrally concentrated with relatively smaller scalelengths and larger concentrations. As one might expect from the above discussion, analyses based on W_{20} appear to give lower (flatter) slopes for the BTFR than those based on the flat region of the rotation curve. The concept of the radial TFR, in which the luminosity is plotted against the rotational velocity at a range of fiducial radii (Yegorova & Salucci 2007), may be helpful for comparing galaxies with different rotation curve morphologies in a consistent manner. Ideally, to relate the baryonic content of disk galaxies to the properties of the dark halos, we would like to use the circular velocity of the dark halo at the virial radius, but for most galaxies this quantity cannot be measured at present (see Courteau et al. 2007 for a useful discussion).

The interpretation of the BTFR is not straightforward. For normal high surface brightness disk galaxies, the rotation speed depends on the contributions to the gravitational potential from both the stellar distribution and the dark matter, including any effects of the stellar distribution on the dark matter (baryonic contraction). This in turn involves the evolution of the stellar disk itself. In gas-rich and LSB galaxies, the contribution of the luminous matter to the potential field is relatively small but, even in this simpler situation, the BTFR involves the ratio of baryon to dark matter mass, the structure of the dark matter halo, and the radial extent or maximum angular momentum of the HI gas. Zwaan et al. (1995) and Sprayberry et al. (1995) constructed a TFR law for LSB galaxies: These galaxies have surface brightnesses that are typically at least a magnitude fainter than the normal galaxies. They found that the TFR for LSB and normal disk galaxies were very similar in slope and zero point. Although this result may seem surprising, it makes sense if interpreted in the context of the BTFR. The stellar luminosity is used as a proxy for the baryonic mass, with some scatter and bias depending on the gas fraction (and adopted stellar M/L ratio). The velocity for these galaxies reflects the circular velocity of the dark matter potential, because the contribution to the gravitational field from the stellar component is relatively insignificant.

The following clever argument of Courteau & Rix (1999) makes use of the scatter in the Tully-Fisher relation. The amplitude of the rotation curve of the self-gravitating exponential disk is

$$V_{\text{disk}} \propto \sqrt{b \Sigma_{\odot}} \propto \sqrt{\frac{M_{\text{disk}}}{b}}. \quad (23)$$

For fixed disk mass M_{disk} we then get by differentiation

$$\frac{\partial \log V_{\text{max}}}{\partial \log b} = -0.5. \quad (24)$$

So at a given absolute magnitude (or mass), a lower scalelength disk should have a higher rotation velocity. If all galaxies were maximum disk, then this anticorrelation should be visible in the scatter of the TFR. It is, however, not observed, and the inference is that on average $V_{\text{disk}} \sim 0.6 V_{\text{total}}$ and galaxies in general do not have maximal disks. We note that this argument ignores the contribution

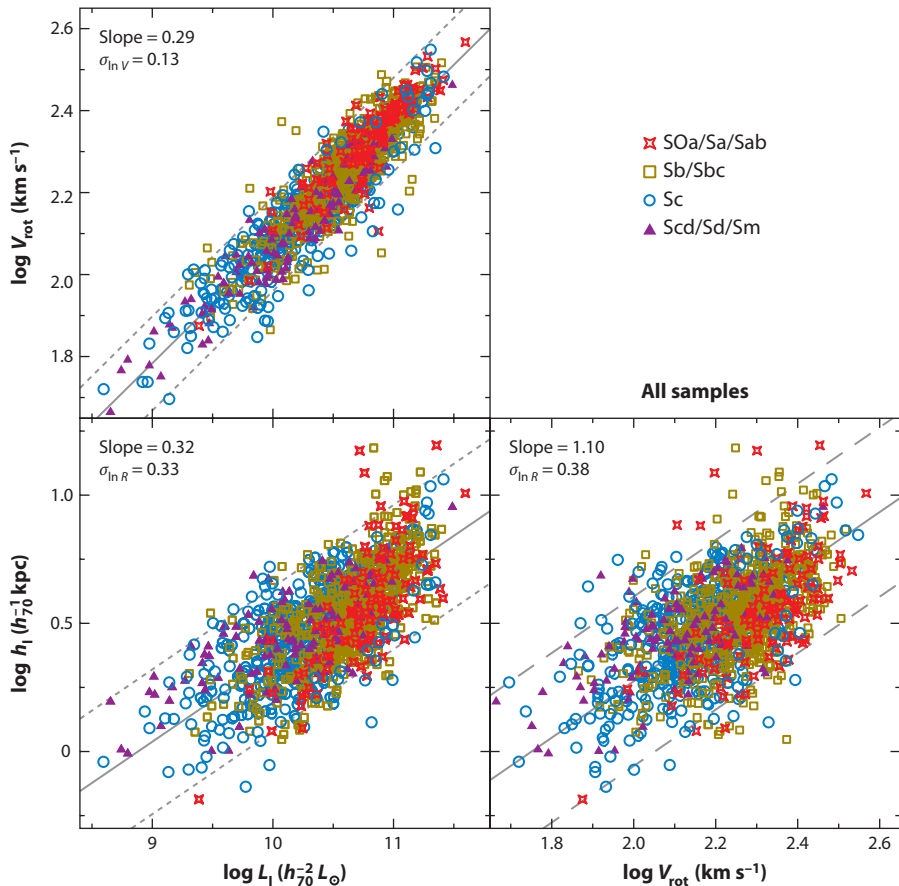


Figure 18

Scaling relations between the rotation velocity V , the scalelength b , and the luminosity L , the latter two in the I -band (From Courteau et al. 2007).

of the gas to the total baryonic mass, which can be significant even for relatively bright galaxies (e.g., Gurovich et al. 2010).

6.2. Scaling Laws Involving the Galaxy Diameter

In their pioneering paper, Tully & Fisher (1977) also considered the relationship between galaxy optical diameter and rotational velocity. Courteau et al. (2007) made an extensive study of the distributions of L and stellar scalelength b (in the I and K bands) and V_{rot} for a sample of 1,300 galaxies. The scalelength reflects the angular momentum distribution of the star-forming baryons but probably includes further complications of the baryonic dissipation and settling to equilibrium.

The scatter in the relations involving b is larger than for the $L-V$ relation (see Figure 18), as one might expect from the additional complexity of the underlying physics and also the difficulty of measuring disk scalelengths accurately. The mean relations found by Courteau et al. (2007) are

$$V_{\text{rot}} \propto L^{0.29}, \quad b \propto L^{0.32}, \quad \text{and} \quad b \propto V_{\text{rot}}^{1.10} \quad (25)$$

in the I -band. The relations involving b show some morphological dependence, but no significant morphological dependence is seen in the $V_{\text{rot}}-L$ relation.

6.3. The Mass-Metallicity Relation

The mass-metallicity relationship pertains to the baryonic component of the galaxies. The relationship between stellar mass or luminosity and metallicity in galaxies goes back at least to Lequeux et al. (1979). A study of a large sample of SDSS galaxies by Tremonti et al. (2004) gives references and demonstrates a tight correlation between the stellar mass and the gas-phase oxygen abundance extending over 3 orders of magnitude in stellar mass and a factor of 10 in oxygen abundance. Kirby et al. (2008) show that the relationship between luminosity and metallicity continues down to the faintest known dwarf spheroidal galaxies with absolute V -magnitudes fainter than -4 . The deeper potential wells of the more massive galaxies are believed to retain more effectively the metal-enriched ejecta of supernovae (Larson 1974, Dekel & Silk 1986), which can be lost via galactic winds. Tassis et al. (2008) have argued, however, that this kind of supernova feedback may not be essential for generating the mass-metallicity relation; the increasingly inefficient conversion of gas into stars in the lower mass galaxies may be responsible.

6.4. The Surface Density–Mass Relation

This relationship again pertains to the baryonic component of the galaxies; as for the mass-metallicity relationship, it provides some constraints on the theory of the evolution of the baryonic component. In the mean, the surface density of galaxies appears to increase with increasing stellar mass or luminosity, as shown first by Kormendy (1985) and followed up by Dekel & Silk (1986) for a sample of nearby ellipticals and irregular galaxies with stellar masses less than about $10^{10.5} M_{\odot}$. For disk galaxies, Gurovich et al. (2010) found a similar relationship: the baryonic (stellar + H i) surface density is observed to increase approximately linearly with W_{20} . Again, this scaling law can be interpreted in terms of supernova-driven loss of gas or as due to increasingly inefficient star formation for systems of lower masses.

6.5. Scalings Laws for Dark Matter Halos

The properties of the dark matter halos of disk galaxies appear to scale with the luminosity of their stellar component. Kormendy & Freeman (2004) analyzed the rotation curves of spirals and dwarf irregular galaxies to estimate parameters for their dark matter halos. They modelled the dark halo density distributions as isothermal spheres with a central core of density ρ_{o} and a core radius r_c . Estimates for the dark halos of dwarf spheroidal galaxies were also included, using the velocity dispersion profiles of these systems. Kormendy & Freeman found that the core density ρ_{o} decreases with luminosity, as $\rho_{\text{o}} \propto L^{-0.28}$: The core densities increase from about $10^{-2.5} M_{\odot} \text{ pc}^{-3}$ for the brighter spirals to a rather high value of about $10^{-0.5} M_{\odot} \text{ pc}^{-3}$ for the fainter dwarf irregular and spheroidal galaxies. The core radius r_c increases with luminosity, as $r_c \propto L^{+0.32}$, so the surface density $\rho_{\text{o}} r_c$ of the dark matter halos is approximately independent of the luminosity of the stellar component. This remarkable observational result was confirmed by Donato et al. (2009) with more recent data for the dark halos of the dwarf galaxies. The surface density $\rho_{\text{o}} r_c$ is constant at about $140 M_{\odot} \text{ pc}^{-2}$ over about 15 mag in stellar luminosity.

The dark halo scaling laws reflect the changing density of the Universe as halos of different masses are formed, with the less massive halos forming earlier. The difference in halo densities indicates that the smallest dwarfs formed about 7 units of redshift earlier than the largest spirals. Djorgovsky (1992) showed that protogalactic clumps, which separate from an evolving density field with power spectrum $|\delta_k|^2 \sim k^n$, have a scaling law between density and radius $\rho \sim r^{-3(3+n)/(5+n)}$.

The observed scaling laws for dark matter halos correspond to $n \approx -2$, close to what is expected for Λ CDM on galactic scales.

7. THICK DISKS

Most spirals, including our Galaxy, have a second thicker disk component surrounding the thin disk. Thick disks were discovered in other galaxies via surface photometry (Burstein 1979, Tsikoudi 1980) and then in the Milky Way through star counts (Gilmore & Reid 1983). It appears that thick disks are very common in disk galaxies and that they are mostly very old. The thick disk is therefore an important component in understanding the assembly of disk galaxies.

7.1. Statistics of Incidence

The photographic surface photometry of van der Kruit & Searle (1981a,b, 1982a) showed that thick disks were common in disk galaxies but perhaps not ubiquitous (see also Fry et al. 1999). At the time, evidence indicated that the thick disk was associated with the presence of a central bulge. A more recent extensive study of a large sample of edge-on galaxies by Yoachim & Dalcanton (2006) showed that thick disks are probably present in all or almost all disk galaxies. They found that the ratio of thick-disk stars to thin-disk stars depends on the luminosity or circular velocity of the galaxy: It is about 10% for large spirals like the Milky Way and rises to about 50% for the smallest disk systems.

Our Galaxy has a thick disk. Star counts by Gilmore & Reid (1983) at high Galactic latitude showed two vertically exponential components: the thin disk and the more extended thick disk. Its scaleheight is about 1,000 pc, compared to about 300 pc for the old thin disk, and its surface brightness is about 10% of the surface brightness of the thin disk, but there is still some disagreement about these parameters.

7.2. Structure of Thick Disks

From within our Galaxy, it is difficult to estimate reliably the scaleheight and scalelength of the thick disk. Values for the scaleheight between about 0.5 and 1.2 kpc have been reported. A recent analysis of the SEGUE photometry gives a relatively short exponential scaleheight of 0.75 ± 0.07 kpc and an exponential scalelength of 4.1 ± 0.4 kpc (de Jong et al. 2010). For comparison, the scaleheight of the thin disk is about 250 to 300 pc; the scalelength of the thin disk is poorly determined but is probably between 2 and 4 kpc. Their model gives the stellar density of the thick disk near the sun to be about $0.0050 M_{\odot} pc^{-3}$, about 7% of the stellar density of the thin disk near the sun (about $0.07 M_{\odot} pc^{-3}$).

Thick disks are not easy to see in galaxy images. **Figure 19** shows that in NGC 4762 [that has a bright thick disk (Tsikoudi 1980)], the outer extent of the faint starlight has an approximate diamond shape, indicating the double exponential light distribution of a thick disk. In **Figure 10**, we see the same thing in the outer outline in the bottom picture for NGC 4565 at the deepest stretch. The luminosity distribution of the edge-on galaxy NGC 891, which is often regarded as an analog for the Milky Way (van der Kruit 1984), shows after subtraction of the disk a light distribution that becomes progressively more flattened at fainter levels (see figure 7 in van der Kruit & Searle 1981b); in van der Kruit (1984), it is shown that this distribution can be interpreted as a superposition of a thin and thick disk plus a small, central bulge. Recent studies show that the scaleheight of its thick disk is 1.44 ± 0.03 kpc, and its radial scalelength is 4.8 ± 0.1 kpc, only slightly longer than that of the thin disk (Ibata, Mouhcine & Rejkuba 2009). The relationship

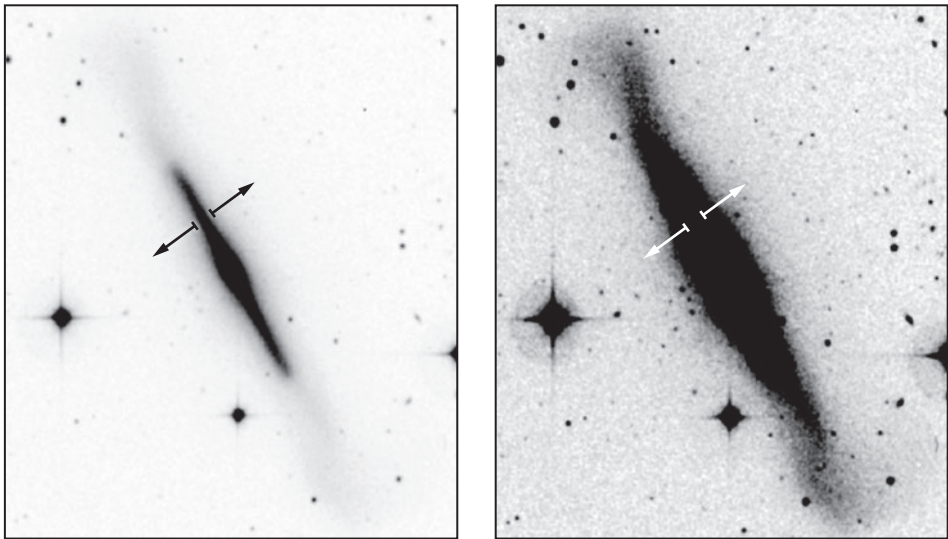


Figure 19

The S0 galaxy NGC 4762, which has a very bright thick disk, as was first described by Tsikoudi (1980). The z extent, indicated by the arrows, is where the thin disk dominates. On the right the outer extent of the thick disk is slanted with respect to the symmetry plane (producing an approximately diamond shape), indicative of a double exponential light distribution. These images were produced with the use of the *Digital Sky Survey*.

between the scalelengths of the thin and thick disk is an important constraint on the various formation mechanisms of thick disks, as discussed below.

7.3. Kinematics and Chemical Properties

Little information is available on the kinematics and chemical properties of thick disks in galaxies other than the Milky Way. The larger scaleheight of the Galactic thick disk means that its velocity dispersion is higher than for the thin disk [about 40 km s^{-1} in the vertical direction near the sun, compared to about 20 km s^{-1} for the thin disk] (e.g., A.C. Quillen, D.R. Garnett, unpublished, arXiv:0004210)]. The stars of the thick disk are usually identified by their larger motions relative to the Local Standard of Rest, but kinematic selection is inevitably prone to contamination by the more abundant thin-disk stars. Recently, it has become clear that the Galactic thick disk is a discrete component, kinematically and chemically distinct from the thin disk. It now appears that thick disk stars can be more reliably selected by their chemical properties.

Near the Galactic plane, the rotational lag of the thick disk relative to the LSR is only about 30 km s^{-1} (Chiba & Beers 2000, Dambis 2009), but its rotational velocity appears to decrease with height above the plane. The stars of the thick disk are old (>10 Gyr) and more metal poor than the thin disk. The metallicity distribution of the thick disk has most of the stars with $[\text{Fe}/\text{H}]$ between about -0.5 and -1.0 , with a tail of metal-poor stars extending to about -2.2 . The thick-disk stars are enhanced in α elements relative to thin-disk stars of the same $[\text{Fe}/\text{H}]$ (e.g., Figure 20, taken from Fuhrmann 2008), indicating a more rapid history of chemical evolution. The thick disk does not show a significant vertical abundance gradient (Gilmore, Wyse & Jones 1995). It appears to be chemically and kinematically distinct from the thin disk.

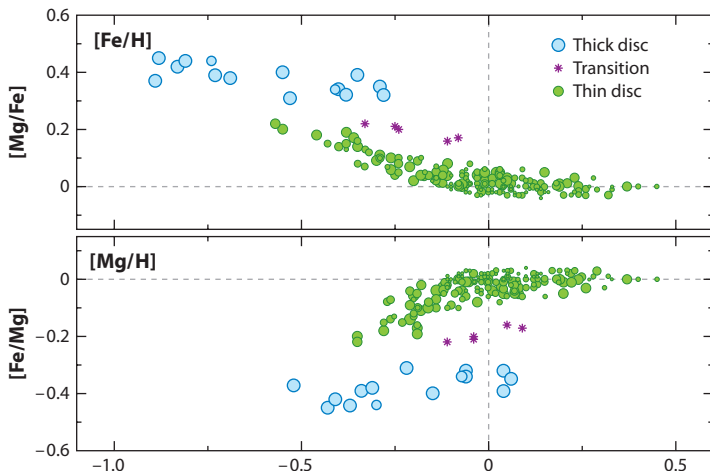


Figure 20

Mg enrichment of the thick disk relative to the thin disk, indicating that the thick disk is a chemically distinct population (From Furhmann 2008).

A decomposition of the kinematics and distribution of stars near the Galactic poles, by Veltz et al. (2008), nicely illustrates the three main kinematically discrete stellar components of the Galaxy: a thin disk with a scaleheight of 225 pc and a mean vertical velocity dispersion of about 18 km s⁻¹; a thick disk with a scaleheight of 1,048 pc and mean velocity dispersion of 40 km s⁻¹; and a halo component with a velocity dispersion of about 65 km s⁻¹.

The old thick disk presents a kinematically recognizable relic of the early Galaxy and is, therefore, a very significant component for studying galaxy formation. Because its stars spend most of their time away from the Galactic plane, the thick disk is unlikely to have suffered much secular heating since the time of its formation. Its dynamical evolution was probably dominated by the changing potential field of the Galaxy associated with the continuing growth of the Galaxy since the time at which the thick disk was formed.

For the thick disks of other galaxies, broadband colors suggest that the thick disks are again old and metal poor relative to their thin disks. Yoachim & Dalcanton (2008) studied the rotation of the thick disks of a small sample of extragalactic thick disks. In one galaxy (FGC 227),¹² they found that the thick disk appeared to be counter-rotating relative to its thin disk. If confirmed, this difficult observation would have important implications for the origin of thick disks.

7.4. Relation of Thick Disk to Other Galactic Components

At this time, there is no convincing evidence that the thick disk is in any way related to the halo or the bulge of its parent galaxy. The almost ubiquitous nature of thick disks, independent of the bulge to disk ratio, argues against any causal relation with the bulge. In the Milky Way, some chemical similarities of bulge and thick-disk stars are observed. For example, the $[\alpha/\text{Fe}]$ ratio of the thin-disk stars near the Sun is somewhat like the enhanced $[\alpha/\text{Fe}]$ ratios seen in bulge stars (Meléndez et al. 2008), but this is probably more a reflection of the rapid star-formation history of both components rather than any deeper relationship. The metal-poor tail of the metallicity distribution of the thick disk reaches down to metallicities usually associated with halo stars ($[\text{Fe}/\text{H}] < -1$), but the kinematics are different [the metal-poor thick-disk stars are rotating more rapidly than the halo stars (e.g., Carollo et al. 2010) and do not hint at any cosmogonic relationship of

¹²FGC is the Flat Galaxy Catalogue of Karachentsev, Karachentseva & Parnovskij (1993).

thick disk and halo]. Gilmore (1995) found that in the Galaxy, the cumulative angular momentum distribution function for stars in the thick disk is rather similar to that of the thin disk, but distinctly different from that of the stellar halo and the bulge.

Thin disks and thick disks do appear to be causally linked: The survey of Yoachim & Dalcanton (2006) shows that all or almost all galaxies selected as having a thin disk also have a thick disk. Thick-disk formation seems to be a normal event in the early formation of thin disks, but the details of how disks form are not yet understood.

7.5. Thick Disk Formation Scenarios

Thick disks appear to be old and very common, puffed up relative to their parent thin disks, and (at least in the case of the Milky Way) to have suffered rapid chemical evolution. Scenarios for their formation include:

- Thick disks come from energetic early star burst events, maybe associated with gas-rich mergers (Samland & Gerhard 2003, Brook et al. 2004).
- Thick disks are the debris of accreted galaxies that were dragged down by dynamical friction into the plane of the parent galaxy and then disrupted (Walker, Mihos & Hernquist 1996; Abadi et al. 2003). To provide the observed metallicity of the Galactic thick disk ($[Fe/H] \sim -0.7$), the accreted galaxies that built up the Galactic thick disk would have been more massive than the Small Magellanic Cloud and would have had to be chemically evolved at the time of their accretion. The possible discovery of a counter-rotating thick disk (Yoachim & Dalcanton 2008) (FGC 227; see above) would favor this mechanism.
- The thick disk's energy comes from the disruption of massive clusters or star-forming aggregates (Kroupa 2002b), possibly like the massive clumps seen in the high redshift clump cluster galaxies. Other researchers have discussed the formation of thick disks through the merging of clumps and heating by clumps in clump cluster galaxies (e.g., Bournaud, Elmegreen & Martig 2009).
- The thick disk may be associated with the effects of radial mixing of stars and gas in the evolving Galaxy (Schönrich & Binney 2009a,b).
- The thick disk represents the remnant early thin disk, heated by accretion events. In this picture, the thin disk begins to form at a redshift of 2 or 3 and is partly disrupted and puffed up during the active merger epoch. Subsequently, the rest of the gas gradually settles to form the present thin disk (e.g., Quinn & Goodman 1986, Freeman 1987).

Sales et al. (2009) have shown that the predicted distribution of orbital eccentricities for nearby thick-disk stars is different for several of these formation scenarios. As large samples of accurate orbital eccentricities become available for thick disk stars, they can be used to exclude some of the proposed formation mechanisms.

8. FORMATION OF DISKS

In this section, we turn to formation models of galaxy disks, describing first formation scenarios and corresponding paradigms and then reviewing briefly observations of disks at high redshift and other matters related to the formation process.

8.1. Disk Formation Scenarios

Stellar disks are close to centrifugal equilibrium, suggesting dissipation of baryons to a near-equilibrium structure before the gas became dense enough to initiate the onset of the main epoch

of star formation. This picture goes back at least to Eggen, Lynden-Bell & Sandage (1962) and Sandage, Freeman & Stokes (1970) in the pre–dark matter era and was followed by many innovative landmark papers in the late 1970s and early 1980s on the cooling of gas and dissipational formation of disks in the potential of the preformed dark matter halo. Rees & Ostriker (1977) discussed the cooling of gas and the thermalizing of infalling gas. White & Rees (1978) described the two-stage theory of galaxy formation, in which the dark matter clustered under the influence of gravity and the gas cooled into the dark matter halos. Fall & Efstathiou (1980) considered the dissipational collapse of a disk within a dark halo, conserving its detailed $M(b)$ distribution as suggested by Mestel (1963). Assuming that the specific angular momenta of the dark matter and gas were similar, they showed that the gas would collapse by at least a factor of 10. Gunn (1982) showed that in this hypothesis approximately exponential stellar disks arise naturally, and van der Kruit (1987) showed that these would then have radial truncations at about 4.5 scalelengths. Blumenthal et al. (1984) discussed the various possible kinds of dark matter (cold, warm, hot) and their implications for the formation of galaxies by cooling. Later versions of this basic picture were discussed by Dalcanton et al. (1997) and Mo, Mao & White (1998). The so-called rotation curve conspiracy—that the properties of disk and halo are precisely those necessary to produce essentially flat, featureless rotation curves and to provide the Tully-Fisher law—was heuristically explained in the context discussed here by Gunn (1987) and Ryden & Gunn (1987).

In summary, this paradigm involves the dark matter halo forming gravitationally and relaxing to virial equilibrium; then infalling gas is shock-heated to the halo virial temperature and then cools radiatively from inside out, gradually building up the disk and forming stars quiescently.

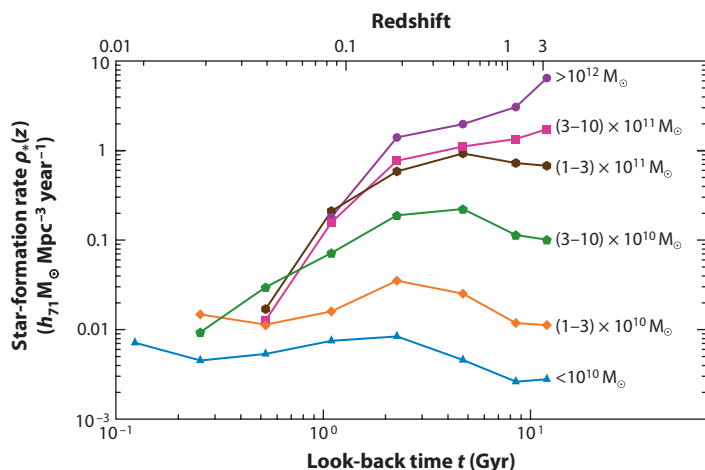
The subsequent star-formation history of disks is very different from galaxy to galaxy. In the S0 galaxies, the star formation has already come to a halt through gas exhaustion or gas stripping. In the Galactic thin disk, star formation began about 10 Gyr ago (Edvardsson et al. 1993; Knox, Hawkins & Hambly 1999), and a wide range of stellar age is seen, indicating that disk formation was an extended process starting about 10 Gyr ago and continuing to the present time. The star-formation history of the disk is not very well constrained, but is consistent with a roughly constant star-formation rate (e.g., Rocha-Pinto et al. 2000) with fluctuations of about a factor of 2 on gigayear timescales. In the lower luminosity systems, the main epoch of star formation did not begin right away, and much of the current star formation in the Universe is now taking place in these smaller disk galaxies. This is the phenomenon of downsizing: star formation in the early Universe occurred mainly in the larger systems and has gradually proceeded to progressively smaller galaxies (see **Figure 21**).

This is nicely shown by Noeske et al. (2007a,b). They analyzed the star-formation rate as a function of stellar mass M_* and redshift. In galaxies that are forming stars, the star-formation rate depends on the stellar mass of the galaxies. The observed range of star-formation rate remains approximately constant with redshift, but the sequence moves to higher star-formation rate with increasing redshift. The dominant mode of evolution since $z = 2$ is a gradual decline of the average star-formation rate. At a given mass, the star-formation rate at $z = 2$ was larger by factors of ~ 4 and ~ 30 than that in star-forming galaxies at $z = 1$ and 0, respectively (Daddi et al. 2007). The star formation drives the growth of disks. Trujillo et al. (2006) studied the evolution of the luminosity-size and stellar mass-size relation in galaxies since $z = 3$ and found that, at a given luminosity, galaxies were three times smaller at $z = 2.5$ than now; at a given M_* , they are two times smaller. In the Local Group, Williams et al. (2009a) directly measured the evolution of the scale length of M33, which has increased from 1 kpc 10 Gyr ago to 1.8 kpc at more recent times.

The present high, specific star-formation rate of many less massive galaxies reflects the late onset of their dominant star-formation episode, after which the star-formation rate gradually

Figure 21

The history of star formation as a function of stellar mass of the galaxy. The curves have been offset by 0.5 in the log, except for the most massive one, where it has been an additional 1.0. The phenomenon of star formation occurring in the early Universe mainly in large systems while later shifting to smaller systems is known as downsizing (From Heavens et al. 2004).



declines. The less massive galaxies appear to have a longer e-folding time and a later onset of their star-formation history.

The color distributions of galaxies reflect this mass dependence of their star-formation history. At low redshifts, the color distribution is bimodal, showing the blue cloud of star-forming galaxies at lower stellar masses and the overlapping red sequence of more luminous systems in which star formation has now stopped or is at a very low rate (Blanton et al. 2003, Kauffmann et al. 2003a). The restframe color distribution is now known to be bimodal at all redshifts $z < 2.5$ (e.g., Brammer et al. 2009). The red sequence persists to beyond $z = 2$, indicating that many galaxies had completed their star-forming lives by this time. Galaxies in the green valley between the red sequence and the blue cloud may be in transition between the two sequences, as blue cloud galaxies whose star formation is running down, but also as red sequence systems in which the star formation has been revitalized (e.g., Beaulieu et al. 2010). However, it seems more likely now that most of these green valley galaxies are reddened star-forming systems.

The bimodality manifests itself in several ways. Blue galaxies, as defined by their color and their star-formation rates, dominate the stellar mass function below a transition mass of about $3 \times 10^{10} M_{\odot}$. It persists to redshifts of at least 2.5. The bulge-to-disk ratio shows a related transition from disk-dominated blue galaxies below the transition mass to spheroid-dominated red sequence galaxies above the transition mass (e.g., Kauffmann et al. 2003b). The surface brightness μ -stellar mass M_* relation changes from $\mu \propto M_*^{0.6}$ at lower masses to $\mu \sim \text{constant}$ at higher masses. The mean mass-metallicity relation also shows a break at the transition mass (e.g., Tremonti et al. 2004). Dalcanton, Yoachim & Bernstein (2004) observed a break in the morphology of dustlanes of edge-on disk galaxies at a similar transition mass, changing from diffuse for lower mass disks to sharply defined for higher mass disks. This could be related to infalling cold gas streams enhancing star formation and turbulence in the less massive galaxies (see Sections 4.4 and 8.3).

The role of mergers in the evolution of disk galaxies remains uncertain. The thin disks of disk galaxies are relatively fragile and are easily puffed up by even minor mergers (Quinn & Goodman 1986, Toth & Ostriker 1992). CDM simulations show a high level of merger activity on all scales. These mergers tend to excite star formation, puff up the disks, and build up spheroidal components in the simulations. This makes it difficult for CDM simulations to generate large spirals like the Milky Way, with relatively small spheroidal components. Although there has been discussion by simulators about the unusually quiescent merger history of the Milky Way, such systems are not unusual. Kormendy et al. (2010) have shown that at least 11 of 19 nearby disk galaxies with circular

velocities >150 km s $^{-1}$ show no evidence for a classical bulge. They argue that pure-disk galaxies are far from rare.

Lotz et al. (2008) studied the evolution of the merger rate since redshift $z = 1.2$. They find that the fraction of galaxies involved in mergers is about 10%, and conclude that the decrease in star-formation rate density since $z = 1$ is a result of the declining star-formation rate in disk galaxies rather than a decrease in major mergers. However, Hammer et al. (2005, 2009) argue, from the episodic star-formation history of most intermediate-mass spirals and from the incidence of peculiar morphologies and anomalous kinematics in a sample of galaxies at median redshift $z = 0.65$, that they have experienced their last major merger event within the past 6–8 Gyr and that reprocessing of spirals by gas-rich mergers may be an important aspect of the formation of present-day disks. From their GOODS galaxy sample, Bundy et al. (2009) show that mergers contribute little to galaxy growth since $z = 1.2$ for galaxies with $M_* < 3 \times 10^{10} M_\odot$. For the more massive galaxies, which are mostly spheroidal systems, mergers are more important; they estimate that about 30% have undergone (mostly dry or gas-free) mergers.

The Milky Way is an important part of assessing the significance of mergers in building up large spiral galaxies. The unique possibility to make very detailed chemical studies of stars in the Milky Way provides an independent opportunity to evaluate the merger history of our large disk galaxy via chemical tagging techniques (Freeman & Bland-Hawthorn 2002).

8.2. Disks at High Redshift

One of the most fundamental observations that the HST made possible is the imaging of galaxies when they were very young. Studies of the Hubble Deep Fields (Williams et al. 1996, 2000; Beckwith et al. 2006) showed observationally that few galaxies, which resemble present-day spirals or ellipticals are present at redshifts >4 . Simulations indicate that disks should be present at redshifts around 2 (e.g., Sommer-Larsen et al. 2003): Is this consistent with observations? If disks are present at these redshifts, what are they like? How do their baryonic mass distributions compare with those of disk galaxies at low redshifts?

Labbé et al. (2003) observed the Hubble Deep Field-South in the near-IR (from the ground) and found six galaxies at redshifts $z = 1.4$ to 3.0 that have disklike morphologies. The galaxies are regular and large in the near-IR (corresponding to rest-frame optical), with face-on effective radii of 5.0–7.5 kpc, which is comparable to the Milky Way. The surface brightness profiles are consistent with an exponential law over 2 to 3 effective radii. The HST morphologies (rest-frame UV) are irregular and show large complex aggregates of star-forming regions (~ 15 kpc across), symmetrically distributed around the centers.

Genzel et al. (2006) described the rapid formation of a luminous star-forming disk galaxy at a redshift of $z = 2.38$. Their integral field unit observations indicate that a large protodisk is channelling gas toward a growing central bulge. The high surface density of gas and the high rate of star formation show a system in rapid assembly, with no obvious evidence for a major merger. Integral-field spectroscopy by Förster Schreiber et al. (2009) of several UV-selected galaxies with stellar masses $\sim 3 \times 10^{10} M_\odot$, star-formation rates of $\sim 70 M_\odot \text{ year}^{-1}$, and redshifts between 1.3 and 2.6 provides rotation curves and indicators of dynamical evolution. The morphology is typically clumpy. About one-third of the galaxies are turbulent and rotation-dominated, another third are compact and dominated by velocity dispersion, whereas the rest are interacting or merging systems. The rotation-dominated fraction is higher for higher masses.

Elmegreen et al. (2009a,b) investigated the relationship to modern spirals of clumpy high-redshift galaxies in the GOODS, GEMS, and Hubble UDF surveys. The clump properties indicate

the gradual dispersal of clumps to form disks and bulges, with little indication of merger activity. The morphological similarity of these systems to modern dwarf irregulars suggests that the clumpy morphology comes from gravitational instability in the turbulent gas. They note that about 50% of these clump cluster galaxies have massive red clumps that could be interpreted as young bulges. We have already discussed the clump cluster galaxies in the context of the formation of the thick disk component (Section 6.5).

Kriek et al. (2009) studied 19 massive galaxies at $z \sim 2.3$: 9 of them are compact quiescent systems and 10 are emission-line systems (6 star-forming galaxies and 4 AGNs). The star-forming galaxies again have clumpy morphologies. In the rest-frame $(U-B) - M_*$ plane, the galaxies appear bimodal: The large star-forming galaxies lie in a blue cloud, and the compact quiescent galaxies in a red sequence. A bimodal distribution similar to that at lower redshifts is already in place at redshifts > 2 .

In summary, it appears that the formation of disk galaxies is already well advanced at redshifts > 2 , but the systems have mostly not yet settled to a quiescent disk in rotational equilibrium. The clumpy structure of the massive star-forming systems is likely to be an important factor in the subsequent evolution of these systems and in the formation of their thick disks and bulges. The role of mergers in building up these disk galaxies may not be as important as it appears to be from CDM simulations.

8.3. Baryon Acquisition by Disk Galaxies

In the scenarios for disk formation that emerged soon after the discovery of dark matter in disk galaxies, the gas was shock-thermalized to the virial temperature and then gradually cooled to form the disk. Simulations (e.g., Sommer-Larsen et al. 1999) suggest that this hot halo is further populated by gas blown out from the disk via feedback into the hot halo. This feedback provides a way to reduce the problem of angular momentum loss that led to unrealistically low angular momenta for disks seen in earlier simulations. These simulations are successful in reproducing the peak in the star-formation rate seen within individual galaxies at $z \sim 2$.

More recent simulations point to the likelihood of cold gas accretion into disk galaxies. Smoothed particle hydrodynamics simulations by Kereš et al. (2005) showed that typically about half of the gas shock-heats to the virial temperature of the potential well ($\sim 10^6$ K in a Milky-Way-like galaxy), whereas the other half radiates its gravitational energy at $T < 10^5$ K. A cold mode of infall is seen for stellar masses $< 2 \times 10^{10} M_\odot$. This cold gas often falls in via the cosmic filaments, allowing galaxies to draw their gas from a large volume. Kereš et al. (2009) found that most of the baryonic mass is acquired through the filamentary cold accretion of gas that was never shock-heated to its virial temperature. This cold accretion is the main driver of the cosmic star-formation history.

Hot halos are seen only for dark halo masses $> 2 - 3 \times 10^{11} M_\odot$. Dekel & Birnboim (2006) ascribed the bimodality of galaxy properties to the nature of the gas acquisition. Galaxies with stellar masses $< 3 \times 10^{10} M_\odot$ are mostly ungrouped star-forming disk systems, whereas the more massive galaxies are mostly grouped old red spheroids. They argue that the bimodality is driven by the thermal properties of the inflowing gas. In halos with masses $< 10^{12} M_\odot$, the disks are built by cold streams, giving efficient early star formation regulated by supernova feedback. In the more massive halos, the infalling gas is shock-heated and is further vulnerable to AGN feedback, shutting off the gas supply and leading to red and dead spheroids at redshift $z \sim 1$. Simulations by Dekel, Sari & Ceverino (2009) showed that the evolution of massive disk systems is governed by interplay between smooth and clumpy cold streams, disk instability, and bulge formation. The streams maintain an unstable gas-rich disk, generating giant clumps that can migrate into the bulge

in a few dynamical times. The streams prolong this clumpy phase for several Gyr. The clumps form stars in dense subclumps and each clump converts to stars in ~ 0.5 Gyr. The star forming disk is extended because the incoming streams keep the outer disk dense and unstable, and also because of angular momentum transport by secular processes within the disk (e.g., Kormendy & Kennicutt 2004). Observationally, the large chemical tagging surveys which will soon begin (HERMES, APOGEE) will be able to evaluate the role of giant clumps in the formation of the thin and thick disks of the Milky Way (e.g., Bland-Hawthorn et al. 2010). The debris of the dispersed giant clumps should be very apparent from the chemical tagging analysis.

The Milky Way is surrounded by a system of infalling high-velocity HI clouds (HVCs) whose nature is not yet fully understood. The associated infall rate is estimated at about $0.2 \text{ M}_\odot \text{ year}^{-1}$ (e.g., Peek, Putman & Sommer-Larsen 2008), an order of magnitude smaller than the current star-formation rate of the Milky Way. Maller & Bullock (2004) proposed that the cooling of the Galactic hot corona is thermally unstable and generates pressure-confined HVCs with masses $\sim 5 \times 10^6 \text{ M}_\odot$, which contribute to fueling the continued star formation of the disk. Binney, Nipoti & Fraternali (2009) argued however that thermal instability of the hot halo is unlikely to be the source of the Galactic HVC system.

Some disk galaxies (e.g., NGC 891: Oosterloo, Fraternali & Sancisi 2007) show thick HI layers surrounding their galactic disks, which is lagging in rotation relative to the gas in the disk. This gas is accompanied by ionized gas (observed in $\text{H}\alpha$) that shares the lag in rotation velocity (Heald et al. 2007, Kamphuis et al. 2007a) and by dust (Kamphuis et al. 2007b). In more face-on systems, this HI appears associated with regions of star formation (e.g., Kamphuis, Sancisi & van der Hulst 1991), indicating that at least a part of it may have originated in the disk. Fraternali & Binney (2008) and Marinacci et al. (2010) suggest that these layers are associated with gas that has been swept up from the hot corona by galactic fountain clouds ejected from the disk by star formation. In this way, the star formation in the disk is self-fueling, through the gas brought down from the hot corona.

Deep HI images of other disk systems show a very extended rotating HI distribution. M83 (see Section 4.3 and **Figure 15**, and <http://www.atnf.csiro.au/people/bkoribal/m83/m83.html>) is an example, with HI extending far beyond the optical extent of the system. Its outermost HI shows spectacular HI arms and filaments, some of which are forming stars at a low level (Bigiel et al. 2010a). It seems unlikely that this structure should be interpreted as spiral structure in an extended HI disk, because the density of the HI is so low. It may represent a slow filamentary infall of HI into the disk. The observed star formation in this outer HI disk indicates that the outer disk is still in the process of construction. NGC 6946 is another more orderly example of such a very extended HI disk (Boomsma et al. 2008).

9. S0 GALAXIES

Hubble (1936) introduced S0 galaxies as the transition type between elliptical galaxies and spirals. Spitzer & Baade (1951) suggested they were spirals stripped of their dust, gas, and arms as a result of collisions in clusters of galaxies. Sandage, Freeman & Stokes (1970) argued that the morphological type of a galaxy is defined at the time of the formation of the old disk stars, and S0 galaxies are those in which, at the time of the completion of the formation of the disk, there was little gas left for star formation. Subsequently, the observation of a high proportion of S0 galaxies in clusters (Oemler 1974), the evolution of blue galaxies populations in clusters with redshift (Butcher & Oemler 1978), and the increasing ratio of S0s compared to spiral in regions of higher galaxy density (Dressler 1980) led to the general acceptance that S0 galaxies in clusters are stripped spirals. Larson, Tinsley & Caldwell (1980) reconsidered the issue. They remarked

that the apparent rate of consumption of gas by star formation leads to the paradoxical situation that spirals exhaust their gas supplies on a timescale considerably less than the Hubble time (see their abstract). The solution they suggested to this was that spirals constantly replenish their gas content from a reservoir in a gaseous envelope remaining from their formation and, therefore, can sustain star formation over a much longer timescale, whereas S0 galaxies would have lost these envelopes early on and, therefore, do run out of gas on a relatively short timescale.

One way to further address the issue of whether S0s are stripped spirals is to investigate the structure and, in particular, the kinematics of disks in S0s in order to investigate whether or not there are differences in the stellar dynamics. We do not fully review the work on S0 galaxies, but concentrate on this aspect and refer to comprehensive reviews of S0 galaxies, for example, those presented by Quilis, Moore & Bower (2000) and Fritze-von Alvensleben (2004); we also point out that the importance of ram-pressure stripping in environments like Virgo has convincingly been demonstrated by Chung et al. (2009).

Although S0s have a relatively bright surface brightness, measurements of their kinematics remained difficult, and this prevented for a long time a detailed understanding of their dynamics. One of the earliest identified and most easily accessible S0s is NGC 3115. Oort (1940), already as early as during the 1930s (!) considered its dynamics; his motivation was to study issues of stability, as he was interested in the origin and maintenance of spiral structure (the first part of the paper concerns the origin of the deviation of the vertex as caused by spiral arms). Although his photometry shows evidence for a disk component (concentration of light near the major axis), he does not treat it as a separate component. The velocity data (only a few points of the rotation curve by Humason as reported in the annual report of the Mount Wilson Observatory) were insufficient for a significant treatment. Oort concludes that, if these data are correct, the distribution of mass does not correspond to that of the light and quotes mass-to-light ratios of order 250. Minkowski (1960) reported, in a review at a meeting on “*Les Recherches Galactiques et Extragalactiques et la Photographie Électronique*” in Paris in 1959, a new rotation curve that showed an initial rise, then a secondary minimum followed by another strong rise. In the discussion after Minkowski’s paper, Oort reported that he was able to reproduce this behavior on the assumption of a proportionality of mass to light and a large velocity dispersion, which was reported also by Minkowski.¹³

Oort urged Maarten Schmidt to remeasure the rotation of NGC 3115 and together they took spectra in 1968 on the 200-inch Hale Telescope. It took until 1974 before Williams (1975) reduced the data. Oort never used this for a detailed dynamical study, his interests having turned to problems of galactic nuclei and cosmology (Oort 1977, 1981, 1983). In the meantime, measurements of the light distribution improved (Miller & Prendergast 1968; Strom et al. 1977, 1978), but although color information seemed to support the existence of color variations and the rotation curve allowed an estimate of the mass of the disk as a fraction of the total ($\lesssim 0.4$), no comprehensive dynamical model was possible without better spectroscopy. The detailed surface photometry study of Tsikoudi (1979) constituted the first attempt to separate photometric components. The most accurate measurements of the stellar kinematics, confirming the flat shape of the stellar rotation and providing also evidence for a supermassive black hole in the center, have been presented by Kormendy & Richstone (1992).

The kinematic data necessary for a detailed dynamical modelling started to become available only in the 1980s, first in the central regions (Rubin, Peterson & Ford 1980) and then over a more

¹³Oort was, however, not satisfied with his solution and never published it. He did illustrate it during his lectures on Stellar Dynamics in Leiden, as the notes of one of us—P.C.K. is a student of Oort—show and mentioned there that he felt that the rotation curve might very well be wrong and needed confirmation.

extended region (Illingworth & Schechter 1982). In the latter study, the kinematics of the disk were estimated from a decomposition of the contributions to the observed velocities and velocity dispersions. The main result of the study was the important deduction, which later was proved to be more general, that in bulges of disk galaxies rotation plays a bigger role in supporting its shape and density distribution than in ellipticals.

Kormendy (1984a,b) was the first to measure the velocity dispersion in the disk of an S0 galaxy. His main aim was to estimate the Toomre (1964) Q -parameter for local stability. Both in NGC 1553 and in the barred S0 NGC 936, he was able to estimate Q and found it to be well above unity (more like 2 or 3). He therefore concluded that S0 galaxies may differ from spirals in that their stellar disks are too hot (in addition to suffering from lack of gas, which would lower the overall Q) to form small-scale structure.

For NGC 3115, the observations of photometry and kinematics have become more sophisticated in recent years (e.g., Capaccioli, Vietri & Held 1988; Silva et al. 1989; Capaccioli et al. 1993; Michard 2007), but the issue has become much more complicated. A simple answer to the question of whether an S0 originated as a spiral that was swept of its gas or a system that formed its disk with little gas that was not replenished has not emerged. *Gemini* multiobject long-slit spectroscopy by Norris, Sharples & Kuntscher (2006) shows that there is a difference between the $[\alpha/\text{Fe}]$ in the bulge (~ 0.3) and the disk (close to solar), whereas the average age of stars in the disk (5–8 Gyr) is significantly less than in the bulge (10–12 Gyr). The fact that the disk is bluer than the bulge would then primarily be an age difference. Star formation in the disk of this archetypal S0 has proceeded at least for some time after the formation of the bulge.

We note that the advent of new techniques has greatly improved the observational possibilities. SAURON can measure kinematic data using integral field spectroscopy, such as in the study of the S0 galaxy NGC 7332 by Falcón-Barroso et al. (2004). In this system, the stellar populations in the disk (but also in the bulge) are again relatively young, so that star formation must have proceeded in the disk until fairly recently. In addition there is evidence for a strong influence by a bar.

Another recent development is the use of PNe to measure the kinematics. This has the advantage that velocities and dispersions can be measured in faint outer parts of galaxies (e.g., Coccato et al. 2009). Comparing photometry, absorption-line, and PNe kinematics shows that there is good agreement between the PNe number density distribution and the stellar surface brightness and also a good agreement between PNe and absorption line kinematics. An application of this technique to an S0 galaxy is the study of NGC 1023 by Noordermeer et al. (2008), where the PNe were measured with a very good distribution over the face of the system. With these data, it is possible to test whether an S0 could result from a minor merger such that its kinematics become dominated by random motions. The inner parts are fitted quite well with a disk that is rotationally supported, but the outer parts would suggest a minor merger event. Information like this on more systems is required to answer the basic questions.

Finally, an interesting approach is that of Aragón-Salamanca, Bedregal & Merrifield (2006) and Barr et al. (2007), who use globular clusters to measuring the fading of S0 galaxies. They do this by comparing the specific frequency of globular clusters (their number per unit luminosity, S_N) between S0s and normal spirals. This innovative and powerful method has led to the picture in which the disk has faded by a factor of three or so. S0s with younger ages have values for S_N that are more like those of spirals. This is consistent with the view that S0s are formed as a result of removal of gas from normal spirals.

Although the kinematics of S0s would suggest that their disks have been present on a long timescale, the evidence for relatively recent star formation indicates that their history is more complicated than previously thought.

DISCLOSURE STATEMENT

The authors are not aware of any affiliations, memberships, funding, or financial holdings that might be perceived as affecting the objectivity of this review.

ACKNOWLEDGMENTS

A major part of this review was written during work visits by P.C.K. to Mount Stromlo Observatory. P.C.K. thanks the Research School for Astronomy and Astrophysics of the Australian National University and its directors for hospitality and facilities over the years in support of such visits. He is grateful to the Governing Board of the University of Groningen for the appointment as distinguished Jacobus C. Kapteyn Professor of Astronomy, and the Faculty of Mathematics and Natural Sciences for an accompanying annual research grant that supported, among other things, his travels to scientific meetings and work visits. Additional financial support was provided from an annual research grant as a member of the Area Board for Exact Sciences of the Netherlands Organisation for Scientific Research (NWO). We are grateful for the detailed and very useful remarks and suggestions by the scientific editor, John Kormendy. K.C.F. is very grateful to many colleagues for discussions of galactic disks, and particularly to Gérard de Vaucouleurs and Allan Sandage. P.C.K. acknowledges many stimulating collaborations, of which he wishes to acknowledge here especially that with Leonard Searle.

LITERATURE CITED

- Abadi MG, Navarro JF, Steinmetz M, Eke VR. 2003. *Ap. J.* 597:21
- Abe F, Bond IA, Carter BS, Dodd RJ, Fujimoto M, et al. 1999. *Astron. J.* 118:261
- Allen RJ, Goss WM, van Woerden H. 1973. *Astron. Astrophys.* 29:447
- Allen RJ, Shu FH. 1979. *Ap. J.* 227:67
- Alloin D, Edmunds MG, Lindblad PO, Pagel BEJ. 1981. *Astron. Astrophys.* 101:377
- Ann HB. 2007. *J. Korean Astron. Soc.* 40:9
- Ann HB, Park J-C. 2006. *New Astron.* 11:293
- Aragón-Salamanca A, Bedregal AG, Merrifield MR. 2006. *MNRAS* 458:101
- Argyle E. 1965. *Astron. J.* 141:750
- Arp HC. 1965. *Ap. J.* 142:402
- Athanassoula E, Sellwood JA. 1986. *MNRAS* 221:213
- Baade W. 1944. *Ap. J.* 100:137
- Babcock HW. 1939. *Lick Obs. Bull.* 19:41
- Bahcall JN. 1986. *Annu. Rev. Astron. Astrophys.* 24:577
- Baldwin JE, Field C, Warner PJ, Wright MCH. 1971. *MNRAS* 154:445
- Banerjee A, Matthews LD, Jog CJ. 2010. *New Astron.* 15:89
- Barbanis B, Woltjer L. 1967. *Ap. J.* 150:461
- Barker MK, Sarajedini A, Geisler D, Harding P, Schommer R. 2007a. *Astron. J.* 133:1125
- Barker MK, Sarajedini A, Geisler D, Harding P, Schommer R. 2007b. *Astron. J.* 133:1138
- Barnes JE. 1988. *MNRAS* 331:699
- Barr JM, Bedregal AG, Aragón-Salamanca A, Merrifield MR, Bamford SP. 2007. *Astron. Astrophys.* 470:173
- Bastian N, Covey KR, Meyer MR. 2010. *Annu. Rev. Astron. Astrophys.* 48:339
- Battaglia G, Fraternali F, Oosterloo T, Sancisi R. 2006. *Astron. Astrophys.* 447:49
- Battener E, Florido E, Jiménez-Vicente J. 2002. *Astron. Astrophys.* 338:313
- Beaulieu SF, Freeman KC, Hidalgo SL, Norman CA, Quinn PJ, et al. 2010. *Astron. J.* 139:984
- Beck R. 2008. In *Formation and Evolution of Galaxy Disks*, ASP Conf. Ser. 396, p. 35
- Beckwith SVW, Stiavelli M, Koekemoer AM, Caldwell JAR, Ferguson HC, et al. 2006. *Astron. J.* 132:1729
- Begeman K. 1987. *HI rotation curves of spiral galaxies*. PhD thesis. Univ. Groningen

- Bell EF, de Jong RS. 2000. *MNRAS* 312:497
- Bell EF, de Jong RS. 2001. *MNRAS* 550:212
- Bellini A, Bedin LR, Piotto G, Milone AP, Marino AF, et al. 2010. *Astron. J.* 140:631
- Bershady MA, Verheijen MAW, Swaters RA, Andersen DR, Westfall KB, Martinsson T. 2010a. *Ap. J.* 716:198
- Bershady MA, Verheijen MAW, Westfall KB, Andersen DR, Swaters RA, Martinsson T. 2010b. *Ap. J.* 716:234
- Bigiel F, Leroy A, Seibert M, Walter F, Blitz L, et al. 2010a. *Ap. J.* 720:31
- Bigiel F, Leroy A, Walter F, Blitz L, Brinks E, et al. 2010b. *Astron. J.* 140:1194
- Binney JJ. 2007. See de Jong 2007, p. 67
- Binney JJ, Nipoti C, Fraternali F. 2009. *MNRAS* 397:1804
- Bland-Hawthorn J, Karlsson T, Sharma S, Krumholz M, Silk J. 2010. *Ap. J.* 721:582
- Bland-Hawthorn J, Vlajić M, Freeman KC, Draine BT. 2005. *Ap. J.* 629:249
- Blanton MR, Hogg DW, Bahcall NA, Baldry IK, Brinkmann J, et al. 2003. *Ap. J.* 594:186
- Block DL, Freeman KC, Puerari I, eds. 2010. *Galaxies and Their Masks*. New York: Springer
- Blumenthal GR, Faber SM, Flores R, Primack JR. 1986. *Ap. J.* 301:27
- Blumenthal GR, Faber SM, Primack JR, Rees MJ. 1984. *Nature* 311:517
- Böker T. 2008. *Ap. J.* 672:L111
- Böker T, Laine S, van der Marel RP, Sarzi M, Rix H-W, et al. 2002. *Astron. J.* 123:1389
- Böker T, Sarzi M, McLaughlin DE, van der Marel RP, Rix H-W, et al. 2004. *Astron. J.* 127:105
- Boomsma R, Oosterloo TA, Fraternali F, van der Hulst JM, Sancisi R. 2008. *Astron. Astrophys.* 490:555
- Bosma A. 1981a. *Astron. J.* 86:1791
- Bosma A. 1981b. *Astron. J.* 86:1825
- Bosma A, Freeman KC. 1993. *Astron. J.* 106:1394
- Bottema R. 1993. *Astron. Astrophys.* 275:16
- Bottema R. 1995. *Astron. Astrophys.* 295:605
- Bottema R. 1996. *Astron. Astrophys.* 306:345
- Bottema R. 1997. *Astron. Astrophys.* 328:517
- Bottema R. 2003. *MNRAS* 344:358
- Bottema R, Shostak GS, van der Kruit PC. 1987. *Nature* 328:401
- Bournaud F, Elmegreen BG, Martig M. 2009. *Ap. J.* 707:L1
- Brammer GB, Whitaker KE, van Dokkum PG, Marchesini D, Labb   I, et al. 2009. *Ap. J.* 706:L173
- Briggs FH. 1990. *Ap. J.* 352:15
- Broeils AH. 1992. *Dark and visual matter in spiral galaxies*. PhD thesis. Univ. Groningen
- Broeils AH, Rhee M-H. 1997. *Astron. Astrophys.* 324:877
- Brook CB, Kawata D, Gibson BK, Freeman KC. 2004. *Ap. J.* 612:894
- Brosche P. 1973. *Astron. Astrophys.* 23:259
- Bruzual G, Charlot S. 2003. *MNRAS* 344:1000
- Bundy K, Fukugita M, Ellis RS, Targett TA, Belli S, Kodama T. 2009. *Ap. J.* 697:1369
- Burbidge EM, Burbidge GR, Shelton JW. 1967. *Ap. J.* 150:783
- Burke BF. 1957. *Astron. J.* 62:90
- Burstein D. 1979. *Ap. J.* 234:829
- Butcher HR, Oemler A. 1978. *Ap. J.* 219:18
- Byun Y-I. 1998. *Cbin. J. Phys.* 36:677
- Byun Y-I, Freeman KC. 1995. *Ap. J.* 448:563
- Camm GL. 1950. *MNRAS* 110:305
- Cantinella B, Haynes MP, Giovanelli R. 2007. *Astron. J.* 134:334
- Capaccioli M, Cappellaro E, Held EV, Vietri M. 1993. *Astron. Astrophys.* 274:69
- Capaccioli M, Vietri M, Held EV. 1988. *MNRAS* 234:335
- Carignan C, Freeman KC. 1985. *Ap. J.* 294:494
- Carlberg RG, Sellwood JA. 1985. *Ap. J.* 292:79
- Carney BW, Yong D, Teixeira de Almeida ML. 2005. *Astron. J.* 130:1111
- Carollo D, Beers TC, Chiba M, Norris JE, Freeman KC, et al. 2010. *Ap. J.* 712:692
- Casertano S. 1983. *MNRAS* 203:735
- Chabrier G. 2003. *Publ. Astron. Soc. Pac.* 115:763

- Chiappini C, Matteucci F, Gratton R. 1997. *Ap. J.* 477:765
- Chiba M, Beers TC. 2000. *Astron. J.* 119:2843
- Chung A, van Gorkom JH, Kenney JDP, Crowl H, Vollmer B. 2009. *Astron. J.* 138:1741
- Cioni ML. 2009. *Astron. Astrophys.* 506:1137
- Coccato L, Gerhard O, Arnaboldi M, Das P, Douglas NG, et al. 2009. *MNRAS* 394:1249
- Cole AA, Tolstoy E, Gallagher JS, Smecker-Hane TA. 2005. *Astron. J.* 129:1465
- Condon JJ. 1992. *Annu. Rev. Astron. Astrophys.* 30:575
- Courteau S. 1996. *Ap. J. Suppl.* 103:363
- Courteau S, de Jong RS. 2009. *Unveiling the Mass.* <http://www.astro.queensu.ca/GalaxyMasses09/programme.php>
- Courteau S, Dutton A, van den Bosch FC, MacArthur LA, Dekel A, et al. 2007. *Ap. J.* 671:203
- Courteau S, Rix H-W. 1999. *Ap. J.* 513:561
- Cuddeford P, Amendt P. 1992. *MNRAS* 256:166
- da Costa GS, Jerjen H. 2002. In *The Dynamics, Structure & History of Galaxies, ASP Conf. Ser.* 273, p. 85
- Daddi E, Dickinson M, Morrison G, Chary R, Cimatti A, et al. 2007. *Ap. J.* 670:156
- Dalcanton JJ, Spergel DN, Summers FJ. 1997. *Ap. J.* 482:659
- Dalcanton JJ, Williams BF, Seth AC, Dolphin A, Holtzman J, et al. 2009. *Ap. J. Suppl.* 183:67
- Dalcanton JJ, Yoachim P, Bernstein RA. 2004. *Ap. J.* 608:189
- Dambis AK. 2009. *MNRAS* 396:553
- Davidge TJ. 2010. *Ap. J.* 718:1428
- Debattista VP, Mayer L, Carollo CM, Moore B, Wadsley J, Quinn T. 2006. *Ap. J.* 645:209
- Debattista VP, Sellwood JA. 1999. *Ap. J.* 513:L107
- Debattista VP, Sellwood J. 2000. *Ap. J.* 543:704
- de Blok WJG. 2010. *Adv. Astron.* 2010:789293
- de Blok WJG, McGaugh SS. 1997. *MNRAS* 290:533
- de Blok WJG, van der Hulst JM. 1998a. *Astron. Astrophys.* 335:421
- de Blok WJG, van der Hulst JM. 1998b. *Astron. Astrophys.* 336:49
- de Blok WJG, Walter F, Brinks E, Trachternach C, Oh S-H, Kennicutt RC. 2008. *Astron. J.* 136:2648
- de Grijs R. 1997. *Edge-on disk galaxies: a structure analysis in the optical and infrared.* PhD thesis. Univ. Groningen. <http://dissertations.ub.rug.nl/FILES/faculties/science/1997/r.de.grijs/c5.pdf>
- de Grijs R. 1998. *MNRAS* 299:595
- de Grijs R, Peletier RF. 1997. *Astron. Astrophys.* 320:L21
- de Grijs R, Peletier RF, van der Kruit PC. 1997. *Astron. Astrophys.* 327:966
- Dehnen W, Binney JJ. 1998. *MNRAS* 298:387
- de Jong JTA, Yanny B, Rix H-W, Dolphin AE, Martin NF, et al. 2010. *Ap. J.* 714:663
- de Jong RS. 1996a. *Astron. Astrophys. Suppl.* 118:557
- de Jong RS. 1996b. *Astron. Astrophys.* 313:45
- de Jong RS. 1996c. *Astron. Astrophys.* 313:377
- de Jong RS, ed. 2007. *Astrophys. Space Sci. Proc.: Island Universes: Structure and Evolution of Disk Galaxies.* Dordrecht: Springer
- de Jong RS, Bell EF. 2009. In *Unveiling the Mass.* http://www.astro.queensu.ca/GalaxyMasses09/data/deJong_GMasses09.pdf
- de Jong RS, Seth AC, Bell EF, Brown TM, Bullock JS, et al. 2007a. *IAU Symp.* 241:503
- de Jong RS, Seth AC, Radburn-Smith DJ, Bell EF, Brown TM, et al. 2007b. *Ap. J.* 667:L49
- de Jong RS, van der Kruit PC. 1994. *Astron. Astrophys. Suppl.* 106:451
- Dekel A, Birnboim Y. 2006. *MNRAS* 368:2
- Dekel A, Sari R, Ceverino D. 2009. *Ap. J.* 703:785
- Dekel A, Silk J. 1986. *Ap. J.* 303:39
- Dennefeld M, Kunth D. 1981. *Astron. J.* 86:989
- de Vaucouleurs G. 1958. *Ap. J.* 128:465
- de Vaucouleurs G. 1959a. *Ap. J.* 130:718
- de Vaucouleurs G. 1959b. *Handb. Fys.* 53:511

- Dickinson M, Giavalisco M, the GOODS Team. 2003. In *ESO Astrophys. Symp.: The Mass of Galaxies at Low and High Redshift*, p. 324
- Disney MJ. 1976. *Nature* 263:573
- Disney MJ, Phillipps S. 1983. *MNRAS* 205:1253
- Disney MJ, Romano JD, Garcia-Appadoo DA, West AAQ, Dalcanton JJ, Cortese L. 2008. *Nature* 455:1082
- Djorgovsky G. 1992. In *Cosmology and Large-Scale Structure in the Universe, ASP Conf. Ser.* 24, p. 19
- Dolphin AE. 2000. *MNRAS* 313:281
- Donato F, Gentile G, Salucci P, Frigerio Martins C, Wilkinson MI, et al. 2009. *MNRAS* 397:1169
- Dressler A. 1980. *Ap. J.* 236:351
- Drimmel R, Spergel DN. 2001. *Ap. J.* 556:181
- Dubinski J, Carlberg RG. 1991. *Ap. J.* 378:496
- Edvardsson B, Andersen J, Gustafsson B, Lambert DL, Nissen PE, Tomkin J. 1993. *Astron. Astrophys.* 275:101
- Edvardsson B, Gustafsson B, Nissen PE, Andersen J, Lambert DL, Tomkin J. 1994. In *Panchromatic View of Galaxies: Their Evolutionary Puzzle*, ed. G Hensler, Ch Theis, J Gallagher, p. 401. Gif Sur Yvette, Fr.: Ed. Front.
- Efstathiou G, Jones BJT. 1979. *MNRAS* 186:133
- Efstathiou G, Lake G, Negroponte J. 1982. *MNRAS* 199:1069
- Eggen OJ, Lynden-Bell D, Sandage AR. 1962. *Ap. J.* 136:478
- Elmegreen BG, Elmegreen DM, Fernandez MX, Lemonias JJ. 2009a. *Ap. J.* 692:12
- Elmegreen BG, Elmegreen DM, Leitner SN. 2003. *Ap. J.* 590:271
- Elmegreen DM, Elmegreen BG, Marcus MT, Shahinyan K, Yau A, Petersen M. 2009b. *Ap. J.* 701:306
- Emerson DT. 1976. *MNRAS* 176:321
- Erwin P, Pohlen M, Beckman JE, Gutierrez L, Aladro R. 2007. In *Pathways Through an Eclectic Universe, ASP Conf. Ser.* 390:251
- Faber SM, Gallagher JS. 1979. *Annu. Rev. Astron. Astrophys.* 17:136
- Falcón-Barroso J, Peletier RF, Emsellem E, Kuntschner H, Fathi K, et al. 2004. *MNRAS* 350:35
- Fall SM, Efstathiou G. 1980. *MNRAS* 193:189
- Famaey B, van Caelenberg K, Dejonghe H. 2002. *MNRAS* 335:201
- Fathi K. 2010. *Ap. J.* 722:L120
- Fathi K, Allen M, Boch T, Hatziminaoglou E, Peletier RF. 2010. *MNRAS* 406:1595
- Ferguson AMN. 2007. In *From Stars to Galaxies: Building the Pieces up to Build up the Universe, ASP Conf. Ser.* 374, p. 239
- Ferguson AMN, Gallagher JS, Wyse RFG. 1998a. *Astron. J.* 116:673
- Ferguson AMN, Irwin M, Chapman S, Ibata R, Lewis G, Tanvir N. 2007. See de Jong 2007, p. 239
- Ferguson AMN, Wyse RFG, Gallagher JS, Hunter DA. 1998b. *Ap. J.* 506:L19
- Ferrarini L, Ford H. 2005. *Space Sci. Rev.* 116:523
- Fich M, Silkey M. 1991. *Ap. J.* 366:107
- Florido E, Battaner E, Guijarro A, Garzón F, Castillo-Morales A. 2006. *Astron. Astrophys.* 455:467
- Florido E, Prieto M, Battaner E, Mediavilla E, Sanchez-Saavedra ML. 1991. *Astron. Astrophys.* 242:301
- Förster Schreiber NM, Genzel R, Bouché N, Cresci G, Davies R, et al. 2009. *Ap. J.* 706:1364
- Fraternali F, Binney JJ. 2008. *MNRAS* 386:935
- Freeman KC. 1970. *Ap. J.* 160:811
- Freeman KC. 1975. In *Galaxies and the Universe, Stars and Stellar Systems*, ed. A Sandage, M Sandage, J Kristian, 9:409. Chicago: Univ. Chicago Press
- Freeman KC. 1987. *Annu. Rev. Astron. Astrophys.* 25:603
- Freeman KC. 1991. In *Dynamics of Disc Galaxies*, ed. B Sundelius, p. 15. Göteborg: Univ. Göteborg
- Freeman KC. 1993. In *The Globular Cluster-Galaxy Connection, ASP Conf. Ser.* 48, p. 608
- Freeman KC. 1999. In *The Low Surface Brightness Universe, ASP Conf. Ser.* 170, p. 3
- Freeman KC. 2007. See de Jong 2007, p. 3
- Freeman KC, Bland-Hawthorn J. 2002. *Annu. Rev. Astron. Astrophys.* 40:487
- Freudenreich HT. 1998. *Ap. J.* 492:495
- Fritze-von Alvensleben U. 2004. *Astrophys. Space Sci. Libr.* 319:81

- Fry AM, Morrison HL, Harding P, Boroson TA. 1999. *Astron. J.* 118:1209
- Funes JG, Corsini EM, eds. 2008. In *Formation and Evolution of Galaxy Disks*, ASP Conf. Ser. 396
- Furhmann K. 2008. *MNRAS* 384:173
- Gadotti DA. 2009. *MNRAS* 393:1531
- García-Ruiz I. 2001. *Warps in disk galaxies*. PhD thesis Univ. Groningen. <http://dissertations.ub.rug.nl/faculties/science/2001/i.garcia-ruiz/>
- García-Ruiz I, Sancisi R, Kuijken KH. 2002. *Astron. Astrophys.* 394:769
- Garnett DR, Shields GA. 1987. *Ap. J.* 317:82
- Gebhardt K, Lauer TR, Kormendy J, Pinkney J, Bower GA, et al. 2001. *Astron. J.* 122:2469
- Genzel R, Tacconi LJ, Eisenhauer F, Förster Schreiber NM, Cimatti A, et al. 2006. *Nature* 442:786
- Gerssen J, Kuijken KH, Merrifield MR. 1997. *MNRAS* 288:618
- Gerssen J, Kuijken KH, Merrifield MR. 2000. *MNRAS* 317:545
- Gilmore G. 1995. *IAU Symp.* 164:99
- Gilmore G, King IR, van der Kruit PC. 1990. *The Milky Way as a Galaxy*, ed. R Buser, I King. Mill Valley, CA: Univ. Sci. Books
- Gilmore G, Reid IN. 1983. *MNRAS* 202:1025
- Gilmore G, Wyse RFG, Jones JB. 1995. *Astron. J.* 109:1095
- Gilmore G, Wyse RFG, Kuijken KH. 1989. *Annu. Rev. Astron. Astrophys.* 27:555
- Gogarten SM, Dalcanton JJ, Williams BF, Roškar R, Holtzman J, et al. 2010. *Ap. J.* 712:858
- Gogarten SM, Dalcanton JJ, Williams BF, Seth AC, Dolphin A, et al. 2009. *Ap. J.* 691:115
- Gomez AE, Delhaye J, Grenier S, Jaschek C, Arenou F, Jaschek M. 1990. *Astron. Astrophys.* 236:95
- Graham AW, de Blok WJG. 2001. *Ap. J.* 556:177
- Gunn JE. 1982. In *Astrophysical Cosmology*, ed. HA Brück, GV Coyne, MS Longair, p. 233. Vatican: Pont. Acad. Sci.
- Gunn JE. 1987. *IAU Symp.* 117:537
- Gunn JE, Gott JR. 1972. *Ap. J.* 176:1
- Gurovich S, Freeman KC, Jerjen H, Staveley-Smith L, Puerari I. 2010. *Astron. J.* 140:663
- Hammer F, Flores H, Elbaz D, Zheng XZ, Liang YC, Cesarsky C. 2005. *Astron. Astrophys.* 430:115
- Hammer F, Flores H, Puech M, Yang YB, Athanassoula E, et al. 2009. *Astron. Astrophys.* 507:1313
- Hammer F, Puech M, Chemin L, Flores H, Lehnert MD. 2007. *Ap. J.* 662:322
- Hänninen J, Flynn C. 2000. *MNRAS* 337:731
- Hänninen J, Flynn C. 2002. *Astron. Astrophys.* 421:1001
- Hawaiian Starlight. 1999. *Exploring the Universe from Mauna Kea*. <http://www.cfht.hawaii.edu/HawaiianStarlight/Posters/NGC891-CFHT-Cuillandre-Coelum-1999.jpg>
- Hayes MP, van Zee L, Hogg DE, Roberts MS, Maddalena RJ. 1998. *Astron. J.* 115:62
- Heald GH, Rand RJ, Benjamin RA, Bershady MA. 2007. *Ap. J.* 663:933
- Heavens A, Panter B, Jimenez R, Dunlop J. 2004. *Nature* 428:625
- Helmi A. 2004. *MNRAS* 351:643
- Helmi A. 2008. *Astron. Astrophys. Rev.* 15:145
- Herrmann KA, Ciardullo R. 2009a. *Ap. J.* 703:894
- Herrmann KA, Ciardullo R. 2009b. *Ap. J.* 705:1686
- Herrmann KA, Ciardullo R, Feldmeier JJ, Vinciguerra M. 2008. *Ap. J.* 683:630
- Herschel W. 1785. *Philos. Trans.* 75:213
- Hohl F. 1971. *Ap. J.* 168:343
- Holmberg EB. 1937. *Ann. Obs. Lund*, No. 6
- Holmberg EB. 1958. *Medd. Lunds Astron. Obs.* II, No. 136
- Hubble EP. 1936. *The Realm of the Nebulae*. New Haven, CT: Yale Univ. Press
- Humason ML, Mayall NU, Sandage AR. 1956. *Astron. J.* 61:97
- Ibata R, Mouhcine M, Rejkuba M. 2009. *MNRAS* 395:126
- Ida S, Kokuba E, Makino J. 1993. *MNRAS* 263:875
- Illingworth G, Schechter PL. 1982. *Ap. J.* 256:481
- Jenkins A. 1992. *MNRAS* 257:620
- Jenkins A, Binney JJ. 1990. *MNRAS* 245:305

- Jiang I-G, Binney JJ. 1999. *MNRAS* 303:L7
- Kalberla PMW, Dedes L, Kerp J, Huad U. 2007. *Astron. Astrophys.* 469:11
- Kalberla PMW, Kerp J. 2009. *Annu. Rev. Astron. Astrophys.* 47:27
- Kalnajs AJ. 1987. *IAU Symp.* 117:289
- Kamphuis JJ, Briggs FH. 1996. *Astron. Astrophys.* 253:335
- Kamphuis JJ, Sancisi R, van der Hulst JM. 1991. *Astron. Astrophys.* 244:L29
- Kamphuis JJ, Sijbring D, van Albada TS. 1996. *Astron. Astrophys.* 116:15
- Kamphuis P, Holwerda BW, Allen RJ, Peletier RF, van der Kruit PC. 2007a. *Astron. Astrophys.* 471:L1
- Kamphuis P, Peletier RF, Dettmar R-J, van der Hulst JM, van der Kruit PC, Allen RJ. 2007b. *Astron. Astrophys.* 468:951
- Kapteyn JC. 1909a. *Ap. J.* 29:46
- Kapteyn JC. 1909b. *Ap. J.* 30:284. Erratum. 1909. *Ap. J.* 30:398
- Kapteyn JC. 1914. *Ap. J.* 40:187
- Kapteyn JC. 1922. *Ap. J.* 55:302
- Kapteyn JC, van Rhijn PJ. 1920. *Ap. J.* 52:23
- Karachentsev ID, Karachentseva VE, Parnovskij SL. 1993. *Astron. Nachr.* 314:97
- Kauffmann G, Heckman TM, White SDM, Charlot S, Tremonti C, et al. 2003a. *MNRAS* 341:33
- Kauffmann G, Heckman TM, White SDM, Charlot S, Tremonti C, et al. 2003b. *MNRAS* 341:54
- Kautsch SJ. 2009. *Publ. Astron. Soc. Pac.* 121:1297
- Kennicutt RC. 1983. *Ap. J.* 272:54
- Kennicutt RC. 1989. *Ap. J.* 344:685
- Kennicutt RC. 1998. *Annu. Rev. Astron. Astrophys.* 36:189
- Kennicutt RC, Armus L, Bendo G, Calzetti D, Dale DA, et al. 2003. *Publ. Astron. Soc. Pac.* 115:928
- Kent S. 1987. *Ap. J.* 93:816
- Kereš D, Katz N, Fardal M, Davé R, Weinberg DH. 2009. *MNRAS* 385:160
- Kereš D, Katz N, Weinberg DH, Davé R. 2005. *MNRAS* 363:2
- Kerr FJ. 1957. *Astron. J.* 62:93
- King IR. 1971. *Publ. Astron. Soc. Pac.* 83:377
- Kirby E, Simon JD, Geha M, Guhathakurta P, Frebel A. 2008. *Ap. J.* 685:L43
- Knapen JH, van der Kruit PC. 1991. *Astron. Astrophys.* 248:57
- Knox RA, Hawkins MRS, Hambly NC. 1999. *MNRAS* 306:736
- Kormendy J. 1977. *Ap. J.* 217:406
- Kormendy J. 1984a. *Ap. J.* 286:116
- Kormendy J. 1984b. *Ap. J.* 286:132
- Kormendy J. 1985. *Ap. J.* 295:73
- Kormendy J. 2007. *IAU Symp.* 245:107
- Kormendy J, Drory N, Bender R, Cornell ME. 2010. *Ap. J.* 723:54
- Kormendy J, Freeman KC. 2004. In *IAU Symp. 220: Dark Matter in Galaxies*, p. 377
- Kormendy J, Kennicutt RC. 2004. *Annu. Rev. Astron. Astrophys.* 42:603
- Kormendy J, McClure RD. 1993. *Astron. J.* 105:1793
- Kormendy J, Norman CA. 1979. *Ap. J.* 233:539
- Kormendy J, Richstone D. 1992. *Ap. J.* 393:559
- Kormendy J, Richstone D. 1995. *Annu. Rev. Astron. Astrophys.* 33:581
- Kregel M, Sancisi R. 2001. *Astron. Astrophys.* 376:59
- Kregel M, van der Kruit PC. 2004a. *MNRAS* 352:787
- Kregel M, van der Kruit PC. 2004b. *MNRAS* 355:143
- Kregel M, van der Kruit PC. 2005. *MNRAS* 358:481
- Kregel M, van der Kruit PC, de Blok WJG. 2004. *MNRAS* 352:768
- Kregel M, van der Kruit PC, de Grijs R. 2002. *MNRAS* 334:646
- Kregel M, van der Kruit PC, Freeman KC. 2004. *MNRAS* 351:1247
- Kregel M, van der Kruit PC, Freeman KC. 2005. *MNRAS* 358:503
- Kriek M, van Dokkum PG, Franx M, Illingworth GD, Magee DK. 2009. *Ap. J.* 705:L71
- Kroupa P. 2001. *MNRAS* 322:231

- Kroupa P. 2002a. *Science* 295:82
- Kroupa P. 2002b. *MNRAS* 330:707
- Kylafis N, Bahcall JN. 1987. *Ap. J.* 317:637
- Labbé I, Rudnick G, Franx M, Daddi E, van Dokkum PG, et al. 2003. *Ap. J.* 591:95
- Lacey CG. 1984. *MNRAS* 208:687
- Larson RB. 1974. *MNRAS* 169:229
- Larson RB. 1976. *MNRAS* 176:31
- Larson RB, Tinsley BM. 1978. *Ap. J.* 219:46
- Larson RB, Tinsley BM, Caldwell CN. 1980. *Ap. J.* 237:692
- Lequeux J, Peimbert M, Rayo JF, Serrano A, Torres-Peimbert S, et al. 1979. *Astron. Astrophys.* 80:155
- Lewis JR, Freeman KC. 1989. *Astron. J.* 97:139
- Lotz J, Davis M, Faber SM, Guhathakurta P, Gwyn S, et al. 2008. *Ap. J.* 672:177
- Luck RE, Kovtyukh VV, Andrievsky SM. 2006. *Astron. J.* 132:902
- Magrini L, Corbelli E, Galli D. 2007. *Astron. Astrophys.* 470:843
- Maller AH, Bullock JS. 2004. *MNRAS* 355:694
- Marinacci F, Binney JJ, Fraternali F, Nipoti C, Ciotti L, et al. 2010. *MNRAS* 404:1464
- Martin DC, Fanson J, Schiminovich D, Morrissey P, Friedman PG, et al. 2008. *Ap. J.* 619:L1
- Martínez-Delgado D, Gabany RJ, Peñarrubia RJ, Rix H-W, Majewski SR, et al. 2009. *Highlights of Spanish Astronomy, Astrophys. Space Sci. Proc.*, p. 163
- Martínez-Delgado D, Peñarrubia RJ, Ganaby RJ, Trujillo I, Majewski SR, Pohlen M. 2008. *Ap. J.* 689:184
- Mathewson DS, Ford VL, Buchhorn M. 1992. *Ap. J. Suppl.* 81:413
- Matthews LD. 2000. *Astron. J.* 120:1764
- Matthews LD, Gallagher JS, van Driel W. 1999. *Astron. J.* 118:2751
- Matthews LD, Uson JM. 2008a. *Astron. J.* 135:291
- Matthews LD, Uson JM. 2008b. *Ap. J.* 688:237
- Matthews LD, van Driel W, Gallagher JS. 1998. *Astron. J.* 116:1169
- Matthews LD, Wood K. 2003. *Ap. J.* 593:721
- McConnachie AW, Irwin MJ, Ibata RA, Dubinski J, Widrow LM, et al. 2009. *Nature* 461:66
- McGaugh SS. 2005. *Ap. J.* 632:859
- McGaugh SS. 2009. In *Unveiling the Mass*. http://www.astro.queensu.ca/GalaxyMasses09/data/McGaugh_GMassas09.pdf
- McGaugh SS, Schombert JM, Bothun GD, de Blok WJG. 2000. *Ap. J.* 533:L99
- McWilliam A. 1990. *Ap. J. Suppl.* 74:1075
- McWilliam A. 1997. *Annu. Rev. Astron. Astrophys.* 35:503
- Meléndez J, Asplund M, Alves-Brito A, Cunha K, Barbuy B, et al. 2008. *Astron. Astrophys.* 484:L21
- Mestel L. 1963. *MNRAS* 126:553
- Meusinger H, Reimann H-G, Stecklum B. 1991. *Astron. Astrophys.* 245:57
- Meyer MJ, Zwaan MA, Webster RL, Staveley-Smith L, Ryan-Weber E, et al. 2004. *MNRAS* 350:1195
- Michard R. 2007. *Astron. Astrophys.* 464:507
- Mignard F. 2000. *Astron. Astrophys.* 354:522
- Mihos JC, McGaugh SS, de Blok WJG. 1997. *Ap. J.* 477:79
- Miller RH, Prendergast KH. 1968. *Ap. J.* 153:35
- Miller RH, Prendergast KH, Quirk WJ. 1970. *Ap. J.* 161:903
- Minchev I, Quillen AC. 2006. *MNRAS* 368:623
- Minkowski R. 1960. *Ann. Astrophys.* 23:385
- Mo H, Mao S, White SDM. 1998. *MNRAS* 295:319
- Morrison HL, Boroson TA, Harding P. 1994. *Astron. J.* 108:1191
- Mould JR. 1984. *Publ. Astron. Soc. Pac.* 96:773
- Navarro JF, Frenk CS, White SDM. 1996. *Ap. J.* 462:563
- Navarro JF, Frenk CS, White SDM. 1997. *Ap. J.* 490:493
- Noeske KG, Faber SM, Weiner BJ, Koo DC, Primack JR, et al. 2007a. *Ap. J.* 660:L47
- Noeske KG, Weiner BJ, Faber SM, Papovich C, Koo DC, et al. 2007b. *Ap. J.* 660:L43
- Noordermeer E, Merrifield MR, Coccato L, Arnaboldi M, Capaccioli M, et al. 2008. *MNRAS* 384:943

- Noordermeer E, Sparke LS, Levine SE. 2001. *MNRAS* 328:1064
- Noordermeer E, van der Hulst JM, Sancisi R, Swaters RA, van Albada TS. 2005. *Astron. Astrophys.* 442:137
- Noordermeer E, van der Hulst JM, Sancisi R, Swaters RA, van Albada TS. 2007. *MNRAS* 376:1513
- Nordström B, Mayor M, Andersen J, Holmberg J, Pont F, et al. 2004. *Astron. Astrophys.* 418:989
- Norris MA, Sharples RM, Kuntscher H. 2006. *MNRAS* 367:815
- O'Brien JC, Freeman KC, van der Kruit PC. 2010a. *Astron. Astrophys.* 515:A61
- O'Brien JC, Freeman KC, van der Kruit PC. 2010b. *Astron. Astrophys.* 515:A62
- O'Brien JC, Freeman KC, van der Kruit PC. 2010c. *Astron. Astrophys.* 515:A63
- O'Brien JC, Freeman KC, van der Kruit PC, Bosma A. 2010. *Astron. Astrophys.* 515:A60
- O'Connell DJK, ed. 1958. *Stellar Populations*. Vatican City: Vatican Obs.
- Oemler A. 1974. *Ap. J.* 194:1
- Olling RP. 1995. *Astron. J.* 110:591
- Olling RP. 1996a. *Astron. J.* 112:481
- Olling RP. 1996b. *Astron. J.* 112:457
- Oort JH. 1932. *Bull. Astron. Inst. Neth.* 6:249
- Oort JH. 1940. *Ap. J.* 91:273
- Oort JH. 1965. In *Stars and Stellar Systems*, Vol. 5, ed. A Blaauw, M Schmidt, ch, 21, p. 455. Chicago: Univ. Chicago Press
- Oort JH. 1977. *Annu. Rev. Astron. Astrophys.* 15:259
- Oort JH. 1981. *Annu. Rev. Astron. Astrophys.* 19:1
- Oort JH. 1983. *Annu. Rev. Astron. Astrophys.* 21:373
- Oosterloo T, Fraternali F, Sancisi R. 2007. *Astron. J.* 134:1019
- Ostriker JP, Peebles PJE. 1973. *Ap. J.* 186:467
- Pacholka W. 2009. APOD (27-Jan-2009). antwrp.gsfc.nasa.gov/apod/ap090127.html
- Pastorini G, Marconi A, Capetti A, Axon DJ, Alonso-Herrero A, et al. 2007. *Astron. Astrophys.* 469:405
- Patterson FS. 1940. *Harvard Bull.* 914:9
- Pease FG. 1914. *Proc. Natl. Acad. Sci. USA* 2:517
- Peebles PJE. 1971. *Astron. Astrophys.* 11:377
- Peek JEG, Putman ME, Sommer-Larsen J. 2008. *Ap. J.* 674:227
- Peletier RF, de Grijs R. 1998. *MNRAS* 300:L3
- Pérez I, Fux R, Freeman KC. 2004. *Astron. Astrophys.* 424:799
- Pohlen M, Balcells M, Lüticke R, Dettmar R-J. 2003. *Astron. Astrophys.* 409:485
- Pohlen M, Dettmar R-J, Lüticke R, Aronica G. 2002. *Astron. Astrophys.* 392:807
- Pohlen M, Trujillo I. 2006. *Astron. Astrophys.* 454:759
- Pohlen M, Zaroubi S, Peletier RF, Dettmar R-J. 2007. *MNRAS* 378:594
- Quilis V, Moore B, Bower R. 2000. *Science* 288:1617
- Quinn P, Goodman J. 1986. *Ap. J.* 309:472
- Rees M, Ostriker J. 1977. *MNRAS* 179:541
- Reid M, Menten KM, Zheng XW, Brunthaler A, Moscadelli L, et al. 2009. *Ap. J.* 700:137
- Reshetnikov V, Battaner E, Combes F, Jiménez-Vicente J. 2002. *Astron. Astrophys.* 382:513
- Reylé C, Marshall DJ, Robin AC, Schulteis M. 2009. *Astron. Astrophys.* 495:819
- Reynolds RH. 1913. *MNRAS* 74:132
- Rix H-W, Zaritsky D. 1995. *Ap. J.* 447:82
- Roberts MS. 2008. In *Frontiers of Astrophysics, ASP Conf. Ser.* 395, p. 283
- Roberts MS, Hayes MP. 1994. *Annu. Rev. Astron. Astrophys.* 32:115
- Roberts MS, Whitehurst RN. 1975. *Ap. J.* 201:327
- Robin AC, Crézé M, Mohan V. 1992. *Ap. J.* 400:L25
- Rocha-Pinto HJ, Scalo J, Maciel WJ, Flynn C. 2000. *Ap. J.* 531:L115
- Rogstad DH, Lockart IA, Wright MCH. 1974. *Ap. J.* 193:309
- Rogstad DH, Shostak SS. 1971. *Astron. Astrophys.* 176:315
- Rosales-Ortega FF, Kennicutt RC, Sánchez SF, Díaz AI, Pasquali A, et al. 2010. *MNRAS* 405:735
- Roškar R, Debattista VP, Brooks AM, Quinn TR, Brook CB, et al. 2010. *MNRAS* 408:783
- Roškar R, Debattista VP, Quinn TR, Stinton GS, Wadsley J. 2008a. *Ap. J.* 684:L79

- Roškar R, Debattista VP, Stinton GS, Quinn TR, Kaufmann T, Wadsley J. 2008b. *Ap. J.* 675:L65
- Rossa J, van der Marel RP, Böker T, Gerssen J, Ho LC, et al. 2006. *Astron. J.* 132:1074
- Rubin VC, Burstein D, Ford WK, Thonnard N. 1985. *Ap. J.* 289:81
- Rubin VC, Peterson CJ, Ford WK. 1980. *Ap. J.* 239:50
- Ruphy S, Robin AC, Epcrtein N, Copet E, Bertin E, et al. 1996. *Astron. Astrophys.* 313:L21
- Ryden BS, Gunn JE. 1987. *Ap. J.* 318:15
- Sackett PD. 1997. *Ap. J.* 483:103
- Sackett PD. 1999. In *Galaxy Dynamics, ASP Conf. Ser.* 182, p. 393
- Sackett PD, Rix H-W, Jarvis BJ, Freeman KC. 1994. *Ap. J.* 436:629
- Saha K, de Jong RS, Holwerda BW. 2009. *MNRAS* 396:409
- Sakai S, Mould JR, Hughes SMG, Huchra JP, Macri LM, et al. 2000. *Ap. J.* 529:698
- Sales LV, Helmi A, Abadi MG, Brook CB, Gómez FA, et al. 2009. *MNRAS* 400:L61
- Salpeter EE. 1959. *Ap. J.* 129:608
- Samland M, Gerhard O. 2003. *Astron. Astrophys.* 399:961
- Sanchez-Saavedra ML, Battaner E, Florido E. 1990. *Ap. Space Sci.* 171:239
- Sancisi R. 1976. *Astron. Astrophys.* 53:159
- Sancisi R. 1983. In *Internal Kinematics and Dynamics of Galaxies, IAU Symp.* 100, p. 55
- Sancisi R, Allen RJ. 1979. *Astron. Astrophys.* 64:73
- Sandage AR. 1961. *The Hubble Atlas of Galaxies*. Washington: Carnegie Inst.
- Sandage AR. 1986. *Annu. Rev. Astron. Astrophys.* 24:421
- Sandage AR. 2005. *Annu. Rev. Astron. Astrophys.* 43:581
- Sandage AR, Eggen OJ. 1969. *Ap. J.* 158:669
- Sandage AR, Freeman KC, Stokes NR. 1970. *Ap. J.* 160:831
- Sandage AR, Lubin LM, VandenBerg DA. 2003. *Publ. Astron. Soc. Pac.* 115:1187
- Sanders RH, McGaugh SS. 2002. *Annu. Rev. Astron. Astrophys.* 40:263
- Satyapal S, Böker T, Mcalpine W, Gliozzi M, Abel NP, et al. 2009. *Ap. J.* 704:439
- Schaye J. 2004. *Ap. J.* 609:667
- Schmidt M. 1959. *Ap. J.* 129:243
- Schmidt M. 1963. *Ap. J.* 137:758
- Schombert JM, Bothun GD. 1987. *Astron. J.* 93:60
- Schönrich R, Binney JJ. 2009a. *MNRAS* 396:203
- Schönrich R, Binney JJ. 2009b. *MNRAS* 399:1145
- Schwarzkopf U, Dettmar R-J. 2001. *Astron. Astrophys.* 373:402
- Schweizer F. 1986. *Science* 231:227
- Searle L. 1973. *Ap. J.* 168:327
- Searle L, Sargent WLW. 1972. *Ap. J.* 173:25
- Searle L, Sargent WLW, Bagnuolo WG. 1973. *Ap. J.* 179:427
- Searle L, Zinn R. 1978. *Ap. J.* 225:357
- Sellwood JA. 2008. In *Formation and Evolution of Galaxy Disks, ASP Conf. Ser.* 396, p. 241
- Sellwood JA. 2011a. In *Planets, Stars and Stellar Systems 5*. In press (arXiv:1006.4855)
- Sellwood JA. 2011b. In *Evolution of Planetary and Stellar Systems*. In press (arXiv:1001.5430)
- Sellwood JA, Binney J. 2002. *MNRAS* 336:785
- Sellwood JA, Carlberg RG. 1984. *Ap. J.* 282:61
- Sérsic JL. 1963. *Bol. Asoc. Argent. Astron.* 6:41
- Seth AC, Dalcanton JJ, de Jong RS. 2005. *Astron. J.* 130:1575
- Shaver PA, McGee RX, Newton LM, Danks AC, Pottasch SR. 1983. *MNRAS* 204:53
- Shen J, Sellwood JA. 2006. *MNRAS* 370:2
- Sheth K, Elmegreen DM, Elmegreen BG, Capak P, Abraham RG, et al. 2008. *Ap. J.* 675:1141
- Sheth K, Regan M, Hinz JL, Gil de Paz A, Menéndez-Delmestre K, et al. 2010. *Publ. Astron. Soc. Pac.* 122:1397
- Shostak GS, van der Kruit PC. 1984. *Astron. Astrophys.* 132:20
- Sicking FJ. 1997. *The thickness of the HI layer in spiral galaxies*. PhD thesis. Univ. Groningen.
<http://dissertations.ub.rug.nl/faculties/science/1997/f.j.sicking/>
- Silva DR, Boroson TA, Thompson IB, Jedrzejewski RI. 1989. *Astron. J.* 98:131

- Skrutskie MF, Cutri RM, Stiening R, Weinberg MD, Schneider S, et al. 2006. *Astron. J.* 131:1163
- Sofue Y. 1986. *Ap. J.* 458:120
- Sofue Y, Rubin VC. 2001. *Annu. Rev. Astron. Astrophys.* 39:137
- Soifer BT, Helou G, Werner M. 2008. *Annu. Rev. Astron. Astrophys.* 46:201
- Sommer-Larsen J, Gelato S, Vedel H. 1999. *Ap. J.* 519:501
- Sommer-Larsen J, Götz M, Portinari L. 2003. *Ap. J.* 596:47
- Soubiran C, Bienaymé O, Mishenina TV, Kovtyukh VV. 2008. *Astron. Astrophys.* 480:91
- Sparke LS, van Moorsel G, Schwarz UJ, Vogelaar M. 2009. *Astron. J.* 137:3976
- Spitzer L, Baade W. 1951. *Ap. J.* 113:413
- Spitzer L, Schwarzschild M. 1951. *Ap. J.* 114:385
- Sprayberry D, Bernstein GM, Impey CD, Bothun GD. 1995. *Ap. J.* 438:72
- Stark DV, McGaugh SS, Swaters RA. 2009. *Astron. J.* 138:392
- Strom KM, Strom SE, Jensen EB, Moller J, Thompson LA, Thuan TX. 1977. *Ap. J.* 212:335
- Strom KM, Strom SE, Wells DC, Romanishin W. 1978. *Ap. J.* 220:62
- Swaters RA. 1999. *Dark matter in late-type dwarf galaxies*. PhD thesis. Univ. Groningen. <http://dissertations.ub.rug.nl/faculties/science/1999/r.a.swaters/>
- Swaters RA, Balcells M. 2002. *Astron. Astrophys.* 390:863
- Swaters RA, Schoenmaker RHM, Sancisi R, van Albada TS. 1999. *MNRAS* 304:330
- Swaters RA, van Albada TS, van der Hulst JM, Sancisi R. 2002. *Astron. Astrophys.* 390:829
- Takamiya T, Sofue Y. 2002. *Ap. J.* 576:L15
- Tamburro D, Rix H-W, Leroy AK, Mac Low M-M, Walter F, et al. 2009. *Astron. J.* 137:4424
- Tassis K, Kravtsov AV, Gnedin NY. 2008. *Ap. J.* 682:888
- Tinsley BM. 1980. *Fundam. Cosmic Phys.* 5:287
- Tinsley BM, Larson RB, eds. 1977. *Evolution of Galaxies and Stellar Populations*. New Haven, CT: Yale Univ. Press
- Toomre A. 1964. *Ap. J.* 13:1217
- Toomre A. 1977. *Annu. Rev. Astron. Astrophys.* 15:437
- Toomre A. 1981. In *The Structure and Evolution of Normal Galaxies*, ed. SM Fall, D Lynden-Bell, p. 111. Cambridge, UK: Cambridge Univ. Press
- Toomre A, Toomre J. 1972. *Ap. J.* 178:623
- Toth G, Ostriker JP. 1992. *Ap. J.* 389:5
- Trachernach C, de Blok WJG, McGaugh SS, van der Hulst JM, Dettmar RJ. 2009. *Astron. Astrophys.* 505:577
- Tremonti CA, Heckman TM, Kauffmann G, Brinchmann J, Charlot S, et al. 2004. *Ap. J.* 613:898
- Trujillo I, Förster Schreiber NM, Rudnick G, Barden M, Franx M, et al. 2006. *Ap. J.* 650:18
- Trujillo I, Martínez-Valpuesta I, Martínez-Delgado D, Peñarrubia J, Gabany RJ, Pohlen M. 2009. *Ap. J.* 704:618
- Tsikoudi V. 1979. *Ap. J.* 234:842
- Tsikoudi V. 1980. *Ap. J. Suppl.* 43:356
- Tully B, Fisher R. 1977. *Astron. Astrophys.* 54:661
- Uson JM, Matthews LD. 2003. *Astron. J.* 125:2455
- van Albada TS, Bahcall JN, Begeman K, Sancisi R. 1985. *Ap. J.* 295:305
- van Albada TS, Sancisi R. 1986. *Philos. Trans. Ser. A* 320:447
- van de Hulst HC, Raimond E, van Woerden H. 1957. *Bull. Astron. Inst. Neth.* 14:1
- van der Hulst JM. 2002. In *Seeing through the Dust: The Detection of HI and the Exploration of the ISM in Galaxies*, *ASP Conf. Ser.* 276, p. 84
- van der Hulst JM, van Albada TS, Sancisi R. 2001. In *Gas and Galaxy Evolution*, *ASP Conf. Ser.* 240, p. 451
- van der Kruit PC. 1976. *Astron. Astrophys.* 49:161
- van der Kruit PC. 1979. *Astron. Astrophys. Suppl.* 38:15
- van der Kruit PC. 1981. *Astron. Astrophys.* 99:298
- van der Kruit PC. 1984. *Astron. Astrophys.* 140:470
- van der Kruit PC. 1986. *Astron. Astrophys.* 157:230
- van der Kruit PC. 1987. *Astron. Astrophys.* 173:59
- van der Kruit PC. 1988. *Astron. Astrophys.* 192:117

- van der Kruit PC. 2001. In *Galaxy Disks and Disk Galaxies*, *ASP Conf. Ser.* 230, p. 119
- van der Kruit PC. 2002. In *The Dynamics, Structure & History of Galaxies*, *ASP Conf. Ser.* 273, p. 7
- van der Kruit PC. 2007. *Astron. Astrophys.* 466:883
- van der Kruit PC. 2008. In *Formation and Evolution of Galaxy Disks*, *ASP Conf. Ser.* 396, p. 173
- van der Kruit PC. 2009. In *Unveiling the Mass*. http://www.astro.queensu.ca/GalaxyMasses09/data/vanderKruit_GMasses09.pdf
- van der Kruit PC, Allen RJ. 1976. *Annu. Rev. Astron. Astrophys.* 14:417
- van der Kruit PC, Allen RJ. 1978. *Annu. Rev. Astron. Astrophys.* 16:103
- van der Kruit PC, de Grijs R. 1999. *Astron. Astrophys.* 352:129
- van der Kruit PC, Freeman KC. 1984. *Ap. J.* 278:81
- van der Kruit PC, Freeman KC. 1986. *Ap. J.* 303:556
- van der Kruit PC, Gilmore G, eds. 1995. *Stellar Populations: IAU Symp.* 164. Dordrecht: Kluwer
- van der Kruit PC, Jiménez-Vicente J, Kregel M, Freeman KC. 2001. *Astron. Astrophys.* 379:374
- van der Kruit PC, Searle L. 1981a. *Astron. Astrophys.* 95:105
- van der Kruit PC, Searle L. 1981b. *Astron. Astrophys.* 95:116
- van der Kruit PC, Searle L. 1982a. *Astron. Astrophys.* 110:61
- van der Kruit PC, Searle L. 1982b. *Astron. Astrophys.* 110:79
- van der Kruit PC, Shostak GS. 1982. *Astron. Astrophys.* 105:351
- van der Kruit PC, Shostak GS. 1984. *Astron. Astrophys.* 134:258
- van der Kruit PC, van Berkel K. 2000. *Astrophys. Space Sci. Libr.*, vol. 246. Dordrecht: Kluwer
- van Woerden H. 1967. In *IAU Symp. 31: Radio Astronomy and the Galactic System*, p. 3
- Velázquez H, White SDM. 1999. *MNRAS* 304:25
- Veltz L, Bienaymé O, Freeman KC, Binney JJ, Bland-Hawthorn J, et al. 2008. *Astron. Astrophys.* 480:753
- Verheijen MAW. 2001. *Astron. J.* 563:694
- Verheijen MAW, Bershady MA, Swaters RA, Andersen DR, Westfall KB. 2007. See de Jong 2007, p. 95
- Verheijen MAW, Sancisi R. 2001. *Astron. Astrophys.* 370:765
- Villumsen JB. 1985. *Ap. J.* 290:75
- Vlajić M, Bland-Hawthorn J, Freeman KC. 2009. *Ap. J.* 697:361
- Wainscoat RJ, Hyland AR, Freeman KC. 1989. *Ap. J.* 337:163
- Wainscoat RJ, Hyland AR, Freeman KC. 1990. *Ap. J.* 348:85
- Walcher CJ, Böker T, Charlot S, Ho LC, Rix H-W, et al. 2006. *Ap. J.* 649:692
- Walcher CJ, van der Marel RP, McLaughlin D, Rix H-W, Böker T, et al. 2005. *Ap. J.* 618:237
- Walker IR, Mihos JC, Hernquist L. 1996. *Ap. J.* 460:121
- Walter F, Brinks E, de Blok WJG, Bigiel F, Kennicutt RC, et al. 2008. *Astron. J.* 136:2563
- Weiner BJ, Sellwood JA, Williams TB. 2001. *Ap. J.* 546:931
- Westfall KB, Bershady MA, Verheijen MAW, Andersen DR, Swaters RA. 2008. In *Formation and Evolution of Galaxy Disks*, *ASP Conf. Ser.* 396, p. 41
- Wevers BMHR. 1984. *A study of spiral galaxies*. PhD thesis. Univ. Groningen
- Wevers BMHR, van der Kruit PC, Allen RJ. 1986. *Astron. Astrophys. Suppl.* 66:505
- White S, Rees M. 1978. *MNRAS* 183:341
- Wielen R. 1977. *Astron. Astrophys.* 60:262
- Williams BF, Dalcanton JJ, Dolphin AE, Holtzman J, Sarajedini A. 2009a. *Ap. J.* 695:L15
- Williams BF, Dalcanton JJ, Seth AC, Weisz D, Dolphin A, et al. 2009b. *Ap. J.* 137:419
- Williams BF, Dalcanton JJ, Stilp A, Gilbert KM, Roškar R, et al. 2010. *Ap. J.* 709:135
- Williams RE, Baum S, Bergeron LE, Bernstein N, Blacker BS, et al. 2000. *Astron. J.* 120:2735
- Williams RE, Blacker B, Dickinson M, van Dyke Dixon W, Ferguson HC, et al. 1996. *Ap. J.* 112:1335
- Williams TB. 1975. *Ap. J.* 199:586
- Woolley R, Martin WL, Penston MJ, Sinclair JE, Aslon S. 1977. *MNRAS* 179:81
- Worthey G, España AL, MacArthur LA, Courteau S. 2005. *Ap. J.* 631:820
- Wyder TK, Martin DC, Barlow TA, Foster K, Friedman PG, et al. 2009. *Ap. J.* 696:1834
- Yegorova I, Salucci P. 2007. *MNRAS* 377:507
- Yin J, Hou JL, Prantzos N, Boissier S, Chang RX, et al. 2009. *Astron. Astrophys.* 505:497
- Yoachim P, Dalcanton JJ. 2006. *Astron. J.* 131:226
- Yoachim P, Dalcanton JJ. 2008. *Ap. J.* 682:1004

- Yoachim P, Roškar R, Debattista VP. 2010. *Ap. J.* 716:L4
- York DG, Adelman J, Anderson JE, Anderson SF, Annis J, et al. 2000. *Astron. J.* 120:1579
- Zaritsky D, Kennicutt RC, Huchra JP. 1994. *Ap. J.* 420:87
- Zaritsky D, Rix H-W. 1997. *Ap. J.* 477:118
- Zwaan MA, van der Hulst JM, de Blok WJG, McGaugh SS. 1995. *MNRAS* 273:L35

Contents

An Interesting Voyage <i>Vera C. Rubin</i>	1
Laboratory Astrochemistry: Gas-Phase Processes <i>Ian W.M. Smith</i>	29
Protoplanetary Disks and Their Evolution <i>Jonathan P. Williams and Lucas A. Cieza</i>	67
The Astrophysics of Ultrahigh-Energy Cosmic Rays <i>Kumiko Kotera and Angela V. Olinto</i>	119
Dark Matter Searches with Astroparticle Data <i>Troy A. Porter, Robert P. Johnson, and Peter W. Graham</i>	155
Dynamics of Protoplanetary Disks <i>Philip J. Armitage</i>	195
The Interstellar Medium Surrounding the Sun <i>Priscilla C. Frisch, Seth Redfield, and Jonathan D. Slavin</i>	237
Comets as Building Blocks <i>Michael F. A'Hearn</i>	281
Galaxy Disks <i>P.C. van der Kruit and K.C. Freeman</i>	301
The First Galaxies <i>Volker Bromm and Naoki Yoshida</i>	373
Cosmological Parameters from Observations of Galaxy Clusters <i>Steven W. Allen, August E. Evrard, and Adam B. Mantz</i>	409
The Chemical Composition of Comets—Emerging Taxonomies and Natal Heritage <i>Michael J. Mumma and Steven B. Charnley</i>	471
Physical Properties of Galaxies from $z = 2-4$ <i>Alice E. Shapley</i>	525

GALACTIC BULGES

Rosemary F. G. Wyse

Department of Physics and Astronomy, The Johns Hopkins University, Baltimore,
Maryland 21218, USA; e-mail: wyse@pha.jhu.edu

Gerard Gilmore

Institute of Astronomy, Madingley Road, Cambridge CB3 0HA, United Kingdom;
Institut d’Astrophysique de Paris, 98bis boulevard Arago, 75014 Paris, France;
e-mail: gil@ast.cam.ac.uk

Marijn Franx

Kapteyn Astronomical Institute, University of Groningen, PO Box 800, 9700AV
Groningen, The Netherlands; e-mail: franx@astro.rug.nl

KEY WORDS: galaxy formation, the Galaxy, extragalactic astronomy, Local Group, dynamical astronomy

ABSTRACT

We discuss the present observational and theoretical understanding of the stellar populations of bulges and their implications for galaxy formation and evolution. The place of bulges as key to the Hubble Sequence remains secure, but some old paradigms are giving way to new ones as observations develop. Detailed studies of Local Group bulges and haloes provide a basis on which we consider higher redshift data. We present the evidence for and against the currently common preconceptions that bulges are old, above solar metallicity in the mean, and simply scaled-down versions of ellipticals. We conclude life is not so simple: Bulges are diverse and heterogeneous, and although their properties vary systematically, sometimes they are reminiscent of disks, sometimes of ellipticals. The extant observational data are, however, limited. New and future surveys will rectify this, and we discuss the questions those data will address.

1. MOTIVATION AND SCOPE OF REVIEW

1.1 *Introduction*

In his introduction to the report of IAU Symposium #1, *Coordination of Galactic Research*, held near Groningen, June 1953, Blaauw noted, “In the discussion

the terms ‘halo’, ‘nucleus’ and ‘disk’ are used to indicate different parts of the Galaxy. These general regions are not defined more precisely. Their introduction proved very useful, and one might rather say that their more exact description is one of the problems of galactic research.” This statement provides an excellent example of the limitations of terminology and of the term galactic bulge in that this component continues to lack a clear definition (nucleus? halo?) of either its structure or its relationship to the other stellar components of the Galaxy. This is compounded by the difficulty of observing bulges even once one has decided which part of the galaxy that is.

The common usage of “bulge,” for example in the term bulge-to-disk ratio, allocates all “non-disk” light in any galaxy that has a “disk” into the bulge. That is, the bulge contains any light that is in excess of an inward extrapolation of a constant scale-length exponential disk. Sandage (Sandage & Bedke 1994, *Carnegie Atlas of Galaxies*; panel S11 and p. 45) emphasizes that “one of the three classification criteria along the spiral sequence is the size of the central amorphous bulge, compared with the size of the disk. The bulge size, seen best in nearly edge-on galaxies, decreases progressively, while the current star formation rate and the geometrical entropy of the arm pattern increases, from early Sa to Sd, Sm and Im types.” This is the clearest convenient description of a bulge, namely a centrally concentrated stellar distribution with an amorphous—smooth—appearance. Note that this implicitly excludes gas, dust, and continuing recent star formation by definition, ascribing all such phenomena in the central parts of a galaxy to the central disk, not to the bulge with which it cohabits. Furthermore, for a bulge to be identified at all it must, by selection, have a central stellar surface density that is at least comparable to that of the disk, and/or it must have a (vertical) scale height that is at least not very much smaller than that of the disk. The fact that this working definition can be applied successfully to the extensive classifications in the *Carnegie Atlas of Galaxies* illustrates some fundamental correctness. Bulges are also clearly very much a defining component whose properties underly the Hubble sequence, and hence the reason why we care—understanding how bulges form and evolve is integral to the questions of galaxy formation and evolution.

This review considers the current widespread beliefs and preconceptions about galaxian bulges—for example, that they are old, metal-rich, and related to elliptical galaxies—in the light of modern data. Our aim is to provide an overview of interesting and topical questions and to emphasize recent and future observations that pertain to the understanding of the formation and evolutionary status of bulges. We begin by considering some common preconceptions.

1.2 Preconception Number 1: Bulges Are Old

The expectation of “old age” arose, as far as we can ascertain, from the interpretation of the observed correlation between stellar kinematics and metallicity

for local stars in the Milky Way by Eggen et al (1962). These authors proposed a model of Galaxy formation by collapse of a galaxy-sized density perturbation, generalized to models wherein the spheroidal components of galaxies—including the entire stellar mass of an elliptical galaxy—formed stars *prior* to the dissipational settling to a disk and so contained the oldest stars (e.g. review of Gott 1977). The high central surface brightnesses of bulges (and of ellipticals), assuming they correspond to high mass densities, also imply a higher redshift of formation, for a fixed collapse factor of the protogalaxy, because at higher redshift the background density was higher (Peebles 1989).

An older component in the central regions of the Milky Way Galaxy clearly exists. The first real work on the bulge (or “nucleus” as it was called at the time) used classical “halo” tracers, such as globular clusters, RR Lyrae, and planetary nebulae. Of course, one must remember that “older” is used here in the sense that the term was used until very recently, which meant much older than the local disk, which contains ongoing star formation. That is, “old” means “there is no obvious AF star population.” The Baade-era concept of “old” meant a turnoff in the F-region, which is of course old only for a very metal-poor system (see Sandage 1986, and the *Carnegie Atlas* for thorough reviews of Baade’s Population concept). Furthermore, the very idea of discriminating between ages of 10 Gyr and 15 Gyr is a recent concept, in spite of the large fractional difference between the two.

Constraints on the redshift of formation of bulges can be obtained by direct observations of high-redshift galaxies, for which morphological information may be obtained with the Hubble Space Telescope (HST) (see Section 4). In general, disentangling the effects of age and metallicity on stellar colors is difficult, even when the stars are resolved and color-magnitude diagrams may be examined. The state-of-the-art mean age determinations for lower redshift bulges and disks are discussed in Section 3, and the interpretations of color-magnitude diagrams are discussed in Section 2. Much ambiguity and uncertainty remains.

Implicit in the Eggen et al (1962) scenario was the hypothesis that the Galactic bulge was simply the central region of the stellar halo, traced at the solar neighborhood by the high-velocity subdwarfs. These stars are old by anyone’s definition. Stellar haloes can be studied easily only in the Local Group, and we discuss the stellar populations in those galaxies in Section 2 below.

1.3 Preconception Number 2: *The Galactic Bulge Is Super-Solar Metallicity*

This belief was strongly supported by study of late M-giants in Baade’s Window (cf Frogel 1988), motivated by the Whitford (1978) paper that compared the spectrum of the Milky Way bulge to that of the integrated light of the central regions of external bulges and giant elliptical galaxies (see Whitford 1986 for

a personal interpretation of his research). Whitford's investigation aimed to determine whether or not the bulge of our galaxy was "normal," i.e. the same as others. Whitford was apparently influenced, as were most people at that time, by the interpretation of the color-magnitude relation of Faber (1973) to assume that bulges and ellipticals were differentiated only by luminosity, which determined the metallicity, and that ages were invariant and *old*, with a turnoff mass of $\sim 1 M_{\odot}$ (Faber 1973), at least for the dominant population. In this case, the most metal-rich stars in a lower luminosity bulge, like that of the Milky Way, could be used as a template for the *typical* star in a giant elliptical.

Whitford (1978) concluded from his data that indeed "the strengths of the spectral features in the sampled areas of the nuclear bulge of the Galaxy are very close to those expected from measures on similar areas of comparable galaxies." However, Whitford's data were, by current standards, of low spectral resolution and were limited to the following: spectra, with a resolution of 32 Å in the blue and 64 Å in the red, for three regions in Baade's Window and for the central regions of five edge-on spirals of type Sa to Sb; lower spectral resolution data for the central regions of M 31; partial data—blue wavelengths only—for one elliptical (NGC3379, E1); and full wavelength coverage spectra for one other elliptical (NGC4976, E4), which he emphasized did not match the Milky Way and was anomalous. Furthermore, the data for Baade's Window in the blue wavelength region—where direct comparison with a "normal" elliptical galaxy was possible—were emphasized to be very uncertain, owing to the large corrections for reddening and foreground (disk) emission. Thus, while the Whitford paper was deservedly influential in motivating comparison between stars in the Milky Way bulge and the integrated population of external galaxies, its detailed conclusions rest on rather poor foundations.

The results of Rich (1988), based on his low-resolution spectra, that the mean metallicity of K/M giants in Baade's Window was twice the solar value, was very influential and widely accepted; however, it is now apparent that line-blending and elemental abundance variations contributed to a calibration error. We discuss below the current status of the metallicity-luminosity relation for bulges and for ellipticals and the detailed chemical abundance distribution for stars in the bulge of the Milky Way. Although super-metal-rich stars clearly exist in the bulge of the Milky Way, they are a minority, and their relationship to the majority population (are they the same age?) remains unknown.

1.4 Preconception Number 3: Bulges Are Similar to Elliptical Galaxies

Bulges and ellipticals have traditionally been fit by the same surface brightness profiles, the de Vaucouleurs $R^{1/4}$ law; for simplicity, one is tempted to assume that bulges are simply scaled-down ellipticals and that they formed the same

way. N-body simulations (e.g. van Albada 1982), together with analytic considerations of “maximum entropy” end states (Tremaine et al 1986), suggested that this was through violent relaxation of a dissipationless, perhaps lumpy, system. These ideas incorporate the proposition (e.g. Toomre 1977, Barnes & Hernquist 1992) that equal-mass mergers destroy preexisting stellar disks and form bulges and ellipticals, of which these latter two are distinguished only by mass.

Furthermore, the stellar kinematics of ellipticals and bulges of the same luminosity are similar, in that each rotates approximately as rapidly as predicted by isotropic oblate models (Davies et al 1983). However, the two general categories of “bulges” and “ellipticals” are becoming clear to be somewhat heterogeneous and may cover systems that formed in a variety of ways.

The above preconceptions may be tested against modern data. We proceed with the systems for which the most detailed data may be obtained, the galaxies in the Local Group, and then outward in distance.

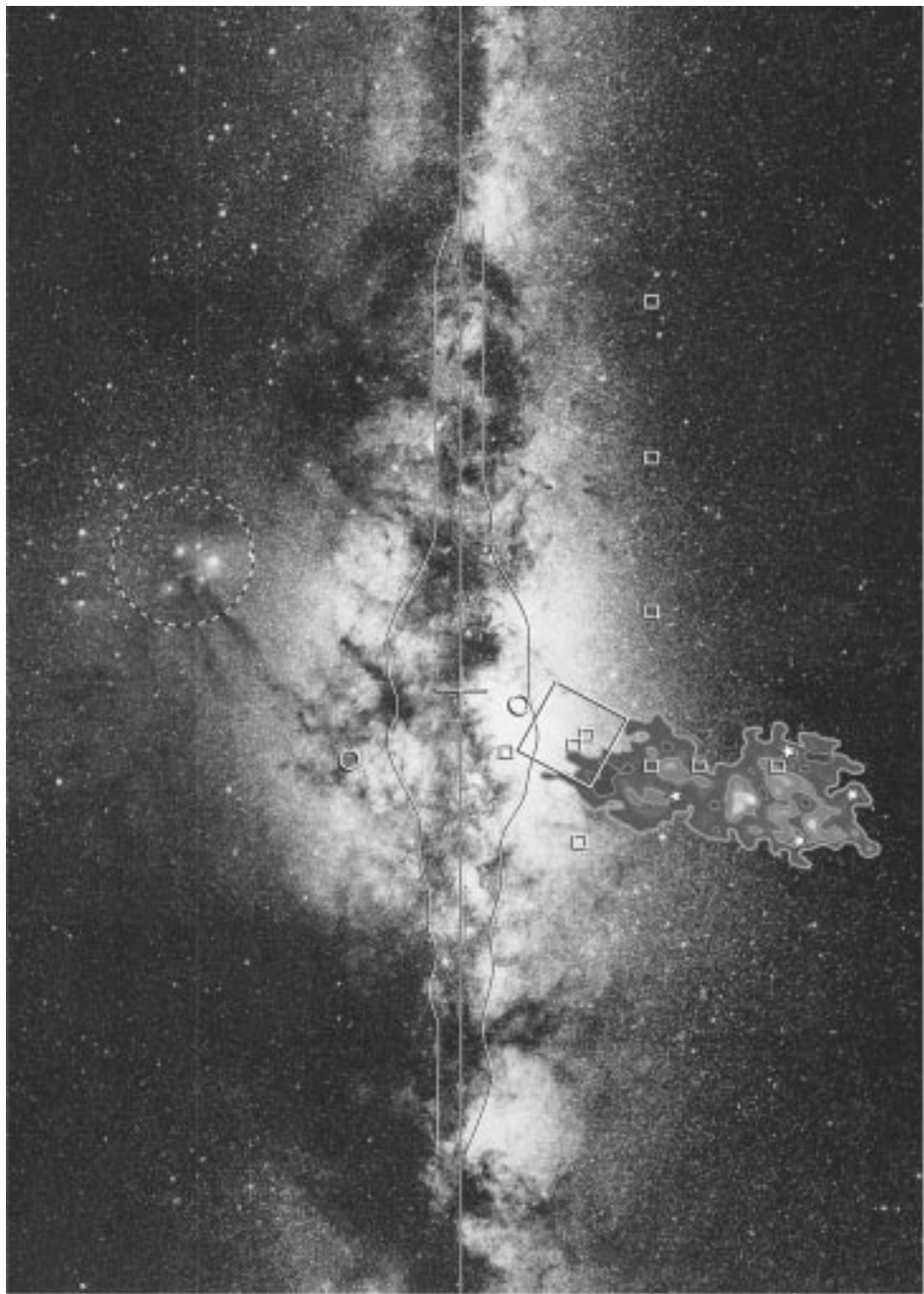
2. RESOLVED BULGES—LOCAL GROUP GALAXIES

The Local Group provides a sample of bulges in which one can determine the stellar distribution functions on a star-by-star basis, which allows a more detailed analysis than is possible based on the integrated properties of more distant bulges/haloes. In this comparison, one must be careful to isolate the essential features because there is much confusing detail, both observational and theoretical, specific to individual galaxies.

Obvious questions that can be addressed most efficiently locally include possible differences, similarities, or smooth(?) gradients in properties—kinematics, chemical abundance distribution, age distribution, scale-lengths, profiles, etc—from inner bulges to outer haloes, and from bulges to inner disks. Different tracers can be used that allow comparisons between, for example, globular clusters and field stars.

2.1 *Milky Way Galaxy*

Let us adopt for the moment the working definition of the bulge as the component constituting the amorphous stellar light in the central regions of the Milky Way. Although one might imagine that the Milky Way bulge can be studied in significantly more detail than is possible in other galaxies, our location in the disk restricts our view such that this is true only several kiloparsecs from the Galactic center. Most of the Galactic bulge is obscured by dust and stars associated with the foreground disk. We illustrate the situation in Figure 1 below.



CHEMICAL ABUNDANCES Chemical abundances of K and M giants in the central regions of the Galaxy have been determined by a variety of techniques, ranging from high-resolution spectra that allow elemental abundance analyses to intermediate-band photometry. Application to Baade's Window—approximately 500-pc projected distance from the Galactic center—determined that the metallicity distribution function (calibrated onto a [Fe/H] scale) of K/M giants is broad, with a maximum at ~ -0.2 dex (i.e. ~ 0.6 of the solar iron abundance) and extending down to at least -1 dex and up to at least $+0.5$ dex (e.g. McWilliam & Rich 1994, Sadler et al 1996). It remains unclear to what extent these upper and lower limits are a true representation of the underlying distribution function and to what extent they are observational bias, set by calibration difficulties and/or sensitivities of the techniques. Furthermore, the identification of foreground disk stars remains difficult.

At larger Galactocentric distances, Ibata & Gilmore (1995a,b) utilized fiber spectroscopy down many lines of sight to mimic “long-slit spectroscopy” of the Galactic bulge, in order to facilitate a direct comparison between the Milky Way bulge and those of external spiral galaxies. They obtained spectra of about 2000 stars; star count models, stellar luminosity classifications, and kinematics were used to isolate about 1500 K/M-giants from 700 pc to 3.5 kpc (projected distance) from the Galactic Center. These authors estimated metallicities from the Mg'b' index, calibrated against local field stars; thus there is a possible zero-point offset of up to ~ 0.3 dex, which is dependent on the element ratios of the Bulge stars compared to the local stars. Ibata & Gilmore truncated their distribution function above the solar value, owing to the great similarity



Figure 1 An optical image of the central Galaxy, adapted from that published by Madsen & Laustsen (1986). The field covered is $70^\circ \times 50^\circ$. The Galactic plane is indicated by the horizontal line, and the Galactic center by the cross in the center of the image. Also shown is an outline of the COBE/DIRBE image of the Galactic center (*smooth solid curve*, from Arendt et al 1994), an approximate outline of the Sagittarius dSph galaxy (*complex curve*, from Ibata et al 1997), with the four Sgr dSph globular clusters identified as asterisks; Baade's Window (*heavy circle below the center*); the field of the DUO microlensing survey, which contains some of the other microlensing fields (*solid square*, overlapping the Sgr dSph rectangle; Alard 1996); the four fields for which deep HST color-magnitude data are available (*open squares*, near Baade's Window); and the six fields surveyed for kinematics and metallicity by Ibata & Gilmore (1995a,b: *black/white outline boxes*). The location of Kepler's supernova is indicated as a circle, north of the Galactic plane. Other features of relevance include the extreme extinction, which prevents optical/near-IR low-resolution observations of the bulge within a few degrees of the plane, and the pronounced asymmetry in the apparent bulge farther from the plane. The dust that generates the apparent peanut shape in the COBE/DIRBE image is apparent. The asymmetry at negative longitudes north of the plane, indicated by a large dotted circle, is the Ophiuchus star formation region, some 160 pc from the Sun. The Sagittarius spiral arm contributes significantly at positive longitudes in the plane.

in low-resolution spectra between foreground K dwarfs and such metal-rich K giants, which leads to an inability to identify contamination of the bulge sample by disk stars. They find that the outer bulge metallicity distribution function peaks at ~ -0.3 dex, and continues down beyond -1 dex (see Figure 2 below).

Minniti et al (1995) present the metallicity distribution function for ~ 250 K/M giants in two fields at projected Galactocentric distances of $R \sim 1.5$ kpc. Their results are calibrated only for stars more metal-poor than ~ -0.5 dex, and one of their fields was selected with a bias against high metallicities. Their data for their unbiased field again shows a broad distribution function, which is approximately flat from -1 to $+0.3$ dex. Minniti et al (1995) also summarize (and list the references to) results from extant photometric chemical abundance determinations (e.g. Morrison & Harding 1993); in general, these agree neither with each other nor with spectroscopic determinations. Further work is clearly needed.

The few large-scale kinematic surveys of the bulge (Ibata & Gilmore 1995a,b, Minniti et al 1995) find no convincing evidence for an abundance-kinematics correlation within the bulge itself, after corrections for halo stars and disk stars (see also Minniti 1996).

The most striking aspects of the bulge K/M giants' metallicity distribution function are its width and the fact that there is little if any radial gradient in its peak (modal) value when one considers only spectroscopic determinations. Further data are required to determine whether or not the wings of the distribution are also invariant. Certainly the very late spectral-type M giants have a significantly smaller scale height than do the K giants (Blanco & Terndrup 1989), a fact that could be a manifestation of either a metallicity gradient in the high-metallicity tail of the distribution function or of an age gradient, with a small scale height, metal-rich, younger population that is concentrated to the Galactic plane. Star formation clearly occurs in the very center of the Galaxy (e.g. Gredel 1996), so that a distinction between inner disk and bulge stellar populations remains problematic, and perhaps semantic, in the inner few hundred parsecs of the Galaxy. External disk galaxies do show color gradients in their bulge components, but the amplitude is luminosity dependent and expected to be small for bulges like that of the Milky Way (Balcells & Peletier 1994).

The little evidence there is concerning the stellar metallicity distribution of older stars in the inner disk is also somewhat confusing. An abundance gradient with the mean rising ~ 0.1 dex/kpc towards the inner Galaxy, but for data only relevant to Galactocentric distances of 4–11 kpc, has been plausibly established for F/G stars of ages up to 10^{10} years (Edvardsson 1993; their table 14—their few older stars show no evidence for a gradient). A similar amplitude of metallicity gradient is seen in open clusters older than 1 Gyr,

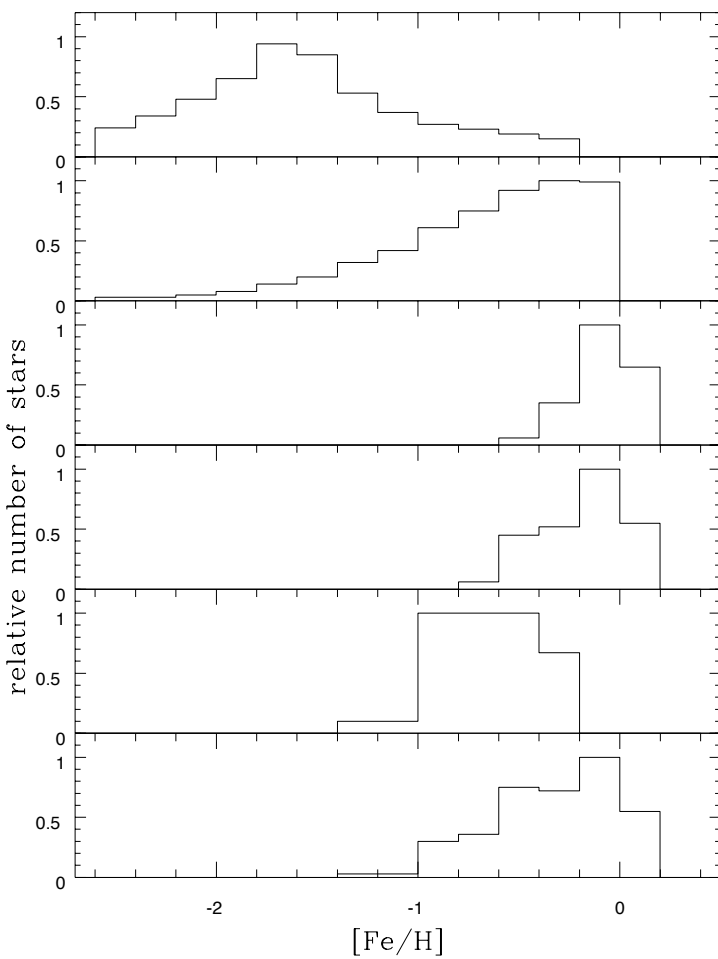


Figure 2 Chemical abundance distribution functions, normalized to unity, derived by Wyse & Gilmore (1995), except where noted. The distributions are, from top to bottom, the solar neighborhood stellar halo (Laird et al 1988); the outer Galactic bulge (Ibata & Gilmore 1995b), truncated at solar metallicity; the younger stars of the solar neighborhood; a volume-complete sample of local long-lived stars; a volume-complete sample of local thick-disk stars; the column integral through the disk abundance distribution for the sum of the long-lived thin disk and the thick disk.

but for clusters that are exterior to the solar circle (e.g. Friel 1995). Earlier data for K giants, however, suggest no radial abundance gradient, with a mean $[Fe/H] \sim -0.3$ from exterior to the Sun to within 1 kpc of the center (Lewis & Freeman 1989), even though such stars should be no older than the F/G sample. Clearly, however, the abundance range that contains most of the bulge stars overlaps that of the disk, with probable disk gradients that are smaller than the range of the bulge metallicity distribution function. This is of particular interest given the correlations, discussed below, between the colors of bulges and inner disks in external galaxies (de Jong 1996, Peletier & Balcells 1996).

As discussed further below, the mean metallicity of field bulge stars is significantly above that of the globular cluster system of the Milky Way, even if only the inner, more metal-rich “disk” globular clusters with mean metallicity of ~ -0.7 dex (e.g. Armandroff 1989) are considered.

A characterization of the width of the metallicity distribution comes from the fact that the distributions for both Baade’s Window (Rich 1990) and for the outer bulge (Ibata & Gilmore 1995b) are consistent with the predictions of the “Simple Closed Box” model of chemical evolution. This is in contrast to the disk of the Milky Way, at least in the solar neighborhood, which has a significantly narrower metallicity distribution and indeed a shortage of low-metallicity stars compared to this model (the “G-Dwarf problem”). This of course does not mean that any or all of the assumptions inherent in the simple closed box model were realized during bulge formation and evolution, but it is rather a way of quantifying the greater width of the observed metallicity distribution in the bulge compared to the disk at the solar neighborhood, two locations that have the same *mean* metallicity.

Elemental abundances provide significantly more information than does metallicity because different elements are synthesized by stars of different masses and hence on different time scales (e.g. Tinsley 1980, McWilliam 1997). Different scenarios for the formation of the bulge could in principle be distinguished by their signatures in the pattern of element ratios (Wyse & Gilmore 1992). The available data are somewhat difficult to interpret, in part owing to small number statistics (e.g. McWilliam & Rich 1994, Sadler et al 1996), but this can be rectified with the coming 8- to 10-m class telescopes.

AGE ESTIMATES RR Lyrae stars, the traditional tracers of an old metal-poor population, are found in significant numbers along bulge lines of sight, at characteristic distances that place them close to the Galactic center (Oort & Plaut 1975). This has been taken as supporting evidence for an old bulge. Indeed, Lee (1992) argued that, for a stellar population of high mean metallicity to produce significant numbers of RR Lyrae stars from the metal-poor tail of the chemical abundance distribution, the population must be older than a metal-poor

population with the same RR Lyrae production rate. Lee hence concluded that the bulge contained the oldest stars in the Galaxy, older than the stars in the field halo. But are the observed RR Lyrae stars indeed part of the metal-rich bulge, or of the metal-poor stellar halo, whose density of course also peaks in the inner Galaxy?

The samples of RR Lyrae available for this experiment have been small. However, a side benefit of the recent interest in microlensing surveys of the Galactic bulge (e.g. OGLE, MACHO, DUO) has been well-defined catalogs of variable stars, including RR Lyraes. In an analysis of the projected spatial distribution of DUO RR Lyrae—which have been segregated statistically by metallicity based on periods and fit to density laws of halo, disk, and bulge—Alard (1996) has found that the great majority of RR Lyrae stars in his catalog are not associated with the bulge, but rather with the thick disk and halo. Nonetheless, a detectable fraction of the most metal-rich RR Lyrae variables of the 1400 discovered by DUO do indeed belong to a concentrated bulge population. These stars comprise only about 7% of the whole RR Lyrae sample. Thus, the microlensing surveys have in fact made the first discovery of true bulge RR Lyrae. The intermediate-abundance RR Lyrae are primarily thick disk, whereas the most metal poor are primarily halo, from this analysis.

Analysis of the variable stars detected by the IRAS satellite (mostly Mira variables) implied a significant intermediate-age population (e.g. Harmon & Gilmore 1988), perhaps that traced by the carbon stars (Azzopardi et al 1988, Westerlund 1991) and the strong red clump population (e.g. Pacynski et al 1994a,b).

Renzini (1994, 1995) has emphasized that the relative strength of the red clump and red giant branches is dependent on helium content as well as on age and argues that age is not an important parameter for stellar populations older than 1 Gyr. Thus, should the bulge stars be of high helium content—as expected if they had been found to be super-metal-rich—then the observed red clump would be consistent with an old age. However, the fact that the mean metallicity of the bulge is now established (from unbiased tracers) to be below the solar value, with a correspondingly much-reduced helium abundance, makes this unlikely.

Understanding the effects of dust along the line of sight to the central regions is crucial. The analysis of infrared (IR) data reduces some of the reddening problems of optical data, but again the interpretation in terms of stellar properties is far from unambiguous. A deep near-IR luminosity function for Baade's window was obtained by Tiede et al (1995). Houdashelt (1996), in a detailed analysis of the available IR photometry and spectroscopy for stars in Baade's Window, concluded that a typical age of perhaps 8 Gyr and mean metallicity of $[Fe/H] \sim -0.3$ are most consistent.

Optical/near-IR color-magnitude diagrams that extend well below the main sequence turnoff region may be used to make quantitative statements about mean age and age ranges of stellar populations: modulo uncertainties in this case that are due to large and highly variable extinction, to extreme crowding in the inner fields, and to the contribution of foreground stars. In spite of these complications, Ortolani et al (1995) concluded, from a comparison of HST color-magnitude data for the horizontal branch luminosity functions of an inner globular cluster with ground-based data towards Baade's Window, that the stellar population of the bulge is as old as is the globular cluster system and, furthermore, shows negligible age range. This contrasts with earlier conclusions based on prerefurbishment HST color-magnitude data for Baade's Window (Holtzman 1993), which suggests a dominant intermediate-age population. Future improved deep HST color-magnitude data are eagerly awaited.

An example of the information that can be obtained is given in Figure 3, which is a V-I, V color-magnitude diagram from WFPC2 data (planetary camera) obtained as part of the Medium Deep Survey (S Feltzing, private communication).

BULGE STRUCTURE The only single-parameter global fit to the surface brightness of the combined halo plus bulge of the Galaxy that implicitly assumes they are a single entity, is that by de Vaucouleurs & Pence (1978). From their rather limited data on the visual surface brightness profile of the bulge/halo interior to the solar Galactocentric distance, when assuming an $R^{1/4}$ -law profile, they derived a projected effective radius of 2.75 kpc, which may be deprojected to a physical half-light radius of 3.75 kpc. As shown by Morrison (1993), the de Vaucouleurs & Pence density profile, extrapolated to the solar neighborhood, is brighter than the observed local surface brightness of the metal-poor halo, which was obtained from star counts, by 2.5 magnitudes. Because the density profile of the outer halo is well described by a power law in density, with index $\rho(r) \propto r^{-3.2}$, and oblate spheroidal axis ratio of about 0.6 (Kinman et al 1966, 1994, Wyse & Gilmore 1989, Larsen & Humphreys 1994), this result actually provides the first, though unappreciated, evidence that the central regions of the galaxy are predominantly bulge light and that the bulge light falls off faster than does the outer halo light. That is, the bulge and halo are not a single structural entity. More generally, because the spatial density distribution of the stellar metal-poor halo is well described by a power law, whereas the inner bulge (see below) is well described by another power law of much smaller scale length, the apparent fit of the single $R^{1/4}$ -law profile must be spurious and misleading.

The limiting factors in all studies of the large-scale structure of the stellar Galactic bulge are the reddening, which is extreme and patchy, and severe crowding. The systematic difference between the best pre-HST photometry

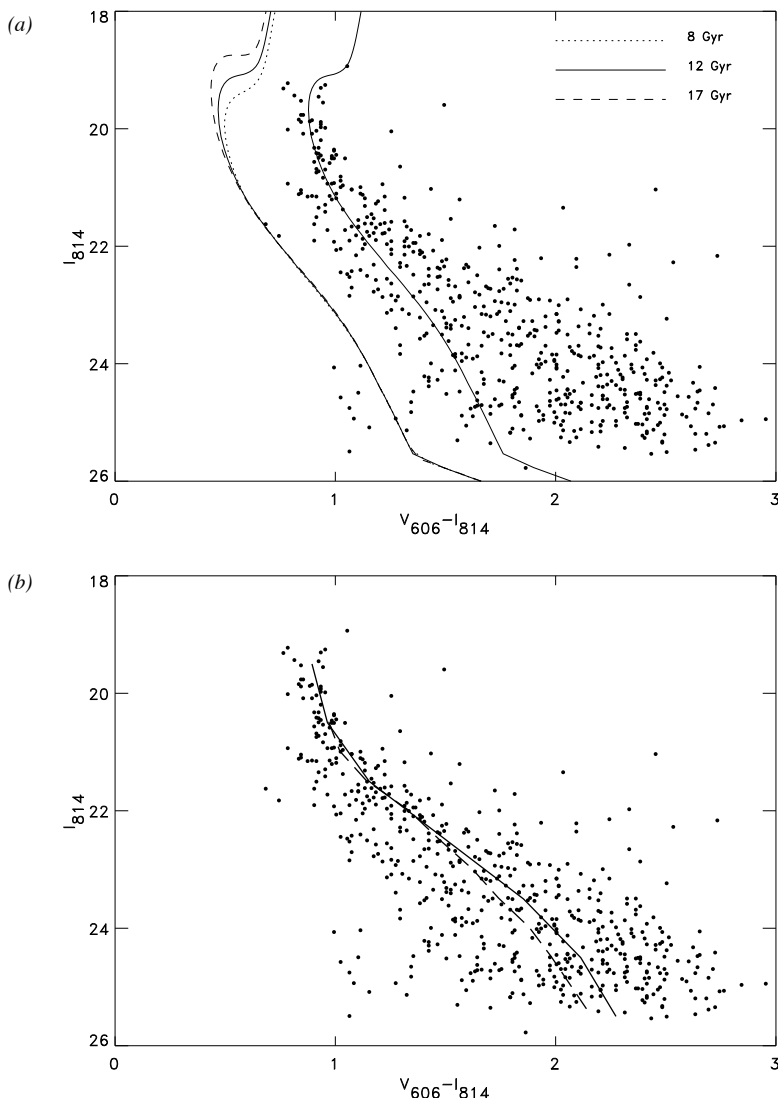


Figure 3 The HST WF/PC2 color-magnitude data for the Galactic bulge, for the field at $(l, b) = (3.6, -7)$ identified in Figure 1, from the Medium Deep Survey. (a) The panel shows the data. Overlaid, from a by-eye fit, is a 12-Gyr isochrone for metallicity $[Fe/H] = -0.25$, from Bertelli et al (1994), together with a range of other ages plotted to one side, to illustrate the precision required and the need for independent determinations of extinction at each point. (b) The panel shows the mean line through the data, excluding extreme points, together with the ridge line from similar HST data for the globular cluster 47 Tucanae (Santiago et al 1996), arbitrarily offset to match the mean line.

in crowded regions and the reality, as seen by HST, is now well appreciated after many studies of globular clusters. Near-IR studies within a few degrees of the Galactic plane show optical extinction that has a random variation, on angular scales down to a few arcseconds, of up to $A_V \sim 35$ mag (e.g. Catchpole et al 1990). At southern Galactic latitudes, however, more than a few degrees from the plane, extinction is both low (typically $E_{B-V} \sim 0.2$) and surprisingly uniform, as is evident in the optical bulge image in Figure 1 and as exploited by Baade. Nonetheless, detailed star-count modeling of the inner galaxy (Ibata & Gilmore 1995a,b; M Unavane, private communication) demonstrates that extinction variations are still larger in their photometric effects than are the photometric signatures of different plausible structural models. This sensitivity to extinction, together with the extreme crowding that bedevils ground-based photometry, is well illustrated by the recent history of structural analyses of the inner Milky Way disk by the OGLE microlensing group, based on low spatial-resolution optical data. Their initial analysis of their data suggested that there is no inner disk in the Galaxy, only prominent foreground spiral structure (Paczynski et al 1994a). After more careful consideration of crowding, and of alternative extinction models, this detection of a “hole” in the disk was retracted (Kiraga et al 1997). The true spatial density distribution of the inner disk remains obscure.

There are many analyses of the surface brightness structure of the bulge, which range from straightforward counts of late-type stars perpendicular to the plane along the minor axis (cf Frogel 1988 for references) through extensive two-dimensional analyses (Kent et al 1991), to detailed inversions of photometric maps (e.g. Blitz & Spergel 1991, Binney et al 1997). In all such cases, extreme reddening near the plane precludes reliable use of low spatial resolution data with $|b| < 2$, irrespective of the techniques used. The zero order properties of the photometric structure of the bulge are fairly consistently derived in all such studies and determine ~ 350 pc for the minor axis exponential scale height, as well as significant flattening, with minor:major axis ratio of ~ 0.5 . Together with a disk scale length of around 3 kpc, this result places the Milky Way galaxy within the scatter of late-type disk galaxies on the correlation between disk and bulge scale lengths of Courteau et al (1996).

Considerable efforts have been expended in the last decade to determine the three-dimensional structure of the Galactic bulge. These efforts began at a serious level with analyses of the kinematics of gas in the inner Galaxy, following the prescient work of Liszt & Burton in the 1980s (see Liszt & Burton 1996 and Burton et al 1996 for recent reviews and introductions to the subject), by Gerhard & Vietri (1986) together with much other work reviewed by Combes (1991). A resurgence of interest in bar models has been motivated by (a) new dynamical analyses (e.g. Binney et al 1991, Blitz et al 1993), (b) the realization

that near-IR data might reflect the pronounced molecular gas asymmetry (Blitz & Spergel 1991), (c) gravitational microlensing results (Paczynski et al 1994b), and (d) the new photometric COBE/DIRBE data (Weiland et al 1994).

It appears that all galaxies in their central regions have non-axisymmetric structures, often multiple structures such as bars within bars (e.g. Shaw et al 1995, Friedli et al 1996). The distinction between inner spiral arms, bars, lenses, local star formation, and the like is perhaps of semantic interest, except in cases where the distortions are of sufficiently large amplitude such as to affect the dynamical evolution. Is the Galaxy like that? The significant question is the existence of a substantial perturbation to the inner density distribution, and gravitational potential, associated with a bar. Secondary questions are the shape of that bar and its relationship to the disk or to the bulge. The extant three-dimensional models of the central regions of the Milky Way derived from the COBE surface photometry depend on systematic asymmetries of the derived “dust-free” surface brightness with longitude of less than 0.4 mag in amplitude, after statistical correction for extinction that is locally some orders of magnitude larger in amplitude (Binney et al 1997). Thus the models are crucially sensitive to reddening corrections made on a scale of 1.5 degrees (the COBE/DIRBE resolution), although reddening varies on much smaller scales (Figure 1).

The models also provide only a smooth description of most of the known foreground disk structure such as can be seen in Figure 1—the Ophiuchus star formation region, the Sagittarius (Sgr) spiral arm, etc—and do not work at low Galactic latitudes. A model of this disk must be subtracted before bulge parameters can be derived. The best available description of the stellar bulge derived this way suggests axis ratios $x:y:z \sim 1.0:0.6:0.4$ (Binney et al 1997).

It is worth noting that this model, although the best currently available, fails to explain either the high spatial frequency structure in the photometric data or the observed high rate of gravitational microlensing towards the inner Galaxy (Bissantz et al 1997), in addition to having remaining difficulties with the details of the gas kinematics in the inner Galaxy. Little evidence exists for non-axisymmetry in the potential from analyses of stellar kinematics—radial velocity surveys find consistency with an isotropic oblate rotator model (e.g. Ibata & Gilmore 1995, Minniti 1996), though with a mild bar allowed (Blum et al 1995). Although evidence for a bar is seen in proper-motion surveys (Zhao et al 1994, who analyzed proper motions from Spaenhauer et al 1992), this is very dependent on the distances assigned to the stars. Thus it must be emphasized that the best available models for the inner Galaxy remain poor descriptors of the very complex kinematics and spatial distribution of the gas (see Liszt & Burton 1996) and of the complex kinematics of some samples of stars (e.g. Izumiura et al 1995).

Analysis of the photometric structure of the inner galaxy is a very active field of research, which promises major progress in the next few years with the availability of the Infrared Space Observatory (ISO) imaging survey data of the inner galaxy (Perault et al 1996). ISO improves on the $\sim 1^\circ$ spatial resolution of COBE, as it has typically 6-arcsec resolution in surveys. These data provide for the first time a detailed census of individual stars and the ISM in the inner Galaxy, with sufficient resolution and sensitivity to see single stars at the Galactic center, thereby allowing the first ever determination of the true three-dimensional spatial distribution of the inner Galaxy.

We consider the kinematics of the Galactic bulge, the halo, and the disk, and their implications for formation models, below (section 5).

2.2 *M 33 (NGC 598)*

The stellar population of M 33 was reviewed by van den Bergh (1991a), to which the reader is referred for details. We discuss the significant developments since then concerning the existence and nature of the stellar halo and bulge.

M 33 shows photometric evidence for nondisk light, in particular in the central regions. However, the nature of this light remains uncertain, as does whether or not there is a central bulge component that is distinct from the stellar halo.

Attempts to fit optical and IR data for the central regions with an $R^{1/4}$ law generally agree with a “bulge-to-disk” ratio of only $\sim 2\%$, or $M_{V,bulge}$ fainter than ~ -15 (Bothun 1992, Regan & Vogel 1994). Regan & Vogel emphasize that a single $R^{1/4}$ provided the best fit to their data. Some evidence is given from ground-based H-band imaging (Minnitti et al 1993) and from HST V-I/I CMD data (Mighell & Rich 1995) for asymptotic giant branch (AGB) stars in the central regions in excess of the number predicted by a simple extrapolation from the outer disk; these stars have been ascribed to a rather young centrally concentrated bulge. However, McLean & Liu (1996) contend that their JHK photometry, after removal of crowded regions, shows no resolved bulge population distinct from the smooth continuation of the inner disk.

Is the $R^{1/4}$ component metal-poor or metal-rich? The giant branch of the HST CMD data is consistent with a broad range of metallicity, ranging from M 15-like to 47 Tuc-like, some 1.5 dex in metallicity. The low end of this metallicity range is consistent with that estimated earlier from ground-based CMD data for fields in the outer “halo,” $[Fe/H] \sim -2.2$ (Mould & Kristian 1986). These outer fields showed a narrow giant branch, which is consistent with a small dispersion in metallicity, and thus the two datasets together are suggestive of a gradient in the mean metallicity and metallicity dispersion. This may be interpreted as evidence for a centrally concentrated more metal-rich component, albeit following the same density profile as the metal-poor

stars. Pritchett (1988) reported a preliminary detection of RR Lyrae stars in M 33, again evidence for old, probably metal-poor, stars.

The semistarlike nucleus of M 33 has a luminosity similar to that of the brightest Galactic globular clusters, $M_V \sim -10$, and a diameter of ~ 6 pc. Analysis of its spectrum (Schmidt et al 1990) demonstrated that its blue color reflects the presence of young stars (age less than 1 Gyr) rather than extremely low metallicity; old and intermediate-age stars with metallicity greater than 0.1 of the solar value dominate. The relation of this nucleus to the “bulge,” if any, is unclear.

The only kinematic data for nondisk tracers in M 33 are for a subset of its ~ 200 “large clusters of concentrated morphology” (Christian 1993), of which perhaps 10% have the colors of the classical old globular clusters of the Milky Way. Of these clusters, 14 have kinematics that are suggestive of halo objects, in that they define a system with little net rotation and with a “hot” velocity dispersion of order $1/\sqrt{2}$ times the amplitude of the HI rotation curve (Schommer et al 1991, Schommer 1993). Estimates of the metallicities and ages of the “populous” clusters, based on spectrophotometry, suggest a wide range of each, with even the “globular clusters” spanning perhaps ~ -2 dex to just under solar metallicity (Christian 1993). Improved estimates from better data are possible and desirable. M 33 has a very large number of globular clusters per unit field halo light, but the meaning of this is unclear.

In summary, M 33 has a low luminosity halo, which is at least in part old and metal-poor. There is no convincing evidence for the existence of a bulge in addition to this halo.

2.3 *M 31 (NGC 224)*

The stellar population of M 31 was reviewed by van den Bergh (1991b), and again we restrict discussion to significant subsequent developments.

The field nondisk population has been studied by several groups, following Mould & Kristian (1986; see also Croots 1986). These authors established, from V and I data that reach several magnitudes down the giant branch, that the bulge/halo of M 31, at 7 kpc from its center, has mean metallicity like the Galactic globular 47 Tuc, $[Fe/H] \sim -0.7$, and a significant dispersion in metallicity, when assuming an old population, down to ~ -2 dex and up towards solar. Similar conclusions have been reached from HST data for the outer regions of M 31 (~ 10 kpc) by Holland et al (1996) and by Rich et al (1996) at ~ 30 kpc from the center, which limits the amplitude of any chemical abundance gradients, assuming always that one is dealing with an old stellar population.

These HST data also established firmly the scarcity of Blue Horizontal Branch (BHB) stars in the halo of M 31, which confirms the suggestion by Pritchett & van den Bergh (1987, 1988). A few BHB stars were found by Holland et al (1996),

who suggest that the horizontal branch (HB) morphology is apparently too red for the derived broad metallicity distribution. If one assumes that the horizontal branch traces a population as old as the Galactic halo globular clusters, then the M 31 field population suffers a severe “second-parameter problem.”

Assuming that the derived broad metallicity distribution is well-established, does this lack of a significant BHB population imply a young age for M31? Age can affect HB morphology in that younger populations are redder at a given metallicity, other things being equal (e.g. Lee 1993, who also demonstrates the effects of many other parameters), so that it is of interest to consider this possibility [while recalling that Richer et al (1996) argue quite convincingly, based on relative ages for those Galactic globular clusters with main sequence turn-off photometry, that age is not the dominant “second parameter” of HB morphology, at least in these systems]. Indeed, the presence of bright stars, identified as intermediate-age AGB stars, has been suggested from (prerefurbishment) WF/PC HST VI data at least within the inner 2 kpc of the bulge (Rich & Michell 1995). Morris et al (1994) argued for a ubiquitous strong luminous AGB component, with a typical age of 5 Gyr, from their ground-based V and I data that reaches the bright giants in various fields of M 31, 16–35 kpc along the major axis of the disk and one probing the halo at 8 kpc down the minor axis (close to the field of Mould & Kristian 1986). Rich et al (1996), and also Holland et al (1996), find no evidence for an extended giant branch in their WF/PC2 HST data for fields in the outer halo, at 10–30 kpc from center, where again the RHB/clump is dominant, with essentially no trace of a BHB. Thus, the data describing possible metallicity/age effects remain unclear.

Large-scale surface photometry of the disk and of the bulge of M 31, in many broadband colors, was obtained and analyzed by Walterbos & Kennicutt (1988). They found that there was no color gradient in the bulge and that the inner disk and the bulge have essentially the same colors, i.e. those of “old, metal-rich stellar populations.” This similarity of broadband colors has subsequently been found for a large sample of external disk galaxies, as discussed in Section 3, and clearly must be incorporated into models of the formation and evolution of bulges (see Section 5 below). Walterbos & Kennicutt also derived structural parameters for the disk and bulge that are consistent with the correlation between scale lengths found for the larger sample of more distant disk galaxies by Courteau et al (1996). In terms of total optical light, the bulge-to-disk ratio of M 31 is about 40%.

Pritchett & van den Bergh (1996) emphasize that a single $R^{1/4}$ -law provides a good fit to their derived V-band surface photometry (from star counts), with no bulge/halo dichotomy. The $R^{1/4}$ component is significantly flattened, with axial ratio of 0.55, which is similar to the value for the metal-poor halo of the Milky Way (Larsen & Humphreys 1994, Wyse & Gilmore 1989).

In contrast to the metal-poor halo of the Milky Way, which is apparently flattened by anisotropic velocity dispersions, the bulge of M 31 has kinematics consistent with an isotropic oblate rotator, with mean rotational velocity of ~ 65 km/s and velocity dispersion of ~ 145 km/s (McElroy 1983), which are typical of external bulges (Kormendy & Illingworth 1982).

Thus, although Baade (1944a,b) identified the “bulge” of M 31 (which we may now define to be field nondisk stars at distances up to 35 kpc from the center of M 31) with Population II (similar to the Milky Way halo), the dominant tracers of the M 31 bulge do not share the characteristics of classical Galactic Population II, as they are neither of low mean metallicity nor have little net rotation (see Wyse & Gilmore 1988 for further development of this point, in the context of thick disks).

There are around 200 confirmed globular clusters associated with M 31 (e.g. Fusi Pecci et al 1993). The distribution of their metallicities has a mean of around -1 dex, which is more metal-poor than the field stars, with a range of perhaps 1 dex on either side (e.g. Huchra et al 1991, Ajhar et al 1996). The inner metal-rich clusters form a rapidly rotating system, whereas the outer metal-poor clusters have more classical “hot” halo kinematics (e.g. Huchra 1993; see also Ashman & Bird 1993 for further discussion of subsystems within the globular clusters). The overall globular cluster system has a projected number density profile that may be fit by a de Vaucouleurs profile (although the central regions fall off less steeply) with an effective radius of $\sim 4\text{--}5$ kpc (Battistini et al 1993). This is more extended than the $R^{1/4}$ fit to the field stars. Thus, in terms of kinematics, metallicity, and structure, there may be evidence for a bulge/halo dichotomy in M 31 if the halo is traced by the globular clusters and the bulge by field stars. Note that, although there are exceptions, the spatial distributions of globular cluster systems and underlying galaxy light are similar to the first order (Harris 1991).

As seems to be the case for any system studied in sufficient detail, the morphology of the very central regions of M 31 is clearly complicated, with twisted isophotes (Stark 1977), gas kinematics that may trace a bar (e.g. Gerhard 1988), inner spiral arms (e.g. Sofue et al 1994), and two nuclei (Bacon et al 1993) that may indicate a tilted inner disk (Tremaine 1995). These phenomena have been modeled recently by Stark & Binney (1994) by a spherical mass distribution plus a weak prolate bar, with the bar containing one third of the mass within 4 kpc (the corotation radius). The association of the bulge with this bar, which one might be tempted to adopt by analogy with the Milky Way, is unclear.

2.4 Large Magellanic Cloud

The Large Magellanic Cloud (LMC) is the nearest barred galaxy, with the bar offset from the kinematic and isophotal center and embedded in an extensive

disk. A minor metal-poor old component of the LMC is seen in deep HST color-magnitude data (Elson et al 1997), but its kinematics and spatial distribution are not yet well known. There is a significant amount of new information, from the several microlensing experiments, which will appear in the literature over the next few years concerning the variable star population of the LMC. Of particular relevance are data for the Long Period Variables (LPVs) and the RR Lyrae. The LPVs are believed to have low-mass progenitors and hence trace older stellar populations, while RR Lyrae variables are the traditional tracers of old metal-poor populations. However, most of the information has yet to be analyzed. There has been no kinematical analysis of the LPVs since that of Hughes et al (1991), who found tentative indications of classical hot halo kinematics. The old globular clusters of the LMC, despite prejudice, have kinematics consistent with being in a rotating disk (e.g. Freeman 1993). Thus, little evidence exists for a bulge or halo population in the LMC, except the observation that an old metal-poor stellar population exists.

2.5 *General Properties of the Local Group Disk Galaxies*

The diversity of properties of bulges, haloes, and disks evident in the four largest disk galaxies in the Local Group is striking. The essential properties seem to be the following. The two latest type galaxies (M 33, LMC) have no convincingly detected bulge, but both have at least some evidence for a small population of very old metal-poor stars. Both have old metal-poor globular clusters. The intermediate-type Milky Way galaxy contains what can be termed both a halo (metal-poor, old, extended, narrow abundance distribution, containing globular clusters) and a bulge (metal-rich, mostly, and perhaps exclusively, fairly old, with a very broad metallicity distribution function, and extremely compact in spatial scale). The earlier type M 31 has a prominent and extended bulge, which is both quite metal-rich and fairly old, and has a broad abundance distribution function. The only evidence for a metal-poor old halo in M 31 comes from its globular clusters and its—very few—RR Lyrae stars and BHB stars. In all cases, haloes are supported against gravitational gradients by their velocity dispersion (pressure-supported systems), very unlike disks, though this is perhaps as much a definition as an observation.

Thus, whereas the Local Group Spiral galaxies have a definable halo:disk ratio, which is apparently rather similar for all three, only the two earlier types have a definable bulge-to-disk ratio, which is greater for M 31 than for the Milky Way.

3. LOW-REDSHIFT UNRESOLVED BULGES

3.1 *Bulges and Ellipticals*

In the most simplified picture of galaxies, a galaxy consists of a bulge that follows an $R^{1/4}$ profile and an exponential disk, whereas elliptical galaxies are

simply the extension of bulges in the limit of bulge-to-disk ratio tending to infinity.

The picture has been complicated by the discovery that most intermediate luminosity ellipticals (as classified from photographic plates) have significant disks (e.g. Bender et al 1988, Rix & White 1990). These disks can be very difficult to detect, especially when seen face-on. Kormendy & Bender (1996) have recently proposed that ellipticals with “disky” isophotes, which tend to be of lower luminosity than those with “boxy” isophotes, are the natural extension of the Hubble sequence of disk galaxies.

Futhermore, many ellipticals show nuclear disks, either from their kinematics or high-resolution imaging (e.g. review of de Zeeuw & Franx 1991). These disks are very concentrated towards the center and are therefore different from the extended disks in normal spiral galaxies. Sometimes these disks have an angular momentum vector opposite to that of the bulge (e.g. IC 1459, Franx & Illingworth 1988), implying that the gas that formed the disk did not have its genesis in the stars of the bulge but was accreted from elsewhere. Notice, however, that some spiral galaxies also show evidence for these “nuclear disks,” including the Milky Way (Genzel et al 1996) and the Sombrero galaxy (Emsellem et al 1996).

HST observations confirm the similarity in some aspects of low-luminosity ellipticals and bulges. Most of these systems have power-law profiles in their inner parts, with steep profile indexes (e.g. Faber et al 1997). In contrast, most high-luminosity ellipticals show “breaks” in their surface brightness distribution within 1kpc or less from the center, i.e. relatively sudden changes where the intensity profiles flatten. It is not clear yet what formation processes have caused these variations, although it has been suggested that the dynamical effects of massive black holes may be responsible (Faber et al 1997). HST imaging of large samples of spirals is needed to determine better the structure of their bulges. Preliminary results (pre-refurbishment) indicate that a significant fraction of bulges in early-type spirals have power-law profiles in their inner parts, while late-type spirals have shallower inner profiles and often an unresolved nucleus (e.g. Phillips et al 1996).

These results suggest caution in the analysis of other data, as bulges are not necessarily the only important component near the center and as the formation histories of the centers of different galaxies may have been quite different from each other. Indeed, the central 1 kpc or so of most, if not all, galaxies clearly contain something unusual—even without the benefit of detailed HST images (e.g. note NGC 4314 in the Hubble Atlas, which is a barred galaxy that has spiral arms in the center of the bar).

Beyond the very central regions, a systematic variation of surface brightness profile with bulge luminosity has been established, in that bulges in late-type spiral galaxies are better fit by exponential profiles than by the de Vaucouleurs

profile, which is appropriate for early-type spirals (e.g. Andredakis et al 1995, de Jong 1995, Courteau et al 1996). HST imaging of late-type spirals is needed to better determine the structure of their bulges. Preliminary results indicate that a significant fraction of bulges in late-type spirals have power-law profiles in their inner parts (e.g. Phillips et al 1996).

Much recent research into the properties of elliptical galaxies has demonstrated the existence of a “fundamental plane” that characterizes their dynamical state (e.g. review of Kormendy & Djorgovski 1989, Bender et al 1993). The bulges of disk galaxies in the range S0–Sc (T0–T5) have also recently been demonstrated to occupy the same general locus in this plane (Jablonka et al 1996). Furthermore, these bulges have a similar Mg2 line strength–velocity dispersion relationship to that of ellipticals, but the bulges are offset slightly to lower line strengths. This offset may be due to bulges having lower metallicity or lower age. Contamination by disk light can produce a similar effect. Jablonka et al argue in favor of a close connection between ellipticals and bulges. Balcells & Peletier (1994) find that bulges follow a color-magnitude relationship similar to that of ellipticals but that bulges have a larger scatter. Furthermore, they find that bulges and ellipticals of the same luminosity do not have the same colors and that bulges are bluer. The offset is similar to that seen by Jablonka et al in the strength of the magnesium index, but Balcells & Peletier interpret it as indicating a real, though complex, difference between bulges and ellipticals. In addition to the data noted above on the central parts of bulges, Balcells & Peletier (1994) find that the amplitude of radial color gradients also varies systematically with bulge luminosity. They interpret their results as consistent with bright bulges ($M_R < -20$) being similar to ellipticals (despite the color zero-point offset), whereas faint bulges are perhaps associated with disks.

The potential well of the outer regions of disk galaxies is clearly dominated by dark matter, whereas the properties of dark matter haloes around elliptical galaxies are less well known (e.g. de Zeeuw 1995). How do properties of bulges scale with dark haloes? Figure 4 shows the ratio of bulge dispersion divided by the circular velocity of the halo (derived from rotation of tracers in the disk) against bulge-to-disk ratios. The square on the right represents elliptical galaxies, derived from models by Franx (1993), which assume a flat rotation curve. The triangle on the left corresponds to the inner regions of pure disks, as derived for a sample of Sa–Sc galaxies by Bottema (1993) (it should be noted that the inner regions of disks are not cold, but warm). Bulges may be seen to lie on a rather smooth sequence between these two extreme points. This suggests that the bulges in galaxies with low bulge-to-disk ratios may have been formed at the same time as the disk, whereas bulges in galaxies with large bulge-to-disk ratios are so much hotter than the disk that it is more likely that they formed separately. More and better data would be valuable to improve the diagram.

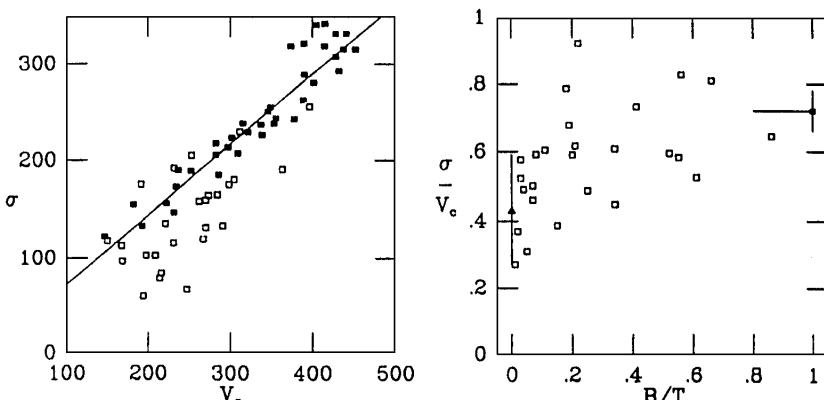


Figure 4 (a) The central velocity dispersion of stellar tracers, σ , against dark halo circular velocity, V_c . Open symbols are bulges; closed symbols are ellipticals. Circular velocities for the ellipticals are derived from models, as described by Franx (1993). (b) The ratio of velocity dispersion in the bulge to dark halo circular velocity, σ/V_c , taken from Franx (1993), plotted as a function of bulge-to-total luminosity (B/T) ratio, for the entire range of Hubble Type. The triangle at left is valid for the inner regions of pure disks, the square at right for ellipticals. Note that systems with low B/T have kinematics almost equal to those of inner disks.

3.2 Bulges and Disks

Astronomical gospel declares that bulges are red and disks are blue. This is generally presumed to be derived from studies of nearby bulges. Unfortunately, there are very few data on which these rather strong statements are based. The observations were difficult to make before the advent of CCD cameras and have been lacking since then until very recently—perhaps because the problem was considered to be solved. Full two-dimensional imaging is needed for accurate bulge/disk decomposition and for exclusion of dusty areas, and large surveys with multicolor information are still rare. Notable exceptions are the recent studies of the colors of “normal” spiral galaxies by de Jong (1995, 1996) and by Balcells & Peletier (1994, Peletier & Balcells 1996).

A relationship between bulges and disks is seen clearly in their colors. We show in Figure 5 the correlation between bulge color and the color of the disk of the same galaxy, for the data of Peletier & Balcells (1996), taken from their table 1. The disk color is measured at two major axis scale lengths, and the bulge color at half an effective radius, or at 5 arcsec, whichever is the larger. Note that bulges are more like their disk than they are like each other, and the very wide range of colors evident. This sample consists of luminous ($M_R \lesssim -21$) nearby disk galaxies that span the range S0–Sbc.

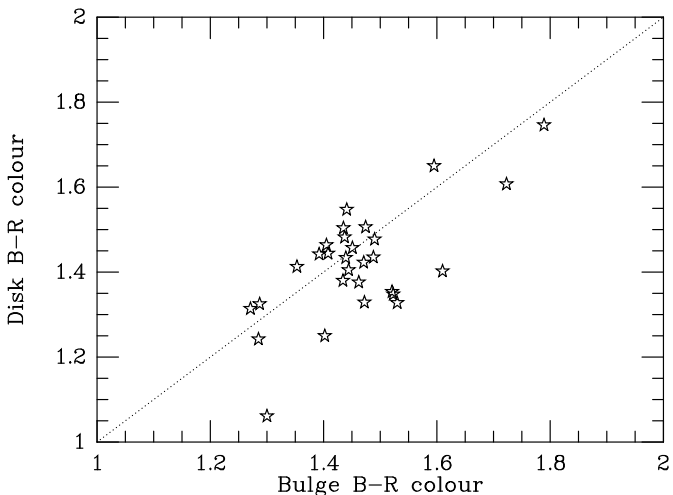


Figure 5 The correlation between bulge color and the color of the disk of the same galaxy, for the data of Peletier & Balcells (1996), taken from their table 1. The disk color is measured at two major axis scale lengths, and the bulge color at half an effective radius, or at 5 arcsec, whichever is the larger. Note that bulges are more like their disk than they are like each other, and the very wide range of colors evident.

The color range for the bulges is noticeably large—almost as large as is the range of colors for the disks. Furthermore, although some bulges are quite red, blue bulges clearly exist, as do red disks. The sample of de Jong (1996) includes the later morphological types of disk galaxies (Sc and Sd) and shows a similar relationship between the colors of bulge and inner disks. These data show that there is little support for sweeping statements such as “bulges are red, and disks are blue.” Color data for the “hidden” disks in elliptical galaxies would be very interesting.

Furthermore, the similarity in color between inner disk and bulge has been interpreted as implying similar ages and metallicities for these two components and an implicit evolutionary connection (de Jong 1996, Peletier & Balcells 1996). Given the difficulties of disentangling the effects of age and metallicity even with resolved bulges, any quantification of “similar” must be treated with caution (see Peletier & Balcells 1996, who derive an age difference of less than 30%, assuming old populations with identical metallicities). We notice in passing that the ages of ellipticals have not been determined yet to high accuracy. Measurements of various absorption line strengths have been interpreted to indicate a wide range of ages of the central regions of ellipticals, with no

correlation between age and luminosity (Faber et al 1995), but this is far from rigorously established because of the coupling of age and metallicity in their effects on line strengths.

A close association between bulges and disks has been suggested by Courteau et al (1996), on the strength of a correlation between the scale lengths of the bulge and disk; they find that bulges have about one-tenth the scale length of disks. This correlation shows considerable scatter, especially for earlier galaxies of type Sa, and relies upon an ability to measure reliably bulge scale lengths that are a small fraction of the seeing. More and better data are anticipated.

3.3 *Bulges in Formation at $z < 0.1$?*

A few local exceptional systems are candidates for young bulges. Gravitational torques during interactions can act to drive gas to the central regions (e.g. Mihos & Hernquist 1994), where it may form stars, and which may, depending on the duration of star formation and of the interaction, be heated into a bulge. Schweizer (1990) discusses local disk galaxies with blue bulges, presenting them as evidence for recent bulge-building in this manner. These galaxies include (the dwarf) NGC 5102, an S0 galaxy with a bluer bulge than disk and strong Balmer absorption lines in its central regions. Classic merger remnants such as NGC 7252 are forming disks in their central parts, which may imply that these galaxies perhaps have evolved into S0s, or early type spirals (e.g. Whitmore et al 1993).

A more dramatic example of gas-rich mergers is Arp 230, which shows classical shells in the bulge component and a young disk rich in gas, as displayed in Figure 6 (D Schiminovich & J van Gorkom, private communication and in preparation).

4. HIGH-REDSHIFT BULGES

Direct searches for the progenitors of local bulges may be made by the combination of statistically complete redshift surveys of the field galaxy population, combined with photometric and especially with morphological data. As an example, the I-band-selected CFHT redshift survey contains galaxies out to redshifts of order unity, and these galaxies may be analyzed in terms of the evolution of the luminosity function of galaxies of different colors, presumed to correlate with morphological type (Lilly et al 1995). The data are consistent with very little evolution in the luminosity function of the red galaxies, over the entire redshift range $0 < z < 1$, and substantial evolution in the blue galaxies' luminosity function, with the color cut dividing the sample into blue and red taken as the rest-frame color of an unevolving Sbc galaxy. This lack of evolution for red galaxies may be interpreted as showing that the stars of

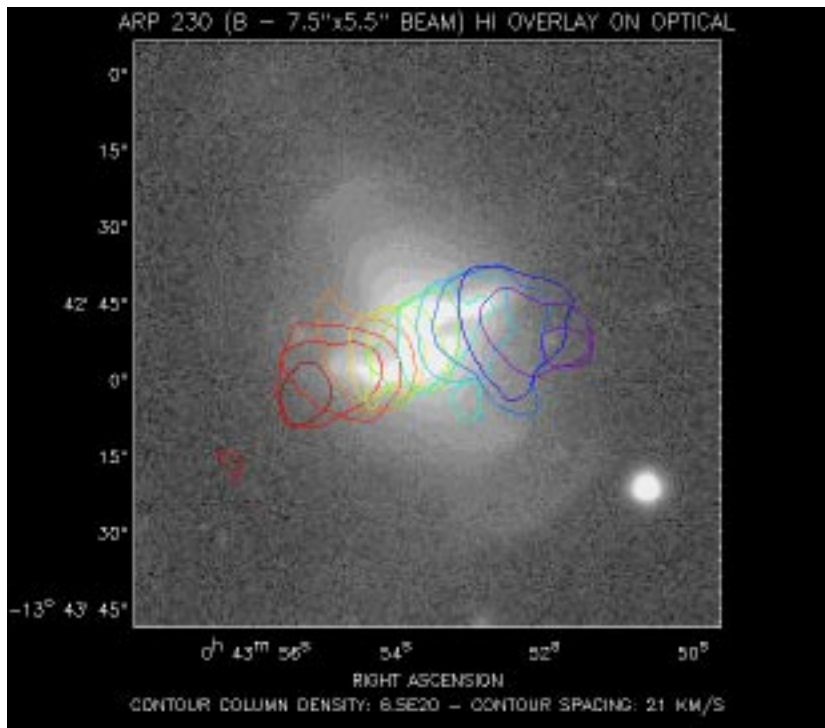


Figure 6 An optical image of Arp 230, with overlaid HI contours. This galaxy shows evidence for shells in its outer bulge, which indicates a recent substantial accretion event, and also has a young gas-rich disk (D Schiminovich & J van Gorkom, private communication).

bulge-dominated systems—the red galaxies—were already formed at redshifts greater than unity, corresponding to a look-back time of greater than half of the age of the universe, or 5–10 Gyr (depending on cosmological parameters).

The high spatial resolution of the HST allows collection of morphological information. Schade et al (1995) obtained HST images for a subset (32 galaxies in total) of the CFHT redshift survey, mostly blue galaxies with $z > 0.5$. They found, in addition to the “normal” blue galaxies with exponential disks and spiral arms and red bulge-dominated galaxies, a significant population of high luminosity ($M_B < -20$) “blue nucleated galaxies” (BNG), with large bulge-to-disk ratio ($B/T \gtrsim 0.5$)—could these be bulges in formation, at look-back times of ~ 5 Gyr? Small number statistics notwithstanding, most of the blue nucleated galaxies are asymmetric and show some suggestions of interactions. Schade et al (1996) found similar results for a larger sample, using just CFHT

images for morphological classification, and confirmed that red galaxies tend to have high bulge-to-disk ratios.

Extending these results to even higher redshifts, and hence studies of progenitors of older present-day bulges, has been achieved by the identification of a sample of galaxies with $z \gtrsim 3$ based on a simple color criterion that selects systems with a Lyman-continuum break, superposed on an otherwise flat spectrum, redshifted into the optical (e.g. Steidel et al 1996a,b). Ground-based spectroscopy of 23 high-redshift candidates provided 16 galaxies at $z > 3$ (Steidel et al 1996b). The observed optical spectra probe the rest-frame 1400- to 1900-Å UV and provide a reasonable estimate of the reddening, and hence dust content, and of the star formation rate. The systems are inferred to be relatively dust-free, with the extinction at ~ 1600 Å typically ~ 1.7 mag, which corresponds to an optical reddening in the galaxies' rest-frame of $E(B - V) \sim 0.3$ mag. Whether the low dust content is a selection effect, perhaps due to fortuitous observational line of sight, or is a general feature of these high-redshift galaxies is not clear. The comoving space density of these systems is large—on the order of half that of bright ($L > L^*$, with L^* the knee of the Schechter luminosity function) galaxies locally, which suggests that not too many of them can be hidden. The star formation rates, assuming a solar neighborhood IMF, are typically $\sim 10 M_\odot/\text{year}$. There are interstellar absorption lines due to various chemical species; these lines may be interpreted as indicative of gas motions in a gravitational potential of characteristic velocity dispersion of ~ 200 km/s, which is typical of normal galaxies today.

Morphological information from optical HST images (Giavalisco et al 1996) for 19 Lyman-break candidates, of which 6 have confirmed redshifts, show that in the rest-frame UV (1400–1900 Å) these systems are mostly rather similar, in contrast to the wide range of morphological types seen at lower redshifts, $z \sim 1$, discussed above. Furthermore, the typical $z \sim 3$ galaxy selected this way is compact, at least in the UV, and has a half-light radius of ~ 2 kpc, which is reminiscent of present-day bulges in the optical. Some of these galaxies show faint surrounding emission that could be interpreted as “disks.” The star formation rates inferred from the spectra build the equivalent of a bulge—say $10^{10} M_\odot$ —over a few billion years, which spans the redshift range from $1 \sim z \sim 4$. Similar results are obtained from $z > 3$ samples derived from the HST Deep Field (Steidel et al 1996a) and for one galaxy at a redshift of $z = 3.43$, the central regions of which do, in fact, fit a de Vaucouleurs profile (Giavalisco et al 1995).

Thus, there is strong evidence that some (parts of some) bulges are formed at $z \gtrsim 3$. However, it is hard to draw definite conclusions about all bulges on the basis of these results because the observations at these redshifts can be biased. If, for example, half of all bulges form at $z \lesssim 0.5$, then we would

simply not observe those at higher redshifts. At higher and higher redshifts, we would simply be selecting older and older bulges. Our conclusions would become strongly biased. This is very similar to the bias for early-type galaxies discussed by van Dokkum & Franx (1996).

5. FORMATION SCENARIOS

5.1 *Are Bulges Related to Their Haloes?*

Analyses of globular cluster systems in external galaxies conclude that they are more metal-poor in the mean than the underlying stellar light, at all radii in all galaxies (Harris 1991). It is worth noting that the Milky Way is sometimes considered an anomaly here, in that the metallicity distribution function for the (metal-poor, also known as halo) globular cluster system is not very different from that of field halo stars, with differences restricted to the wings of the distributions (e.g. Ryan & Norris 1991). It is important to note, however, that this comparison is done in the Milky Way at equivalent halo surface brightness levels well below those achievable in external galaxies. The higher surface brightness part of the Milky Way, that part which is appropriate to compare to similar studies in other galaxies, is the inner bulge. As discussed above, the metallicity there is well above that of the globular clusters. The Milky Way is typical. More importantly, this (single) test suggests the possibility that *all* spiral galaxies that have globular cluster systems have a corresponding field halo, which in turn is systematically more metal-poor and extended than is the more metal-rich observable bulge.

If this is true, the Local Group galaxies are typical, and the concept of “stellar halo” must be distinguished from that of “stellar bulge.” In addition, although haloes seem ubiquitous, they are always of low luminosity and seem generally more extended than bulges. Bulges are not ubiquitous, as they are only found in earlier type galaxies, and cover a very wide range of luminosities. This is, in fact, clearly seen in the Hubble classification criteria from Sa to Sc types.

What is the evolutionary relationship, if any, between bulges and haloes? The Milky Way is an ideal case to study this because it has both bulge and halo. We noted above that the bulge is more metal-rich and possibly younger than the halo, contrary to the argument of Lee (1992). What of its dynamics?

In the Milky Way, the bulge stars do show significant net rotation (e.g. Ibata & Gilmore 1995b, Minniti et al 1995), but the very concentrated spatial distribution of these stars leads to low angular momentum orbits. Indeed, the angular momentum (per unit mass) distribution of the bulge is very similar to that of the stellar halo and very different from that of the disk (Wyse & Gilmore 1992, Ibata & Gilmore 1995b); see Figure 7. As discussed below, this is suggestive of the Eggen et al (1962) scenario, with the bulge as the central region of the

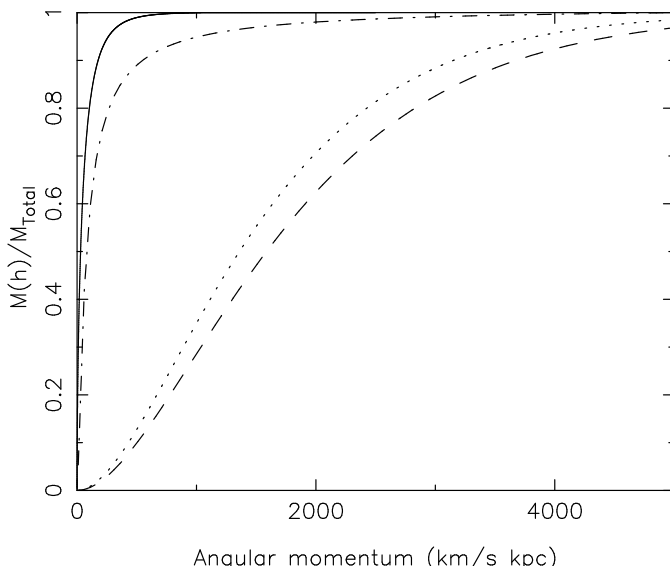


Figure 7 Cumulative distribution functions of specific angular momentum for the four major Galactic stellar populations. The solid curve is the distribution for the bulge, from Ibata & Gilmore (1995b). The other curves are taken from Wyse & Gilmore (1992): The dashed-dotted curve represents the halo, the dotted curve represents the thick disk, and the dashed curve represents the thin disk. It is clear that the halo and bulge are more like each other than they are like the disk components.

halo but formed with significantly more dissipation. Furthermore, the available estimates of the masses of the stellar halo and bulge give a ratio of $\sim 1:10$, which is (coincidentally?) about the ratio predicted by models in which the bulge is built up by gas loss from star-forming regions in the halo (e.g. Carney et al 1990, Wyse 1995). The real test of this model is determination of the *rate* of formation and chemical enrichment of the stars in each of the halo and bulge. This is feasible and only requires good data on element ratios (e.g. Wyse & Gilmore 1992).

5.2 Accretion/Merging

DESTRUCTION OF DISKS BY MERGERS The current paradigm of structure formation in the universe is the hierarchical clustering of dominant dissipationless dark matter; galaxies as we see them form by the dissipation of gas into the potential wells of the dark matter, with subsequent star formation (e.g. Silk & Wyse 1993). The first objects to collapse under self-gravity are the highest density perturbations on scales which are characteristic of dwarf galaxies,

and globular clusters, though globular clusters seem, on chemical evolution grounds, not to be the first objects to have formed. Large galaxies form by the merging of many smaller systems. The merging rate of the dissipationless dark haloes is reasonably straightforward to calculate (e.g. Lacey & Cole 1993). Unfortunately, many badly understood parameters are involved in the physics of gaseous heating/cooling and star formation, which determine how the baryonic components evolve. In the absence of understanding, the naive separation of different stellar components of galaxies is achieved by the following prescription (Baugh et al 1996, Kauffmann 1996): Star formation occurs in disks, which are destroyed during a merger with a significantly larger companion, with “significant” meaning a free parameter to be set by comparison with observations. In such a merger, all the extant “disk” stars are reassigned to the “bulge,” the cold gas present is assumed to be driven to the center and fuel a burst of star formation, and a new disk is assumed to grow through accretion of intergalactic gas. Ellipticals are simply bare bulges, which are more likely in environments that prevent the subsequent reaccretion of a new disk—environments such as clusters of galaxies (e.g. Gunn & Gott 1972). One consequence (see Kauffmann 1996) of this prescription is that late-type spirals, which have a large disk-to-bulge ratio, should have older bulges than do early-type spirals, since to have a larger disk the galaxy must have been undisturbed and able to accrete gas for a longer time. This does not appear compatible with the observations discussed above. Bulge formation is highly likely to be more complex than this simple prescription.

ACCRETION OF DENSE STELLAR SATELLITES The central regions of galaxies are obvious repositories of accreted systems, as they are the bottom of the local potential well, provided that the accreted systems are sufficiently dense to survive tidal disruption while sinking to the center (e.g. Tremaine et al 1975). Should the accreted systems be predominately gaseous, then the situation is simply that described by Eggen et al (1962), with the chemical evolution modified to include late continuing infall. [It is worth noting that late infall of gas narrows resulting chemical abundance distribution functions (e.g. Edmunds 1990), and at least the Milky Way bulge has an observed very broad distribution.] We now consider models of bulge formation by accretion of small stellar systems.

As discussed above, the mean metallicity of the Galactic bulge is now reasonably well established at $[Fe/H] \sim -0.3$ dex (McWilliam & Rich 1994, Ibata & Gilmore 1995b, McWilliam 1997), with a significant spread below -1 dex and above solar. Thus, satellite galaxies that could have contributed significantly to the bulge are restricted to those of high metallicity. Given the fairly well-established correlation between mean metallicity and galaxy luminosity/velocity dispersion (e.g. Bender et al 1993, Lee et al 1993, Zaritsky et al

1994), only galaxies of luminosity comparable to the bulge can have been responsible. That is, one is immediately forced to a degenerate model, in which most of the stellar population of the bulge was accreted in one or a few mergers of objects like the Magellanic Clouds or the *most* luminous dwarf spheroidals (dSph). Because the metallicity distribution of the bulge is very broad, significantly broader than that of the solar neighborhood, a compromise model is viable, in which only the metal-poor tail of the bulge abundance distribution function has been augmented by accretion of lower luminosity satellite galaxies. Quantification of this statement awaits more robust measurement of the tails of the bulge metallicity distribution function and of appropriate element ratios.

Limits on the fraction of the bulge that has been accreted can be derived from stellar population analyses, following the approach utilized by Unavane et al (1996) concerning the merger history of the Galactic halo.

The Sagittarius dSph galaxy was discovered (Ibata et al 1994) through spectroscopy of a sample of stars selected purely on the basis of color and magnitude to contain predominantly K giants in the Galactic bulge. After rejection of foreground dwarf stars, the radial velocities isolated the Sagittarius dwarf galaxy member stars from the foreground bulge giants. The technique (serendipity) used to discover the Sagittarius dSph allows a real comparison between its stellar population and that of the bulge. Not only the radial velocities distinguish the dwarf galaxy, but also its stellar population—as seen in Figure 8 (taken from Ibata et al 1994), *all* giant stars redder than $B_J - R \gtrsim 2.25$ have kinematics that place them in the low velocity-dispersion component, i.e. in the Sagittarius dwarf. This is a real quantifiable difference between the *bulge* field population and this, the most metal-rich of the Galactic satellite dSph galaxies.

Furthermore, the carbon star population of the bulge can be compared with those of typical extant satellites. In this case, there is a clear discrepancy between the bulge and the Magellanic Clouds and dSph (Azzopardi & Lequeux 1992), in that the bulge has a significantly lower frequency of carbon stars.

Thus, although accretion may have played a role in the evolution of the bulge of the Milky Way, satellite galaxies like those we see around us now cannot have dominated. However, accretion is the best explanation for at least one external bulge—that of the apparently normal Sb galaxy NGC 7331, which is counter-rotating with respect to its disk (Prada et al 1996). It should also be noted that for S0 galaxies—those disk galaxies that at least in some models have suffered the most merging—Kuijken et al (1996) have completed a survey for counter-rotating components in the disks and found that only 1% of S0 galaxies contain a significant population of counter-rotating disk stars. This is a surprisingly low fraction and suggests some caution prior to adopting late merger models as a common origin of early-type systems.

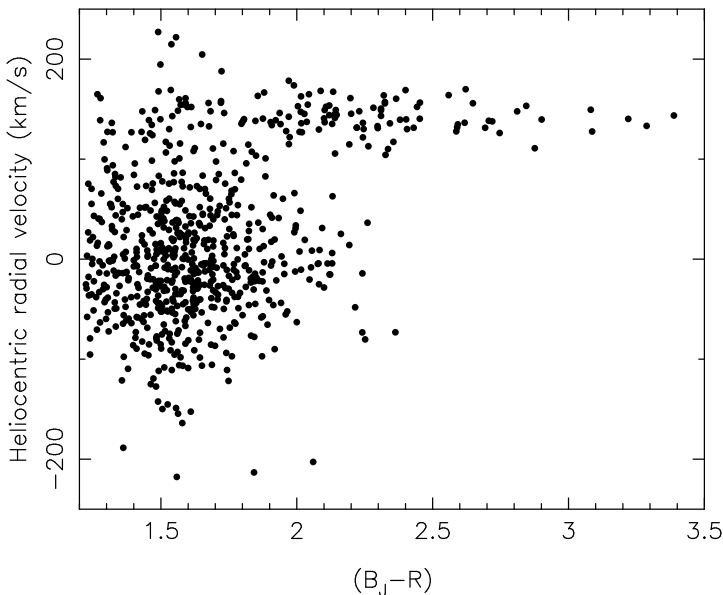


Figure 8 Heliocentric radial velocities of the sample of stars observed by Ibata et al (1994), towards $\ell = -5^\circ$, $b = -12^\circ$, -15° , and -20° . The stars with velocities less than about 120 km/s are predominately bulge K giants. Those with velocities between about 120 and 180 km/s are members of the Sagittarius (Sgr) dSph galaxy, which was discovered from this figure. Note the real difference between the color distributions of bulge and Sgr members. Thus, the bulge cannot be built up by merger of several galaxies like the Sgr dwarf.

5.3 Disk–Bars–Bulges, Etc

Recall that the broadband color distributions of disk galaxies show smooth continuity across the transition between disk and bulge. In the mean, there is approximate equality between the colors of the inner disk and the bulge in any one galaxy (de Jong 1996, Peletier & Balcells 1996). These data may be interpreted as showing similar mean age and metallicity for inner disk and bulge (de Jong 1996, Peletier & Balcells 1996), but the degeneracy of age and of metallicity on the colors of stellar populations cause uncertainties (see, for example, Peletier & Balcells 1996). Courteau et al (1996) find further that the scale lengths of disk and bulge are correlated. They argue that this relationship implies that the bulge formed via secular evolution of the disk. In principle this is possible if disks are bar-unstable and bars are themselves unstable, and if significant angular-momentum transport is feasible.

The secular evolution of collisionless stellar disks has been studied in some detail recently, in particular through three-dimensional N-body simulations (Combes et al 1990, Raha et al 1991; see Combes 1994 and Pfenniger 1993 for interesting reviews). These simulations demonstrated that not only are thin disks often unstable to bar formation, but bars themselves can be unstable, in particular to deformations out of the plane of the disk, perhaps leading to peanut-shaped bulges. The kinematics of stars in “peanut bulges” lend some observational support for the association of peanut bulges with bars (Kuijken & Merrifield 1995). Thus stars initially in the inner disk end up in the bulge, which provides a natural explanation for the continuity observed in the properties of the stellar populations in disks and in bulges.

Merritt & Sellwood (1994; see also Merrifield 1996) provided a detailed description of the physics of instabilities of stellar disks. They demonstrated that the buckling instability of the stellar bar that produces a peanut bulge (Combes et al 1990, Raha et al 1991) is a collective phenomenon, similar to a forced harmonic oscillator. Thus the instability involves the bar in general, not only stars on special resonant orbits, as had been earlier proposed (e.g. Combes et al 1990). Not all instabilities form peanuts, which is just as well for this class of model for bulge formation, because, although box/peanut bulges are perhaps fairly common, comprising 20% of galaxies (Shaw 1987), the subset of these that rotate on cylinders is small (e.g. Shaw 1993 and references therein). Relevant photometric studies show that the light in a peanut bulge is additional to that in a smooth underlying disk, not subtracted from it (e.g. Shaw et al 1990, Shaw 1993), which rather weakens the case for these models.

The extant simulations of bar instabilities also find that a very small mass concentration at the center of the galaxy can destroy a bar. Such a mass concentration is very likely, since inflow, driven by gravitational torques, is probable after a bar is formed. Hasan & Norman (1990) suggested that a sufficiently large central mass concentration could eventually destroy the bar. Norman et al (1996) used three-dimensional N-body simulations to follow the evolution of a bar-unstable disk galaxy and attempted to incorporate the effects of gas inflow by allowing the growth of a very centrally concentrated component. Indeed, in time the fraction of material in this central component is sufficient to destroy the bar, fattening it into a “bulge-like” component. Bulges may be built up by successive cycles of disk instability–bar formation–bar dissolution (Hasan et al 1993). The time scales and duty cycles are not clear. Some simulations (e.g. Friedli 1994) find that as little as 1% of the mass in a central component is sufficient to dissolve a bar. This is a potential problem, as Miller (1996) points out, since the fact that one observes bars in around 50% of disk galaxies means that bars cannot be too fragile. A numerical example supporting Miller’s

important point is provided by Dehnen (1996), who finds that his bar is stable even with a cuspy density profile in the underlying disk. The simulations are clearly not yet mature.

A further potential problem with the general applicability of this scenario of bulge formation is the different light profiles of bars in galaxies of different bulge-to-disk ratio—early-type disk galaxies have bars with flat surface density profiles (e.g. Noguchi 1996, Elmegreen et al 1996), whereas late-type galaxies have bars with steeper surface brightness profiles than their disks. The Courteau et al correlation, that bulge scale lengths are around one-eighth that of disks, was found for a sample of late-type galaxies. In this scenario, the color of a bar should also be the same color as its surrounding disk, so that the subsequent bulge is the same color as the disk. While colors of bars are complicated by dust lanes and associated star formation, barred structures are often identified by means of color maps (e.g. Quillen et al 1996), suggesting problems for this class of model.

Specific counter-examples to models where the bulge forms through secular evolution of the inner disk are the high-luminosity but low surface brightness disk galaxies, such as Malin 1 (McGaugh et al 1995), which have apparently “normal” bulges (e.g. surface brightnesses and scale lengths typical of galaxies with high surface brightness disks) that clearly could not have formed by a disk instability.

Dissipationless formation of bulges from disks suffers yet a further problem, in that the phase space density of bulges is too high (Ostriker 1990, Wyse 1997). This also manifests itself in the fact that the spatial densities of bulges are higher than those of inner disks. Thus one must appeal to dissipational processes to form bulges, such as gas flows. The presence of color gradients in some external bulges would support a dissipative collapse with accompanying star formation (e.g. Balcells & Peletier 1994). Indeed, Kormendy (1993) has argued that many bulges are actually inner extensions of disks, formed through gas inflow from the disk, with later *in situ* star formation. This complicates the interpretation of the similarity between the colors of bulges and inner disks, which was a natural product of a stellar instability to form bulges from disk stars. One should note also that should bulges indeed not be formed at high redshift, then dissipation is also implicated in the production of the high spatial densities of their central regions.

It is also important to note that the term bar is used no less generically than is the term bulge. There is a fundamental, and rarely clarified, difference between a detectable perturbation to the luminosity distribution and a substantial $m = 2$ perturbation to the galactic gravitational potential. Inspection of the delightful pictures in the *Carnegie Atlas of Galaxies* (Sandage & Bedke 1994) suggests a continuum of structures, with all degrees of symmetry and asymmetry (i.e. $m =$

1, 2, . . .) and relative amplitudes. When is a bar fundamentally more than the region where spiral arms meet the center? More important for the continuing debate about the center of the Milky Way, is it true that all these structures are seen in the cold disks only? Is there such a thing as a bar-bulge?

6. CONCLUSIONS

In the Local Group, all spiral galaxies, and probably all disk galaxies, have an old metal-poor spatially extended stellar population that we define to be a stellar halo. These seem to be the first stars formed in what would later become the galactic potential, though the possibility of later accretion of a *minor* fraction remains viable. The bulges of Local Group spiral galaxies are more diverse in properties, ranging from the very luminous, intermediate metallicity and very spatially extended bulge of M 31 through the intermediate luminosity, centrally concentrated bulge of the Milky Way, to no firm detection of a bulge in M 33.

In general, well-studied bulges are reasonably old, have a near-solar mean abundance, though with a very wide abundance distribution function, which is of importance, and are consistent with isotropic oblate rotator models for their kinematics, in which the basic support is provided by random motions and the flattening is consistent with additional rotational effects. Given these properties, bulges are most simply seen as the more dissipated descendants of their haloes.

However, diversity is apparent. All bulges of disk galaxies are not old, super-metal-rich, and simply small elliptical galaxies. This is not to say that such systems do not exist, but rather that bulges are heterogeneous. Higher luminosity bulges seem to have a closer affinity to ellipticals, whereas lower luminosity bulges prefer disks. But even this statement does not apply to all the properties of the stellar populations of bulges.

This diversity, together with the surprisingly limited database available concerning the photometric, structural, and kinematic properties of bulges, precludes firm conclusions. Much new and much needed data are about to become available, with the advent of 6- to 10-m class telescopes, with their exceptionally efficient spectrographs, and wide field array imaging systems on smaller telescopes. It will be interesting to see if the next review on bulges will be entitled “Disks and Ellipticals.”

ACKNOWLEDGMENTS

RFGW and GG thank the North Atlantic Treaty Organization for a collaborative grant. RFGW acknowledges the support of the NASA Astrophysics Theory Program and the Seaver Institution, and she thanks the UC Berkeley Astronomy Department and Center for Particle Astrophysics, and the Institute

of Astronomy, Cambridge, for hospitality during some of the writing of this review.

Visit the *Annual Reviews* home page at
<http://www.annurev.org>.

Literature Cited

- Ajhar A, Grillmair C, Lauer T, Baum W, Faber S, et al. 1996. *Astron. J.* 111:1110–27
- Alard C. 1996. PhD thesis. Univ. Paris VI
- Andredakis YC, Peletier RF, Balcells M. 1995. *MNRAS* 275:874–88
- Armandroff T. 1989. *Astron. J.* 97:375–89
- Ashman K, Bird C. 1993. *Astron. J.* 106:2281–90
- Azzopardi M, Lequeux J. 1992. In *The Stellar Populations of Galaxies*, IAU Symp. 149, ed. B Barbuy, A Renzini, pp. 201–6. Dordrecht: Kluwer
- Azzopardi M, Lequeux J, Rebeirot E. 1988. *Astron. Astrophys.* 202:L27–L29
- Baade W. 1944. *Ap. J.* 100:137–46
- Bacon R, Emsellem E, Monnet G, Nieto J-L. 1994. *Astron. Astrophys.* 281:691–717
- Balcells M, Peletier R. 1994. *Astron. J.* 107:135–52
- Barnes J, Hernquist L. 1992. *Annu. Rev. Astron. Astrophys.* 30:705–42
- Battistini P, Bonoli F, Casavecchia M, Ciotti L, Frederici L, Fusi-Pecci F. 1993. *Astron. Astrophys.* 272:77–97
- Baugh CM, Cole S, Frenk CS. 1996. *MNRAS* 283:1361–78
- Bender R, Burstein D, Faber S. 1993. *Ap. J.* 411:153–69
- Bender R, Doeberleiner S, Moellenhoff C. 1988. *Astron. Astrophys. Suppl.* 74:385–426
- Bertelli G, Bressan N, Chiosi C, Fogatto F, Nasi E. 1994. *Astron. Astrophys. Suppl.* 106:275–302
- Binney J, Gerhard O, Spergel D. 1997. *MNRAS* In press
- Binney JJ, Gerhard O, Stark AA, Bally J, Uchida KI. 1991. *MNRAS* 252:210–18
- Bissantz N, Englmaier P, Binney J, Gerhard O. 1997. *MNRAS* In press
- Blanco V, Tendrup D. 1989. *Astron. J.* 98:843–52
- Blitz L, Binney J, Lo KY, Bally J, Ho PTP. 1993. *Nature* 361:417–24
- Blitz L, Spergel DN. 1991. *Ap. J.* 379:631–38
- Blitz L, Teuben P, eds. 1996. In *Unsolved Problems of the Milky Way*, IAU Symp. 169. Dordrecht: Kluwer
- Bothun G. 1992. *Astron. J.* 103:104–9
- Bottema R. 1993. *Astron. Astrophys.* 275:16–36
- Burton W, Hartmann D, West S. 1996. See Blitz & Teuben 1996, pp. 447–68
- Buta R, Elmegreen BG, Crocker DA, eds. 1996. *Barred Galaxies, IAU Colloq. 157, ASP Conf. Ser. 91*. San Francisco: Astron. Soc. Pac.
- Carney B, Latham D, Laird J. 1990. In *Bulges of Galaxies*, ed. B Jarvis, D Tendrup, pp. 127–35. Garching: Eur. Space Obs.
- Catchpole R, Whitelock P, Glass I. 1990. *MNRAS* 247:479–90
- Christian C. 1993. See Smith & Brodie 1993, pp. 448–57
- Combes F. 1991. *Annu. Rev. Astron. Astrophys.* 29:195–238
- Combes F. 1994. In *The Formation and Evolution of Galaxies*, ed. C Munoz-Turon, F Sanchez, pp. 317–98. Cambridge: Cambridge Univ. Press
- Combes F, Debbasch F, Friedli D, Pfenniger D. 1990. *Astron. Astrophys.* 233:82–95
- Courteau S, de Jong R, Broeils A. 1996. *Ap. J. Lett.* 457:L73–L76
- Crotts A. 1986. *Astron. J.* 92:292–301
- Davies RL, Efstathiou GP, Fall SM, Illingworth G, Schechter P. 1983. *Ap. J.* 266:41–57
- Dehnen M. 1996. In *New Light on Galaxy Evolution*, ed. R Bender, RL Davies, p. 359. Dordrecht: Kluwer
- de Jong R. 1995. PhD thesis. Univ. Groningen
- de Jong R. 1996. *Astron. Astrophys.* 313:45–64
- Dejonghe H, Habing H, eds. 1993. In *Galactic Bulges, IAU Symp. 153*. Dordrecht: Kluwer
- de Vaucouleurs G, Pence W. 1978. *Astron. J.* 83:1163–74
- de Zeeuw PT. 1995. See van der Kruit & Gilmore 1995, pp. 215–26
- de Zeeuw PT, Franx M. 1991. *Annu. Rev. Astron. Astrophys.* 29:239–74
- Edmunds M. 1990. *MNRAS* 246:678–87
- Edvardsson B, Andersen J, Gustafsson B, Lambert DL, Nissen P, Tomkin J. 1993. *Astron. Astrophys.* 275:101–52
- Eggen O, Lynden-Bell D, Sandage A. 1962. *Ap. J.* 136:748–66
- Elmegreen B, Elmegreen D, Chromey F, Haselbacher D, Bissell B. 1996. *Astron. J.* 111:2233–37
- Elson R, Gilmore G, Santiago B. 1997. *MNRAS* In press

- Emsellem E, Bacon R, Monnet G, Poulain P. 1996. *Astron. Astrophys.* 312:777–96
- Faber SM. 1973. *Ap. J.* 179:731–54
- Faber SM, Trager S, Gonzalez J, Worthey G. 1995. See van der Kruit & Gilmore 1995, pp. 249–58
- Faber SM, Tremaine S, Ajhar EA, Byun Y-I, Burstein D, et al. 1997. *Ap. J.* In press
- Franx M. 1993. See Dejonghe & Habing 1993, pp. 243–62
- Franx M, Illingworth G. 1988. *Ap. J.* 327:L55–L59
- Freeman KC. 1993. See Smith & Brodie 1993, pp. 27–38
- Friedli D. 1994. In *Mass Transfer Induced Activity in Galaxies*, ed. I Shlosman, pp. 268–73. Cambridge: Cambridge Univ. Press
- Friedli D, Wozniak H, Rieke M, Martinet L, Bratschi P. 1996. *Astron. Astrophys. Suppl.* 118:461–79
- Friel E. 1995. *Annu. Rev. Astron. Astrophys.* 33:381–414
- Frogel J. 1988. *Annu. Rev. Astron. Astrophys.* 26:51–92
- Fusi-Peccia F, Cacciari C, Federici L, Pasquali A. 1993. See Smith & Brodie 1993, pp. 410–19
- Genzel R, Thatte N, Krabbe A, Kroker H, Tacconi-Garman L. 1996. *Ap. J.* 472:153–72
- Gerhard OE. 1988. *MNRAS* 232:P13–P20
- Gerhard OE, Vietri M. 1986. *MNRAS* 223:377–89
- Giavalisco M, Macchetto D, Madau P, Sparks B. 1995. *Ap. J. Lett.* 441:L13–L16
- Giavalisco M, Steidel C, Macchetto D. 1996. *Ap. J.* 470:189–94
- Gott JR. 1977. *Annu. Rev. Astron. Astrophys.* 15:235–66
- Gredel R, ed. 1996. *The Galactic Center. ASP Conf. Ser.*, Vol. 102
- Gunn J, Gott JR. 1972. *Ap. J.* 176:1–20
- Harmon R, Gilmore G. 1988. *MNRAS* 235:1025–47
- Harris W. 1991. *Annu. Rev. Astron. Astrophys.* 29:543–80
- Hasan H, Norman C. 1990. *Ap. J.* 361:69–77
- Hasan H, Pfenniger D, Norman C. 1993. *Ap. J.* 409:91–109
- Holland S, Fahlman G, Richer HB. 1996. *Astron. J.* 112:1035–45
- Holtzman JA, Light RM, Baum WA, Worthey G, Faber SM, et al. 1993. *Astron. J.* 106:1826–38
- Houck J. 1996. *PASP* 108:828
- Huchra J. 1993. See Smith & Brodie 1993, pp. 420–31
- Huchra J, Kent S, Brodie J. 1991. *Ap. J.* 370:495–504
- Hughes SA, Wood P, Reid IN. 1991. *Astron. J.* 101:1304–23
- Ibata R, Gilmore G. 1995a. *MNRAS* 275:591–604
- Ibata R, Gilmore G. 1995b. *MNRAS* 275:605–27
- Ibata R, Gilmore G, Irwin M. 1994. *Nature* 370:194–96
- Izumiura H, Deguchi S, Hashimoto O, Nakada Y, Onaka T, et al. 1995. *Ap. J.* 453:837–63
- Jablonka P, Martin P, Arimoto N. 1996. *Astron. J.* 112:1415–22
- Kauffmann G. 1996. *MNRAS* 281:487–92
- Kent S, Dame TM, Fazio G. 1991. *Ap. J.* 378:131–38
- Kinman T, Suntzeff N, Kraft R. 1994. *Astron. J.* 108:1722–72
- Kinman T, Wirtanen CA, Janes K. 1966. *Ap. J. Suppl.* 13:379–409
- Kiraga M, Paczynski B, Stanek K. 1997. Preprint
- Kormendy J. 1993. See Dejonghe & Habing 1993, pp. 209–30
- Kormendy J, Bender R. 1996. *Ap. J. Lett.* 464:L119–22
- Kormendy J, Djorgovski S. 1989. *Annu. Rev. Astron. Astrophys.* 27:235–78
- Kormendy J, Illingworth G. 1982. *Ap. J.* 256:460–80
- Kuijken K, Fisher D, Merrifield M. 1996. *MNRAS* 283:543–50
- Kuijken K, Merrifield M. 1995. *Ap. J. Lett.* 443:L13–L16
- Lacey C, Cole S. 1993. *MNRAS* 262:627–49
- Larsen J, Humphreys R. 1994. *Ap. J. Lett.* 436:L149–52
- Lee MG, Freedman W, Mateo M, Thompson I, Rath M, Ruiz M-T. 1993. *Astron. J.* 106:1420–62
- Lee Y-W. 1992. *Astron. J.* 104:1780–89
- Lee Y-W. 1993. See Smith & Brodie 1993, pp. 142–55
- Lewis J, Freeman KC. 1989. *Astron. J.* 97:139–62
- Lilly S, Tresse L, Hammer F, Crampton D, Le Fevre O. 1995. *Ap. J.* 455:108–24
- Liszt H, Burton WB. 1996. See Blitz & Teuben 1996, pp. 297–310
- Madsen C, Laustsen S. 1986. *ESO Messenger* 46:12
- McElroy D. 1983. *Ap. J.* 270:485–506
- McGaugh S, Schombert J, Bothun G. 1995. *Astron. J.* 109:2019–34
- McLean I, Liu T. 1996. *Ap. J.* 456:499–503
- McWilliam A. 1997. *Annu. Rev. Astron. Astrophys.* 35:503–56
- McWilliam A, Rich M. 1994. *Ap. J. Suppl.* 91:749–91
- Merrifield M. 1996. See Buta et al 1996, pp. 179–87
- Merritt D, Sellwood J. 1994. *Ap. J.* 425:551–67
- Mighell K, Rich RM. 1995. *Astron. J.* 110:1649–64
- Mihos JC, Hernquist L. 1994. *Ap. J.* 425:L13–L16

- Miller RH. 1996. See Buta et al 1996, pp. 569–74
- Minniti D. 1996. *Ap. J.* 459:175–80
- Minniti D, Olszewski E, Liebert J, White SDM, Hill JM, Irwin M. 1995. *MNRAS* 277:1293–311
- Minniti D, Olszewski E, Rieke M. 1993. *Ap. J. Lett.* 410:L79–L82
- Morris PW, Reid IN, Griffiths W, Penny AJ. 1994. *MNRAS* 271:852–74
- Morrison H. 1993. *Astron. J.* 106:578–90
- Morrison H, Harding P. 1993. See Dejonghe & Habing 1993, pp. 297–98
- Mould JR, Kristian J. 1986. *Ap. J.* 305:591–99
- Noguchi K. 1996. See Buta et al 1996, pp. 339–48
- Norman C, Sellwood J, Hasan H. 1996. *Ap. J.* 462:114–24
- Oort J, Plaut L. 1975. *Astron. Astrophys.* 41:71–86
- Ortolani S, Renzini A, Gilmozzi R, Marconi G, Barbay B, et al. 1995. *Nature* 377:701–4
- Ostriker JP. 1990. In *Evolution of the Universe of Galaxies*, *ASP Conf. Ser.*, ed. R Kron, 10:25. San Francisco: Astron. Soc. Pac.
- Paczynski B, Stanek KZ, Udalski A, Szymanski M, Kaluzny J, et al. 1994a. *Astron. J.* 107:2060–66
- Paczynski B, Stanek KZ, Udalski A, Szymanski M, Kaluzny J, et al. 1994b. *Ap. J. Lett.* 435:L113–16
- Peebles PJE. 1989. In *The Epoch of Galaxy Formation*, ed. CS Frenk, R Ellis, T Shanks, A Heavens, J Peacock, pp. 1–14. Dordrecht: Kluwer
- Peletier R, Balcells M. 1996. *Astron. J.* 111:2238–42
- Perault M, Omont A, Simon G, Seguin P, Ojha D, Blommaert J, et al. 1996. *Astron. Astrophys.* 315:L165–68
- Pfenniger D. 1993. See Dejonghe & Habing 1993, pp. 387–90
- Phillips A, Illingworth G, Mackenty J, Franx M. 1996. *Astron. J.* 111:1566–74
- Prada F, Gutierrez CM, Peletier RF, McKeith CD. 1996. *Ap. J. Lett.* 463:L9–L12
- Pritchett CJ. 1988. In *The Extragalactic Distance Scale*, *ASP Conf. Ser.*, ed. C Pritchett, S van den Bergh, 4:59–68. San Francisco: Astron. Soc. Pac.
- Pritchett CJ, van den Bergh S. 1987. *Ap. J.* 316:517–29
- Pritchett CJ, van den Bergh S. 1988. *Ap. J.* 331:135–44
- Pritchett CJ, van den Bergh S. 1996. See Blitz & Teuben 1996, pp. 39–46
- Quillen A, Ramirez S, Frogel J. 1996. *Ap. J.* 470:790–96
- Raha A, Sellwood J, James R, Kahn FD. 1991. *Nature* 352:411–12
- Regan M, Vogel S. 1994. *Ap. J.* 434:536–45
- Renzini A. 1995. See van der Kruit & Gilmore 1995, pp. 325–36
- Rich RM. 1988. *Astron. J.* 95:828–65
- Rich RM. 1990. *Ap. J.* 362:604–19
- Rich RM, Michell K. 1995. *Ap. J.* 439:145–54
- Rich RM, Michell K, Freedman W, Neill J. 1996. *Astron. J.* 111:768–76
- Richer HB, Harris WE, Fahlman GG, Bell RA, Bond HE, et al. 1996. *Ap. J.* 463:602–8
- Rix H-W, White SDM. 1990. *Ap. J.* 362:52–58
- Ryan S, Norris J. 1991. *Astron. J.* 101:1865–79
- Sadler E, Rich RM, Terndrup D. 1996. *Astron. J.* 112:171–85
- Sandage A. 1986. *Annu. Rev. Astron. Astrophys.* 24:421–58
- Sandage A, Bedke J. 1994. *The Carnegie Atlas of Galaxies*. Carnegie Inst. Wash. Publ. 638. 750 pp.
- Santiago B, Elson R, Gilmore G. 1996. *MNRAS* 281:1363–74
- Schade D, Lilly S, Crampton D, Hammer F, Lefevre O, Tresse L. 1995. *Ap. J. Lett.* 451:L1–L4
- Schade D, Lilly S, Lefevre O, Hammer F, Crampton D. 1996. *Ap. J.* 464:79–91
- Schmidt A, Bica E, Alloin D. 1990. *MNRAS* 243:620–28
- Schommer RA. 1993. See Smith & Brodie 1993, pp. 458–68
- Schommer RA, Cristian C, Caldwell N, Bothun G, Huchra J. 1991. *Astron. J.* 101:873–83
- Schweizer F. 1990. In *Dynamics and Interactions of Galaxies*, ed. R Wielen, pp. 60–71. Berlin: Springer-Verlag
- Shaw M. 1987. *MNRAS* 229:691–706
- Shaw M. 1993. *MNRAS* 261:718–52
- Shaw M, Axon D, Probst R, Gately I. 1995. *MNRAS* 274:369–87
- Shaw M, Dettmar R, Bartledress A. 1990. *Astrophys. J.* 240:36–51
- Silk J, Wyse RFG. 1993. *Phys. Rep.* 231:293–67
- Smith G, Brodie J, eds. 1993. In *The Globular Cluster – Galaxy Connection*. San Francisco: Astron. Soc. Pac.
- Sofue Y, Yoshida S, Aoki T, Soyano T, Tarusawa K, et al. 1994. *PASJ* 46:1–7
- Stark AA. 1977. *Ap. J.* 213:368–73
- Stark AA, Binney J. 1994. *Ap. J. Lett.* 426:L31–L33
- Steidel C, Giavalisco M, Dickinson M, Adelberger KL. 1996a. *Astron. J.* 112:352–58
- Steidel C, Giavalisco M, Pettini M, Dickinson M, Adelberger KL. 1996b. *Ap. J. Lett.* 462:L17–L21
- Tinsley BM. 1980. *Fundam. Cosmic Phys.* 5:287–388
- Toomre A. 1977. In *The Evolution of Galaxies and Stellar Populations*, ed. RB Larson, B

- Tinsley, pp. 401–416. New Haven: Yale Univ. Obs.
- Tremaine S. 1995. *Astron. J.* 110:628–34
- Tremaine S., Henon M., Lynden-Bell D. 1986. *MNRAS* 219:285–97
- Tremaine SD, Ostriker JP, Spitzer L. 1975. *Ap. J.* 196:407–11
- Unavane M., Wyse RFG, Gilmore G. 1996. *MNRAS* 278:727–36
- van Albada T. 1982. *MNRAS* 201:939–55
- van den Bergh S. 1991a. *PASP* 103:609–22
- van den Bergh S. 1991b. *PASP* 103:1053–68
- van der Kruit, Gilmore G, eds. 1995. *Stellar Populations, IAU Symp. 164*. Dordrecht: Kluwer
- van Dokkum PG, Franx M. 1996. *MNRAS* 281:985–1000
- Walterbos R, Kennicutt R. 1988. *Astron. Astrophys.* 98:61–86
- Weiland JL, Arendt RG, Berriman GB, Dwek E, Freudenreich HT, et al. 1994. *Ap. J.* 425:L81–L84
- Westerlund B, Lequeux J, Azzopardi M, Rebeiro E. 1991. *Astron. Astrophys.* 244:367–72
- Whitford A. 1978. *Ap. J.* 226:777–89
- Whitford A. 1986. *Annu. Rev. Astron. Astrophys.* 24:1–22
- Whitmore BC, Schweizer F, Leitherer C, Borne K, Robert C. 1993. *Astron. J.* 106:1354–70
- Wyse RFG. 1995. See van der Kruit & Gilmore 1995, pp. 133–50
- Wyse RFG. 1997. Preprint
- Wyse RFG, Gilmore G. 1988. *Astron. J.* 95: 1404–14
- Wyse RFG, Gilmore G. 1989. *Comments Astrophys.* 8:135–44
- Wyse RFG, Gilmore G. 1992. *Astron. J.* 104:144–53
- Wyse RFG, Gilmore G. 1995. *Astron. J.* 110:2771–87
- Zaritsky D, Kennicutt R, Huchra J. 1994. *Ap. J.* 420:87–109
- Zhao H, Spergel DN, Rich RM. 1994. *Astron. J.* 108:2154–63



CONTENTS

A PHYSICIST COURTS ASTRONOMY, <i>Charles H. Townes</i>	xiii
ETA CARINAE AND ITS ENVIRONMENT, <i>Kris Davidson and Roberta M. Humphreys</i>	1
THE SUN'S VARIABLE RADIATION AND ITS RELEVANCE FOR EARTH, <i>Judith Lean</i>	33
LUMINOUS SUPERSOFT X-RAY SOURCES, <i>P. Kahabka and E. P. J. van den Heuvel</i>	69
OBSERVATIONAL SELECTION BIAS AFFECTING THE DETERMINATION OF THE EXTRAGALACTIC DISTANCE SCALE, <i>P. Teerikorpi</i>	101
MODEL ATMOSPHERES OF VERY LOW MASS STARS AND BROWN DWARFS, <i>France Allard, Peter H. Hauschildt, David R. Alexander, and Sumner Starrfield</i>	137
DENSE PHOTODISSOCIATION REGIONS (PDRs), <i>D. J. Hollenbach and A. G. G. M. Tielens</i>	179
HIGH-VELOCITY CLOUDS, <i>B. P. Wakker and H. van Woerden</i>	217
LOW SURFACE BRIGHTNESS GALAXIES, <i>Chris Impey and Greg Bothun</i>	267
OPTICAL SPECTRA OF SUPERNOVAE, <i>Alexei V. Filippenko</i>	309
COMPACT GROUPS OF GALAXIES, <i>Paul Hickson</i>	357
FAINT BLUE GALAXIES, <i>Richard S. Ellis</i>	389
VARIABILITY OF ACTIVE GALACTIC NUCLEI, <i>Marie-Helene Ulrich, Laura Maraschi, and C. Megan Urry</i>	445
ABUNDANCE RATIOS AND GALACTIC CHEMICAL EVOLUTION, <i>Andrew McWilliam</i>	503
MIXING IN STARS, <i>M. Pinsonneault</i>	557
PARSEC-SCALE JETS IN EXTRAGALACTIC RADIO SOURCES, <i>J. Anton Zensus</i>	607
GALACTIC BULGES, <i>Rosemary F. G. Wyse, Gerard Gilmore, and Marijn Franx</i>	637

(continued)

vii

INDEXES

Subject Index	677
Cumulative Index of Contributing Authors, Volumes 25–35	691
Cumulative Index of Chapter Titles, Volumes 25–35	694

Formation and Properties of Persisting Stellar Bars

F. Combes¹ and R. H. Sanders²

¹ Ecole Normale Supérieure (ERA 762), Paris et Observatoire de Paris-Meudon, F-92190 Meudon, France

² Kapteyn Laboratory, Groningen, The Netherlands

Received February 21, accepted July 22, 1980

Summary. Long time-scale three dimensional N -body simulations of galaxies composed of two components, a self-consistent disk and a spheroidal halo, demonstrate that bars develop over a large range of halo mass to disk mass ratio (M_h/M_d). Such non axisymmetric systems dynamically evolve at a rate which depends upon M_h/M_d . For systems with low mass haloes ($M_h/M_d \leq 1$), strong bars quickly form but then weaken to a quasi steady state in less than twenty rotation times. For systems with high halo mass, the bar strength is still increasing after 20 rotation times. This suggests that the strong bars observed in SBb galaxies have not persisted since the epoch of galaxy formation but have developed more recently in systems with $M_h/M_d \geq 2$.

Key words: galactic structure – star – stellar dynamics

I. Introduction

The presence of barred structure seems to be a very general attribute of disk galaxies. Perhaps half of all spirals should be classified as barred or intermediate barred (de Vaucouleurs, 1963). This high frequency of occurrence and the fact that bars (at least in early-type systems) consist of an old stellar population, suggest that bars are long-lived and fundamental components of the mass distributions of disk systems. Moreover, there is evidence that some galaxies contain bars which represent very strong deviations from axial symmetry. This conclusion is based on a comparison of gas dynamical calculations with the observed gas distributions and motions in SBb systems (Sanders and Tubbs, 1980). These calculations imply that the bars in such galaxies have the following characteristics:

1. they are strong, with the maximum tangential force exceeding 30% of the local axisymmetric force.
2. they cannot be represented by a single $m=2$ distortion of a disk. Higher order harmonics must be present in a Fourier expansion of mass or potential distribution.
3. the overall mass distribution must be centrally condensed with present respect to the bar. The bar extends beyond the peak in the rotation curve of an axially symmetrized mass distribution.
4. such bars must be rotating rather rapidly, with corotation at a radius which is not more than twice the radius of the maximum tangential force due to the bar.

Numerical and analytical calculations during the past decade have established that cold self-gravitating disks are unstable to the formation of bars (Hohl and Hockney, 1969; Miller et al.,

1970; Kalnajs, 1972; James and Sellwood, 1978). Bars generated in numerical experiments form in one or two rotation times but then seem to weaken over several additional rotation times (see Hohl, 1975), i.e. there is a suggestion of continuing dynamical evolution of these non-axisymmetric systems in a time scale longer than a rotation or dynamical time scale. Indeed, recent 3 D calculations by Hohl and Zang (1979) demonstrate very clearly that systems with bars are continuing to dynamically evolve after five rotation times. Therefore it is reasonable to ask how strong bars evolve in disk systems.

It is well known that the presence of a hot spheroidal halo affects the overall stability of the disk against bar forming modes (Ostriker and Peebles, 1973). This suggests that the presence of a halo would have significant influence on the growth and evolution of bars. We investigate this possibility in the present paper by means of numerical N -body calculations. We follow the time evolution of several disk systems embedded in rigid haloes. The free parameter in these calculations is the halo mass to disk mass ratio. The essential difference between the present and previous numerical calculations is the length of time over which galactic evolution is followed. In four cases we numerically follow the evolution for 20 rotation time scales or about $5 \cdot 10^9$ yr. This is done because the essential question which we investigate is the influence of the halo on the long-term evolution of the bar phenomenon. In addition we determine the dynamical characteristics of long-lived bars (strength, angular velocity, degree of central concentration, presence of resonances), and we compare these results with the models required to excite the observed gas response in SBb galaxies (Sanders and Tubbs, 1980).

II. The Physical Model

Galactic disks embedded in spherical haloes are simulated by three-dimensional (3 D) N -body calculations. The model galaxy is composed of two components: a three dimensional disk of 16,000 mass points, representing the flattened star population, and a spherically symmetric and more centrally concentrated rigid component representing a bulge-halo. Initially, both disk and halo have a potential of the form (cf. Toomre, 1963):

$$\phi = \phi_0 (1 + r^2/a^2)^{-1/2} \quad (1)$$

where a is the radial scale length of a given component (a_d and a_h for disk and halo respectively). Therefore, there are two dimensionless free parameters in our model, the ratios of radial scale lengths and the ratio of disk to halo masses: a_h/a_d and M_h/M_d . In the present calculations, only the mass ratio is varied. Below we consider the initial properties of the disk and halo:

Send offprint requests to: F. Combes (Meudon)

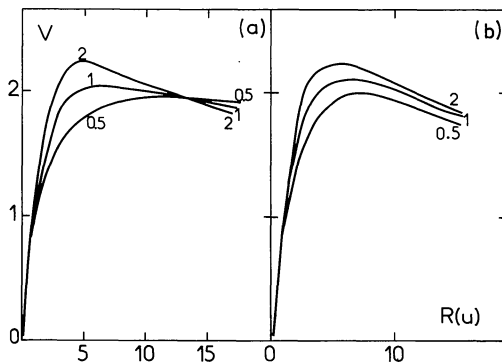


Fig. 1. Initial rotation curves for three of the simulated models. Curves are labelled by the halo-to-disk mass ratio. The actual initial rotation curves b), are very similar to the theoretical curves a), the difference comes mainly from the truncation of the disk. The unit of length may be taken as 1 kpc, so that the velocity unit is 100 km s^{-1}

Disk Component

Particles in the disk are randomly distributed such that their surface density follows the radial law of a truncated Toomre disk,

$$\mu = \mu_0 (1 + r^2/a_d^2)^{-3/2} \quad r < r_d \quad (2)$$

where r_d is the maximum radius of the disk. The surface density at the origin μ_0 , is determined by fixing the total mass M_d of the disk inside the radius r_d . The distribution in the z -direction has the following dependence at each radius r :

$$\varrho(r, z) = \varrho(r, 0) \operatorname{sech}^2(z/h(r)) \quad (3)$$

where $h(r)$ is the scale height in the z -direction

$$h(r) = h_0 (1 - r^2/r_d^2)^{1/2}. \quad (4)$$

The scale height in the central region h_0 is typically 1 kpc or $0.06 r_d$. The Z distribution is truncated at the limits of the grid and is normalized according to the radial distribution of the surface density (Eq. 2). This z -exponential law corresponds to the equilibrium distribution of a one dimensional plane parallel system (cf. Spitzer, 1968).

Initially, particles are given a systematic tangential velocity. There are no radial or z -velocities and the tangential velocity dispersion is zero; therefore, the disk is completely cold in the sense of Ostriker and Peebles (1973). The actual initial rotation curve for the ensemble of particles which is computed by the model is not very different from that of the untruncated Toomre disk (Fig. 1). The discrepancy is due primarily to the truncation of the disk and to a lesser extent to a non-Newtonian force law at distances less than about one or two cell-lengths. When M_h/M_d is high, these two effects are smeared out by the presence of the halo, whose potential is computed exactly and which is not truncated.

In a few test runs the particles were given an initial random motion sufficient to prevent local axisymmetric instabilities (Toomre, 1964). After one or two dynamical times the behavior of those initially warm systems was identical to the initially completely cold systems, due to the overwhelming importance of non-axisymmetric modes in relaxing the systems.

Any choice of initial conditions for the disk is, of course, arbitrary; however, since galactic disks presumably form by dis-

sipationnal collapse of a gas cloud with high specific angular momentum (cf. Eggen et al., 1962), it is expected that disks may initially be rather cold.

Halo

This is the spherical and centrally condensed rigid potential included to stabilize or partially stabilize, the disk. The stabilizing effect is the same when this halo-component is made self-consistent, as shown by Hohl (1978). The potential of the halo [cf. Eq. (1)], is normalized such that the halo mass interior to the radius r_d is M_h . The quantity M_h/M_d is the ratio of halo to disk mass inside the same radius r_d .

The chosen halo potential (1) leads to a density distribution:

$$\varrho_h(r) = \varrho_0 (1 + r^2/a_h^2)^{-5/2}.$$

The ratio of halo to disk length scales (a_h/a_d) is chosen to be 0.25 and is not varied. This assumes that the halo should be identified with the observed bulges in spiral galaxies (the halo is the extension of the bulge) and therefore, this spheroidal component is distinct from proposed massive extensive haloes providing flat rotation curves at large radii (Ostriker et al., 1974). Such extensive haloes would have little dynamical effect in the inner regions of the galaxies considered here.

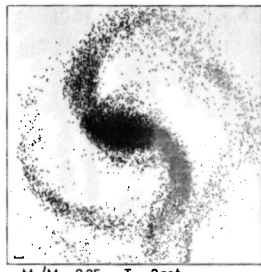
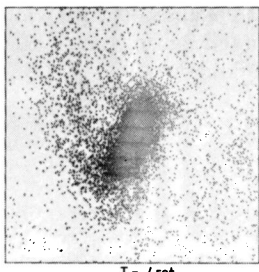
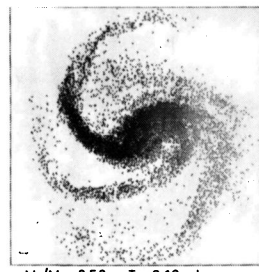
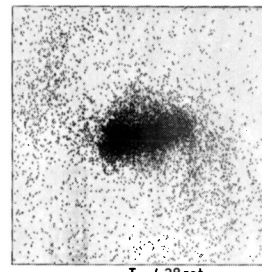
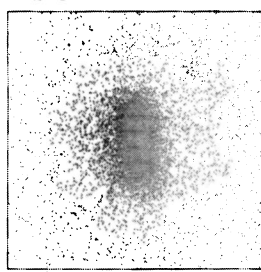
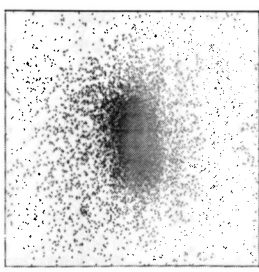
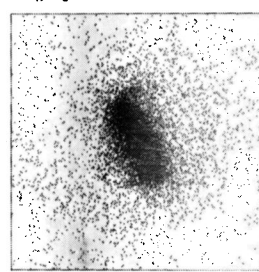
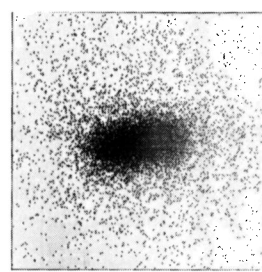
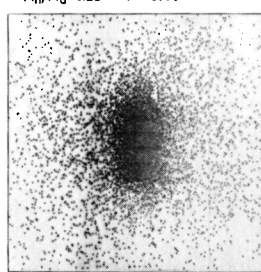
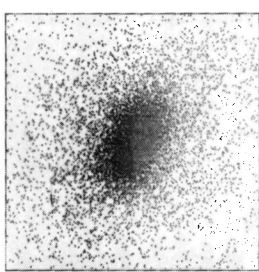
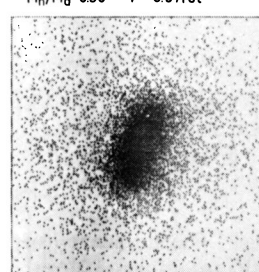
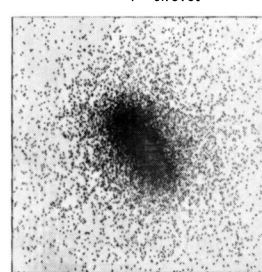
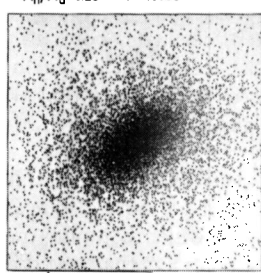
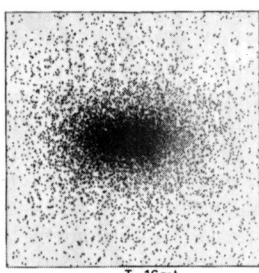
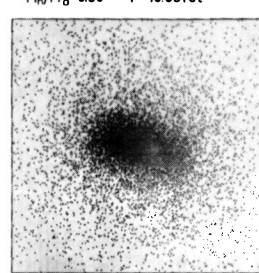
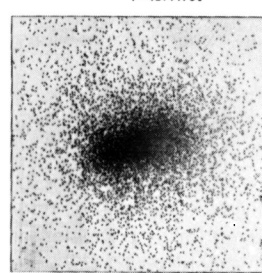
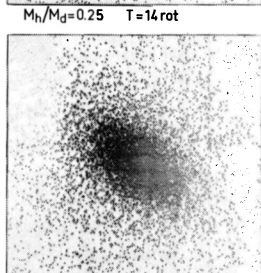
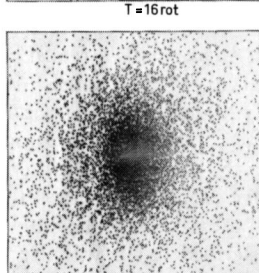
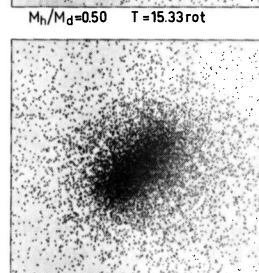
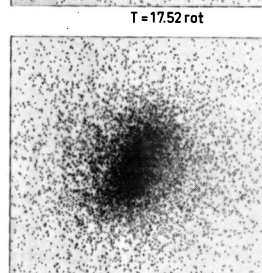
III. Technique

In our 3 D N -body calculations, the gravitational potential is obtained by the rapid Fourier transform method (see e.g. Hohl and Hockney, 1969). At each integration step, density is computed at each point of a grid of $32 \times 32 \times 16$ cells: each particle contributes to the density of the eight nearest grid points, according to the well-known CIC procedure (Birdsall and Fuss, 1969). Fourier transforms of density and potential are then carried out on a $64 \times 64 \times 32$ grid. The potential function between two particles is the Newtonian law (r^{-1}), but with a cut off at short distances and at distances larger than the total grid which contains the galaxy. The fact that the potential for distances less than one cell is taken as constant, suppresses violent close encounters and simulates a galaxy with a realistically long two-body relaxation time (see Hohl, 1973; Combes, 1980). The interaction between periodically reproduced images is avoided in the usual way (Hohl and Hockney, 1969). The force acting on each particle is computed from the gravitational potential of the nearest grid points. To avoid the excitation of the 4-fold symmetrical mode in computing the potential in a cube, only particles interior to the largest cylinder inscribed in the grid are taken into account (cf. Hohl, 1972). The particles which pass outside this boundary are advanced according to a Keplerian approximation of the force corresponding to the total interior mass.

The time step Δt is chosen to satisfy the relation:

$$V_{\max} \Delta t \lesssim L \quad (5)$$

where V_{\max} is the maximum of the rotation curve and L is the cell length in the plane of the galaxy. This means that particles cannot jump more than one cell in one time step. According to this constraint, a rotation time (defined at $r = 0.5 r_d$) contains about 50 time steps in all our runs. This constraint (5) gives also a computational lower limit to the radial scale length of the halo: for a given halo mass, the computation time becomes prohibitively long if $a_h < 3 L$.

 $M_h/M_d=0.25 \quad T=2\text{rot}$  $T=4\text{rot}$  $M_h/M_d=0.50 \quad T=2.19\text{rot}$  $T=4.38\text{rot}$  $M_h/M_d=0.25 \quad T=6\text{rot}$  $T=8\text{rot}$  $M_h/M_d=0.50 \quad T=6.57\text{rot}$  $T=8.76\text{rot}$  $M_h/M_d=0.25 \quad T=10\text{rot}$  $T=12\text{rot}$  $M_h/M_d=0.50 \quad T=10.95\text{rot}$  $T=13.14\text{rot}$  $M_h/M_d=0.25 \quad T=14\text{rot}$  $T=16\text{rot}$  $M_h/M_d=0.50 \quad T=15.33\text{rot}$  $T=17.52\text{rot}$  $M_h/M_d=0.25 \quad T=18\text{rot}$  $T=20\text{rot}$  $M_h/M_d=0.50 \quad T=19.71\text{rot}$  $T=21.9\text{rot}$ **Fig. 2**

Figs. 2–5. Particle plots of the four runs at various epochs: $M_h/M_d=0.25, 0.5, 1.0$, and 2.0 . A cell length is indicated by tick marks. In the first two cases, the disk radius (r_d) was half the grid radius

IV. Results of Experiments

Four cases with different ratios of halo to disk masses were run with the same ratio a_h/a_d (0.25). For these four cases, the ratio M_h/M_d was 0.25, 0.5, 1.0, 2.

The cases $M_h/M_d=1, 2$ were run with the disc of particles filling the computational grid. The number of escaped particles, i.e. particles advanced only approximately, was always under 15%. The number of escaped particles increases very quickly as the halo mass decreases, since the disk then undergoes more violent

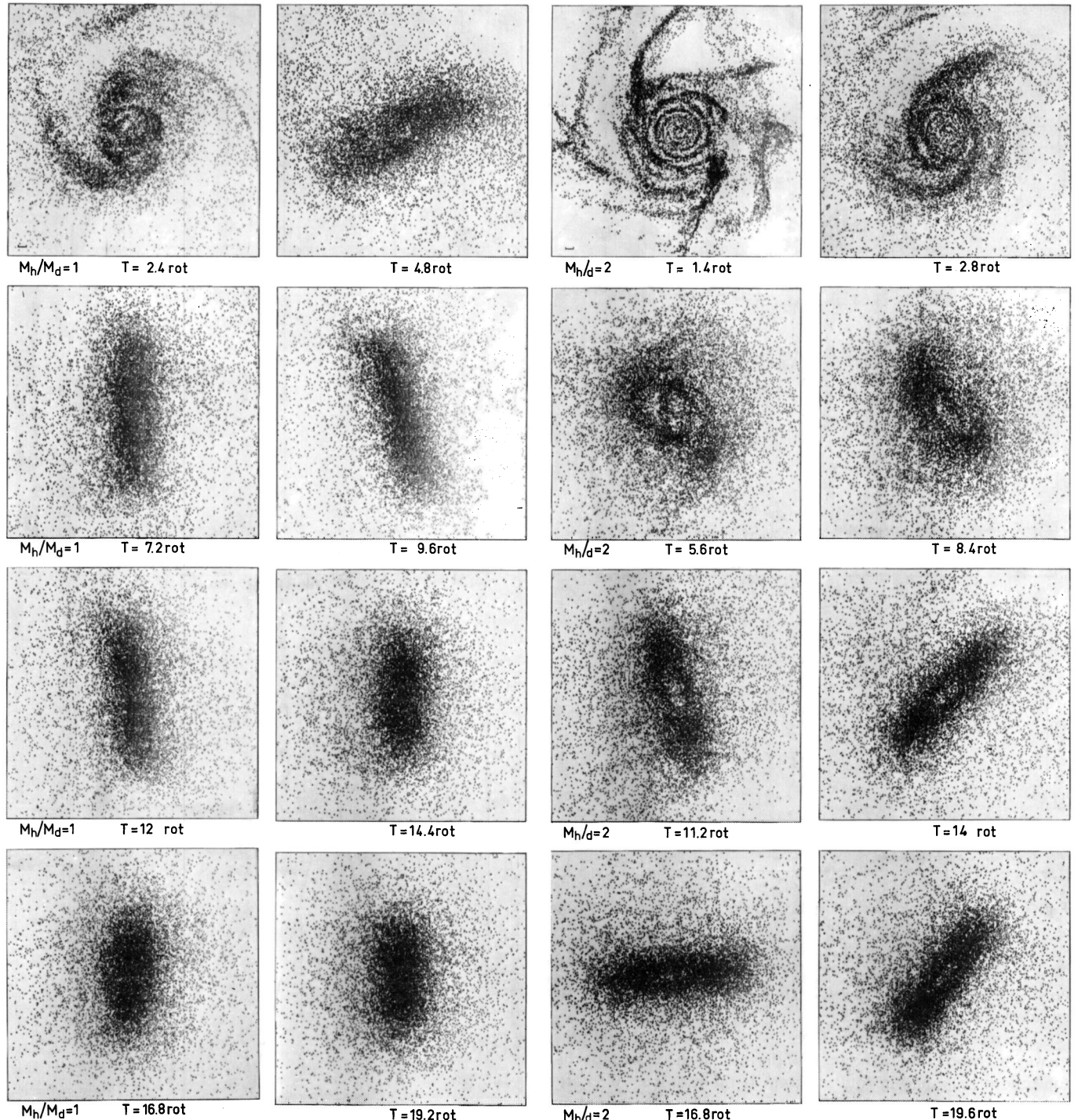


Fig. 4.

Fig. 5.

instabilities. For the $M_h/M_d = 0.25$ and 0.5 cases, the large number of escaped particles leads us to reduce the radius of the disk in units of the grid cell length, by a factor of 2, so that the number of escaped particles was reduced below 20%. A test run for the case $M_h/M_d = 1$ was carried out with the reduced grid radius and this run was identical to the run in which the disk fills the grid; therefore a finer scale is justified in the large M_h/M_d cases.

If the unit of length in the calculations is assumed to be 1 kpc (the initial disk has a maximum radius of 16 kpc), and the total mass of the galaxy (halo and disk inside 16 kpc) is taken to be $10^{11} M_\odot$, then the maximum rotational velocity is about 220 km s⁻¹. Then condition (5) requires a time step of about $5 \cdot 10^6$ yr. One rotation time at the half-grid radius ($r_{\frac{1}{2}} = 8$ kpc) is typically $2.5 \cdot 10^8$ yr. Since all cases were run for 20 rotation times, this

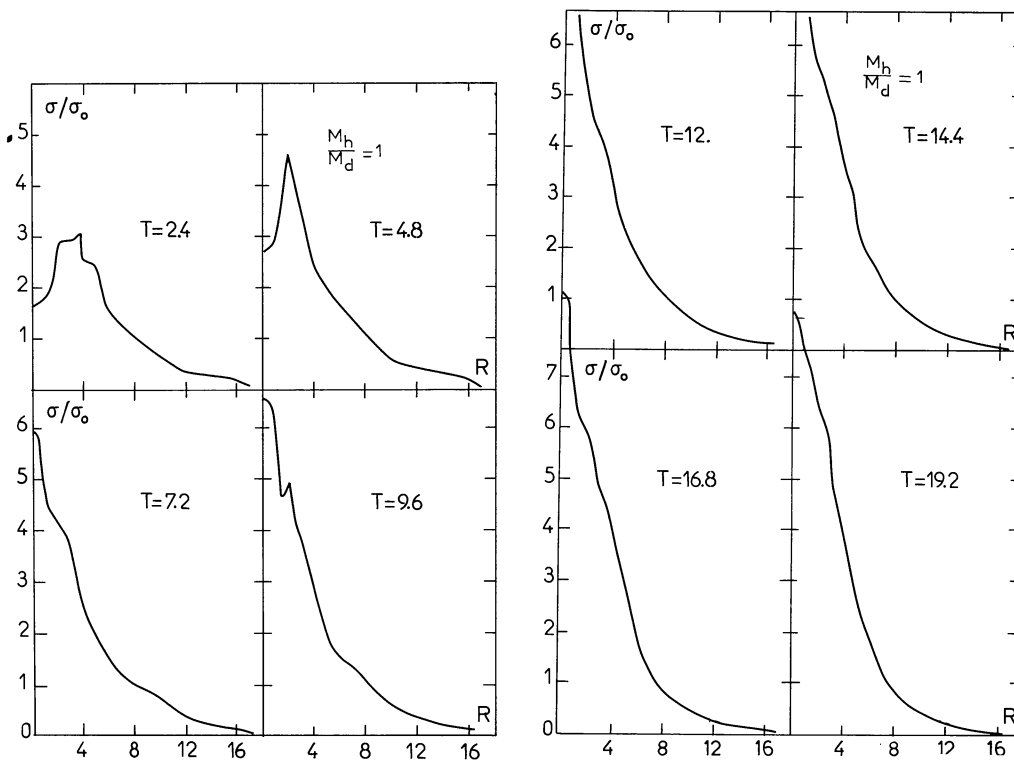


Fig. 6. Evolution of surface density distribution for the model $M_h/M_d=1$

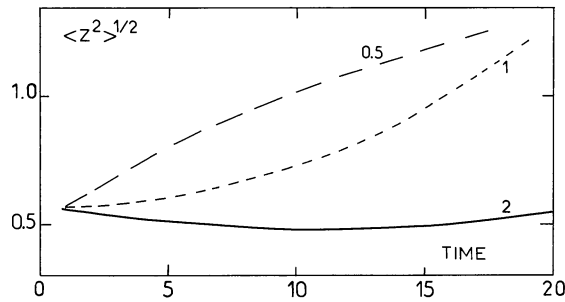


Fig. 7. Mean thickness of the galaxy disks as a function of time

corresponds to a total physical time scale of $5 \cdot 10^9$ yr for the simulations.

The results are shown in Figs. 2–5. These are particle plots viewed perpendicular to the plane of the disk, at successive epochs; the time is reckoned in rotation time at the radius $r = 0.5 r_d$ for each case. Pictures are shown more frequently at the beginning of the runs when the evolution is faster. In all cases bars are seen to develop from an apparent $m=2$ instability. The growth time scale of the bar increases with M_h/M_d which is consistent with previous results (Hockney and Brownrigg, 1974; Miller, 1978). In all the cases, bars are seen to persist for 20 rotation times. We can see for the case $M_h/M_d=2$, there develops a small hole in the central density. This may be due to the fact that particles in the central cells tend to move radially outward due to their high centrifugal forces that cannot be exactly balanced by the model.

The evolution of the radial distribution of the surface density is also more rapid when the halo is less massive. The case of $M_h/M_d=1$ is shown in Fig. 6. It is seen that particles tend to gather in the center and to evolve towards an exponential radial

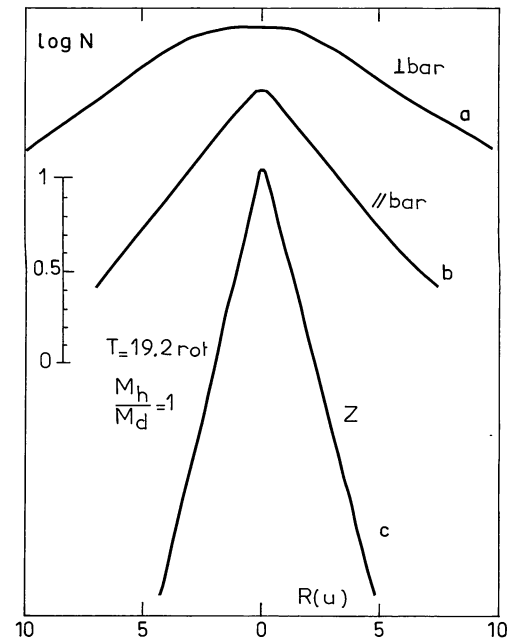


Fig. 8. Density profiles across the bar for the case $M_h/M_d=1$ and $T=19.2$ rotations, when the galaxy is seen edge-on: a) strip along the plane ($z=0$), along the larger length of the bar, and b) along the smaller length of the bar, c) strip perpendicular to the plane, when the galaxy exhibits the perpendicular box shape (smaller section of the bar)

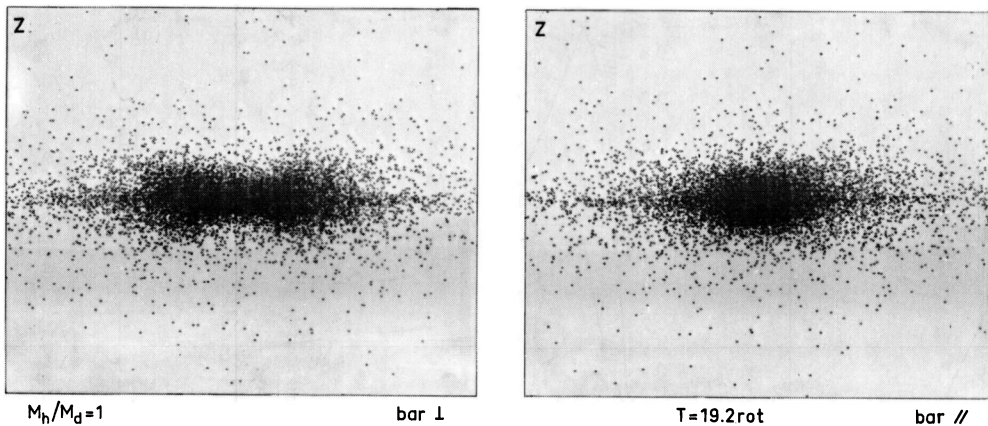


Fig. 9. Edge-on views of the bar, for the case $M_h/M_d=1$, at the end of the simulation. Note the box shape morphology of the galaxy in the view perpendicular to the major axis of the bar

distribution. In this case, the maximum surface density doubles in ten rotations, but then does not increase over the final 10 rotations, indicating that a steady-state has been reached. This behavior is similar to that found in earlier experiments (cf. Hohl, 1972, Miller and Smith, 1979). For the other values of M_h/M_d , the behaviour of surface density distribution is similar apart from the time scales.

The mean thickness of the disks as a function of time is displayed in Fig. 7, for three cases of M_h/M_d . In all cases, the thickness is increasing, but this increase is only very slight in the case $M_h/M_d=2$. This behaviour, which was also detected by Hohl (1978), is probably related to the stabilizing effect of the halo.

In all cases, bars appear relatively narrow. The axial ratios in the plane range from 2 to 3. In Fig. 8, are shown density profiles along and across the bar for the case $M_h/M_d=1$, $T=7.2$ rotations. It is interesting to note the peculiar morphology of a barred galaxy, when viewed edge-on. In Fig. 9 we see the case $M_h/M_d=1$, at the end of the simulation ($T=19.2$ rot.). Similar shapes occur in all other cases. In a view where the galaxy is edge-on and the line of sight is parallel to the long axis of the bar, the system looks like a box (to be compared to NGC 7332); and in a view where the line of sight is perpendicular to the long axis of the bar (Fig. 9), it is easy to recognize a peanut-shape morphology, very similar to the edge-on S 0 galaxy NGC 128 (Hubble Atlas, Sandage, 1961). From the computation of the z -oscillation frequency of the particles as a function of radius ($v_z(r)$), it is found that there exist high order resonances between the bar motion and the z -motions of the particles; in particular, the 4th order resonance ($\Omega_b=\Omega-v_z/4$), always occurs at the radius of highest thickness of the peanut shape. The peculiar shapes occurring in NGC 128 and in other galaxies (see Freeman, 1977), can thus be a consequence of the presence of a bar.

V. Analysis of Results

A) Definitions

To quantitatively follow the formation and evolution of a bar, it is useful to compute the Fourier transform of the potential of the system in polar coordinates. We may write the potential, in the plane of the galaxy ($z=0$), as:

$$\Phi(r, \varphi) = \Phi_0(r) + \sum_m \Phi_m(r) \cos [m(\varphi - \varphi_m)]. \quad (6)$$

It is convenient to represent each amplitude by the corresponding ratio Q_m ,

$$Q_m(r) = -m\Phi_m/r \frac{\partial\Phi_0}{\partial r} \quad (7)$$

which is the amplitude of the m^{th} harmonic in terms of the mean axisymmetric force. We also define Q_t as:

$$Q_t(r) = \left(\frac{\partial\Phi}{\partial\varphi} \right)_{\max} / r \frac{\partial\Phi_0}{\partial r}. \quad (8)$$

This quantity, the maximum tangential force in terms of the mean radial force, is a measure of the strength of the bar. The variation of the phase φ_m with radius, discriminates between bars and spiral arms; for instance, in a bar-like potential, the phase φ_2 is the same at all radii. The quantity $\partial\varphi_2/\partial t$ is the angular velocity of the pattern, Ω_p .

For bar distortion of a disk there exist resonances which are identical to the Lindblad resonances discussed for spiral structure. An essential dynamical property is the number of resonances implied by the angular velocity of the pattern Ω_p . The zeroth order epicyclic frequency k

$$k = \left(3\Omega^2 + \frac{\partial^2\Phi_0}{\partial r^2} \right)^{1/2} \quad (9)$$

and the critical frequencies $\Omega+k/2$ and $\Omega-k/2$ are evaluated in these calculations as a function of radius.

A basic dynamical property of N -body systems is the relative energy in systematic bulk motions. A convenient measure of this property is the ratio of mean ordered kinetic energy to total potential energy; i.e.

$$t = \frac{T_{\text{bulk}}}{|W|}.$$

This parameter seems to be related to the stability of the system against bar forming modes (see Ostriker and Peebles, 1973). We determine this parameter for our models by first computing the kinetic energy in systematic motions:

$$T_{\text{bulk}} = \frac{1}{2} m \sum_{i=1}^N V_i^2$$

where m is the mass of each particle and V_i is the average stream velocity at the position of the i^{th} particle. The mean stream ve-

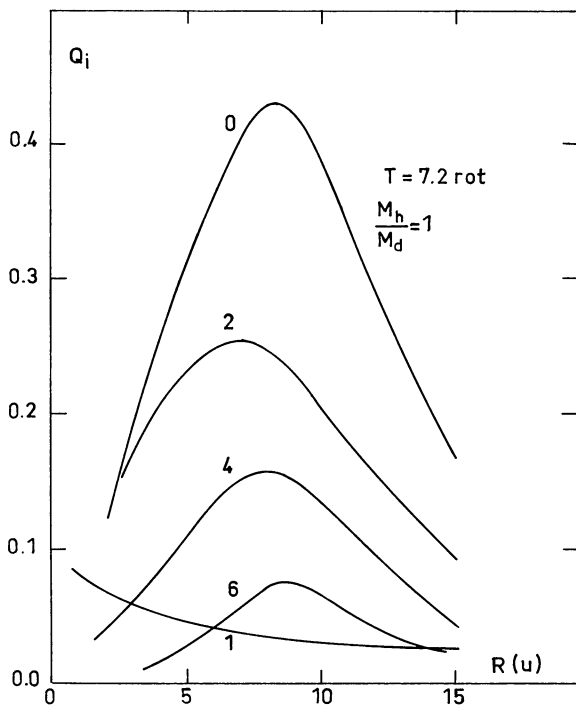


Fig. 10. Fourier analysis of the bar potential on the $Z=0$ plane. The ratio Q_i of tangential forces to the radial axisymmetric force for harmonics $i=1, 2, 4, 6, 8$ are plotted as a function of radius for $M_h/M_d=1$ at $T=7.2$ rotations. The total tangential force Q_t (code 0) is also shown

locity is computed by averaging over the velocities of all particles within one or two cell lengths depending upon the distance to the center; i.e. the size of the averaging box regularly increases from center to periphery to include reasonable numbers of particles per averaging box. Because the halo is considered to have no systematic motion, this parameter applies to the entire system, halo plus disk. We also evaluate t_d , the ratio of mean ordered kinetic energy, to twice the total kinetic energy in the disk alone, in the absence of a halo, $t_d=t$. In other words, t_d would be the value of t measured by an observer who does not know about the existence of a halo. When the parameters t and t_d reach a stable value, the system may be considered to be in a quasi-stationary state.

For a system in equilibrium, the Virial theorem should be verified. Here, since the potential is not computed exactly, essentially because of the cut-off at small distances, the theorem is not expected to be verified exactly. We found a departure of about 15% for the flattened and self-consistent component of our models. The underestimate of potential leads then to an estimate of t which is accurate within only 15%.

B) Analysis

First we consider the Fourier analysis of the tangential force at one epoch of the simulations $M_h/M_d=1$. The quantities Q_t and Q_m ($m=1, 2, 4, 6, 8$) are shown in Fig. 10 as a function of radius at $t=7.2$ rotations. As is obvious from Fig. 4, the bar has become well-developed by this time. It is seen that the bar is quite strong

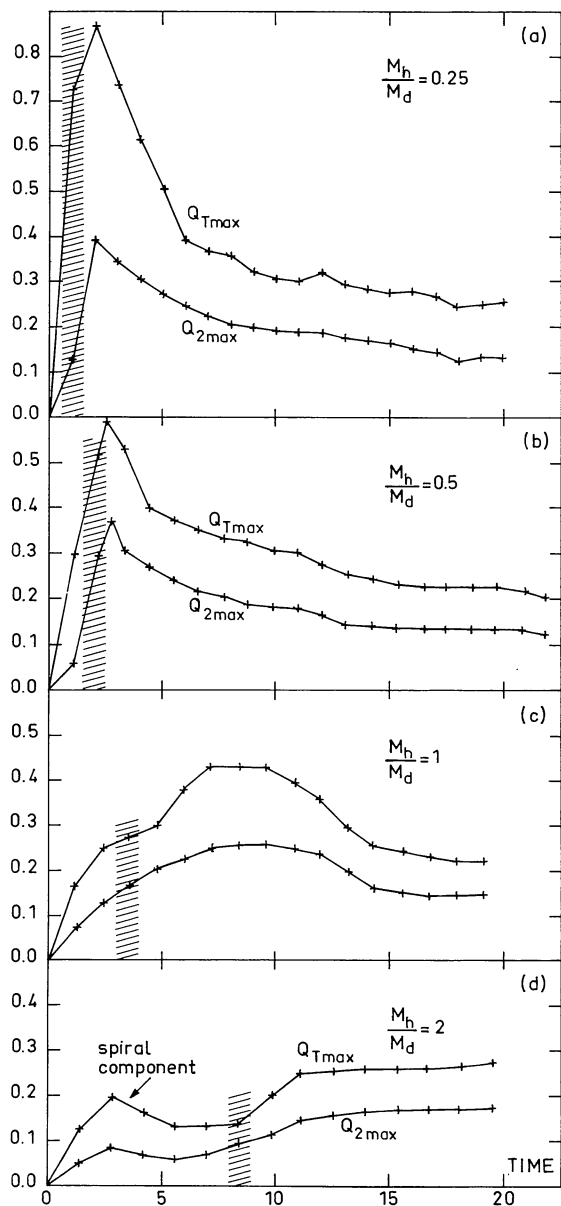


Fig. 11. Evolution of the strength of the bar perturbation as a function of time (represented by $Q_{t\max}$ and $Q_{2\max}$) for the four cases. Shaded regions indicate the period of bar formation

with a maximum tangential force of 43% of the mean axisymmetric force at a radius (r_{\max}) of 9 units (i.e. $Q_{t\max} = 0.43$).

The dominant Fourier component is $m=2$, but higher order components also make a significant contribution to the force. The ratio $Q_{t\max}/Q_{2\max}$ is a measure of the contribution of higher order harmonics to the tangential force, and in this case is

$$Q_{t\max}/Q_{2\max} = 1.7.$$

The phases of all even Fourier components do not vary with radius (within 1%), thus the potential is created by a true bar pattern. The first order Fourier component of the tangential force (Q_1) is small but non zero over the grid. The phase of this component, however, varies randomly with radius and suggests that the $m=1$ term is an artifact of statistical fluctuation in the particle density.

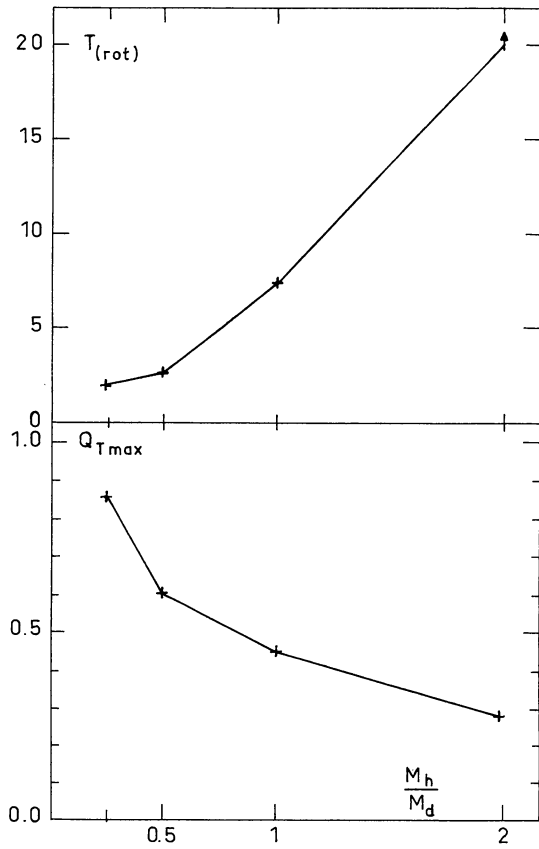


Fig. 12. **a** Plot of the peak strength of the bar ($Q_{t\max}$ and $Q_{2\max}$) as a function of the halo-to-disk mass ratio (M_h/M_d).
b Plot of the growth time of the bar for all cases

The time evolution of the bar strength for the four cases ($M_h/M_d=0.25, 0.5, 1, 2$) is shown in Fig. 11. This is a plot of the maximum values of Q_t and Q_2 as a function of time. The period of bar development is indicated by the hatched lines and it is seen that the bar develops later for greater halo to disk mass ratios. In all cases, a spiral perturbation develops initially, but it is a transient phase. In case $M_h/M_d=2$, the spiral phase lasts for about four rotations and is very distinct from the bar phase.

In the cases $M_h/M_d=0.25, 0.5, 1$, the bar strength, as measured by $Q_{t\max}$ and $Q_{2\max}$, reaches its greatest value several rotations after the development of the bar and then decreases to an apparent steady state value.

In the case $M_h/M_d=2$, the bar strength still seems to increase at the end of the calculations; the time scale for the growth of the bar is longer in this case. The time scale for the bar strength (Q_t) to reach its maximum value is a strong function of M_h/M_d as is apparent in Fig. 12.

It is evident from Fig. 11 that reasonably strong bars persist in all cases for more than twenty rotation times (i.e. $> 5 \cdot 10^9$ yr). The maximum strength of the bar (the largest value of Q_t max over the time of the simulation) is an apparent function of the halo to disk mass ratio (Fig. 12).

The angular velocity of the bar (derived directly from the Fourier analysis of the force) is plotted in Fig. 13 as a function of time for the three cases. It is seen that the angular velocity generally decreases with time, i.e., the bars rotate slower as they

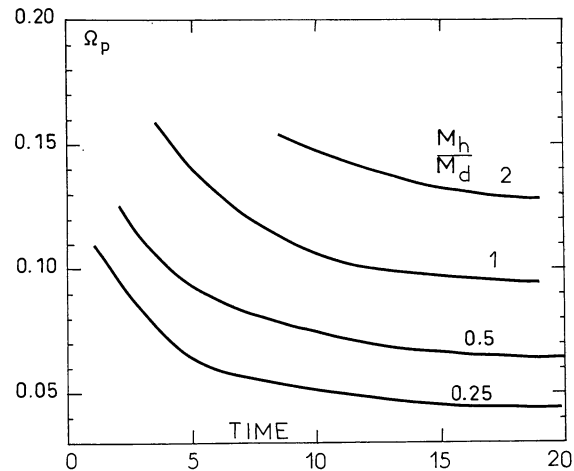


Fig. 13. Evolution of the pattern angular velocities for all cases. With standard units (see caption to Fig. 1) the unit of Ω_p is 100 km s/kpc

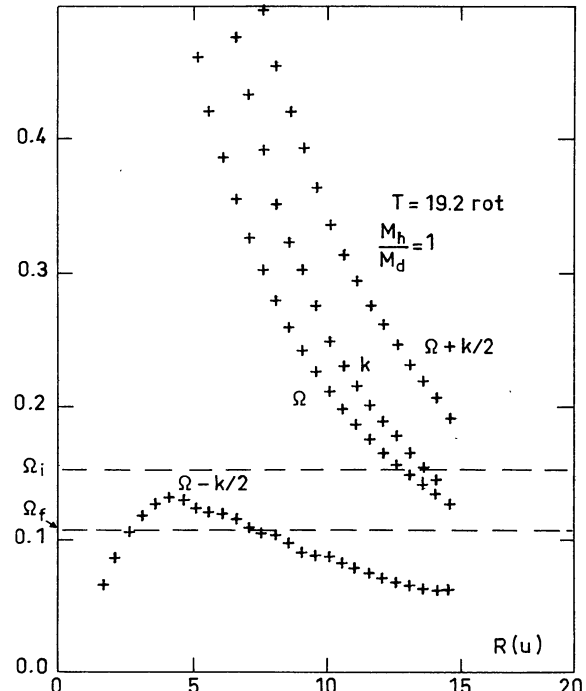


Fig. 14. The initial and final angular velocities of the bar perturbation are compared to the disk frequencies k , Ω , $\Omega - k/2$, and $\Omega + k/2$ for the case $M_h/M_d=1$

evolve towards a steady-state. The angular velocity Ω and the $\Omega - k/2$ curve are shown in Fig. 14 as a function of radius at the final epoch in the case $M_h/M_d=1$. These curves are very similar for the other models. Also shown in this figure are the initial and final values of Ω_p . Corotation initially lies at a radius of 13 units and then over the course of bar evolution, it moves beyond the grid radius to about 16.5 units, based upon an extrapolation of the angular velocity. Initially there are no inner resonances, but resonances appear at about $t=7$ rotations (shortly before the

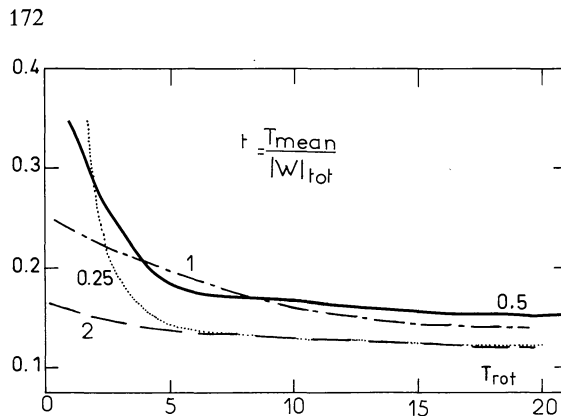


Fig. 15. Estimation of the stability of galaxies, through the ratio t =ratio of mean ordered kinetic energy to total potential energy. According to Ostriker and Peebles (1973) the stability criterium is $t \lesssim 14$

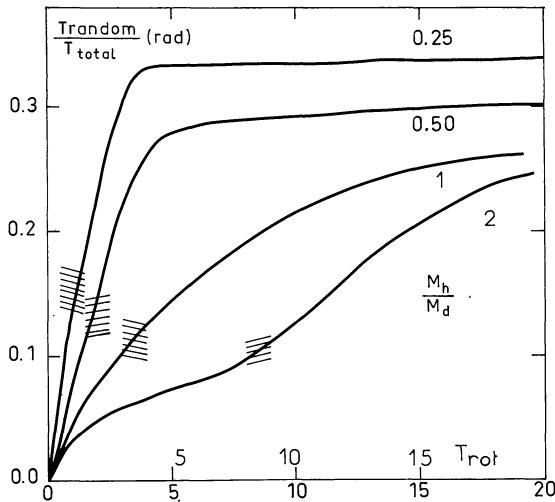


Fig. 16. Evolution of the random kinetic energy in the radial direction in terms of the total kinetic energy, for all models. The appearance of the bar (shaded regions) corresponds to a heating of the systems

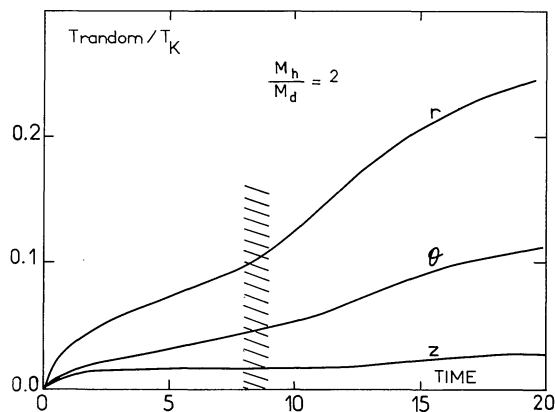


Fig. 17. Evolution of random kinetic energy in the radial, azimuthal and z directions, in terms of the total kinetic energy, for the case $M_h/M_d=2$. The shaded region represents the epoch of formation of the bar. The heating of the system due to the bar is anisotropic

bar reaches its maximum strength); by the end of the simulation there seems to exist two inner resonances at $r=2.5$ and $r=7$ units. However, it should be emphasized that the calculation of $\Omega-k/2$ is based upon a first order expansion about the mean axisymmetric field. When the bar strength becomes larger and particle orbits more elongated this approximation is less accurate and should not be used for the determination of the existence or location of resonances. With the errors of determination of $\Omega-k/2$, it appears that once the bar has become well developed, the bar angular velocity lies near the peak of the $\Omega-k/2$ curve (see Sanders, 1977).

It should be noted that the location of possible resonances is within the bar. If we let r_p be the radius of the peak of $\Omega-k/2$,

$$\frac{r_{\max}}{r_p} = 2.2.$$

That is, the maximum tangential force due to the bar occurs well beyond the possible resonances. This also demonstrates that the overall mass distribution is centrally condensed with respect to the bar.

In Fig. 15, the parameter t is plotted for the three cases. This illustrates the decrease of energy in systematic motions (i.e. the heating of the systems) during the dynamical evolution. All systems are initially cold and unstable to the formation of a bar by the Ostriker-Peebles criterion.

In cases $M_h/M_d=0.5, 1$, the rapid development of a bar quickly heats the systems. For the case $M_h/M_d=2$, the longer growth time of the bar leads to a more gradual heating. In case $M_h/M_d=1, 2$, the final value of t is near the Ostriker-Peebles criterium for stability ($t \sim 0.11$) but in the case $M_h/M_d=0.5$, the system is somewhat above this limit ($t=0.16$).

From the plots of t as a function of time, we see that the case $M_h/M_d=2$ is still heating at the end of the calculation, while the other two cases have reached a quasi-steady state. This also apparent from Fig. 16, which is a plot of the kinetic random radial energy in terms of the total kinetic energy as a function of time in the three cases. The importance of the bar in the heating of the system is illustrated by the hatchings which correspond again to the region of bar formation. The lack of continued heating after 10 rotations for $M_h/M_d=0.25, 0.5, 1$, suggests that no further relaxation is going on; in particular, that numerical relaxation is not a significant effect.

The appearance of the bar heats the system in an anisotropic way. This is shown in Fig. 17, where the time evolution of random kinetic energy in all three directions (r, φ, z) is plotted for the case $M_h/M_d=2$. Here the bar appears between 8 and 9 rotations, and the heating due to the bar is unambiguously distinguished from the initial relaxation. This heating only increases the velocity dispersions in the plane (r, φ) and not perpendicular to the plane. This anisotropic heating is similar to that found by Hohl and Zang (1979).

VI. Conclusion

In the present calculations, a purely axisymmetric disk is not obtained for a large range of the halo mass to disk mass ratio: $0.25 \leq M_h/M_d \leq 2$. Indeed in all cases the bar structure remains quite strong at the end of twenty rotations, with the maximum tangential force of the order of 25% of the axisymmetric force at the radius of maximum tangential forcing. This is consistent with the observed presence of bar components at some level in many

if not most spiral galaxies (de Vaucouleurs, 1963). It is also evident from the present calculations that non axisymmetric systems evolve on a time scale which is much longer than a dynamical time scale but much shorter than the usual two-body relaxation time. The rate of this evolution depends on the ratio of halo mass to disk mass and systems with a larger fraction of total mass in a halo component evolve more slowly. For example, in the case $M_h/M_d=0.25$, the peak bar strength is reached after only two rotations, while in the case $M_h/M_d=2$, the bar strength is still increasing after 20 rotations (Fig. 11). The general character of evolution is the same in all cases, with the bar strength rising to a maximum and then decreasing; however the peak bar strength and relative variations of the bar strength are much larger for those cases with low halo mass (see Fig. 12). It should be emphasized that bars do weaken after reaching a maximum strength, and the time scale for this weakening is comparable to the bar growth time. The decrease of bar strength is accompanied by the general heating of the system as evidenced by the approach of the Ostriker-Peebles parameter t_{0p} to ~ 0.14 . It appears that the bars reach a quasi-stationary state after some time; for example in the case of $M_h/M_d=0.25$, the bar strength after rapidly decreasing by a factor 2 in only three rotations, decreases by only 10% in the final 10 rotations. This continuing dissolution of the quasi-stationary bar, if real, would result in the approach to axial symmetry on a Hubble time (50 rotations) in the cases where $M_h/M_d \leq 1$. However, this longer time scale weakening may be due to an effective two-body relaxation and remains to be confirmed by long time scale calculations with more particles.

The rapid growth of bar followed by weakening and approach to a quasi-stationary state on the same time scale was qualitatively evident in previous calculations (see Hohl, 1975). The measure of bar strength, Qt , quantitatively demonstrates this effect in the present calculations.

In all cases the formation of the bar is accompanied by the development of an anisotropic velocity distribution. This is most evident in the case $M_h/M_d=2$ because of the long growth time scale of the bar (Fig. 17). This phenomenon is also seen in the calculations of Hohl and Zang (1979). The subsequent heating of the system, during the weakening of the bar is less dramatic, and appears to be more isotropic. In all cases, when the bar has formed, the disk viewed edge-on has the peculiar "box" or "peanut" shaped appearance depending on the angle between the bar and the line of sight (see Fig. 9). This might be due to high order resonances between the bar motion and the z -oscillations of the particles in the disk. These forms are observed in a few edge-on galaxies, for example NGC 128 and NGC 7332, and can be the indication of the existence of a bar.

It is suggested by gas-dynamical calculations that bars observed in SB_b galaxies represent strong deviations from axial symmetry ($Qt > 0.3$). Such bars are produced in these calculations for $M_h/M_d \leq 1$ but only for a time short compared to a Hubble time; i.e. for $M_h/M_d \leq 1$, strong bars appear to be a transient phenomenon. However, in the case $M_h/M_d=2$, the bar strength is still increasing after 20 rotation times, or about one half a Hubble time. This suggests that the bars observed in SB_b gal-

axies have not persisted since the epoch of galaxy formation, but have developed more recently in systems with $M_h/M_d \geq 2$. It is possibly the rate of global dynamical evolution of non axisymmetric systems which determines whether or not a disk galaxy will now appear as a barred or unbarred galaxy, and this rate of evolution depends strongly on M_h/M_d . Therefore, the fraction of the galactic mass in a hot halo is likely to be a critical parameter in determining the morphology of galaxies. In systems with low M_h/M_d , bars develop rapidly but then weaken leaving a hot disk with a weak oval distortion. In systems with very high M_h/M_d (possibly $M_h/M_d \sim 4$ judging from calculations by James and Sellwood, 1978) the evolution is so long that a stationary bar may not develop in a Hubble time.

References

- Birdsall, C.K., Fuss, D.: 1969, *J. Comput. Phys.* **3**, 494
 Berman, R.H., Mark, J.W.K.: 1979, *Astron. Astrophys.* **77**, 31
 Combes, F.: 1980, unpublished thesis, Paris University
 Eggen, O.J., Lynden-Bell, D., Sandage, A.: 1962, *Astrophys. J.* **136**, 748
 Freeman, K.C.: 1977, in I.A.U. Symp. no. 77 Structure and Properties of Nearby Galaxies ed. E. M. Berkhuijsen and R. Wielebinski, Boston, Reidel, p. 3
 Hockney, R.W., Brownrigg, D.R.K.: 1974, *Monthly Notices Roy. Astron. Soc.* **167**, 351
 Hohl, F.: 1972, *J. Comput. Phys.* **9**, 10
 Hohl, F.: 1973, *Astrophys. J.* **184**, 353
 Hohl, F.: 1975, IAU Symp. **69**, 349
 Hohl, F.: 1978, *Astron. J.* **83**, 768
 Hohl, F., Hockney, R.W.: 1969, *J. Comput. Phys.* **4**, 306
 Hohl, F., Zang, T.A.: 1979, *Astron. J.* **84**, 585
 James, R.A., Sellwood, J.A.: 1978, *Monthly Notices Roy. Astron. Soc.* **182**, 331
 Kalnajs, A.J.: 1972, *Astrophys. J.* **175**, 63
 Miller, R.H.: 1978, *Astrophys. J.* **224**, 32
 Miller, R.H., Prendergast, K.H., Quirk, W.J.: 1970, *Astrophys. J.* **161**, 90
 Miller, R.H., Smith, B.F.: 1979, *Astrophys. J.* **227**, 785
 Ostriker, J.P., Peebles, P.J.E.: 1973, *Astrophys. J.* **186**, 467
 Ostriker, J.P., Peebles, P.J.E., Yahil, A.: 1974, *Astrophys. J.* **193**, L1
 Sandage, A.R.: 1961, The Hubble Atlas of Galaxies, Carnegie Institution of Washington
 Sanders, R.H.: 1977, *Astrophys. J.* **217**, 916
 Sanders, R.H., Tubbs, A.D.: 1980, *Astrophys. J.* **235**, 803
 Sellwood, J.A.: 1979 (preprint)
 Spitzer, L.: 1968, Diffuse matter in Space, p. 179
 Toomre, A.: 1963, *Astrophys. J.* **138**, 385
 Toomre, A.: 1964, *Astrophys. J.* **139**, 1217
 de Vaucouleurs, G.: 1963, *Astrophys. J. Suppl.* **8**, 31

Late-type galaxies observed with SAURON: two-dimensional stellar and emission-line kinematics of 18 spirals

Katia Ganda,¹★ Jesús Falcón-Barroso,² Reynier F. Peletier,¹ Michele Cappellari,² Eric Emsellem,³ Richard M. McDermid,² P. Tim de Zeeuw² and C. Marcella Carollo⁴

¹*Kapteyn Astronomical Institute, Postbus 800, 9700 AV Groningen, the Netherlands*

²*Leiden Observatory, Postbus 9513, 2300 RA Leiden, the Netherlands*

³*Centre de Recherche Astrophysique de Lyon – Observatoire, 9 Avenue Charles André, 69230 Saint Genis Laval, France*

⁴*Eidgenössische Technische Hochschule Zurich, Hönggerberg HPF G4.3, CH-8092 Zurich, Switzerland*

Accepted 2005 December 2. Received 2005 November 21; in original form 2005 October 4

ABSTRACT

We present the stellar and gas kinematics of a sample of 18 nearby late-type spiral galaxies (Hubble types ranging from Sb to Sd), observed with the integral-field spectrograph SAURON at the 4.2-m William Herschel Telescope. SAURON covers the spectral range 4800–5380 Å, allowing us to measure the H β , Fe, Mg b absorption features and the emission in the H β line and the [O III] $\lambda\lambda 4959, 5007$ Å and [N I] $\lambda\lambda 5198, 5200$ Å doublets over a 33×41 -arcsec 2 field of view. The maps cover the nuclear region of these late-type galaxies and in all cases include the entire bulge. In many cases the stellar kinematics suggests the presence of a cold inner region, as visible from a central drop in the stellar velocity dispersion. The ionized gas is almost ubiquitous and behaves in a complicated fashion: the gas velocity fields often display more features than the stellar ones, including wiggles in the zero-velocity lines, irregular distributions, ring-like structures. The line ratio [O III]/H β often takes on low values over most of the field, probably indicating a wide-spread star formation.

Key words: galaxies: bulges – galaxies: evolution – galaxies: formation – galaxies: kinematics and dynamics – galaxies: spiral.

1 INTRODUCTION

From a theoretical point of view, we have a well-defined paradigm for the formation of disc galaxies within the cold dark matter hierarchical structure formation scenario (Fall & Efstathiou 1980; Silk 2003): discs quietly settle and cool inside dark matter haloes, while bulges form through mergers of multiple haloes. However, some of the observed properties of spiral galaxies suggest a larger complexity in their formation history. The presence of bulges is not ubiquitous and their nature can be ambiguous. Evidence has accumulated in the past years showing that many bulges have a disc-like, sometimes exponential radial fall-off of the stellar density (Andredakis & Sanders 1994; Andredakis, Peletier & Balcells 1995; de Jong 1995; Courteau, de Jong & Broeils 1996; Carollo & Stiavelli 1998; Seigar et al. 2002; MacArthur, Courteau & Holtzman 2003). Numerical simulations seem to suggest that the dissolution of bars inside the discs may trigger the formation of three-dimensional stellar structures with roughly exponential profiles (Combes et al. 1990; Pfenniger & Norman 1990; Raha et al. 1991; Norman, Sellwood & Hasan 1996); this could mean that some bulges form through the evolution of dynamical instabilities in the disc. Quite recently, the quality of imaging data made available through *Hubble Space Tele-*

scope (HST) boosted the study of the inner regions of spiral galaxies, showing that they can host a variety of structures: bulges, nuclear star clusters, stellar discs, small bars, double bars, star forming rings (Carollo et al. 1997; Carollo, Stiavelli & Mack 1998; Carollo 1999; Pérez-Ramírez et al. 2000; Böker et al. 2002; Carollo et al. 2002; Falcón-Barroso, Peletier & Balcells 2002; Laine et al. 2002; Allard, Peletier & Knapen 2005), without there being an agreement about their origin and evolutionary pattern. Ongoing large projects like the panchromatic Spitzer Infrared Nearby Galaxies Survey (SINGS) (Kennicutt et al. 2003) which makes use of observations at infrared, visible and UV wavelengths represent a very useful approach to building a comprehensive picture of galactic structure, but at the moment rely mostly on imaging. Looking at disc galaxies from a spectroscopic perspective would add kinematic information and insight into stellar populations which cannot come from imaging, and could help us tracing their star formation and mass assembly histories.

Contrary to the massive spheroids, the stellar populations and kinematics of late-type disc-dominated galaxies are poorly known, due to the difficulty of reliably measuring and interpreting such diagnostics in low surface brightness environments which are so full of dust, star formation and substructures, not much attention has been paid to the spectroscopic counterpart of all the mentioned imaging that has been carried out. There are a few exceptions to this

*E-mail: katia@astro.rug.nl

statement: Böker et al. (2001) started a project on Space Telescope Imaging Spectrograph (STIS) long-slit spectroscopy of 77 nearby late-type spiral galaxies previously imaged with *HST*/Wide Field Planetary Camera 2 (WFPC2); first results are discussed in Böker et al. (2003); Walcher et al. (2005) analysed UV slit-spectroscopy of the nuclei of nine late-type spirals; these studies are mainly focused on the nature of the innermost components, in particular on the nuclear star clusters.

We are currently engaged in a study aimed at investigating the properties of the nuclear regions of very late-type galaxies. In such environments, long-slit spectra are too limited to be useful for modelling and interpretation and have generally been used only to discuss the properties of emission lines (see e.g. Matthews & Gallagher 2002, who measure the position–velocity curve of 21 extreme late-type spiral galaxies using the H α emission line). Here, we present deep integral-field spectroscopy that not only makes it easier to study the kinematics and physical properties of stars and gas, but also allows to study and model the stellar populations.

We were granted six nights at the William Herschel Telescope (WHT) of the Observatorio del Roque de los Muchachos in La Palma, Spain, to obtain two-dimensional spectroscopy with the integral-field Spectrographic Areal Unit for Research on Optical Nebulae (SAURON), which was custom built for a representative census of elliptical and lenticular galaxies, and Sa bulges (the so-called SAURON survey, see Bacon et al. 2001 and de Zeeuw et al. 2002, hereafter, respectively, Paper I and Paper II). The present work can be regarded as a natural extension of the SAURON survey towards the end of the Hubble sequence. Our purpose was to use SAURON in order to map the stellar and gaseous (H β , [O III], [N I]) kinematics and the absorption line-strength distributions of the indices H β , Mg, Fe, in the region 4800–5380 Å. In this paper, we present the observations and data reduction and the resulting kinematical maps for 18 Sb–Sd galaxies. The data and maps will be made available via the SAURON website (<http://www.strw.leidenuniv.nl/sauron>).

The paper is structured as follows. Section 2 describes the sample selection and characteristics. Section 3 summarizes the observations and data reduction. Section 4 describes the methods applied to calculate the stellar and gaseous kinematics from our spectra. Section 5 carries out a comparison with previous measurements. Section 6 presents and discusses the kinematical maps and looks in particular at the behaviour of the stellar velocity dispersion. Finally, Section 7 summarizes the results. Detailed modelling and interpretation of the data will come in future papers.

2 THE SAMPLE

Our sample galaxies were optically selected ($B_T < 12.5$, according to the values given in de Vaucouleurs et al. 1991, hereafter RC3) with *HST* imaging available from WFPC2 and/or Near Infrared Camera and Multi-Object Spectrometer (NICMOS). In practice, the galaxies were chosen from objects lists of recent imaging projects with *HST* (Carollo et al. 1997, 1998; Böker et al. 2002; Carollo et al. 2002; Laine et al. 2002). Their morphological type ranges between Sb and Sd, following the classification reported in NASA/IPAC Extragalactic Database (NED)¹ (from RC3). Galaxies in close interaction and Seyferts were discarded. Only galaxies with $0 < \text{right ascension} < 15^{\text{h}}$ and $\delta > -20^{\circ}$ were selected, to fulfil a visibility criterion during the allocated nights. The resulting sample contains 18 nearby galaxies.

In Table 1 we list properties already measured and available through public catalogues, while in Fig. 1 we represent graphically the range spanned by our sample galaxies in a number of global and nuclear properties. This can be useful for a visual comparison with the galaxies of the SAURON survey (see figs 1 and 3 of Paper II). Panel (a) shows the distribution of the selected galaxies in the plane $M_B - \epsilon_{25}$. M_B is the absolute magnitude in the B band and ϵ_{25} is the ellipticity, derived from the axial ratio at the 25 mag arcsec $^{-2}$ isophotal level in B . This panel shows that there is a lack of high-ellipticity objects, indicating that our disc galaxies are generally far from being edge-on systems. Panel (b) plots the effective $B - V$ colour versus the central velocity dispersion σ ; a relatively tight trend is recognizable, since galaxies with higher velocity dispersions tend to be redder. Panel (c) plots the effective $B - V$ colour versus the morphological type; colours become bluer with later types. Panel (d) shows the distribution of our galaxies in the Tully–Fisher plane: M_B versus the inclination-corrected rotation velocity, obtained as $W_{20_c} = W_{20}/\sin(i)$, where W_{20} is the 21-cm line width at 20 per cent of the peak and i the inclination between line of sight and polar axis. The overplotted solid line is the Tully–Fisher relation, as determined by Verheijen (2001) for the B band from a sample of 45 galaxies with measured H I global profile: $M_B = -2.91 - 6.8 \log(W_{20_c})$. In the figure, all the galaxies with inclination below 45° are marked with an asterisk, since the reported relation was established on the basis of higher-inclination objects, one can see that all the galaxies that deviate most from the red line have low inclination, although not all of the low-inclination galaxies are deviant. Panel (e) presents the relation between total luminosity (absolute blue magnitude M_B) and central velocity dispersion; the galaxies cover a range of ≈ 100 in luminosity and a factor of ≈ 5 in velocity dispersion and become more luminous with increasing velocity dispersion. To conclude, panel (f) plots M_B against the morphological type; the luminosity tends to decrease as the galaxies become later in type, as shown also by de Jong (1996). The quantities plotted in this figure are all derived from catalogues, mainly from RC3 and HyperLeda,² (for a description and a list of references, see caption to Table 1), except for the central velocity dispersion. Since previously existing central velocity dispersion values are available only for six of the galaxies in our sample, we decided to measure the central velocity dispersion from our own spectra. The measured spectra in a central aperture (2.4×2.4 arcsec 2) were combined to give an averaged spectrum from which we computed the stellar kinematics, using methods which we will present and discuss later in this paper. The resulting σ values are taken as central velocity dispersions, listed in Table 1 and used in Fig. 1. In Section 5, we will provide a qualitative comparison between our central velocity dispersions and the literature values, for the six galaxies for which we could find references.

3 OBSERVATIONS AND DATA REDUCTION

Observations of the 18 late-type galaxies were carried out in 2004 January 20–26, using the integral-field spectrograph SAURON attached to the 4.2-m WHT. For each of the 18 galaxies, Table 2 lists the number of 1800-s exposures that we took.

We used the low spatial resolution mode of SAURON, giving a field of view (FOV) of 33×41 arcsec 2 . The spatial sampling of individual exposures is determined by an array of 0.94×0.94 -arcsec 2 lenses. This produces 1431 spectra per pointing over the

¹ <http://nedwww.ipac.caltech.edu>

² <http://leda.univ-lyon1.fr>

Table 1. Properties of our 18 galaxies. (1) Galaxy identifier. (2) Hubble type (RC3 through NED). (3) Numerical morphological type (RC3). (4) Heliocentric neutral hydrogen velocity in km s^{-1} (RC3, via VizieR). (5) Absolute blue magnitude M_B in mag (quoted from HyperLeda), computed from the corrected apparent magnitude and the distance modulus (also listed in HyperLeda); a Virgocentric flow model with $v_{\text{virgo}} = 208 \text{ km s}^{-1}$, a Hubble constant $H_0 = 70 \text{ km s}^{-1} \text{ Mpc}^{-1}$ and the correction to the Local Group centroid of Yahil, Tammann & Sandage (1977) are adopted. (6) Effective $(B - V)_e$ colour in mag; values marked with ‘L’ have been taken from HyperLeda, the others from RC3. (7) Projected diameter at the isophotal level of 25 mag arcsec $^{-2}$ in the B band, in arcsec (RC3). (8) Effective radius R_e in the B band, in arcsec (RC3). (9) Ellipticity ϵ_{25} of the contour of 25 mag arcsec $^{-2}$ B surface brightness (RC3). (10) Disc inclination in degrees, calculated from the axis ratio listed in RC3. (11) PA of the major axis, in degrees (RC3); values marked with ‘g’ are taken from Grosbøl (1985). (12) Central velocity dispersion σ in km s^{-1} , from our own measurement (averaging the spectra in a central 2.4×2.4 -arcsec 2 aperture and measuring the kinematics on the resulting spectrum, as explained in the text). (13) Width of the 21-cm neutral hydrogen line at 20 per cent of the peak in km s^{-1} (RC3), corrected for the disc inclination, as listed in column (10).

NGC (1)	Type (2)	T (3)	V_{21} (4)	M_B (5)	$(B - V)_e$ (6)	d_{25} (7)	R_e (8)	ϵ_{25} (9)	i (10)	PA (11)	σ (12)	$W_{20 \text{ c}}$ (13)
488	SA(r)b	3.0	2269	-21.71	0.96	315	52	0.260	42	15	196	675
628	SA(s)c	5.0	656	-20.29	0.64	629	144	0.088	24	25	54	190
772	SA(s)b	3.0	2458	-22.23	0.86	435	77	0.411	54	130	120	583
864	SAB(rs)c	5.0	1560	-20.54	0.63	281	97	0.241	41	20	65	356
1042	SAB(rs)cd	6.0	1373	-19.83	0.62	281	95	0.224	39	43 ^g	55	179
2805	SAB(rs)d	7.0	1734	-20.75	0.54	379	128	0.241	41	125	46	181
2964	SAB(r)bc	4.0	1321	-19.74	0.75	173	26	0.451	57	97	101	372
3346	SB(rs)cd	6.0	1260	-18.89		173		0.129	29	111 ^g	48	338
3423	SA(s)cd	6.0	1011	-19.54		228	36	0.149	32	10	49	337
3949	SA(s)bc	4.0	798	-19.60	0.49 ^L	173		0.425	55	120	61	338
4030	SA(s)bc	4.0	1460	-20.27	0.88 ^L	250		0.276	44	27	100	503
4102	SAB(s)b?	3.0	837	-19.38	0.97 ^L	181		0.425	55	38	150	385
4254	SA(s)c	5.0	2407	-22.63	0.65	322	56	0.129	29	62 ^g	72	537
4487	SAB(rs)cd	6.0	1037	-19.12		250		0.324	47	75	51	297
4775	SA(s)d	7.0	1567	-19.81		128		0.067	21	52 ^g	42	342
5585	SAB(s)d	7.0	305	-18.32	0.49	345	102	0.354	50	30	42	204
5668	SA(s)d	7.0	1583	-19.65	0.70	199	38	0.088	24	164 ^g	53	280
5678	SAB(rs)b	3.0	1922	-21.30	0.88 ^L	199		0.510	61	5	103	452

SAURON FOV; another 146 lenses sample a region 1.9 arcmin away from the main field in order to measure simultaneously the sky background. SAURON delivers a spectral resolution of 4.2 Å full width at half-maximum (FWHM) and covers the narrow spectral range 4800–5380 Å (1.1 Å pixel $^{-1}$). This wavelength range includes a number of important stellar absorption lines (e.g. H β , Fe, Mg b) and potential emission lines as well (H β , [O III], [N I]). For a more exhaustive description of the instrument, see Paper I and in particular Table 1 there.

For each galaxy, two to six largely overlapping exposures of 1800 s were typically obtained (Table 2). An offset of a few arcseconds, which corresponds to a few spatial elements, was introduced between consecutive exposures to avoid systematic errors due, for example, to bad CCD regions. Fig. 2 outlines the (approximate) position of the SAURON pointings overlaid on R -band Digital Sky Survey images of our galaxies, showing that our observations cover the nuclear regions.

3.1 Data reduction

We reduced the SAURON observations using the dedicated software XSAURON developed at the Centre de Recherche Astronomique de Lyon (CRAL; Paper I). During the observing run, arc exposures were taken before and after each galaxy exposure for wavelength calibration purposes. Tungsten lamp exposures were also taken every night in order to build the extraction mask. At the telescope, we had a misalignment of $\approx 1^\circ$ between the columns of the CCD and the dispersion direction. To correct for this misalignment and avoid interference patterns due to uneven sampling of the data, we decided to rectify the spectra by rotating all of the frames by the

same amount ($\approx 1^\circ$) and in the opposite sense to the mentioned misalignment, at a very early stage of the reduction, by means of the IRAF³ tasks geomap and geotran, available from the IMAGES.IMMATCH package. The reduction steps include thus bias and dark subtraction, rotation of all the frames, extraction of the spectra using the fitted mask model, wavelength calibration, low-frequency flat-fielding, cosmic ray removal, homogenization of the spectral resolution over the FOV, sky subtraction and flux calibration of the spectra, although the data were not necessarily collected under photometric conditions. The individually extracted and calibrated data cubes were finally merged by truncating the wavelength domain to a common range, recentering the exposures using reconstructed images and combining the spectra, while correcting also for the effect of atmospheric refraction. In this process, the data cubes were spatially resampled to a common grid, so that the final merged data cube is sampled on to a rectangular grid with 0.8×0.8 -arcsec 2 pixels. The improvement in spatial sampling with respect to the individual data cubes is due to the dithering of exposures.

4 ANALYSIS AND METHODS

In order to ensure the measurement of reliable stellar kinematics, we spatially binned our merged data cubes using the Voronoi two-dimensional binning algorithm of Cappellari & Copin (2003), creating compact bins with a minimum signal-to-noise ratio (S/N) $_{\star} \approx$

³ IRAF is distributed by the National Optical Astronomy Observatories, which are operated by the Association of Universities for Research in Astronomy, Inc., under cooperative agreement with the National Science Foundation.

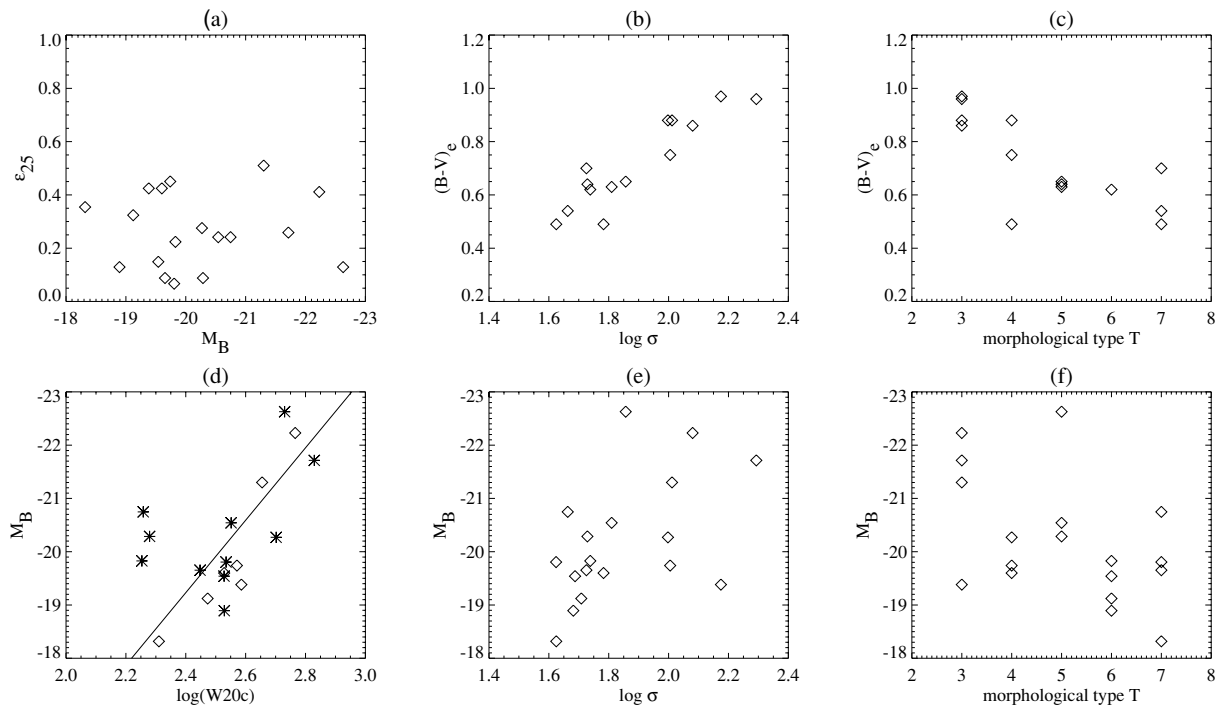


Figure 1. (a) Distribution of the 18 spiral galaxies in the plane ellipticity ϵ_{25} – absolute blue magnitude M_B ; (b) effective $B - V$ colour versus central velocity dispersion σ (in logarithmic units; we note here once and for all that throughout the paper we will refer to decimal logarithms simply as logarithms); (c) effective $B - V$ colour versus morphological type; (d) absolute magnitude M_B versus the inclination-corrected rotation velocity (in logarithmic units); the overplotted solid line indicates the standard Tully–Fisher relation (see the text for further details); (e) M_B plotted versus central velocity dispersion σ (in logarithmic units); (f) M_B versus morphological type. The numerical values for the plotted quantities are derived from public catalogues (see Table 1), except the values for σ , that come from our own measurements, as explained in the text.

Table 2. Number of exposures of 1800 s each per galaxy.

NGC	#	NGC	#
488	3	3949	3
628	1+4 ^a	4030	5
772	5	4102	5
864	4	4254	2
1042	4	4487	4
2805	6	4775	4
2964	2	5585	5
3346	6	5668	5
3423	6	5678	4

^a For the first exposure of NGC 628 we pointed the telescope on a star offset by ≈ 13 arcsec with respect to the galaxy centre; so we have 2 slightly different pointings on this galaxy.

60 per resolution element. However, most of the spectra in the central regions have a $(S/N)_*$ greater than 60, so a large fraction of the original spatial elements remains unbinned.

4.1 Stellar kinematics

We measured the stellar kinematics on each spectrum in our binned data cubes using the penalized pixel fitting (pPXF) method by Cappellari & Emsellem (2004). A linear combination of template stellar spectra, convolved with a line-of-sight velocity distribution described as a Gauss–Hermite expansion (Gerhard 1993; van der

Marel & Franx 1993), is fitted to each galaxy spectrum by χ^2 minimization in pixel space, using a penalty term to suppress noise. While fitting, the spectral regions that are potentially affected by nebular emission (corresponding to the H β , [O III], [N I] lines) are masked out. A low-order polynomial (generally of order 6) is also included in the fit to account for small differences in the flux calibration between the galaxy and the template spectra. This allows us to derive the mean velocity (V), velocity dispersion (σ) and the higher-order Gauss–Hermite moments (h_3 and h_4). As stellar templates we used a library of single-age, single-metallicity population models from Vazdekis (1999), from which we selected 39 models characterized by $1.00 \leqslant \text{Age} \leqslant 17.78$ Gyr, $-1.68 \leqslant [\text{Fe}/\text{H}] \leqslant +0.20$. This is similar to what has been done by Falcón-Barroso et al. (2006, hereafter Paper VII) for the analysis of the 24 Sa galaxies part of the SAURON survey.

As we will show in Section 6, our galaxies display stellar velocity dispersions often lower than those measured in the early-type galaxies of the SAURON survey (Emsellem et al. 2004, hereafter Paper III). SAURON has an instrumental dispersion of 108 km s^{-1} , while our measured velocity dispersions are in many cases below that level (see the central values for σ listed in Table 1). Thus, one might be concerned that velocity dispersions significantly below the instrumental dispersion cannot be reliably measured. This issue has already been addressed in Paper III: it reports tests of the uncertainties on the measured σ via Monte Carlo simulations which prove that for a spectrum with $(S/N)_* \approx 60$ and $\sigma \approx 50 \text{ km s}^{-1}$, the pPXF method will output velocity dispersions differing from the intrinsic one by no more than 10 km s^{-1} , a value within the measured error.

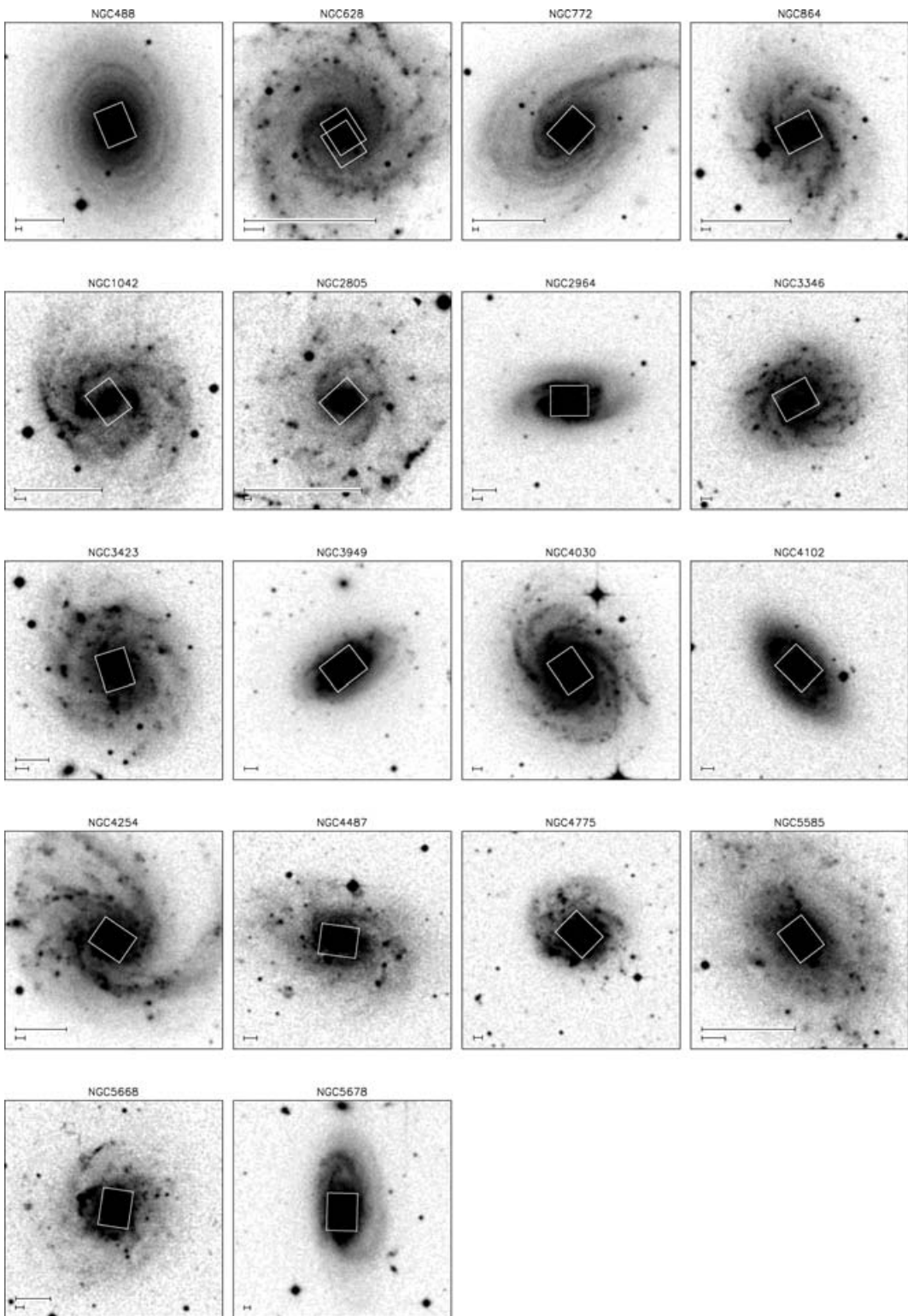


Figure 2. *R*-band Digital Sky Survey images of all 18 late-type spirals in the sample. The size of each image is 4×4 arcmin 2 and the orientation is such that north is upwards and east is towards left-hand side. Overplotted on each image are the positions of the SAURON pointings. The small bar at the bottom left-hand corner of each image corresponds to the linear length of 1 kpc; when the effective radius is available from RC3 (Table 1), another bar indicating the size of $1R_e$ is provided, above the 1-kpc bar.

Another technical issue related to the low velocity-dispersion values is that when the observed velocity dispersion is less than about 2 pixels ($\sigma \leqslant 120$ km s $^{-1}$), it becomes more difficult to measure the Gauss–Hermite moments h_3 and h_4 at our minimum ($S/N)_* \approx 60$;

in those cases the penalization in pPXF then biases the solutions towards a Gaussian (Cappellari & Emsellem 2004). In practice, one expects the measured higher moments to be significant only in the galactic regions where the velocity dispersion or ($S/N)_*$ are high.

4.2 Gas kinematics

Nebular emission is almost ubiquitous in our sample of 18 spiral galaxies. Thus, we have decided to apply a ‘double-binning scheme’, in order to compute the gas kinematics on bins smaller than the ones with $(S/N)_* = 60$ on which we calculated the stellar kinematics as described above. The large amount of gas in fact allows us to reliably measure the kinematics of emission lines at a lower S/N level, and having smaller bins prevents loss of spatial resolution, especially in the outer regions. To do this, we proceed as follows.

We call ‘star bins’ the previously introduced Voronoi bins with minimum $(S/N)_* = 60$. We first reconstruct the gas map by running pPXF on each single unbinned spectrum (single-lens spectrum) keeping fixed the stellar kinematics at the values determined for the star bin to which the spectrum belongs, thus fitting only for the stellar template and polynomial coefficients; this is done again by masking out the spectral regions potentially affected by emission. We recover the gas spectrum by subtracting the best fit from the original spectrum. For each gas spectrum we compute the $(S/N)_{\text{gas}}$ of the [O III] line taking the peak of the considered gas spectrum over the [O III] region and dividing by the noise, calculated on the gas spectrum over the emission-free part of the SAURON range. For the $(S/N)_{\text{gas}}$ determination, we could have used one of the other emission lines in the SAURON spectral range, e.g. H β or [N I], but they both present disadvantages compared to [O III]. In fact, the lines of the [N I] doublet are normally quite weak, and it is difficult to measure their kinematics and amplitude; the H β emission can instead be contaminated by stellar absorption at the same wavelength. At this stage, we bin the merged data cube to a minimum $(S/N)_{\text{gas}}$ of 5, according to the $(S/N)_{\text{gas}}$ values found for each single gas spectrum. We end up with a ‘gas-binned’ data cube. We call these bins ‘gas bins’.

In a second step, we determine the gas kinematics for each gas bin. We proceed by running pPXF on the average of all the star-binned spectra that have some spatial intersection with the considered gas bin. This is the input stellar kinematics for our determination of the gas kinematics.

The actual computation of the gas kinematics parameters requires a careful separation of the line emission from the stellar absorption. We follow the procedure described in Sarzi et al. (2006; hereafter Paper V) and in Paper VII that has been fully tested on the SAURON survey galaxies. For each gas-binned spectrum, the method relies on an iterative search for the emission-line velocities and velocity dispersions, while linearly solving at each step for the line amplitudes and the optimal combination of the stellar templates. The fit is performed over each ‘gas-binned’ spectrum, and no masking is applied, in contrast to the stellar kinematics determination. A multiplicative Legendre polynomial of order 6 is included in the fit to correct for small differences in the flux calibration between the galaxy spectrum and the library of models.

Most of our galaxies have conspicuous gas emission, so we proceed by fitting the H β and [O III] lines independently, in order to detect differences in the kinematics of the two lines, if present. The [N I] lines are instead forced to share the same kinematics with H β (see Paper V and Paper VII for details on the method).

We have visually inspected the emission-line profiles in our data cubes in order to assess the applicability of our fitting method, which fits a single Gaussian profile to each line in the SAURON wavelength range. In the large majority of cases, we did not find deviations from pure Gaussians. Only NGC 2964 and 4102 present complex line profiles, but limited to specific regions possibly related to activity (see the description of individual objects in Section 6.4). This lack

of complex line profiles may well be caused by the limited instrumental spectral resolution. For completeness, in Fig. 3 we show for NGC 4102 a spectrum where the [O III]5007 Å line does not resemble a single Gaussian and a spectrum where the line profiles instead do not differ from the Gaussian fit; there we present also the [O III] flux and velocity maps, in order to spatially locate the mentioned spectra.

5 COMPARISON WITH PUBLISHED MEASUREMENTS

The methods described in the previous sections were used to measure the stellar and gaseous kinematics and the amount of gas emission for the 72 galaxies of the SAURON survey (Paper III, Paper V and Paper VII). The quoted papers showed that the methods give results in agreement with previous measurements.

We also carried out a direct comparison with previous work. As already mentioned in Section 2, measurements of the stellar velocity dispersion are available for one-third of our sample. In addition, those few references are very heterogeneous and in some cases do not give all the information required to perform a careful and systematic comparison. In any case, we can qualitatively investigate the agreement of the central aperture velocity dispersion listed in Table 1 with the literature. The left-hand panel of Fig. 4 plots our measurements against the average of the existing values⁴ (if more than one). Overplotted with a dotted line is the 1:1 relation. Uncertainties in the literature values are taken from the references; as for our own measurements, we give an estimate of the errors by running pPXF on the single-lens spectra within our aperture and looking at the scatter in the resulting velocity dispersions. The agreement is generally satisfactory; the only deviant galaxy is NGC 4254, for which the only references we could find date back from the 1980s (Whitmore, Kirshner & Schechter 1979; Tonry & Davies 1981).

In the case of the gas measurements, as a source for our literature comparison we choose the Palomar spectroscopic survey of Ho, Filippenko & Sargent (1995, 1997), which includes 11 out of our 18 galaxies. We compare the [O III]/H β line ratio and the width of the forbidden emission, represented by the [O III] and [N II]6583 Å lines of the SAURON and Palomar samples, respectively. To perform a proper comparison, we measured the [O III]/H β line ratio and [O III] FWHM on central spectra obtained extracting from our data cubes a central aperture that matches the size ($2 \times 4 \text{ arcsec}^2$) and orientation of the Palomar long-slit observations. Uncertainties in the [N II] FWHM in the Palomar survey are typically ≈ 10 per cent, except for NGC 3346 and 3949, where Ho et al. (1997) report only the 3σ upper limit; for the [O III]/H β line ratio, the quoted uncertainties are around 30–40 per cent, except the case of NGC 488, where the uncertainty is ≈ 50 per cent. For our SAURON data, errors on the [O III] line width come from the fitting procedure and vary in percentage from galaxy to galaxy, while an upper limit on the uncertainties on the [O III]/H β line ratio comes from the typical errors on the line fluxes estimate given in Paper V.

The central panel of Fig. 4 plots the SAURON against Palomar [O III]/H β line ratio. The agreement appears to be reasonable, with all the galaxies lying on the 1:1 relation (indicated by the dotted line in Fig. 4) within the error bar, with the exception of NGC 3949. The right-hand panel compares the FWHMs of the forbidden lines, and the agreement appears to be less satisfactory. In particular,

⁴ From Shapiro, Gerssen & van der Marel (2003) for NGC 4030 and from HyperLeda for NGC 488, 628, 772, 2964 and 4254.

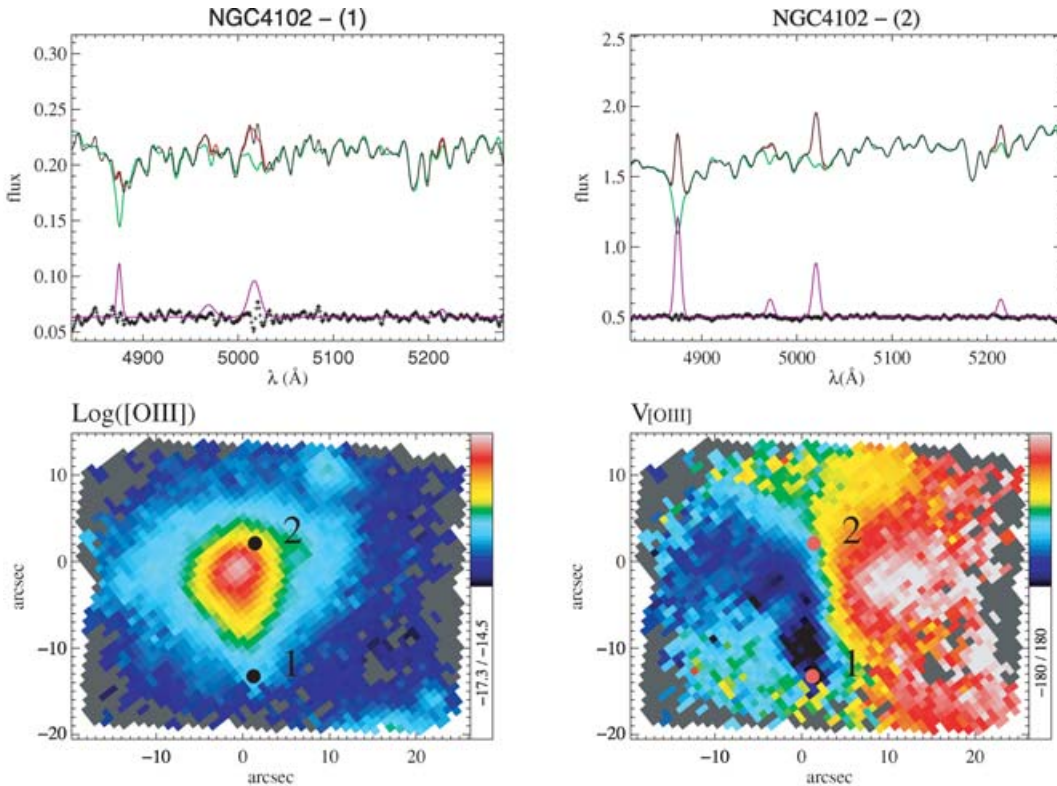


Figure 3. In the top left-hand panel we show for NGC 4102 a spectrum where the [O III] lines are only badly fitted by a single Gaussian; in the plot, the black solid line represents the galaxy spectrum; the red line is the full spectrum fit; the green solid line is the best-fitting combination of stellar templates, convolved with the kinematics; at the bottom of the panel, the purple line is the pure-emission spectrum and the black dotted line represents the residuals from the fit; a constant has been added to both. Along the vertical axis, the flux is in units of $10^{-16} \text{ erg cm}^{-2} \text{ s}^{-1}$. The top right-hand panel shows a spectrum for the same galaxy where there are no deviations from Gaussianity in the line profiles. This is an example of the typical behaviour of our spectra and also illustrates the quality of fit that we obtain. In the second row, the [O III] flux (in $\text{erg cm}^{-2} \text{ s}^{-1}$ and logarithmic scale) and velocity (in km s^{-1}) maps are shown (bottom left- and right-hand panels, respectively); the location of the two representative spectra is marked on the maps with a dot. For a description of the maps, we refer the reader to Section 6.1.

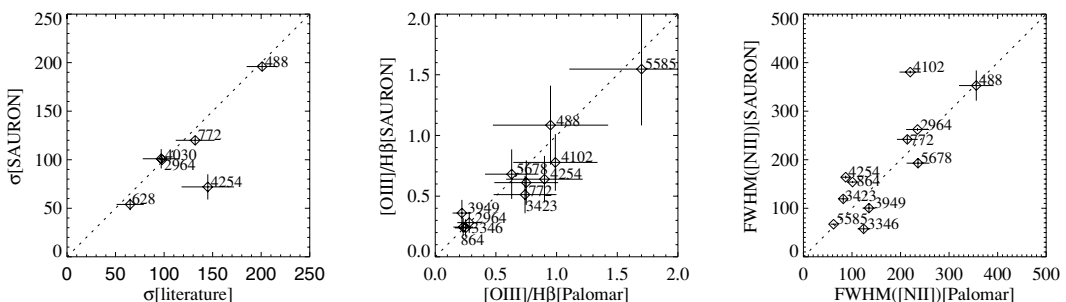


Figure 4. Literature comparison for stars (left-hand panel) and gas measurements (central and right-hand panels). Left-hand panel: SAURON against literature central stellar velocity dispersion (in km s^{-1}); central panel: SAURON against Palomar [O III]/H β line ratio; right-hand panel: SAURON against Palomar forbidden line width (in km s^{-1}). In each of the plots, the dotted line marks the 1:1 relation and the NGC galaxy identifiers are indicated close to the corresponding symbol; see the text for further details.

NGC 4102 lies well above the 1 : 1 relation; this is due to the broadening of the [O III] lines in this galaxy, where the single Gaussian used in our method fails to reproduce the line profile, as demonstrated at the end of the previous section. We stress the fact that the Palomar slit was oriented in the direction of the galactic region where the lines are double peaked (see Sections 4.2 and 6.4.12); our extracted aperture tests then that region and thus it is not a surprise that the comparison is not very accurate. In fact, a tight correlation between the widths of the [O III] and [N II] lines is expected if the

lines are produced in low-density regions (Ho et al. 1997), and it is not clear that this condition is satisfied in all objects.

6 OBSERVED STELLAR AND GAS KINEMATICS

This section presents our results for the 18 spiral galaxies and points out and briefly describes some interesting features detectable in the maps. We first show the maps (Section 6.1), then discuss some

properties of the stellar and gaseous kinematics of the sample as a whole (Sections 6.2 and 6.3), and in the end give a detailed description of the individual galaxies (Section 6.4).

6.1 Stellar and gas flux and kinematics: the maps

Figs 5(a)–(r) present the flux and kinematical maps of stars and gas for our sample of 18 spiral galaxies, obtained as explained in Sections 4.1 and 4.2. For each object, in the first row we give the unsharp-masked optical image of the galaxy from *HST*⁵ together with the UGC number when available, the FK5 2000 coordinates, the absolute blue magnitude, the ellipticity and the morphological type; NGC 772 represents an exception in that respect, since an optical space-based image is not available: we therefore show the unsharp-masked SAURON image instead; the second row contains the total intensity reconstructed by collapsing the SAURON spectra in the wavelength direction (in mag arcsec⁻², with an arbitrary zero-point), and the stellar velocity and velocity dispersion (in km s⁻¹); the third and fourth rows contain, respectively, the H β and [O III] flux (in erg cm⁻² s⁻¹ and logarithmic scale) and kinematics (velocity and velocity dispersion, in km s⁻¹); finally, the fifth row presents the line ratio [O III]/H β , in logarithmic scale, and the stellar h_3 and h_4 kinematical moments. Overplotted on each map are the isophotal contours. All the plotted velocities are systemic velocity subtracted; the same systemic velocity is assumed for stars and gas. No inclination correction to the kinematics has been applied, thus the plotted velocities are in all cases projected velocities. The stellar kinematics is shown on the (S/N)_{*} = 60 star bins, while the gas parameters are plotted on the (S/N)_{gas} = 5 gas bins. In each figure, the arrow and its associated dash at the top of the page, close to the galaxy name, indicate the orientation of the maps, pointing to the north and east directions, respectively.

To display the gas maps, we have chosen to consider as real a detection of emission when the amplitude over noise (hereafter A/N) of the line, defined as the fitted emission amplitude divided by the noise in the residual spectrum (galaxy spectrum – best fit over the whole SAURON range), is larger than 4 (see also Paper V and Paper VII). The bins below this threshold are displayed using a dark grey colour. Despite this cut in A/N, the gas detection covers in most cases a very large fraction of the SAURON field.

In NGC 4030 and 4102, we detected also significant emission from the [N I] doublet; however, in the large majority of our galaxies [N I] is very weak and hard to measure: since we would not learn more about our galaxies considering also the [N I] maps, we decided not to include them in Figs 5(a)–(r).

6.2 Stellar kinematics

All the objects show rotation, as expected. An interesting feature is the quite frequent central decline in σ (NGC 628, 772, 2805, 3346, 3949 and 5668). We measured also the higher moments h_3 and h_4 , but unfortunately our spectra contain information only for the most early-type galaxies in our sample (NGC 488, 772, 4030 and 4102) which are generally the objects with the highest (S/N)_{*}, where penalization does not play an important role (see Section 4.1 and Cappellari & Emsellem 2004). Some objects display misaligned

photometric and kinematical axes (NGC 864, 3346 and 4487), a possible indication of non-axisymmetric structures such as bars. In other cases, the situation is less clear, due to the presence of twists in the rotation axis (NGC 772, 2964, 3949, 4254 and 5678). In many galaxies our measurements indicate very low velocity dispersions, as seen also on the basis of the central values reported in Table 1 and Fig. 1.

6.2.1 Radial behaviour of the stellar velocity dispersion

We addressed the radial behaviour of the stellar velocity dispersion σ by measuring the radial σ profiles and their slopes and correlating these with the morphological type. For each of our galaxies, we computed a σ profile by averaging the stellar velocity dispersion map on elliptical annuli orientated as the galaxy isophotes; for some strongly barred galaxies, the chosen orientation does not coincide with the position angle (PA) quoted in Table 1, which refers to the outermost isophotes. The ellipticity of the concentric ellipses is instead taken in all cases from Table 1. The distance between consecutive annuli is 0.8 arcsec along the minor axis, corresponding to the pixel size of the unbinned SAURON cubes. In order to take into account the galaxy size, we rescaled the radial coordinate by dividing it by the disc scalelength. The values for the disc scalelength h_r come from one-dimensional fitting of the photometric profiles that we extracted from space- and ground-based images via isophotal analysis. The details of this photometric analysis will be given in a future paper. We then estimated the σ gradient across the field by fitting a straight line to the data points by means of a least-squares algorithm. Fig. 6 illustrates the results. For each galaxy the computed σ profile is plotted against the scale-free radius r/h_r ; the solid lines overplotted are the best-fitting straight lines, the slope of which is indicated in a corner of each panel. One can see that for some galaxies a straight line is clearly not an optimal description of the data, at least not over the whole radial range considered, but it serves as an indication of a global trend. The dotted line drawn on each plot marks the $r = 1.2$ arcsec line, which represents the edge of the squared aperture within which the central σ values reported in Table 1 were computed. In Fig. 7, we plot the slope of these scale-free fits against the morphological type of the galaxy. A weak global trend can be recognized: the slope tends to increase with later types, indicating that it is more probable for later-type galaxies to have a central region colder than the surroundings, rather than a hotter one. In the figure, we labelled with (B) the galaxies classified as barred (B and AB in Table 1), but we do not detect any significant correlation with bar classification.

The velocity-dispersion profile is determined by the mass distribution of the galaxy, the anisotropy of the velocity distribution and the viewing angle. Galaxies with more concentrated light distribution will have larger central peaks in their σ profiles. Elliptical galaxies generally have σ profiles decreasing outwards (see e.g. D'Onofrio et al. 1995), and this is also the case for many early-type spirals (Paper VII), as a result of a centrally concentrated bulge. Here, we see that for the later type spiral galaxies there is no sign anymore in the σ profile of this central mass concentration, which is indeed expected for galaxies with lower bulge/disc ratios: for later types bulges are smaller and have lower surface brightness (see e.g. Falcón-Barroso et al. 2002). In some cases, however, we see that σ is increasing outwards, which is a sign of cooler central mass concentration. Emsellem et al. (2001), Márquez et al. (2003), Shapiro et al. (2003) and Paper VII have shown that these central σ -drops are quite common, and are in general associated with disc-like

⁵ We used WFPC2 images taken with the F606W filter for NGC 488, 628, 864, 1042, 2964, 3423, 3949, 4030, 4102, 4254, 4487, 5585 and 5668 and with the F814W filter for NGC 2805, 3346, 4775 and 5668.

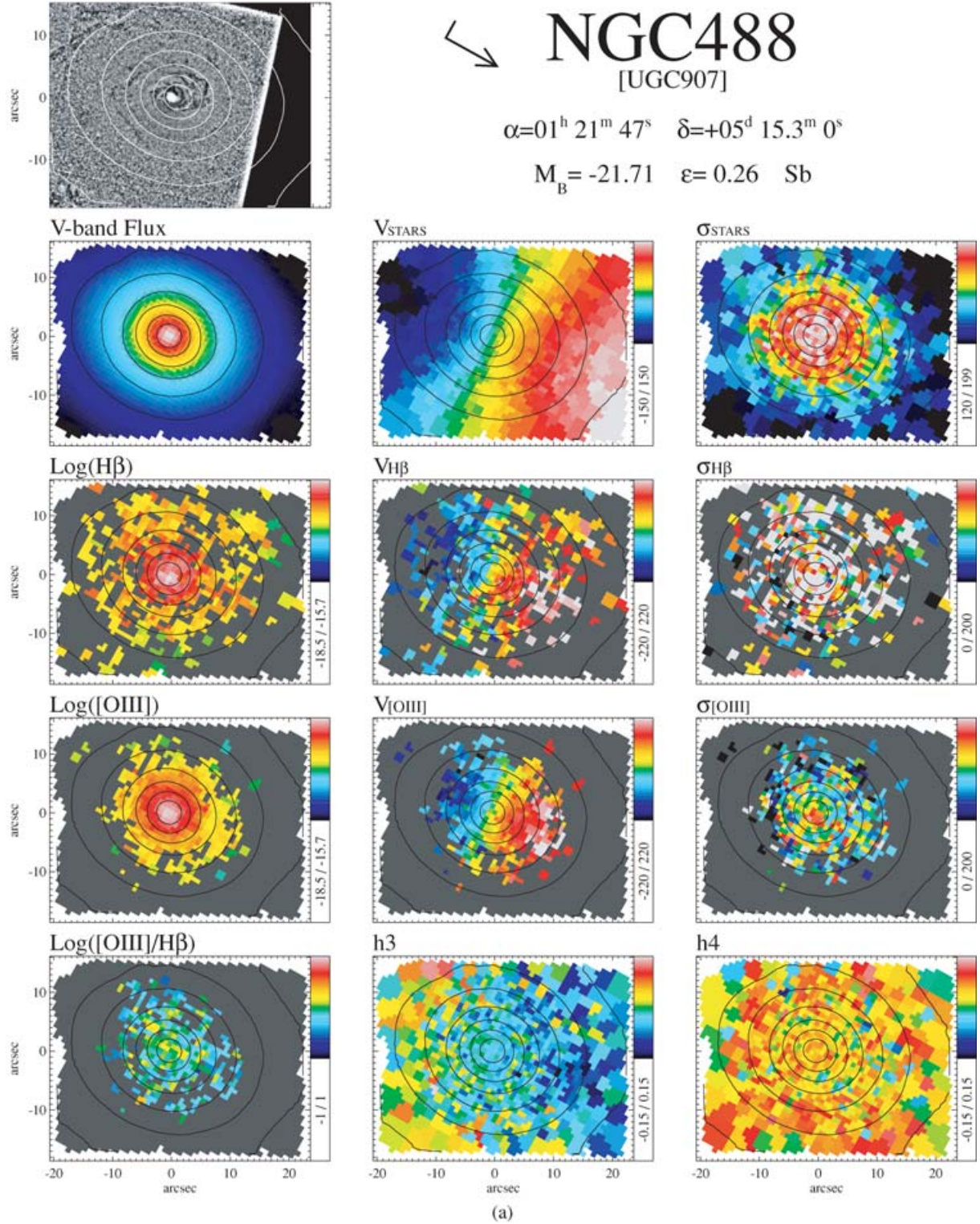


Figure 5. (a) Maps of stellar and gaseous kinematics for NGC 488. First row: unsharp-masked image and some astrometric information; second row: stellar flux (in mag arcsec $^{-2}$, with an arbitrary zero-point), velocity and velocity dispersion (in km s $^{-1}$); third and fourth row: respectively H β and [O III] fluxes (in erg s $^{-1}$ cm $^{-2}$ and logarithmic scale), velocity and velocity dispersion (in km s $^{-1}$); fifth row: [O III]/H β line ratio (in logarithmic scale), stellar h_3 and h_4 moments. The ranges are indicated in the box on the right-hand side of each map. In the gas maps, the dark grey colour is used for the bins with A/N below the selected threshold. (b) As in Fig. 5(a) for NGC 628. (c) As in Fig. 5(a) for NGC 772. (d) As in Fig. 5(a) for NGC 864. (e) As in Fig. 5(a) for NGC 1042. (f) As in Fig. 5(a) for NGC 2805. (g) As in Fig. 5(a) for NGC 2964. (h) As in Fig. 5(a) for NGC 3346. (i) As in Fig. 5(a) for NGC 3423. (j) As in Fig. 5(a) for NGC 3949. (k) As in Fig. 5(a) for NGC 4030. (l) As in Fig. 5(a) for NGC 4102. (m) As in Fig. 5(a) for NGC 4254. (n) As in Fig. 5(a) for NGC 4487. (o) As in Fig. 5(a) for NGC 4775. (p) As in Fig. 5(a) for NGC 5585. (q) As in Fig. 5(a) for NGC 5668. (r) As in Fig. 5(a) for NGC 5678.

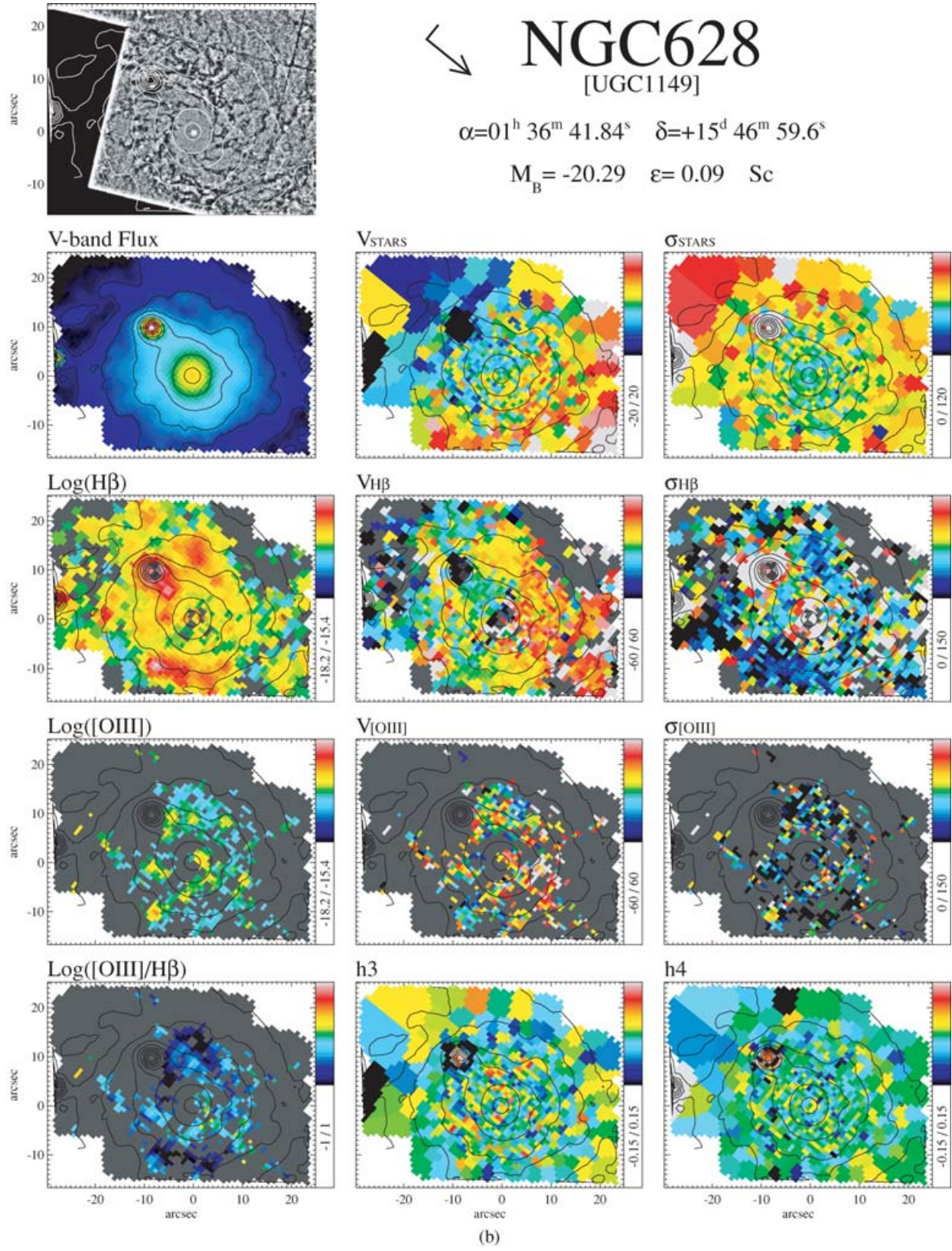


Figure 5 – continued

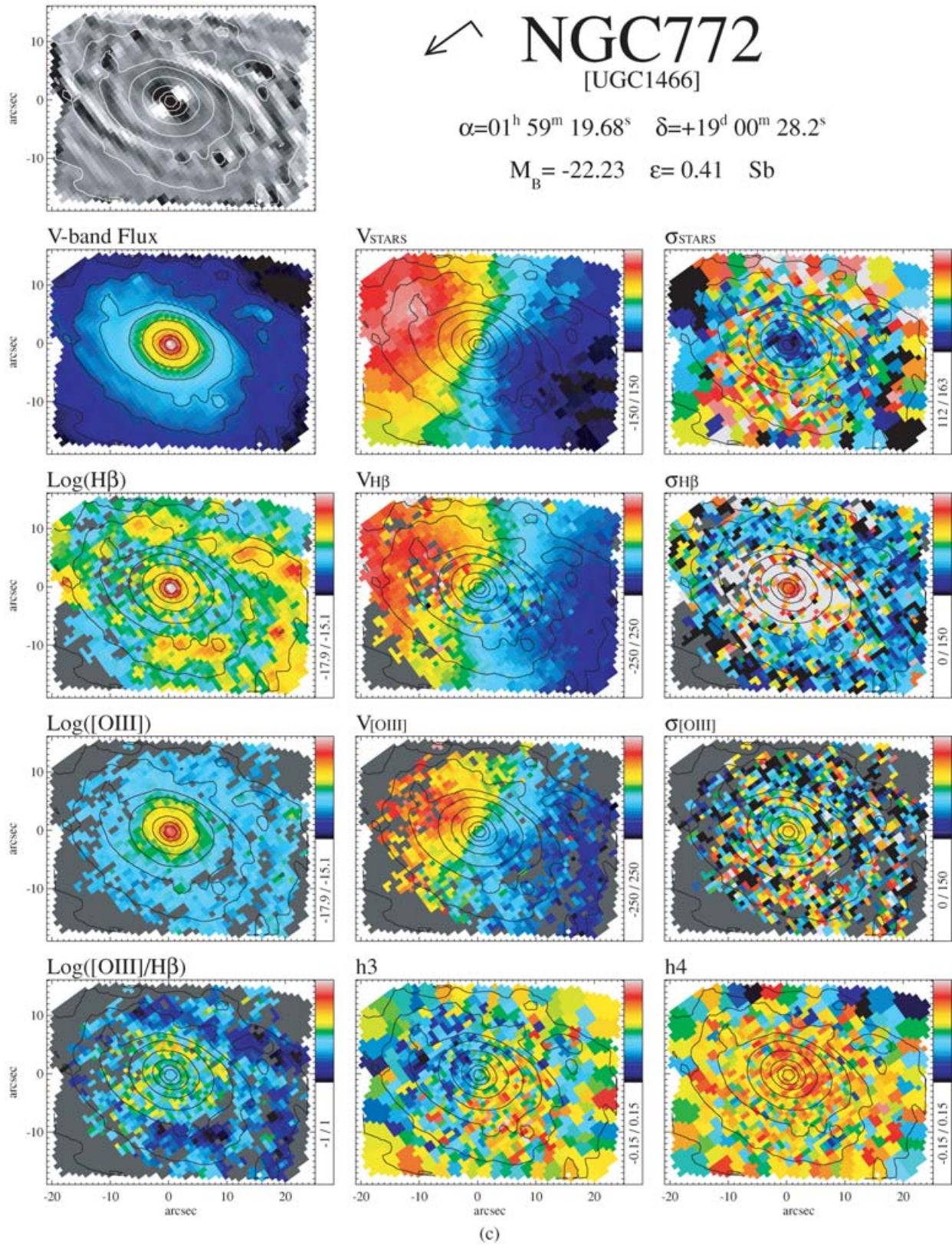


Figure 5 – continued

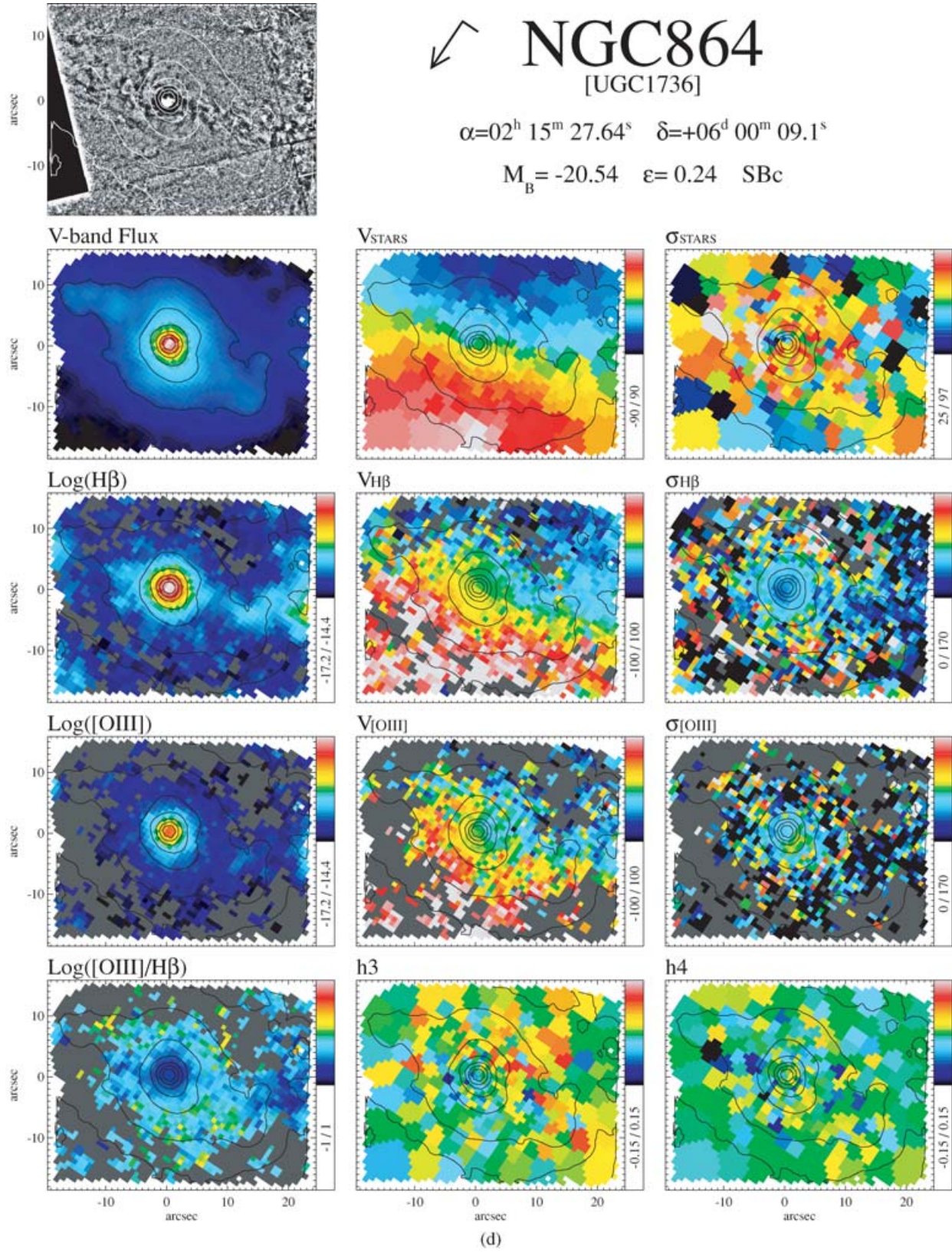


Figure 5 – continued

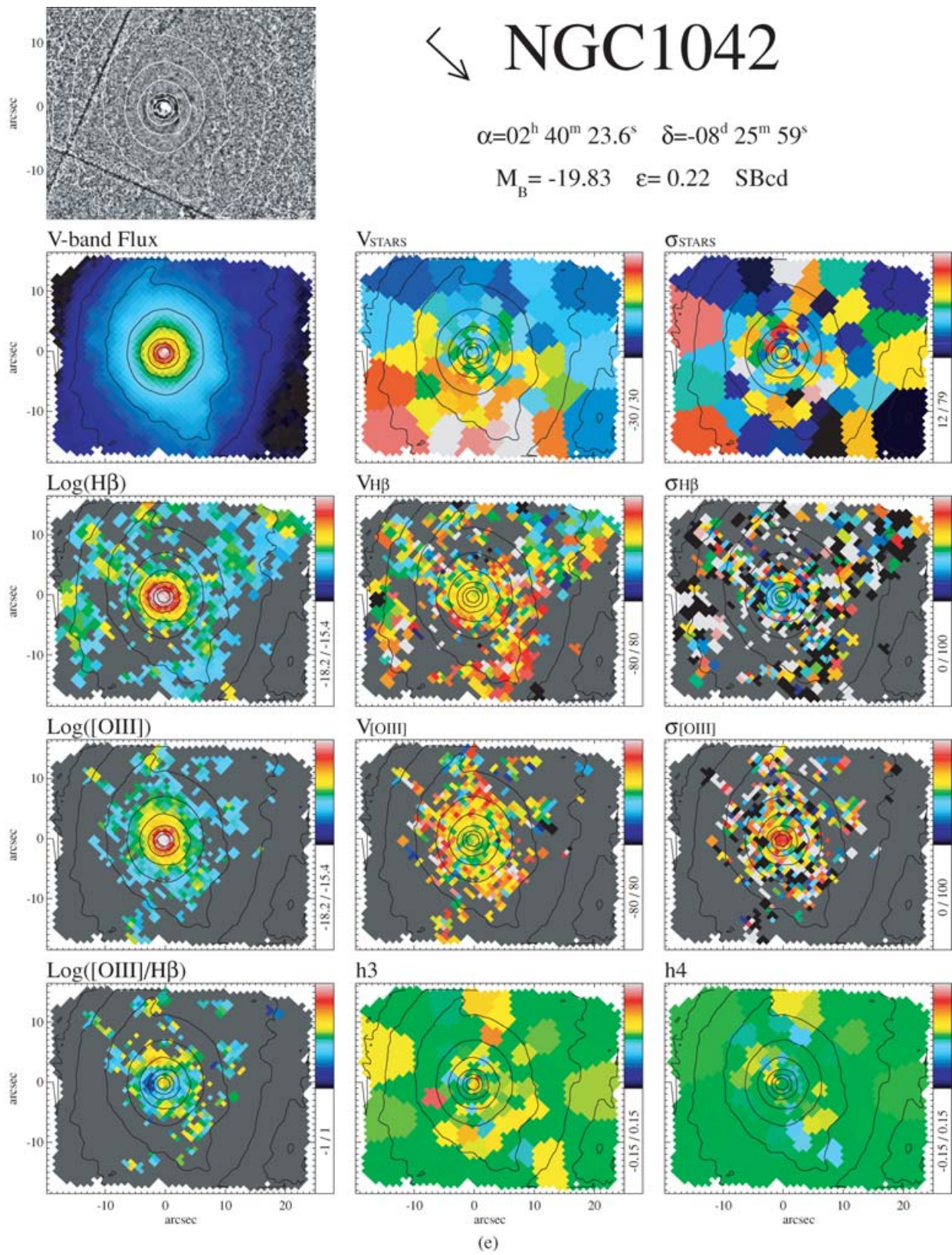


Figure 5 – continued

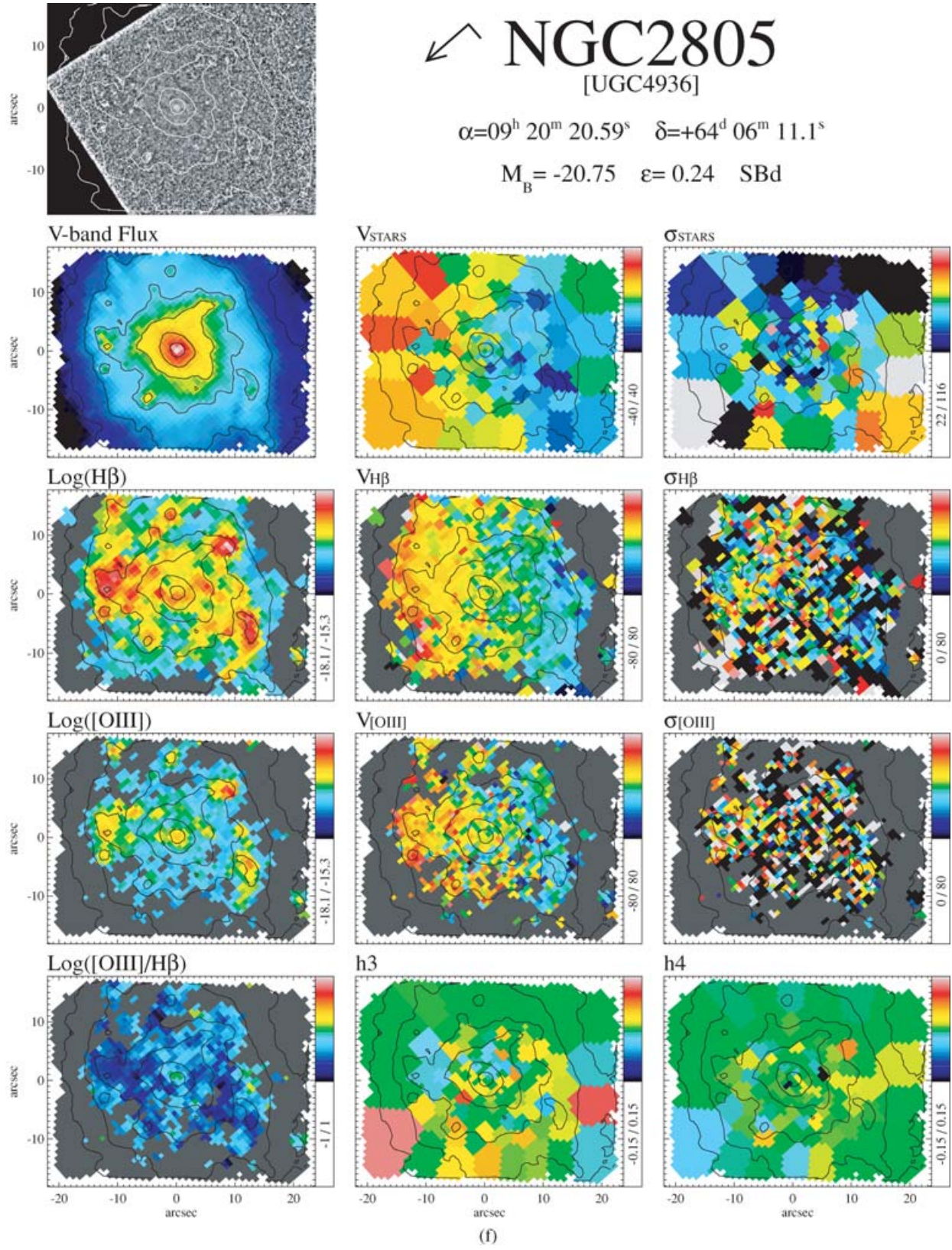


Figure 5 – continued

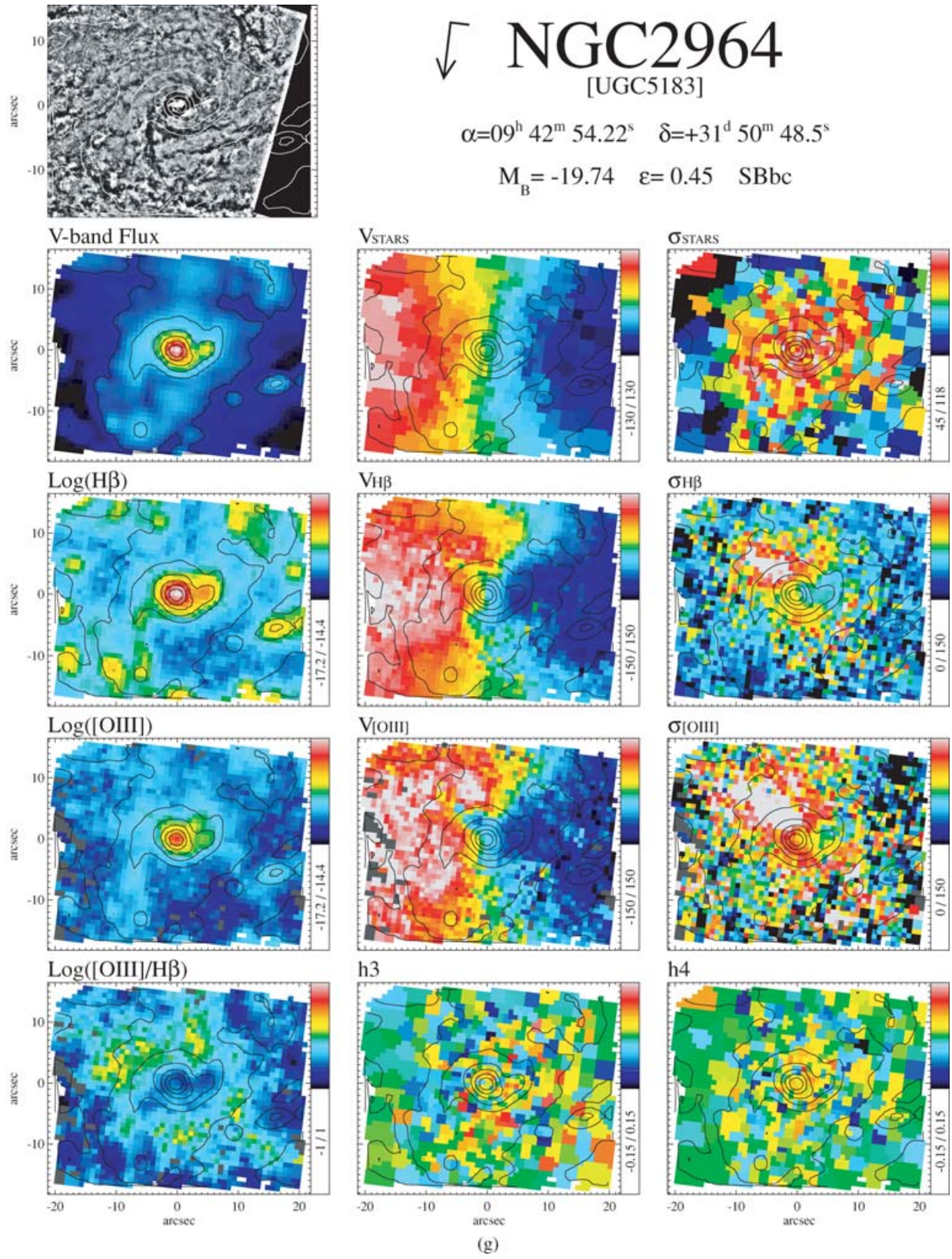


Figure 5 – continued

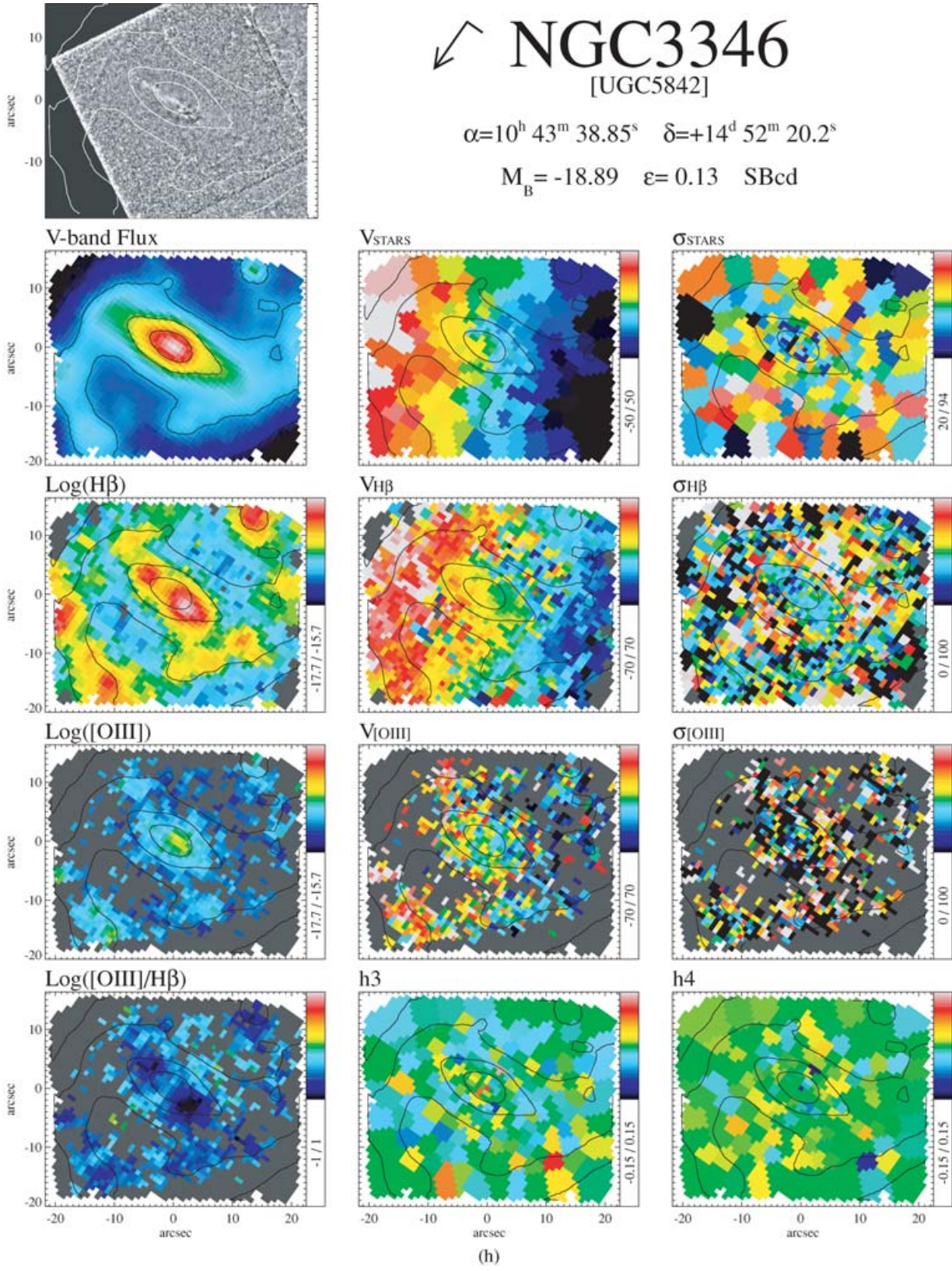


Figure 5 – continued

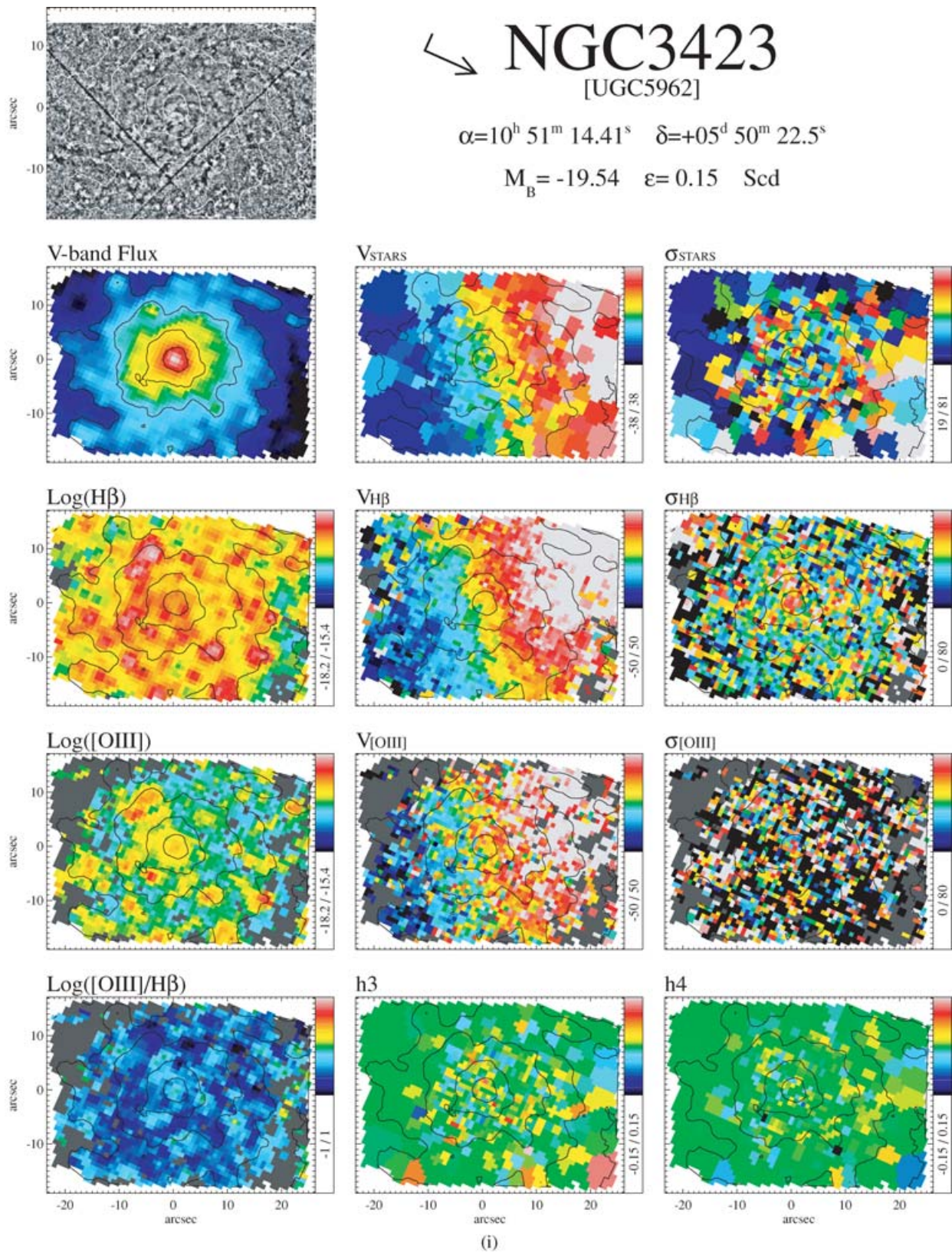


Figure 5 – continued

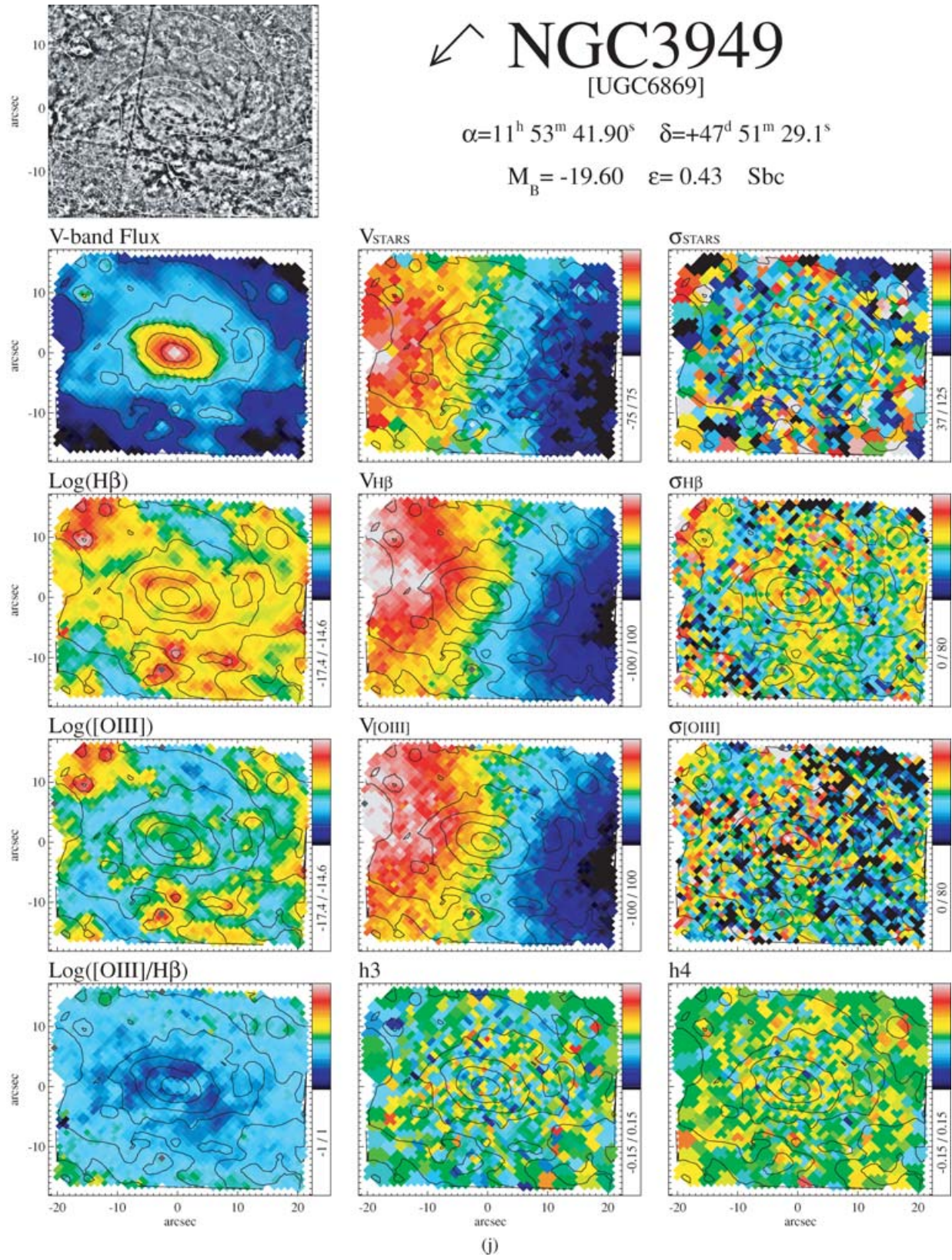
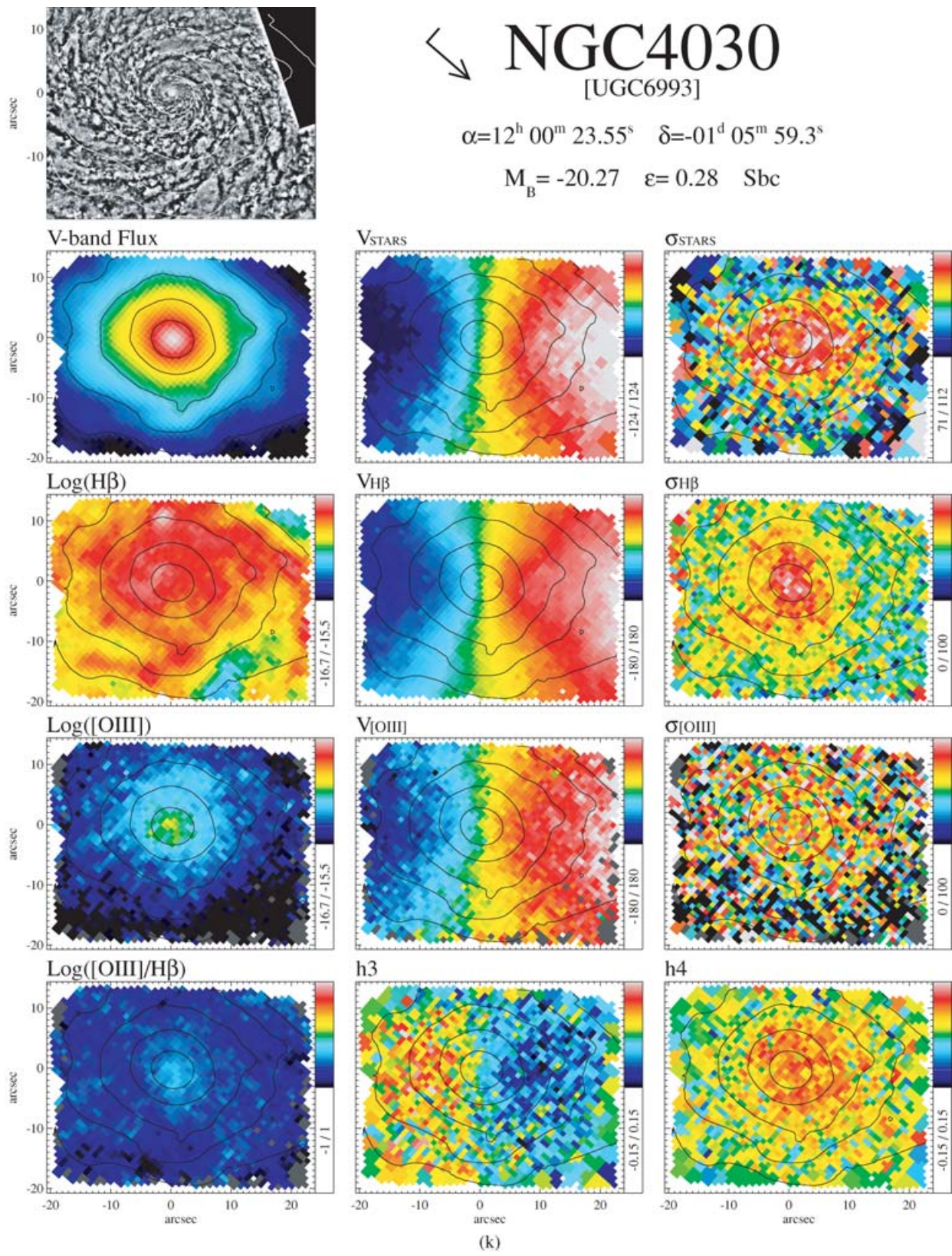


Figure 5 – continued

**Figure 5 – continued**

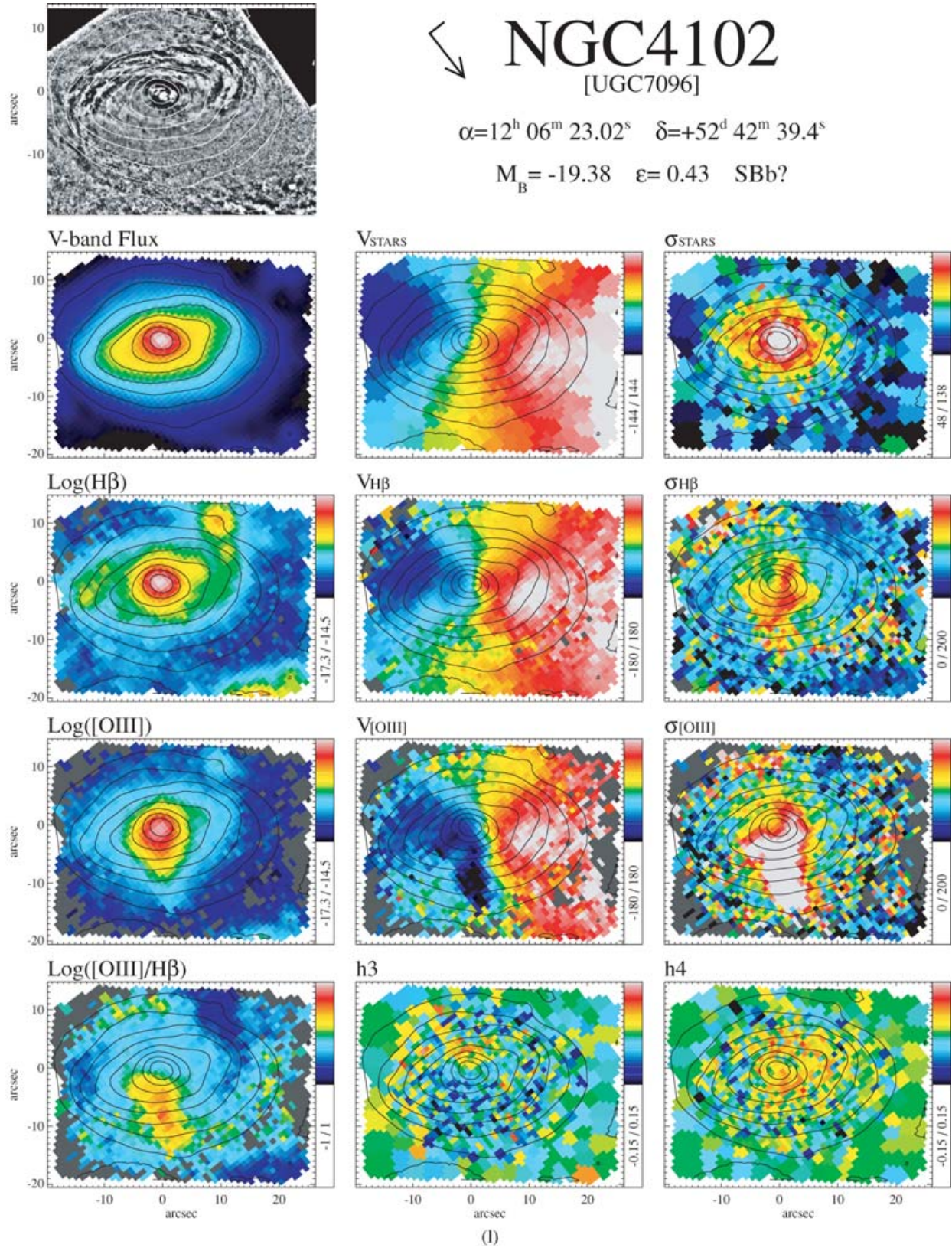
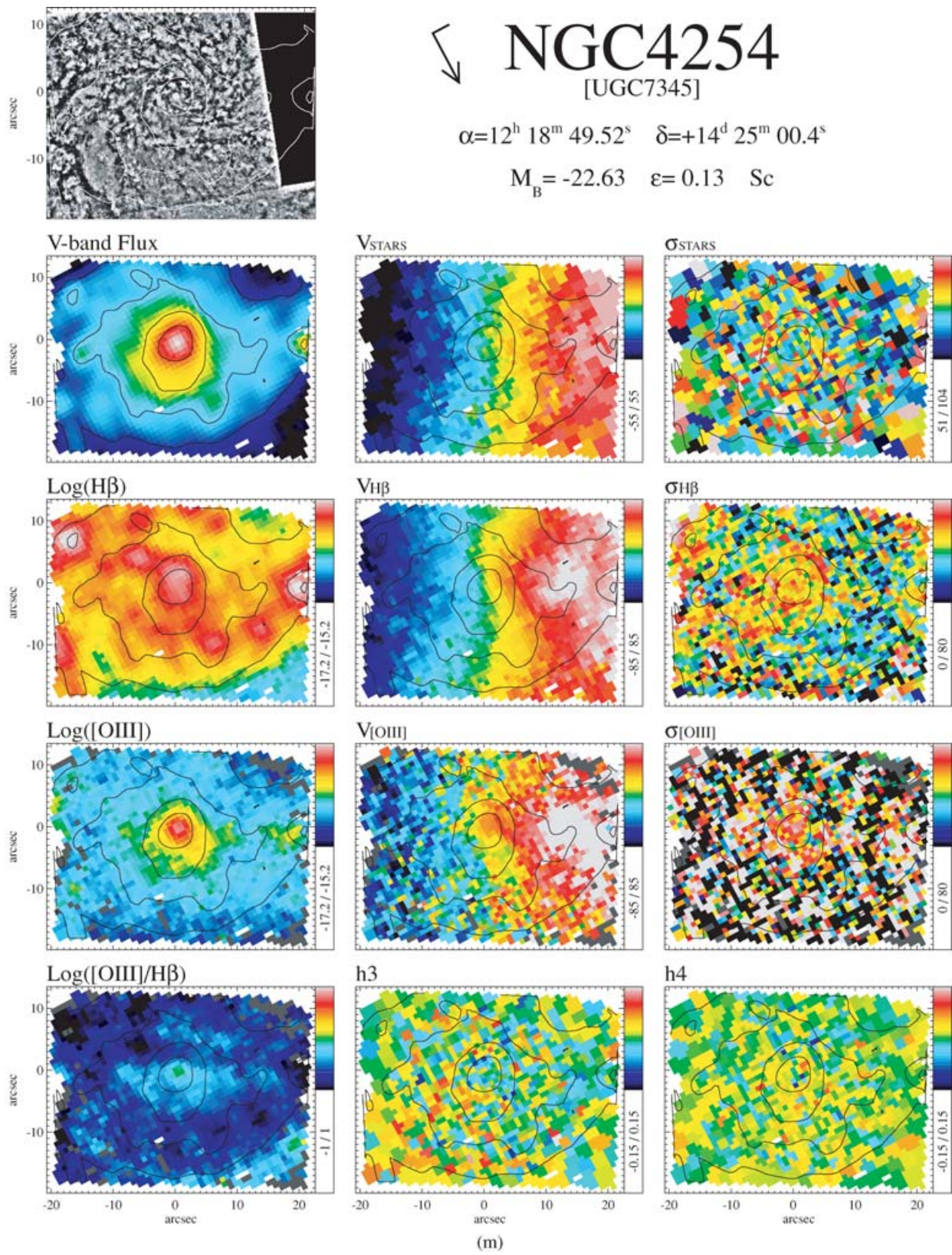


Figure 5 – continued

**Figure 5 – continued**

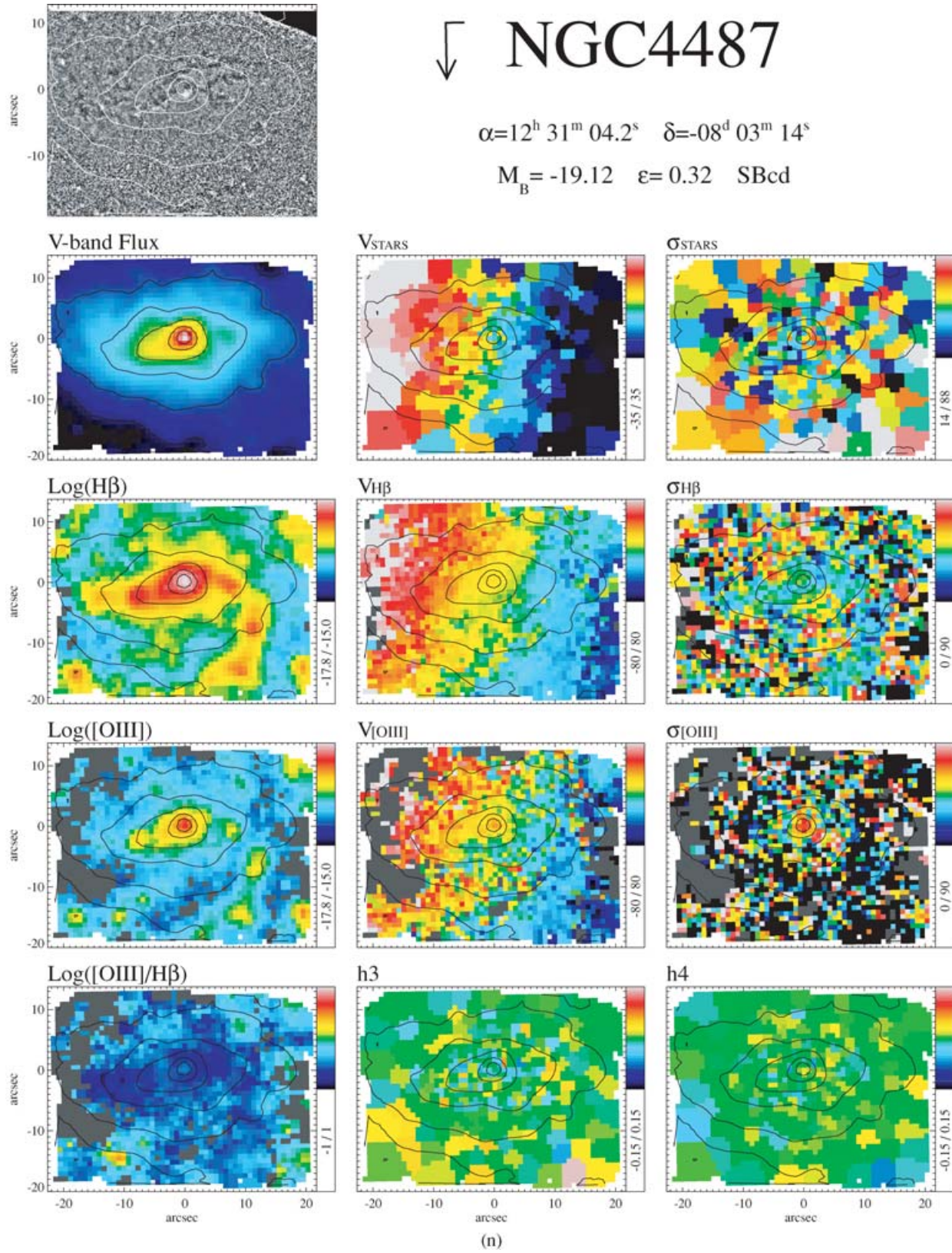


Figure 5 – continued

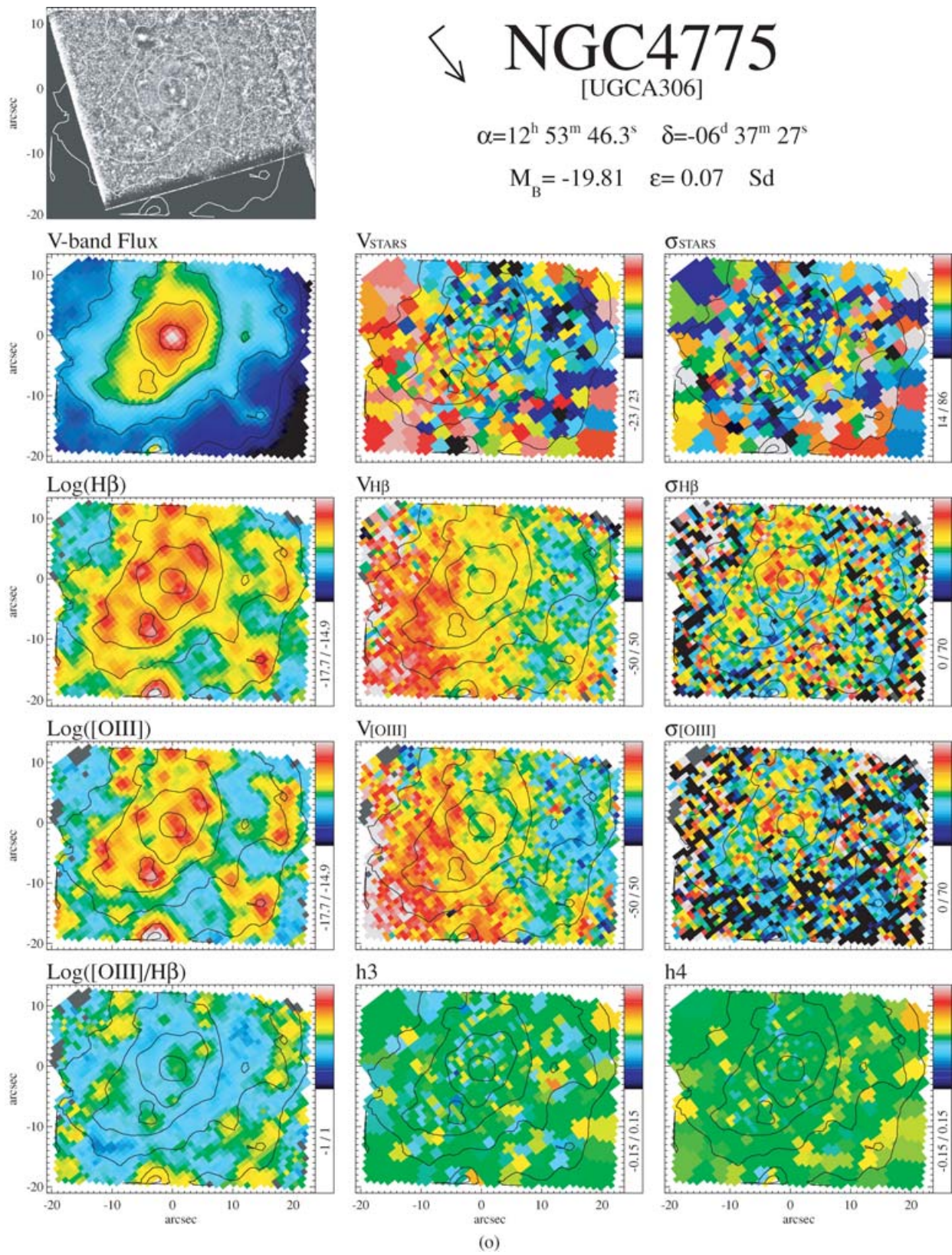


Figure 5 – continued

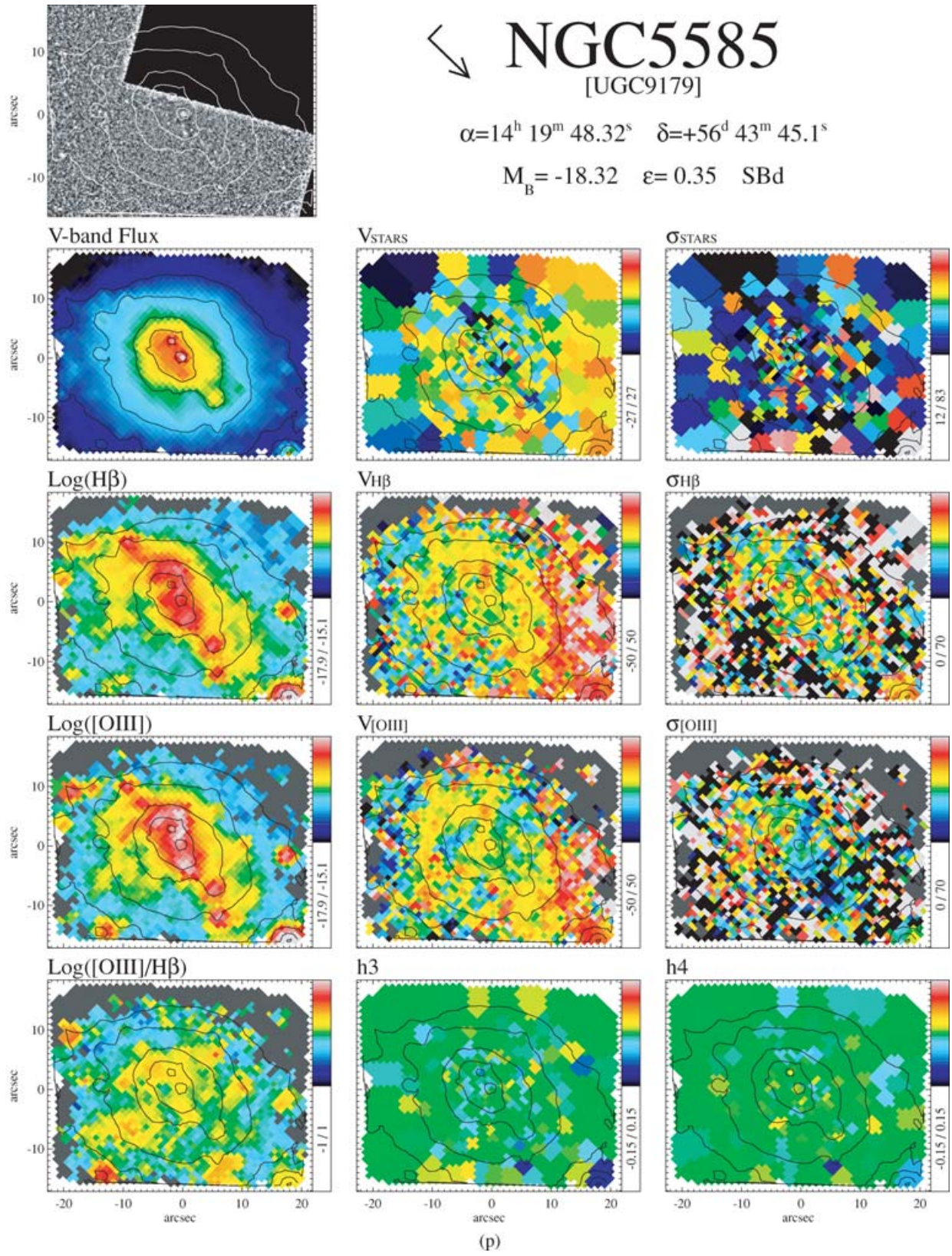


Figure 5 – continued

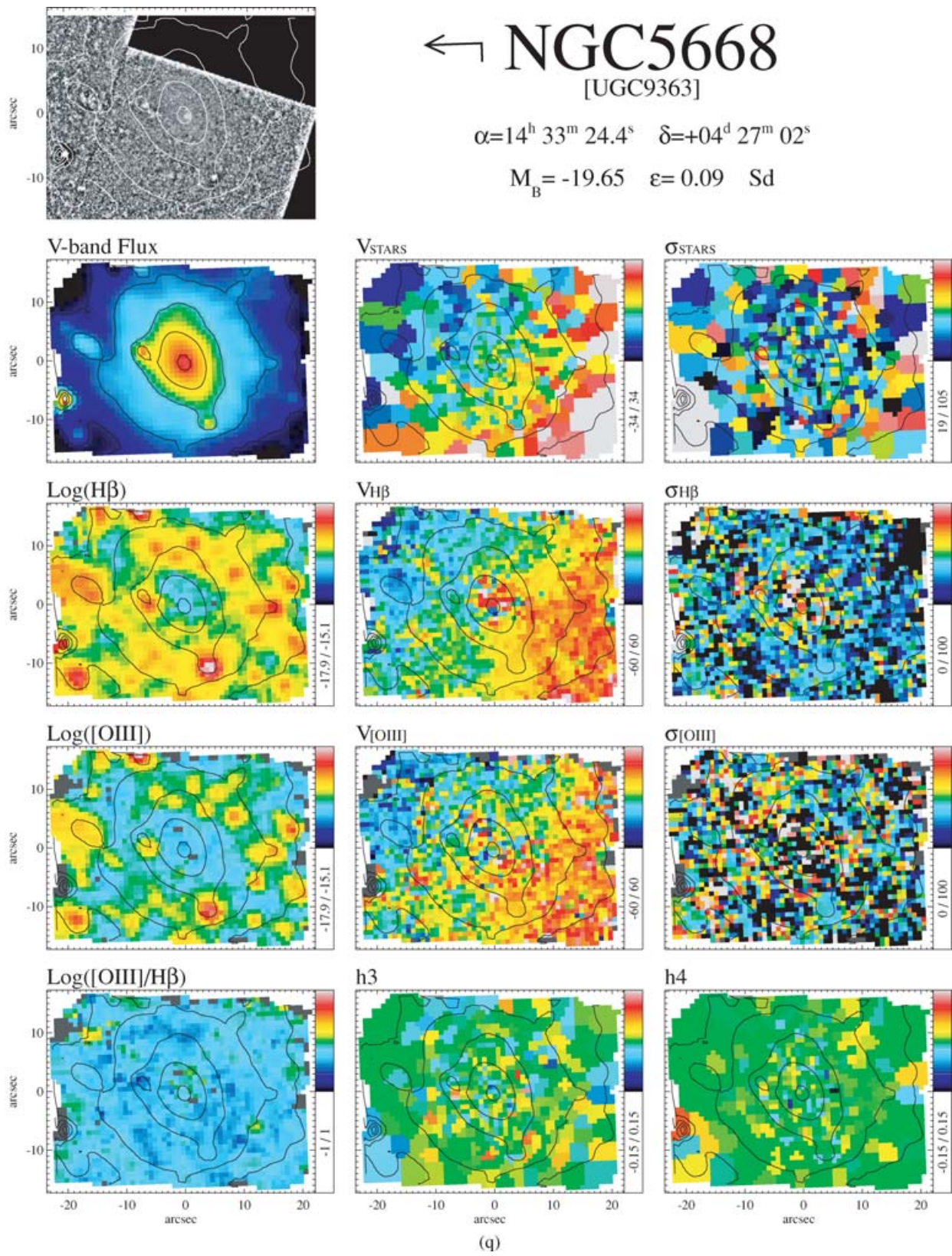


Figure 5 – continued

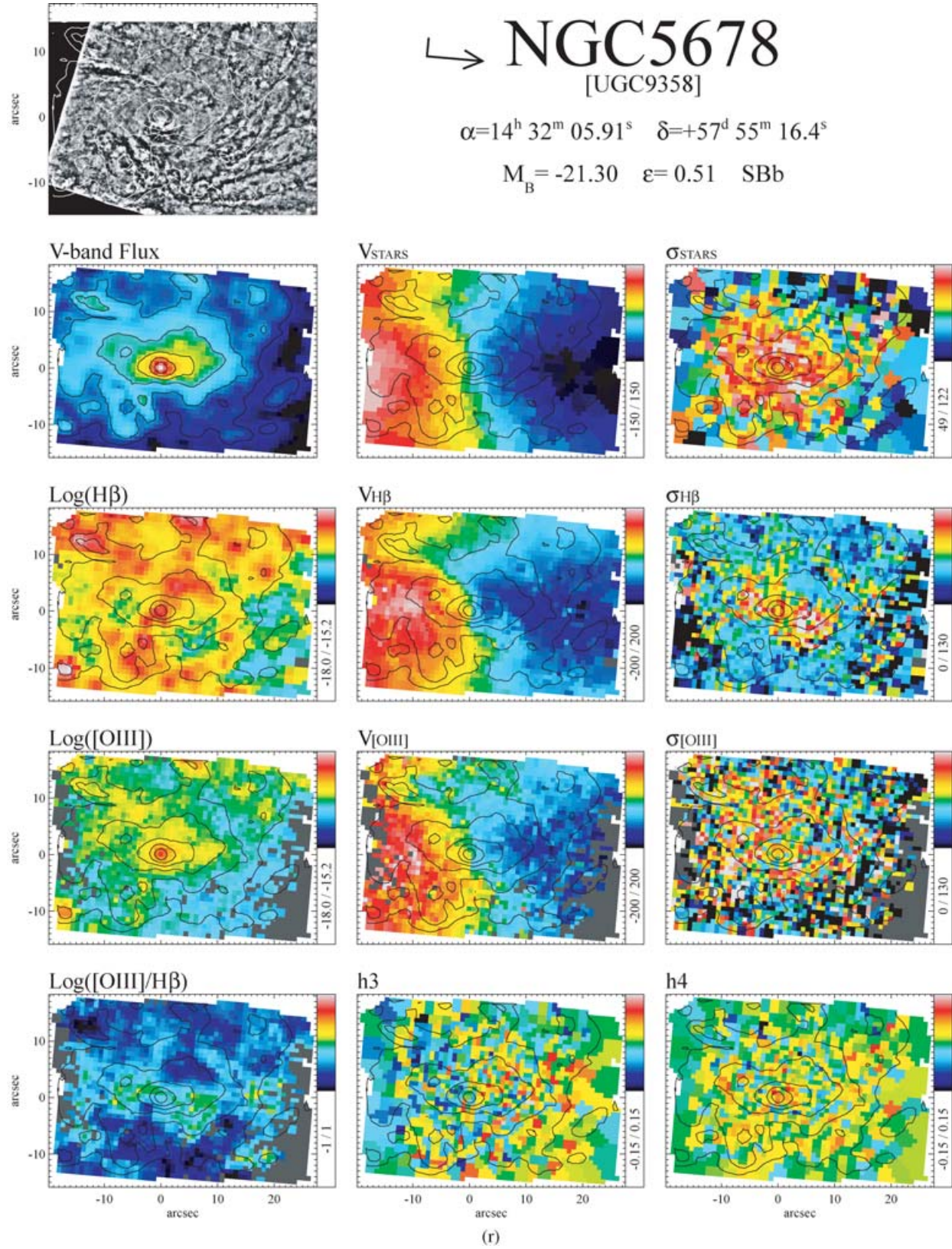


Figure 5 – continued

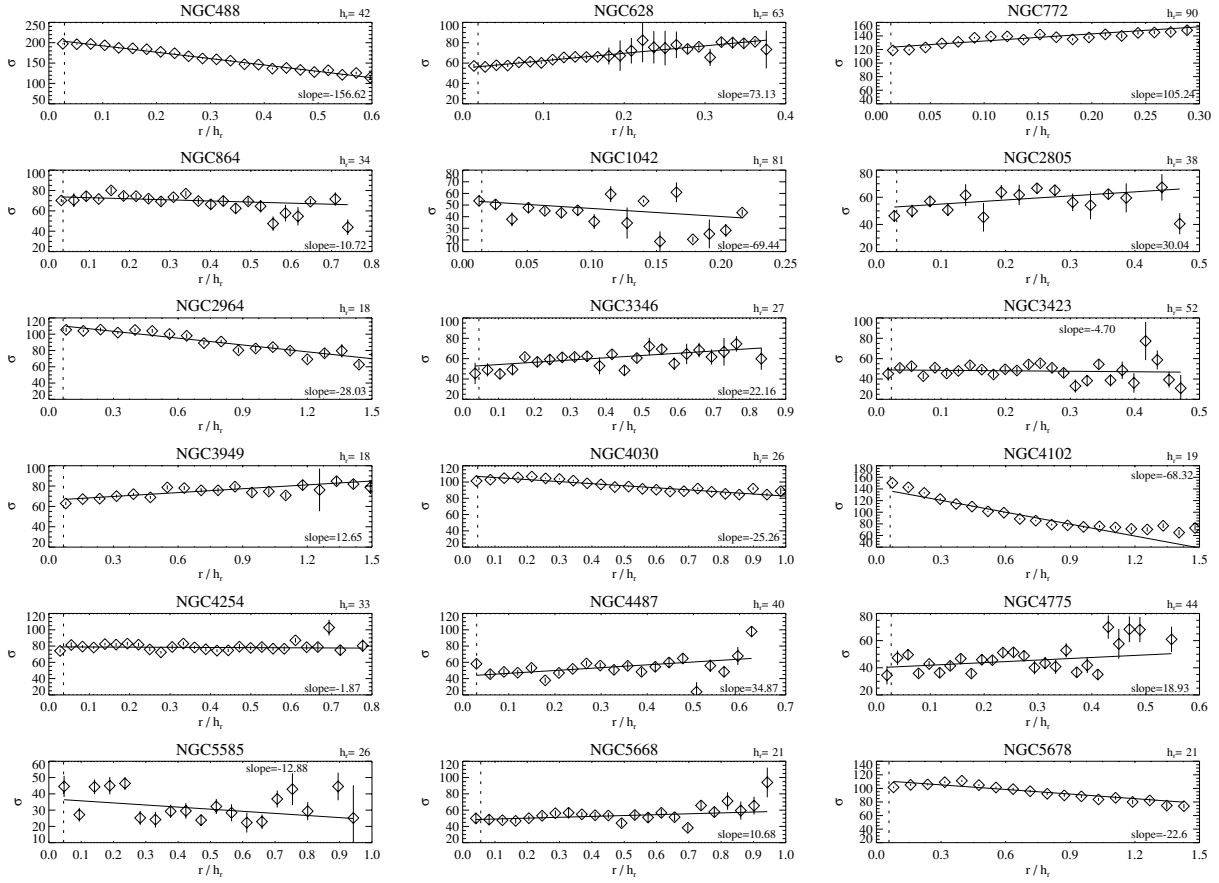


Figure 6. The plots present galaxy by galaxy the radial profile of stellar velocity dispersion (in km s^{-1}), calculated on elliptical annuli as explained in the text; on the horizontal axis we plot a scale-free radius, obtained dividing our radial coordinate (semimajor axis of the ellipses in arcsec) by the disc scalelength h_r (also expressed in arcsec and written above each plot). A straight line is fitted to the velocity dispersion profiles; the solid lines overplotted are the best-fitting straight lines, the slope of which is recorded in a corner of each panel; the dotted vertical line indicates in each panel the $r = 1.2$ arcsec line within which the central values of Table 1 were calculated.

structures. They are most likely due to stellar discs formed from gas that has been accreted towards the centre. This is in agreement with simulations by Wozniak et al. (2003). Our measurements show that also galaxies as late as Sd present velocity dispersion drops. The fact that the velocity dispersion profiles are flat or rising does not necessarily mean that these galaxies have no bulge – by detailed modelling in a future paper we will be able to answer this question.

6.2.2 Qualitative comparison with HST photometry

It is not straightforward to connect our kinematic results with photometry. In the last decade, analysis based on *HST* imaging (Carollo et al. 1997, 1998; Peletier et al. 1999; Böker et al. 2002; Carollo et al. 2002; Laine et al. 2002) revealed that late-type galaxies do not necessarily possess classical bulges⁶; they can instead host small-scale structures such as nuclear bars, nuclear star clusters, point-like sources. We cross-correlated the above-mentioned samples with our own and tried to look for kinematical signatures of the photometric features that they detected in the images. In Table 3 we tabulate the results of this comparison, based on a review of the relevant litera-

ture, on the appearance of our maps [Figs 5(a)–(r), Section 6.1] and of the radial behaviour of σ as well (Fig. 6).

According to Böker et al. (2002), NGC 1042, 2805, 3346, 3423, 4487, 4775, 5585 and 5668 host a nuclear star cluster and do not have a stellar bulge; our data show that the central regions of these objects are indeed cold. For any speculation on nuclear star clusters, caution is needed, since the nuclear star clusters detected with *HST* imaging have a spatial scale usually much smaller than the SAURON resolution. There are also cases where our observations nicely support the photometrical results: NGC 488 has a classical $r^{1/4}$ bulge (Carollo et al. 1997), and our maps show a hot, extended central region; NGC 4030 has also a large stellar bulge – although classified as ‘irregular’ and ‘exponential’ (Carollo et al. 1998) – and our data show a hot nuclear region. To conclude, the examples show that there is a correspondence between the photometric lack of a stellar bulge and the kinematical measurement that the inner regions are cold. At the moment this is a qualitative statement that requires further investigation. As previously stated, in a future paper we will study deeper the relation between the kinematical structures and the shape of the photometrical profiles.

6.3 Gas kinematics

In our data, the gas rotates usually faster than the stars and around the same axis; the gas velocity fields are much more complicated

⁶ We note here that Carollo et al. (1997, 1998, 2002) refer to a definition of classical bulge as a centrally concentrated stellar distribution with an amorphous, smooth appearance. This implicitly excludes gas, dust and continuing recent star formation (Wyse, Gilmore & Franx 1997).

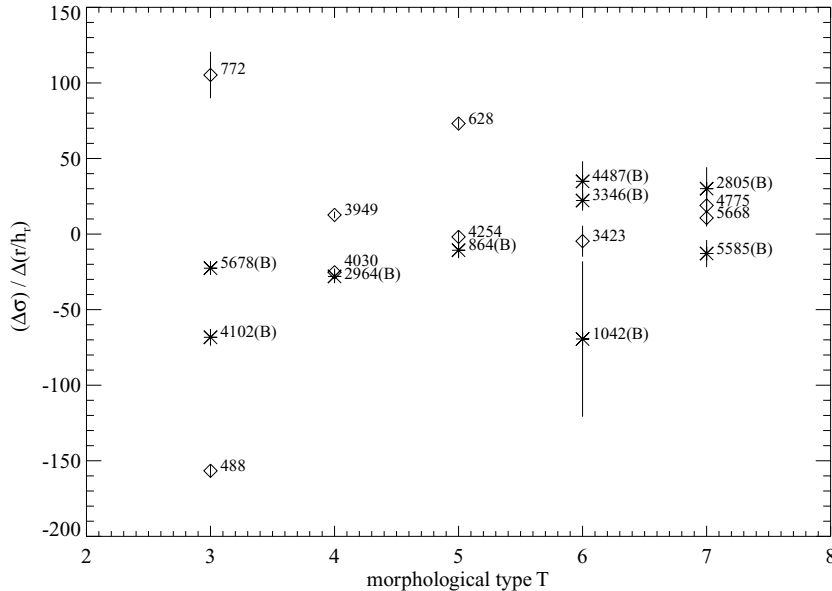


Figure 7. The fitted slope $\Delta\sigma/\Delta(r/h_r)$ of the velocity dispersion profiles is plotted here as a function of morphological type; the values for this slope are those indicated in the panels in Fig. 6. The galaxies classified as barred are here labelled with (B) and represented by asterisks; the NGC galaxy identifiers are indicated close to the corresponding symbol.

Table 3. Comparison with *HST* photometry. References in the table: C97, Carollo et al. 1997; C98, Carollo et al. 1998; C02, Carollo et al. 2002; B02, Böker et al. 2002. Abbreviations: $r^{1/4}$ b, de Vaucouleurs bulge; irb, irregular bulge (when a galaxy possess a central dense component but does not have a featureless appearance); expb, exponential bulge; nuc, nuclear compact source; nsc, nuclear star cluster; sf, nuclear star forming region. For a more accurate description of the photometric features, we refer the reader to the quoted papers.

NGC	<i>HST</i>	References	SAURON
488	$r^{1/4}$ b	C97	Hot central region
1042	nsc	B02	Low σ over the field
2805	nsc	B02	Cold central region
2964	sf, nuc	C97, C02	σ enhanced in the centre
3346	nsc	B02	Cold central region
3423	nsc	B02	Low σ over the field
3949	nuc	C02	Cold central region
4030	irb, expb	C98	Hot central region
4102	irb	C97	Hot central region
4487	nsc	B02	Cold central region
4775	nsc	B02	Low σ over the field
5585	nsc	B02	Low σ over the field
5668	nsc	B02	Cold inner region
5678	nuc	C02	Hot central region

Table 4. The table reports galaxy by galaxy the decimal logarithm of the global fluxes in the H β and [O III] emission lines, in erg s $^{-1}$ cm $^{-2}$.

NGC	log $FH\beta$	log $F[O\text{ III}]$	NGC	log $FH\beta$	log $F[O\text{ III}]$
488	-13.72	-13.79	3949	-12.32	-12.59
628	-13.34	-14.12	4030	-12.51	-13.18
772	-13.18	-13.59	4102	-12.69	-12.85
864	-13.03	-13.53	4254	-12.48	-13.13
1042	-13.84	-13.92	4487	-12.91	-13.40
2805	-13.32	-13.84	4775	-12.64	-12.70
2964	-12.60	-13.03	5585	-12.98	-12.89
3346	-13.47	-14.14	5668	-12.89	-13.15
3423	-12.93	-13.45	5678	-12.80	-13.33

differences between the velocity fields in the two lines, while the velocity dispersion is usually higher in H β ; exceptions to this statement will be highlighted in the description of the individual galaxies (Section 6.4). The differences between the two lines are particularly strong in the case of NGC 4102 (see also Fig. 3 and the related text), which is classified as a low-ionization nuclear emission-line region (LINER). Overall, the sample galaxies display low [O III]/H β ratios over most of the SAURON field, suggesting star formation, as expected in spiral galaxies.

6.4 Notes on individual galaxies

Here, we comment individually on the galaxies of our sample; for each of them, we first summarize the known properties from previous work, then we describe the most interesting features seen in our SAURON maps, shown in Section 6.1.

6.4.1 NGC 488

NGC 488 is the most ‘elliptical-like’ galaxy in our sample; it is an unbarred Sb galaxy with a very regular tightly wound spiral pattern, with a pitch angle of only 5° (Kormendy 1984; Gerssen,

Kuijken & Merrifield 1997), and a large and smooth central bulge. According to Carollo et al. (1997), this is a classical $r^{1/4}$ bulge. The rotation curve has been measured using H α and [N II]6583 Å data by Peterson (1980) out to a radius of 20 kpc, where he found that the velocity reaches ≈ 363 km s $^{-1}$, and continues to increase outwards. This galaxy has been studied using photometric and kinematic data to construct a dynamical model of bulge and disc (Fuchs 1997), concluding that the disc is dynamically cold.

The SAURON maps show regular stellar and gaseous rotation, with stars and gas rotating fast around the photometric minor axis and stellar velocity dispersion smoothly increasing towards the centre (consistent with the presence of the large bulge), to reach the highest value in our sample (around 200 km s $^{-1}$, see also Table 1 and Fig. 6). The gas turns out to be quite patchy (H β) and centrally concentrated.

6.4.2 NGC 628

NGC 628, also known as M74, is a well-studied grand-design spiral galaxy classified as Sc. It is known to be surrounded by an elliptical ring of neutral hydrogen extending well beyond the optical disc, out to $\approx 3R_{H_0}$ (isophotal radius at the 26.5 mag arcsec $^{-2}$ surface brightness level), lying in a plane which is $\approx 15^\circ$ inclined with respect to the plane of the bright inner disc (see Roberts 1962; Briggs et al. 1980; Briggs 1982). The origin of the warped velocity field of the outer galaxy has been debated, since the apparent isolation of this galaxy makes it difficult for tidal disruption to be responsible for the warp. UV observations of NGC 628 have shown spiral arms with a more symmetrical appearance than in the optical; Chen et al. (1992) identified in the UV a possible companion 7.6 arcmin south-west from the nucleus, which could have helped to clarify the origin of the outer warp, but later it turned out to be a spurious detection. From both near-infrared (NIR) spectroscopy of CO absorption and submillimetric imaging of CO emission, a circumnuclear ring of star formation has been seen (Wakker & Adler 1995, James & Seigar 1999). These rings are believed to exist as a result of a barred potential; Seigar (2002) claims that ground-based NIR images suggest the presence of an oval distortion at ≈ 2 kpc from the centre, which could be part of the dissolution of a bar and responsible for the circumnuclear ring. On the basis of their analysis of *HST* *H*-band images, Laine et al. (2002) found a bar on a ≈ 100 -pc scale; this would then be a case of nested bars.

From the stellar population side, Cornett et al. (1994) concluded that the star formation history of NGC 628 varies with galactocentric distance; Natali, Pedichini & Righini (1992) suggested that the galaxy could be seen as an inner and an outer disc characterized by different stellar populations; according to them, the transition between the two regions is located at ≈ 8 –10 kpc from the centre.

NGC 628 can be resolved from the ground into individual supergiants and H II regions (Sohn & Davidge 1996). Many previous studies focused on the H II regions; Belley & Roy (1992) derived redshifts, H β emission-equivalent widths and metallicities for 130 H II regions; Ivanov et al. (1992) classified a similar number of stellar associations. Sohn & Davidge (1996) studied a large number (more than 300) of stellar objects in the disc of NGC 628, measuring brightness and colours, finding some recent star formation and getting an estimate of the distance modulus (29.3 mag).

Our observations of NGC 628 are disturbed by the presence of a foreground star which falls close to the centre (≈ 13 arcsec southern); as mentioned in the caption to Table 2 our first exposure on this galaxy was centred on this foreground star. During our last two

exposures, the observing conditions were not optimal: the seeing went up to ≈ 2 arcsec.

From our data we can measure slow projected rotation around the minor axis, as expected for an almost face-on object. The stellar velocity dispersion decreases in the central zones, indicating a cold central region, maybe an inner disc. Photometric observations at UV wavelengths from Cornett et al. (1994) did not show evidence for a bulge: the nucleus of NGC 628 has the appearance of disc material in the UV. The ionized gas rotates in a way similar to the stars; the H β distribution turns out to be more extended than the [O III] distribution, both of them suggesting an annular structure.

6.4.3 NGC 772

NGC 772, named also Arp78, forms a pair at 3.3 arcmin with the E3 galaxy NGC 770. It is an Sb galaxy characterized by a particularly strong spiral arm; it is known to have faint H II regions (Oey & Kennicutt 1993) and extended H I, to a radius ≈ 75 kpc (Rao & Briggs 1993).

The unsharp-masked SAURON image (no optical *HST* image is available) displays a well-defined dust pattern, with the dust following the spiral arms. From the stellar kinematical maps, we can see that in the central region there is a clear drop in the stellar velocity dispersion and h_3 turns out to anticorrelate with the velocity, as expected for a rotating disc; the stellar velocity map shows rotation around the photometric minor axis and a mildly S-shaped zero-velocity line. The gas, especially in H β , rotates in a more complex way than the stars, with a very strongly S-shaped zero-velocity line, and its distribution follows the spiral arm pattern. The [O III] velocity field is instead much more regular. The gas velocity dispersion in the H β line is flat and low beyond ≈ 10 arcsec, enhanced in an annular region around the centre and depressed again in the nucleus – although still well higher than in the outer parts. All of this is also seen in the [O III]/H β map, where we can recognize regions with very low values corresponding to the spiral arms and to low values in the ionized-gas velocity dispersion.

6.4.4 NGC 864

Nuclear radio emission has been found in this barred Sc spiral galaxy (Ulvestad & Ho 2002); the nuclear radio source has diffuse morphology, with linear size of ≈ 300 pc.

The SAURON maps show rotation both in the stellar and gaseous components, around the photometric major axis, e.g. the rotation axis is oriented as the bar; but looking at a larger-scale image (see e.g. Fig. 2) we can see that the major axis of the bar turns out to be the global minor axis when considering the whole optical galaxy. The stellar velocity dispersion is flat and low over the entire SAURON FOV. The gas flux follows the nucleus plus bar structure, as visible especially in the H β case. The line ratio [O III]/H β is also structured in a similar way, assuming low values along the bar and in particular in the central ≈ 4 -arcsec circle, which could indicate a star forming nucleus. Interestingly, this region corresponds to a local minimum in the H β velocity dispersion map, which assumes in the centre lower values than the dispersion in [O III], differently to what happens in most of our galaxies.

6.4.5 NGC 1042

This Scd galaxy forms a pair with the Sc galaxy NGC 1035 at a separation of 22 arcmin (corresponding to 177 kpc). It has a bright,

small nucleus and otherwise low surface brightness. Neutral hydrogen has been detected at positions corresponding to the optical centre and two adjacent regions (Bottinelli & Gouguenheim 1980).

In our data, this galaxy has a quite poor S/N, so that the stellar binning is quite heavy. There are some indications of slow projected stellar rotation, but in general the kinematical maps are difficult to interpret. The gas is quite patchy and does not cover, at the chosen A/N level, the whole SAURON field. In contrast to what is seen in the majority of our galaxies, the velocity dispersion in [O III] is higher than in H β , especially in the central region.

6.4.6 NGC 2805

NGC 2805 is an Sd galaxy seen nearly face-on and it is the brightest member of a multiple interacting system containing also NGC 2814 (Sb), NGC 2820 (Sc) at 13 arcmin and IC2458 (I0). According to Hodge (1975), in this group the H II regions appear distorted on the side of the galaxy opposite to the companion. H I has been detected (Reakes 1979; Bosma et al. 1980) and there are claims that the outer H I layers are warped (see e.g. Bosma et al. 1980). The galaxy seems to be also optically disturbed, since the spiral arms appear to be broken up into straight segments.

From our SAURON data, we find slow projected stellar velocities and a central drop in velocity dispersion. The gas has a clumpy distribution and rotates consistently with the stars. The line ratio [O III]/H β is low all over the field, possibly indicating ongoing star formation everywhere.

6.4.7 NGC 2964

NGC 2964 is a barred Sbc galaxy and forms a non-interacting pair with the I0 galaxy NGC 2968 at 5.8 arcmin. From *HST* images Carollo et al. (1997) detected a resolved central compact component, possibly star forming. CO has been detected by Braine et al. (1993); they suggested that the galaxy might contain an unresolved nuclear ring.

Our data reveal a variety of features in this galaxy. The stars rotate in a quite regular way, although a twist in the zero-velocity line can be seen very close to the edge of the field, on both sides. The stellar velocity dispersion increases smoothly towards the centre. Two-dimensional maps of stellar velocity and velocity dispersion for this galaxy have recently been published by Batcheldor et al. (2005). Although their maps deliver a lower spatial resolution than ours and a smaller FOV, there is a global agreement between the two observations. They also provide central values for the higher Gauss–Hermite moments h_3 and h_4 ; the latter value is larger than ours.

The ionized gas has a clumpy distribution, which could suggest a spiral arm structure, and complex kinematics in both lines, with a very irregular zero-velocity line and with the velocity dispersion peaking in an off-centre region. The velocity dispersion in [O III] is enhanced with respect to H β . Overall, the gas motions are consistent with the stellar rotation. In the region of the gas- σ peak, the spectra show also complex line profiles; in some bins we find double-peaked lines in the [O III] spectral region (see discussion in Section 4.2). It could be that we are seeing the regular gas motion together with an ionization cone, caused by a central active galactic nucleus (AGN), as is probably also the case in NGC 4102. Up to now, NGC 2964 has not been classified as an AGN yet. The double-peaked line shape characterizes only a few spectra, so we applied our standard method which fits single Gaussians to the emission lines. The [O III]/H β

line ratio is small over most of the field, and is enhanced in a ring-like structure (see also Braine et al. 1993) surrounding an elongated nuclear region where the ratio becomes low again. This could be a star forming region, in accordance with Carollo et al. (1997).

6.4.8 NGC 3346

This is a barred Scd galaxy, for which only little information is available from the literature. The SAURON data show regular stellar rotation around an axis slightly misaligned with respect to the direction perpendicular to the bar, with complicated structures in the very inner regions; the stellar velocity dispersion is everywhere low and flat, and it seems to be depressed in a central region elongated in the same direction as the bar; the map is quite patchy. The ionized gas is concentrated along the bar and the spiral arms and rotates similarly to the stars, although the gas velocity fields appear quite patchy. The H β distribution is more extended than [O III]. The line ratio [O III]/H β is depressed along the bar, particularly in bubble-shaped spots, as the H β velocity dispersion does as well; these could be star forming regions.

6.4.9 NGC 3423

Also for this Scd galaxy there is not much literature to refer to. In the SAURON maps we measure slow projected stellar rotation and low velocity dispersion. The gas shows a clumpy distribution and rotates faster than the stars and around the same axis. [O III]/H β is everywhere low, possibly indicating wide-spread star formation.

6.4.10 NGC 3949

NGC 3949 is an Sbc galaxy in the Ursa Major cluster. Optical images show a diffuse extended halo (Tully et al. 1996). It has been observed with the Westerbork Synthesis Radio Telescope (Verheijen 1997): H I is detected well beyond the optical galaxy.

The SAURON maps show rotation both in the stellar and gaseous components. The stellar velocity dispersion indicates a cold inner region. This galaxy is part of the sample observed by Batcheldor et al. (2005); as in the case of NGC 2964, their reported central h_4 value is larger than ours. Integral-field observations of NGC 3949 are presented also by Westfall et al. (2005); their central values for the stellar velocity dispersion are in good agreement with ours; the agreement at larger radii and in the gas velocity dispersion is less satisfactory. The gas has a complex and clumpy distribution and its velocity fields present the same characteristics as the stellar one: global rotation and irregular zero-velocity line. The global appearance of the previously mentioned H I velocity field resembles our SAURON velocity maps. Overall, [O III]/H β is low, especially in a circumnuclear region. No correspondence between the line ratio and the highly complex gas velocity-dispersion maps is evident.

6.4.11 NGC 4030

Carollo et al. (1998) analysed the *HST* images of NGC 4030, and found tightly wound flocculent spiral structure reaching the nucleus and an irregular, exponential bulge. Our observations of NGC 4030 have a very high S/N, so that the data are of extremely good quality. The kinematical behaviour of this Sbc galaxy is characterized by very regular rotation of stars and gas around the minor axis. The velocity dispersion increases smoothly moving inwards, becoming possibly flat in the nuclear region (see Fig. 6), and the stellar h_3

anticorrelates with the velocity, as expected for a rotating disc. Our gas flux maps show a central concentration, although in H β some structure is visible that could be related to the spiral arms and/or dust lanes pattern: as can be seen in the unsharp-masked image and as already noticed by Carollo et al. (1998), the spiral arms and dust lanes structures extend down to the innermost scales. From long-slit H α optical spectroscopy extended over ≈ 80 per cent of the optical image, Mathewson & Ford (1996) derive a rotation curve with maximum rotation velocity of $\approx 236 \text{ km s}^{-1}$. Our gas velocity regularly increases going outwards, up to a value of $\approx 180 \text{ km s}^{-1}$ at the edges of the field. Since the outermost radius of our data is smaller than the one of the quoted observations, there is not necessarily a disagreement.

6.4.12 NGC 4102

NGC 4102 shows a bright central bar from which two tightly wound and dusty spiral arms depart (Verheijen 1997). In the NED data base, this object is classified as a LINER; it is known to be a powerful far-infrared galaxy (Young et al. 1989) and also to have a strong nuclear radio source (Condon et al. 1982). Devereux (1989) classified it as one of the most powerful nearby starburst galaxies. From optical spectroscopy of the ionized swept-up gas, Boer (1994) determined the time-scale of the central starburst wind to be of the order of 10^6 yr – a young starburst. Gonçalves, Véron-Cetty & Véron (1999) recognized a weak Seyfert2 component, mainly detected by the broadening of the [O III] lines. NGC 4102 has also been observed in CO: Jogee & Kenney (1996) found a compact CO morphology and a CO velocity field characterized in the inner 200 pc by purely circular motion, and a sharp discontinuity in gas kinematics at larger radii, around 3 arcsec; this could be due to streaming motions along the bar. H I has been detected in absorption against the bright central radio source (Verheijen 1997).

The signs of all the documented activity going on in this galaxy are detectable also in our SAURON maps: the gas kinematics turn out to be extremely complicated. As mentioned in the discussion in Section 6.3, this is the only case in our sample with a significant difference between the kinematics of the H β and [O III] lines: the H β velocity field resembles more closely the stellar one, although it is more irregular, while the [O III] maps trace more likely the outflowing gas. This can be also seen by looking at the gas flux maps: in [O III] the central gaseous concentration appears to be elongated in a north-western direction, which is not the case in the H β distribution, that follows instead the spiral arm pattern. The [O III] velocity dispersion is also elongated in the same direction. Together with NGC 2964, this is the only galaxy in our sample where we find emission lines that are not well fitted by single Gaussians (see the discussion in Section 4.2 and Fig. 3). The complex line profiles are found only in the region corresponding to the maximum difference between the H β and [O III] kinematics (which is also, as already noticed, the region of the [O III] σ peak and flux elongation); there the [O III] lines turn out to be broadened, in accordance with Gonçalves et al. (1999). According to our measurements, the [O III]/H β line ratio is then enhanced in the outflow region, as expected for an active object. As for the stellar kinematics, we do not see signs of activity there: the stars behave in a much more quiet way, with regular rotation and velocity dispersion increasing from the outer parts towards the centre.

6.4.13 NGC 4254

NGC 4254, known also as M99, is one of the brightest spiral galaxies in the Virgo cluster. Its optical appearance is characterized by

the one-arm structure: the arms to the north-west are much less defined than the southern arm. This kind of spiral structure could be related to an external driving mechanism, but for NGC 4254 there are no close companions and no evident signs of past interactions (Rauscher 1995). Phookun, Vogel & Mundy (1993) carried out H I and H α observations of this Sc galaxy, detecting non-disc H I emission, coming mostly from a region to the north of the galaxy and contiguous with it in the plane of the sky; according to the authors, the non-disc H I corresponds to 3 per cent of the total H I mass; they do not find H α emission corresponding to the non-disc gas, which indicates little or no star formation there. They interpreted these observational results as infall of a disintegrating gas cloud; this could have caused the asymmetry in the spiral structure. H α intensity and velocity fields are presented also in Chemin et al. (2006), confirming the asymmetry in the prominent spiral structure and detecting streaming motions along the arms. There are also claims for the presence of a weak bar with a PA of $\approx 60^\circ$, although NGC 4254 is classified as unbarred (Sakamoto et al. 1999, from analysis of the molecular gas distribution).

We observed this galaxy under bad seeing conditions (≈ 3 arcsec). Our kinematic maps reveal regular stellar rotation, although the stellar zero-velocity line is twisting towards the edges of the field. The gas flux follows the spiral pattern, which is particularly evident in the H β case and can be seen also in the [O III]/H β line ratio, which assumes particularly low values in bubble-shaped regions along the arms. The gas rotation globally resembles the stellar motions, but presents more complex structures, with S-shaped zero-velocity lines, which could be related to the mentioned possible bar; Fourier analysis of the velocity field will help clarifying this. Velocity dispersion in [O III] is higher than in H β , as particularly visible in the central region.

6.4.14 NGC 4487

This Scd galaxy forms a pair with the Scd galaxy NGC 4504, at a separation of 35 arcmin (corresponding to ≈ 165 kpc). Two principal arms of the grand-design type are recognizable in the images; one of the two is less well defined than the other and splits into broad segments which cover one side of the disc. The spiral pattern shows up also in our gas flux maps. The stars and gas rotate around an axis misaligned with respect to the photometric minor axis. The stellar and gaseous velocity dispersions are everywhere very low. In the [O III]/H β map regions of possible star formation can be recognized, in the centre and along the spiral arm, in correspondence to a drop in the H β velocity dispersion. Contrary to what happens in the majority of our galaxies, in the very centre the velocity dispersion in H β is lower than that in [O III].

6.4.15 NGC 4775

Very little is known about this low-inclination and very late-type (Sd) galaxy. Our maps, although based on 4×1800 -s exposures, are quite patchy and not easy to interpret; they suggest very slow stellar and gaseous projected rotation, as expected for an almost face-on galaxy, low stellar and gaseous velocity dispersion and a clumpy gas distribution in both H β and [O III] lines.

6.4.16 NGC 5585

NGC 5585 is a barred Sd galaxy; together with NGC 5204 (Sm), NGC 5474 (Scd), NGC 5477 (Sm), HoIV (Im) and M101 (Scd) it

forms the M101 group. It is highly resolved into individual stars and H II regions. In this galaxy, Coté, Carignan & Sancisi (1991) detected H I extended out to more than twice the optical radius; the H I velocity field turned out to be strongly warped; using these data and the *B*-band luminosity profiles, they constructed a mass model finding that the contribution of the dark matter component dominates the rotation curve at almost all radii, also when using a maximum-disc method. Later, Blais-Ouellette et al. (1999) pointed out that using two-dimensional H α Fabry-Pérot spectroscopy one can better constrain the orientation parameters and the rotation curve in its rising part, reducing by 30 per cent the dark to luminous matter ratio.

In our SAURON maps, there is not much information about the stellar velocity (patchy map). There are some hints of slow projected rotation. The stellar σ decreases moving outwards from the central region, although the map appears patchy and has everywhere low values. The gas distribution follows the bar morphology; along the bar some spots can be seen where the flux in [O III] is larger than that in H β . The [O III]/H β line ratio is enhanced in a region elongated in a roughly perpendicular direction to the one defined by the bar.

6.4.17 NGC 5668

NGC 5668 is another Sd galaxy, which has a high rate of star formation, as indicated by its large far-infrared and H α luminosities (Schulman et al. 1996, and references therein); the mentioned authors observed it in H I and detected high-velocity clouds of neutral hydrogen. High-velocity clouds were found also in the ionized gas and interpreted as regions with vertical motions related to ongoing star forming processes in the disc, as pointed out by Jiménez-Vicente & Battaner (2000) on the basis of Fabry-Pérot H α observations.

Our SAURON data indicate very slow stellar projected rotation velocities and a cold inner region. The gas distribution is clumpy, defining a ring-like structure also characterized by slightly lower [O III]/H β values compared to the surroundings.

6.4.18 NGC 5678

Not much is known from previous work on this barred and very dusty Sb galaxy. According to our SAURON data, the stars rotate in a rather regular way around the minor axis, although the zero-velocity line is strongly bent. The stellar velocity dispersion increases moving inwards, and becomes flatter in the nuclear region (see Fig. 6). The gas has instead a complex distribution, more structured in H β than in [O III], with kinematics consistent with the stars, but a zero-velocity line more disturbed and wiggling, similar to what we see in NGC 2964. Over a large part of the field, the velocity dispersion in the [O III] line is higher than in H β .

7 CONCLUSIONS

Two-dimensional kinematics and stellar population analysis of spiral galaxies towards the end of the Hubble sequence (Hubble types later than Sb) is still a relatively unexplored field: late-type spirals are very complex objects, often faint and full of substructures, as recently proved by analysis of *HST* images. They have been the targets of a few photometric and long-slit optical spectroscopic observations, but measurements of their two-dimensional kinematics were still missing. We have started a project on a sample of

18 such objects using integral-field spectroscopic observations obtained with SAURON. This allowed us to measure the stellar kinematics, the flux and kinematics of the H β 4861 Å and [O III] $\lambda\lambda$ 4959, 5007 Å emission lines and the strength of the H β , Fe and Mgb absorption features over a two-dimensional area covering the central region of our galaxies.

In this paper, we discussed the first results from this study, presenting the two-dimensional kinematics for stars and ionized gas. The majority of our galaxies is shown to be kinematically cold and to possess a considerable amount of ionized gas, covering in most cases a large part of the SAURON FOV and frequently following bar or spiral arm patterns in the spatial distribution. A quite common feature of our measured stellar kinematic maps is a central depression in the velocity dispersion, which assumes very often low values; we measured the velocity dispersion profiles and correlated their slopes with the morphological type: later-type galaxies tend to have velocity dispersion profiles which increase outwards. This implies small bulge/disc ratios and the presence of inner, occasionally star forming, disc-like structures. We also qualitatively compared the characteristics of our maps with the properties of the galaxy known from literature *HST* isophotal analysis: the main conclusion common to spectroscopy and photometry is that the kinematic detection of a cold inner region turns out to be often related to the lack of a classical stellar bulge and the presence of small-scale structures (nuclear star clusters, inner rings, inner bars). The gaseous component turns out to be almost ubiquitous and kinematically highly complex, displaying in many cases irregular velocity fields, with the kinematic axis twisting or bending or wiggling, or even without a clear sense of rotation, possibly because of the dust which strongly affects these objects. They also host intense star formation, often spread over the whole region we have observed, as suggested by the low values in the [O III]/H β line ratio maps.

In follow-up papers we will model the observed kinematic fields in detail, present the line-strength maps for these same galaxies, consider the bulge–disc decomposition and compare our results with those for the 24 Sa bulges in the SAURON survey.

ACKNOWLEDGMENTS

We kindly acknowledge Anna Pasquali and Ignacio Ferreras for their help during the early stages of this project. We thank Marc Balcells, Marc Sarzi and Kristen Shapiro for a careful reading of and commenting on the draft. We also thank the referee Torsten Böker for useful comments and suggestions which improved the paper. The SAURON-related projects are made possible through grants 614.13.003, 781.74.203, 614.000.301 and 614.031.015 from NWO and financial contributions from the Institut National des Sciences de l’Univers, the Université Claude Bernard Lyon I, the Universities of Durham, Leiden and the Netherlands Research School for Astronomy NOVA. KG acknowledges support for the Ubbo Emmius PhD program of the University of Groningen. JFB acknowledges support from the Euro3D Research Training Network, funded by the EC under contract HPRN-CT-2002-00305. MC acknowledges support from a VENI grant 639.041.203 awarded by the Netherlands Organization for Scientific Research (NWO). This project made use of the HyperLeda and NED data bases. Part of this work is based on data obtained from the STScI Science Archive Facility. The Digitized Sky Surveys were produced at the Space Telescope Science Institute under US Government grant NAGW-2166. The images of these surveys are based on photographic data obtained using the Oschin Schmidt Telescope on Palomar Mountain and the UK Schmidt Telescope.

REFERENCES

- Allard E. L., Peletier R. F., Knapen J. H., 2005, *ApJ*, 633, L25
- Andredakis Y., Sanders R., 1994, *MNRAS*, 267, 283
- Andredakis Y. C., Peletier R. F., Balcells M., 1995, *MNRAS*, 275, 874
- Bacon R. et al., 2001, *MNRAS*, 326, 23 (Paper I)
- Batcheldor D. et al., 2005, *ApJS*, 160, 76
- Belley J., Roy J.-R., 1992, *ApJS*, 78, 61
- Blais-Ouellette S., Carignan C., Amram P., Coté C., 1999, *AJ*, 118, 2123
- Boer B., 1994, in Shlosman I., ed., *Mass Transfer Induced Activity in Galaxies*. Cambridge Univ. Press, Cambridge, p. 308
- Böker T., Laine S., van der Marel R. P., Sarzi M., Rix H.-W., Ho L. C., Shields J. C., 2001, *A&AS*, 199, 705
- Böker T., Laine S., van der Marel R. P., Sarzi M., Rix H.-W., Ho L. C., Shields J. C., 2002, *AJ*, 123, 1389
- Böker T., van der Marel R. P., Gerssen J., Walcher J., Rix H.-W., Shields J. C., Ho L. C., 2003, *SPIE*, 4384, 57
- Bosma A., Casini C., Heidmann H., van der Hulst J. M., van Woerden H., 1980, *A&A*, 89, 345
- Bottinelli L., Gouguenheim L., 1980, *A&A*, 88, 108
- Braine J., Combes F., Casoli F., Dupraz C., Gerin M., Klein U., Wielebinski R., Brouillet N., 1993, *A&AS*, 97, 887
- Briggs F. H., Wolfe A. M., Krumm N., Salpeter E. E., 1980, *ApJ*, 238, 510
- Briggs F. H., 1982, *ApJ*, 259, 544
- Cappellari M., Copin Y., 2003, *MNRAS*, 342, 345
- Cappellari M., Emsellem E., 2004, *PASP*, 116, 138
- Carollo C. M., 1999, *ApJ*, 523, 566
- Carollo C. M., Stiavelli M., 1998, *AJ*, 115, 2306
- Carollo C. M., Stiavelli M., de Zeeuw P. T., Mack J., 1997, *AJ*, 114, 2366
- Carollo C. M., Stiavelli M., Mack J., 1998, *AJ*, 116, 68
- Carollo C. M., Stiavelli M., Seigar M., de Zeeuw P. T., Dejonghe H., 2002, *AJ*, 123, 159
- Chen P. C. et al., 1992, *ApJ*, 395, 41
- Chemin L. et al., 2006, *MNRAS*, in press (astro-ph/0511417)
- Combes F., Debbasch F., Friedli D., Pfenniger D., 1990, *A&A*, 233, 82
- Condon J. J., Condon M. A., Grisler G., Puscell J. J., 1982, *ApJ*, 252, 102
- Cornett R. H. et al., 1994, *ApJ*, 426, 553
- Coté S., Carignan C., Sancisi R., 1991, *AJ*, 102, 904
- Courteau S., de Jong R., Broeils A. H., 1996, *ApJ*, 457, 73
- de Jong R., 1995, PhD thesis, Univ. Groningen, the Netherlands
- de Jong R., 1996, *A&A*, 313, 45
- de Vaucouleurs G., de Vaucouleurs A., Corwin H. G. Jr., Buta R. J., Paturel G., Fouqué P., 1991, *Third Reference Catalogue of Bright Galaxies*. Springer-Verlag, New York (RC3)
- de Zeeuw P. T. et al., 2002, *MNRAS*, 329, 513 (Paper II)
- Devereux N. A., 1989, *ApJ*, 346, 126
- D’Onofrio M., Zaggia S. R., Longo G., Caon N., Capaccioli M., 1995, *A&A*, 296, 319
- Emsellem E., Greusard D., Combes F., Friedli D., Leon S., Pécontal E., Wozniak H., 2001, *A&A*, 368, 52
- Emsellem E. et al., 2004, *MNRAS*, 352, 721 (Paper III)
- Falcón-Barroso J., Peletier R. F., Balcells M., 2002, *MNRAS*, 335, 741
- Falcón-Barroso J. et al., 2006, *MNRAS*, submitted (Paper VII)
- Fall S. M., Efstatithiou G., 1980, *MNRAS*, 193, 189
- Fuchs B., 1997, *A&A*, 328, 43
- Gerhard O. E., 1993, *MNRAS*, 265, 213
- Gerssen J., Kuijken K., Merrifield M. R., 1997, *MNRAS*, 288, 618
- Gonçalves A. C., Véron-Cetty M.-P., Véron P., 1999, *A&AS*, 135, 437
- Grosbøl P. J., 1985, *A&AS*, 60, 261
- Ho L. C., Filippenko A. V., Sargent W. L., 1995, *ApJS*, 98, 477
- Ho L. C., Filippenko A. V., Sargent W. L., 1997, *ApJS*, 112, 315
- Hodge P. W., 1975, *ApJ*, 202, 619
- Ivanov G. R., Popravko G., Efremov I. N., Tikhonov N. A., Karachentsev I. D., 1992, *A&AS*, 96, 645
- James P. A., Seigar M. S., 1999, *A&A*, 350, 791
- Jiménez-Vicente J., Battaner E., 2000, *A&A*, 358, 812
- Jogee S., Kenney J. D. P., 1996, *ASPC*, 91, 230
- Jones L., 1997, PhD thesis, Univ. North Carolina
- Kennicutt R. C. et al., 2003, *PASP*, 115, 928
- Kormendy J., 1984, *ApJ*, 286, 132
- Laine S., Shlosman I., Knapen J. H., Peletier R. F., 2002, *ApJ*, 567, 92
- MacArthur L., Courteau S., Holtzman J., 2003, *ApJ*, 582, 689
- Márquez I., Masegosa J., Durret F., González Delgado R. M., Moles M., Maza J., Pérez E., Roth M., 2003, *A&A*, 409, 459
- Matthews L. D., Gallagher J. S., 2002, *ApJS*, 141, 492
- Mathewson D. S., Ford V. L., 1996, *ApJS*, 107, 97
- Natali G., Pedichini F., Righini M., 1992, *A&A*, 256, 79
- Norman C., Sellwood J. A., Hasan H., 1996, *ApJ*, 462, 114
- Oey M. S., Kennicutt R. C., 1993, *ApJ*, 411, 137
- Peletier R. F., Knapen J. H., Shlosman I., Pérez-Ramírez D., Nadeau D., Doyon R., Rodriguez Espinosa J. M., Pérez García A. M., 1999, *ApJS*, 125, 363
- Pérez-Ramírez D., Knapen J. H., Peletier R. F., Laine S., Doyon R., Nadeau D., 2000, *MNRAS*, 317, 234
- Peterson C. J., 1980, *AJ*, 85, 226
- Pfenniger D., Norman C., 1990, *ApJ*, 363, 391
- Phookun B., Vogel S. N., Mundy L. G., 1993, *ApJ*, 418, 113
- Raha N., Sellwood J. A., James R. A., Kahn F. D., 1991, *Nature*, 352, 411
- Rao S., Briggs F., 1993, *ApJ*, 419, 515
- Rauscher B. J., 1995, *AJ*, 109, 1608
- Reakes M., 1979, *MNRAS*, 187, 525
- Roberts M. S., 1962, *AJ*, 67, 437
- Sakamoto K., Okumura S. K., Ishizuk S., Scoville N. Z., 1999, *ApJS*, 124, 403
- Sarzi M. et al., 2006, *MNRAS*, in press (doi:10.1111/j.1365-2966.2005.09839.x) (astro-ph/0511307) (Paper V)
- Schulman E., Bregman J. N., Brinks E., Roberts M. S., 1996, *AJ*, 112, 960
- Seigar M. S., 2002, *A&A*, 393, 499
- Seigar M. S., Carollo C. M., Stiavelli M., de Zeeuw P. T., Dejonghe H., 2002, *AJ*, 123, 184
- Shapiro K. L., Gerssen J., van der Marel R. P., 2003, *AJ*, 126, 2707
- Silk J., 2003, *Astrophys. Space Sci.*, 284, 663
- Sohn Y.-J., Davidge T. J., 1996, *AJ*, 111, 2280
- Tonry J., Davis M., 1981, *ApJ*, 246, 666
- Tully R. B., Verheijen M. A. W., Pierce M. J., Huang J.-S., Wainscoat R. J., 1996, *AJ*, 112
- Ulvestad J. S., Ho L. C., 2002, *ApJ*, 581, 925
- van der Marel R. P., Franx M., 1993, *ApJ*, 407, 525
- Vazdekis A., 1999, *ApJ*, 513, 224
- Verheijen M., 1997, PhD thesis, Univ. Groningen, the Netherlands
- Verheijen M., 2001, *ApJ*, 563, 694
- Wakker B. P., Adler D. S., 1995, *AJ*, 109, 134
- Walcher C. J. et al., 2005, *ApJ*, 618, 237
- Westfall K. B., Bershady M. A., Verheijen M. A. W., Andersen D. R., Swaters R. A., 2005, preprint (astro-ph/0508552)
- Whitmore B. C., Kirshner R. P., Schechter P. L., 1979, *ApJ*, 234, 68
- Wozniak H., Combes F., Emsellem E., Friedli E., 2003, *A&A*, 409, 469
- Wyse R. F. G., Gilmore G., Franx M., 1997, *ARA&A*, 35, 637
- Yahil A., Tammann G. A., Sandage A., 1977, *ApJ*, 217, 903
- Young J. S., Xie S., Kenney J. D. P., Rice W. L., 1989, *ApJS*, 70, 699

Morphological classification of the OSU Bright Spiral Galaxy Survey

L. F. Whyte,¹★ R. G. Abraham,² M. R. Merrifield,¹ P. B. Eskridge,³
J. A. Frogel⁴ and R. W. Pogge⁴

¹School of Physics and Astronomy, University of Nottingham, Nottingham NG7 2RD

²Department of Astronomy and Astrophysics, University of Toronto, 60 St George Street, Toronto, ON, M5S 3H8, Canada

³Department of Physics & Astronomy, Minnesota State University, Mankato, MN 56003, USA

⁴Department of Astronomy, The Ohio State University, 140 W. 18th Avenue, Columbus, OH 43210, USA

Accepted 2002 July 15. Received 2002 July 15; in original form 2002 March 4

ABSTRACT

To quantify the distribution of bar shapes in spiral galaxies, we have analysed 113 *H*-band and 89 *B*-band galaxy images from the Ohio State University Bright Spiral Galaxy Survey. Parameters measuring bar shape and position along the Hubble sequence were obtained in each waveband. Evidence was found for a bimodality in the distribution of bar shape, implying that barred and unbarred galaxies are not just the extrema of a single distribution, and that any evolution between these two states must occur on a rapid time-scale. Objective bar shapes measured in the *H*-band were found to be more closely related to visual classifications than *B*-band bar strengths, as the *B*-band images are somewhat compromised by localized star formation, especially in later type systems. Galaxies were found to be more centrally concentrated in the infrared. Later type galaxies showed greater asymmetry in the optical than the infrared, presumably again owing to localized star formation, but on average the bar shapes in the two bands were found to be the same.

Key words: galaxies: fundamental parameters – galaxies: structure.

1 INTRODUCTION

For over 75 yr, bright galaxies have been classified using Hubble's (1926) tuning fork. Modifications and refinements have been made, but the original scheme, defining 'early' to 'late' types by the size of the bulge, and the smoothness and pitch angle of the spiral arms, has proved to be a remarkably robust starting point. Hubble's second parameter, whether or not a galaxy contains a central bar, has also proved a useful defining feature in describing the morphologies of galaxies. However, the existence of galaxies with differing degrees of 'barring' led de Vaucouleurs (1959) to introduce an intermediate category, SAB, between strongly barred SB galaxies and unbarred SA galaxies. This finer gradation raises the natural question of whether galaxies really are naturally divided into barred and unbarred systems, or whether some continuum exists. This issue is clearly of significance in trying to understand the still-disputed origins of the bars found in a large fraction of galaxies (see, for example, Sellwood 1999).

In an attempt to address this question, Abraham & Merrifield (2000) made a quantitative assessment of the morphologies of galaxies in the Frei et al. (1996) catalogue. They discovered that if these galaxies are plotted in a two parameter 'Hubble space,' with a measure of position along the Hubble sequence on the *x*-axis and barri-

ness on the *y*-axis, then the galaxies naturally split into the classical bifurcated tuning fork seen in Hubble's original work, with the barred galaxies forming a remarkably tight sequence in this space. The bimodal nature of the barring parameter then implies that barred and unbarred galaxies do form distinct populations. However, there were two significant shortcomings in this analysis.

First, the Frei et al. (1996) catalogue was not selected in a manner well-suited to this type of analysis. Indeed, since it was chosen to contain a broad range of galaxy types, one might well imagine that the most strongly barred galaxies were included to represent this type of system, while galaxies with no central distortion in their isophotes were selected to represent unbarred systems. Thus, one could imagine that the criteria upon which the catalogue was selected could introduce exactly the type of bimodal distribution observed.

Secondly, the observations for the Frei et al. (1996) catalogue were all at optical wavelengths. Light in this part of the spectrum can be dominated by relatively small amounts of recent star formation, so the perceived morphology may not be representative of the underlying structure a galaxy. Hackwell & Schweizer (1983), and more recently Block et al. (1994), have shown that the optical appearance of a galaxy can be totally different from its infrared morphology, which is more representative of the bulk of the stellar distribution of the galaxy. Thus, even such basic properties as whether or not a galaxy contains a bar may be difficult to establish at optical wavelengths. Indeed, it is notable in Abraham & Merrifield's (2000) analysis that unbarred late-type galaxies, where contamination by

*E-mail: pxlfw@nottingham.ac.uk

recent star formation is more of an issue, have tended to be classified as intermediate ‘SAB’ galaxies, perhaps reflecting the difficulty in classifying the bariness of these systems. A further indication of the potentially misleading nature of optical classifications of bariness comes from the simple statistic that at visible wavelengths only ~ 50 – 60 per cent of galaxies are classified as barred (Sellwood & Wilkinson 1993), whereas at infrared wavelengths the fraction is ~ 70 per cent (Mulchaey & Regan 1997; Knapen, Shlosman & Peletier 2000; Eskridge et al. 2000).

In this paper, we address these issues by carrying out a morphological analysis of data from the Ohio State University Bright Spiral Galaxy Survey.¹ The galaxies in this sample have well defined selection criteria, and should prove representative of bright spiral galaxies in the local Universe, removing the first concern expressed above. Further, galaxy images are available at both near-infrared and optical wavelengths, so the morphological properties can be determined using the more robust infrared data, and tested against the morphologies derived in the optical.

The remainder of the paper is laid out as follows. In Section 2, the data set is briefly described. Section 3 describes the measures adopted to quantify each position of a galaxy in Hubble space, while Section 4 presents the results of applying this analysis. Conclusions are discussed in Section 5.

2 THE OSU BRIGHT SPIRAL GALAXY SURVEY

The sample of galaxies used in this investigation were taken from the Ohio State University Bright Spiral Galaxy Survey (OSUBSGS). 205 galaxies were observed in B , V , R , J , H and K bands at five different observatories, using 1.2–2.4 m telescopes. A full description of the survey can be found in Eskridge et al. (2002). The spiral galaxies were selected for the survey from Third Reference Catalogue of Bright Galaxies (RC3) (de Vaucouleurs et al. 1991) subject to the constraints that they have a B -band magnitude $B \leq 12$ and a diameter $D \leq 6.5$ arcmin.

In this paper a total of 196 H -band, and 166 B -band galaxy images were investigated. However before the classification parameters could be measured, the foreground stars in each image had to be removed. Stars were replaced with an average of the surrounding pixels. All images were closely examined for suitability and were rejected if they had too many foreground stars; had bright stars near the centre; or had large bright stars elsewhere causing saturation over a significant portion of the galaxy image.

As it is almost impossible to determine whether a galaxy that lies close to edge-on is barred on the basis of photometry alone, we follow Abraham et al. (1999) and only use galaxies whose axial ratios imply an inclination $i < 60^\circ$. In the B -band images, galaxies with strong dust or star formation features (e.g. NGC 2442), could not be satisfactorily fitted by any kind of ellipse-fitting model, and were therefore also rejected. In total 89 B -band and 113 H -band images were found to be suitable, with a total of 72 galaxies having images in both bands. Fig. 1 shows that the sub-sample is slightly deficient of very late-type systems (as a result of the rejection of heavily dust-obscured galaxies), but is otherwise representative of the nearby bright spiral galaxy population found in the RC3.

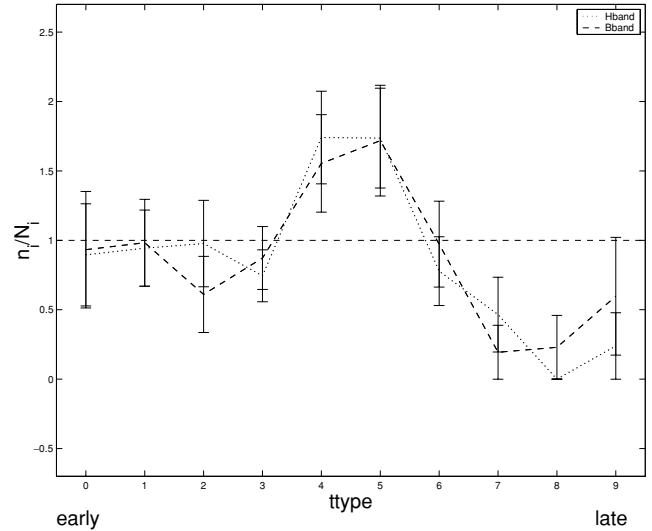


Figure 1. Distribution of galaxy Hubble types in the H - and B -band subsamples of OSUBSGS, in comparison with the RC3. N_i is the normalized number of galaxies in the RC3, while n_i is the normalized number of galaxies in the OSUBSGS subsamples, so for an unbiased sample $n_i/N_i = 1$.

3 CLASSIFICATION PARAMETERS

In order to classify the galaxies, we adopt the framework described in detail in Abraham & Merrifield (2000). This methodology defines a two-dimensional Hubble space where the x -coordinate measures position along the early-to-late sequence, while the y -coordinate measures, in a quantitative way, the degree to which a galaxy is barred. This parameter space provides a quantitative framework for investigating Hubble’s tuning fork: if the original scheme were strictly valid, we might expect to find galaxies separated into one-dimensional barred and unbarred sequences, with weakly barred galaxies perhaps lying at the lower edge of the barred distribution.

We assume that the distribution of light corresponds to a thin disc that is intrinsically axisymmetric at large radii, and define the centre of galaxy as the pixel with the maximum flux. A quantitative measure of asymmetry, A , was obtained by subtracting the image of the galaxy from a version that had been rotated through 180° (Abraham et al. 1996). We define the early-to-late (x) axis using the central concentration parameter, C , defined in Abraham et al. (1994) and closely related to the parameter defined by Doi, Fukugita & Okamura (1993). This parameter closely tracks bulge-to-disc ratios and has been shown to provide a quantitative substitute for more orthodox visual classifications of position along the Hubble sequence (Abraham et al. 1996). The concentration parameter is simply the flux ratio between an inner and a outer ellipse. The outer ellipse is selected using second-order moments obtained by a 2σ cut above the sky noise, σ . The inner ellipse is calculated by a similar moment analysis, but at a radius of only 30 per cent of the outer ellipse.

Assuming that the galaxy is intrinsically axisymmetric at large radii, the axial ratio of the outer ellipse can be used to define the galaxy inclination, which is also important for determining the bar shape (y) axis. Following Abraham & Merrifield (2000) we define the bar strength as;

$$f_{\text{bar}} = \frac{2}{\pi} \left[\arctan \left(\frac{b}{a} \right)^{-\frac{1}{2}}_{\text{bar}} - \arctan \left(\frac{b}{a} \right)^{+\frac{1}{2}}_{\text{bar}} \right], \quad (1)$$

where $(b/a)_{\text{bar}}$ is the intrinsic axial ratio of the putative bar, calculated from its apparent axial ratio and the inclination of the galaxy

¹The subset of the OSUBSGS used was the Early Data Release, available online at <http://www.astronomy.ohio-state.edu/~survey/EDR/>.

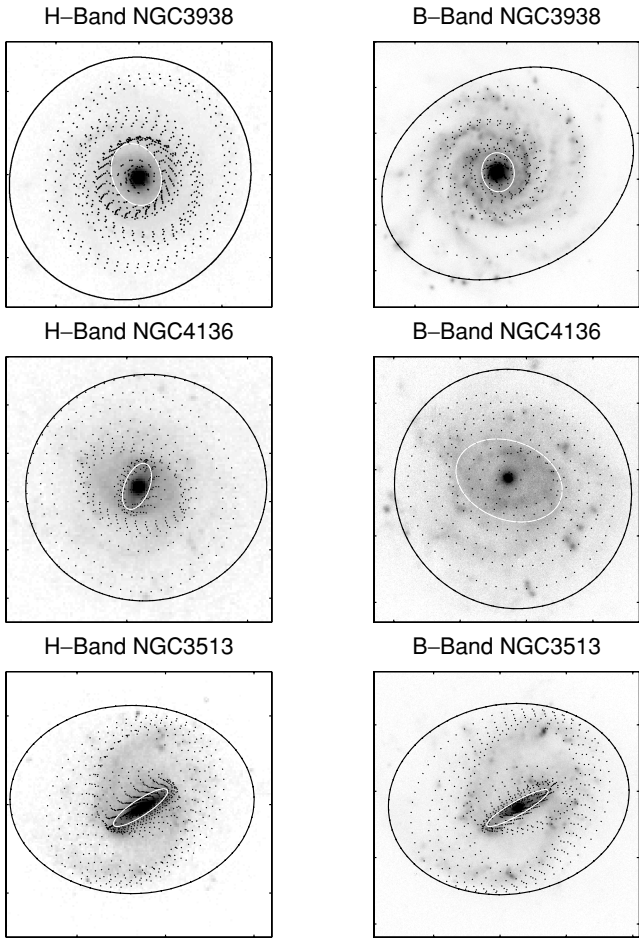


Figure 2. Ellipse fits for H - and B -band images. The solid black line is the outer ellipse used to determine the galaxy inclination, and for calculations of C and f_{bar} . The white ellipse is the inner ellipse used for measuring f_{bar} . The dashed lines are isophotes fitted to different intensity slices separated by 1σ in the sky noise.

using equation (2) of Abraham et al. (1999). To make sure that we do not miss any small high surface brightness or large low surface brightness bars, the whole range of radii is searched starting with the outer isophote (defined as for C) and working inwards. The inner ellipse is then defined as the isophote with the minimum $(b/a)_{\text{bar}}$ (i.e. the maximum value of f_{bar}). Fig. 2 shows several examples of the ellipse fits.

In order to discriminate between barred and unbarred galaxies, Abraham et al. (1999) proposed that systems with $(b/a)_{\text{bar}}^2 < 0.5$ could be classified as barred. This corresponds to $f_{\text{bar}} < 0.11$, which we will use to determine the fraction of barred galaxies in the OSUBSGS. It should be stressed that this cut-off does not represent any underlying physical process within spiral galaxies, but merely provides a useful visual criterion for defining a galaxy as barred.

4 RESULTS

Fig. 3 displays the distribution of the optical and near-infrared samples in the two dimensional Hubble space. A slight anticorrelation is observed between C and f_{bar} in both infrared and optical bands. As discussed in Abraham & Merrifield (2000), such a trend occurs naturally as the presence of a strong bulge (and hence large value of

C) will tend to wash out any bar signature, whereas in galaxies with weak bulges even quite modest bars will still be strongly detected.

In terms of their qualitative bar classifications, the galaxies are reasonably well divided in both optical and near-infrared Hubble space, with SA galaxies distributed across the bottom, SB galaxies across the top, and SAB galaxies bridging the gap between the two. The bimodal split between barred and unbarred galaxies is far less apparent in these figures than was found by Abraham & Merrifield (2000). However, there is still evidence for such a split even in this more objectively defined sample. The histograms of f_{bar} in Fig. 4 show a dip in the number of galaxies at $f_{\text{bar}} \sim 0.2$, the same value as the gap found in Abraham & Merrifield's (2000) analysis of the Frei sample. The dip is at a greater significance level (~ 95 per cent) in the infrared data than in the optical, which suggests that the optical bar shapes are more compromised by the effects of star formation, dust obscuration, etc.

This impression is borne out by the fact that there is a tighter grouping of the visual classifications, particularly the SB galaxies, in the infrared data than in the optical (despite the fact that the visual classifications were based on optical images). The 5 per cent of cases where the visual and automated classifications disagree strongly were inspected individually. In almost all cases the discrepancy arises because the automated fit is being compromised by bright star-forming features. In some cases, these features are localized regions, but in others (such as NGC 4136, see Fig. 2) the fit is drawn to tightly wrapped spiral arms, which are identified as the strongest non-circular features, rather than the bar that we seek. It should be noted that for galaxies with two or more bars, the automated process would pick out the most elliptical bar, not necessarily the primary outer bar (although no such cases were found in this sample). We could have intervened in the bar analysis to prevent such misfits, but such subjective judgements are contrary to the ethos of this approach, as they could easily introduce subjective biases in the analysis.

There are thus at least two non-physical sources of scatter in the distribution of f_{bar} . First, the intrinsic limitations of the automated fitting process (particularly at optical wavelengths) mean that there is an uncertainty introduced in the derived value of bar shape. Secondly, the correlation between C and f_{bar} means that a projection of this two-dimensional space on to the f_{bar} -axis will tend to smear out intrinsically sharp features in Hubble space when viewed in one dimension. Hence, the true divide between barred and unbarred galaxies is likely to be rather more dramatic than we see in Fig. 4.

In order to compare the fraction of barred galaxies in the optical and infrared, only the 72 galaxies for which images in both bands were available were used. We find that 74 per cent of galaxies are barred in the optical, with this fraction increasing to 79 per cent in the near-infrared. Visual classification of the entire OSUBSGS sample, performed by Eskridge et al. (2000) found only 72 per cent of galaxies to be either strongly or weakly barred in the H -band, while only 64 per cent were classified as barred in the RC3 (B -band). Overall there is a good correlation between optical and NIR bar shape. Obscuration from dust and star formation did cause some late-type galaxies to appear more barred in the NIR than the optical. A few galaxies did appear to be significantly more barred in the optical than NIR, as isophotes fitted around H II regions can occasionally give the appearance of a bar.

Automated classification finds a slightly higher fraction of barred galaxies in both bands than visual classification. This could mean that smaller bars are occasionally overlooked when visual classifications are made. However the difference in fractions in this case is probably owing to the value of f_{bar} selected to separate barred

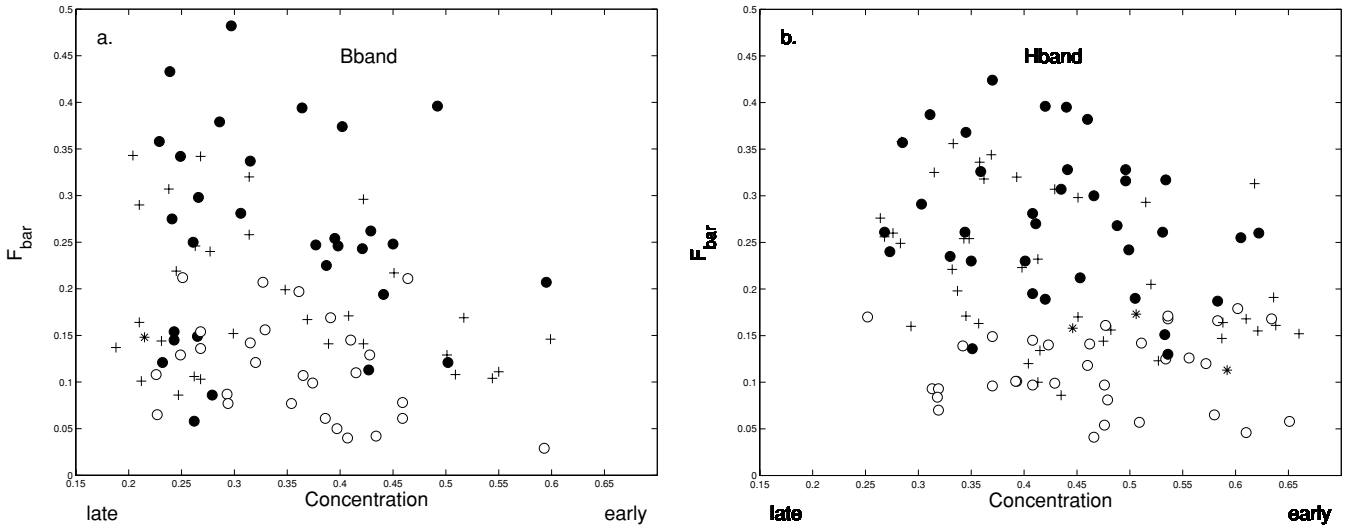


Figure 3. Distribution of optical and near-infrared samples in ‘Hubble space.’ SA galaxies are represented by circles, SAB galaxies by crosses, SB galaxies by filled circles, and unclassified galaxies by asterisks.

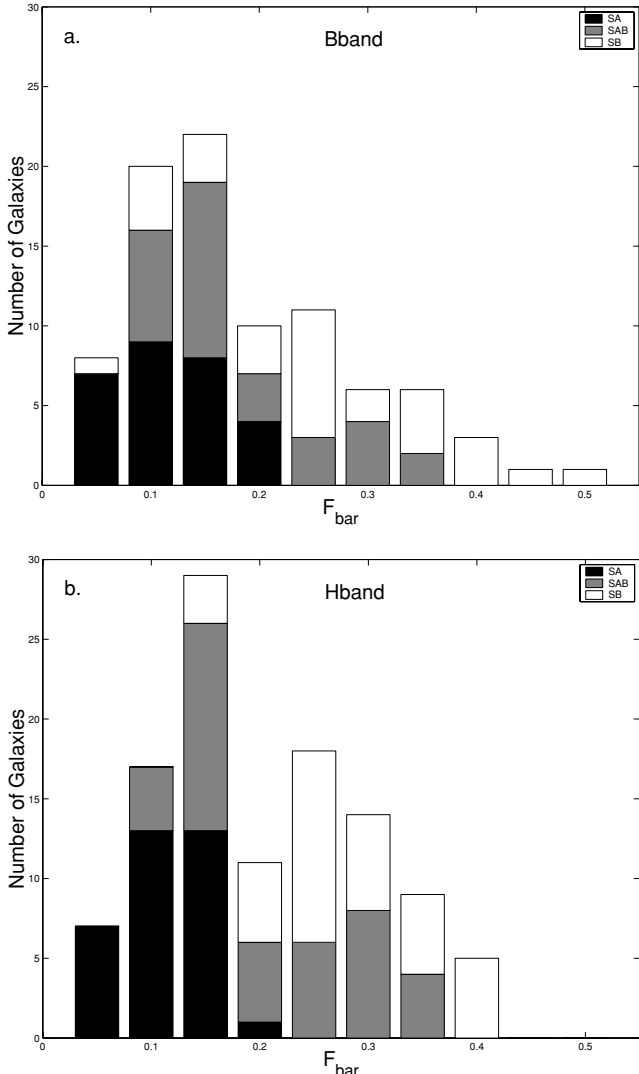


Figure 4. Histogram of bar shape distribution in (a) optical and (b) near-infrared.

from unbarred galaxies. Indeed, if we increase the proposed value of $f_{\text{bar}} < 0.11$ to $f_{\text{bar}} < 0.14$, we find that 61 per cent of galaxies are barred in the B -band and 71 per cent in the H -band. These fractions are in good agreement with those found by Eskridge et al. (2000).

Having established that the optical properties of galaxies introduce more dispersion in their objective classifications than occurs in the infrared, we now look briefly at possible systematic differences between the two data sets. Fig. 5 shows the fractional variation in asymmetry, bar shape and central concentration between the optical and infrared data as a function of mean concentration (the average of the concentrations in the two bands). There is a clear trend in asymmetry in the sense that although high concentration (early type) galaxies have similar asymmetries, the low concentration (late type) galaxies are systematically more asymmetric in the optical than the infrared. Patchy, asymmetric star formation occurs more commonly in later type galaxies, so this result again reflects the fact that optical data are more affected by star formation than infrared observations. Bar shape does not seem to be systematically affected in the same way. Although patchy star formation increases the scatter in bar shape in low concentration galaxies, it only marginally lowers the bar shapes in the optical compared to their infrared values. Concentration, on the other hand, does change systematically between the optical and infrared in the sense that galaxies are on average more centrally concentrated in the infrared. This variation could be an indicator of opacity in the central regions of these galaxies, which suppresses the optical emission – as recently discussed in White, Keel & Conselice (2000), this remains a controversial issue. However, it could also simply reflect the star formation in the discs of these galaxies, which will augment the optical emission at large radii, lowering the concentration observed in this band.

5 DISCUSSION

This study has placed a well-defined sample of spiral galaxies in the Hubble space of early-to-late type and bar shape. The main conclusion is that there are significant signs of bimodality in the bar shape parameter, similar to those found by Abraham & Merrifield’s (2000). Since the current analysis is based on a sample with more objective selection criteria, this bimodality is unlikely to be attributable

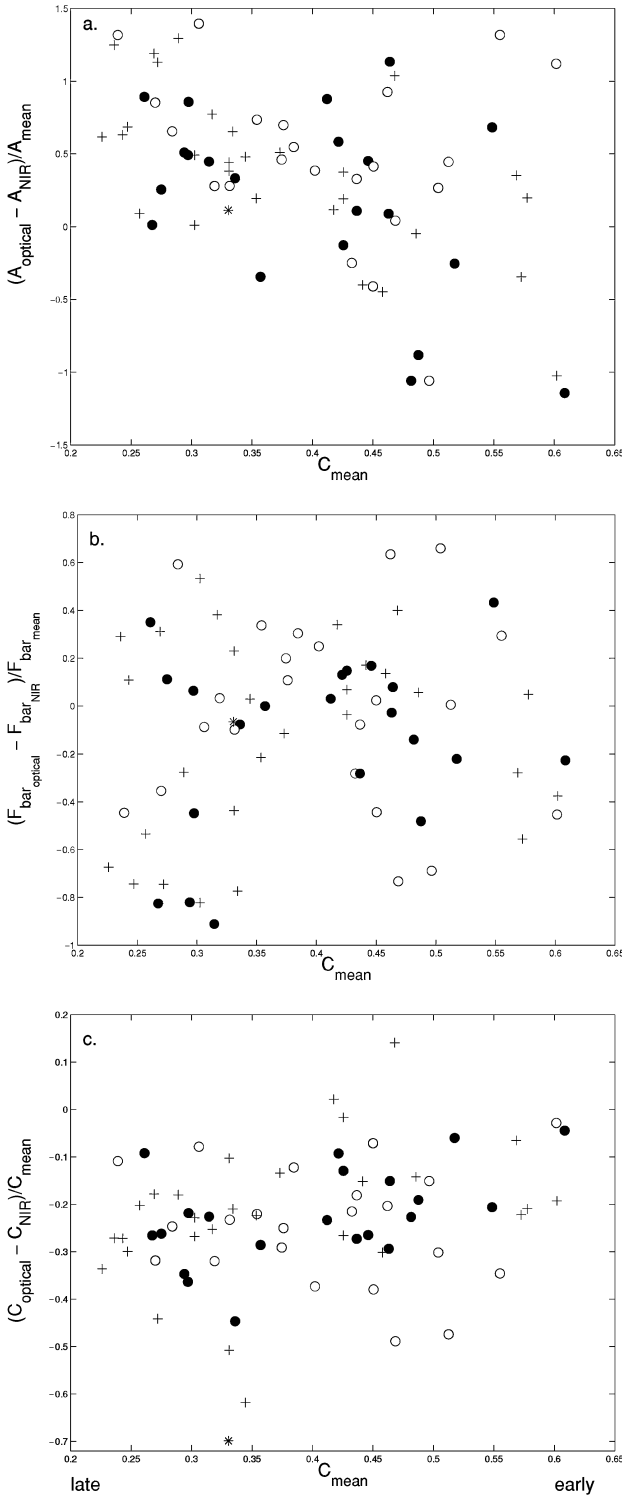


Figure 5. Variation between the optical and infrared data of (a) the asymmetry index, (b) the bar shape parameter, and (c) the central concentration parameter, plotted as a function of the concentration of the galaxy. SA galaxies are represented by circles, SAB galaxies by crosses, SB galaxies by filled circles, and unclassified galaxies by asterisks.

to selection effects. This therefore suggests that barred and unbarred galaxies exist as distinct populations, rather than as the extremes of a continuum.

Barred and unbarred galaxies are remarkably similar in all their other properties such as size, luminosity, Tully–Fisher relation, etc.,

(e.g. Debattista & Sellwood 2000). Therefore it seems unlikely that barred and unbarred galaxies are two separate types of system with no evolution between the two. Further, a variety of mechanisms have shown up in numerical simulations that may cause bars to form and dissolve in real disc galaxies (e.g. Athanassoula 2002). Thus, there are good reasons to believe that evolution should occur between these two populations. The existence of a gap between them then implies that such evolution must occur on a time-scale that is short compared to the cosmological lifetimes of the galaxies (just as the Hertzsprung gap in the stellar colour–magnitude diagram indicates the haste with which stars evolve through this region of parameter space).

The comparison between optical and near-infrared morphologies is also instructive. Some measures of galaxy morphology, such as central concentration and asymmetry, vary systematically between the optical and near-infrared. However the bar shape parameter remains approximately the same, albeit with greater scatter in the optical because of localized star formation, etc. This discovery has an important implication for studies of bar shape as a function of redshift, which indicate that barred galaxies are extremely rare for $z \geq 0.5$ (Abraham et al. 1999; Van den Bergh et al. 2000). One possible explanation for this rarity is that it might be attributed to bandshifting effect, since the I -band images used in these studies correspond to B -band rest-frame emission for $z \sim 0.8$. Thus, if bars were systematically weaker in the B band than at red wavelengths, then one would expect to see such a decrease in bar fraction with redshift. This matter is discussed in greater detail by Van den Bergh et al. (2002). Since there is no such systematic variation in bar shape with waveband, this explanation now seems unlikely; it would appear that bars are intrinsically rarer at higher redshifts.

These conclusions have been drawn from a relatively small sample of galaxies, necessarily limiting their confidence. However, with the advent of large surveys like the Sloan Digital Sky Survey (York et al. 2000), much larger samples of galaxies are becoming available. Since the morphological parameters used in this analysis are reasonably robust, they can be applied to rather more distant galaxies than traditional classifications, opening up a larger region of space to such studies, and hence allowing much larger samples to be gathered. With these larger samples, objective morphological analysis should provide definitive answers to many of the questions where this study has only been able to scratch the surface.

ACKNOWLEDGMENTS

This work made use of data from the Ohio State University Bright Spiral Galaxy Survey, which was funded by grants AST-9217716 and AST-9617006 from the United States National Science Foundation, with additional support from the Ohio State University.

REFERENCES

- Abraham R. G., Merrifield M. R., 2000, AJ, 120, 2835
- Abraham R. G., Valdes F., Yee H. K. C., Van Den Bergh S., 1994, ApJ, 432, 75
- Abraham R. G., Tanvir N. R., Santiago B. X., Ellis R. S., Glazebrook K., Van Den Bergh S., 1996, MNRAS, 279, L47
- Abraham R. G., Merrifield M. R., Ellis R. S., Tanvir N. R., Brinchmann J., 1999, MNRAS, 308, 569
- Athanassoula L., 2002, in ASP Conf. Ser., Disks of Galaxies: Kinematics, Dynamics and Perturbations. Astron. Soc. Pac., San Francisco, in press
- Block D. L., Bertin G., Stockton A., Grosbol P., Moorwood A. F. M., Peletier R. F., 1994, A&A, 288, 365

- Brinchmann J. et al., 1998, *ApJ*, 499, 112
 de Vaucouleurs G., 1959, in Flugge S., ed., *Handbuch der Physik LIII, Astrophysik IV, Sternsysteme*. Springer-Verlag, Berlin, p. 275
 de Vaucouleurs G., de Vaucouleurs A., Corwin H. G. Jr., Buta R. J., Paturel G., Fouque P., 1991, *Third Reference Catalogue of Bright Galaxies Vol. 1–3. XII*. Springer-Verlag, Berlin
 Debattista V., Sellwood J., 2000, *ApJ*, 543, 704
 Doi M., Fukugita M., Okamura S., 1993, *MNRAS*, 264, 832
 Eskridge P. B. et al., 2000, *AJ*, 119, 536
 Eskridge P. B. et al., 2002, *ApJS*, 143, in press (astro-ph/0206320)
 Frei Z., Guhathakurta P., Gunn J. E., Tyson J. A., 1996, *AJ*, 111, 174
 Hackwell J. A., Schweizer F., 1983, *ApJ*, 265, 643
 Hubble E., 1926, *ApJ*, 64, 321
 Knapen J. H., Shlosman I., Peletier R. F., 2000, *ApJ*, 529, 93K
 Mulchaey J. S., Regan M. W., 1997, *ApJ*, 482, L135
 Sellwood J. A., 1999, in Combes F., Mamon G. A., Charmadaris V., eds, ASP Conf. Ser. Vol. 197, *Dynamics of Galaxies: from the Early Universe to the Present*. Astron. Soc. Pac., San Francisco, p. 3
 Sellwood J. A., Wilkinson A., 1993, *Rep. Prog. Phys.*, 56, 173
 Van den Bergh S., Cohen J. C., Hogg D. W., Blanford R., 2000, *AJ*, 120, 2190
 Van den Bergh S., Abraham R. G., Whyte L. F., Merrifield M. R., Eskridge P., Frogel J. A., Pogge R., 2002, *AJ*, 123, 2913
 White R. E., Keel W. C., Conselice C. J., 2000, *ApJ*, 542, 761
 York D. G. et al., 2000, *AJ*, 120, 1579

This paper has been typeset from a $\text{\TeX}/\text{\LaTeX}$ file prepared by the author.

Stellar populations in bulges of spiral galaxies[★]

Bhasker K. Moorthy[†] and Jon A. Holtzman

Department of Astronomy, New Mexico State University, PO Box 30001, MSC 4500, Las Cruces, New Mexico 88003, USA

Accepted 2006 June 19. Received 2006 June 19; in original form 2005 December 12

ABSTRACT

We present line strengths in the bulges and inner discs of 38 galaxies in the local Universe, including several galaxies whose bulges were previously identified as being disc like in their colours or kinematics, to see if their spectral properties reveal evidence for secular evolution. We find that red bulges of all Hubble types are similar to luminous ellipticals in their central stellar populations. They have large luminosity-weighted ages, metallicities, and α/Fe ratios. Blue bulges can be separated into a metal-poor class that is restricted to late types with small velocity dispersion and a young, metal-rich class that includes all Hubble types and velocity dispersions. Luminosity-weighted metallicities and α/Fe ratios are sensitive to central velocity dispersion and maximum disc rotational velocity. Red bulges and ellipticals follow the same scaling relations. We see differences in some scaling relations between blue and red bulges and between bulges of barred and unbarred galaxies. Most bulges have decreasing metallicity with increasing radius; galaxies with larger central metallicities have steeper gradients. Where positive age gradients (with the central regions being younger) are present, they are invariably in barred galaxies. The metallicities of bulges are correlated with those of their discs. While this and the differences between barred and unbarred galaxies suggest that secular evolution cannot be ignored, our results are generally consistent with the hypothesis that mergers have been the dominant mechanism responsible for bulge formation.

Key words: galaxies: bulges – galaxies: elliptical and lenticular, cD – galaxies: evolution – galaxies: formation – galaxies: spiral – galaxies: stellar content.

1 INTRODUCTION

Bulges are important relics of the galaxy formation process. An analysis of their structure, kinematics, dynamics, and stellar content can potentially reveal the physical mechanisms responsible for the formation and evolution of galaxies, as well as the nature of the Hubble sequence. Similarities between bulges and ellipticals have long been recognized but recent observations suggest that at least some bulges may be related to discs. This has led to the suggestion that the large bulges of early-type spirals are more similar to ellipticals, while late-type bulges are more disc like (Wyse, Gilmore & Franx 1997). As a consequence of these observations, formation scenarios have emerged for bulges that are either identical to those for ellipticals or involve the secular evolution of discs. However, the degree to which formation mechanisms are homogeneous is still open to question.

Early models for elliptical formation involved the monolithic collapse of a primordial gas cloud (Larson 1974; Carlberg 1984;

Arimoto & Yoshii 1987). This model naturally explains several observed properties of ellipticals, including the mass–metallicity relation and the presence of metallicity gradients, but large-scale collapse is inconsistent with present-day cold dark matter (CDM) cosmology and with recent observations showing that massive ellipticals were not fully assembled until after $z = 1$ (Bell et al. 2004; Faber et al. 2005). It is now widely believed that ellipticals formed hierarchically through mergers of smaller fragments (Kauffmann, White & Guiderdoni 1993). Mergers are frequently caught in the act (van Dokkum et al. 1999; Ferreiro & Pastoriza 2004), and photometric and kinematic evidence for past mergers is abundant in ellipticals (Emsellem et al. 2004; van Dokkum 2005). The merger model has been extended to bulges due to the many observed similarities between bulges and ellipticals. For example, Carollo et al. (1997) found that bulges were well fitted by the $R^{1/4}$ law used for ellipticals. The Fundamental Plane relation of bulges is nearly the same as that of ellipticals, with late types perhaps lying below early types (Falcón-Barroso, Peletier & Balcells 2002).

In the secular evolution scenario, bulges are produced through radial and vertical transport of disc material as the result of instabilities and resonances (see Kormendy & Kennicutt 2004, for a review). These models come in several flavours, most of which involve bars. Simulations that do not include gas have found that

[★]Based on observations obtained with the Apache Point Observatory 3.5-m telescope, which is owned and operated by the Astrophysical Research Consortium.

[†]E-mail: bmoorthy@nmsu.edu

bars can buckle, heating the inner disc and increasing its scaleheight to resemble a bulge. Hydrodynamical simulations have found that bars can transport gas towards the centre, triggering intense star formation (Pfenniger 1993; Friedli & Benz 1995; Norman, Sellwood & Hasan 1996; Noguchi 2000; Immeli et al. 2004). The presence of neighbours may also drive this (Kannappan, Jansen & Barton 2004). Support for secular evolution comes from observed correlations between the scalelengths of bulges and their discs (Courteau, de Jong & Broeils 1996; MacArthur, Courteau & Holtzman 2003). It has also been found that the light profiles of many bulges are closer to exponential than $R^{1/4}$ (Andredakis & Sanders 1994; de Jong 1996a; Balcells et al. 2003; MacArthur et al. 2003; de Jong et al. 2004). Furthermore, the ratio of rotational to random motions in bulges is often typical of discs (Kormendy & Illingworth 1982; Kormendy & Kennicutt 2004). Comparisons between the morphology and kinematics of observed galaxies with simulated ones have shown that boxy and peanut-shaped (b/p) bulges are bars viewed at high inclination (Bureau & Freeman 1999; Aronica et al. 2003; Chung & Bureau 2004; Athanassoula 2005). Athanassoula (2005) distinguished between b/p bulges, which are formed through the buckling of the bar, and what she called ‘discy bulges’, which are smaller cold components that formed out of the gas driven inwards by the bar.

Bulges that could have been formed through secular evolution are often referred to as ‘pseudobulges’ to distinguish them from the ‘classical’ bulges that may have formed through mergers. Since pseudobulge signatures are generally found in late-type spirals, Kormendy & Kennicutt (2004) suggested that early-type spirals (Sa, Sab, and some S0) contain classical bulges, while late-type spirals (Sb, Sc and some S0) contain pseudobulges. On the theoretical side, Pfenniger (1993) found that secular evolution can produce small bulges but not those having a characteristic radius much larger than the disc scalelength. However, it is not at all clear that the spectrum of observed bulge properties points towards two distinct formation scenarios. Since the stability of bars continues to be debated (Debattista et al. 2004; Shen & Sellwood 2004; Bournaud, Combes & Semelin 2005), it is also not clear whether or not pseudobulges should exist only in present-day barred galaxies.

Stellar population (SP) studies can potentially place important constraints on the formation mechanisms. A successful formation scenario has to reproduce the observed distribution of ages and metallicities. In a collapse model, bulges and ellipticals are universally old and have radial metallicity gradients. In his dissipative collapse simulation, Carlberg (1984) found that the steepness of the metallicity gradient was correlated with galaxy properties, such as mass and luminosity. If ellipticals and bulges formed through mergers, it is important to keep in mind that their assembly histories might be very different from their star formation histories. Λ CDM simulations suggest that most-massive ellipticals (and therefore presumably bulges) were not fully assembled until recently ($z < 1$), whereas the bulk of star formation occurred much earlier ($z > 2$) in the progenitor galaxies (De Lucia et al. 2006). This is consistent with observational studies of merger activity, number counts, and the luminosity function (Faber et al. 2005; van Dokkum 2005). De Lucia et al. found that the star formation histories of massive ellipticals peak at $z \sim 5$, while those of less-massive ellipticals peak at progressively smaller redshifts and are more extended. These simulations predict a mass–metallicity relation, with the most-massive ellipticals having solar metallicity and the least-massive ones being a factor of 10 smaller in metallicity. Gradients in SPs are difficult to model within the framework of hierarchical formation. Mergers

between discs can presumably preserve existing gradients in the subcomponents and produce new gradients through gas infall, but mixing from successive mergers might erase any correlations between gradients and global properties. White (1980) found that the metallicity gradient in a disc galaxy was halved after three mergers with similar-sized discs. However, Bekki & Shioya (1999) found that more-massive galaxies had steeper metallicity gradients. The impact of secular evolution on gradients is not straightforward. Since the resulting pseudobulge has a smaller scalelength than the progenitor disc, an existing disc gradient could become amplified (A Klypin, private communication). However, mixing during secular evolution can have the effect of washing out existing gradients. Adding gas only complicates the picture. If gas is fuelled towards the central regions by bars, this could result in a nucleus that is younger and more metal rich than the outer regions of the bulge. Simulations by Friedli, Benz & Kennicutt (1994) resulted in a flattening of metallicity gradients in all but the innermost regions where a starburst, fuelled by infalling gas, produced a metal-rich nucleus.

Abundance ratios can place additional constraints. Mg and other α -elements are primarily produced in Type II supernovae (SNe II), while a substantial fraction of the Fe-peak elements, Fe and Cr, are produced in Type Ia supernovae (SNe Ia). Therefore, α -enhancement is generally attributed to a cessation of star formation before the bulk of SNe Ia occurred. Through chemical evolution modelling, Thomas (1999) found that a clumpy collapse model produced uniform α -enhancement or positive gradients (increasing α/Fe with radius), while a merger model produced uniformly solar α/Fe or negative gradients. For the case of secular evolution, Immeli et al. (2004) made different predictions for abundance ratios in bulge stars, depending on whether it is the gas disc or the stellar disc which first becomes unstable. In the former case, gas clumps merge together and spiral inwards, causing massive starbursts and producing large α/Fe ratios. In the latter case, a bar forms and then channels gas towards the centre. This occurs on long time-scales, resulting in smaller α/Fe ratios.

The only bulges where individual stars can be resolved are those of the Milky Way (MW) and M31. The majority of the stars in the MW bulge are old ($t \geq 7$ Gyr), although young ($t \leq 200$ Myr) and intermediate-age (200 Myr $\leq t \leq 7$ Gyr) stars are also detected (Ibata & Gilmore 1995; Sadler, Rich & Terndrup 1996; Feltzing & Gilmore 2000; van Loon et al. 2003; Zoccali et al. 2003). As a barred late-type spiral, the MW might be a good candidate for secular evolution. However, the MW bulge is dominated by old stars unlike the MW disc at the solar neighbourhood. If the bulge was produced through a rearrangement of disc stars, either this must have occurred several Gyr ago or the inner disc must have a considerably different age distribution than the disc at the solar neighbourhood. The young stars in the bulge are mainly found in the innermost regions. While the gas that formed them could have been driven by a bar, it could just as well have been provided by a recent merger. The mean metallicity of the Galactic bulge is slightly subsolar (Minniti 1996; Feltzing & Gilmore 2000; van Loon et al. 2003; Zoccali et al. 2003; Fulbright, McWilliam & Rich 2006). The stellar content of M31’s bulge is not as well understood as that of the MW since we cannot reach its main-sequence turn-off. Observations of giant stars are consistent with M31’s bulge being similar in age to the MW bulge and slightly more metal rich (Rich 1999; Jablonka et al. 2000; Davidge 2001; Stephens et al. 2003; Sarajedini & Jablonka 2005).

SPs in more distant bulges have to be studied through photometry or spectroscopy of integrated light. An important limitation of such studies is that integrated light is dominated by the most-luminous stars. Colours have been studied more extensively as they have the

advantage of higher signal-to-noise ratio (S/N). Pioneering work by Balcells & Peletier (1994) found that colour variations from galaxy to galaxy are much larger than colour differences between disc and bulge in each galaxy. Similarly, de Jong (1996b) found that bulge and disc colours are correlated and that the colour differences between bulge and disc suggested that the SPs did not vary much from one to the other. Unfortunately, colour studies suffer from degeneracies between ages, metallicities, and extinction.

Line strengths are nearly insensitive to dust (MacArthur 2005), provide information on the abundances of several elements and molecules, and allow for breaking the age–metallicity degeneracy. Worthey (1994) obtained line strengths for a range of single-age, single-metallicity SPs (SSPs) on the Lick/IDS system (Burstein et al. 1984; Faber et al. 1985) and found that while individual indices are sensitive to both age and metallicity, the relative sensitivity varies from index to index. Spectral indices have also been defined at high resolution (Vazdekis 1999), allowing better age determinations than otherwise possible. One of the limitations of the original models is that they were calibrated using galactic stars that do not cover an adequate range of metallicity and α/Fe ratio for interpreting the spectra of early-type galaxies (they contain very few, if any, stars that are both metal rich and α -enhanced). Much progress has since been made in extending Lick indices to non-solar abundance ratios using synthetic spectra or by calibrating with globular clusters that, like early-type galaxies, are both metal rich and α -enhanced (Tripicco & Bell 1995; Trager et al. 2000a; Thomas, Maraston & Bender 2003; Thomas, Maraston & Korn 2004; Lee & Worthey 2005).

Line strengths have been used extensively to characterize the SPs of ellipticals. The luminosity-weighted ages of massive ellipticals are large (~ 10 Gyr) while those of low-mass ellipticals ($\sigma \lesssim 130 \text{ km s}^{-1}$) are, on average, smaller (~ 5 Gyr), with a large spread (Caldwell, Rose & Concannon 2003; Nelan et al. 2005; Thomas et al. 2005). Ellipticals in low-density environments appear to show larger scatter in their SPs than those in clusters (Rose et al. 1994; Trager et al. 2000a; Vazdekis et al. 2001; Proctor & Sansom 2002; Denicoló et al. 2005; Thomas et al. 2005). These observations go against the collapse model and confirm, at least qualitatively, the prediction of the merger model by Kauffmann (1996). Mg-sensitive indices in ellipticals are more tightly correlated with central velocity dispersion than Fe-sensitive indices, resulting in a correlation between Mg/Fe and σ_0 (Bender, Burstein & Faber 1993). Worthey & Collobert (2003) found that the Mg– σ relation of ellipticals is consistent with these objects having been formed through around 50 mergers with merger probability constant or mildly declining with time.

There have been fewer studies of line strengths in bulges. Integrated light studies on the bulges of the MW and M31 have arrived at similar ages and metallicities as the resolved studies (Puzia et al. 2002; Puzia, Perrett & Bridges 2005). Both bulges have large SSP ages. M31 is slightly supersolar in SSP metallicity, while the MW is solar. Both are α -enhanced with M31 being more so in line with its larger σ_0 . Early studies on extragalactic bulges found them to be similar to ellipticals in their central line strengths (Idiart, de Freitas Pacheco & Costa 1996; Jablonka, Martin & Arimoto 1996). Proctor & Sansom (2002) found that bulges have smaller average luminosity-weighted age than ellipticals. These authors did not find the correlation predicted by Kauffmann (1996) for bulges and suggested that it might have been erased by secular evolution in late types. The largest sample of bulges to date was that of Prugniel, Maubon & Simien (2001), who identified three classes of bulges: (i) young bulges which are small, have ionized gas, low velocity dispersions, and low metallicity; (ii) old bulges that are α -enhanced and

follow the mass–metallicity relation of ellipticals; and (iii) bulges that have a mixture of young and old populations, which are less α -enhanced than those of class (ii), and deviate from the Mg₂ relation of ellipticals. Prugniel et al. and Proctor et al. found that both Fe and Mg were correlated with σ_0 in bulges, resulting in the lack of a tight correlation between Mg/Fe and σ_0 in bulges. Prugniel et al. (2001) found that Mg₂ in bulges is more tightly correlated with the V_{max} of the disc than with σ , indicating that the SPs are more sensitive to the total galaxy potential (i.e. the dark matter halo) than the bulge potential.

Studies with spatial resolution offer several advantages over studies that only sample the central region. First, differential studies of ages and abundances are more reliable than absolute estimates. Secondly, formation models invariably make predictions for the global properties of galaxies which are better traced by mean observed quantities than central ones; observations with spatial resolution allow estimation of mean values. Finally, as mentioned already, population gradients can place additional constraints on formation mechanisms.

Line-strength gradients have been studied extensively in ellipticals. Carollo, Danziger & Buson (1993) and Forbes, Sánchez-Blázquez & Proctor (2005) found strong correlations between gradients and physical properties, while others found weak (Mehlert et al. 2003) or no (Kobayashi & Arimoto 1999) correlations. There have been relatively few studies on gradients in bulges. Fisher, Franx & Illingworth (1996) found steeper metallicity gradients along the minor-axes of nine edge-on S0s than along the major-axes, suggesting different formation mechanisms for the bulge and the disc. Goudfrooij, Gorgas & Jablonka (1999) found that gradients were correlated with luminosity in 16 bulges. Proctor, Sansom & Reid (2000) found that gradients correlated with velocity dispersion, albeit with a sample of only four galaxies, while Jablonka, Gorgas & Goudfrooij (2002) found no such correlation. Integral field spectroscopy has enabled the acquisition of 2D line strengths in bulges with results just starting to emerge (e.g. Sil’chenko et al. 2003; Falcón-Barroso et al. 2004). Recent work by Ryder, Fenner & Gibson (2005) showed that tunable filters might be another way to obtain 2D line strengths.

In this paper, we present line strengths and line-strength gradients in the bulges and inner discs of 38 galaxies. Our sample, described in Section 2, was chosen to span a range of bulge properties and specifically targeted several galaxies with blue bulges and similar bulge/disc colours and/or disc-like kinematics in an attempt to look for SP signatures of secular evolution. Section 3 describes the observations and data analysis. Section 4 describes the SP results and Section 5 discusses their implications for bulge formation scenarios. Section 6 contains a summary. The structure, kinematics, and dynamics and how they relate to the SPs will be discussed in a future paper (hereafter Paper II).

2 THE GALAXY SAMPLE

We selected a sample that included some bulges that are similar in colour to their discs and others that are considerably redder as a control. Colour was chosen as the primary selection criterion because this has so far been the best-studied property of bulges. de Jong (1996b, hereafter DJ) and Peletier & Balcells (1997, hereafter PB) obtained colour gradients of galaxies from the Uppsala General Catalog (Nilson 1973) with major-axes larger than 2 arcmin. We selected 17 galaxies from PB and 14 from DJ. The two samples complement each other nicely in their sky coverage and sampling

of Hubble types. The DJ galaxies are nearly face-on while the PB galaxies are highly inclined.

We also included three galaxies, NGCs 2787, 3384 and 3945, which were previously found to possess disc-like structural and kinematical properties (Busarello et al. 1996; Erwin et al. 2003; Pinkney et al. 2003; Sil'chenko et al. 2003). All three are barred S0 galaxies with inner discs or bars that are more luminous than the surrounding bulge. One of the PB galaxies, NGC 7457, is also known to have disc-like kinematics (Kormendy 1993; Pinkney et al. 2003). Michard & Marchal (1994) found small bar-like distortions in this galaxy and Emsellem et al. (2004) found nearly-cylindrical rotation which is seen in boxy bulges (Bertola & Capaccioli 1977; Kormendy & Illingworth 1982; Falcón-Barroso et al. 2004) and in simulations of edge-on bars (Combes et al. 1990; Sellwood 1993; Athanassoula & Misiriotis 2002).

This project initially began in collaboration with some members of the ENEAR survey (Wegner et al. 2000). Therefore, the first five galaxies we observed were from their sample: NGCs 4472, 2775, 3544, 3831 and 5793. NGC 4472, a bright elliptical in the centre of the Virgo cluster, was included for comparison with previous studies. The other four galaxies were selected to span a wide range in inclination and bulge-to-disc ratio.

Several reasons for including both high- and low-inclination galaxies are listed below.

(1) Minor-axis observations of highly inclined galaxies offer minimum disc contamination in the outer regions of the bulge.

(2) In moderately inclined galaxies, there is actually more disc contamination along the minor-axis than the major-axis for the same solid angle. To estimate the degree of disc contamination, we obtained spectra along both major- and minor-axes for some of our inclined galaxies.

(3) Major-axis observations of inclined galaxies allow for the measurement of rotation which can provide additional information about the structure of the galaxy.

(4) Low-inclination galaxies have less disc contamination in the central regions and allow for clear identification of bars, rings, and other morphological features. Including both high- and low-inclination galaxies allows for a comparison between bars and b/p bulges.

(5) In highly inclined galaxies, the bulge and disc can be distinguished based on their shapes (spheroidal versus flat). In face-on galaxies, this is not possible and so bulges are generally defined as the excess light on top of the inward extrapolation of an exponential disc. SPs and kinematics offer two additional and independent means of distinguishing between bulges and discs in face-on galaxies.

12 out of our 20 low-inclination galaxies are barred. Some of our highly inclined galaxies were classified by Lüticke, Dettmar & Pohlen (2000) into peanut-shaped, boxy, nearly boxy, or elliptical bulges. For our remaining highly inclined galaxies, we determined the shapes using their technique. This yielded 10 b/p bulges and eight elliptical bulges. Therefore, the fraction of barred galaxies in low-inclination galaxies is approximately equal to the fraction of b/p bulges in highly inclined galaxies. While peanut-shaped bulges are easily identified, it is not always easy to distinguish an elliptical bulge from one that is slightly boxy. For instance, Lüticke et al. classified NGC 5838's bulge as elliptical but Michard & Marchal (1994) described it as boxy.

Table 1 contains basic data on our galaxies. The column 'Morphological type' describes the shape of the bulge if the galaxy is highly inclined (boxy, peanut, or elliptical) and whether or not it

is barred if it is not highly inclined. Identifications marked with an asterisk are those of Lüticke et al., while those without asterisks are our identifications.

When comparing SPs in galaxies with different colours, it is important to keep in mind that colour is correlated with the global dynamical properties of a galaxy. Fig. 1 shows the bulge $B - K$ colours as a function of central velocity dispersions, and maximum disc rotational velocities of our galaxies where available. The bulge and disc colours are from DJ and PB. Bulge colour is defined to be the colour at half the K -band bulge effective radius or 5 arcsec, whichever is larger. Disc colour is defined to be the colour at two disc scalelengths. We found that it is useful to subdivide bulges according to whether they are redder or bluer than $B - K = 4$; these are shown as red and blue points. Section 3.3 describes how the rotation curves and velocity dispersion profiles were obtained. Central velocity dispersion was measured on approximately 4-arcsec spectral bins [3.3, 4.2 and 3.8 arcsec for Double Imaging Spectrograph (DIS) I, II and III, respectively]. The maximum disc rotational velocity shown is the average of visual estimates on either side of the major-axis. In this and subsequent plots, the point shape represents the Hubble type; the circles are S0 galaxies; the hexagons are S0a and Sa galaxies; the pentagons are Sab galaxies; the squares are Sb galaxies; and the triangles are Sbc and Sc galaxies. The filled symbols are barred galaxies. The thin open symbols are elliptical bulges if highly inclined and unbarred galaxies if not highly inclined. The thick open symbols are b/p bulges.

Bulge colours correlate more tightly with V_{\max} than with σ_0 . Galaxies with $V_{\max} > 200 \text{ km s}^{-1}$ host red bulges while those with $V_{\max} < 165 \text{ km s}^{-1}$ host blue bulges. Both red and blue bulges are found in nearly the full range of central velocity dispersions spanned by our galaxies although there is an overabundance of red bulges in large σ galaxies and vice versa.

3 OBSERVATIONS AND DATA ANALYSIS

3.1 Observations

Observations were made with the DIS on the ARC 3.5-m telescope at Apache Point Observatory between 2000 January and 2004 February. The spectrograph uses a dichroic to split the light into separate blue and red channels. During this period, the instrument was upgraded in several phases with the installation of new detectors and optics. Table 2 gives the specifications of each configuration and Table 3 describes the spectroscopic observations. DIS I gave us continuous wavelength coverage from 4000 to 7500 Å while DIS II and DIS III gave us continuous coverage from 3700 to 7500 Å. A 5 arcmin \times 1.5 arcsec slit was used in all the observations. On each night, we observed a quartz lamp for flat-fielding, arc lamps for wavelength calibration, and two to five spectrophotometric standards for flux calibration. On several nights, Lick standard stars from Worthey et al. (1994) were observed to allow us to transform our line indices to the Lick/IDS system.

For most of the highly inclined galaxies, we obtained spectra along both major- and minor-axes. For the unbarred low-inclination galaxies, we obtained major-axis profiles except for NGC 2916 for which we obtained a minor-axis profile instead because there was a bright star along the major-axis. For the clearly barred galaxies, we placed the slit along the bar. For IC 302 and NGC 2487, this is different from the position angle of the major-axis. In NGC 5375, the bar happens to be along the major-axis. We could not identify a major-axis in NGC 266 or NGC 5020, but the slit must have been

Table 1. The galaxy sample. DJ denotes de Jong (1996b), PB denotes Peletier & Balcells (1997), and EN denotes the ENEAR survey (Wegner et al. 2000). The morphological types are from the NED. The B magnitudes are from RC3 (de Vaucouleurs et al. 1991). The bulge and disc colours are from DJ and PB. Bulge colour is defined to be the colour at half the K -band bulge effective radius or 5 arcsec, whichever is larger. Disc colour is defined to be the colour at two disc scalelengths. b/a is the red major- over minor-axis ratio taken from the sources listed. The recessional velocities shown are the RC3 heliocentric velocities corrected to the Local Group according to Karachentsev & Makarov (1996). The 21-cm values were used where both 21-cm and optical velocities were available. Since no RC3 data were available for NGC 3831, the B magnitude and optical heliocentric velocity were taken from Fairall et al. (1992). The scale was obtained assuming $H_0 = 70$. The distance to NGC 3384 was determined by Cepheid observations (Tanvir, Ferguson & Shanks 1999).

Galaxy	Source	Type	Morphological type	m_B (mag)	$(B - K)_B$	$(B - K)_D$	b/a	V_{LG} (km s $^{-1}$)	Scale (kpc arcsec $^{-1}$)
IC 267	DJ	SBb	Unbarred	13.63	4.6	4.24	0.71	3577	0.25
IC 302	DJ	SBbc	Barred	13.59			0.92	5950	0.41
IC 1029	PB	SAb	Elliptical*	13.64	3.89	3.77	0.24	2520	0.17
NGC 266	DJ	SBab	Barred	12.33	4.6	3.85	0.94	4908	0.34
NGC 765	DJ	SABbc	Barred	13.60	4.4	3.82	1.00	5117	0.37
NGC 1642	DJ	SA(rs)c	Unbarred?	13.28	4.0	3.26	1.00	4579	0.32
NGC 2487	DJ	SBb	Barred	13.10	4.1	3.53	0.92	4758	0.33
NGC 2599	DJ	SAa	Unbarred	13.12	4.0	3.8	1.00	4651	0.32
NGC 2775	EN	SAab	Unbarred	11.13			0.85	1173	0.08
NGC 2787		SB0+	Barred	11.77				696	0.06
NGC 2916	DJ	SAab	Unbarred	12.42	4.2	3.59	0.74	3618	0.25
NGC 3384		SB0-	Barred	10.63				735	0.06
NGC 3544	EN	SABA	Unbarred?	12.99			0.30	3354	0.23
NGC 3681	DJ	SAB(r)bc	Barred	12.25	3.8	3.47	1.00	1239	0.08
NGC 3728	DJ	SAb	Unbarred	13.80	4.2	3.7	0.75	6904	0.48
NGC 3831	EN	SAB0+	Boxy*	14.5			0.24	4715	0.33
NGC 3883	DJ	SAb	Barred	13.10	4.1	3.44	0.91	6937	0.48
NGC 3945		SB0+	Barred	11.38				1220	0.09
NGC 4472	EN	E2		9.30				744	0.05
NGC 5020	DJ	SABbc	Barred	12.50	3.6	3.11	0.85	3284	0.23
NGC 5326	PB	SAa	Unbarred	12.92	4.05	3.97	0.50	2573	0.18
NGC 5362	PB	SAb	Unbarred	13.14	3.56	3.24	0.37	2314	0.16
NGC 5375	DJ	SBab	Barred	12.40	3.9	3.47	0.81	2418	0.17
NGC 5389	PB	SABO/a	Boxy*	13.10	4.12	4.10	0.20	1996	0.14
NGC 5422	PB	SA0	Elliptical*	12.81	4.17	4.09	0.20	1921	0.13
NGC 5577	PB	SAbc	Elliptical*	13.05	3.84	3.54	0.28	1702	0.12
NGC 5689	PB	SBO/a	Boxy?*	12.54	4.14	4.12	0.25	2295	0.16
NGC 5707	PB	SAab	Elliptical*	13.38	4.24	3.92	0.25	2354	0.16
NGC 5719	PB	SABab	Boxy?*	13.1	4.54	3.84	0.36	1676	0.12
NGC 5746	PB	SABB	Peanut*	11.38	4.42	4.50	0.16	1676	0.12
NGC 5793	EN	SABB	Boxy?	14.30			0.37	3387	0.23
NGC 5838	PB	SA0-	Boxy?*	11.74	4.21	4.11	0.35	1338	0.09
NGC 5987	PB	SAb	Elliptical	13.00	4.46	4.14	0.40	3207	0.22
NGC 6246A	DJ	SABC	Unbarred	14.10	3.9	3.23	0.91	5495	0.38
NGC 6368	PB	SAb	Elliptical*	13.10	4.84	4.58	0.20	2904	0.20
NGC 7311	PB	SAab	Elliptical	13.36	4.35	4.07	0.50	4762	0.33
NGC 7332	PB	SAB0	Boxy*	12.11	3.75	3.58	0.26	1584	0.11
NGC 7457	PB	SAB0-	Boxy?	11.86	3.69	3.50	0.52	1115	0.08
NGC 7537	PB	SAbc	Elliptical*	13.65	3.88	3.62	0.34	2888	0.20

placed close to it as we see substantial rotation. We did not detect any rotation in five galaxies: IC 302 and NGCs 765, 2487, 2916 and 6246A, due to their inclinations being too low.

We obtained images in B , V and R for bulge-to-disc decomposition (B/D) on six nights using the SPIcam detector on the same telescope. Typical exposure times were 600 s for B , 180 s for V , and 120 s for R . Superbiases and twilight flats were obtained on each night.

3.2 Basic reductions

Data reduction was carried out using the XVISTA software package. For the imaging, basic reduction included bias subtraction and flat-fielding. For the spectroscopy, flat-fields were constructed using a median of five to 10 bright quartz lamp exposures; the mean

spectral response was divided out. Wavelength calibration was performed using He, Ne, and Ar arc lamp exposures, using a fifth-order polynomial for both blue and red channels. Flux calibration was performed using a spline fit to published spectra of the spectrophotometric standards (Massey et al. 1988). Line curvature along the slit was measured using the lamp exposures and a simple row-by-row shift was stored for subsequent corrections. Similarly, spatial distortion in the spectrograph was measured using standard star exposures and the correction was stored.

Since spatial distortion includes a component due to differential refraction unless the slit is perpendicular to the parallactic angle, this component was calculated and removed from the standard star measurements. Differential refraction causes a mixture of light loss and positional shift along the slit as a function of wavelength depending

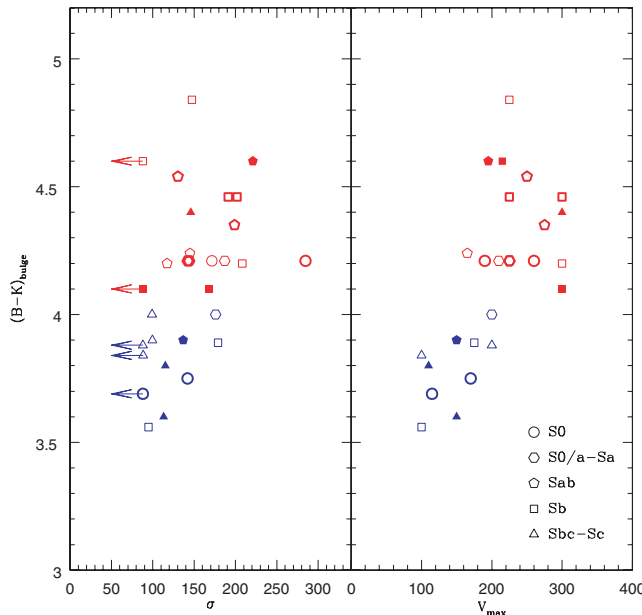


Figure 1. Bulge colour versus central velocity dispersion and maximum disc rotational velocity. The velocities are from this work while the colours are from PB and DJ. The central velocity dispersions were measured within an aperture of approximately 4 arcsec. See Table 1 for the definition of bulge colour. Bulges are shown in red or blue according to whether they are redder or bluer than $B - K = 4$. The filled symbols are barred galaxies. The thin open symbols are elliptical bulges if highly inclined and unbarred galaxies if not highly inclined; the thick open symbols are b/p bulges.

on the orientation of the slit to the parallactic angle. Light loss from differential refraction has a negligible effect on line strengths since they are defined over a relatively narrow range in wavelength. Positional changes as a function of wavelength need to be considered to ensure that the indices at different wavelengths are being compared at the same physical location. To do this, we calculate the expected shift from differential refraction depending on the orientation of the slit, assuming typical atmospheric parameters, and correct the position of the spectra as a function of wavelength accordingly. This is done for both flux calibration stars and the galaxy spectra; additionally, the corrected calibration stars provide a measurement of distortion that we also apply to the galaxies. An alternative, and perhaps more standard, approach would be to just ‘straighten’ each object based on the centroid or peak of the object. We felt that the calculated positional correction might be more accurate in the case of more diffuse galaxies, especially at wavelengths with lower S/N; in practice, they yield similar corrections.

Each galaxy frame was subtracted by the overscan and superbias, flat-fielded, and trimmed to remove the overscan region. The line curvature and spatial distortion corrections were applied. Multiple

observations of each galaxy were then co-added, rejecting cosmic ray outliers in the process. Where multiple observations were not available, cosmic rays were removed by eye using a spatial median filter. Variance frames were propagated throughout the reduction process. To combine the red and blue channels, the red galaxy spectra were rescaled to spatially match the blue spectra. The spectra were then extracted in approximately 1-arcsec bins near the centre of the galaxy and using larger bins farther out. An average of sky values measured on both sides of the galaxy was subtracted from each slice. Wavelength and flux calibrations were applied and both red and blue frames were rebinned to 3 \AA pixel^{-1} . Finally, the spectra were de-redshifted and the red and blue sides were combined. The blue spectrum was used out to a wavelength of 5600 \AA and the red from 5450 \AA . In the overlap region between 5450 and 5600 \AA , an average of red and blue values was used. In some galaxies, there is a discontinuity in the overlap region that arises from the difficulty of accurately combining the two channels for extended objects; fortunately, none of our absorption features falls within this region.

On our last observing run (2004 February 15), the light on star frames was too extended to be explained by seeing alone. The excess light, which we believe is scattered light, had a spectral energy distribution similar to that of the mated stellar spectrum but without any narrow spectral features presumably because it is significantly defocused. Since adding a constant to a spectrum decreases the equivalent width (EW) of an absorption feature and since the relative contribution of the scattered light to galaxy light increases with distance from the galaxy centre, this introduces an artificial negative gradient in the line-strength profiles. To correct for the scattered light, we fit the 2D stellar spectrum with a smoothed stellar spectrum along the wavelength direction and a fifth-order polynomial along the spatial direction, masking out the central 20 pixels (8.4 arcsec). This spatial profile, combined with the smoothed spectral profile of the galaxy, was subtracted from each galaxy frame. One galaxy that was observed on the problematic night, NGC 3384, has previously measured index profiles. Applying the correction resulted in much better agreement with the published values (see Section 3.7). No scattered light correction was applied on any of the other nights, since the correction derived for those nights did not affect the line-strength profiles significantly.

3.3 Measuring and correcting for rotation and velocity dispersion

We measured rotation and velocity dispersion in the stellar components of our galaxies using the ppxf package (Cappellari & Emsellem 2004). SSP spectra were constructed using the SP models by Bruzual & Charlot (2003, hereafter BC03) assuming a Chabrier initial mass function. The ppxf routine fits each galactic extraction with a linear combination of SSP spectra, shifting and broadening these to match the galaxy’s rotation and velocity dispersion,

Table 2. Spectrograph specifications during our observing runs.

Detector	Observation dates (M/D/Y–M/D/Y)	Grating	Dispersion (\AA pixel^{-1})	Approximate resolution (\AA)	Scale (arcsec pixel^{-1})
DIS I blue	1/10/00–2/11/02	Medium	3.18	5.7	1.086
DIS I red	1/10/00–2/11/02	Medium	3.53	8.6	0.605
DIS II blue	4/13/02–10/09/02	Low	3.05	8.6	0.600
DIS II red	4/13/02–04/07/03	Medium	3.13	7.8	0.605
DIS III blue	03/06/03–02/15/04	Low	2.42	7.7	0.419
DIS III red	05/29/03–02/15/04	Medium	2.31	6.9	0.396

Table 3. Spectrographic observations.

Galaxy	Axis	Position angle	Date (M/D/Y)	Exposure time (s)
IC 267		-25	12/22/03	1 × 2400 1 × 1230
IC 302	Bar	8	10/9/02	2 × 2400
IC 1029	Major	152	5/30/03	3 × 2400
NGC 266	Bar	0	9/17/02	2 × 2400
NGC 765		15	12/22/03	3 × 2400
NGC 1642		0	12/1/03	2 × 2400
NGC 2487	Bar	45	2/11/02	3 × 2400
NGC 2599		-90	2/11/02	3 × 2400
NGC 2775	Major	66	1/10/00	3 × 1200
	Minor	156	1/10/00	3 × 1200
NGC 2787	Major	109	2/15/04	2 × 2400
NGC 2916	Minor	-80	12/1/03	2 × 2400 1 × 900
NGC 3384	Major	50	2/15/04	2 × 2400
NGC 3544	Major	-84	1/10/00	3 × 1200
	Minor	6	4/25/00	3 × 1200
NGC 3681	Bar	-25	2/11/02	3 × 2400
NGC 3728	Major	20	3/6/03	3 × 2400
NGC 3831	Major	24	4/25/00	3 × 1200
	Minor	114	5/3/00	3 × 1800
NGC 3883	Major	-14	3/7/03	3 × 2400 1 × 1200
NGC 3945	Major	-22	2/15/04	2 × 2400 1 × 1800
NGC 4472		67	1/10/00	3 × 1200
NGC 5020	Bar	38	3/6/03	2 × 2400
NGC 5326	Major	-44	5/4/00	4 × 1800
	Minor	-134	2/11/02	2 × 2400
NGC 5362	Major	-92	6/16/01	4 × 2400
NGC 5375	Bar	-10	4/7/03	1 × 2400 1 × 1200
NGC 5389	Major	3	5/2/00	4 × 1800
	Minor	-87	5/2/00	3 × 1800
NGC 5422	Major	-26	5/2/00	2 × 1200
	Minor	64	5/3/00	2 × 1800 2 × 1500
NGC 5577	Major	56	1/10/00	3 × 1200 2 × 1500
NGC 5689	Major	-93	6/17/01	3 × 2400
	Minor	0	4/13/02	2 × 2400
NGC 5707	Major	39	5/29/03	2 × 2400 1 × 1200
NGC 5719	Major	-90	5/30/03	3 × 2400
NGC 5746	Major	-9	4/17/02	3 × 2400
	Minor	-99	4/17/02	3 × 2400
NGC 5793	Major	-35	5/4/00	1 × 1800
	Minor	55		2 × 1500
NGC 5838	Major	42	6/8/02	2 × 2400
NGC 5987	Major	-109	5/30/03	1 × 2400 1 × 2700
NGC 6246A		-90	2/19/01	2 × 1800
			2/20/01	2 × 1800
NGC 6368	Major	47	6/29/03	1 × 2400 1 × 2100
NGC 7311	Major	24	7/1/03	1 × 2400
		15	10/12/01	1 × 2400
NGC 7332	Major	-24	7/3/00	4 × 1800
NGC 7457	Major	-38	7/1/03	1 × 2400 1 × 1257
NGC 7537	Major	-100	10/12/01	4 × 2400

respectively. The fit was performed within the wavelength range 4800–5400 Å, with the emission lines H β , [O III] 4959, and [O III] 5007 masked out. The profiles will be presented in Paper II.

The galaxy spectrum at each location was shifted by the measured stellar rotation before measuring the line indices. To correct the indices for velocity dispersion, line strengths were measured on an SSP template that was broadened by the measured velocity dispersion and another template that was broadened only to the instrumental resolution. These templates were also constructed using a linear combination of BC03 SSP spectra with emission lines masked out, but the wavelength range for the fit was 4000–6600 Å, to include all the Lick indices. The same templates were used for emission correction (following section). The measured absorption-line EWs were multiplied by the ratio of the unbroadened line strength to the broadened one; for magnitudes, the correction factor is the difference between these two quantities.

3.4 Measuring and correcting for emission

Some absorption indices can be severely affected by line-filling by emission. These include the Balmer indices, Fe5015 (due to [O III] 5007 emission), and Mgb (due to [N I] 5199 emission). To correct for this, we subtracted the template described in the previous section from each galaxy spectrum. If on the residual spectrum, H α was found to be in emission at the 5 σ level and a local maximum was detected at H β , a Gaussian was fitted to the H β emission and subtracted from the galaxy spectrum. This procedure was repeated for Hy and H δ . [O III] 5007 and [N I] 5199 were subtracted out if they were found to be in emission at the 3 and 4 σ levels, respectively. A larger threshold was used for [N I] 5199 because this feature lies at the edge of the Mg₂ absorption feature and spurious discontinuities often show up there due to template mismatch.

EWs were measured for several emission lines to study the nature of the ionized gas in bulges and inner discs. The galaxy continuum, obtained by smoothing the galaxy spectrum, was added to the emission spectrum described above before measuring the EWs.

3.5 Lick index measurements

The final galaxy spectra were broadened to 9.5-Å full width at half-maximum (FWHM), which is approximately equal to the Lick resolution, and rebinned to a dispersion of 0.125 Å pixel⁻¹. Variable broadening as prescribed in Worthey & Ottaviani (1997) was tried and found not to produce significantly different results. The strengths of 25 absorption features were measured using the latest bandpasses from Guy Worthey's webpage. The EW or magnitude of each feature was computed following Trager et al. (1998).

Spectral indices were measured on Lick standard stars, exactly as done for the galaxies, to transform our line strengths to the Lick/IDS system. Such transformations are necessary because our detector differs in resolution from the IDS and because the IDS spectra were not flux calibrated. Twenty-four stars ranging in spectral type from F5V to K7III were used in deriving the transformations for DIS I and 22 stars (also ranging in spectral type from F5V to K7III) were used for DIS III. By imaging one of the stars at several positions along the slit, it was determined that the line strengths do not vary significantly with slit position. Fig. 2 compares the indices we obtained for the stars with those obtained using the IDS. Linear least-squares fits were performed on these data to obtain the transformation terms. The final EWs and magnitudes were computed as follows:

$$\text{EW} = \frac{\text{EW}_{\text{raw}} T_0 / T + B}{A}$$

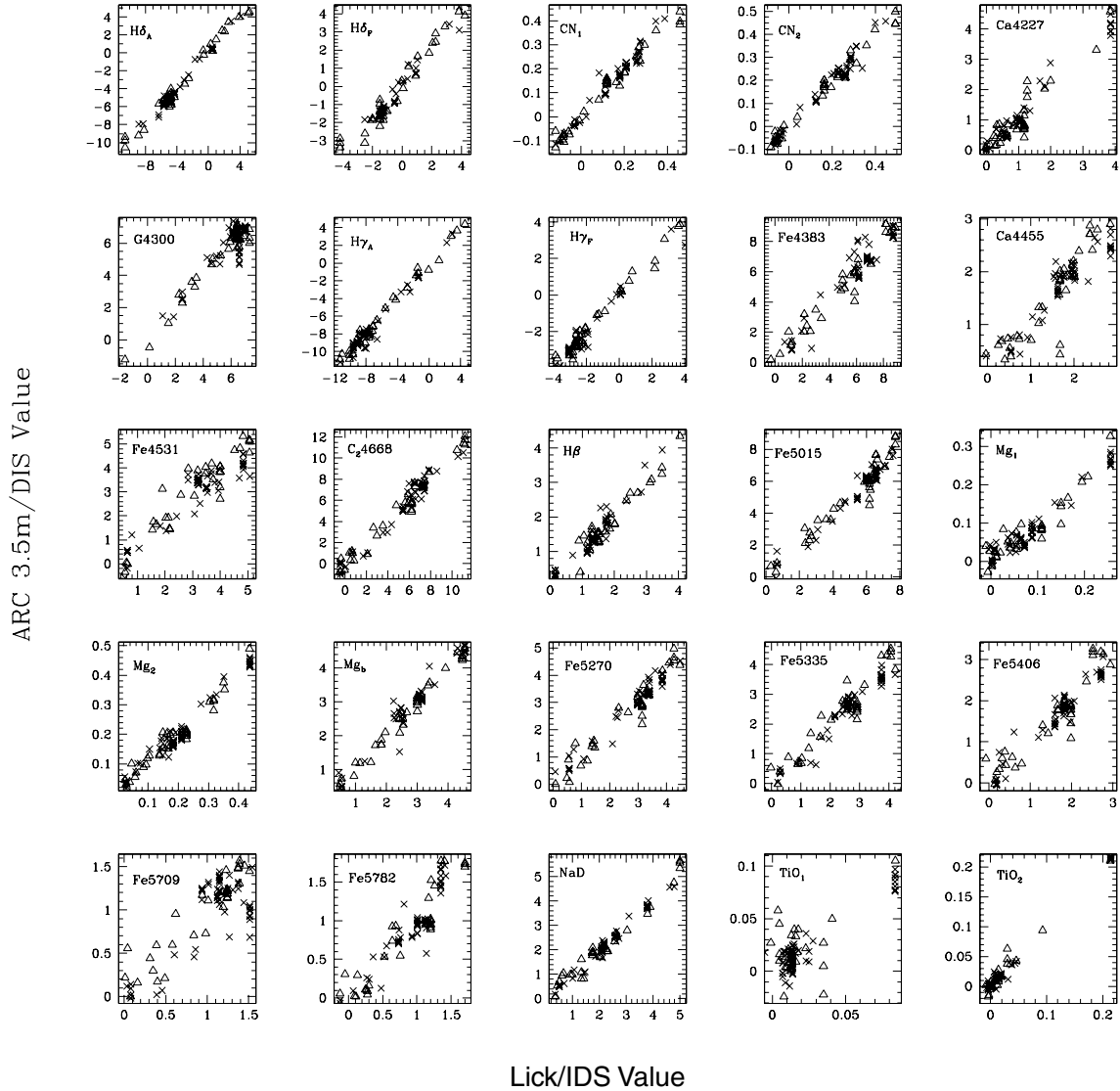


Figure 2. Comparison of indices obtained on standard stars using our instrument and using the Lick/IDS instrument. Each point is a Lick standard star. The triangles are DIS I. The crosses are DIS III. DIS III transformations were used for DIS II.

$$\text{mag} = \frac{\text{mag}_{\text{raw}} + T_0 - T + B}{A},$$

where T_0 and T are the index values measured on the unbroadened and broadened templates, respectively (their ratio or difference is the velocity dispersion correction factor). The transformation terms A and B are given in Table 4 along with the rms scatter in applying the transformations to the stars. DIS III transformations were used for DIS II since the same gratings were used in both setups.

The flux response of the detector changes rapidly at the long-wavelength end of the blue channel, making measurements there difficult. Only the Mg_1 and Mg_2 indices were affected by this, but severely so, since their continuum bandpasses are far apart and the red continuum bandpass lies right where our flux response is steepest. This resulted in large scatter in the transformations of these indices. For the other indices, the scatter in the transformations is similar or slightly larger than that obtained by Proctor & Sansom (2002).

3.6 Comparison with the literature

Fig. 3 shows comparisons of Lick indices between this work and the most recently published values for NGC 4472. There is excellent agreement in the Ca4227, $\text{H}\beta$, Fe5015, $\langle \text{Fe} \rangle$, and Fe5270 profiles between this work and all the published values. Our other index profiles are systematically offset from at least one of the other two studies but the offset is within the uncertainties of transforming our data to the Lick system. In general, our results agree better with the long-slit data from Vazdekis et al. (1997) than the IFU data from Peletier et al. (1999). Nearly all our central values agree with those of Trager et al. Emission correction was not responsible for any disagreement among studies since NGC 4472 does not have much emission.

The first column of Fig. 4 shows index comparisons between this work (triangles), azimuthally averaged IFU data from Sil'chenko (1999; asterisks), and SAURON data extracted along the major-axis from Falcón-Barroso et al. (2004; squares) for NGC 7332.

Table 4. Transformations to the Lick/IDS system. The terms ‘A’ and ‘B’ are described in Section 3.5. ‘rms’ refers to the rms scatter in applying the transformations to the standard stars.

Index	DIS I			DIS II/III		
	A	B	rms	A	B	rms
H δ_A	0.915	-0.198	0.615	0.872	0.620	0.385
H δ_F	0.831	-0.215	0.518	0.854	0.247	0.297
CN ₁	1.015	0.001	0.029	0.844	-0.005	0.022
CN ₂	0.987	-0.007	0.025	0.830	-0.017	0.026
Ca4227	0.949	-0.013	0.384	0.726	-0.022	0.288
G4300	0.909	-0.868	0.501	0.741	-0.772	0.696
H γ_A	1.020	0.025	0.534	0.818	0.250	0.608
H γ_F	0.982	0.046	0.328	0.820	0.078	0.342
Fe4383	1.031	0.578	0.616	0.818	0.547	0.705
Ca4455	0.982	0.233	0.374	0.813	0.296	0.241
Fe4531	0.842	-0.381	0.549	0.856	-0.281	0.537
C ₂ 4668	0.924	-0.748	0.652	0.879	-0.079	0.615
H β	1.060	-0.009	0.239	0.814	-0.298	0.200
Fe5015	0.911	-0.033	0.640	0.861	0.081	0.364
Mg ₁	0.905	0.009	0.027	1.000	0.024	0.020
Mg ₂	1.002	0.023	0.026	0.974	0.036	0.021
Mgb	1.047	0.107	0.157	0.825	-0.105	0.244
Fe5270	0.865	-0.239	0.372	0.888	0.238	0.230
Fe5335	0.813	-0.232	0.387	0.817	-0.415	0.244
Fe5406	0.864	-0.067	0.364	0.793	-0.107	0.222
Fe5709	0.975	-0.040	0.172	0.712	-0.475	0.322
Fe5782	0.774	-0.016	0.218	0.784	0.007	0.169
NaD	0.941	0.115	0.304	0.933	-0.181	0.142
TiO ₁	1.317	0.015	0.021	1.035	0.014	0.010
TiO ₂	0.868	-0.016	0.010	0.934	-0.010	0.006

All the central values are in agreement. The slope of our H β and Fe5270 profiles are steeper than Falcón-Barroso et al.’s but not as steep as Silchenko’s. Our Mgb and Fe5015 profiles agree reasonably well with Falcón-Barroso’s but Silchenko’s Mgb profile is again steeper.

The second column of Fig. 4 shows index comparisons between this work, long-slit data from Fisher et al. (1996; crosses), IFU data from Sil’chenko et al. (2003; asterisks), and SAURON data from de Zeeuw et al. (2002; squares) for NGC 3384. Here also, Sil’chenko’s profile is averaged azimuthally while de Zeeuw et al.’s is an extraction along the major-axis. This galaxy was observed on the night in which scattered light was corrected for as described in Section 3.2. Fisher et al.’s profiles are in good agreement with those from SAURON. Our Mgb and Fe5270 profiles agree marginally with published values. In the central regions, our H β profile falls in between de Zeeuw et al.’s and Sil’chenko et al.’s. Outside about 15 arcsec, our profile falls steeply, possibly due to inadequate scattered light correction, while de Zeeuw et al.’s stays flat. Our Fe5335 profile is much steeper than the published ones especially outside 15 arcsec (again likely due to inadequate scattered light correction).

The third column of Fig. 4 compares profiles for NGC 7457 with IFU data from Sil’chenko et al. (2002) and archival SAURON data which were also presented in Silchenko et al.’s paper. Silchenko et al.’s values are systematically smaller in the central regions than those obtained by others except for the case of Fe5335, where they are in agreement with ours. Our values have larger scatter but are otherwise in agreement with the SAURON values. The agreement among studies is worst for H β although this galaxy has little or no Balmer emission. The 2D SAURON map shows a negative gradient along the major-axis but not along the minor-axis, while Sil’chenko

et al.’s 2D map shows no gradients whatsoever; our values are in better agreement with SAURON’s than Sil’chenko et al.’s.

3.7 Absorption-line indices and SSP models

We have measured all 25 Lick indices in our galaxies as a function of galactocentric radius. In this paper, we concentrate on a subset of these indices which are sensitive to age, metallicity, and α/Fe . The most age-sensitive indices are the Balmer indices H β , H γ_A , H γ_F , H δ_A and H δ_F . Of these, H β suffers most from line-filling by emission, while the H δ indices are the least affected. On the other hand, H β offers the most orthogonality with respect to metallicity-sensitive indices. Using a combination of the Balmer indices, we can obtain more reliable age estimates than with just one index. For metal lines, we compute the indices Mgb/ $\langle \text{Fe} \rangle$ and [MgFe]’ as discussed in Thomas, Maraston & Bender (2003, hereafter TMB); the former is directly related to α/Fe , and [MgFe]’ traces metallicity without any sensitivity to α/Fe . Individually, [MgFe]’ and the Balmer indices are degenerate in age and metallicity but together they can break the degeneracy since each index has a different age–metallicity dependence.

The integrated-light spectrum of an object is a linear combination of SSPs. Some objects, such as globular clusters, are well represented by a single SSP while galaxies are generally not. Still, one can characterize the SPs of a galaxy by an ‘equivalent SSP’. Since the integrated light from a galaxy is weighted by luminosity, its SSP age and metallicity are likely to be different from the mass-weighted age and metallicity of its stars. SSP values are useful parametrizations of the SPs but cannot be interpreted as true ages and metallicities, since galaxies most likely contain a range of both. To avoid overinterpreting our data, we focus on the line strengths, mentioning SSP values only to illustrate dramatic differences between objects or regions within an object (i.e. 2 versus 10 Gyr as opposed to 8 versus 12 Gyr). Different line strengths in different objects (or within an object) imply different SPs; the SSP models allow us to infer the underlying source of the differences.

3.8 Bulge-to-disc decomposition

1D and 2D B/D was performed on our images. The disc and bulge were simultaneously fitted with an exponential and an $\exp(r^{1/n})$ profile, respectively. Initial fits were made using the fixed values of n of 1, 2, 3 and 4; the best fit of these was used as a starting guess in a final fit where n was allowed to vary as a free parameter. The results from the 1D decomposition were used as starting guesses for the 2D decomposition. In the 2D fits, both the bulge and disc components were allowed to be elliptical. This resulted in an overestimation of bulge size in most of our low-inclination barred galaxies (IC 302 and NGCs 266, 765, 3681, 3883 and 5375). A two-component bulge/disc model, such as ours, also overestimates the bulge component of our three S0s with luminous inner discs (NGCs 2787, 3384 and 3945) as previously found by Erwin et al. (2003). We pay close attention to these effects when studying the line-strength profiles in the bulge- and disc-dominated regions (Section 4.2). It was found through visual inspection that the best-fitting bulge and disc components of the other galaxies were reasonable. Fig. 5 shows the light profiles of our galaxies along with the best-fitting bulge and disc components.

The B/D used here primarily serves to determine the relative contribution of bulge and disc light as a function of radius; while B/D is notoriously difficult, especially when allowing for a Sersic

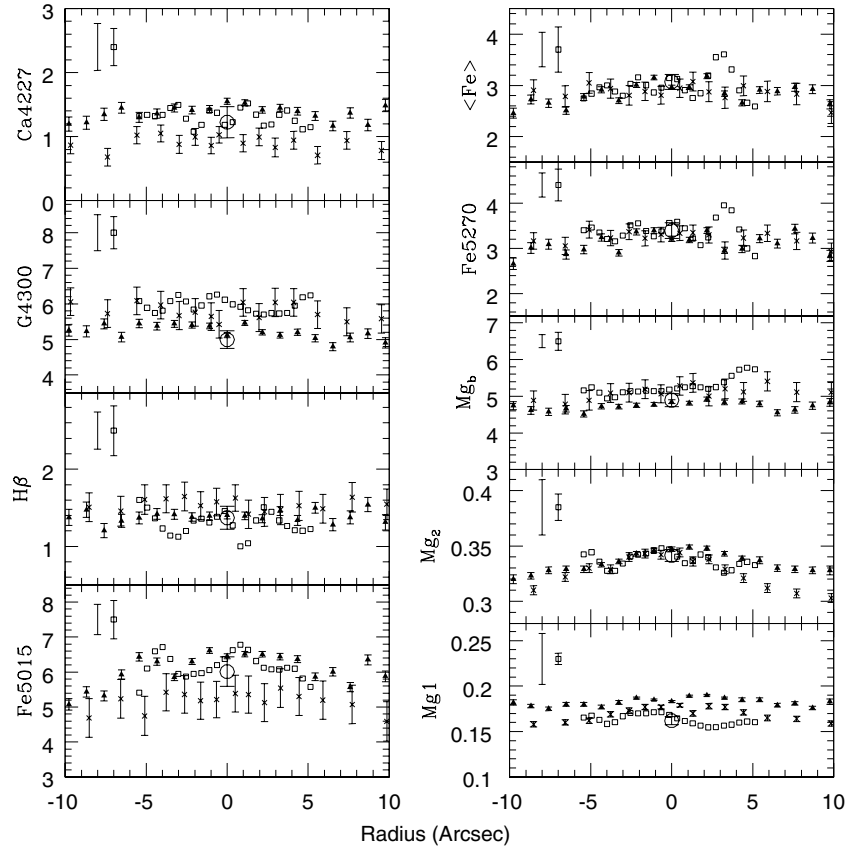


Figure 3. Comparison of line-strength gradients between this work and published values for NGC 4472. The triangles are from this work. The large circles are from Trager et al. (1998). The open squares are IFU data from Peletier et al. (1999) and the crosses are long-slit data from Vazdekis et al. (1997). At the top of each figure, the error bars without points represent the scatter in stars from our transformations to the Lick system; the error bars with squares indicate uncertainties in Peletier et al.’s data, including those involved in transforming to the Lick system.

bulge, this ratio is determined more robustly than the derived values of bulge effective radius and Sersic index.

Throughout this paper, the term ‘disc’ refers to the exponential outer region of the luminosity profile and the term ‘bulge’ refers to the excess light in the inner regions that was fitted with a Sersic profile. It is possible that these photometrically determined components do not correspond to a cold and a hot component, a flat and a spheroidal component, or a young and an old component. Through simulations, Abadi et al. (2003) found that while the stars of a simulated galaxy were well fitted by a Sersic + exponential profile, the hot and cold components were not well fitted individually by a Sersic and an exponential profile, respectively. Instead both were Sersic in the inner regions and exponential farther out. Using our kinematic information, we address this issue in Paper II. The structural properties and how they relate to the SPs will also be presented in that paper.

4 RESULTS

4.1 Central line strengths

Fig. 6 shows the measured central values of $H\beta$ and $[MgFe]'$ for our sample as well as published values for the MW (Puzia et al. 2002), M31 (Puzia et al. 2005), other bulges (Proctor & Sansom 2002) and elliptical galaxies (Trager et al. 1998; Proctor & Sansom 2002; Nelan et al. 2005). Symbol type and size denote Hubble type and central velocity dispersion, respectively. Most of Trager et al.’s and Proctor

et al.’s ellipticals have large σ_0 but those of Nelan et al. (2005) populate all the σ_0 bins. Early- and late-type bulges preferentially populate the intermediate- σ_0 and small- σ_0 bins, respectively. S0s are found in all σ_0 bins. TMB’s SSP models are superimposed on the plot. If a point has an accompanying vertical line segment, its location relative to the model grid was determined using an average of the other four Balmer indices instead of $H\beta$. The other end of the line segment shows the $H\beta$ value. If the difference between these is large, this is due most likely to errors in $H\beta$ emission correction since the galaxies whose $H\beta$ values lie outside the model grid have strong $H\beta$ emission. Two galaxies have $H\beta$ values that put them outside the plot range. These are NGCs 2787 and 5719 with $H\beta$ values of -0.506 and 0.607 , respectively. If a point does not have an accompanying vertical line segment, its location relative to the model grid does not change much depending on which Balmer index is plotted versus $[MgFe]'$.

Our central indices were measured on spectral extractions binned to match Trager et al.’s $1.4 \times 4\text{-arcsec}^2$ aperture and Proctor et al.’s $1.25 \times 3.6\text{-arcsec}^2$ aperture as closely as possible (1.5×3.3 , 1.5×4.2 and $1.5 \times 3.8\text{ arcsec}^2$ for DIS I, II and III, respectively). Nelan et al. used 2-arcsec-diameter fibres. Nelan et al.’s large- σ_0 galaxies have systematically smaller $[MgFe]'$ than those of Trager et al. and Proctor et al. Line-strength gradients are likely to be responsible for the offset. While the three studies used similar angular apertures, Nelan et al.’s galaxies are considerably more distant ($c\zeta \sim 15\,000\text{ km s}^{-1}$ for Nelan et al., 3000 km s^{-1} for Trager et al., and 2000 km s^{-1} for Proctor et al.). Since Nelan et al. sampled a larger portion of each

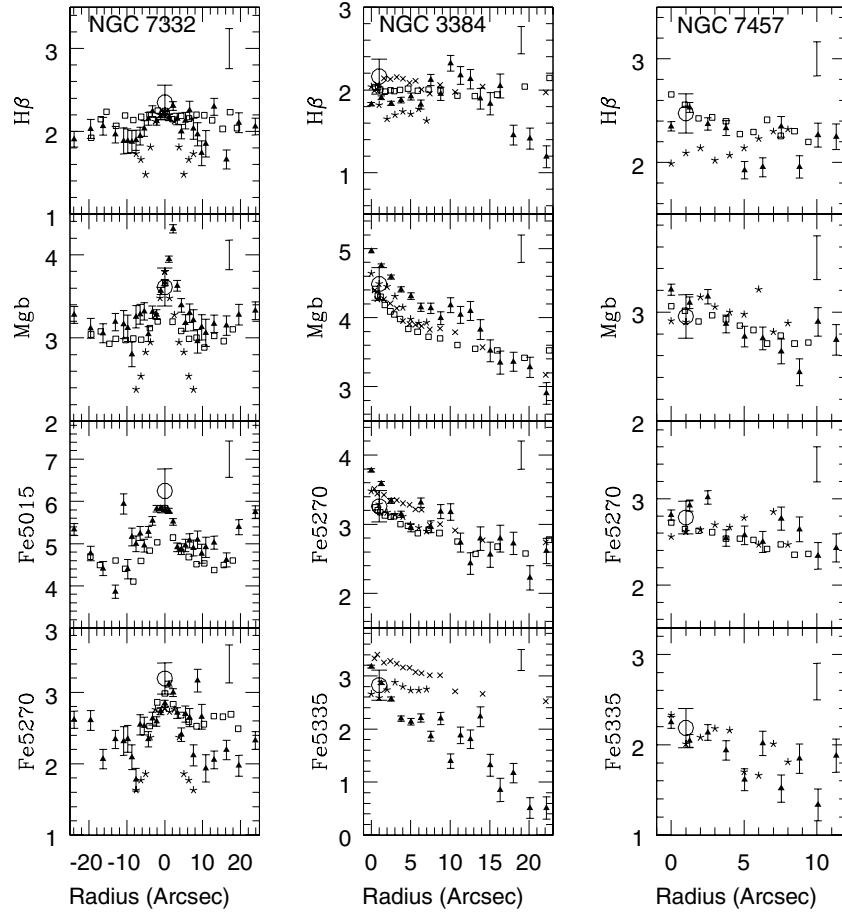


Figure 4. Comparison of line-strength gradients between this work and published values for NGCs 7332, 3384 and 7457. The triangles are from this work. The asterisks are azimuthally averaged IFU data from Sil'chenko (1999), Sil'chenko et al. (2003), and Sil'chenko et al. (2002) for NGCs 7332, 3384 and 7457, respectively. The squares are SAURON data extracted along the major-axis from Falcón-Barroso et al. (2004), de Zeeuw et al. (2002) and Sil'chenko et al. (2002). For NGC 3384, the crosses are long-slit data from Fisher et al. (1996).

galaxy and since early-type galaxies have decreasing [MgFe] with radius, we would expect them to obtain smaller ‘central’ values for [MgFe]. Kuntschner et al. (2006) computed aperture corrections to Mgb and Fe5015 in early-type galaxies and found the magnitude of the correction to be similar in these two indices. Assuming that Nelan et al.’s galaxies are a factor of 5 farther than those of Trager et al. and assuming that [MgFe] has a similar correction as Mgb and Fe5015, yields an [MgFe] value of 3.8 for Nelan et al.’s largest- σ_0 bin. This brings its SSP metallicity close to those of the large- σ_0 ellipticals from Trager et al. and Proctor et al.

Bulges can be broadly classified into three groups according to which region of Fig. 6 they populate: the old metal-rich (OMR, lower right-hand panel) region, the young metal-rich (YMR, upper right-hand panel) region with ages less than 3 Gyr and supersolar metallicity, or the metal-poor (MP, left-hand panel) region with subsolar metallicity. This classification scheme is analogous to that of Prugniel et al. with our MP, OMR and YMR classes corresponding to their A, B and C classes, respectively. The bulges of the MW and M31 lie in the MP region.

Membership in a region is closely related to bulge colour. Most of the red bulges populate the OMR region while all but one of the bulges in the MP region are blue. The exception is IC 267 (the red open square with [MgFe] = 1.65). This bulge has strong Balmer emission which suggests that its red colour is due to dust from recent

star formation as opposed to an old SP. Colour does not uniquely represent the SPs of blue bulges; some bulges are blue because they are metal poor while others are blue because they are young. To distinguish the two classes of blue bulges in subsequent plots, the MP bulges are marked with an additional blue dot.

Besides colour, central line strengths are sensitive to Hubble type. All the early-type (S0–Sab) bulges have large central metallicities. The blue early types are in the YMR region, while the red early types are in the OMR region. Bulges of late-type spirals are more heterogeneous in their central line strengths than those of early types. The MP region is populated exclusively by late types, but late types are also found in the other two regions. Ellipticals populate all three regions of the plot.

Much of the variation in central line strengths is due to correlations between the line strengths and the global kinematics. The largest- σ_0 galaxies, which include a large fraction of Trager et al.’s and Proctor et al.’s ellipticals, exclusively populate the OMR region. As σ_0 decreases, SSP age and SSP metallicity decrease in Nelan et al.’s ellipticals; this appears to be true in our bulges and those of Proctor et al. as well but at fixed σ_0 , the scatter in SSP age and SSP metallicity among bulges is large. Caldwell et al. (2003) also found that small- σ_0 ellipticals have, on average, smaller SSP ages and metallicities than large- σ_0 ellipticals; unfortunately, we cannot include their data in Fig. 6 because they did not measure the

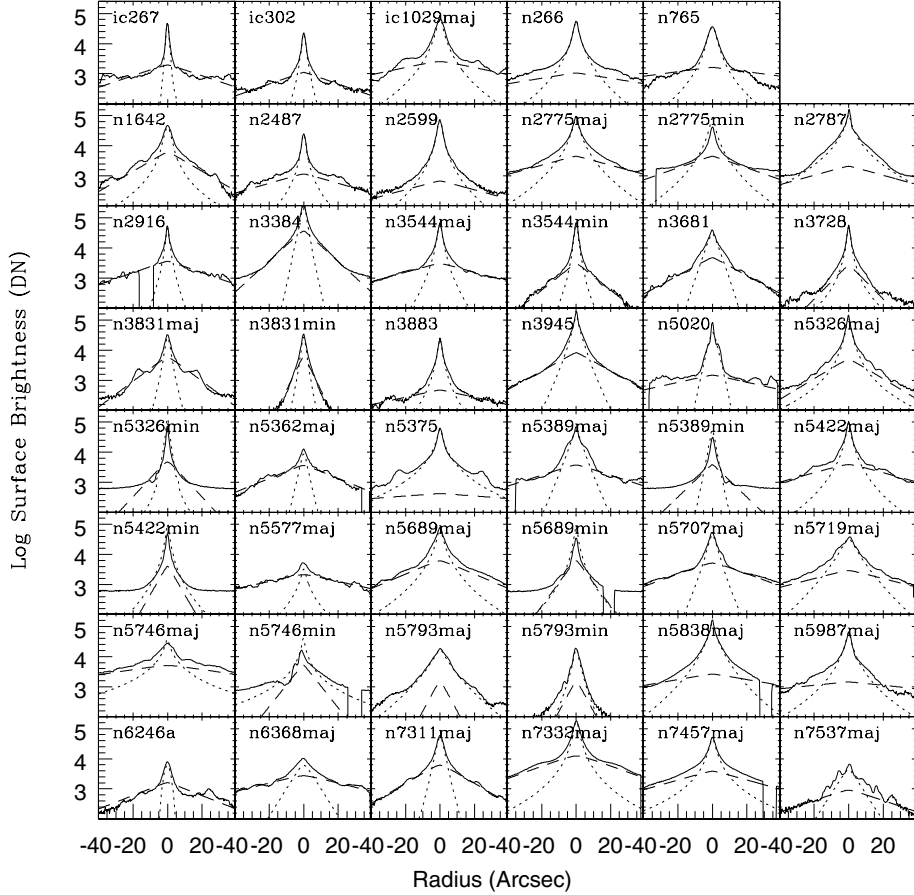


Figure 5. Results of 2D B/D. The light profile of each galaxy is shown as a solid line, the best-fitting bulge as a dotted line, and the best-fitting disc as a dashed line. The position angles are the same as those used for the spectroscopy (Table 3).

same indices. The OMR region is populated almost exclusively by large- σ_0 [$\log(\sigma_0) > 2.2$] galaxies, while the MP region is populated exclusively by small- σ_0 [$\log(\sigma_0) < 2$] galaxies. The YMR region is populated by small- and intermediate- σ_0 galaxies.

The different types of bulges (MP, YMR and OMR) and ellipticals form a continuous and overlapping sequence on a plot of [MgFe]' versus central velocity dispersion (Fig. 7, top left-hand panel). In both bulges and ellipticals, [MgFe]' is correlated with σ_0 at the low- σ_0 end. As σ_0 increases beyond $\log(\sigma_0) > 2.2$, [MgFe]' remains constant. Bulges show larger scatter than ellipticals in the [MgFe]'- σ_0 relation.

[MgFe]' is also correlated with the maximum disc rotational velocity (Fig. 7, top right-hand panel), as previously found by Prugniel et al. However, the blue bulges with $\log V_{\max} > 2.2$ are significant outliers in the [MgFe]'- V_{\max} , having smaller central values of [MgFe]' than their red counterparts.

Balmer indices are anticorrelated with σ_0 and weakly anticorrelated with V_{\max} (middle panel of Fig. 7). Residuals in the H β - σ_0 and H β - V_{\max} relations are correlated with colour such that at a given σ_0 and V_{\max} , blue bulges have larger H β values than red bulges.

At fixed σ_0 , age and metallicity are known to be anticorrelated in ellipticals (Trager et al. 2000b; Proctor & Sansom 2002), a result which has important consequences for the origin of the red sequence (See Section 5.1). This is clearly seen in Fig. 6. Nearly all the green and magenta crosses belong to the two largest- σ_0 bins. Of these, the ones with the largest SSP age (~ 15 Gyr) have the smallest SSP metallicity ($[Z/H] \sim 0.2$), while those with the smallest SSP age (~ 3 Gyr) have the largest SSP metallicity ($[Z/H] \sim 0.7$). A similar

anticorrelation does not appear to exist for bulges; if it does exist, there is considerably larger scatter than in ellipticals.

In bulges and ellipticals, the α/Fe ratio as indicated by Mgb/(Fe), is correlated with σ_0 and V_{\max} (bottom panel of Fig. 7). In these two plots, the region within the inner horizontal lines corresponds to models with solar α/Fe for metallicities $-1.35 \leq [Z/\text{H}] \leq 0.35$ and ages from 8 to 15 Gyr; the region within the outer lines represents models with the same metallicities and ages from 3 to 15 Gyr (from fig. 4 of TMB). Red bulges and ellipticals show good overlap in the Mgb/(Fe)- σ_0 diagram. With a few exceptions, blue bulges are consistent with having solar α/Fe . Consequently, most blue bulges have smaller Mgb/(Fe) ratios than red bulges or ellipticals at a given value of σ_0 or V_{\max} . One of the blue bulges, NGC 6246A, has supersolar α/Fe , large age, and small metallicity ($[Z/\text{H}] \sim -0.8$) like MW halo stars. The other two blue bulges with supersolar α/Fe have supersolar metallicity like the majority of red bulges.

There are hints of possible differences between barred and unbarred galaxies in some of the scaling relations. At fixed σ_0 and V_{\max} , barred galaxies appear to have larger central values of [MgFe]' than unbarred galaxies (or galaxies with elliptical-shaped bulges). b/p bulges generally lie between and exhibit larger scatter than barred and unbarred/elliptical bulges in the [MgFe]'- σ_0 and [MgFe]'- V_{\max} diagrams. The central regions of b/p bulges could be contaminated by the foreground disc resulting in smaller values of [MgFe]' than those of the low-inclination barred galaxies. Barred galaxies appear to have smaller H β than unbarred galaxies at fixed σ_0 and V_{\max} . No striking difference is seen between barred and unbarred galaxies in the scaling relations involving Mgb/(Fe). Note that the parame-

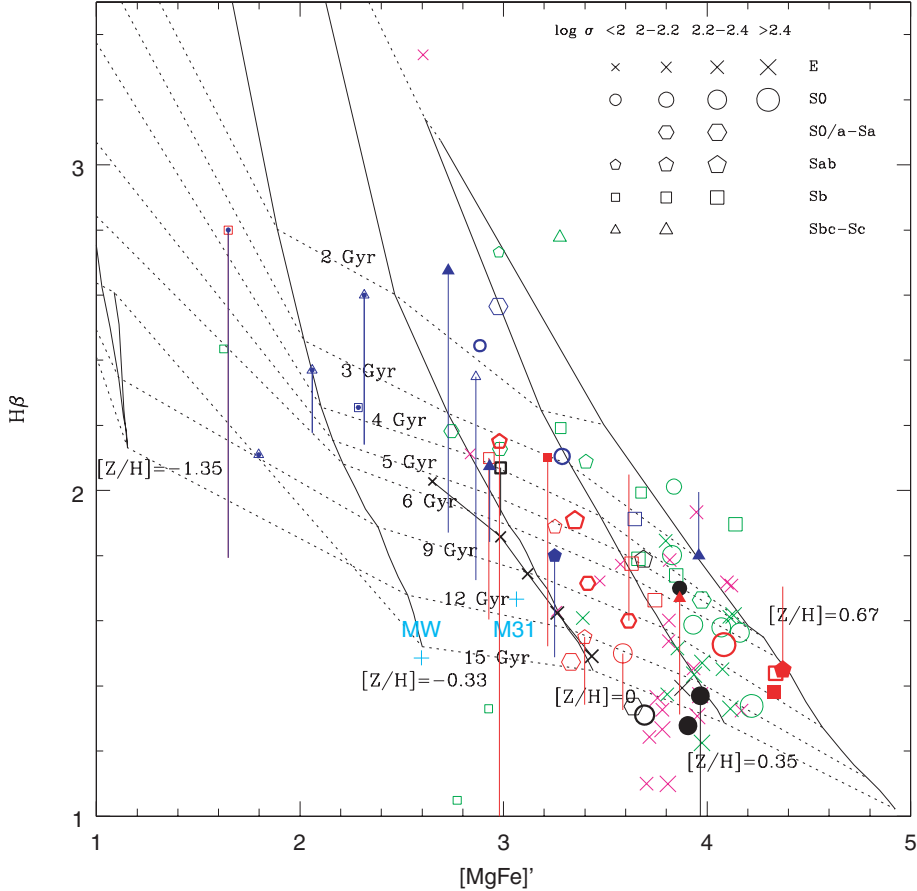


Figure 6. $H\beta$ versus $[MgFe]'$ in the central regions of bulges and ellipticals. Symbol type and size denote Hubble type and central velocity dispersion, respectively, as shown in the legend. The bold black crosses connected by lines are from Nelan et al. (2005). Each bold cross represents the mean of approximately 700 early-type galaxies. The magenta crosses are galaxies from Trager et al. (1998) that were classified as elliptical and had $H\beta$ uncertainty less than 0.2 and velocity dispersion uncertainty less than or equal to 10 km s^{-1} . The green symbols are bulges and ellipticals from Proctor & Sansom (2002). The MW (Puzia et al. 2002) and M31 (Puzia et al. 2005) are shown as '+' symbols. Bulges from this work are shown in blue or red as in Fig. 1 or in black if no colour information is available. As in Fig. 1, the filled symbols are barred galaxies, the thick open symbols are b/p bulges, and the thin open symbols are unbarred galaxies or elliptical-shaped bulges. Our five metal-poor (MP) bulges are marked with an additional blue dot. TMB's models are superimposed on the plot. If a point has an accompanying vertical line segment, its location relative to the model grid was determined using an average of the other four Balmer indices, instead of $H\beta$. The other end of the line segment shows the $H\beta$ value. If a point does not have an accompanying vertical line segment, its location relative to the model grid does not change much depending on which Balmer index is plotted versus $[MgFe]'$.

ter space defined by morphology, kinematics, and dynamics is only sparsely sampled in this study. A considerably larger galaxy sample is required to definitively determine whether or not barred and unbarred galaxies follow the same scaling relations.

The central regions of our three barred S0s with disc-like structure and kinematics (filled black circles) have supersolar SSP metallicities and α/Fe ratios and two of the three have large SSP ages. If all discs formed stars on long time-scales (several Gyr), we would expect them to have small α/Fe ratios, like the MW disc at the solar neighbourhood, since interstellar medium (ISM)-enrichment would eventually be dominated by SNe Ia. The ‘luminous inner discs’ of these S0s have not had such a star formation history. Peletier et al. (1999) found that the Sombrero galaxy is also dominated by a fast rotating disc whose $[Mg/\text{Fe}]$ is similar not to other discs but to ellipticals of similar mass as the Sombrero.

4.2 Line-strength gradients

Figs 8 and 9 show $[Mg/\text{Fe}]$ profiles in our galaxies. The open squares and filled triangles show points that were and were not corrected for

$[\text{N I}]$ 5199 emission, respectively; the correction was seldom performed. The solid and dotted vertical lines indicate where the ratio of bulge to disc light is 2 and 1/2, respectively, as determined from the B/D. We performed linear least-squares fits to the $[Mg/\text{Fe}]$ profiles separately in the bulge- and disc-dominated regions, selecting the points to include based on the B/D but making exceptions where they seemed appropriate (such as when the bar was fit as a bulge; see Section 3.8). We usually avoided the transition region from bulge to disc dominance. The best-fitting lines are shown in red. The discrepancy due to scattered light between our Fe5335 profile of NGC 3384 and published ones (see Section 3.6) does not affect $[Mg/\text{Fe}]$ significantly. The $[Mg/\text{Fe}]$ profile obtained by Fisher et al. (1996) for NGC 3384 (green curve in Fig. 8) shows good agreement with ours.

Most galaxies have negative $[Mg/\text{Fe}]$ gradients (decreasing $[Mg/\text{Fe}]$ with increasing radius) in the bulge-dominated region. $[Mg/\text{Fe}]$ generally decreases steadily from the galaxy centre to the solid vertical lines, beyond which the slope of the profile changes. In low-inclination galaxies and along the major-axes of inclined galaxies, $[Mg/\text{Fe}]$ is usually larger just outside the solid vertical lines than

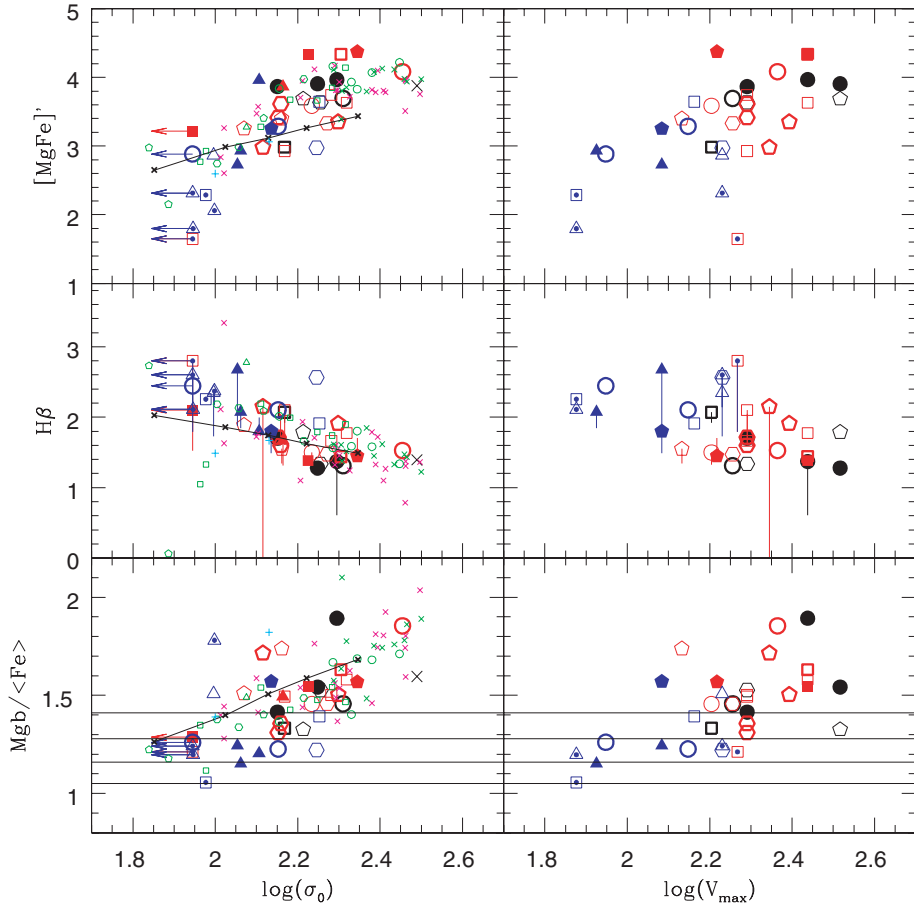


Figure 7. Central line strengths versus central velocity dispersion and maximum disc rotational velocity. The symbols are as in Fig. 6, except that the large symbols represent values obtained in this work and the small symbols represent published values. The arrows represent upper limits for galaxies whose velocity dispersions are close to or below our resolution limit. IC 302 and NGCs 765, 2487, 2916 and 6246A are not shown on the right-hand panel, since their inclinations are too low to measure rotation. In the bottom panel, the region within the inner horizontal lines corresponds to models with solar α/Fe for metallicities $-1.35 \leq [\text{Z}/\text{H}] \leq 0.35$ and ages from 8 to 15 Gyr (from fig. 4 of TMB). The region within the outer horizontal lines represents models with the same metallicities and ages from 3 to 15 Gyr.

inside it (NGC 5987 is a good example), suggesting that the outer bulge has a smaller line strength than the inner disc. The fact that we can identify distinct bulge and disc components in the $[\text{MgFe}]'$ profiles suggests that disc contamination is not significant within the solid vertical lines.

The galaxies that do not have negative $[\text{MgFe}]'$ gradients in the bulge-dominated region are generally those with small bulges (solid vertical lines are located at a radius of less than 5 arcsec). In four of these (IC 267 and NGCs 3831, 5577 and 6246A), there is the hint of a positive gradient while the rest (NGCs 2916, 5362 and 6368) are consistent with having little or no gradient. Since the profiles are always different inside and outside the solid lines, they cannot be explained by disc contamination. Two galaxies with larger bulge-dominated regions, NGCs 3681 and 5707, also do not have negative $[\text{MgFe}]'$ gradients in the bulge. They do, however, have a negative gradient in the transition region from bulge to disc dominance.

Another test for disc contamination is how the major- and minor-axis profiles vary as a function of inclination. Low-inclination galaxies should have identical profiles if there are no azimuthal differences in line strengths. The major- and minor-axis profiles of NGC 2775, the only low-inclination galaxy for which both were obtained, are indeed identical. At intermediate inclinations, one ex-

pects more disc contamination on one side of the minor-axis (the dusty side) than the major-axis for the same solid angle. In the three intermediate inclination galaxies for which we have major- and minor-axis spectra (NGCs 3544, 5326 and 5389), this effect is clearly seen; the minor-axis profile is asymmetric outside the solid vertical lines with the profile turning over at a smaller galactocentric distance on the dusty (left hand) side than that on the dust-free side. Within the solid lines, there is good agreement in gradient slopes between major- and minor-axes, indicating that disc contamination is not significant. In edge-on galaxies, it is difficult to estimate the degree of disc contamination in the central region; but away from the centre, there is more disc contamination along the major-axis than along the minor-axis. In two of our edge-on galaxies (NGCs 5422 and 5689), the minor-axis profile continues to decrease beyond the distance at which the major-axis profiles turn over briefly (due to the inner disc having larger $[\text{MgFe}]'$ than the outer bulge, as discussed above). The profiles of our other two edge-on galaxies (NGCs 5746 and 5793) are too noisy to determine if this effect is present. Previously, Fisher et al. (1996) noted differences in major- and minor-axis index profiles in S0s, with the major-axis profiles flattening off at large radii, while the minor-axis profiles continue to decrease.

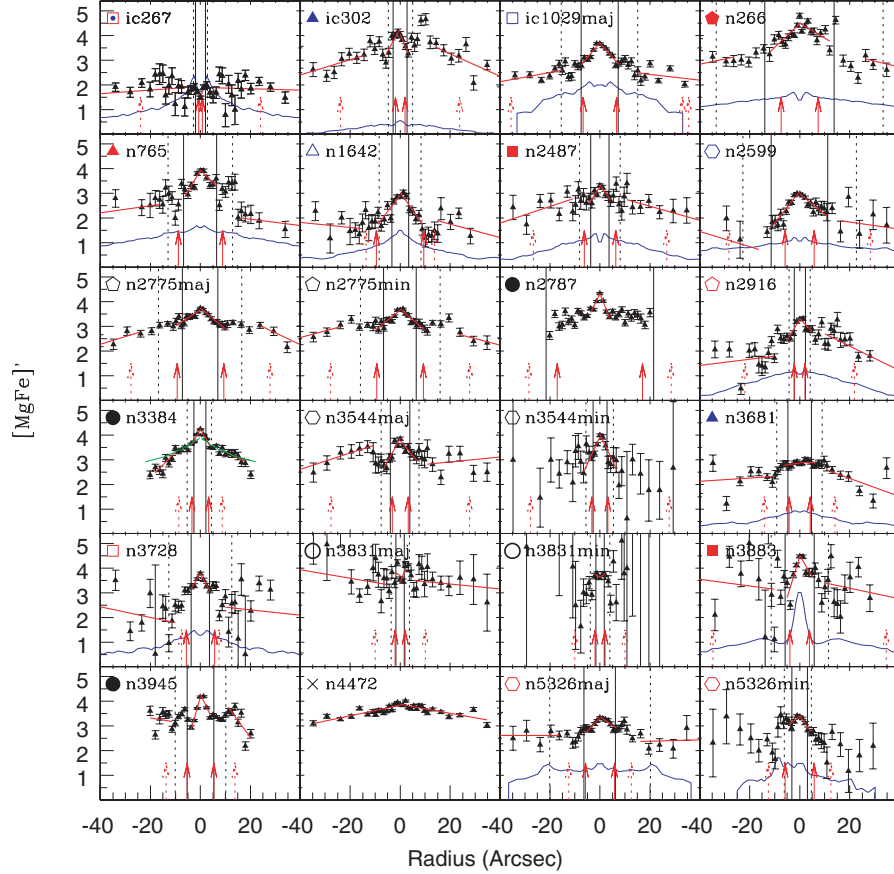


Figure 8. $[\text{MgFe}]'$ profiles in our galaxies. The open squares and filled triangles show points that were and were not corrected for $[\text{N I}]$ 5199 emission, respectively. For NGC 3384, the green curve shows the profile obtained by Fisher et al. (1996). At the top left-hand side of each plot are symbols denoting the galaxy type (as in Fig. 6) as well as the NGC or IC identifiers. The solid and dotted vertical lines indicate where the ratio of bulge to disc light is 2 and 1/2, respectively, as determined from the B/D. The solid and dotted red arrows indicate the location of the bulge effective radius and disc scalelength, respectively. Results from linear least-squares fits performed separately in the bulge- and disc-dominated regions are shown in red. The blue lines are colour profiles ($B - K - 3$) from PB and DJ. $B - K$ was not available for IC 302; $V - H - 3$ is shown instead.

The slopes of $[\text{MgFe}]'$ gradients within the bulge along the major-axis are shown in Fig. 10 as a function of the central $[\text{MgFe}]'$, central velocity dispersion, and maximum disc rotational velocity. Galaxies with large central values have correspondingly large negative gradients, while the three galaxies with the smallest central values, namely IC 267 and NGCs 5577 and 6246A, have positive gradients. Gradients are weakly correlated with the global kinematics, perhaps slightly more tightly with V_{\max} than with σ_0 . Proctor (2002) also found that index gradients in bulges were correlated with central velocity dispersion and more tightly with central indices. It does not appear as if the tightness of the correlation between gradients and the global kinematics would improve if some Hubble types (for instance, early types) were excluded but this result needs to be confirmed with a larger galaxy sample.

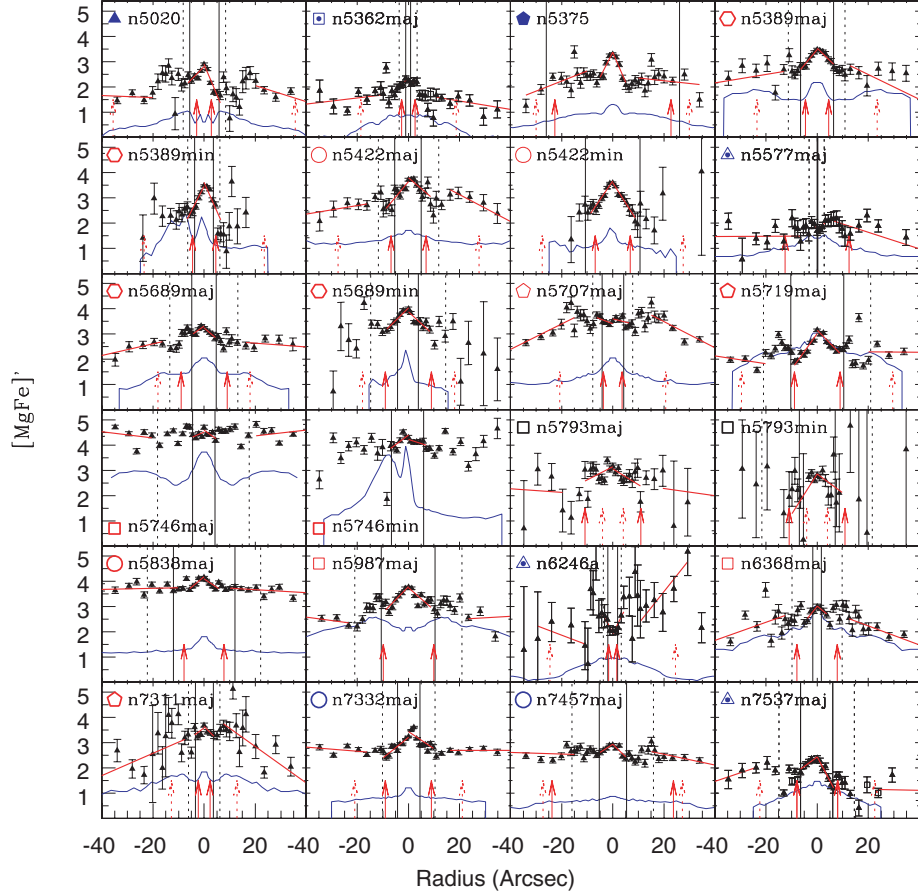
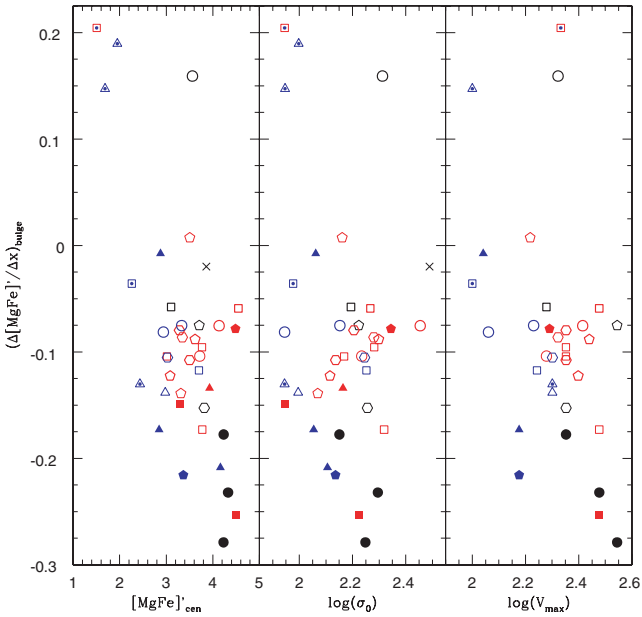
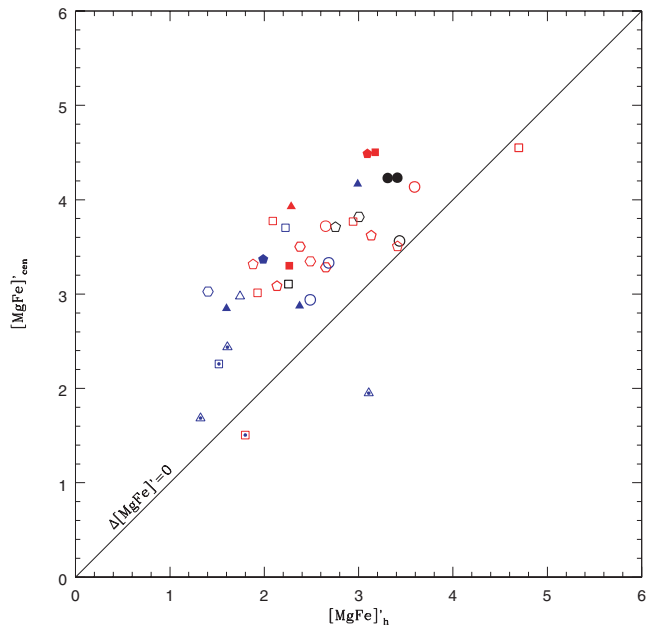
Most galaxies also have negative gradients in the disc-dominated region but it is shallower than that of the bulge. Some galaxies (e.g. NGCs 5746, 5838 and 7332) have no gradient in the disc.

The $[\text{MgFe}]'$ value at one disc scalelength (computed using the results of our least-squares fits) is correlated with the central value (Fig. 11). This indicates that the metallicity of the disc is correlated with that of the bulge. This correlation holds for all galaxies, not just the late types or those with bars, blue bulges, or bulges identified as having disc-like structural or kinematical properties.

4.2.1 Separating age and metallicity effects

Figs 12 and 13 show gradients in the $H\delta_A$ index. The $H\delta$ profiles show less scatter than the lower-order Balmer indices since they are less affected by emission. The squares and filled triangles show points that were and were not corrected for emission, respectively. Least-squares fits were performed on the Balmer indices exactly in the same manner as for the $[\text{MgFe}]'$ profiles. The fit results for $H\delta_A$ are shown in red in Fig. 12. Gradient slopes computed on individual indices were combined to disentangle the effects of age and metallicity. This is shown in Fig. 14 for the $[\text{MgFe}]' - H\delta_A$ index combination. A red arrow is drawn from the galaxy centre to the edge of the bulge-dominated region (on either side of the galaxy) and a blue arrow is drawn from there to the disc scalelength.

The majority of galaxies (at least 29 out of 38) have negative metallicity gradients in the bulge-dominated region. NGCs 3681, 3831, 5362, 5707 and 7311 show little or no metallicity gradient in the bulge. Three of the five MP bulges (IC 267 and NGC 5577 and 6246A) have positive metallicity gradients. The remaining two galaxies (NGCs 5746 and 5793, both edge-on with b/p bulges) show internal discrepancies in the fit results. Except for its minor-axis $H\delta_A$ profile, NGC 5746 is consistent with having little or no metallicity gradient. The minor-axis profiles of NGC 5793 consistently

Figure 9. $[\text{MgFe}]'$ profiles in our galaxies (continued). The symbols are as in Fig. 6.Figure 10. $[\text{MgFe}]'$ gradient within the bulge-dominated region versus the central value of $[\text{MgFe}]'$, central velocity dispersion, and maximum disc rotational velocity. For galaxies with major- and minor-axis observations, the gradient along the major-axis is shown. The symbols are as in Fig. 6.Figure 11. The central value of $[\text{MgFe}]'$ versus the value at one disc scale-length computed using the results from a least-squares fit to the $[\text{MgFe}]'$ profiles. The solid line shows where objects would lie if their bulges and discs were identical in $[\text{MgFe}]'$. The symbols are as in Fig. 6.

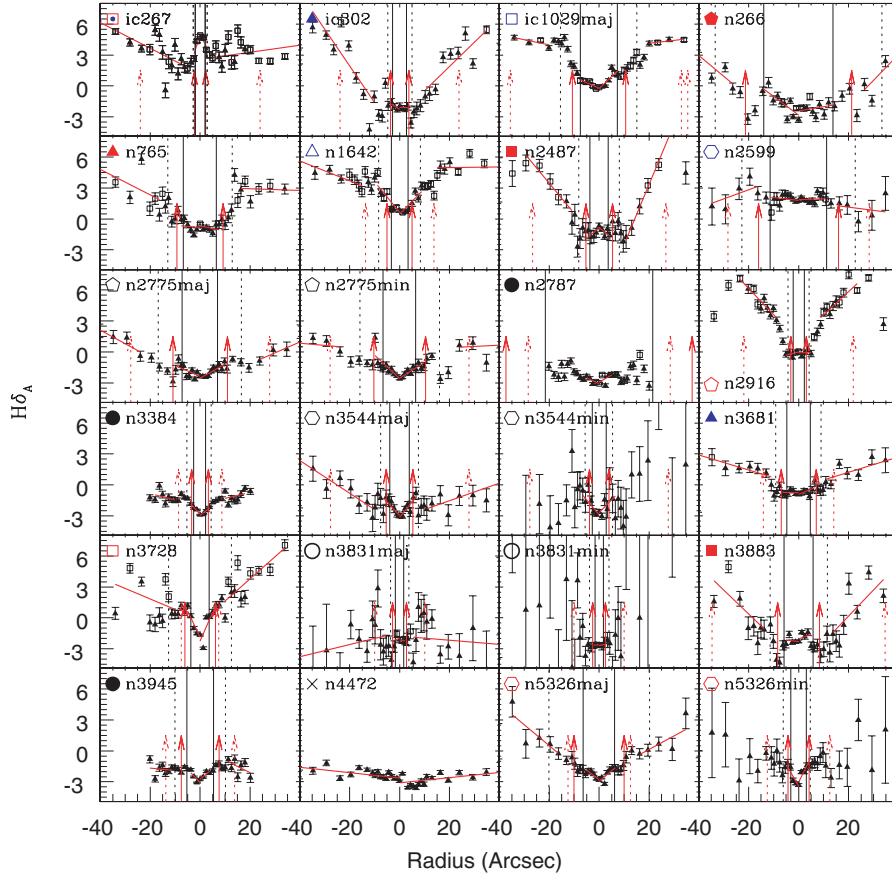


Figure 12. $H\delta_A$ profiles in our galaxies. The symbols are as in Fig. 6.

show a negative metallicity gradient but the major-axis profiles show none.

The majority of galaxies are consistent with having little or no age gradient within the bulge. At least 10 galaxies (IC 302 and NGCs 266, 765, 2487, 2599, 2916, 3883, 5020, 5375 and 5838) have a positive age gradient (larger age with increasing radius). Of these, seven are barred and one has a b/p bulge. At least five galaxies (NGCs 3728, 5577, 6246A, 7311, and the major-axis of NGC 5793) have a negative age gradient in the bulge.

The Balmer indices show large scatter in the disc-dominated regions, making it difficult to determine whether metallicity and age gradients are present. Plots of gradients in the five Balmer indices versus $[MgFe]'$ (such as Fig. 14) do not show consistent results for approximately half the galaxies. Of the other half, most have a negative age gradient and little or no metallicity gradient. Most discs are solar or subsolar in metallicity but NGCs 5746 and 5838 are supersolar well into the disc-dominated region.

4.2.2 Comparison with colour gradients

The blue lines in Figs 8 and 9 are colour profiles ($B - K - 2$) from PB and DJ. The shapes of the $[MgFe]'$ and colour profiles agree often but not always. Where discrepancies exist, they can usually be explained, at least qualitatively, by differences in age- and metallicity-sensitivity between $[MgFe]'$ and $B - K$ colour, with $B - K$ being more age-sensitive. For instance, NGC 266, 2487, 2916 and 3728 show a positive colour gradient but a negative $[MgFe]'$ in the central 5 arcsec. Of these, NGCs 266 and 2487 show a negative $H\delta_A$ gradient in the central region which indicates a positive age

gradient (a negative $H\delta_A$ gradient could also be caused by a positive metallicity gradient but that is ruled out by the negative $[MgFe]'$ gradient). NGC 2916's $H\delta_A$ profile is flat in the central 5 arcsec which, combined with its negative $[MgFe]'$ gradient, also indicates a positive age gradient. A negative metallicity gradient combined with a positive age gradient can explain the differences in $[MgFe]'$ and colour gradients in these galaxies. This explanation is not satisfactory for NGC 3728 whose $[MgFe]'$ and Balmer profiles suggest a negative metallicity gradient and little or no age gradient, while its colour profile suggests a positive gradient in age, metallicity, or both.

De Jong (1996b) noted that it is not possible to identify distinct bulge and disc components using the colour profiles. However, it is possible to do so using the $[MgFe]'$ profiles. As mentioned earlier, the slopes of the $[MgFe]'$ profiles are almost always distinct inside and outside the bulge-dominated region, with the former usually having a steeper negative gradient. Eleven out of the 14 DJ galaxies and 15 out of the 17 PB galaxies have negative $[MgFe]'$ gradients in the bulge-dominated region. The majority of the PB galaxies (12 out of 17 as opposed to four out of the 14 DJ galaxies) also show a negative colour gradient in the bulge-dominated region. The systematic difference in colour gradients between the PB and DJ samples is likely due to different amounts of extinction at different inclinations since the PB galaxies have large inclinations while the DJ galaxies have small ones.

If we compare the gradient in $[MgFe]'$ from the galaxy centre to the disc scalelength (computed using the fit results) with the colour gradient (read from the profiles), we find that these two quantities are not tightly correlated (Fig. 15). This could be due to a combination

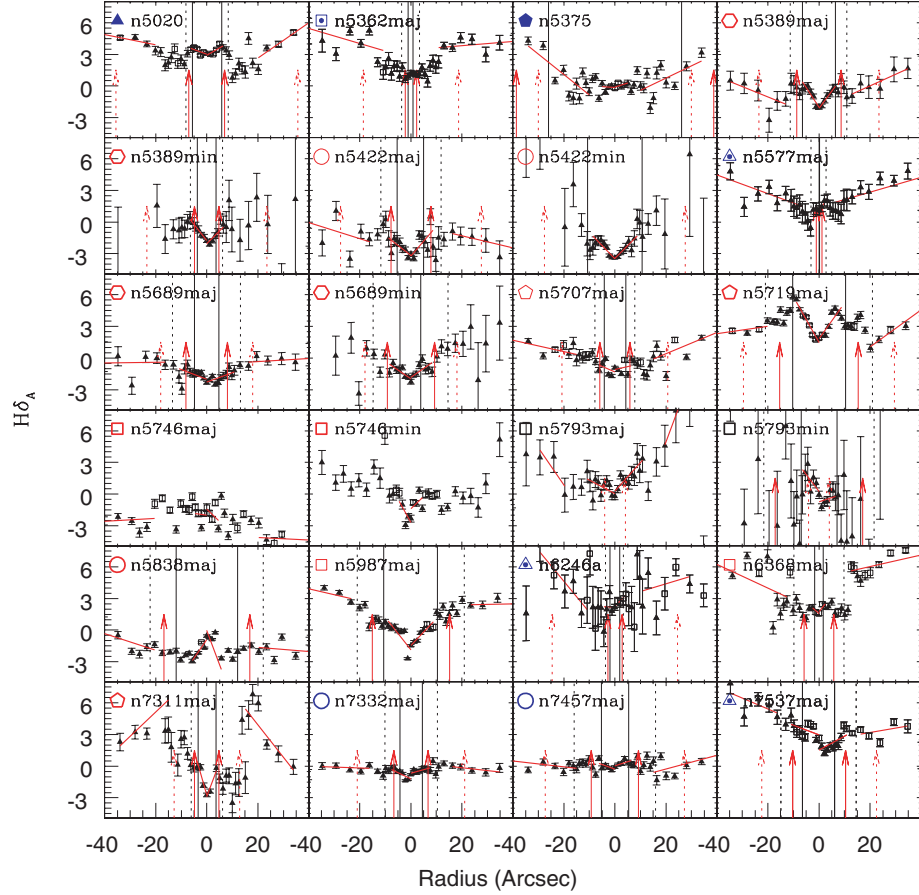


Figure 13. $H\delta_A$ profiles in our galaxies (continued). The symbols are as in Fig. 6.

of different age–metallicity sensitivities between $[\text{Mg}/\text{Fe}]'$ and $B - K$ colour and the influence of dust on the colour profiles.

Gadotti & dos Anjos (2001) found a greater prevalence of null or positive colour gradients in barred galaxies than in unbarred galaxies. They interpreted their result as evidence for gradients being erased by bar-driven mixing. We do not see any systematic difference between barred and unbarred galaxies with regard to their gradients. Also, if bars homogenized the SPs, we might expect a smooth transition in the line-strength profiles from the bulge to the bar. However, the outer bulges of barred galaxies have lower $[\text{Mg}/\text{Fe}]'$ than the inner bar, the same way the outer bulges of unbarred galaxies have lower $[\text{Mg}/\text{Fe}]'$ than the inner disc.

4.2.3 Abundance ratio gradients

Most galaxies either have a positive gradient or no gradient in $\text{Mgb}/(\text{Fe})$ within the bulge-dominated region (Figs 16 and 17). The disc-dominated regions generally have solar α/Fe . Since the red-bulge galaxies have supersolar α/Fe in the centre, they have a negative gradient in the bulge–disc transition. The blue–bulge galaxies have solar α/Fe in the centre. These either have uniformly solar α/Fe or a positive gradient in the bulge and a negative gradient in the bulge–disc transition. Recall that what is marked as the bulge-dominated region in some galaxies (e.g. NGCs 266 and 5375) is actually a bar and that the true bulge-dominated region is smaller. The elliptical galaxy, NGC 4472, is uniformly supersolar in α/Fe .

There are a few galaxies that have supersolar α/Fe in the disc-dominated region. NGCs 266, 5707 and 5746 are nearly uniformly

supersolar. The disc of NGC 5838 is supersolar but less enhanced than its bulge.

For NGC 3384, we obtain a positive gradient in $\text{Mgb}/(\text{Fe})$ while Fisher et al. (1996; green curve in Fig. 16) found no gradient. The discrepancy could be due to scattered light in our data. The other two objects affected by scattered light are NGCs 2787 and 3945. NGC 2787 shows no gradient in $\text{Mgb}/(\text{Fe})$. NGC 3945 has an asymmetric positive gradient. This could not be due entirely to scattered light since the scattered profile was symmetric.

4.3 Emission lines in bulges

Fig. 18 shows profiles of $\text{H}\alpha$ and $[\text{N II}] 6583$ emission strength in our galaxies. We detect emission in the central regions of all our galaxies except the S0s, NGCs 3384 and 7457. The locations of our galaxies in the Baldwin et al. (1981) (hereafter BPT) diagram of emission-line ratios are shown in Fig. 19 for objects with central emission-line EW smaller than -0.5 \AA (the negative sign denotes emission) in $\text{H}\alpha$, $[\text{N II}] 6583$, $\text{H}\beta$, and $[\text{O III}] 5007$. The dashed curve shows the demarcation between starburst galaxies and active galactic nuclei (AGN) as defined by Kauffmann et al. (2003). The majority of our emission-line galaxies are AGN. If the emission in these galaxies is due entirely to the AGN, we would expect it to be restricted to the centre of the galaxy. However, in the three of these (NGCs 2599, 5719 and 7537), it is not centrally peaked. In the other five (NGCs 266, 2916, 3831, 5793 and 6368), the emission peaks at the centre and decreases steadily out to the edge of the bulge-dominated region, beyond which it rises again. Therefore, all

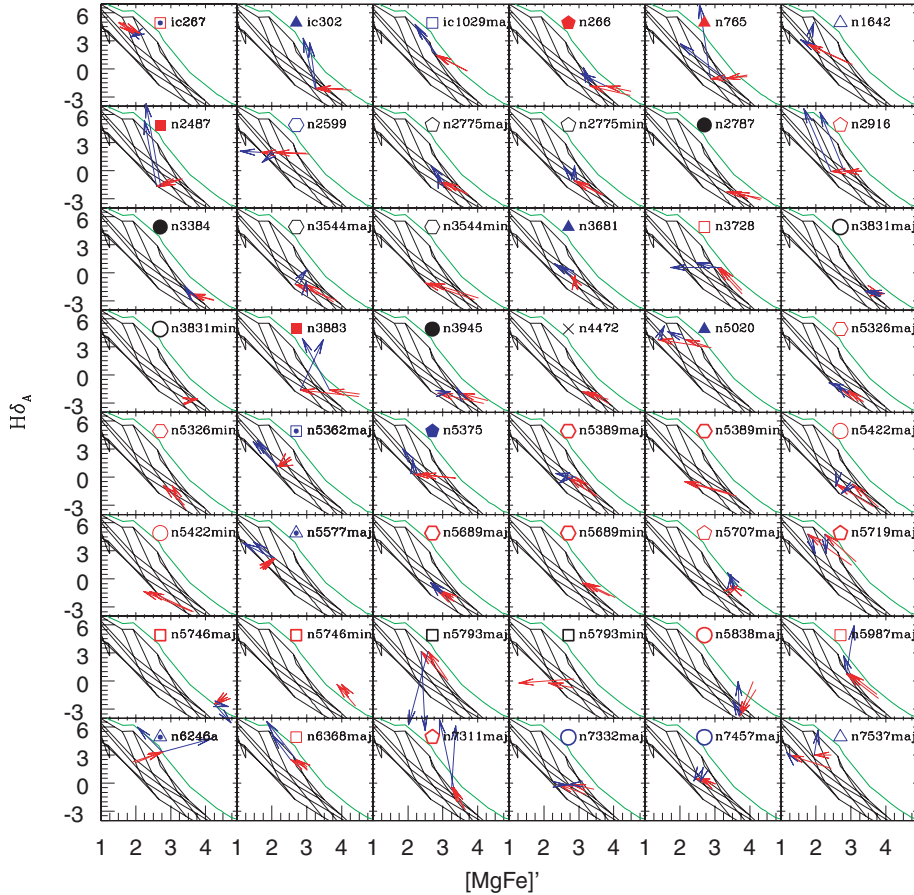


Figure 14. Gradients in $H\delta_A$ and $[MgFe]'$. The red arrows are drawn from the galaxy centre to the edge of the bulge-dominated region on either side of the galaxy. The blue arrows are drawn from the edge of the bulge-dominated region to the disc scalelength. The symbols are as in Fig. 6. TMB models with solar α/Fe , age = 1, 2, 3, 6 and 15 Gyr, and $[Z/H]$ = -1.35, -0.33, 0, 0.35 and 0.67 are overlaid. Unlike $H\beta$, the higher-order Balmer indices are not independent of α/Fe . α -enhanced models are parallel to the solar models, lying above and to the right-hand side. The green curves show models with age = 1 Gyr and $[Z/H]$ = 0.67 for $[\alpha/Fe]$ = 0.3.

or most of the AGN also have active star formation in the bulge-dominated region.

AGN have previously been found to have a larger fraction of young stars than quiescent galaxies (Raimann et al. 2001, 2003). In agreement with these results, we find that most of the AGN have small SSP ages (< 4 Gyr). The only one with a large SSP age (~ 15 Gyr) is NGC 3831. This could be due to errors from emission correction or from the young component not dominating the total luminosity. Prugniel et al. (2001) found that bulges with emission were small and metal poor. The star-forming region of our BPT diagram is populated by four blue bulges. They have similar SPs as Prugniel et al.'s emission-line galaxies except that one of them (NGC 6246A) has a large SSP age, again possibly due to errors in emission correction.

We see a wide range of behaviours in the emission-line profiles. In some galaxies, such as NGCs 3681 and 5362, there is strong emission in the disc-dominated region but little or no emission in the bulge-dominated region as would be expected if discs continue to form stars while bulges do not. The only galaxies with little or no emission in the disc-dominated region are S0s. In other cases, there is emission throughout the galaxy but it is weaker in the bulge-dominated region (e.g. NGCs 1642, 2916, 5020 and 7537). This is consistent with a quiescent bulge and a star-forming disc coexisting in the central regions with the ratio of bulge to disc dominance

decreasing with radius. Alternatively, the bulge and disc could both be forming stars but the disc does so more actively. Finally, in some cases (e.g. IC 267 and NGCs 266 and 5793), the emission lines are strongest at the centre.

5 THE FORMATION OF BULGES

As mentioned in the Introduction section, present-day Λ CDM cosmology argues against the monolithic collapse scenario as does observational evidence for the recent and continuing mass assembly of ellipticals. Of the main proposed formation scenarios, that leaves mergers and secular evolution as possibilities for bulges.

However, the collapse model continues to receive much attention under the claim that it better reproduces the observed line-strength profiles of ellipticals. We investigate whether or not this is true for bulges. Gradients in the index Mg_2 have been computed in galaxies formed in collapse and merger simulations, allowing for direct comparisons with our data (Fig. 20). The points are our data. The solid lines are two remnants from major disc-disc mergers by Bekki & Shioya (1999) with initial disc masses of $10^{10} M_\odot$ (bottom curve in Mg_2 ; top curve in $H\beta$) and $10^{12} M_\odot$. The remnants are 13.1 Gyr old. The dotted lines are two collapse models by Angeletti & Giannone (2003) with final ages of 13 Gyr (top curve) and 2 Gyr. We focus on the gradient slopes, assuming that changes in mass and

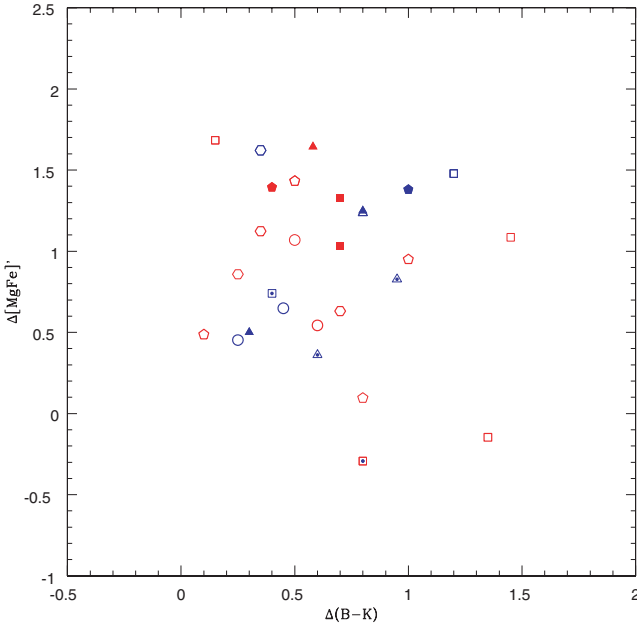


Figure 15. $[\text{Mg}/\text{Fe}]'$ gradient versus $B - K$ colour gradient, where a gradient is defined as the difference between the value at the centre of the galaxy and the value at the disc scalelength. The symbols are as in Fig. 6.

formation epoch mainly shift the models up or down. The collapse models predict steeper Mg_2 profiles than the merger models. Within the bulge-dominated region, some of our profiles agree with one of the merger models (e.g. NGCs 765 and 7311), while others agree with one of the collapse models (e.g. NGC 3728 and the minor-axes of NGCs 5326 and 5422). There are also cases, mostly among blue bulges, where the observed profile is flatter than the merger models (e.g. IC 302). However, the majority of galaxies fall between the collapse and merger models.

Bekki & Shioya also computed $H\beta$ profiles in their models (Fig. 21). Nearly all our galaxies have flat $H\beta$ profiles within the bulge-dominated region as predicted by the models. The profiles of the oldest bulges agree with the models in their zero-points as well, while younger bulges lie above the models.

Through chemical evolution modelling, Thomas et al. (1999) studied α/Fe ratios in ellipticals that formed through a fast (~ 1 Gyr) collapse of star-forming clumps and through mergers of MW-like spirals. The main difference between the two models was that the merging spirals had several Gyr of Fe-enrichment, while the gas involved in the collapse was not pre-enriched in Fe. The large central α/Fe ratios found in massive ellipticals were reproduced in the collapse model. The merger model does not produce supersolar α/Fe assuming a Salpeter initial mass function, unless the merger happened early, before the progenitors acquired much Fe. Metallicity and α/Fe are anticorrelated in the collapse model; since ellipticals have negative gradients in metallicity, the model predicts that they

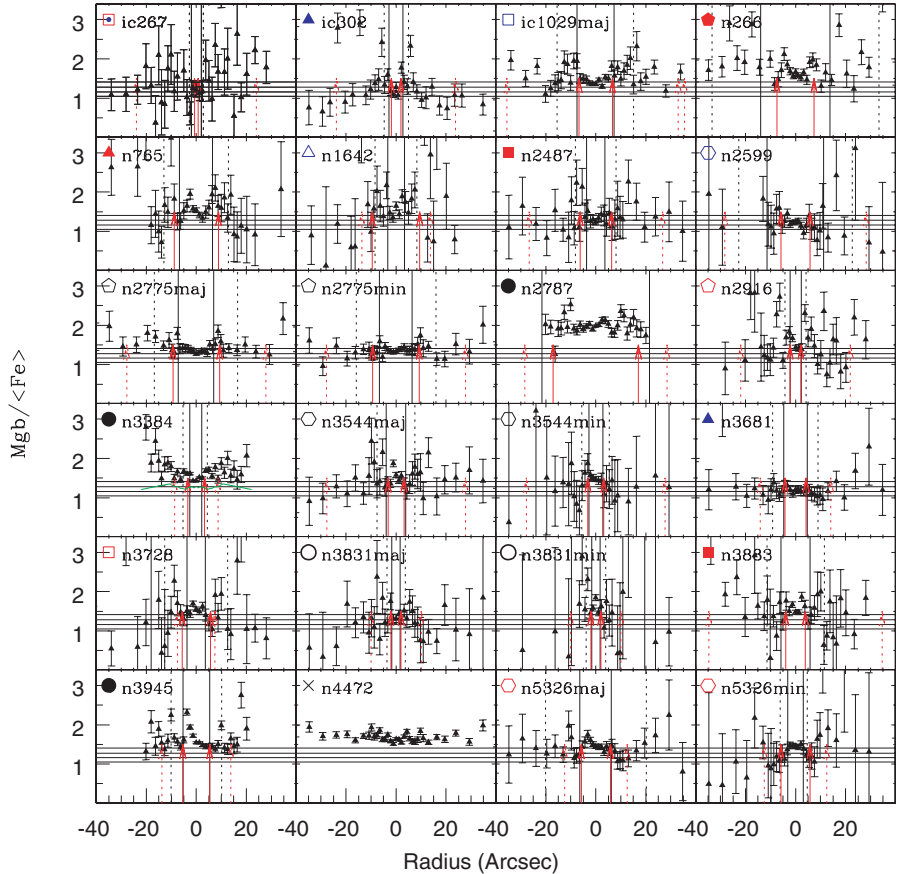


Figure 16. Mgb/Fe profiles in our galaxies. For NGC 3384, the green curve shows the profile obtained by Fisher et al. (1996). The symbols are as in Fig. 6. The horizontal lines are as in Fig. 7.

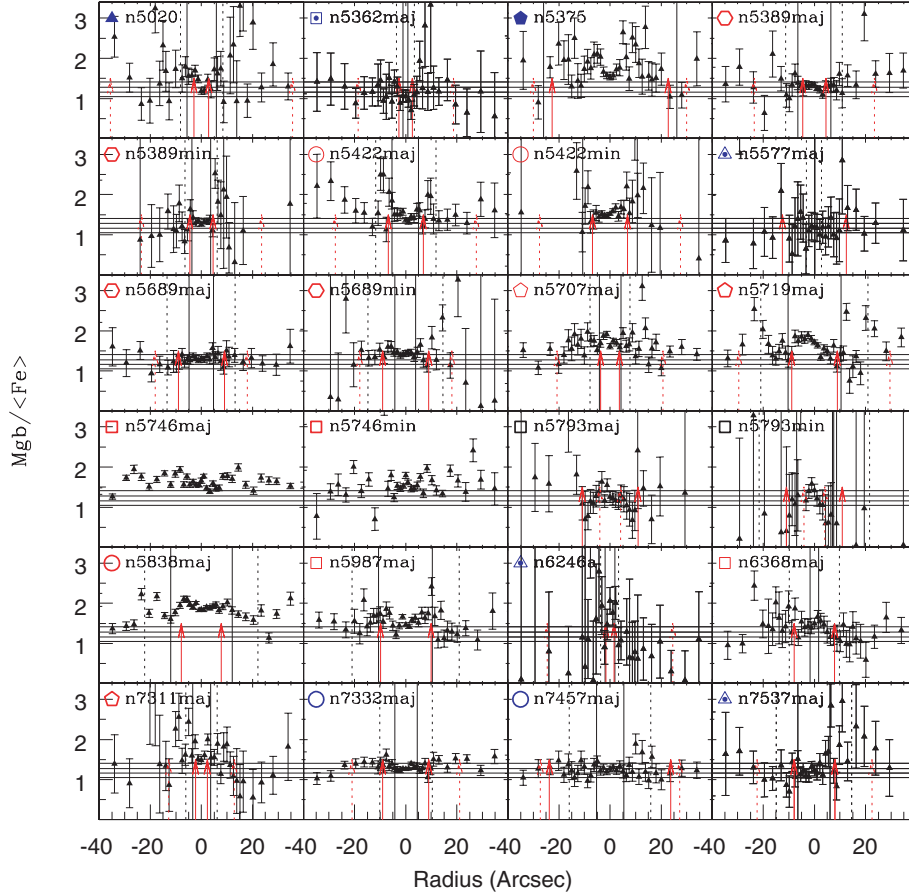


Figure 17. $Mg_b/\langle Fe \rangle$ profiles in our galaxies (continued). The symbols are as in Fig. 6. The horizontal lines are as in Fig. 7.

should have a positive gradient in α/Fe . The merger model produces solar α/Fe in the outer regions. Therefore, uniformly solar α/Fe is consistent with the merger model while positive gradients are consistent with the collapse model. Pipino et al. (2005) also found positive α/Fe gradients in a model where ellipticals are formed through the infall of gaseous lumps. Since our blue bulges have uniformly solar α/Fe , they are consistent with the predictions of the merger model. Several of the red bulges have positive gradients as predicted by the collapse model. Most of the remaining bulges have uniformly supersolar α/Fe , which is difficult to reproduce in any of the models.

In summary, both collapse and merger models have limited success in reproducing the line-strength profiles of individual galaxies but neither explain the full range of behaviours seen in the data. It is important to note that hierarchical models are only beginning to make robust predictions for SPs, successfully reproducing properties traditionally thought to favour the collapse model, such as the mass–metallicity relation. As advancements continue to be made in incorporating gas dynamics, star formation, and chemical evolution in cosmologically motivated merger models, it will be interesting to see if the line-strength profiles will be reproduced as well.

5.1 Mergers

In a recent paper, Faber et al. (2005) argued that massive red ellipticals could not have formed entirely through major mergers of gas-rich components or through dry mergers but through a combination of the two. Ellipticals of the same mass and colour could

have formed in different ways: through early gas-rich mergers of low-mass objects followed by dry mergers or through recent gas-rich mergers of more-massive objects. Objects that arrived on the red sequence early-on and have been gaining mass through dry mergers will have larger SSP ages than those that have arrived on the red sequence near their present mass as the result of recent gas-rich mergers. The former will also have smaller metallicities since their last gas-rich mergers were of lower-mass progenitors with correspondingly lower metallicities according to the gas-phase mass–metallicity relation (Kobulnicky et al. 2003; Tremonti et al. 2004). The predicted anticorrelation between age and metallicity at fixed σ_0 is seen in ellipticals. If such an anticorrelation exists for bulges, it is not nearly as tight as that of ellipticals. This suggests that an additional formation mechanism might be required to explain the SPs of bulges.

Recent semi-analytic models incorporating the Millennium Simulation of cosmic structure growth find a correlation between stellar metallicity and stellar mass, with the most-massive galaxies having roughly solar metallicity (De Lucia et al. 2006). This is qualitatively consistent with the observed $[MgFe] - \sigma_0$ and $[MgFe] - V_{max}$ relations. Massive ellipticals and bulges have supersolar central metallicity which is in apparent contradiction with De Lucia et al.’s results. However, they also have negative metallicity gradients. The arrows in Fig. 12, which extend to approximately the bulge effective radius, fall around solar metallicity in the massive red bulges. The metallicity at the effective radius is more representative, than the central value, of the mean metallicity. Therefore, the data are not inconsistent with the models.

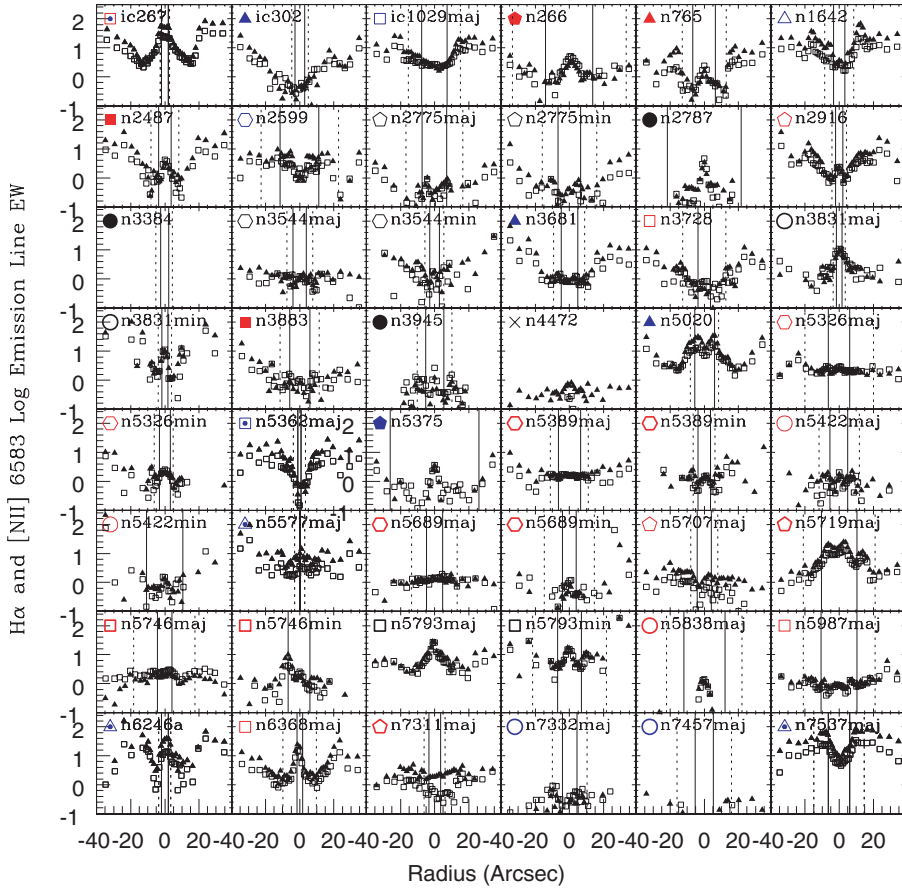


Figure 18. Profiles of emission-line strengths in bulges. The triangles are H α . The squares are [N II] 6583. The symbols are as in Fig. 6.

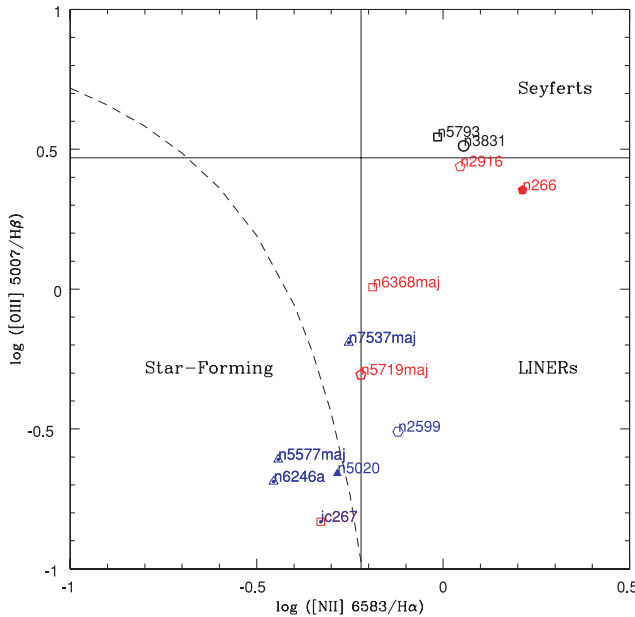


Figure 19. Bulges on the BPT (Baldwin et al. 1981) diagram in which the emission-line flux ratio [O III] 5007/H β is plotted against the ratio [N II] 6583/H α . The symbols are as in Fig. 8. The dashed curve shows the demarcation between starburst galaxies and AGN as defined by Kauffmann et al. (2003). We adopt the commonly used definition of LINERS having [O III] 5007/H β < 3 and [N II] 6583/H α > 0.6 and Seyferts having [O III] 5007/H β > 3 and [N II] 6583/H α > 0.6.

De Lucia et al. also found in their simulations that less-massive ellipticals had more extended star formation histories than their massive counterparts. This is consistent with the observed $\alpha/\text{Fe}-\sigma_0$ and $\alpha/\text{Fe}-V_{\max}$ correlations. These correlations can be produced in starbursts induced by gas-rich mergers. During the starburst, SNe II enrich the ISM with α -elements. If star formation is somehow quenched before SNe Ia contribute much Fe, the α/Fe ratio increases. Subsequent dry mergers might add scatter to the $\alpha/\text{Fe}-V_{\max}$ relations by increasing V_{\max} without altering α/Fe . The effect of dry mergers on the $\alpha/\text{Fe}-\sigma_0$ relation is less certain. Simulations find that dry mergers increase the velocity dispersion but that the increase is more dramatic in the outer regions than at the centre (Colín et al. 2004).

The differences between blue and red bulges at fixed σ_0 can also be explained by mergers. At fixed σ_0 , blue bulges have smaller SSP ages than their red counterparts which suggests that they have undergone gas-rich mergers more recently. The progenitors of the blue bulges have then had more time to acquire Fe. Since the progenitors have small α/Fe ratios, so do the remnants. This is seen in the simulations by Thomas et al. (1999), who found that gas-rich mergers cannot produce large α/Fe ratios, unless they happened early in the chemical evolution of the progenitors.

5.2 Secular evolution

In dissipationless secular evolution, the bulge is formed through the vertical and radial redistributions of disc stars. In this process, existing gradients can either become amplified since the resulting (pseudo)bulge has a smaller scalelength than the progenitor disc or

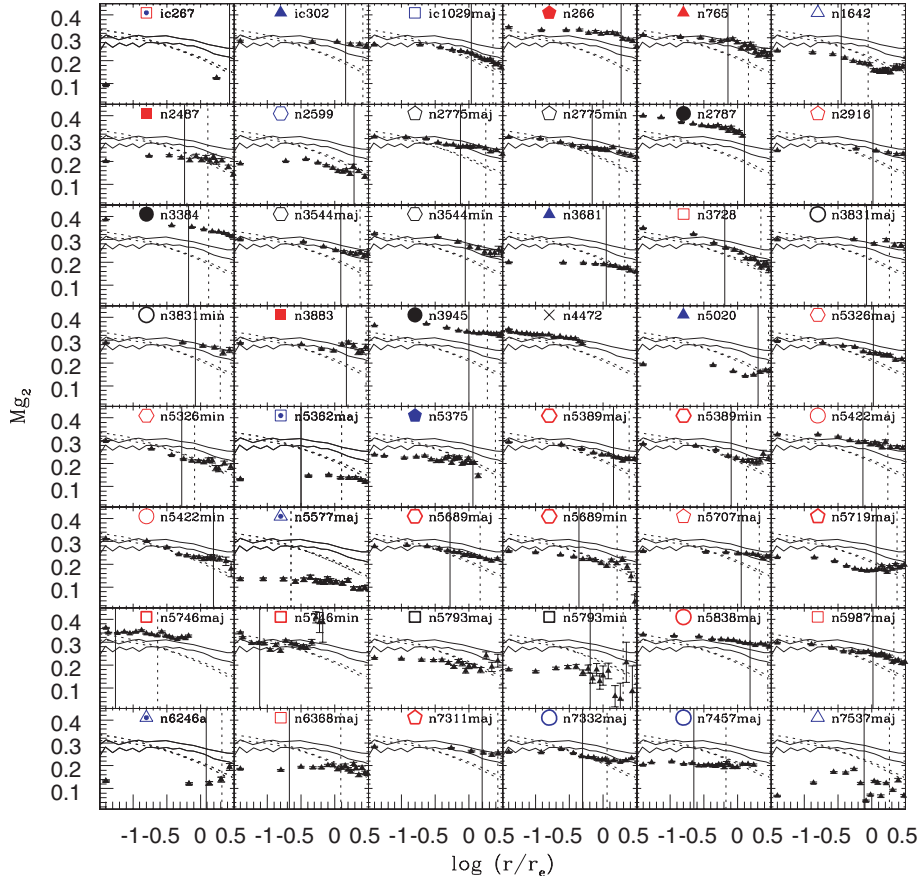


Figure 20. Comparison of Mg_2 profiles between this work and numerical simulations. The solid lines are merger models by Bekki & Shioya (1999) with final age 13.1 Gyr and initial disc masses of $10^{10} M_\odot$ (bottom curve) and $10^{12} M_\odot$. The dotted lines are collapse models by Angeletti & Giannone with final age 13 Gyr (top curve) and 2 Gyr. The symbols are as in Fig. 6.

erased as a consequence of disc heating. However, if the disc has no gradient, then the bulge also should not have one. This process cannot be ruled out based on $[Mg/Fe]$ gradients, since the majority of galaxies show negative gradients in the disc-dominated region. However, the majority of red bulges have solar α/Fe in the disc-dominated region, despite having supersolar α/Fe in the bulge. Therefore, they could not have been produced through purely dissipationless secular evolution. If secular evolution with gas infall has been responsible for the formation of these objects, the star formation time-scales must have been identical (at fixed σ_0) in this scenario as in merger-induced star formation since red bulges and ellipticals follow the same $\alpha/Fe-\sigma_0$ relation. Furthermore, the star formation must have been completed several Gyr ago since red bulges have large SSP ages. This goes for the three barred S0s with disc-like structural and kinematical properties (NGCs 2787, 3384 and 3945) as well. These objects are identical to ellipticals of comparable σ_0 in their SPs and two of them have among the largest central SSP ages observed.

Note that the α/Fe ratios of the blue bulges are consistent with dissipationless secular evolution. Unfortunately, neither mergers nor secular evolution can be ruled out for blue bulges based on their α/Fe ratios.

Secular evolution with gas infall is supported by the frequency of barred galaxies with age gradients. Of the 10 galaxies whose central regions are younger than the outer regions, seven are barred and one has a b/p bulge. Bar-driven gas infall could lead to extended

star formation in the central region, producing the observed age gradient.

If bars are long lived and the chemical imprints of secular evolution are different from those of mergers, we would expect the bulges of barred galaxies to have different abundance patterns than those of unbarred galaxies. We see hints of such differences in index- σ_0 and index- V_{\max} relations. At fixed σ_0 and V_{\max} , barred galaxies appear to have larger central metallicities.

The metallicities of bulges and their discs are correlated. This is naturally explained in processes that involve the bulge being formed from the disc. However, this correlation holds for all galaxies, not just those with bars, blue bulges, or bulges identified as having disc-like structure and kinematics. Therefore, either all bulges formed secularly and some had their bars destroyed or the other bulge/disc formation mechanisms also produce this correlation.

5.3 Evolution of galaxy populations

Small- σ bulges fall into two categories: YMR bulges with little or no star formation and MP bulges which are actively forming stars. This suggests that the MP bulges would have migrated to the YMR region by the time their star formation is quenched. Will this be the scenario for all metal-poor bulges (including that of the MW) or is the observed anticorrelation between emission strength and metallicity the result of small number statistics? Are there really no metal-poor bulges that do not have emission? Extending this type

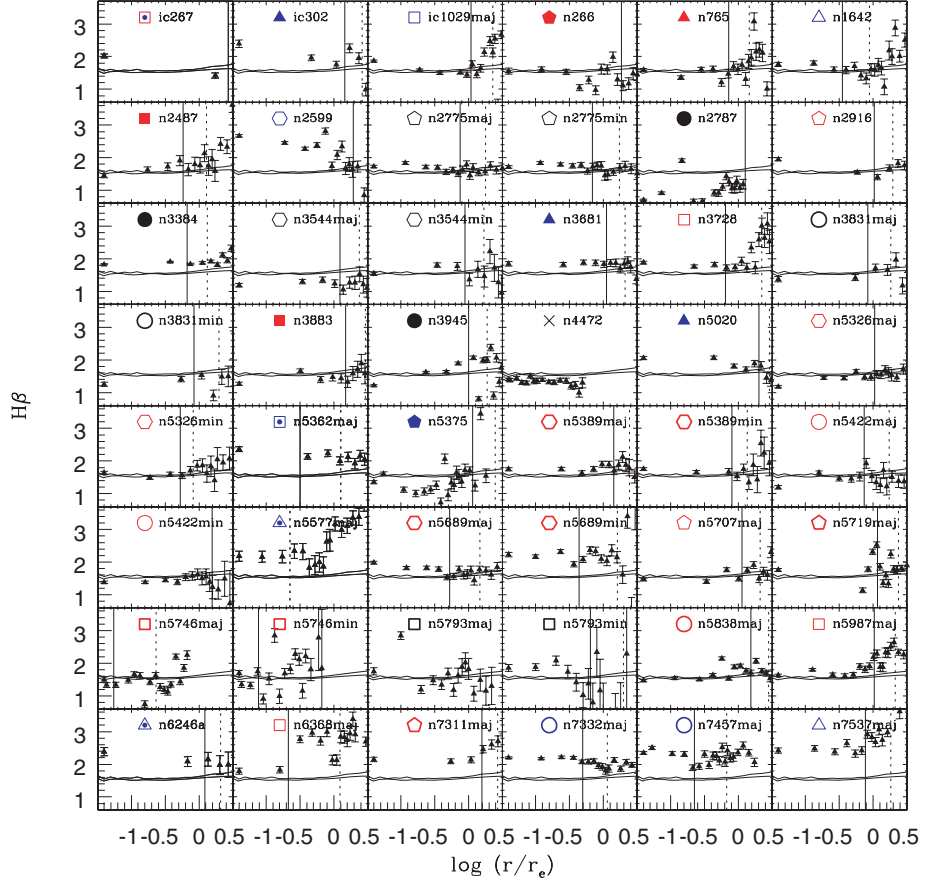


Figure 21. Comparison of $H\beta$ profiles between this work and merger models by Bekki & Shioya (1999) with initial disc masses of $10^{10} M_\odot$ (bottom curve) and $10^{12} M_\odot$. The symbols are as in Fig. 6.

of study to large galaxy samples should shed light into the evolution of small- σ bulges.

While all five of the MP galaxies are late types (Sb–Sc), three of the seven YMR galaxies are early types (S0–Sa). Perhaps, the mechanisms that trigger and quench the star formation are also responsible for transforming galaxies from late to early types. As the YMR bulges age, they will move down to the OMR region.

6 SUMMARY

We have studied line strengths in the bulges and inner discs of 38 galaxies in the local Universe. Our galaxies span a wide range of Hubble types, central velocity dispersions, maximum disc rotational velocities, and inclinations. The low-inclination galaxies include barred and unbarred objects; the edge-on galaxies include those with and without b/p bulges. We included several galaxies whose bulges were previously identified as being disc like in their colours or kinematics to see if their spectral properties reveal evidence for secular evolution. We use the $[MgFe]$ index and five Balmer indices to characterize the luminosity-weighted metallicities and ages of the SPs and the $Mgb/(Fe)$ index to characterize the α/Fe ratios. Our main results are the following.

- (i) The central regions of bulges range in SSP metallicity from $[Z/H] = -0.8$ to $+0.7$ dex and in SSP age from less than 2 to greater than 15 Gyr.
- (ii) The central ages and metallicities are sensitive to bulge colour which is in turn sensitive to central velocity dispersion and maximum disc rotational velocity.

(iii) Red bulges of all Hubble types are similar to luminous ellipticals in their central SPs. They have large SSP ages and are supersolar in SSP metallicity and α/Fe .

(iv) Blue bulges can be separated into two classes: a metal-poor class that is restricted to late types with small velocity dispersion and a young, metal-rich class that includes all Hubble types and velocity dispersions. The metal-poor blue bulges are actively forming stars, while the metal-rich ones are not. Low-luminosity ellipticals exhibit a similar range of SSP ages and metallicities as blue bulges.

(v) Luminous ellipticals and the different types of bulges form a continuous and overlapping sequence on diagrams of metallicity- and age-sensitive indices versus σ_0 . At fixed σ_0 , there is no systematic difference between bulges and ellipticals on these diagrams but bulges exhibit larger scatter. At fixed σ_0 , age and metallicity are more tightly anticorrelated in ellipticals than in bulges.

(vi) α/Fe in red bulges is correlated with σ_0 and V_{max} . Red bulges and ellipticals follow the same $\alpha/Fe-\sigma_0$ relation.

(vii) Most blue bulges (11 out of 14) are consistent with having solar α/Fe . At fixed σ_0 , blue bulges have smaller α/Fe than red bulges and ellipticals.

(viii) Barred galaxies appear to have larger central metallicities than unbarred galaxies of the same σ_0 and V_{max} .

(ix) Most galaxies show a steady decrease in metallicity-sensitive indices with radius. The slope of the gradient is correlated with the central value and therefore with the global kinematics. The bulge- and disc-dominated regions are distinct in their line-strength profiles, with the discs generally having shallower slopes. The smallest bulges do not have negative line-strength gradients; some of these

have flat profiles in the central region while others have positive gradients.

(x) There is a correlation between [MgFe]⁺ strength in the bulge and the disc. This correlation holds for all galaxies, not just those with bars, blue bulges, or bulges identified as having disc-like structural or kinematical properties.

(xi) Where positive age gradients (with the central regions being younger) are present, they are invariably in barred galaxies. This suggests that bar-driven star formation has occurred. However, several red bulges in barred galaxies have large central SSP ages (although it could be younger than those in the outer regions) which means there has been no significant bar-driven star formation for several Gyr.

(xii) Four galaxies have supersolar α/Fe in the disc-dominated region. The rest are consistent with having solar α/Fe in the disc.

(xiii) Objects identified as having disc-like structural or kinematical properties do not have notably different SPs than other bulges. They follow the same scaling relations as the red bulges and ellipticals and have metallicity gradients. The three barred S0s identified as having bulges with disc-like structural and kinematical properties are also α -enhanced and therefore do not resemble the majority of the discs, including the MW disc at the solar neighbourhood.

(xiv) Colour profiles agree frequently but not always with line-strength profiles. Where discrepancies exist, they are likely due to differences in age- and metallicity-sensitivity between colours and line strengths and to the colours being affected by dust. Consequently, colour gradients do not necessarily correlate with [MgFe]⁺ gradients.

Overall, our results are consistent with the hypothesis that mergers have been the dominant mechanism responsible for the formation of bulges. However, some of the observations, such as the correlation between bulge and disc metallicity, pose significant challenges to the merger scenario. Furthermore, the possibility that barred galaxies follow different scaling relations than unbarred galaxies and are overrepresented among galaxies with age gradients supports the secular evolution picture.

Central line strengths on a statistically significant sample of ellipticals and bulges of barred and unbarred spirals would be invaluable in determining whether more than one formation mechanism is required for bulges. The necessary data are already available in the data bases of large surveys such as the Sloan Digital Sky Survey (SDSS). Spatially resolved studies on a smaller, representative sample, would allow for better comparisons between gradients in different types of galaxies.

ACKNOWLEDGMENTS

It is a pleasure to thank Anatoly Klypin, Jason Peterson, Jesús Falcón-Barroso, Mike Hudson, Jenica Nelan, Reynier Peletier, Claudia Maraston, Daniel Thomas, Scott Trager, and Guy Worthey for helpful discussions or assistance with the data analysis. We would also like to thank the anonymous referee for suggestions that greatly improved this manuscript. Partial funding was provided by the New Mexico Space Grant Consortium. This research has made use of the NASA/IPAC Extragalactic Data base (NED) which is operated by the Jet Propulsion Laboratory, California Institute of Technology, under contract with the National Aeronautics and Space Administration.

REFERENCES

- Abadi M. G., Navarro J. F., Steinmetz M., Eke V. R., 2003, ApJ, 597, 21
- Andredakis Y. C., Sanders R. H., 1994, MNRAS, 267, 283
- Angeletti L., Giannone P., 2003, A&A, 403, 449
- Arimoto N., Yoshii Y., 1987, A&A, 173, 23
- Aronica G., Athanassoula E., Bureau M., Bosma A., Dettmar R.-J., Vergani D., Pohlen M., 2003, AP&SS, 284, 753
- Athanassoula E., 2005, MNRAS, 358, 1477
- Athanassoula E., Misiriotis A., 2002, MNRAS, 330, 35
- Balcells M., Peletier R. F., 1994, AJ, 107, 135
- Balcells M., Graham A. W., Domínguez-Palmero L., Peletier R. F., 2003, ApJ, 582, L79
- Baldwin J. A., Phillips M. M., Terlevich R., 1981, PASP, 93, 5 (BPT)
- Bekki K., Shioya Y., 1999, ApJ, 513, 108
- Bell E. F. et al., 2004, ApJ, 608, 752
- Bender R., Burstein D., Faber S. M., 1993, ApJ, 411, 153
- Bertola F., Capaccioli M., 1977, ApJ, 211, 697
- Bournaud F., Combes F., Semelin B., 2005, MNRAS, pp L89+
- Bruzual G., Charlot S., 2003, MNRAS, 344, 1000 (BC03)
- Bureau M., Freeman K. C., 1999, AJ, 118, 126
- Burstein D., Faber S. M., Gaskell C. M., Krumm N., 1984, ApJ, 287, 586
- Busarello G., Capaccioli M., D'Onofrio M., Longo G., Richter G., Zaggia S., 1996, A&A, 314, 32
- Caldwell N., Rose J. A., Concannon K. D., 2003, AJ, 125, 2891
- Cappellari M., Emsellem E., 2004, PASP, 116, 138
- Carlberg R. G., 1984, ApJ, 286, 403
- Carollo C. M., Danziger I. J., Buson L., 1993, MNRAS, 265, 553
- Carollo C. M., Stiavelli M., de Zeeuw P. T., Mack J., 1997, AJ, 114, 2366
- Chung A., Bureau M., 2004, AJ, 127, 3192
- Colín P., Klypin A., Valenzuela O., Gottlöber S., 2004, ApJ, 612, 50
- Combes F., Debbasch F., Friedli D., Pfenniger D., 1990, A&A, 233, 82
- Courteau S., de Jong R. S., Broeils A. H., 1996, ApJ, 457, L73
- Davidge T. J., 2001, AJ, 122, 1386
- de Jong R. S., 1996a, A&AS, 118, 557
- de Jong R. S., 1996b, A&A, 313, 377 (DJ)
- de Jong R. S., Simard L., Davies R. L., Saglia R. P., Burstein D., Colless M., McMahan R., Wegner G., 2004, MNRAS, 355, 1155
- De Lucia G., Springel V., White S. D. M., Croton D., Kauffmann G., 2006, MNRAS, 366, 499
- de Vaucouleurs G., de Vaucouleurs A., Corwin H. G., Buta R. J., Paturel G., Fouque P., 1991, Third Reference Catalogue of Bright Galaxies, Vols 1–3. Springer-Verlag, Berlin, Heidelberg, New York, p. 7
- de Zeeuw P. T. et al., 2002, MNRAS, 329, 513
- Debattista V. P., Carollo C. M., Mayer L., Moore B., 2004, ApJ, 604, L93
- Denicoló G., Terlevich R., Terlevich E., Forbes D. A., Terlevich A., 2005, MNRAS, 358, 813
- Emsellem E. et al., 2004, MNRAS, 352, 721
- Erwin P., Beltrán J. C. V., Graham A. W., Beckman J. E., 2003, ApJ, 597, 929
- Faber S. M., Friel E. D., Burstein D., Gaskell C. M., 1985, ApJS, 57, 711
- Faber S. M. et al., 2005, ApJ, submitted (astro-ph/0506044)
- Fairall A. P. et al., 1992, AJ, 103, 11
- Falcón-Barroso J., Peletier R. F., Balcells M., 2002, MNRAS, 335, 741
- Falcón-Barroso J. et al., 2004, MNRAS, 350, 35
- Feltzing S., Gilmore G., 2000, A&A, 355, 949
- Ferreiro D. L., Pastoriza M. G., 2004, A&A, 428, 837
- Fisher D., Franx M., Illingworth G., 1996, ApJ, 459, 110
- Forbes D. A., Sánchez-Blázquez P., Proctor R., 2005, MNRAS, 361, L47
- Friedli D., Benz W., 1995, A&A, 301, 649
- Friedli D., Benz W., Kennicutt R., 1994, ApJ, 430, L105
- Fulbright J. P., McWilliam A., Rich R. M., 2006, ApJ, 636, 821
- Gadotti D. A., dos Anjos S., 2001, AJ, 122, 1298
- Goudfrooij P., Gorgas J., Jablonka P., 1999, AP&SS, 269, 109
- Ibata R. A., Gilmore G. F., 1995, MNRAS, 275, 605
- Idiart T. P., de Freitas Pacheco J. A., Costa R. D. D., 1996, AJ, 112, 2541
- Immeli A., Samland M., Gerhard O., Westera P., 2004, A&A, 413, 547

- Jablonka P., Martin P., Arimoto N., 1996, AJ, 112, 1415
- Jablonka P., Courbin F., Meylan G., Sarajedini A., Bridges T. J., Magain P., 2000, A&A, 359, 131
- Jablonka P., Gorgas J., Goudfrooij P., 2002, AP&SS, 281, 367
- Kannappan S. J., Jansen R. A., Barton E. J., 2004, AJ, 127, 1371
- Karachentsev I. D., Makarov D. A., 1996, AJ, 111, 794
- Kauffmann G., 1996, MNRAS, 281, 487
- Kauffmann G., White S. D. M., Guiderdoni B., 1993, MNRAS, 264, 201
- Kauffmann G. et al., 2003, MNRAS, 346, 1055
- Kobayashi C., Arimoto N., 1999, ApJ, 527, 573
- Kobulnicky H. A. et al., 2003, ApJ, 599, 1006
- Kormendy J., 1993, in Dejonghe H., Habing H. J., eds, IAU Symp. 153, Galactic Bulges. Kluwer, Dordrecht, p. 209
- Kormendy J., Illingworth G., 1982, ApJ, 256, 460
- Kormendy J., Kennicutt R. C., 2004, ARA&A, 42, 603
- Kuntschner H. et al., 2006, MNRAS, 369, 497
- Lütticke R., Dettmar R.-J., Pohlen M., 2000, A&AS, 145, 405
- Larson R. B., 1974, MNRAS, 166, 585
- Lee H.-c., Worthey G., 2005, ApJS, 160, 176
- MacArthur L. A., 2005, ApJ, 623, 795
- MacArthur L. A., Courteau S., Holtzman J. A., 2003, ApJ, 582, 689
- Massey P., Strobel K., Barnes J. V., Anderson E., 1988, ApJ, 328, 315
- Mehlert D., Thomas D., Saglia R. P., Bender R., Wegner G., 2003, A&A, 407, 423
- Michard R., Marchal J., 1994, A&AS, 107, 187
- Minniti D., 1996, ApJ, 459, 175
- Nelan J. E., Smith R. J., Hudson M. J., Wegner G. A., Lucey J. R., Moore S. A. W., Quinney S. J., Suntzeff N. B., 2005, ApJ, 632, 137
- Nilson P., 1973, Uppsala general catalogue of galaxies. Acta Universitatis Upsaliensis. Nova Acta Regiae Societatis Scientiarum, Series V
- Noguchi M., 2000, MNRAS, 312, 194
- Norman C. A., Sellwood J. A., Hasan H., 1996, ApJ, 462, 114
- Peletier R. F., Balcells M., 1997, New Astron., 1, 349 (PB)
- Peletier R. F., Vazdekis A., Arribas S., del Burgo C., García-Lorenzo B., Gutiérrez C., Mediavilla E., Prada F., 1999, MNRAS, 310, 863
- Pfenniger D., 1993, in Dejonghe H., Habing H. J., eds, IAU Symp. 153, Galactic Bulges. Kluwer, Dordrecht, p. 387
- Pipino A., Kawata D., Gibson B. K., Matteucci F., 2005, A&A, 434, 553
- Pinkney J. et al., 2003, ApJ, 596, 903
- Proctor R. N., Sansom A. E., 2002, MNRAS, 333, 517
- Proctor R. N., Sansom A. E., Reid I. N., 2000, MNRAS, 311, 37
- Prugniel P., Maubon G., Simien F., 2001, A&A, 366, 68
- Puzia T. H., Saglia R. P., Kissler-Patig M., Maraston C., Greggio L., Renzini A., Ortolani S., 2002, A&A, 395, 45
- Puzia T. H., Perrett K. M., Bridges T. J., 2005, A&A, 434, 909
- Raimann D., Storchi-Bergmann T., Bica E., Alloin D., 2001, MNRAS, 324, 1087
- Raimann D., Storchi-Bergmann T., González Delgado R. M., Cid Fernandes R., Heckman T., Leitherer C., Schmitt H., 2003, MNRAS, 339, 772
- Rich R. M., 1999, in Hubeny I., Heap S., Cornett R., eds, ASP Conf. Ser., Vol. 192, Spectrophotometric Dating of Stars and Galaxies. Astron. Soc. Pac., San Francisco, p. 215
- Rose J. A., Bower R. G., Caldwell N., Ellis R. S., Sharples R. M., Teague P., 1994, AJ, 108, 2054
- Ryder S. D., Fenner Y., Gibson B. K., 2005, MNRAS, 358, 1337
- Sadler E. M., Rich R. M., Terndrup D. M., 1996, AJ, 112, 171
- Sarajedini A., Jablonka P., 2005, AJ, 130, 1627
- Sellwood J. A., 1993, in Dejonghe H., Habing H. J., eds, IAU Symp. 153, Galactic Bulges. Kluwer, Dordrecht, p. 391
- Shen J., Sellwood J. A., 2004, ApJ, 604, 614
- Sil'chenko O. K., 1999, AJ, 117, 2725
- Sil'chenko O. K., Afanasiev V. L., Chavushyan V. H., Valdes J. R., 2002, ApJ, 577, 668
- Sil'chenko O. K., Moiseev A. V., Afanasiev V. L., Chavushyan V. H., Valdes J. R., 2003, ApJ, 591, 185
- Stephens A. W. et al., 2003, AJ, 125, 2473
- Tanvir N. R., Ferguson H. C., Shanks T., 1999, MNRAS, 310, 175
- Thomas D., 1999, MNRAS, 306, 655
- Thomas D., Maraston C., Bender R., 2003, MNRAS, 339, 897 (TMB)
- Thomas D., Maraston C., Korn A., 2004, MNRAS, 351, L19
- Thomas D., Maraston C., Bender R., de Oliveira C. M., 2005, ApJ, 621, 673
- Trager S. C., Worthey G., Faber S. M., Burstein D., Gonzalez J. J., 1998, ApJS, 116, 1
- Trager S. C., Faber S. M., Worthey G., González J. J., 2000a, AJ, 119, 1645
- Trager S. C., Faber S. M., Worthey G., González J. J., 2000b, AJ, 120, 165
- Tremonti C. A. et al., 2004, ApJ, 613, 898
- Trippico M. J., Bell R. A., 1995, AJ, 110, 3035
- van Dokkum P. G., 2005, AJ, 130, 2647
- van Dokkum P. G., Franx M., Fabricant D., Kelson D. D., Illingworth G. D., 1999, ApJ, 520, L95
- van Loon J. T. et al., 2003, MNRAS, 338, 857
- Vazdekis A., 1999, ApJ, 513, 224
- Vazdekis A., Peletier R. F., Beckman J. E., Casuso E., 1997, ApJS, 111, 203
- Vazdekis A., Kuntschner H., Davies R. L., Arimoto N., Nakamura O., Peletier R., 2001, ApJ, 551, L127
- Wegner G., da Costa L. N., Alonso M. V., Bernardi M., Wilmer C. N. A., Pellegrini P. S., Rité C., Maia M., 2000, in Courteau S., Willick J., eds, ASP Conf. Ser., Vol. 201, Cosmic Flows Workshop. Astron. Soc. Pac., San Francisco, p. 62
- White S. D. M., 1980, MNRAS, 191, 1p
- Worthey G., 1994, ApJS, 95, 107
- Worthey G., Ottaviani D. L., 1997, ApJS, 111, 377
- Worthey G., Collobert M., 2003, ApJ, 586, 17
- Worthey G., Faber S. M., Gonzalez J. J., Burstein D., 1994, ApJS, 94, 687
- Wyse R. F. G., Gilmore G., Franx M., 1997, ARA&A, 35, 637
- Zoccali M. et al., 2003, A&A, 399, 931

This paper has been typeset from a $\text{\TeX}/\text{\LaTeX}$ file prepared by the author.

Structural properties of pseudo-bulges, classical bulges and elliptical galaxies: a Sloan Digital Sky Survey perspective

Dimitri A. Gadotti[★]

Max-Planck-Institut für Astrophysik, Karl-Schwarzschild-Str. 1, D-85748 Garching bei München, Germany

Accepted 2008 November 14. Received 2008 November 13; in original form 2008 October 9

ABSTRACT

We have performed 2D bulge/bar/disc decompositions using g , r and i -band images of a representative sample of nearly 1000 galaxies from the Sloan Digital Sky Survey. We show that the Petrosian concentration index is a better proxy for the bulge-to-total ratio than the global Sérsic index. We show that pseudo-bulges can be distinguished from classical bulges as outliers in the Kormendy relation. We provide the structural parameters and distributions of stellar masses of ellipticals, classical bulges, pseudo-bulges, discs and bars, and find that 32 per cent of the total stellar mass in massive galaxies in the local universe is contained in ellipticals, 36 per cent in discs, 25 per cent in classical bulges, 3 per cent in pseudo-bulges and 4 per cent in bars. Pseudo-bulges are currently undergoing intense star formation activity and populate the blue cloud of the colour–magnitude diagram. Most (though not all) classical bulges are quiescent and populate the red sequence of the diagram. Classical bulges follow a correlation between the bulge Sérsic index and bulge-to-total ratio, while pseudo-bulges do not. In addition, for a fixed bulge-to-total ratio, pseudo-bulges are less concentrated than classical bulges. Pseudo-bulges follow a mass–size relation similar to that followed by bars, and different from that followed by classical bulges. In the fundamental plane, pseudo-bulges occupy the same locus as discs. While these results point out different formation processes for classical and pseudo-bulges, we also find a significant overlap in their properties, indicating that the different processes might happen concomitantly. Finally, classical bulges and ellipticals follow offset mass–size relations, suggesting that high-mass bulges might not be simply high-mass ellipticals surrounded by discs.

Key words: galaxies: bulges – galaxies: evolution – galaxies: formation – galaxies: fundamental parameters – galaxies: photometry – galaxies: structure.

1 INTRODUCTION

The central components of disc galaxies have proven deceptively simple. The early view of galaxy bulges as scaled ellipticals is far from complete. Even the mere definition of a galaxy bulge is still prone to debate. Yet bulges hold crucial clues to galaxy formation and evolution. Current views discern between bulges formed through violent processes, such as hierarchical clustering via minor mergers, named classical bulges, and those formed through longer time-scales, via disc instabilities and secular evolution processes, named pseudo-bulges (see Wyse, Gilmore & Franx 1997; Kormendy & Kennicutt 2004, for reviews). Given their dissimilar origins, it is naturally expected that these different bulge categories should be structurally distinct.

In fact, previous work have showed evidence that pseudo-bulges, when compared to classical bulges, tend to show younger stellar

populations, kinematics supported by rotation and less-concentrated surface brightness profiles, similar to those of discs, which can be parametrized by the corresponding Sérsic indices (see e.g. Carollo et al. 1997; Gadotti & dos Anjos 2001; Kormendy et al. 2006; Drory & Fisher 2007; Fisher & Drory 2008, and references therein). In relatively inclined galaxies, pseudo-bulges are seen to be more flattened than classical bulges, and as flattened as discs. Some pseudo-bulges display a characteristic box/peanut shape if the galaxy is viewed edge-on. Such box/peanut bulges are believed to be the inner parts of bars that have evolved and buckled off the plane of the disc (see e.g. Athanassoula 2005, and references therein). Such evidence is, however, limited. Since such studies brought along new perceptions, proofs of concept, and because pseudo-bulges are less conspicuous than classical bulges, they had to focus on a detailed analysis of small samples, often with high-resolution data. For instance, pseudo-bulges often host nuclear bars and/or nuclear spiral arms, which are difficult to identify without images of high physical spatial resolution, or a careful analysis.

[★]E-mail: dgadotti@mpa-garching.mpg.de

Ellipticals would be formed through major mergers. The gas content in galaxies, as a dissipative component and the material to form new stars, is likely to play an important role in minor/major mergers and secular evolution, and adds considerable complexity to these views. A more complete picture of galaxy formation and evolution demands a deep understanding of the consequences of such diverse processes, as well as the structural properties of the different galaxy components. It is still necessary to understand better how these different formation processes result in evolutionary and structural differences, how these differences translate into observables and how this framework can be incorporated by theoretical developments. Questions such as how structurally different ellipticals, classical bulges and pseudo-bulges are, how different the host galaxies of classical and pseudo-bulges are, how often disc galaxies host pseudo-bulges as compared to classical bulges, how are their masses distributed, and in which conditions pseudo-bulges are important, remain to be properly answered. Time is ripe for more extensive studies on the properties of bulges and ellipticals, taking advantage of large data sets, such as the Sloan Digital Sky Survey (SDSS), which are becoming more commonly available.

We have performed a detailed structural analysis of a sample of nearly 1000 galaxies from the SDSS. Through such a work, we were able to determine Sérsic indices, scalelengths and effective surface brightness for elliptical galaxies, classical bulges and pseudo-bulges, and scalelengths and central surface brightness for discs, taking into account the presence of a bar when necessary, as well as the bulge-to-total and disc-to-total luminosity ratios, in three different bandpasses (g , r and i). We have also determined colours and stellar masses for each galaxy component separately. Such structural parameters are explored throughout this paper, combined with several other physical properties obtained for the SDSS sample of galaxies. (A similar set of parameters was also obtained for bars, which are investigated in a separate paper.)

Allen et al. (2006) and Benson et al. (2007) have recently performed a detailed structural analysis using large data sets. While their samples are substantially larger than ours, our methodology aims at a more careful analysis. For instance, we have included a bar component in the models fitted, since, as shown in Gadotti (2008), if the bar is not taken into account in the modelling of barred galaxies, bulge properties can be significantly affected. We have produced fits in multiple bands for every galaxy, which have allowed us to estimate the colours of the different components. With such colours, we were able to directly estimate mass-to-light ratios for the different components, which result in more accurate stellar mass estimates. Finally, we have selected a sample of galaxies suitable for such image decompositions, and each fit was performed and checked individually. All this care assures us that the results from our analysis are trustworthy to carry the investigations we aimed for.

A common practice in studies on bulges is to define pseudo-bulges as those with a Sérsic index lower than a given threshold. However, the use of Sérsic indices to distinguish pseudo-bulges from classical bulges is likely to generate considerable ambiguity, as the dynamical range of this parameter is small, compared to the uncertainty in individual measurements (see discussion in Durbala et al. 2008; Gadotti 2008). Instead, we have used the Kormendy relation (Kormendy 1977) to identify pseudo-bulges. Some degree of structural similarity between classical bulges and ellipticals is borne out by such relation, which is followed by both kinds of systems. In contrast, pseudo-bulges, being structurally different, do not follow a similar relation. Therefore, our identification of pseudo-bulges is not only more reliable but also better physically motivated. It is also important to point out that, due to the fact

that our models include a bar component, the pseudo-bulges we identify in this study are not those pseudo-bulges associated with the box/peanut morphology.

This paper is organized as follows. The next section describes the sample selection and properties. Section 3 describes the methodology implemented to produce the fits. Results are presented in Section 4, separated in several subsections. We discuss various aspects of our main findings in Section 5, including a comparison with previous work. Finally, we summarize our work and major conclusions in Section 6. Throughout this work, we have used the following cosmological parameters: $H_0 = 75 \text{ km s}^{-1} \text{ Mpc}^{-1}$, $\Omega_M = 0.3$ and $\Omega_\Lambda = 0.7$. Unless noted, photometric measurements refer to the i band. All logarithms are base 10.

2 SAMPLE SELECTION AND PROPERTIES

We aimed for a sample which is concomitantly suitable for structural analysis based on an image decomposition and a fair representation of the galaxy population in the local universe. We thus drew the sample from all objects spectroscopically classified as galaxies in the SDSS Data Release 2 (DR2), applying the following criteria. We first selected all galaxies with redshift in the range $0.02 \leq z \leq 0.07$. This provides a sample with a statistically meaningful number of galaxies, whose images have a relatively comparable physical spatial resolution. Images of closer galaxies have a level of detail much richer than those of galaxies at $z \approx 0.05$, as observed within SDSS. On the other hand, images of farther galaxies have a physical spatial resolution which is often not adequate to study their structural properties in some detail.

Secondly, since dwarf galaxies are not an object of our study, we excluded all galaxies with stellar masses below $10^{10} M_\odot$. Galaxy stellar masses were obtained from Kauffmann et al. (2003b). At this stage, we have a volume-limited sample, i.e. a sample which includes all galaxies more massive than $10^{10} M_\odot$ in the volume defined by our redshift cuts and the DR2 footprint. From now on, we will refer to this sample as our parent sample.

Finally, we chose objects with an axial ratio $b/a \geq 0.9$, where a and b are, respectively, the semimajor and semiminor axes of the galaxy, taken from the SDSS data base (these are measured at the 25 mag arcsec $^{-2}$ isophote in the g band.). This criterion assures us that our galaxies are very close to face-on, meaning that effects from dust attenuation, as well as projection effects, are minimized, and that bars can be distinctly seen, avoiding erroneous fits, and leading to a more reliable determination of the structural parameters and colours of the separate galaxy components. It also implies that we do not need to worry about inclination corrections. These criteria resulted in a sample of 3375 objects. The images of each of these galaxies were individually inspected to remove from the sample those galaxies which are either not truly face-on,¹ substantially disturbed by a companion or a merger, overly faint or irregular, have images too close to the border of the CCD frame, as well as duplicate entries and those images where the presence of a bright star renders them unfit. We also rejected galaxies with $a < 4$ arcsec, as we deemed these galaxies too small for a detailed parametric image decomposition. This ensured that, for the vast majority of the sample, the effective radius of the bulge is larger than the point spread function (PSF) half width at half-maximum (HWHM). Hence, reliable conclusions can be drawn even for small bulges (see discussion

¹ Axial ratios from SDSS measurements are not always correct. Galaxies with b/a clearly below 0.9 were removed from the sample.

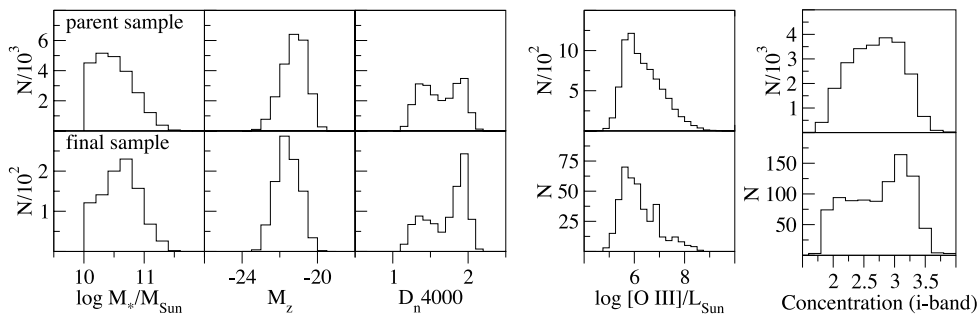


Figure 1. Distributions of galaxy properties for the parent sample (top panels) and the final sample (bottom panels). From left- to right-hand panel: dust-corrected stellar mass, k -corrected z -band absolute magnitude, D_n4000 (corrected for [Ne III] contamination), extinction-corrected [O III] 5007 Å luminosity for AGN and the Petrosian concentration index. The first three parameters were taken from Kauffmann et al. (2003b), [O III] luminosities from Kauffmann et al. (2003a) and concentration from the SDSS data base. The [O III] luminosity has been used in previous work as an indicator of the accretion rate on to the central black hole (Heckman et al. 2004).

further below). Our final sample contains 963 galaxies, of which 407 contain active galactic nuclei (AGN – mostly type 2). The AGN classification is taken from Kauffmann et al. (2003a).

Most of the galaxies in the final sample have $0.04 < z < 0.06$. At this distance, 1 arcsec corresponds roughly to 1 kpc. Since the SDSS spectra are taken through a circular aperture of 3 arcsec in diameter, this means that, for the majority of our galaxies, the spectra obtained represent the central, bulge-dominated part of the galaxy, with a little disc contamination. This will become clearer further below, where the effective radius of bulges is presented. Since the mean PSF full width at half-maximum (FWHM) in SDSS images is ≈ 1.5 arcsec, the typical physical spatial resolution in the images of our final sample is about 1.5 kpc. Most of these galaxies also have $0.9 \leq b/a < 0.95$. In many cases, this means that bulge and disc have slightly different geometrical properties, such as ellipticity ϵ (i.e. $1 - b/a$) and position angle. These differences are helpful when fitting models to the images, since they provide further constraints to the models of the different galaxy components. Finally, their typical stellar mass is similar to that of the Milky Way (i.e. $\approx 5 \times 10^{10} M_\odot$ – Sommer-Larsen & Dolgov 2001).

Let us now check whether our final sample is a fair representation of the galaxy population in the parent, volume-limited sample, and whether our selection criteria to reach the final sample introduce any bias that have to be accounted for. With this aim, we plot in Fig. 1 the distributions of several relevant properties of the galaxies in both samples. One sees that these distributions are reasonably similar, in particular those of the AGN [O III] luminosity. However, it is also apparent that the final sample includes a somewhat larger fraction of massive, brighter, quiescent and more concentrated galaxies. The more stringent criterion to reach the final sample from our parent sample is the axial ratio cut. Thus, we now investigate whether this criterion is the cause of such differences. The top panel of Fig. 2 shows the distributions of the axial ratio for galaxies in the parent sample, separated according to their concentration C . From our structural analysis below, we find that most ellipticals, and few disc galaxies, have $C > 3$. Conversely, most disc-dominated galaxies, and few ellipticals, have $C < 2.5$. We thus use these thresholds to separate ellipticals and disc galaxies. It is evident that, due to their different *intrinsic* axial ratios, such galaxies have different distributions of the observed axial ratio, in such a way that the fraction of elliptical galaxies increases at higher values of b/a . Therefore, it is indeed the axial ratio cut at $b/a \geq 0.9$ that produces the differences seen in Fig. 1. Some of the results presented below depend on the fraction of elliptical galaxies in the sample, and are

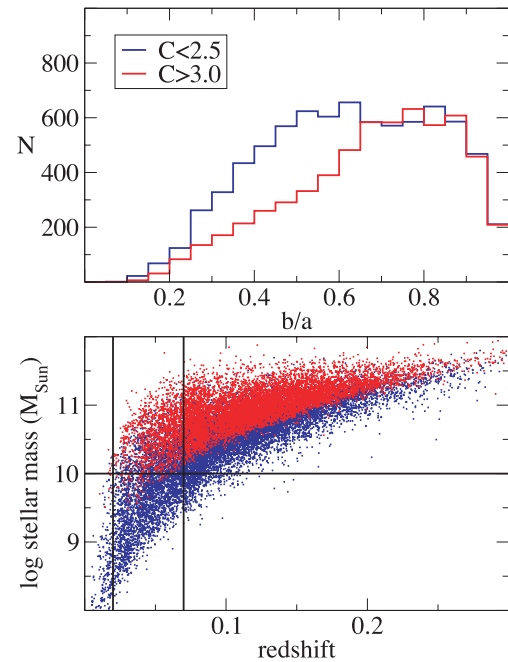


Figure 2. Top panel: distribution of isophotal axial ratios for galaxies in the parent sample with a concentration index below 2.5 (blue line) and above 3 (red line). Bottom panel: stellar mass plotted against redshift for all spectroscopically classified galaxies in SDSS DR2. Black lines indicate our cuts in mass and redshift. Blue and red dots correspond to galaxies with low and high dust-corrected z -band mass-to-light ratios, respectively.

thus affected by this selection effect. We can correct these results for such effect by comparing the fraction of galaxies with $C > 3$ in the parent sample, regardless of axial ratio, to that of galaxies with both $C > 3$ and $b/a \geq 0.9$. This provides us with a fairly good indication of how larger the fraction of elliptical galaxies in our final sample is compared to our parent, volume-limited sample. It turns out that this difference is a factor of 1.3. Such correction factor will be applied when necessary with an explicit mention.

Given our axial ratio cut, one might also question whether the results in this work concern galaxies which are intrinsically more eccentric than average. To check that we have also selected 30 systems with $C > 2.5$ (i.e. mostly bulge-dominated and elliptical galaxies) and $0.5 < b/a < 0.7$, which otherwise comply with all

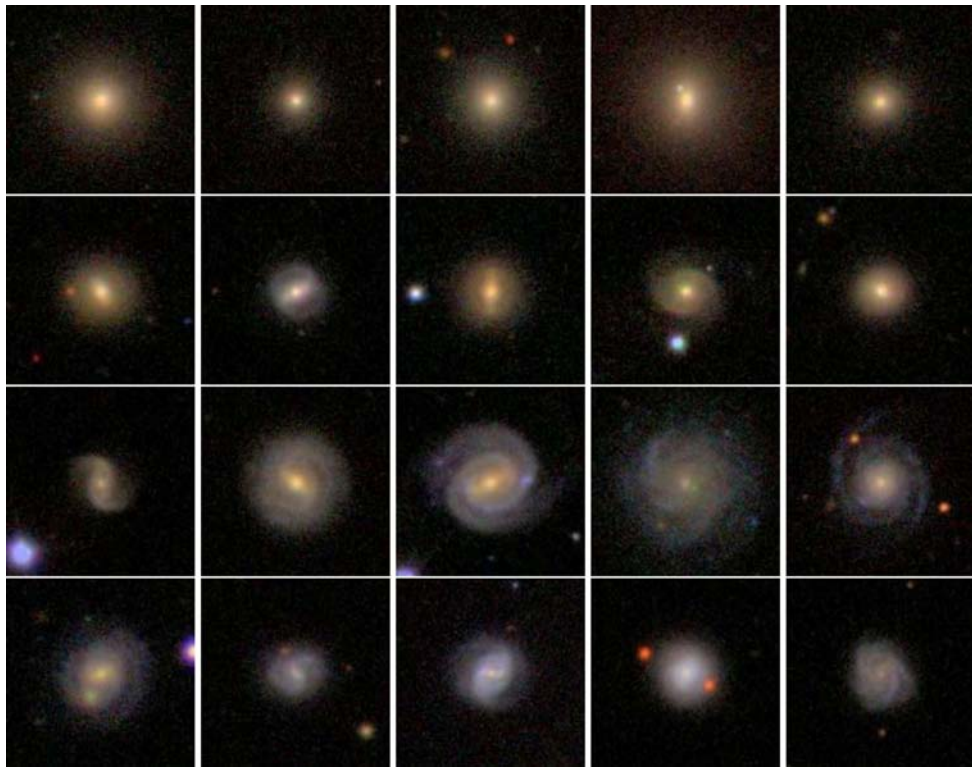


Figure 3. Examples of galaxies in our sample. The four rows show from top to bottom panel, respectively, elliptical galaxies, galaxies with classical bulges, galaxies with pseudo-bulges and bulgeless galaxies. For the three last rows, the first three columns from left show barred galaxies. This grouping is based on the results from our parametric image decompositions.

other selection criteria of the final sample, and analyse them in a similar fashion. One could also ask if we are missing galaxies with very strong bars due to our cut in axial ratio. This would happen if the outer disc of the galaxy is not detected. We argue that this is not the case, based on the fact that the strongest bars we find, considering the bar-to-total luminosity ratio, are about as strong as the strongest ones found in other studies (Sellwood & Wilkinson 1993; Reese et al. 2007; Durbala et al. 2008; Gadotti 2008).

Finally, we also need to check if there is a bias in our parent sample against galaxies close to both its low-mass and high-redshift cuts, which could occur due to magnitude limits in the survey. This is done by plotting galaxy mass against redshift for all spectroscopically classified galaxies in DR2 in the lower panel of Fig. 2. Since such a bias might depend on galaxy colour, we plot separately galaxies with low and high dust-corrected z -band mass-to-light ratio (from Kauffmann et al. 2003b), using the peak of its distribution as boundary between the two groups. One sees that there is no clear need for such a volume correction, i.e. our parent sample includes effectively all galaxies more massive than $10^{10} M_{\odot}$ in the defined volume.

We have also compared the distributions of other physical parameters, such as stellar surface density and metallicity, r -band light-weighted age, number of neighbours and the fluxes and equivalent widths of important emission lines in AGN, derived by Kauffmann et al. (2003a,b, 2004) and Gallazzi et al. (2005), in both our parent and final samples. These distributions are generally similar. We thus conclude that, after accounting for the effects introduced with our axial ratio cut, our final sample is a fair representation of the population of galaxies and AGN in the local universe with stellar masses larger than $10^{10} M_{\odot}$. This means that conclusions based

on this sample are generally pertinent to galaxies that satisfy these conditions.

Fig. 3 shows examples of galaxies in our sample. Each row corresponds to a different galaxy category, concerning the central component. Elliptical galaxies are shown in the top row. The remaining rows show, from top to bottom panel, respectively, galaxies with classical bulges, galaxies with pseudo-bulges and bulgeless galaxies. This grouping is based on the results from our parametric image decompositions below.

3 IMAGE DECOMPOSITION

The fitting of each galaxy image in our sample was done using BUDDA v2.1, which is able to fit up to four different galactic components to a galaxy image, namely bulge, disc, bar, and a central source, usually adopted to account for the emission from bright, type 1 AGN. Details on the code technical aspects and capabilities can be found in de Souza, Gadotti & dos Anjos (2004) and Gadotti (2008). In particular, the latter discusses more specifically the treatment of the bar component. Here, we briefly recall the functions used to describe each component.

The model components are described by concentric, generalized ellipses (see Athanassoula et al. 1990):

$$\left(\frac{|x|}{a}\right)^c + \left(\frac{|y|}{b}\right)^c = 1, \quad (1)$$

where x and y are the pixel coordinates of the ellipse points, a and b are the extent of its semimajor and semiminor axes, respectively, and c is a shape parameter. The centre of the component, given by the coordinates x_0 and y_0 , is also fitted by the code, and is the same

for all components fitted. Position angles and ellipticities were fitted by the code for every component, each one having a single position angle and ellipticity. When $c = 2$ one has a simple, pure ellipse. When $c < 2$ the ellipse is discy, and when $c > 2$ the ellipse is boxy. Bulges and discs were fitted using pure ellipses, but c was left free to fit bars, since bars are better described by boxy ellipses.

Each component also has to follow a surface brightness radial profile. The disc profile is described by an exponential function (Freeman 1970):

$$\mu_d(r) = \mu_0 + 1.086r/h, \quad (2)$$

where r is the galactocentric radius, μ_0 is the disc central surface brightness and h is the disc characteristic scalelength.

The bulge profile is described by a Sérsic function (Sérsic 1968, see Caon, Capaccioli & D'Onofrio 1993):

$$\mu_b(r) = \mu_e + c_n \left[\left(\frac{r}{r_e} \right)^{1/n} - 1 \right], \quad (3)$$

where r_e is the effective radius of the bulge, i.e. the radius that contains half of its light, μ_e is the bulge effective surface brightness, i.e. the surface brightness at r_e , n is the Sérsic index, defining the shape of the profile, and $c_n = 2.5(0.868n - 0.142)$. When $n = 4$ the profile is a de Vaucouleurs function (de Vaucouleurs 1948), while $n = 1$ corresponds to an exponential bulge. Elliptical galaxies were fitted with a single ‘bulge’ component.

The bar profile is also described by a Sérsic function. For the bar,

$$\mu_{\text{bar}}(r) = \mu_{e,\text{bar}} + c_{n,\text{bar}} \left[\left(\frac{r}{r_{e,\text{bar}}} \right)^{1/n_{\text{bar}}} - 1 \right], \quad (4)$$

where $c_{n,\text{bar}} = 2.5(0.868n_{\text{bar}} - 0.142)$, and the other parameters have similar definitions as for the bulge. Another bar parameter fitted by the code is the length of the bar semimajor axis, L_{bar} , after which the bar profile is simply truncated and drops to zero.

Using the models obtained with BUDDA, we have calculated the absolute magnitude of each different galaxy component in all galaxies in the sample in the g , r and i bands. We have thus also calculated the integrated colours of each component separately.

To avoid unreliable results that very often arise from automated image decomposition, we applied BUDDA to each galaxy individually. Erroneous fits are particularly likely to arise, if not followed closely, when fitting barred galaxies. In such cases, the number of parameters fitted can be as high as 18, and the topology of the distribution of χ^2 for many possible models is very complex. We thus adopted a procedure to produce each fit, which is as follows.

First, we needed to produce the image to be fitted. To this end, a cutout was created from the original SDSS galaxy image, with the galaxy in the centre, and containing enough sky background in order not to remove the galaxy outskirts. Usually, this means that the image size on a side is about twice the apparent diameter of the galaxy. Before fitting, each image was cleaned of spurious objects such as foreground stars. The sky background and PSF FWHM values given by SDSS were checked and corrected when necessary, which rarely occurred. When needed, the sky background was estimated by calculating the median pixel value of several areas free from objects in the galaxy image. When the PSF FWHM given by SDSS was deemed erroneous, we have made new estimates by fitting a Moffat profile (Moffat 1969) to a number of suitable stars near the galaxy, and choosing the median value found. The images were fitted without subtracting the mean background value. This is important, because a proper calculation of the χ^2 , and thus a

reliable determination of the uncertainties, is based on the statistics concerning all photons that reached the detector. Evidently, the value of the background is given to the code, and the model components are determined taking it into account.

Secondly, before starting the fit, it is necessary to provide the code with initial guesses for all parameters to be fitted. The coordinates of the pixel with highest intensity were chosen as input to x_0 and y_0 . The geometrical parameters were roughly estimated by visual inspection of the image and the corresponding isophotal contours. When deemed necessary, these parameters were also calculated using the intensity moments in a few different circular apertures centred at the galaxy centre. Finally, the initial guesses for the parameters of the surface brightness profiles were estimated through the inspection of a pixel-by-pixel radial intensity profile of the galaxy. Tests with artificial images of unbarred disc galaxies with high and low spatial resolution in de Souza et al. (2004) showed that BUDDA is generally able to reliably retrieve the correct structural parameters. In Gadotti (2008), further tests with similar images showed that the uncertainties estimated by the code for each fitted parameter are realistic. In Appendix A, we perform new tests, and check how the fits in this study depend on the input parameters, using SDSS r -band images of 20 barred galaxies in our sample. The choice for barred galaxies assures that the results from these tests concern typically difficult fits. The results are encouraging. They show that, in most cases, the code converges to similar results (generally consistent within the estimated uncertainties) for input parameters varying up to a factor of 4. Furthermore, wrong fits can, in general, be recognized by their unusually high χ^2 values.

A critical point at this stage is to decide on which components the model of the galaxy should include. With this aim, the inspection of the galaxy image, isophotal contours and intensity profile was also very helpful. A bulge component was included in the model if the intensity profile is clearly not a single exponential function. In the absence of bars or spiral arms, it might not be clear only by inspecting the image if a galaxy has or not a disc component. The latter might become easier to identify when checking the isophotal contours for significant differences in position angle and/or ellipticity between the inner and outer parts of the galaxy. In addition, an outer exponential component in the intensity profile is naturally also an indication of the presence of a disc. A disc was included in the model whenever one of such signatures was found. To check for the presence of a bar, we first inspected the galaxy image. If in doubt, we then looked for the typical bar signatures in the isophotal contours and the intensity profile, i.e. respectively, an elongated structure with constant position angle and a flat ledge in the profile (see e.g. Gadotti et al. 2007). A bright AGN could be discerned if the profile has a cusp in the centre. However, even bright AGN are smoothed out if the physical spatial resolution of the image is not high enough (see Gadotti 2008). Accordingly, none of our images presents such a feature, and thus no galaxy in our sample required an AGN component in the fit.

Evidently, however, some cases are less clear, and one cannot rule out the possibility of us fitting a truly elliptical galaxy with a model containing bulge and disc, or conversely, fitting an unbarred lenticular galaxy with only a bulge model. In some of the latter cases, a first fit resulted in a bad match to the galaxy image, usually a bulge with an obviously too low Sérsic index. In most of these cases, another fit, including a disc component, produced a better match, revealing the true nature of the galaxy. To check that our decision on whether or not adding a disc component in a given fit is reliable, we have performed the following tests. We

randomly selected 20 galaxies judged as ellipticals and produced test fits with a disc component. Conversely, we randomly selected 20 galaxies judged as unbarred lenticulars and produced test fits without a disc component. It turned out that, for the ellipticals, only one test fit resulted in a lower χ^2 , and, for the lenticulars, two test fits resulted in similar χ^2 values. Nevertheless, none of such cases is significantly improved fits, and most of these test fits resulted in unmistakably worse matches to the galaxy images. Furthermore, the disc component found in the tested ellipticals never contributes with more than a few per cent of the total galaxy luminosity. It should also be mentioned that, due to the limited physical spatial resolution of our images, we likely missed most bars shorter than $L_{\text{bar}} \approx 2-3$ kpc, typically seen in very late type spirals (later than Sc – Elmegreen & Elmegreen 1985). The whole of these faint bars is typically within two to four seeing elements, and thus they do not imprint clear signatures in either the isophotal contours or the intensity profile. Note that, in contrast, bulges with r_e of the order of one seeing HWHM can still be identified in the intensity profile, since they usually contain a much larger fraction of the galaxy light than these short and faint bars.

This procedure was performed using several suitable tasks in IRAF.² The fits to each galaxy were first done in the r band, until a satisfactory model is achieved. Then, the same input parameters which resulted in the final r -band fit were used to fit the g - and i -band images, with the luminosity parameters scaled accordingly. In addition, in some cases, geometrical parameters such as ellipticities and position angles were kept fixed at the values found with the r -band image. A model was deemed incorrect if any of the fitted parameters assumed a value which is clearly wrong, but this was uncommon. A typical case concerns the bulge Sérsic index. If n was found to be outside the range $0.8 \leq n \leq 6$, then a new set of input parameters was tried in a new fit. Usually, the subsequent fits returned values for n within this range, as well as smaller uncertainties in the fitted parameters, and a lower χ^2 . In these cases, we stucked to the new fit. In some other cases, however, the resulting model did not change after changing the initial parameters. When this happened, we considered the model appropriate. Only occasionally, a more detailed comparison between galaxy image and model was done, e.g. by comparing both intensity profiles.

Fig. 4 shows examples of the fits obtained for six galaxies in the sample. These include an elliptical galaxy, two galaxies with a classical bulge (one barred galaxy and one unbarred), two galaxies with a pseudo-bulge (again barred and unbarred) and a bulgeless galaxy. The distinction between classical bulges and pseudo-bulges is explained in details in Section 4.2. One sees that the fits are generally quite good, even though the physical spatial resolution of the images is restricted, and despite the fact that, given the size of our sample, we could not make a thorough comparison between galaxy and model before accepting the fit to every single galaxy in the sample. This would require an unreasonable amount of time to complete the study for the whole sample. The discrepancies between galaxy and model are usually below 0.3 mag arcsec⁻² and are mainly caused by substructures such as spiral arms, rings, lenses and bar ansae. It is clear that, if we cannot ascertain that the fits are excellent for a single specific galaxy, the results from the fits are, on average, trustworthy, and thus suitable for statistical studies.

² IRAF is distributed by the National Optical Astronomy Observatories, which are operated by the Association of Universities for Research in Astronomy, Inc., under cooperative agreement with the National Science Foundation.

4 RESULTS

4.1 A comparison between different bulge-to-total indicators

The morphological (Hubble) type of a galaxy is related to several physical parameters that are an indication of the galaxy formation and evolution processes (e.g. Roberts & Haynes 1994). One of the basic features on which the morphological classification of a galaxy hinges on is the relative importance of the bulge component to the overall light distribution of the galaxy (Hubble 1926). Thus, it is of the utmost importance to be able to measure how relevant is the bulge component within a given galaxy in an objective and quantitative fashion, even if there is some scatter in the relation between measured bulge prominence and visually determined Hubble type (e.g. Laurikainen et al. 2007; Graham & Worley 2008). Because it is difficult to objectively define the latter, the former is advantageous.

In this work, since we have performed a detailed decomposition of each galaxy image into its main components, bulge prominence is readily accessible from the bulge-to-total luminosity ratio B/T , calculated from the models obtained with BUDDA. However, the employment of such techniques to very large samples of galaxies presents serious challenges, as automated procedures are prone to large uncertainties. Thus, other parameters, which are not so difficult to determine, have been suggested as a measure of bulge prominence. One of such parameters is the Petrosian concentration index, defined as the ratio $R90/R50$, where $R90$ and $R50$ are, respectively, the radii enclosing 90 and 50 per cent of the galaxy luminosity (see Kauffmann et al. 2003b, and references therein). Another possibility is to fit the entire galaxy as a single component, with a Sérsic function, and then use the Sérsic index so obtained (e.g. Blanton et al. 2005a,b; Häussler et al. 2007).

Since we have measurements of B/T and the bulge Sérsic index for all galaxies in our sample, we can test how well concentration index and galaxy Sérsic index relate to B/T and how all these connected parameters relate to each other. This is done in Figs 5 and 6. The concentration index is taken from the SDSS data base and galaxy Sérsic index from Blanton et al. (2005a). The latter are updated values after the finding of a systematic bias in the values in Blanton et al. (2003). Fig. 5 shows that concentration correlates poorly with the bulge Sérsic index. Although one sees a tendency in the sense that bulges with higher values for n reside in galaxies with higher $R90/R50$, the spread is very large. This might be partly due to the fact that n is related only to the bulge component, whereas $R90/R50$ depends on the overall structure of the whole galaxy. Another issue is that n can have high uncertainties compared to its dynamical range. Fig. 5 also shows that $R90/R50$ is well correlated with B/T . Interestingly, the correlation gets notably better when the bar contribution to the total galaxy luminosity is taken into account. The correlation coefficient for $R90/R50 \times B/T$ is 0.82, while that for $R90/R50 \times (B + \text{Bar})/T$ is 0.86. Although bars are more extended structures than bulges, they are usually significantly less extended than discs, which explain the better correlation of $R90/R50$ with $(B + \text{Bar})/T$. This means that there is an additional uncertainty when using $R90/R50$ as a proxy for B/T , as one galaxy with small bulge but massive bar can have a higher value of $R90/R50$ than an unbarred, but otherwise similar, galaxy. It is worth noting that concentration rises linearly with $(B + \text{Bar})/T$ up to $(B + \text{Bar})/T \approx 0.6$, after which it stays roughly constant at ≈ 3 , a value of concentration similar to that of massive elliptical galaxies. A linear fit to the data points with $0 < (B + \text{Bar})/T \leq 0.6$ gives

$$R90/R50 = 1.93(\pm 0.02) + 2.02(\pm 0.05) \times (B + \text{Bar})/T. \quad (5)$$

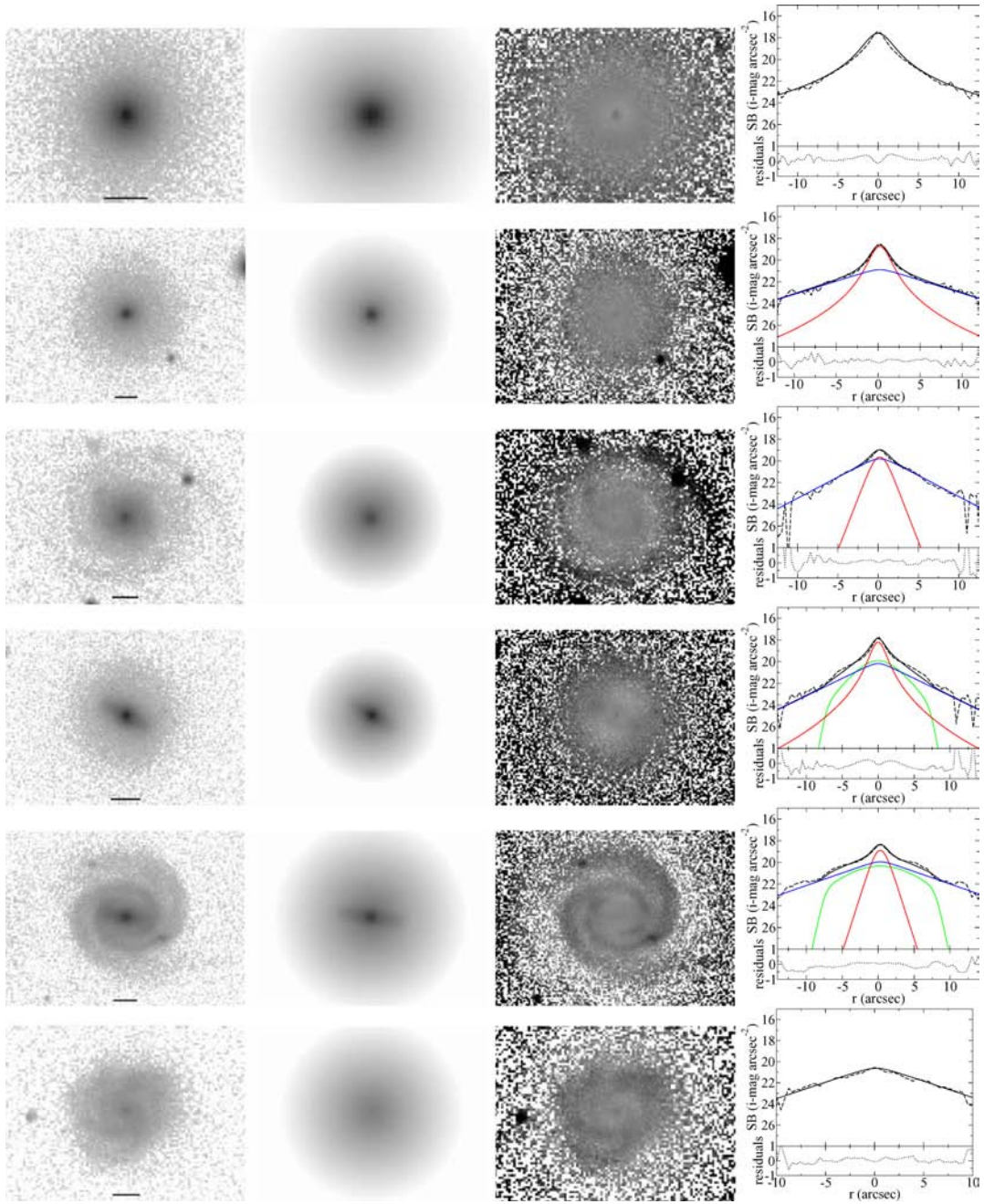


Figure 4. Examples of fits obtained. Each row refers to a single galaxy, showing, from left- to right-hand panel: the original i -band galaxy image, the model image obtained with BUDDA, the residual image and surface brightness profiles. Horizontal lines in the galaxy images mark a length of 5 kpc at the galaxy distance. The first two images have intensities transformed to magnitudes per square arcsec, and are displayed with the same levels in all rows. The residual images are obtained by subtracting the model image from the original image, and are displayed with a much narrower range in intensity, which is also the same in all rows, in order to enhance residual substructures. In the residual images, darker pixels indicate where the galaxy is brighter than the model, whereas whiter pixels indicate where the model is brighter than the galaxy. The surface brightness profiles were obtained from cuts along the galaxy major axis, or along the bar major axis when there is a bar. The dashed line corresponds to the original galaxy image, whereas the black solid line corresponds to the model. When there is more than a single component, red, blue and green lines refer, respectively, to bulge, disc and bar. The dotted line in the bottom panel shows the residuals (galaxy – model). These results correspond to, from top to bottom panel, respectively, an elliptical galaxy, a galaxy with a classical bulge, a galaxy with a pseudo-bulge, a barred galaxy with a classical bulge, a barred galaxy with a pseudo-bulge and a bulgeless galaxy.

Fig. 6 shows how the galaxy Sérsic index relates to the bulge Sérsic index, concentration, B/T and $(B + \text{Bar})/T$. All plots show a very large spread. In particular, the galaxy Sérsic index is systematically higher than the bulge Sérsic index by, on average, ≈ 0.8 . Moreover, the galaxy Sérsic index is a poor proxy for B/T . From the previous figure, one sees that the concentration index is much more

reliable in this respect. The correlation coefficients for the galaxy Sérsic index as a function of B/T and $(B + \text{Bar})/T$ are, respectively, 0.43 and 0.45.

Nevertheless, it should be noted that both the galaxy and bulge Sérsic indices in Figs 5 and 6 are corrected for seeing effects, whereas the concentration index is not. It does seem, however, that

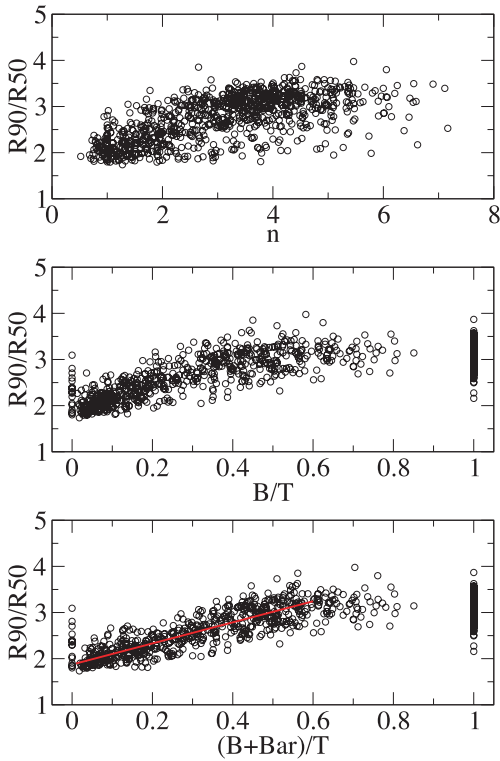


Figure 5. The concentration index ($R90/R50$) plotted against the bulge Sérsic index n (top panel), the bulge-to-total ratio B/T (middle panel) and the added contributions of bulge and bar to the total galaxy luminosity $(B + \text{Bar})/T$ (bottom panel). The correlation between concentration and n is remarkably poorer than that with B/T . Interestingly, the latter correlation is improved when the bar contribution is taken into account. Elliptical galaxies and bulgeless galaxies can be readily identified in the middle panel at $B/T = 1$ and 0, respectively. The red line in the bottom panel is a linear fit to the data points with $0 < (B + \text{Bar})/T \leq 0.6$. For galaxies with B/T , or $(B + \text{Bar})/T$, greater than ≈ 0.6 , $R90/R50$ is roughly constant at ≈ 3 .

seeing effects on the concentration index are small at low redshifts (Blanton et al. 2003). For a sample with a narrow range in redshift, as ours, such effects seem to be practically negligible, since the systematic variation of the average physical size of the PSF is relatively small. We verified this by plotting $R90/R50$ against redshift and finding no correlation whatsoever. Seeing effects would only introduce an uncertainty at each measurement, which is small compared to the spread in concentration seen at each B/T , or $(B + \text{Bar})/T$, in Fig. 5.

4.2 Identifying pseudo-bulges

As mentioned in Introduction, studies on the properties of pseudo-bulges are often characterized by having a physical spatial resolution higher than that of the SDSS images used here. It is thus legitimate to be concerned on how well can we in fact distinguish pseudo-bulges from classical bulges. One key aspect of this assessment is the comparison between the effective radius of the bulge r_e and the PSF HWHM of the corresponding image. Gadotti (2008) showed that the structural properties of bulges can be reliably retrieved provided that r_e is larger than ~ 80 per cent of the PSF HWHM. This was gauged by fitting the images of very nearby galaxies, at a relatively high physical spatial resolution, and through the fitting of the same galaxies using artificially redshifted images. Fig. 7 shows

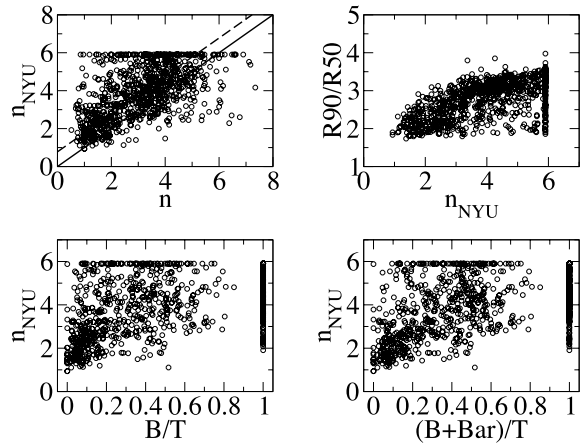


Figure 6. Top left-hand panel: the galaxy Sérsic index from Blanton et al. (2005a) plotted against our measurements of the bulge Sérsic index; top right-hand panel: the concentration index plotted against the galaxy Sérsic index; bottom left-hand panel: the galaxy Sérsic index plotted against B/T and bottom right-hand panel: the galaxy Sérsic index plotted against $(B + \text{Bar})/T$. The solid line in the top left-hand panel depicts a perfect correspondence. The dashed line is a linear fit to all data points, fixing the slope of the fit to 1. Although there is a very large spread, it is clear that the galaxy Sérsic index is systematically higher than the bulge Sérsic index by, on average, ≈ 0.8 .

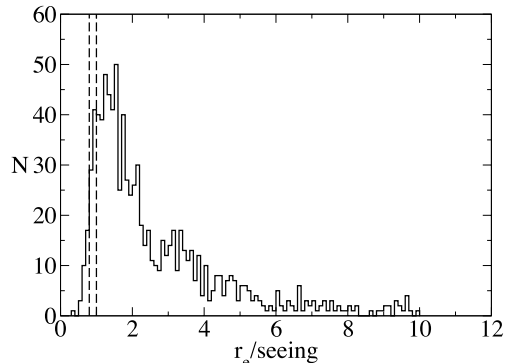


Figure 7. Distribution of the ratio between bulge effective radius and PSF HWHM for all galaxies in the sample (excluding bulgeless galaxies). The two vertical dashed lines mark the positions where this ratio is 0.8 and 1. Only 3 per cent (10 per cent) of the bulges have effective radii below 0.8 (1) times the PSF HWHM.

that only 3 per cent of our bulges do not satisfy this criterion. If one wants to be more stringent and extend this limit to 100 per cent of the seeing radius, one still sees that only 10 per cent of our bulges are below the threshold. We have not excluded these bulges from this study but have verified that their inclusion or removal does not result in any significant change in the results presented here. This gives us confidence that the structural properties we have obtained are generally reliable even for the less conspicuous bulges. Note that our decompositions are seeing corrected.

The top two panels in Fig. 8 show the mean effective surface brightness within the effective radius $\langle \mu_e \rangle^3$ plotted against the

³ Note that $\langle \mu_e \rangle$ is not equal to μ_e , which is the effective surface brightness at the effective radius. In plots such as Fig. 8 and the fundamental plane (discussed further below), $\langle \mu_e \rangle$ must be used, since it takes into account differences in the light (mass) distribution within different systems.

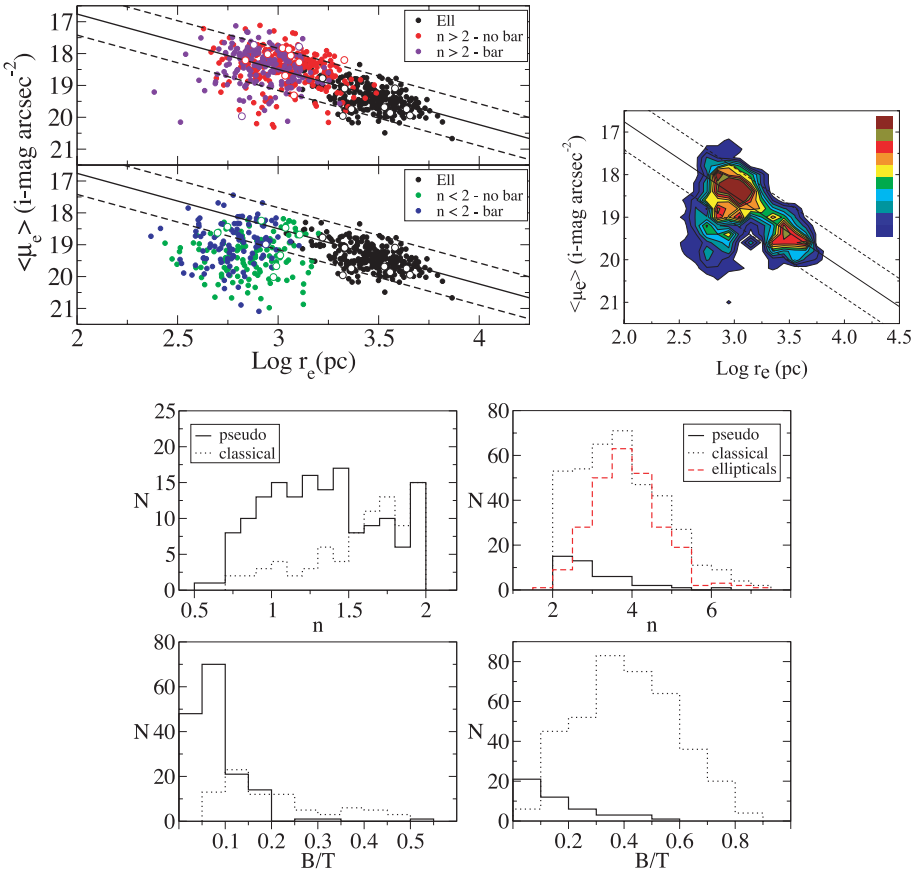


Figure 8. The graphical representation of our criterion to distinguish classical and pseudo-bulges. The two contiguous panels at the top show the mean effective surface brightness *within* the effective radius plotted against the logarithm of the effective radius. The two panels display elliptical galaxies and, separately, bulges with the Sérsic index above and below 2. Barred and unbarred galaxies are also indicated. The solid line is a fit to the elliptical galaxies and the two dashed lines point out its $\pm 3\sigma$ boundaries. Bulges that lie below the lower dashed line are classified as pseudo-bulges, *independently* of their Sérsic index. Bigger, white-filled circles represent systems with $0.5 < b/a < 0.7$, with similar colour coding. They do not show any clear distinct patterns. The separate panel at the top shows a density plot with all data points taken altogether. It shows that ellipticals, classical and pseudo-bulges indeed appear as independent groups in the Kormendy relation. The four histograms at the bottom show the distributions of the Sérsic index n and bulge-to-total luminosity ratio B/T for classical bulges and pseudo-bulges with $n < 2$ (left-hand panel) and $n \geq 2$ (right-hand panel). While the threshold in the Sérsic index can be considered as an approximation to identify pseudo-bulges, it is clear that it can generate many misclassifications. Our criterion can recognize more precisely pseudo-bulges, as those which are structurally different from classical bulges and ellipticals (also shown in the top right histogram).

effective radius for the bulges and elliptical galaxies in our sample. Massive elliptical galaxies follow a well-defined relation between $\langle \mu_e \rangle$ and r_e , which is given by the solid line, constructed from a fit to the data. The two dashed lines are the fit's $\pm 3\sigma$ boundaries (over the zero-point and keeping the slope fixed). This relation is known as the Kormendy relation (Kormendy 1977) and, in fact, one of the possible projections of the fundamental plane (we explore the fundamental plane relations in more detail in Section 4.4). The slope of the Kormendy relation we find here is similar (consistent within the uncertainties) to that found by Pierini et al. (2002) using H -band images. Many bulges also follow this relation. If bulges are separated according to their Sérsic index n , one sees that most of the bulges with $n \geq 2$ follow the ellipticals' relation, whereas most of those with $n < 2$ do not, lying below the relation. This is expected, since exponential bulges are often pseudo-bulges, which are believed to be structurally different from classical bulges and ellipticals (see e.g. Carollo 1999; Kormendy & Kennicutt 2004, and references therein). However, many of the bulges with $n < 2$ do seem to follow the same relation of ellipticals. Conversely, several bulges with $n \geq 2$ fall below this relation. It is thus clear that although

the Sérsic index threshold can be considered as an approximation to identify pseudo-bulges (see e.g. Fisher & Drory 2008), it can introduce many misclassifications. Since pseudo-bulges are expected to be structurally different from classical bulges, and to lie below the $\langle \mu_e \rangle - r_e$ relation for ellipticals, we can use the lower dashed line in Fig. 8 to be the dividing line between classical bulges and pseudo-bulges. This means that pseudo-bulges satisfy the following inequality:

$$\langle \mu_e \rangle > 13.95 + 1.74 \times \log r_e, \quad (6)$$

where $\langle \mu_e \rangle$ and r_e are measured in the SDSS i band and r_e is in parsec. In fact, in this diagram, discs also occupy the region below the relation defined by ellipticals (Pierini et al. 2002), which is consistent with the expectation that pseudo-bulges are built from disc instabilities. From Fig. 8, one also sees that barred and unbarred galaxies behave in a similar fashion in what concerns their positions in the $\langle \mu_e \rangle - r_e$ relation. The histograms in Fig. 8 show the distributions of n and B/T for classical bulges and pseudo-bulges with $n < 2$ and $n \geq 2$ in separate panels. They show that our criterion to separate these two bulge categories can identify bulges with $n < 2$,

but with high values of B/T , as classical bulges. These bulges have often values of n close to 2. Conversely, we are also able to identify pseudo-bulges with $n \geq 2$. These bulges often show low values of B/T and also values for n close to 2. These results indicate that some bulges can be erroneously classified as classical or pseudo, if one uses the Sérsic index for such classification, just for being by chance (due to measurement uncertainties) in the wrong side of the Sérsic index threshold. One sees that, as expected, pseudo-bulges show a distribution of n unlike that of classical bulges and ellipticals. In addition, the distribution of n for classical bulges is wide, and ranges from values typical of ellipticals to values in the gap between pseudo-bulges and ellipticals. Furthermore, one also sees that classical bulges have a peak in B/T around 0.4, while the corresponding value for pseudo-bulges is about 0.1.

Although it is clear that bulges with low and high Sérsic index occupy different loci in the $\langle\mu_e\rangle - r_e$ projection, Fig. 8 suggests that there is a more significant difference between all bulges and ellipticals than between the different bulges. To check that we have performed 2D Kolmogorov–Smirnov tests (Fasano & Franceschini 1987; Press et al. 1992). The tests show that, in fact, *in this projection*, ellipticals differ more from bulges (taken altogether) than bulges with high Sérsic index differ from bulges with low Sérsic index. In this context, we have checked, using the tests described in Section 3, that if a lenticular galaxy is mistaken by an elliptical, the shift in r_e could be at most only 0.04 dex. Thus, although such an effect, if present, would indeed bring ellipticals closer to bulges in the Kormendy relation, its amplitude is too small. In light of these results, one could ask whether a separation between classical and pseudo-bulges in the Kormendy relation is rather artificial. The density plot in Fig. 8 suggests that it is not: pseudo-bulges appear as an independent group of points, as do classical bulges and ellipticals.

Previous studies also indicate that pseudo-bulges show star-forming activity, as opposed to classical bulges, which are constituted mainly by old stellar populations (e.g. Gadotti & dos Anjos 2001; Fisher 2006). We can check this difference within our sample using both the $D_n(4000)$ index provided in Kauffmann et al. (2003b) and the SDSS fibre colour (i.e. the colour measured within the fibre aperture). The $D_n(4000)$ index is based on the 4000 Å discontinuity seen in optical spectra of galaxies, and it is not sensitive to dust attenuation effects. Young stellar populations have low values of $D_n(4000)$, as compared to old stellar populations. The fibre colours are integrated over the central region of the galaxy and can suffer from dust reddening. In Fig. 9, we show the distributions of $D_n(4000)$ and fibre $g - i$ colour for pseudo-bulges and classical bulges. The result is striking. Our pseudo-bulges do indeed show values of $D_n(4000)$ lower than those for classical bulges, indicating a higher level of star formation activity. Their distributions are also significantly apart (except for a tail of classical bulges showing star-forming activity). In fact, the peaks of the $D_n(4000)$ distributions for pseudo-bulges and classical bulges coincide with the peaks in the bimodal distribution of $D_n(4000)$ seen in both our parent and final samples (see Fig. 1). Such bimodality was also found by Allen et al. (2006), who concluded that it is produced by bulge-dominated galaxies on the one hand and disc-dominated galaxies on the other hand. More recently, Drory & Fisher (2007) suggested that such bimodality is a result of the two different bulge families: pseudo-bulges are hosted by galaxies with high overall star formation activity, whereas classical bulges reside in galaxies that underwent violent relaxation processes in the past, such as mergers, and thus have formed most of their stars in these past events. Both suggestions are not mutually exclusive, since galaxies

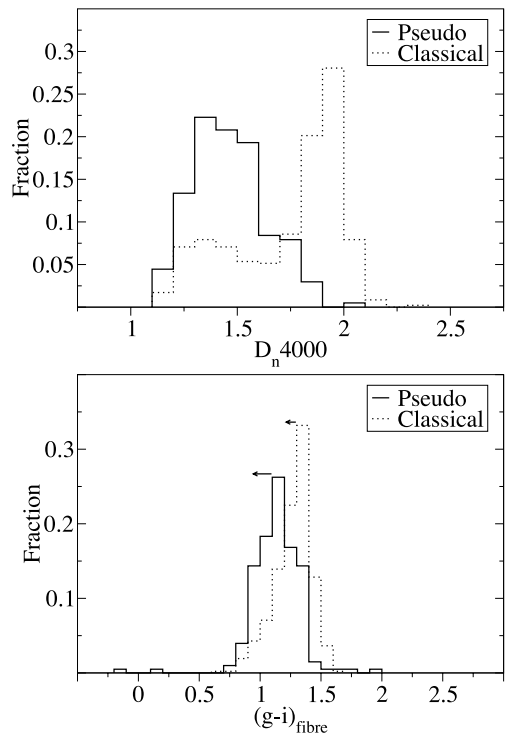


Figure 9. Distributions of $D_n(4000)$ (top panel) and fibre $g - i$ colour (bottom panel) for pseudo-bulges and classical bulges. The arrows in the bottom panel indicate an upper limit on how dust reddening could affect the colours of each bulge category, on average.

with pseudo-bulges are often disc-dominated galaxies, as opposed to bulge-dominated galaxies, which often host classical bulges. In fact, our results indicate that the most disc-dominated galaxies almost always host pseudo-bulges, which are almost always under current intense star-forming activity, whereas classical bulges are mostly quiescent and reside mainly in more bulge-dominated galaxies. Interestingly enough, star-forming classical bulges form a group of points of their own in the density plot of Fig. 8, between the lower dashed line and the solid line. We will come back to these points further below. We have verified that if one separates bulges using their Sérsic index with a threshold at $n = 2$, the resulting $D_n(4000)$ distributions are similar, and one also sees a tail of star-forming bulges with $n \geq 2$. In this case, however, the peaks of such distributions are slightly closer, and the distribution for bulges with $n < 2$ is broader than that of our pseudo-bulges. This gives support to our criterion to identify pseudo-bulges.

The colour distributions are also separated, though in a less dramatic way. Pseudo-bulges show bluer colours than classical bulges, on average, but the difference in the mean colour values amounts only to 0.2 mag. Evidently, dust reddening does play a role in making these distributions more similar, as compared to those of $D_n(4000)$. Some dust attenuation is expected even in face-on galaxies (e.g. Driver et al. 2008). The fact that the colour distribution of pseudo-bulges is wider than that of classical bulges is also a result of dust attenuation. On one hand, there are those pseudo-bulges with not much dust attenuation, whose intense star formation shows up as the resulting blue colours (and the blue tail in the distribution). And, on the other hand, there are those pseudo-bulges with dust-obscured star formation that produce the red colours seen in the red tail of the distribution. One can have an estimate of the dust reddening in

our bulges, using estimates of the total galaxy dust attenuation in Kauffmann et al. (2003b) as an upper limit (i.e. considering that all dust attenuation in the galaxy strikes the bulge light). We calculated the average dust attenuation in the i band using the results for the z band in Kauffmann et al. (2003b), and assuming that dust attenuation goes as $\lambda^{-0.7}$ (where λ is the observed wavelength). The average i -band attenuation we thus find for our elliptical galaxies and galaxies with classical and pseudo-bulges is, respectively, 0.04, 0.16 and 0.48 mag. This corresponds to $g - i$ colour excesses of, respectively, 0.02, 0.08 and 0.15 mag. The colour excess for classical and pseudo-bulges are indicated by the arrows in the lower panel of Fig. 9. Interestingly, the difference in the position of the peaks of the $D_n(4000)$ distributions amounts to 0.60, while the corresponding difference for fibre $g - i$ colour is, as mentioned above, 0.20 mag (without any dust correction) and 0.27 mag (with the upper limit dust correction).

Since the $D_n(4000)$ values and fibre colours are taken from SDSS spectra, which are themselves taken through a *fixed* fibre aperture of 3 arcsec (thus 1.5 arcsec in radius), and since pseudo-bulges are often smaller than classical bulges, one might ask whether the striking difference in $D_n(4000)$ between pseudo-bulges and classical bulges in our sample is only due to aperture effects. One could argue that, due to the smaller extent of pseudo-bulges within the fibre aperture, the $D_n(4000)$ values (and similarly the fibre colours) for pseudo-bulges are contaminated with star formation in the disc. In fact, the average effective radius of pseudo-bulges and classical bulges is, respectively, 0.82 and 1.14 arcsec. However, one must bear in mind that bulge light dominates over disc light through ≈ 2 times the bulge effective radius from the galaxy centre. This is borne out in our surface brightness profiles, and has also been found by others (see e.g. Moriondo, Giovanelli & Haynes 1998; Morelli et al. 2008). Nevertheless, to be reassured that the difference seen in $D_n(4000)$ is not just a spurious effect, we have verified that the difference in the mean values of $D_n(4000)$ for pseudo-bulges and classical bulges is similar when all bulges are separated in bins of similar effective radius. In particular, we have verified that all results from Fig. 9 hold if one considers only bulges with $r_e > 1$, or 1.5 arcsec, where little disc contamination is expected. Furthermore, we have also verified that the SDSS fibre colours are, in fact, much more similar to the integrated bulge colours, as calculated with the determined BUDDA models for the g - and i -band images, than the corresponding disc colours. We thus conclude that one cannot blame disc contamination within the SDSS spectra to explain the higher star formation activity and bluer colours seen in our pseudo-bulges.

Our sample was designed in a way to minimize dust effects. In fact, most of our galaxies have dust attenuation measurements in the low end of the distribution of dust attenuation for the whole sample of more than 10^5 galaxies in Kauffmann et al. (2003b). Nevertheless, it is clear that the high star formation activity seen in pseudo-bulges is accompanied to some extent with dust obscuration. Could this somehow affect the structural parameters obtained? To answer this question, we plot in Fig. 10 the bulge structural parameters obtained with the g -band images against the same parameters obtained with the i -band images. Dust has more pronounced effects in bluer bands and thus, if there are some systematic effects caused by dust in our decompositions, these should show up in these plots, in particular for pseudo-bulges. For instance, dust attenuation could, in principle, result in systematically lower values for n , as well as smaller values for r_e , in the g band, as compared to those in the i band. Fig. 10 shows no substantial systematic effects. We thus conclude that our decompositions are not significantly disturbed by dust. This is consistent with the findings in Moriondo et al. (1998), who found that

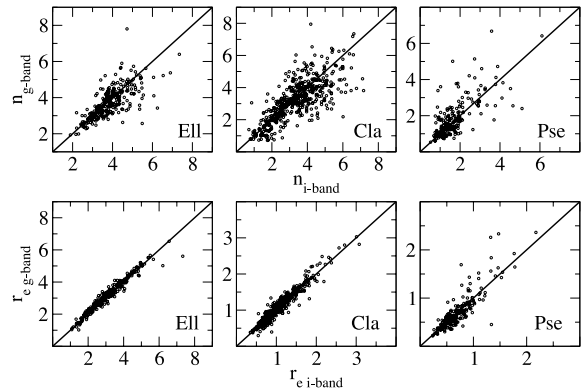


Figure 10. Comparison between structural parameters of elliptical galaxies and bulges obtained in the g and i bands. Top panel: the Sérsic index and bottom panel: effective radius. The solid lines depict a one-to-one correspondence. Bulges are separated according to our classification between classical and pseudo-bulges. The absence of systematic effects indicates that dust does not play a significant role in the overall results of the decompositions.

bulge structural parameters do not change significantly with galaxy inclination.

4.3 Scaling relations

Fig. 11 shows the relations between the bulge Sérsic index and bulge-to-total luminosity ratio, effective surface brightness and effective radius for pseudo-bulges, classical bulges and ellipticals. The relations between the bulge-to-total luminosity ratio and effective surface brightness and effective radius are also shown. It is striking how these three stellar systems populate well defined and

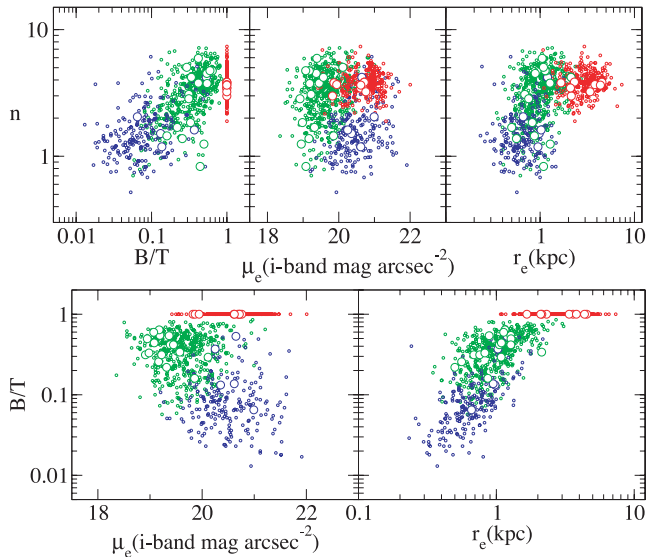


Figure 11. The bulge Sérsic index plotted against the bulge-to-total luminosity ratio (top left-hand panel), bulge effective surface brightness (top centre panel) and bulge effective radius (top right-hand panel). And the bulge-to-total luminosity ratio plotted against bulge effective surface brightness (bottom left-hand panel) and effective radius (bottom right-hand panel). Blue, green and red circles represent, respectively, pseudo-bulges, classical bulges and ellipticals, with $b/a \geq 0.9$. Bigger, white-filled circles with similar colour coding represent systems with $0.5 < b/a < 0.7$. They follow similar patterns.

separate regions in some of these diagrams. Systems with larger n tend to be more conspicuous and extended. One sees a correlation between n and B/T for classical bulges but not as much for pseudo-bulges, corroborating the results from Fisher & Drory (2008), who arrived at a similar conclusion using a smaller sample. It is worth noting that n rises with r_e for bulges but it is rather constant for ellipticals. Furthermore, there is a correlation between B/T and r_e for both classical and pseudo-bulges, although they seem to follow offset relations. Ellipticals tend to be more extended than bulges and have lower effective surface brightness than classical bulges. Note that no difference is seen in Fig. 11 when comparing galaxies with different axial ratios. We have also found that systems with larger n and B/T tend to be in more massive galaxies, although the scatter is large.

In Fig. 12, we show that, as expected, galaxies with more extended bulges or discs tend to be more luminous and massive. This is also true for systems with lower axial ratios. One might also ask whether a similar relation is found if one considers the component mass, rather than the total mass in the galaxy. Although several stellar systems seem to follow such a relation, there might be exceptions, such as globular clusters (see Burstein et al. 1997; Kissler-Patig, Jordán & Bastian 2006; Barmby et al. 2007). This is answered in Fig. 13. One sees that such a correlation indeed exists for pseudo-bulges, classical bulges, bars and discs, separately, regardless of galaxy axial ratio. This figure also shows fits to the data, where scalelengths go as $\propto M^\alpha$, where α is a constant that defines the slope of the relation and M is the component stellar mass. The

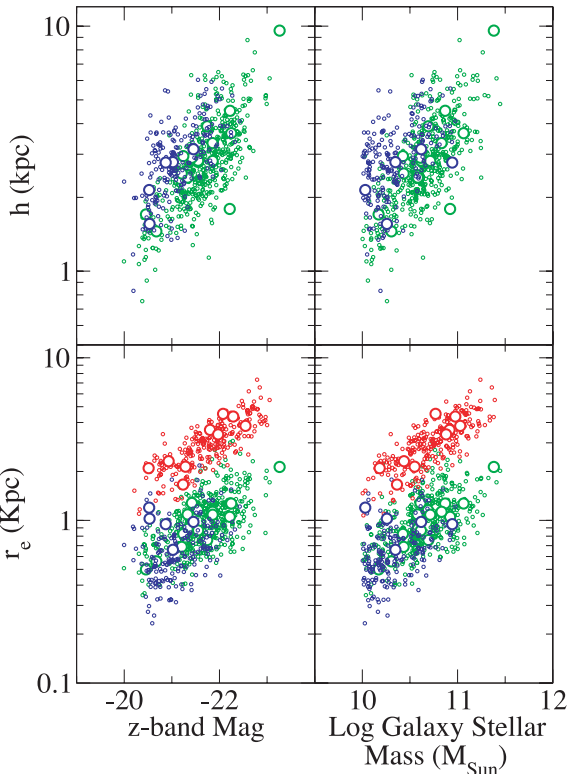


Figure 12. Disc scalelength and bulge effective radius plotted against galaxy z band absolute magnitude (k -corrected to $z = 0.1$) and dust-corrected stellar mass from Kauffmann et al. (2003b). Blue, green and red circles represent, respectively, galaxies with pseudo-bulges, galaxies with classical bulges and ellipticals, with $b/a \geq 0.9$. Bigger, white-filled circles with similar colour coding represent systems with $0.5 < b/a < 0.7$. They follow similar patterns.

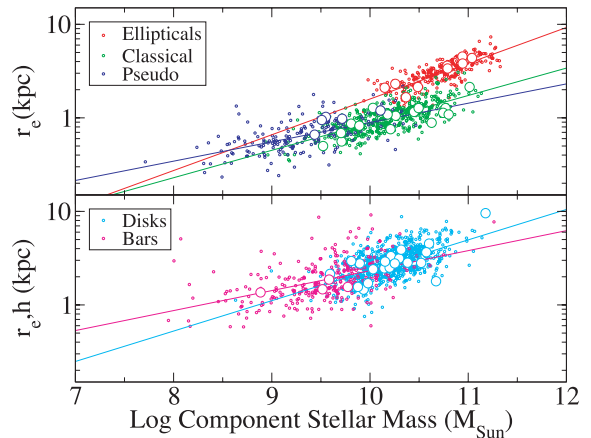


Figure 13. The scalelengths of elliptical galaxies, classical bulges, pseudo-bulges, discs and bars, plotted against the corresponding component stellar mass, as indicated. The solid lines are fits to the data. Bigger, white-filled circles represent systems with $0.5 < b/a < 0.7$, with similar colour coding. They show a similar behaviour.

values we have found for α for bars, discs, pseudo-bulges, classical bulges and ellipticals are, respectively, 0.21, 0.33, 0.20, 0.30 and 0.38, with a mean 1σ uncertainty of 0.02; thus α seems to increase for more massive components. It is interesting to note that bars and pseudo-bulges share a very similar value of α (and these are the only components that do so), which is different from that of classical bulges at a 5σ level. This not only suggests a different formation mechanism for classical and pseudo-bulges, but also reveals a close connection between pseudo-bulges and bars. Such a connection is expected if pseudo-bulges indeed form through disc instabilities. None the less, despite such difference in slope, the locus occupied by classical bulges in such diagram continues rather smoothly from the locus of pseudo-bulges. This suggests that although there might be two different dominant formation processes for classical and pseudo-bulges, there can be a significant number of cases where the different processes are at play concomitantly. Thus, the sequence drawn by pseudo-bulges and classical bulges could represent a sequence where the dominant process changes rather smoothly from one end to the other.

Another striking feature in Fig. 13 concerns ellipticals. They are more offset from classical bulges than classical bulges are offset from pseudo-bulges, as 2D Kolmogorov–Smirnov tests indicate. In fact, one sees that most classical bulges cannot be considered as ellipticals that happen to be surrounded by a disc, at least not ellipticals more massive than $10^{10} M_\odot$. How robust this result is against the possible systematic effects from the decompositions? We explore now two possibilities. The first is that some of the ellipticals could actually be lenticulars whose discs were not identified in the preparation of the fits. As mentioned in Section 3, we produced test fits in which a disc component was forced in 20 ellipticals, and found that in only one case the inclusion of a disc could be justified. However, such a disc contributes with only a few per cent of the total galaxy luminosity, and the resulting shift in r_e , towards lower values, is only of the order of a few hundred parsec. The second possibility is that the input values given to the code to fit r_e are systematically larger for ellipticals. We have thus performed yet another test, again producing test fits for 20 ellipticals but this time with the input values for r_e cut by half. In most cases, the result was similar to the original fit (which incidentally attests the robustness of the code). In a few cases, the shift in the final value for r_e is again only a few

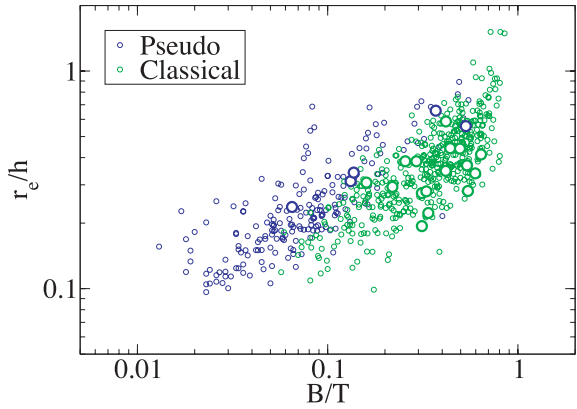


Figure 14. Ratio between the scalelengths of bulges and discs r_e/h plotted against B/T for pseudo-bulges and classical bulges. Although there is some scatter, it is evident that both quantities are correlated, which rules out the concept of a scale-free Hubble sequence. Interestingly, pseudo-bulges and classical bulges seem to follow offset relations. For the same B/T , pseudo-bulges have on average higher values of r_e/h . Bigger, white-filled circles with similar colour coding are pseudo-bulges and classical bulges in galaxies with $0.5 < b/a < 0.7$, and portray similar patterns.

hundred parsec towards lower values; and in all such cases, the resulting χ^2 is substantially worse than that of the original fit. We thus conclude that such systematic effects could, in principle, bring some of the low-mass ellipticals closer to classical bulges in Fig. 13, but the result that at least a significant fraction of classical bulges cannot be considered as (massive) ellipticals surrounded by discs seems to be robust. Note that Fisher & Drory (2008) argue that classical bulges resemble *low-luminosity* ellipticals.

With these data, we can test previous claims that the Hubble sequence is scale-free, i.e. the relation between the scalelengths of bulges and discs does not vary with Hubble type (Courteau, de Jong & Broeils 1996). In this context, Graham & Prieto (1999) showed that fixing the bulge Sérsic index, when fitting galaxy surface brightness profiles, can lead to an overestimate or an underestimate of r_e , depending on the true value of n . Since n is a free parameter in our decompositions, our results are not subject to such systematic biases. In Fig. 14, we plot r_e/h against B/T for pseudo-bulges and classical bulges. This figure shows clearly that r_e/h and B/T are correlated, and thus the Hubble sequence is not scale-free, if it is a B/T sequence. Balcells, Graham & Peletier (2007) and Laurikainen et al. (2007) reached similar results, though with much smaller samples. Fig. 14 also indicates that the relations for pseudo-bulges and classical bulges are offset: for a constant B/T , pseudo-bulges have on average higher values of r_e/h .

It is well known that galaxies can be separated depending on the locus they occupy in a colour–magnitude diagram. Some galaxies follow a tight colour–magnitude relation, in the sense that more luminous galaxies are redder, known as the red sequence, whereas others spread beside the red sequence, originating a swarm of points known as the blue cloud (see e.g. Gladders et al. 1998; Bell et al. 2007, and references therein). Such a diagram is a powerful tool, able to provide clues on the formation and evolutionary processes of galaxies (see e.g. De Lucia et al. 2007). Drory & Fisher (2007), based on a careful analysis of a sample of 39 galaxies, suggested that galaxies with pseudo-bulges populate the blue cloud, while galaxies with classical bulges populate the red sequence. But colour can be subject to dust attenuation effects, and galaxy magnitude is actually used as a proxy to galaxy stellar mass. Since we have

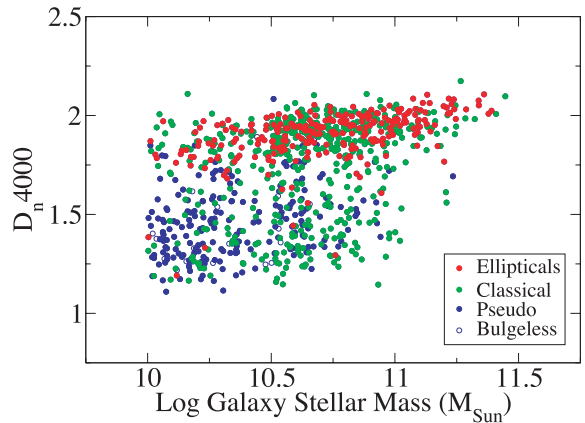


Figure 15. The 4000 Å break index plotted against galaxy dust-corrected stellar mass. Virtually all elliptical galaxies are found in the red sequence, while practically all galaxies with pseudo-bulges, and bulgeless galaxies, are found in the blue cloud. Galaxies with classical bulges can be found in both the red sequence and the blue cloud, although the majority of them occupy the red sequence.

measurements of $D_n(4000)$, an efficient, dust-insensitive index to identify stellar populations with different mean ages, as well as carefully modelled stellar masses, we can go a step further and plot $D_n(4000)$ against galaxy stellar mass, as is done in Fig. 15. It should be noted that often one uses the *total* galaxy colour in the colour–magnitude diagram, whereas our $D_n(4000)$ values correspond to the *central* galaxy colour. That is, however, an asset, since, as argued in Section 4.2, the light that goes through the SDSS fibre, from which $D_n(4000)$ is measured, is in our sample *mostly* emitted by stars in the bulge, meaning that our Fig. 15 is mainly a comparison between ellipticals, classical bulges and pseudo-bulges, avoiding in most cases effects resulting from disc light. None the less, we have verified that similar results emerge if we plot the colour–magnitude diagram in its usual form, using dereddened $g - i$ Petrosian colours from the SDSS data base and absolute magnitudes from Kauffmann et al. (2003b). In such case, however, the blue cloud is not as detached from the red sequence as in Fig. 15, most likely due to dust attenuation. Our results clearly show that virtually all elliptical galaxies are found in the red sequence; and practically all galaxies with pseudo-bulges, and bulgeless galaxies, are found in the blue cloud. However, although most of the galaxies with classical bulges do indeed populate the red sequence, a significant fraction of them are found in the blue cloud (see also Fig. 9).

4.4 The fundamental plane

Elliptical galaxies follow well-defined relations between their effective radius r_e , mean effective surface brightness $\langle \mu_e \rangle$ and central velocity dispersion σ_0 , known as the fundamental plane (FP). Furthermore, it is possible to show that such relations arise in virialized systems (Djorgovski & Davis 1987; Dressler et al. 1987; Bender, Burstein & Faber 1992). Thus, the FP provides important clues on the formation processes of stellar systems. Bender et al. (1992) proposed a formulation of the FP, defining a space, whose three axes, κ_1 , κ_2 and κ_3 , are defined in terms of r_e , $\langle \mu_e \rangle$ and σ_0 , and are proportional to important physical parameters: κ_1 is proportional to the logarithm of the mass, κ_2 is proportional mainly to the logarithm of the surface brightness and κ_3 is proportional to the logarithm of

the mass-to-light ratio. Here, mass means *dynamical* mass, i.e. the stellar mass plus the dark matter mass content.

What is the locus occupied by pseudo-bulges and classical bulges in the FP? We can answer this question using r_e and $\langle \mu_e \rangle$ from our decompositions, and velocity dispersion measurements from the SDSS data base. We have chosen to use the estimates provided in the Data Release 6 (DR6), which are based on results from a direct fit to the spectra. In earlier releases, the estimates are an average of results from direct-fitting and Fourier-fitting, but the latter systematically overestimates the velocity dispersion for low-mass galaxies (Bernardi et al. 2003a; their fig. 17). In fact, we have verified that the velocity dispersion estimates from DR2 are systematically larger (by $\sim 10\text{--}20$ per cent) than those from DR6, for the galaxies in our sample, when the velocity dispersion is below $\approx 150 \text{ km s}^{-1}$. Due to the limited spectral resolution of the SDSS spectra, it is recommended to use only spectra with signal-to-noise ratio above 10, and without warning flags. We have verified that only one galaxy in our sample does not comply with the former criterion, and only eight do not comply with the latter. Before we can use these measurements, we have to apply aperture corrections due to the fact that these velocity dispersions are obtained through a fixed fibre aperture of 3 arcsec, which is physically different from galaxy to galaxy, depending on their distances. We thus used the prescription provided by Jorgensen, Franx & Kjaergaard (1995) and converted the SDSS velocity dispersion measurements to the velocity dispersion at 1/8 of r_e , σ_8 . This empirical prescription is based on measurements for elliptical and lenticular galaxies, and it is unclear if it is also valid for disc-dominated galaxies. However, the corrections applied are small, and do not affect our results significantly.

We thus calculated κ_1 , κ_2 and κ_3 for elliptical galaxies, classical bulges and pseudo-bulges, using the definitions in Bender et al. (1992), and applying an offset in surface brightness to facilitate comparison with Bender et al. (1992) and Burstein et al. (1997), who used measurements in the B band (the same procedure was also done by Bernardi et al. 2003b). The top panels of Fig. 16 show that the relation we have found for κ_3 against κ_1 , considering only elliptical galaxies, is similar to that found by Bernardi et al. (2003b), which used SDSS i -band data for a sample of nearly 9000 early-type galaxies. Bernardi et al. (2003b) used estimates of the velocity dispersion that includes Fourier-fitting results, which, as mentioned above, overestimate the velocity dispersion for low-mass galaxies. Accordingly, their relation is somewhat less steep than ours, even though they have excluded estimates below 100 km s^{-1} . We find that

$$\kappa_3 = 0.27\kappa_1 - 0.11. \quad (7)$$

In addition, classical bulges also seem to follow the same relation, although somewhat offset to higher κ_3 values, regardless of the galaxy being barred or unbarred (see also Falcón-Barroso, Peletier & Balcells 2002). Classical bulges follow more closely the relation found by Bernardi et al. (2003b). It should be noted that their sample also includes early-type *disc* galaxies. To select their sample of early-type galaxies, they have included only galaxies with the concentration index $R90/R50$ larger than 2.5. This does not mean, however, that their sample contains only elliptical galaxies. In fact, we have checked that 99 per cent of our ellipticals have $R90/R50 > 2.5$, but this is also the case for 76 per cent of our galaxies with classical bulges and 8 per cent of our galaxies with pseudo-bulges. Bernardi et al. (2003a) also used other criteria to avoid including late-type galaxies in their sample, but it is unlikely that these criteria excluded most of the galaxies with classical bulges. This can also

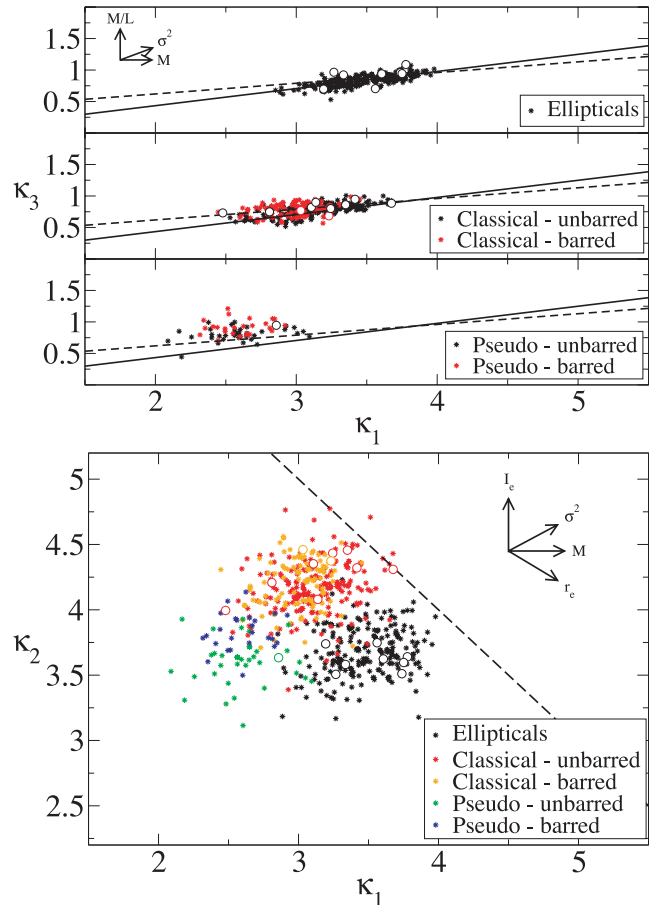


Figure 16. Elliptical galaxies, classical bulges and pseudo-bulges in the κ -space formulation of the fundamental plane (FP). The top three panels show the edge-on view of the FP, κ_3 plotted against κ_1 , while the bottom panel shows its nearly face-on view, κ_2 plotted against κ_1 . Barred and unbarred galaxies are also indicated. In the top panels, the solid line is a fit to our ellipticals, while the dashed line is the fit obtained by Bernardi et al. (2003b) for nearly 9000 early-type galaxies. The dashed line in the bottom panel shows the limit of the zone of avoidance. The arrows indicate how some important physical parameters vary across the FP. Bigger, white-filled circles represent systems with $0.5 < b/a < 0.7$, with similar colour coding.

explain why our relation for ellipticals is slightly different from theirs.

Pseudo-bulges in both barred and unbarred galaxies lie significantly and systematically above these relations. This offset cannot be attributed to effects due to dust attenuation alone. Even considering the upper limit for dust attenuation discussed in Section 4.2, such a correction will bring the points down vertically by 0.19 in κ_3 , while one sees that the offset is ≈ 0.3 , on average. In this projection, 2D Kolmogorov-Smirnov tests indicate that pseudo-bulges differ more from classical bulges than ellipticals differ from classical bulges or bulges altogether. Pseudo-bulges also lie in a locus in the $\kappa_2 \times \kappa_1$ projection of the FP which is different from those of both ellipticals and classical bulges (bottom panel of Fig. 16). Again, correcting for upper limit dust effects would put pseudo-bulges up along the κ_2 axis only by 0.27. In this projection, the statistical tests indicate that pseudo-bulges differ from classical bulges as much as ellipticals differ from classical bulges or bulges altogether. In both projections, pseudo-bulges lie in regions close to those occupied by disc-dominated galaxies (see Pierini et al. 2002). We note that barred

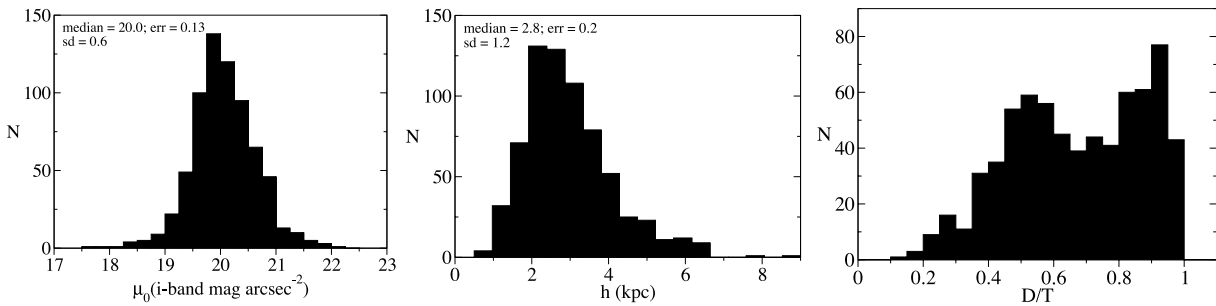


Figure 17. Distributions of μ_0 , h and D/T for all disc galaxies in the sample. The first two panels also show the values of the median and standard deviation of each distribution, as well as the mean 1σ uncertainty in individual measurements. Bin sizes are $\approx 2\sigma$.

galaxies tend to be more separated from their unbarred counterparts in the case of galaxies with pseudo-bulges, as compared to galaxies with classical bulges. Barred galaxies seem to have slightly higher values of both κ_2 and κ_3 , on average. This is also confirmed with the statistical tests. Finally, it is also worth noting that, as expected from the results in Section 4.3, systems with lower axial ratios seem to generally share the same properties as those with $b/a \geq 0.9$.

4.5 Discs

Fig. 17 shows the distributions of the disc parameters (μ_0 , h and D/T). It is worth noting that the distribution of disc-to-total ratio shows two peaks which match the peaks in the bulge-to-total ratio distributions for classical bulges and pseudo-bulges (shown in Fig. 8). The two peaks in the distribution of D/T are at about 0.5 and 0.9. Bars account typically for 10 per cent of the galaxy luminosity. In Fig. 18, we show the scaling relation between disc scalelength and central surface brightness. When one separates galaxies by their bulge type (classical versus pseudo), one sees that, on average, galaxies with pseudo-bulges have more extended discs, with fainter central surface brightness, as compared with galaxies hosting classical

bulges, albeit with significant overlap. A Kolmogorov–Smirnov test rejects the null hypothesis of no difference between such distributions at a 92 per cent confidence level. It is also interesting to ask how the stellar mass in discs varies between these two galaxy classes. The stellar mass in discs of galaxies with pseudo-bulges is, on average, $1.15 \times 10^{10} M_\odot$, whereas that in discs of galaxies with classical bulges is $1.93 \times 10^{10} M_\odot$, thus a factor of 1.7 larger. A similar factor (1.8) corresponds to bars, when present. We can also ask how do their bulge masses compare. The stellar mass within pseudo-bulges is typically $2.2 \times 10^9 M_\odot$, whereas in classical bulges this is $1.41 \times 10^{10} M_\odot$ (see Table 4), thus a factor of 6.4 larger. Hence, in terms of stellar mass, there is more similarity between discs (and bars) in galaxies with pseudo-bulges and those in galaxies with classical bulges, than between classical and pseudo-bulges themselves. Furthermore, the mean difference between the total galaxy mass of galaxies hosting pseudo-bulges and of those with classical bulges is a factor of 2. Therefore, if one scales down a typical galaxy with a classical bulge, dividing the mass of each of its components by 2, one ends up with a galaxy that has a disc (and a bar) with mass similar to that of the corresponding component in galaxies with pseudo-bulges. However, the bulge of such scaled-down galaxy is around three times more massive than the typical pseudo-bulge. If we assume that the physical processes that lead to the formation of discs and bars are the same regardless of the resulting bulge, then this difference suggests that the formation processes of classical bulges and pseudo-bulges are typically distinct.

4.6 A compendium of galaxy structural parameters

The full results from our decompositions are given in Tables 1 and 2. Table 3 shows the parameters describing the distributions (median and standard deviation), as well as the mean 1σ uncertainty in individual measurements, of μ_e , r_e and n for elliptical galaxies, classical bulges and pseudo-bulges.

Evidently, theoretical work on galaxy formation and evolution should comply with these results, either by predicting compatible structural properties or by using these results as a starting point to build realistic models. The same thing can be said about the masses of the different components, and their mass distributions, which are presented in the next section. These results are also useful to test automated procedures of bulge/disc/bar 2D decomposition, with no checking or direct human intervention at the decomposition of every single object. An automated code able to reproduce these results using the same input data (i.e. the same images) should be deemed successful and reliable to be used with much larger

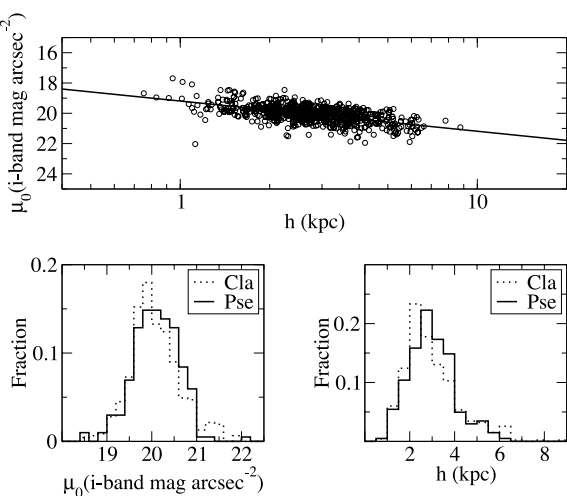


Figure 18. Scaling relation between disc scalelength and central surface brightness. The histograms at the bottom show that galaxies with pseudo-bulges have more extended discs, with fainter central surface brightness, on average, as compared with galaxies hosting classical bulges, albeit with significant overlap. A Kolmogorov–Smirnov test rejects the null hypothesis of no difference between such distributions at a 92 per cent confidence level.

Table 1. Structural parameters of bulges, discs and bars in our sample from *i*-band image fits. Galaxy identifications, uncertainties and similar tables in the *g* and *r* bands are also available. The printed version of the paper contains only a sample. The full table is available online as Supporting Information.

μ_0 (1)	h (2)	μ_e (3)	r_e (4)	n (5)	$\mu_{e,\text{bar}}$ (6)	$r_{e,\text{bar}}$ (7)	ϵ_{bar} (8)	n_{bar} (9)	L_{bar} (10)	c (11)	B/T (12)	D/T (13)	Bar/T (14)	χ^2 (15)	$\text{Seeing}_{\text{HWHM}}$ (16)	z (17)
19.41	2.10	19.72	1.24	1.29	0.0	0.0	0.0	0.0	0.0	0.0	0.35	0.64	0.0	1.14	1.32	0.067
19.16	2.40	19.89	1.82	3.54	0.0	0.0	0.0	0.0	0.0	0.0	0.48	0.51	0.0	1.42	0.68	0.047
19.25	2.18	20.54	0.52	0.94	0.0	0.0	0.0	0.0	0.0	0.0	0.03	0.96	0.0	1.65	0.45	0.043
0.0	0.0	20.19	2.73	2.57	0.0	0.0	0.0	0.0	0.0	0.0	1.0	0.0	0.0	1.03	0.91	0.063
0.0	0.0	20.46	3.12	4.32	0.0	0.0	0.0	0.0	0.0	0.0	1.0	0.0	0.0	1.02	0.82	0.056
18.95	2.42	20.89	1.33	0.82	0.0	0.0	0.0	0.0	0.0	0.0	0.08	0.91	0.0	1.66	0.94	0.065
0.0	0.0	21.23	2.32	4.53	0.0	0.0	0.0	0.0	0.0	0.0	1.0	0.0	0.0	1.18	0.67	0.046
0.0	0.0	19.69	1.63	5.15	0.0	0.0	0.0	0.0	0.0	0.0	1.0	0.0	0.0	1.56	0.94	0.044
0.0	0.0	19.97	2.08	3.78	0.0	0.0	0.0	0.0	0.0	0.0	1.0	0.0	0.0	1.61	0.65	0.045
0.0	0.0	19.55	1.36	4.50	0.0	0.0	0.0	0.0	0.0	0.0	1.0	0.0	0.0	1.29	0.68	0.047
20.03	2.59	21.52	0.65	1.72	20.92	1.39	0.69	0.51	2.11	3.0	0.02	0.92	0.04	1.67	0.55	0.047
0.0	0.0	20.64	2.03	3.12	0.0	0.0	0.0	0.0	0.0	0.0	1.0	0.0	0.0	1.83	1.00	0.047
21.41	3.21	20.22	1.45	6.48	0.0	0.0	0.0	0.0	0.0	0.0	0.69	0.31	0.0	1.30	0.56	0.047
0.0	0.0	21.05	1.98	2.47	0.0	0.0	0.0	0.0	0.0	0.0	1.0	0.0	0.0	1.24	0.51	0.042
0.0	0.0	20.86	2.38	4.01	0.0	0.0	0.0	0.0	0.0	0.0	1.0	0.0	0.0	1.28	0.66	0.046
20.17	1.84	20.94	2.02	4.18	20.56	1.73	0.63	0.74	5.08	2.4	0.58	0.29	0.12	1.54	0.61	0.042
20.78	3.25	21.36	0.58	1.17	0.0	0.0	0.0	0.0	0.0	0.0	0.03	0.96	0.0	0.91	0.71	0.049
0.0	0.0	20.16	1.48	3.17	0.0	0.0	0.0	0.0	0.0	0.0	1.0	0.0	0.0	1.53	0.55	0.047
20.80	3.91	21.07	2.11	3.01	20.01	1.52	0.62	0.86	4.15	2.36	0.0	0.0	0.0	1.76	0.95	0.046
20.33	2.6	21.66	1.77	3.88	0.0	0.0	0.0	0.0	0.0	0.0	0.34	0.65	0.0	2.02	0.94	0.045

Columns (1) and (2) show the disc central surface brightness and scalelength, respectively. Columns (3) to (5) give, respectively, bulge effective surface brightness, effective radius and the Sérsic index. Bar parameters are given in columns (6) to (11), respectively, effective surface brightness, effective radius, ellipticity, the Sérsic index, semimajor axis and boxiness. Bulge-to-total, disc-to-total and bar-to-total luminosity ratios are given in columns (12), (13) and (14), respectively. The χ^2 value of the fit is shown in column (15). Finally, columns (16) and (17) show, respectively, the seeing HWHM of the observation and the galaxy redshift. Intensities are in units of mag arcsec $^{-2}$ and lengths in kpc. Seeing is in arcsec.

samples, which are lately becoming commonly available. The results from our image decompositions are available for download.⁴ These include all structural parameters of bulges, discs and bars in the *g*, *r* and *i* bands, absolute magnitudes and integrated $g - i$ and $r - i$ colours of each component separately, as well as model images for the whole galaxy and for each component separately.

4.7 The stellar mass and luminosity budgets at $z \sim 0$

With the $g - i$ integrated colour of each galaxy component, we have obtained the corresponding mass-to-light ratio in the *i* band, using the results found by Kauffmann et al. (2007, see their fig. 15). They showed that the mass-to-light ratio in the *i* band is well correlated with $g - i$ colour over a range of more than a factor of 10 in the mass-to-light ratio and with a scatter of less than 0.1 dex. They found that the $g - i$ colour is the colour that shows the tightest relation with the mass-to-light ratio. Furthermore, Bell & de Jong (2001) showed that the combined effects of stellar age and dust attenuation are such that the stellar masses obtained here with these mass-to-light ratios are not significantly affected by dust.

With the mass-to-light ratio and the total luminosity of each component, we were thus able to calculate the stellar mass content in each component separately. Interestingly, we have verified that the total mass in each galaxy, calculated by adding the masses of the individual galaxy components, agrees very well with the galaxy stellar mass estimated in Kauffmann et al. (2003b), with a scatter of less than 0.02 dex. The parameters that characterize the stellar mass distributions of each galaxy component (median and standard

deviation) are shown in Table 4. All such distributions are skewed towards lower mass values.

We were also able to compute the fraction of the total stellar mass content in our galaxies contained within each component separately, thus obtaining the stellar mass budget in the local universe for massive galaxies (more massive than $10^{10} M_\odot$). The following figures take into account the selection effect due to our axial ratio cut discussed in Section 2. Elliptical galaxies contain 32 per cent of the total stellar mass, and the corresponding values for discs, bulges and bars are, respectively, 36, 28 and 4 per cent. Classical bulges contain 25 per cent of the total stellar mass, while pseudo-bulges contain 3 per cent. Hence, 11 per cent of the stellar mass in bulges are in pseudo-bulges, the remaining being in classical bulges. The uncertainty in these fractions from Poisson statistics only is between 1 and 2 per cent points.

The corresponding luminosity fractions are as follows: 27 per cent of the total luminosity from the galaxies in our sample (in the *i* band) come from elliptical galaxies, 46 per cent from discs, 24 per cent from bulges and 3 per cent from bars. Classical bulges emit 20 per cent of the total luminosity, while pseudo-bulges account for 4 per cent. Hence, 16 per cent of the luminosity from bulges come from pseudo-bulges, the remaining coming from classical bulges.

As expected, luminosity ratios, such as the bulge-to-total ratio B/T , change in different bands. For pseudo-bulges, the median value of B/T in the *g* band is 0.053, whereas in the *i* band it is 0.075. For classical bulges, the median value of B/T in the *g* band is 0.349, and in the *i* band is 0.377. The median value of Bar/T also increases from 0.087 in the *g* band to 0.095 in the *i* band. The median value of D/T decreases from 0.702 in the *g* band to 0.684 in the *i* band.

It is also worth noting the fraction in number corresponding to the different galaxy categories. From the total number of galaxies in

⁴ See <http://www.mpa-garching.mpg.de/~dimitri/buddaonsdss/buddaonsdss.html>.

Table 2. Absolute magnitudes and integrated colours of bulges, discs and bars in our sample from the BUDDA models. The printed version of the paper contains only a sample. The full table is available online as Supporting Information.

$M_d(g)$ (1)	$M_d(r)$ (2)	$M_d(i)$ (3)	$M_b(g)$ (4)	$M_b(r)$ (5)	$M_b(i)$ (6)	$M_{\text{bar}}(g)$ (7)	$M_{\text{bar}}(r)$ (8)	$M_{\text{bar}}(i)$ (9)	$(g-i)_d$ (10)	$(r-i)_d$ (11)	$(g-i)_b$ (12)	$(r-i)_b$ (13)	$(g-i)_{\text{bar}}$ (14)	$(r-i)_{\text{bar}}$ (15)
-19.74	-20.57	-20.96	-19.33	-19.93	-20.33	0.0	0.0	0.0	1.22	0.38	1.00	0.39	0.0	0.0
-20.17	-20.87	-21.34	-19.40	-20.68	-21.26	0.0	0.0	0.0	1.17	0.46	1.86	0.58	0.0	0.0
-20.17	-20.64	-20.93	-15.81	-16.86	-17.23	0.0	0.0	0.0	0.76	0.29	1.42	0.37	0.0	0.0
0.0	0.0	0.0	-20.67	-21.39	-21.73	0.0	0.0	0.0	0.0	0.0	1.06	0.34	0.0	0.0
0.0	0.0	0.0	-20.61	-21.37	-21.82	0.0	0.0	0.0	0.0	0.0	1.21	0.45	0.0	0.0
-20.69	-21.25	-21.54	-15.50	-18.43	-18.97	0.0	0.0	0.0	0.84	0.29	3.47	0.53	0.0	0.0
0.0	0.0	0.0	-19.17	-20.13	-20.53	0.0	0.0	0.0	0.0	0.0	1.35	0.4	0.0	0.0
0.0	0.0	0.0	-19.86	-20.79	-21.33	0.0	0.0	0.0	0.0	0.0	1.46	0.53	0.0	0.0
0.0	0.0	0.0	-20.15	-20.99	-21.42	0.0	0.0	0.0	0.0	0.0	1.27	0.43	0.0	0.0
0.0	0.0	0.0	-19.50	-20.51	-20.95	0.0	0.0	0.0	0.0	0.0	1.44	0.43	0.0	0.0
-19.89	-20.34	-20.61	-14.60	-16.17	-16.75	-16.76	-17.07	-17.42	0.71	0.26	2.15	0.57	0.66	0.34
0.0	0.0	0.0	-19.25	-20.10	-20.67	0.0	0.0	0.0	0.0	0.0	1.42	0.56	0.0	0.0
-18.31	-19.23	-19.64	-19.26	-20.12	-20.51	0.0	0.0	0.0	1.32	0.41	1.24	0.39	0.0	0.0
0.0	0.0	0.0	-18.99	-19.80	-20.15	0.0	0.0	0.0	0.0	0.0	1.15	0.35	0.0	0.0
0.0	0.0	0.0	-19.66	-20.31	-20.70	0.0	0.0	0.0	0.0	0.0	1.03	0.38	0.0	0.0
-18.84	-19.48	-19.80	-19.46	-20.22	-20.53	-17.72	-18.74	-18.82	0.96	0.32	1.07	0.30	1.09	0.07
-19.67	-20.16	-20.39	-15.23	-16.32	-16.74	0.0	0.0	0.0	0.72	0.23	1.51	0.42	0.0	0.0
0.0	0.0	0.0	-19.17	-20.01	-20.40	0.0	0.0	0.0	0.0	0.0	1.23	0.38	0.0	0.0
-19.41	-20.19	-20.68	-19.33	-20.35	-20.62	-17.87	-18.82	-19.14	1.27	0.49	1.28	0.26	1.27	0.32
-19.39	-20.19	-20.34	-19.01	-17.96	-19.66	0.0	0.0	0.94	0.14	0.65	1.70	0.0	0.0	0.0

Columns (1) to (3) show the disc absolute magnitude in the g , r and i bands, respectively. Columns (4) to (9) show the same parameters for bulge and bar, respectively, as indicated. Columns (10) and (11), (12) and (13) and (14) and (15) give the integrated $(g-i)$ and $(r-i)$ colours of disc, bulge and bar, respectively, as indicated.

Table 3. Parameters describing the distributions (median and standard deviation), as well as the mean 1σ uncertainty in individual measurements, of μ_e , r_e and n for elliptical galaxies, classical bulges and pseudo-bulges from the i -band decompositions.

	μ_e (mag arcsec $^{-2}$)			r_e (kpc)			n		
	Median	SD	1σ	Median	SD	1σ	Median	SD	1σ
Elliptical	20.8	0.4	0.10	3.0	1.0	0.15	3.8	0.9	0.5
Classical	19.6	0.4	0.05	1.0	0.4	0.03	3.4	1.3	0.4
Pseudo	20.5	0.5	0.07	0.7	0.3	0.03	1.5	0.9	0.2

Table 4. Parameters describing the distributions (median and standard deviation) of the stellar mass in elliptical galaxies, classical bulges, pseudo-bulges, discs and bars.

	Median ($10^{10} M_\odot$)	SD ($10^{10} M_\odot$)
Ellipticals	5.15	4.37
Classical	1.41	1.98
Pseudo	0.22	0.99
Discs	1.66	1.62
Bars	0.40	0.61

our sample, 22 per cent are ellipticals, 76 per cent are disc galaxies with bulges and 2 per cent are bulgeless galaxies (i.e. pure discs). Within disc galaxies with bulges, 68 per cent host classical bulges, while 32 per cent have pseudo-bulges. Bars are found in 42 per cent of all disc galaxies.

5 DISCUSSION

5.1 Comparison with previous work

Allen et al. (2006) also performed parametric decomposition of a large sample of galaxy images. As mentioned in Introduction,

their sample is significantly larger than ours, but our methodology aims at a more careful analysis. They found that the stellar mass content in the local universe is distributed as 13 per cent in elliptical galaxies, 58 per cent in discs, 26 per cent in classical bulges, 1.5 per cent in pseudo-bulges and the remainder in low-luminosity blue spheroids (Driver et al. 2007a, see also Benson et al. 2007 who found that 35–51 per cent of the stellar mass is in discs). The figures do not change substantially when dust is taken into account (Driver et al. 2007b). A direct comparison with our results is difficult, since their sample was not selected with a cut in stellar mass. As we avoided low-mass galaxies, it is natural to expect that we find a larger fraction of the local stellar mass in ellipticals, and a corresponding lower fraction in discs. Interestingly, however, their fraction of stellar mass in classical bulges is similar to what we find. This is somewhat unexpected, considering the different sample selection criteria, since their sample should contain a larger fraction of disc-dominated galaxies than our sample. This might be explained by the absence of a bar component in their models. As discussed in Gadotti (2008), it is possible to obtain good (but wrong) fits for barred galaxies, with no bar component in the model, because the bulge model absorbs the bar. Thus, their bulge-to-total luminosity ratios could be overestimated. They have considered pseudo-bulges as those with $B/T < 0.5$ and $r_e/h < 0.5$, and found them to be

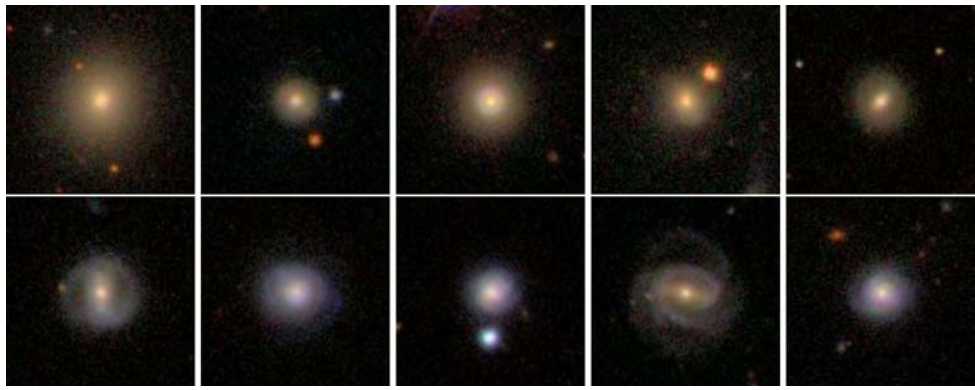


Figure 19. Examples of galaxies hosting classical bulges with $D_n(4000) \geq 1.7$ (top panel) and $D_n(4000) < 1.7$ (bottom panel). It is evident that the latter shows more often spiral structure and blue discs.

generally bluer than the remaining bulges. From our Fig. 14, one sees that such criteria still include many classical bulges. However, they found a stellar content in pseudo-bulges smaller than ours, albeit within the uncertainties. A possible explanation for that could be that a number of their pseudo-bulges were smoothed out by the PSF. Although they have secured that the galaxies in their sample have effective radii larger than the PSF HWHM, it was shown in Gadotti (2008) that it is the effective radius of the *bulge* that has to be considered, and not that of the whole galaxy. This issue is aggravated in Benson et al. (2007), who used SDSS images up to a redshift of 0.3.

In order to try a more meaningful comparison with the results in Driver et al. (2007a), we can assume that all galaxies with stellar masses below $10^{10} M_\odot$ are pure discs. This certainly underestimates the stellar mass content in bars and pseudo-bulges, but can give us a reasonable assessment of the distribution of stellar mass in discs, ellipticals and classical bulges, as if we have made no mass cut. Using the stellar mass function derived by Bell et al. (2003), using *g*-band data for a local sample of SDSS galaxies, we find that 22 per cent of the stellar mass in the local universe is in galaxies with stellar masses below $10^{10} M_\odot$. If all this mass is in discs, then our local stellar mass budget becomes as follows. Discs contain 50 per cent of the stellar mass, ellipticals contain 25 per cent of stellar mass, classical bulges and pseudo-bulges contribute with, respectively, 20 and 2 per cent, and finally bars contain 3 per cent of the stellar mass. One thus sees a more reasonable agreement, although we find a somewhat larger mass fraction in ellipticals.

In Gadotti (2008), it was argued, with indirect means, that the stellar mass content in bars at $z \sim 0$ is ≈ 12 per cent of the total stellar mass (see also Weinzierl et al. 2008), which is a factor of 3 larger than what we find here. This discrepancy can be explained, at least partially, by two factors. First, the bar fraction assumed in the previous work is 70 per cent, which is typically found in studies dedicated to estimate this value (see e.g. Eskridge et al. 2000), whereas the fraction of disc galaxies with bars in this work is 42 per cent. Secondly, we have selected our galaxy sample avoiding galaxies with low stellar mass. Thus, the stellar mass budget we find concerns massive galaxies, and it is thus biased in favour of ellipticals, which cannot contain the bars we are addressing here. The fact that our bar fraction is low can also be explained by two factors. First, as discussed in Section 3, we miss most of the short bars, due to the limited spatial resolution in SDSS images. Secondly, bar fraction seems to be larger in low-mass galaxies than in more massive galaxies (Barazza, Jogee & Marinova 2008).

5.2 Classical bulges with star formation

One interesting finding from Figs 9 and 15 is that while pseudo-bulges show almost always intense star formation, classical bulges can either be quiescent or forming young stars. This indicates that galaxies with classical bulges can be further divided according to their values of $D_n(4000)$. We have thus separated classical bulges in two different categories, namely those with $D_n(4000) < 1.7$ and those with $D_n(4000) \geq 1.7$, and find that these categories have typically different bulge-to-total ratios and stellar masses. Galaxies hosting classical bulges with $D_n(4000) < 1.7$ have median values of $B/T = 0.26$ and mass equal to $0.8 \times 10^{10} M_\odot$, whereas those with $D_n(4000) \geq 1.7$ have median values of $B/T = 0.42$ and mass equal to $1.8 \times 10^{10} M_\odot$. This suggests that the former are dominated by early-type spirals whereas the latter are mostly lenticular galaxies. To verify that we have inspected randomly selected samples of these two galaxy categories and concluded that, in fact, galaxies hosting classical bulges with $D_n(4000) < 1.7$ show more often spiral structure and blue discs than galaxies hosting classical bulges with $D_n(4000) \geq 1.7$ (see Fig. 19). In addition, we show in Fig. 20 that these galaxies have markedly different distributions of the concentration index $R90/R50$. Furthermore, galaxies with pseudo-bulges also show a distribution of $R90/R50$ distinct from that of both categories of galaxies with classical bulges. Elliptical galaxies, however, have a $R90/R50$ distribution more similar to that of galaxies with classical bulges and $D_n(4000) \geq 1.7$. We thus see three peaks in the distribution of concentration. A related finding is reported in Bailin & Harris (2008). As expected, the median Sérsic index of star-forming classical bulges is 2.8, thus lower than that of quiescent classical bulges, for which it is 3.6.

A plausible explanation for the existence of galaxies hosting classical bulges with conspicuous star formation activity is the co-existence of a classical bulge and a pseudo-bulge in the same galaxy. This would naturally occur if, after the formation of the classical bulge (e.g. via a minor merger), the galaxy disc develops an instability (such as a bar) able to induce the observed central star formation through processes of secular evolution.⁵ Since pseudo-bulges are about an order of magnitude less massive than classical bulges (see

⁵ Another possibility is that star-forming classical bulges are those caught during a minor merger that enhances central star formation and will eventually help building the bulge. However, note that we have rejected galaxies with disturbed morphologies (Section 2).

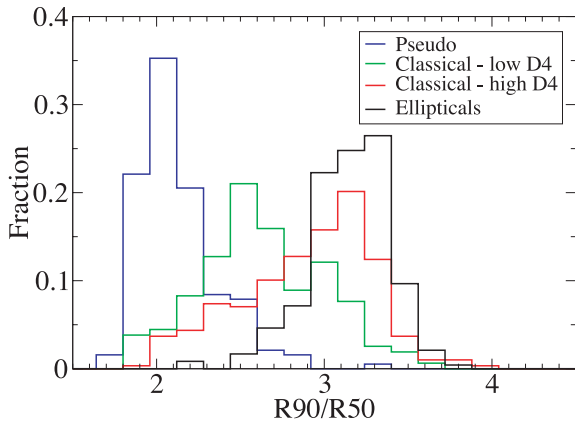


Figure 20. Distribution of concentration ($R90/R50$) for pseudo-bulges, classical bulges with $D_n(4000) < 1.7$, classical bulges with $D_n(4000) \geq 1.7$ and elliptical galaxies.

Table 4), such *composite bulges* would have the structural signature of a classical bulge, concurrent with the star formation activity of a pseudo-bulge, as observed. The fact that the $D_n(4000)$ values of star-forming classical bulges and pseudo-bulges are similar (see Fig. 9) is consistent with this picture. Interestingly, we find that 34 per cent of galaxies with classical bulges have $D_n(4000) < 1.7$ (50 per cent of which hosting bars), the remainder having $D_n(4000) \geq 1.7$ (with a fraction of barred galaxies of 40 per cent). Such excess of bars among star-forming classical bulges is also generally consistent with the picture of a composite bulge. In this context, it is worth noting that classical bulges with star formation lie between pseudo-bulges and classical bulges without star formation in the density plot of Fig. 8 (i.e. between the lower dashed line and the solid line), and also have intermediate masses, as mentioned above (see also Table 4). They thus bridge pseudo-bulges and classical bulges without star formation in the mass-size relation in Fig. 13. If such a picture is correct, then the Hubble classification could be understood as mainly a sequence that goes from elliptical galaxies successively to disc galaxies with classical bulges, composite bulges and pseudo-bulges.

5.3 Formation of bulges and ellipticals

The results in Section 4 all corroborate previous ideas that bulges, as identified through their photometrical properties, are present in two main classes, with distinct structural properties, indicating different formation processes. Those more similar to elliptical galaxies, namely classical bulges, seem to be formed through violent processes, such as hierarchical clustering, whereas those dissimilar bulges, namely pseudo-bulges, seem to be still under formation processes, more likely as a result of their host galaxies' slow internal evolution, which involves disc instabilities and angular momentum transfer.

These inferences are borne out by the fact that pseudo-bulges, when compared to their classical counterparts, have currently intense star formation activity (Figs 9 and 15), are less concentrated at the fixed bulge-to-total ratio (Fig. 14) and occupy the same locus in the FP as discs (Fig. 16). The bulge Sérsic index correlates with the bulge-to-total ratio for classical bulges but not for pseudo-bulges (Fig. 11). In addition, pseudo-bulges follow a mass-size relation similar to that followed by bars, and different from that followed by classical bulges (Fig. 13). Furthermore, the discs (and bars) in

galaxies that host pseudo-bulges are not as different from those in galaxies that host classical bulges as pseudo-bulges are different from classical bulges, in what concerns their relative stellar masses (Section 4.5). This suggests that disc and bar formations are similar in both galaxy classes, whereas bulge formation is distinct.

However, we have also found indications that the processes that lead to the formation of classical and pseudo-bulges might happen concomitantly. In this context, the processes that lead to the formation of a pseudo-bulge are dominant at one end, while those that lead to the formation of a classical bulge are dominant at the other end, across the bulge population. This is suggested by the significant overlap in the distributions of bulges with $n > 2$ and $n < 2$ in the Kormendy relation (Fig. 8), which is in fact statistically more significant than the overlap in the distributions of ellipticals and bulges altogether, as discussed in Section 4.2. We have also found classical bulges with young stellar populations, typical of pseudo-bulges (Fig. 9). Furthermore, although classical and pseudo-bulges have significantly different slopes for their mass-size relations, such relations join smoothly with pseudo-bulges at the low-mass end, and with classical bulges at the high-mass end (Fig. 13).

Classical bulges seem to bear some structural similarity to ellipticals, since they follow the same Kormendy relation (Fig. 8), and occupy a similar locus in the edge-on view of the FP (Fig. 16). However, they also follow offset mass-size relations (Fig. 13). This could, in principle, challenge the idea that classical bulges are simply ellipticals that happen to be surrounded by a disc. It should be noted, though, that this result concerns only massive ellipticals. Low-luminosity ellipticals could, if surrounded by a disc, resemble classical bulges, but this cannot be evaluated with the present data. We have verified that accounting for systematic effects could bring some of the low-mass ellipticals closer to the relation followed by classical bulges. Our tests indicate that such systematic effects should be restricted to about 10 per cent of the ellipticals. In the worst case scenario that all ellipticals are affected by systematic effects, the offset between the mass-size relations of classical bulges and ellipticals would still be present, but restricted to high-mass systems. Thus, the result that high-mass bulges cannot be considered as high-mass ellipticals surrounded by discs seems to be robust. We note that in the face-on view of the FP (Fig. 16), pseudo-bulges, classical bulges and ellipticals occupy three significantly distinct loci, which should provide clues to the different formation and evolution processes.

6 SUMMARY AND CONCLUSIONS

We have determined several structural parameters for elliptical galaxies, bulges, discs and bars through reliable multiband image fitting of a representative sample of nearly 1000 local, massive galaxies in the SDSS. We showed that the Petrosian concentration index is a better proxy for the bulge-to-total ratio than the global Sérsic index.

We showed that, while the bulge Sérsic index can be considered as a criterion to distinguish pseudo-bulges from classical bulges, a more reliable, and physically motivated, separation can be made using the Kormendy relation. While classical bulges follow the relation set by ellipticals, pseudo-bulges do not, independently of their Sérsic index. This shows that classical bulges bear some structural similarity to elliptical galaxies, while pseudo-bulges are structurally different.

Using $D_n(4000)$, which is insensitive to dust attenuation, we demonstrated that pseudo-bulges are currently undergoing intense star formation activity, and that virtually all pseudo-bulges are

located in the blue cloud of the colour–magnitude diagram. In contrast, most (but not all) classical bulges are quiescent and populate the red sequence of the diagram. We presented evidence of different formation mechanisms for classical and pseudo-bulges. Classical bulges follow a correlation between the Sérsic index and bulge-to-total ratio, while pseudo-bulges do not. The latter are less concentrated than the former at the fixed bulge-to-total ratio. The locus occupied by pseudo-bulges in the fundamental plane is different from that of classical bulges, and it is the same as that of discs. Furthermore, pseudo-bulges follow a mass–size relation different from that of classical bulges, and similar to that of bars. Altogether, this indicates that pseudo-bulges are formed through slow, non-violent processes, such as those expected from disc instabilities, whereas classical bulges are formed through violent processes, such as the merging of smaller units. We verified, however, a significant overlap in the properties of classical and pseudo-bulges, which suggests that the different formation processes might happen concomitantly, with different processes being dominant in different cases.

We found that classical bulges and ellipticals follow offset mass–size relations, suggesting that high-mass bulges cannot be considered as high-mass ellipticals that happen to be surrounded by a disc.

We provided distributions and typical values (including uncertainties in individual measurements) of all structural parameters obtained (with the exception of bar parameters, which will be addressed in a separate paper). We calculated the stellar mass content and distribution for each galaxy component, and showed that, considering galaxies more massive than $10^{10} M_{\odot}$, in the local universe, 32 per cent of the total stellar mass is contained in ellipticals, and the corresponding values for discs, bulges and bars are, respectively, 36, 28 and 4 per cent. Classical bulges contain 25 per cent of the total stellar mass, while pseudo-bulges contain 3 per cent. We also provided the corresponding luminosity and number fractions. In particular, we find that approximately a third of disc galaxies hosts pseudo-bulges. Such figures should be reproduced by successful models of galaxy formation and evolution.

ACKNOWLEDGMENTS

I am grateful to Guinevere Kauffmann for her support throughout this work and many useful discussions. Her input is greatly appreciated. It is a pleasure to thank Simone Weinmann for her help in producing Fig. 6 and useful discussions, and Jarle Brinchmann for producing the cutouts and detailed image headers of our parent sample. I have benefitted from useful and stimulating discussions with Lia Athanassoula, Eugene Churazov, Peter Erwin, David Fisher, Alister Graham, Tim Heckman, Jochen Liske, Daniele Pierini and Simon White throughout the writing of this paper. I thank an anonymous referee for comments that helped to improve the paper. DAG is supported by the Deutsche Forschungsgemeinschaft priority program 1177 ('Witnesses of Cosmic History: Formation and Evolution of Galaxies, Black Holes and their Environment') and the Max Planck Society. The Sloan Digital Sky Survey (SDSS) is a joint project of The University of Chicago, Fermilab, the Institute for Advanced Study, the Japan Participation Group, The Johns Hopkins University, Los Alamos National Laboratory, the Max-Planck Institute for Astronomy (MPIA), the Max-Planck Institute for Astrophysics (MPA), New Mexico State University, Princeton University, the United States Naval Observatory and the University of Washington. Apache Point Observatory, site of the SDSS telescopes, is operated by the Astrophysical Research Consortium (ARC). Funding for the project has been provided by the Alfred P. Sloan Foundation, the

SDSS member institutions, the National Aeronautics and Space Administration, the National Science Foundation, the US Department of Energy, the Japanese Monbukagakusho and the Max Planck Society. The SDSS Web site is <http://www.sdss.org/>.

REFERENCES

- Allen P. D., Driver S. P., Graham A. W., Cameron E., Liske J., de Propris R., 2006, MNRAS, 371, 2
 Athanassoula E., 2005, MNRAS, 358, 1477
 Athanassoula E., Morin S., Wozniak H., Puy D., Pierce M. J., Lombard J., Bosma A., 1990, MNRAS, 245, 130
 Bailin J., Harris W. E., 2008, MNRAS, 385, 1835
 Balcells M., Graham A. W., Peletier R. F., 2007, ApJ, 665, 1104
 Barazza F. D., Jogee S., Marinova I., 2008, ApJ, 675, 1194
 Barmby P., McLaughlin D. E., Harris W. E., Harris G. L. H., Forbes D. A., 2007, AJ, 133, 2764
 Bell E. F., de Jong R. S., 2001, ApJ, 550, 212
 Bell E. F., McIntosh D. H., Katz N., Weinberg M. D., 2003, ApJS, 149, 289
 Bell E. F., Zheng X. Z., Papovich C., Borch A., Wolf C., Meisenheimer K., 2007, ApJ, 663, 834
 Bender R., Burstein D., Faber S. M., 1992, ApJ, 399, 462
 Benson A. J., Džanović D., Frenk C. S., Sharples R., 2007, MNRAS, 379, 841
 Bernardi M. et al., 2003a, AJ, 125, 1817
 Bernardi M. et al., 2003b, AJ, 125, 1866
 Blanton M. R. et al., 2003, ApJ, 594, 186
 Blanton M. R., Eisenstein D., Hogg D. W., Schlegel D. J., Brinkmann J., 2005a, ApJ, 629, 143
 Blanton M. R. et al., 2005b, AJ, 129, 2562
 Burstein D., Bender R., Faber S., Nolthenius R., 1997, AJ, 114, 1365
 Caon N., Capaccioli M., D'Onofrio M., 1993, MNRAS, 265, 1013
 Carollo C. M., 1999, ApJ, 523, 566
 Carollo C. M., Stiavelli M., de Zeeuw P. T., Mack J., 1997, AJ, 114, 2366
 Courteau S., de Jong R. S., Broeils A. H., 1996, ApJ, 457, L73
 De Lucia G. et al., 2007, MNRAS, 374, 809
 de Souza R. E., Gadotti D. A., dos Anjos S., 2004, ApJS, 153, 411
 de Vaucouleurs G., 1948, Ann. Astrophys., 11, 247
 Djorgovski S., Davis M., 1987, ApJ, 313, 59
 Dressler A., Lynden-Bell D., Burstein D., Davies R. L., Faber S. M., Terlevich R., Wegner G., 1987, ApJ, 313, 42
 Driver S. P., Allen P. D., Liske J., Graham A. W., 2007a, ApJ, 657, L85
 Driver S. P., Popescu C. C., Tuffs R. J., Liske J., Graham A. W., Allen P. D., de Propris R., 2007b, MNRAS, 379, 1022
 Driver S. P., Popescu C. C., Tuffs R. J., Graham A. W., Liske J., Baldry I., 2008, ApJ, 678, L101
 Drory N., Fisher D. B., 2007, ApJ, 664, 640
 Durbala A., Sulentic J. W., Buta R., Verdes-Montenegro L., 2008, MNRAS, 136, 773
 Elmegreen B. G., Elmegreen D. M., 1985, ApJ, 288, 438
 Eskridge P. B. et al., 2000, AJ, 119, 536
 Falcón-Barroso J., Peletier R. F., Balcells M., 2002, MNRAS, 335, 741
 Fasano G., Franceschini A., 1987, MNRAS, 225, 155
 Fisher D. B., 2006, ApJ, 642, L17
 Fisher D. B., Drory N., 2008, AJ, 136, 773
 Freeman K. C., 1970, ApJ, 160, 811
 Gadotti D. A., 2008, MNRAS, 384, 420
 Gadotti D. A., dos Anjos S., 2001, AJ, 122, 1298
 Gadotti D. A., Athanassoula E., Carrasco L., Bosma A., de Souza R. E., Recillas E., 2007, MNRAS, 381, 943
 Gallazzi A., Charlot S., Brinchmann J., White S. D. M., Tremonti C. A., 2005, MNRAS, 362, 41
 Gladders M. D., Lopez-Cruz O., Yee H. K. C., Kodama T., 1998, ApJ, 501, 571
 Graham A. W., Prieto M., 1999, ApJ, 524, L23
 Graham A. W., Worley C. C., 2008, MNRAS, 388, 1708
 Häussler B. et al., 2007, ApJS, 172, 615

- Heckman T. M., Kauffmann G., Brinchmann J., Charlot S., Tremonti C., White S. D. M., 2004, ApJ, 613, 109
- Hubble E. P., 1926, ApJ, 64, 321
- Jorgensen I., Franz M., Kjaergaard P., 1995, MNRAS, 276, 1341
- Kauffmann G. et al., 2003a, MNRAS, 346, 1055
- Kauffmann G. et al., 2003b, MNRAS, 341, 33
- Kauffmann G., White S. D. M., Heckman T. M., Ménard B., Brinchmann J., Charlot S., Tremonti C., Brinkmann J., 2004, MNRAS, 353, 713
- Kauffmann G. et al., 2007, ApJS, 173, 357
- Kissler-Patig M., Jordán A., Bastian N., 2006, A&A, 448, 1031
- Kormendy J., 1977, ApJ, 218, 333
- Kormendy J., Kennicutt R. C., Jr, 2004, ARA&A, 42, 603
- Kormendy J., Cornell M. E., Block D. L., Knapen J. H., Allard E. L., 2006, ApJ, 642, 765
- Laurikainen E., Salo H., Buta R., Knapen J. H., 2007, MNRAS, 381, 401
- Moffat A. F. J., 1969, A&A, 3, 455
- Morelli L. et al., 2008, MNRAS, 389, 341
- Moriondo G., Giovanelli R., Haynes M. P., 1998, A&A, 338, 795
- Pierini D., Gavazzi G., Franzetti P., Scodellaggio M., Boselli A., 2002, MNRAS, 332, 422
- Press W. H., Teukolsky S. A., Vetterling W. T., Flannery B. P., 1992, Numerical recipes in FORTRAN. The Art of Scientific Computing, 2nd edn. Cambridge Univ. Press, Cambridge
- Reese A. S., Williams T. B., Sellwood J. A., Barnes E. L., Powell B. A., 2007, AJ, 133, 2846
- Roberts M. S., Haynes M. P., 1994, ARA&A, 32, 115
- Sellwood J. A., Wilkinson A., 1993, Rep. Prog. Phys., 56, 173
- Sérsic J. L., 1968, Atlas de Galaxias Australes. Observatorio Astronomico, Cordoba, Argentina
- Sommer-Larsen J., Dolgov A., 2001, ApJ, 551, 608
- Weinzirl T., Jogee S., Khochfar S., Burkert A., Kormendy J., 2008, preprint (arXiv:0807.0040)
- Wyse R. F. G., Gilmore G., Franx M., 1997, ARA&A, 35, 637

APPENDIX A: FIT SENSITIVITY TO INPUT PARAMETERS

As mentioned in Section 3, image fitting often involves finding a χ^2 global minimum in a very complex multidimensional parameter space. This means that, in principle (and depending on the algorithm used), fits can be very sensitive to the initial guesses given to the

fitting code to start the first iteration. To avoid erroneous results, we have opted to produce and check each fit individually. Nevertheless, this alone does not mean that we find the most appropriate set of input parameters in all cases.

In order to check how sensitive the results of our fits are to the set of initial guesses provided to BUDDA, we have performed the following tests. We have randomly selected 20 barred galaxies, and produced test fits, in which the input values for μ_0 , h , μ_e , r_e and n used in the corresponding final fits are increased by a factor of 2 (for 10 of these galaxies) or decreased by a factor of 2 (for the remaining 10 galaxies). The choice for barred galaxies assures that the results from these tests concern typically difficult fits. Also note that a factor of 2 is rather large, and that 20 galaxies correspond to 7 per cent of our barred galaxies. Fig. A1 shows the results from these test fits, as compared to those from the final fits. Error bars are 1σ uncertainties estimated by BUDDA. Its current version does not provide estimates of the uncertainty in B/T . Thus, for B/T , typical error bars are shown, calculated through error propagation using the uncertainties in μ_e , r_e and n , and assuming that the main source of error in B/T comes from determining the total bulge luminosity. Through similar tests with BUDDA, Durbala et al. (2008) found comparable uncertainties in B/T (albeit somewhat smaller).

One sees that, in most cases, the code converges to similar results, even for input parameters varying by a factor of 4. In fact, most results are consistent within the estimated uncertainties. All outliers come from the few fits that resulted in notably high χ^2 values. Furthermore, these results reinforce the findings in Gadotti (2008) by indicating that disc parameters are particularly robust, and that B/T is a more robust parameter than n , which can have large uncertainties compared to its dynamical range. These results also argue in favour of our method to identify pseudo-bulges, at least for statistical studies such as ours, since μ_e and r_e are also more stable than n .

These results do not mean that any reasonable set of input parameters is appropriate. But they show that, by creating input parameters through a careful inspection of each galaxy individually, we are able to achieve robust results. In fact, as noted above, wrong fits often result in significantly higher χ^2 values (see leftmost panel in Fig. A1).

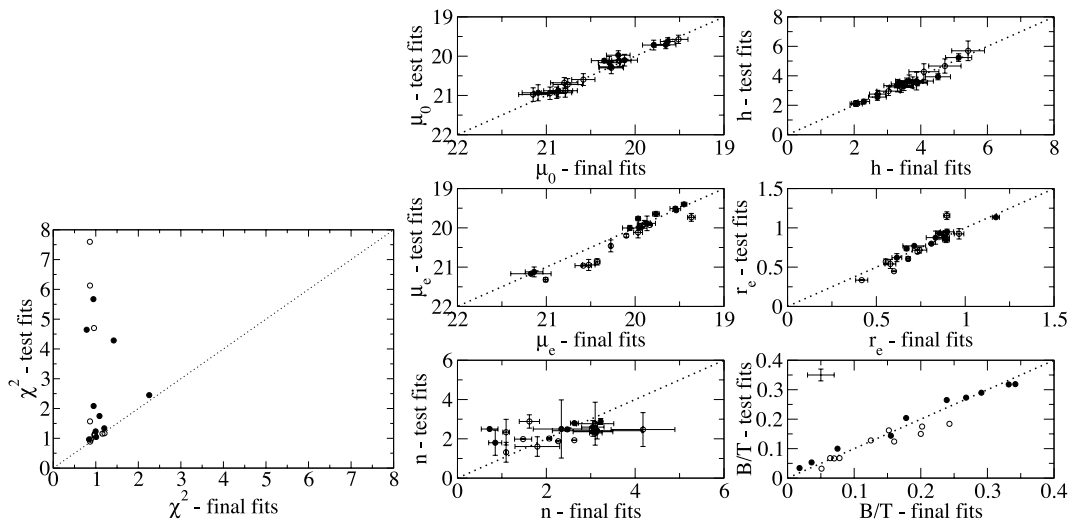


Figure A1. Comparison between the results from test and final fits in 20 barred galaxies. Filled circles refer to tests where the input parameters were multiplied by two, while empty circles refer to tests where the input parameters were divided by two. Error bars are 1σ uncertainties estimated by the fitting code. For B/T , typical error bars are shown, calculated through error propagation using the uncertainties in μ_e , r_e and n .

turning them, generally, easy to recognize in our procedure. Only 2.5 per cent of our final fits have $\chi^2 > 2$.

SUPPORTING INFORMATION

Additional Supporting Information may be found in the online version of this article.

Table 1. Structural parameters of bulges, discs and bars in our sample from *i*-band image fits. Galaxy identifications, uncertainties and similar tables in the *g* and *r* bands are also available.

Table 2. Absolute magnitudes and integrated colours of bulges, discs and bars in our sample from the BUDDA models.

Please note: Wiley-Blackwell are not responsible for the content or functionality of any supporting materials supplied by the authors. Any queries (other than missing material) should be directed to the corresponding author for the article.

This paper has been typeset from a TeX/LaTeX file prepared by the author.

The Classification of Spiral Nebulae.

IN *The Observatory* for June 1927, Mr. J. H. Reynolds has criticised a classification of nebulae which I published recently as a preface to some rather general statistical investigations*. Mr. Reynolds is a friend whose acquaintance with nebulae is very extensive and whose criticisms I shall always welcome. Many of his comments are certainly well founded, but there are a few which I believe should be answered.

THE CLASSIFICATION.

The classification under discussion arranges the extra-galactic nebulae in a sequence of expanding forms. There are two sections in the sequence, comprising the elliptical nebulae and the spirals respectively, which merge into one another. The elliptical nebulae range from the globular E₀ to the lenticular E₇, the cypher indicating the ellipticity of the image (omitting the decimal point) as derived from the ratio of the axes. The spirals might possibly be treated in the same way, but the ratio of the axes is insensitive as a criterion and is replaced by conspicuous structural features. Of these there are three which determine positions in the sequence: (1) the relative size of the unresolved nuclear region, (2) the extent to which the arms are unwound (the openness or angle of the spiral), (3) the degree of condensation in the arms. These three criteria are quite independent, but as an empirical fact of observation they develop in the same direction, and can be treated as various aspects of a single process. This correlation leads directly to the sequence as a basis for classification †. The criteria are not always consistent, it is true, but the combined evidence usually serves to establish general positions without much uncertainty. The "spread," in short, is reasonably small compared to the "length" of the sequence.

The sequence of the spirals is subdivided into three sections of approximately equal "length," termed "early," "intermediate," and "late," respectively. This is an arbitrary procedure, and is adopted merely because it is possible to distinguish the middle section from the two ends. The nomenclature, it is emphasized,

* *Mt. Wilson Contr.*, No. 324; *Astrophysical Journal*, lxiv. p. 321, 1926.

† The "barred spirals," a distinct type, were arranged in a similar subordinate series. Their numbers are a small fraction of the numbers of normal spirals.

refers to position in the sequence, and temporal connotations are made at one's peril. The entire classification is purely empirical and without prejudice to theories of evolution—comparison with theories will be the more significant for this very reason. Moreover, since the classification was devised primarily for statistical studies, the orientation of nebulae was ignored in so far as this was possible.

In actual practice the system works very well. Among upward of a thousand spirals which I have examined, not more than a dozen have refused to fit into the sequence, and in less than ten per cent. has there been any considerable doubt as to their general position. Since reading Mr. Reynolds' criticisms I have reclassified the 290 spirals listed in the paper on which he comments. In only eight cases do the revised types differ from those originally assigned, and some of these are obvious mistakes in the latter. Even admitting an unconscious bias on the part of the author, this is satisfactory for statistical purposes.

Finally, a statistical investigation of Holetschek's nebulae, including all the brighter and a representative collection of the fainter ones down to a definite limiting magnitude over about three-fifths of the sky, has furnished quantitative results which justify the classification in a very evident manner. The sequence, which was derived from structural features alone, presents a smooth progression in mean surface brightness and in diameters for a given total luminosity. Moreover, among the nebulae of a given type, or stage in the sequence, the mean surface brightness is constant, since the total luminosity varies with the square of the diameter. As a result of these numerical relations, the extra-galactic nebulae can be reduced to a standard type and treated statistically as a homogeneous group. There are residuals of course, and at times they are considerable, yet the correlations are evident and, in the opinion of the author, fully justify the general scheme of the classification.

THE CRITICISMS.

(1) Mr. Reynolds disagrees with this conclusion, declaring that "the classification of the spirals is altogether too simple for the great range in types to be found. . . ." A great range in structural details is admitted, and for this very reason a first general classification should be as simple as possible. In actual practice, however, three separate criteria were employed. That the three combine to establish a general sequence is an observational fact

and the reason for choosing the sequence as the basis of classification. Other possible criteria were examined, and discarded because they exhibited no apparent correlations among themselves.

Mr. Reynolds' objections, I suppose, can be stated in another way—that the residuals about the path of the sequence are so large as to destroy the significance of the sequence. This involves quantitative tests, and considerable data may be found in the paper under discussion. Mr. Reynolds does not comment upon the actual results; he criticizes the method by which they were derived, questioning the validity of combining Holetschek's visual magnitudes, measured with a 6-inch refractor, with angular diameters measured on photographs with large reflectors.

The essential features of the investigation were a homogeneous list of diameters and a homogeneous list of magnitudes. Since the distribution of luminosity over the images varies continuously throughout the sequence of types from the compact globular nebulae to the open spirals, it was necessary to use total luminosities in order to treat all types in a uniform manner. Holetschek's list contains the best approximations to total luminosities which we possess in large numbers, and no systematic errors are known that are large enough to invalidate the general order of results of statistical analysis. His values compare favourably, for instance, with the photographic ones which Shapley and Miss Ames derived from Harvard plates for some 60 nebulae in the Virgo Cluster*, among which are represented all stages in the sequence of types. Even where the bulk of the luminosity is confined to the nuclear region, the measured values are still fair approximations to the total magnitudes. I see no reason why this list should not be combined with a list of diameters derived from a moderately homogeneous group of photographic plates. If this conclusion is admitted, the residuals from the correlation curves become significant, and in a general way they justify the classification, at least as a basis for preliminary statistical studies.

(2) Mr. Reynolds, after mentioning only one of the criteria used in my classification of spirals, the degree of condensation, continues:—"There are at least two other criteria which should be taken into account in any classification which is to be used statistically, as Hubble has done in the paper mentioned. No classification would be complete unless the development of the

* *Harvard Circular*, No. 294, 1926

spiral form itself were taken into consideration." On this last we would seem to agree, for I have devoted the first two of my three criteria to it.

Mr. Reynolds, however, has something else in mind, for he adds:— "It (the development of the spiral form) is to a certain degree an indication of age, as a spiral developed through two revolutions of the spiral with many subsidiary arms must have taken longer to develop than the rudimentary examples developed only through half a revolution. It by no means follows that this criterion is in agreement with the development of condensations. . . ."; and he mentions M 33 as a "condensed" spiral developed through a little over half a revolution. Certainly the number of revolutions shows no pronounced correlation with the degree of condensation in the arms. In fact it is not conspicuously correlated with any of the other general features of spirals (except perhaps the thinness of the arms), and for this reason was rejected as a criterion of classification in favour of the openness or angle of the arms. The infrequent cases where the arms can be traced through two revolutions are found among the spirals most similar to the lenticular nebulae, as well as among those most dissimilar.

Mr. Reynolds' statement concerning the age of spirals appears to be an intuitive judgment, and as such has little bearing on an empirical investigation. In the same spirit, however, the openness of the spiral arms might be suggested as a criterion of age with fully as much justification as the number of revolutions—and there is no obvious correlation between the two. There is no need to labour over the point. The number of revolutions is a feature of interest, and eventually it may prove to be of critical importance. At present, however, the significance has not been established, and in the absence of correlations with other general features, it does not seem profitable to use it as a major criterion of classification.

(3) The other criterion which Mr. Reynolds wishes to include and which he feels to be of still greater importance, is the "general apparent mass of the spiral." He differentiates, it will be remembered, between the "massive" spirals, such as M 33, and the "filamentous," such as M 74*. I believe that this is a very significant distinction which may lead to quantitative criteria of absolute dimensions when it is worked out in detail. Its position in a general classification, however, will then be similar to that of

* *Monthly Notices of the R. A. S.* lxxxv. p. 142, 1924.

absolute magnitudes in the sequence of stellar spectra. It will serve to subdivide the general classes, and will be taken into account by subscripts to the class symbols. If this view is correct, the significance of "apparent mass" will be admitted and welcomed without prejudice to the sequence of types.

I hope Mr. Reynolds will continue his investigations along these lines and develop the criterion in a quantitative manner. So far as one can judge from the stars involved in spirals, and these are at present the only indications we have as to distances of individual nebulae, the "massive" spirals are indeed larger systems than the "filamentous." M₃₁ and M₁₀₁ represent about the extreme range in total luminosities of which we are reasonably certain. As yet we have only glimpses of the general luminosity function of extra-galactic nebulae, although the objects whose distances are established, the differences in luminosity between nebulae and their brightest stars, and the frequency distribution of luminosities in a half dozen clusters of nebulae, all indicate a range of the order of perhaps five magnitudes. Further investigations, I venture to believe, must proceed along statistical lines, and a classification adapted to that type of research is very desirable.

(4) Finally, Mr. Reynolds believes that the edge-on spirals are not adequately dealt with in my classification. He urges that they be incorporated into a separate class and further described according to the ratio of the axes and pattern of the absorption. Some precision is certainly sacrificed by including the edge-on objects on the same footing as the others, but the amount can easily be exaggerated. The early-type spirals are readily identified, and most of the difficulty is confined to distinguishing between the intermediate and the late types. Even among these latter, a considerable proportion can be placed with some confidence on the basis of the degree of condensation in the arms and the distribution of luminosity over the image. The heavy peripheral belts of absorption which sometimes obscure the condensations are for the most part confined to the earlier types, where the classification can be estimated on other criteria. Among the 290 spirals classified in the paper under criticism, less than a dozen gave trouble because of their orientation. In these cases the uncertainties were but moderate fractions of the run of the sequence, and, in general discussions of spirals, the errors should tend to cancel out. The difficulties, I believe, are scarcely sufficient to warrant the introduction of an arbitrary class which would destroy the homogeneity

of a classification suitable for statistical discussions of numerical data.

This last aspect of the question seems to me to be of considerable importance. A simple homogeneous system has been formulated which classifies the great majority of nebulae in a fairly definite manner and which, by quantitative tests, has proved to be suitable for statistical investigations. Other systems may handle these matters in a more effective or significant manner, but, until they are formulated and tested, I see no reason for abandoning the present scheme, even though it does ignore some interesting details of structure.

EDWIN HUBBLE.

Mt. Wilson Observatory,
1927, July.

The Satellite Question.

(Reprinted by kind permission of the Proprietors of *Punch.*)

AT an extraordinary meeting of the Solar Branch of Celestial Bodies, Ltd., the proposed Satellites Disputes Bill came up for discussion.

The Sun having occupied the focus, the minutes of the last meeting were read by the secretary (Mercury) and duly approved.

The Sun rose and said he wished to call their attention to the unsatisfactory conduct of certain of the satellites. These, he complained, were in the habit of interposing periodically between their primaries and himself, with the result that he suffered eclipse and lost prestige and dignity. This eclipse policy, he continued, had been deliberately adopted by the Satellites' Union. There could be no excuse for it, as, with the whole of the heavens at their disposal, satellites might easily arrange their orbits so as to avoid this annoyance.

He wished to make his own position as luminous as possible. His business was to provide central heating and lighting for the whole solar system. He endeavoured to give satisfaction. Personally he resented any attempts, whether organised or not, to interfere with the execution of his duties. He would instance the total eclipse programme which had been attempted on June 29th. He had recently received many complaints from the Earth that on that planet they were not receiving their due quota

THE STRUCTURE OF CLASSICAL BULGES AND PSEUDOBULGES: THE LINK BETWEEN PSEUDOBULGES AND SÉRSIC INDEX

DAVID B. FISHER*

Department of Astronomy, The University of Texas at Austin,
 1 University Station C1400, Austin, Texas 78712
 dbfisher@astro.as.utexas.edu

AND

NIV DRORY

Max-Planck-Institut für Extraterrestrische Physik, Giessenbachstraße, 85748 Garching, Germany
 drory@mpe.mpg.de
Submitted to ApJ

ABSTRACT

In this paper we study the properties of pseudobulges (bulges that appear similar to disk galaxies) and classical bulges (bulges which appear similar to E-type galaxies) in bulge-disk decompositions. We show that the distribution of bulge Sérsic indices, n_b , is bimodal, and this bimodality correlates with the morphology of the bulge. Pseudobulges have $n_b \lesssim 2$ and classical bulges have $n_b \gtrsim 2$ with little-to-no overlap. Also, pseudobulges do not follow the correlations of Sérsic index with structural parameters or the photometric projections of the fundamental plane in the same way as classical bulges and elliptical galaxies do. We find that pseudobulges are systematically flatter than classical bulges and thus more disk-like in both their morphology and shape. We do not find significant differences between different bulge morphologies that we are collectively calling pseudobulges (nuclear spirals, nuclear rings, nuclear bars, and nuclear patchiness) appear to behave similarly in all parameter correlations. In Sérsic index, flattening, and bulge-to-total ratio, the distinction appears to be between classical bulges and pseudobulges, not between different pseudobulge morphologies. The Sérsic index of the pseudobulges does not correlate with B/T , in contrast to classical bulges. Also, the half-light radius of the pseudobulge correlates with the scale length of the disk; this is not the case for classical bulges. The correlation of Sérsic index and scale lengths with bulge morphology suggests that secular evolution is creating pseudobulges with low-Sérsic index, and that other processes (e.g. major mergers) are responsible for the higher Sérsic index in classical bulges and elliptical galaxies.

Subject headings: galaxies: bulges — galaxies: formation — galaxies: structure — galaxies: fundamental parameters

1. INTRODUCTION

Historically, all bulges were assumed to be little elliptical galaxies residing in the centers of galactic disks. Thus it was also assumed that all bulges were dynamically hot stellar systems. Recent work puts this assumption in question. Many bulges have disk-like features that do not resemble E-type galaxies.

Classical bulges are dynamically hot, and relatively featureless; they appear similar to the end products of galaxy major mergers. They are easily recognized as having morphologies very similar to E-type galaxies.

In contrast, many bulges have features that are not found in elliptical galaxies, but in galactic disks. These features include the following: kinematics dominated by rotation (Kormendy 1993); flattening similar to that of their outer disk (Fathi & Peletier 2003; Kormendy 1993); mid-IR colors of the bulge are similar to those of the outer disk (Fisher 2006); nuclear bar (Erwin & Sparke 2002); nuclear ring and/or nuclear spiral (Carollo et al. 1997); near-exponential surface brightness profiles (Andredakis & Sanders 1994). Bulges with such properties are called *pseudobulges*. All of these phenomena are manifestations of stellar systems that are dynamically cold. However, the extent to which these features exist simultaneously in all pseudobulges is not yet well-

understood. For a review of the properties of pseudobulges see Kormendy & Kennicutt (2004) (KK04 hereafter).

In this paper, we refer to the super-set of the two systems simply as *bulges*. We note that in this paper the term *pseudobulge* refers to bulges with morphology reminiscent of disk galaxies; there is no *a priori* assumption about their formation mechanism.

Investigating the link between bulge morphology and bulge structural parameters is the main interest of this article. More precisely, those bulges with morphologies that are reminiscent of disks (such as nuclear rings, nuclear bars and nuclear spirals) are expected to have lower Sérsic index than those bulges with smooth light distributions resembling E-type galaxies. We will investigate whether this expectation holds and whether the distribution of bulge Sérsic indices is dichotomous.

Determining whether a critical Sérsic index that discriminates between classical bulges and pseudobulges exists, and what its value is, impacts our understanding of bulge formation in at least two ways. First, the distribution of Sérsic indices would constrain formation theories of classical bulges and pseudobulges. Also, the existence of a critical Sérsic index would robustly establish a method for distinguishing pseudobulges from classical bulges without using high-resolution imaging or kinematic data, neither of which is currently available in large surveys.

In the last ten years, the subject of surface brightness pro-

*For complete version with appendix and high resolution images, please visit <http://spitzer.as.utexas.edu/~twitch/Papers/papers.html>

files of bulges and elliptical galaxies has experienced a shift of paradigm. Traditionally, surface brightness profiles of elliptical galaxies and bulges were all thought to be of a single shape that is well-characterized by the de Vaucouleurs $r^{1/4}$ profile. Caon et al. (1994) show that surface brightness profiles of elliptical galaxies are better fit by Sérsic profiles (Sérsic 1968), which generalize the exponent in the de Vaucouleurs profile to a free parameter. Also, Andredakis & Sanders (1994) show that many bulge-disk galaxies are better described by a double exponential than an inner $r^{1/4}$ profile with an outer exponential. Andredakis et al. (1995) generalize this to show that bulge-disk galaxies are better fit by inner Sérsic profiles with outer exponential disks than double exponentials profiles. The Sérsic function plus outer disk model for bulge-disk galaxies reads

$$I(r) = I_0 \exp \left[-(r/r_0)^{1/n_b} \right] + I_d \exp \left[-(r/h) \right], \quad (1)$$

where I_0 and r_0 represent the central surface brightness and scale length of the bulge, I_d and h represent the central surface brightness and scale length of the outer disk, and n_b represents the bulge Sérsic index.

It is not surprising that Sérsic profiles fit bulge surface brightness profiles better than $r^{1/4}$ -profiles, since the Sérsic function has more flexibility due to the extra parameter. However, the new parameter, n_b , correlates with many properties of the stellar systems to which it is fit, including but not limited to the following: velocity dispersion σ (Khosroshahi et al. 2000), absolute magnitude (Graham et al. 1996), and effective radius (Caon et al. 1994). Many authors have shown that these correlations extend to bulges of bulge-disk galaxies (Graham 2001; MacArthur et al. 2003; de Jong et al. 2004; Thomas & Davies 2006). Additionally, Andredakis et al. (1995) show that the Sérsic index of bulges correlates with Hubble type, decreasing from $n_b \sim 3.7$ for S0 galaxies to $n_b \sim 1.6$ in Sbc-Sd galaxies. Therefore it is reasonable to assume that it has physical significance. The Sérsic index is often referred to as the shape parameter, as it is generally taken as a surrogate for properties such as concentration of the surface brightness profile. For a review of the properties of Sérsic profiles see Graham & Driver (2005).

The tentative assumption is that the Sérsic index of a bulge reflects the classical bulge - pseudobulge dichotomy. Lower Sérsic index might indicate that a bulge is more likely to be a pseudobulge. We do not understand the mechanism that is responsible for determining the Sérsic indices in pseudobulges (or classical bulges). Yet, it seems plausible that the light distribution be similar to that of a disk, since so many other of the properties of pseudobulges are similar to those of galactic disks. Courteau et al. (1996) use bulge-disk decompositions of 243 galaxies to show that the 85% of bulges in Sb-Sc galaxies are better fit by the double exponential than cuspier $r^{1/4}$ models. Thus, the common conclusion is that pseudobulges are marked by near exponential Sérsic index (KK04). Scarlata et al. (2004) shows with STIS acquisition images that bulges with surface brightness profiles more resembling exponential profiles are more likely to have disk-like morphology (e.g. spiral arms), yet there is significant scatter to this claim, in their sample. They go on to show that the distribution of central slopes of surface brightness profiles of the bulges in their sample is bimodal when plotted against absolute magnitude.

It is yet unknown where pseudobulges should lie in other parameter correlations, such as fundamental plane projec-

tions. We do not expect that pseudobulges occupy a significantly different location than classical bulges in fundamental plane parameter space, since the fundamental plane is not known to be bimodal. Many studies of the locations of bulges in structural parameter space exist (e.g. Bender et al. 1992; Graham 2001; MacArthur et al. 2003; de Jong et al. 2004; Thomas & Davies 2006), and no significant bimodal behavior is noticed. Carollo (1999) remarks, though, that pseudobulges deviate more from the $\mu_e - r_e$ relation (Kormendy 1977). We will investigate this further in this paper. Kormendy (1993) shows that the majority of bulges are rounder than the outer parts of the disks they reside in, yet a significant minority are as flat as their associated outer disk. A few bulges are even flatter than their outer disk. This behavior correlates with Hubble type; bulges in later type galaxies have flattening more similar to that of the associated outer disk. Fathi & Peletier (2003) carried out bulge-disk decompositions of 70 galaxies on higher-resolution data finding a similar result.

As discussed in KK04, pseudobulges are characterized principally by having less random motion per unit stellar light. They are rotation-dominated systems (Kormendy 1993; Kormendy & Kennicutt 2004). Thus it makes sense that they be flatter. The relative flatness of a bulge to its associated outer disk has also been suggested as a pseudobulge indicator (KK04). We will test this hypothesis in this paper by comparing the flatness of bulges with disk like morphologies to that of bulges with morphologies like those of elliptical galaxies.

The properties of pseudobulges are in stark contrast to the expected end result of the hierarchical merging process; one does not expect violent relaxation to produce spiral structure and dynamics that is dominated by ordered motion. Further scenarios for the formation of bulges have been suggested. Clump instabilities in disks at high redshift can form bulge-like structures in simulations (Noguchi 1999). It is also plausible that gas rich accretion could form dynamically cold bulges. Internal evolution of disks can drive gas and stars to the center of a disk galaxy as well. The population of bulges as a whole and any one particular bulge may be the result of more than one of these processes.

However, the connections between bulge and disk stellar populations (Peletier & Balcells 1996; MacArthur et al. 2004), inter-stellar medium (Regan et al. 2001; Fisher 2006) and scale lengths (Courteau et al. 1996) may suggest that pseudobulges form through processes intimately linked to their host disks. Furthermore, Drory & Fisher (2007) find that classical bulges occur in red-sequence galaxies and pseudobulges occur in blue cloud galaxies. Kormendy & Kennicutt (2004) reviews the case that pseudobulges are not the result of major mergers, but rather that internal disk-evolution may be responsible for them. However, that bulges can form out of the internal evolution of a disk is not a new idea; see, for example, Hohl (1975).

Simulations suggest that if disk galaxies do not experience major mergers, they may evolve by redistribution of energy and angular momentum driven by non-axisymmetries such as bars, ovals, and spiral structure (Simkin et al. 1980; Pfenniger & Friedli 1991; Debattista et al. 2004), resulting in star formation and bulge-like stellar densities, thus forming pseudobulges. Indeed, a correlation between central star formation rate and the presence of bars and ovals has been detected (e.g. Sheth et al. 2005; Jogee et al. 2005; Fisher 2006). Also, Peebles & Martini (2006) find that galaxies with nuclear rings and/or nuclear spirals are more strongly barred. Thus we also investigate the possible connection between

driving mechanisms and structural properties.

It is, thus, possible that the absence of a classical bulge in a galaxy indicates that the galaxy has not experienced a major merger since the formation of the disk. In this context, pseudobulges may be thought of as more similar to pure disk galaxies that have a surface brightness profile which breaks from the outer exponential profile to a more steep inner surface brightness profile. Though the frequency of pseudobulges has not yet been robustly calculated, if they are common then this implies that many disk galaxies did not suffer major mergers since their formation.

This paper is organized as follows. In § 2 we present the observational data we use, and we discuss the surface brightness fitting procedure. In § 3 we present results on the location of pseudobulges and classical bulges in various structural parameter correlations. In § 4 we discuss the flatness of pseudobulges and classical bulges. In § 5, we discuss behavior of different bulge morphologies (nuclear bars, nuclear spirals, and nuclear rings) in various parameter correlations. In § 6 we summarize and discuss these results. Finally, the appendix includes an image of each galaxy, all decompositions and a discussion of the robustness of our decomposition and fitting procedure.

2. METHODS AND OBSERVATIONS

2.1. The Sample

The aim of this work is to establish whether or not pseudobulges – recognized by the presence of disk-like morphological features as motivated and discussed in KK04 – can be distinguished from classical bulges simply by structural features in their surface brightness profiles, most prominently their profile shape. Thus we ask whether bulges that contain disk-like morphologies (pseudobulges) have lower Sérsic index and higher flattening ratios than bulges with elliptical-like morphologies (classical bulges). Answering this question requires high resolution imaging (preferably in the optical bands) to detect the nuclear spirals, bars, and rings; and we need surface brightness profiles with large dynamic range in radius to accurately determine the parameters in Eq. 1 for a bulge-disk decomposition.

We choose galaxies observable from the northern hemisphere that have data in the *Hubble Space Telescope* (HST) archive. We limit our selection to galaxies closer than ~ 40 Mpc to resolve features in the bulge.

The link between non-axisymmetries (barred and oval distortions) and secular evolution motivates us to create a sample containing roughly equal numbers of galaxies with a driving agent (galaxies with a bar and/or an oval) and galaxies without a driving agent. Detection of oval distortions are discussed in Kormendy (1982). They are identified by nested shelves in the surface brightness profile usually having different position angles. We identify bars by consulting the Carnegie Atlas of Galaxies (Sandage & Bedke 1994) and the RC3 (de Vaucouleurs et al. 1991). If a galaxy has both a bar and an oval, we call that galaxy barred. Additionally, we look for bars and ovals in all galaxies using K-band images from 2MASS (Skrutskie et al. 2006). Note that we do not distinguish grand design spirals as a possible secular driver, though they may be able to generate a similar but less extreme effect as bars do (KK04). We use 39 undriven (no bar and no oval) galaxies and 38 driven galaxies (30 barred and 8 ovaled), a total of 77 galaxies.

In Fig. 1 we show the distribution of global properties of the

galaxies in our sample; these are also listed in Table 1. The distribution of the distances of the galaxies in our sample is heavily peaked at 16 Mpc due to the Virgo cluster and has a standard deviation of 6 Mpc. We derive total magnitudes by 2D integration of our surface brightness profiles. The distribution of absolute V magnitudes ranges mostly from -19 to -22 with a median value of -20.5.

KK04 compiles data from several different studies to generate preliminary statistics on how the frequency of pseudobulges varies along the Hubble Sequence. They suggest that both pseudobulges and classical bulges exist at intermediate Hubble Types (S0 to Sbc). There appears to be a transition from classical bulges being more frequent at early types (S0-Sb) to pseudobulges being more frequent at later types (Sbc - Sd). They further suggest that classical bulges will be almost non-existent at Hubble types Sc and later. In the right panel of Fig. 1, we show the distribution of Hubble Types (taken from Sandage & Bedke 1994) of the galaxies in our sample. To test for differences between pseudobulges and classical bulges we choose to sample the range of Hubble type from S0 to Sc. If we combine this with our choice of evenly sampling driven and undriven galaxies, we expect that our sample should overemphasize pseudobulges. The distribution of Hubble types is as follows: 13 S0, 2 S0a, 18 Sa, 6 Sab, 20 Sb, 11 Sbc, 9 Sc. We will also use 24 E type galaxies from Kormendy et al. (2006) as early-type sample in some parameter correlations.

2.2. Identification of pseudobulges

We define “bulges” photometrically as excess light over the inward extrapolation of the surface brightness profile of the outer disk. The region of the galaxy where this excess light dominates the profile is the bulge region. We classify galaxies as having a pseudobulge by their morphology within this bulge region; if the bulge is or contains any of the following features: a nuclear bar, a nuclear spiral, and/or a nuclear ring, then the bulge is called a pseudobulge. Conversely, if the bulge better resembles an elliptical galaxy (relatively featureless isophotes), then the bulge is called a classical bulge. This method is discussed in KK04. The existence/absence of visibly identifiable disk-like structure in a bulge correlates with properties of the bulge and the whole galaxy. The same method is shown to be successful in identifying bulges with higher specific star formation rates (Fisher 2006) and globally bluer galaxies (Drory & Fisher 2007).

Fig. 2 shows high-resolution HST images of the bulge region of all galaxies in our sample. All images are taken in close-to V band filters. Note first that classical bulges (for example NGC 1398, NGC 2775, NGC 2880, and NGC 3115, all in the rightmost column of the first page of the figure) have a smooth stellar light profile. There is no reason evident in the images to think that any of these galaxies harbor a pseudobulge. The bulges fit the description of E-type galaxies. On the other hand, NGC 4030 shows a face-on nuclear spiral (bottom row on the second page). The spiral dominates the radial profile for more than a kiloparsec. NGC 4736 (fourth page, second row) also has a nuclear spiral pattern but also has a nuclear bar; note how the spiral arms seem pinched vertically in the image. Moellenhoff et al. (1995) study this nuclear bar in more detail using dynamical modeling. NGC 4371 (third page, middle row) is an S0 galaxy with at least one nuclear bar. NGC 3351 (second page, third row) has a prominent nuclear ring that heavily distorts the surface brightness profile (see Fig. 4); this nuclear ring is quite well known (Sandage

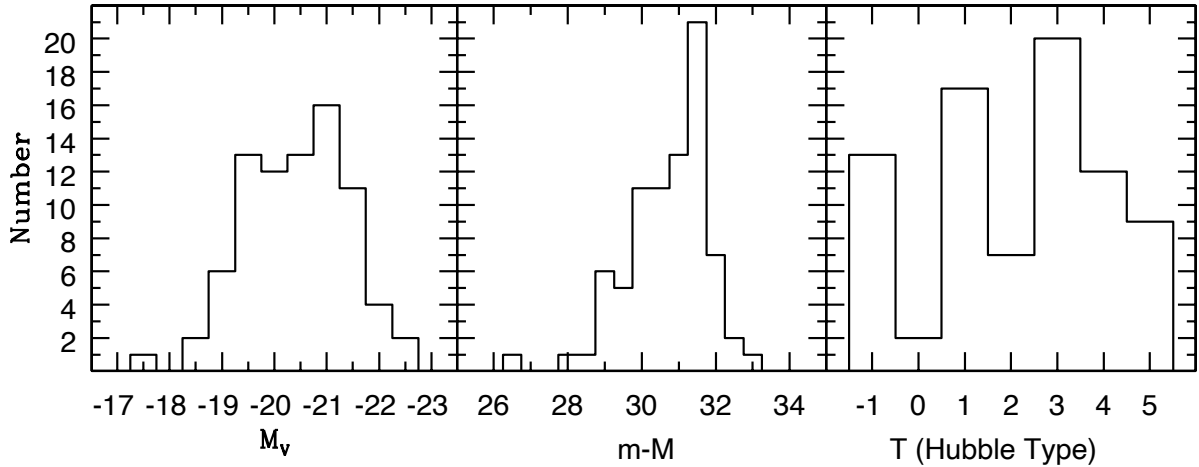


FIG. 1.— The distribution of absolute magnitude (left), distance modulus (middle), and Hubble Type (right) for all 77 galaxies in our sample.

[1961]. The bulge of NGC 2903 (first page, bottom row) shows a chaotic nuclear region; it appears nearly spiral but is not regular enough over a significant radial range to call it a nuclear spiral.

In this paper we classify bulges with near- V -band images (F547M, F555W, & F606W). Thus our method is subject to the effects of dust obscuration. However, the structures used to identify pseudobulges are usually experiencing enhanced star formation rates (Fisher 2006). Pseudobulges are, therefore, easier to detect in the optical band passes where the mass-to-light ratios are more affected by young stellar populations, rather than in the near infrared where the effects of dust are less pronounced. It is important to note that classical bulges may have dust in their center, as do many elliptical galaxies (Lauer et al. 2005). In fact, many classical bulges shown in Fig. 2 have some dust lanes in their bulges. The presence of dust alone is not enough to classify a galaxy as containing a pseudobulge; instead, it must be of a disk-like nature.

2.3. Data Sources and Surface Photometry

As stated in the introduction, the Sérsic function provides better fits and more information over two-parameter fitting functions describing surface brightness profiles of bulges and elliptical galaxies. However, this information comes at the price of more detailed observations. Saglia et al. (1997) shows that replacing an $r^{1/4}$ -model with a Sérsic model makes little difference in residuals, unless one has data with high dynamic range in radius. Further, the coupling between parameters in the Sérsic function can be quite high (Graham & Colless 1997). Thus again, it is necessary to fit the decomposition (Eq. 1) to large radial range in order to minimize these degeneracies. For each galaxy we therefore combine multiple data sources together: high-resolution HST imaging in the center, and ground based wide-field images covering the outer disk. Comments on data sources follow. Table 1 lists the sources of data used for each galaxy.

All profiles contain HST data sources. PC2 data has a small field-of-view ($\sim 18 \times 18$ arcsec 2); thus, it is critical to supplement PC2 data with wide field data. ACS/WFC has proven to be an excellent instrument for obtaining large radial fitting range. It provides a reasonable sized field-of-view ($\sim 100 \times 100$ arcsec 2) at high spatial resolution (0.049 arcsec

pixel $^{-1}$).

For as many galaxies as possible we obtain wide field images from the Prime-Focus-Camera on the McDonald 0.8 m telescope. This instrument provides a large unvignetted field of view (45×45 arcmin 2), and a single CCD detector. Therefore, we can more accurately carry out sky-subtraction. These data generally are the deepest. We also include images from the Sloan Digital Sky Survey (Adelman-McCarthy et al. 2006), 2Micron All Sky Survey (2MASS) and the Isaac Newton Group (ING) Archive. Individual data sources are noted in Table 1.

All raw data (McDonald 0.8 m & ING data) are bias-subtracted, flat-fielded, and illumination corrected. We subtract the sky background by fitting a plane to a smoothed version of the image where the galaxy and bright stars have been removed.

We calculate Johnson V -band magnitude zero points using the transformations in Holtzman et al. (1995) for the WFPC2 images and Sirianni et al. (2005) for the ACS images. SDSS g and r profiles are converted to a single V -band profile for each galaxy using the transformations in Smith et al. (2002). Other profiles are simply shifted to match in surface brightness. These transformations are derived on galactic disk stars, not galaxies. Further, the calculations require color information. We use colors from Hyper-LEDA, which refer to colors of the entire galaxies, and the galaxies in our sample most certainly have non-zero color gradients. Therefore the absolute values of surface brightness in this paper are not expected to be consistent to more than 0.3 mag. However, this does not affect our conclusions which are based the structure in the profiles and not on absolute magnitude. We check that our total magnitudes are consistent with those published in the RC3 and Hyper-LEDA.

We use the isophote fitting routine of Bender & Moellenhoff (1987). We identify and mask interfering foreground objects in each image. Then we fit ellipses to isophotes by least squares. Here, isophotes are sampled by 256 points equally spaced in an angle θ relating to polar angle by $\tan\theta = (a/b)\tan\phi$, where ϕ is the polar angle and b/a is the axial ratio. The software determines six parameters for each ellipse: relative surface brightness, center position, major and minor axis lengths, and position angle along the major axis.

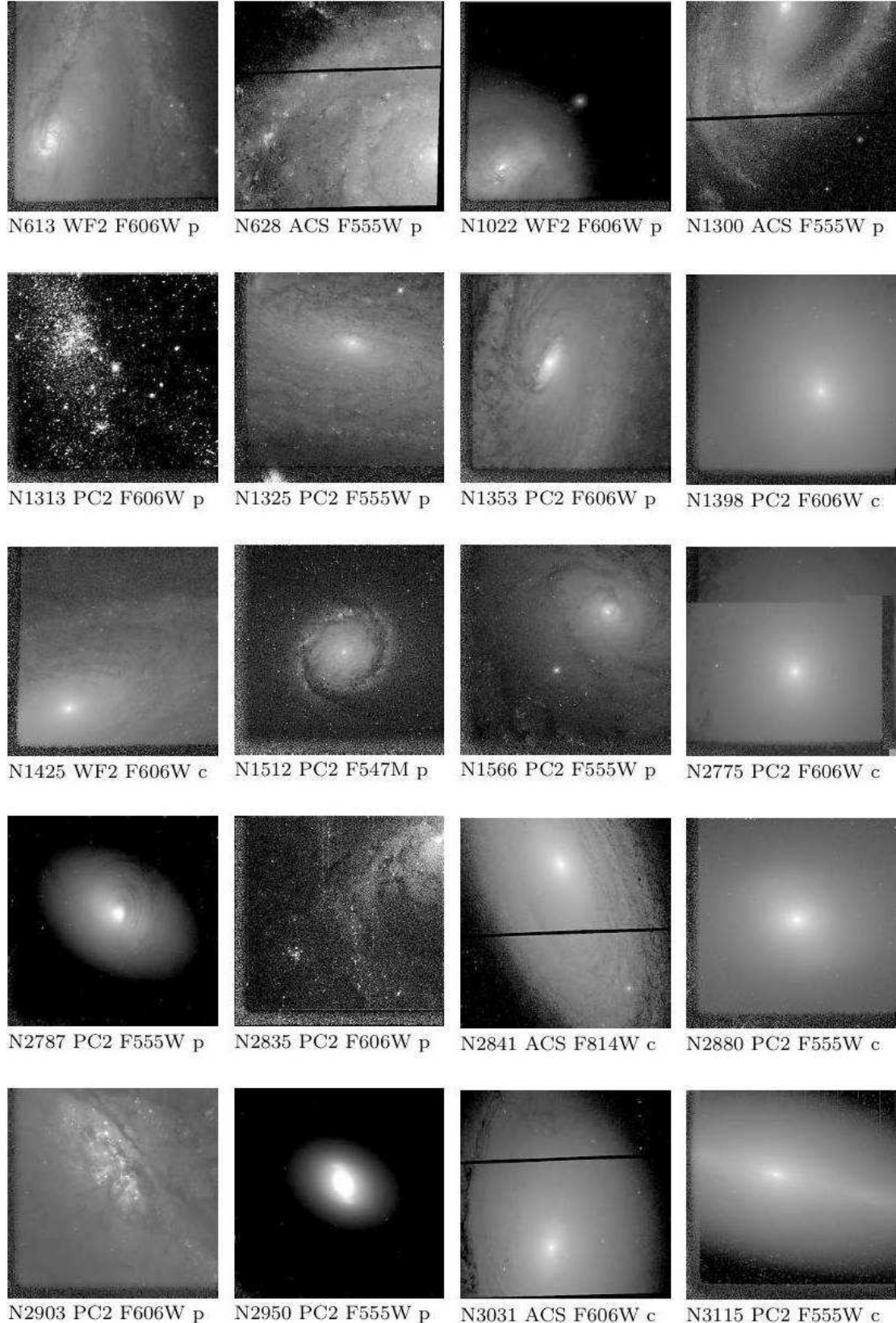


FIG. 2.— High-resolution *HST* images of all bulges in our sample. The images are scaled logarithmically, and the range of shown intensities is chosen to emphasize those features which motivate the bulge classification. For all galaxies we give the galaxy name, imaging instrument used, filter, and the classification. We label bulges classified as classical by ‘c’ and pseudobulges by ‘p’. The images show the inner 40 arcsec (ACS), 36 arcsec (PC2), and 80 arcsec (WF2) of the galaxies.

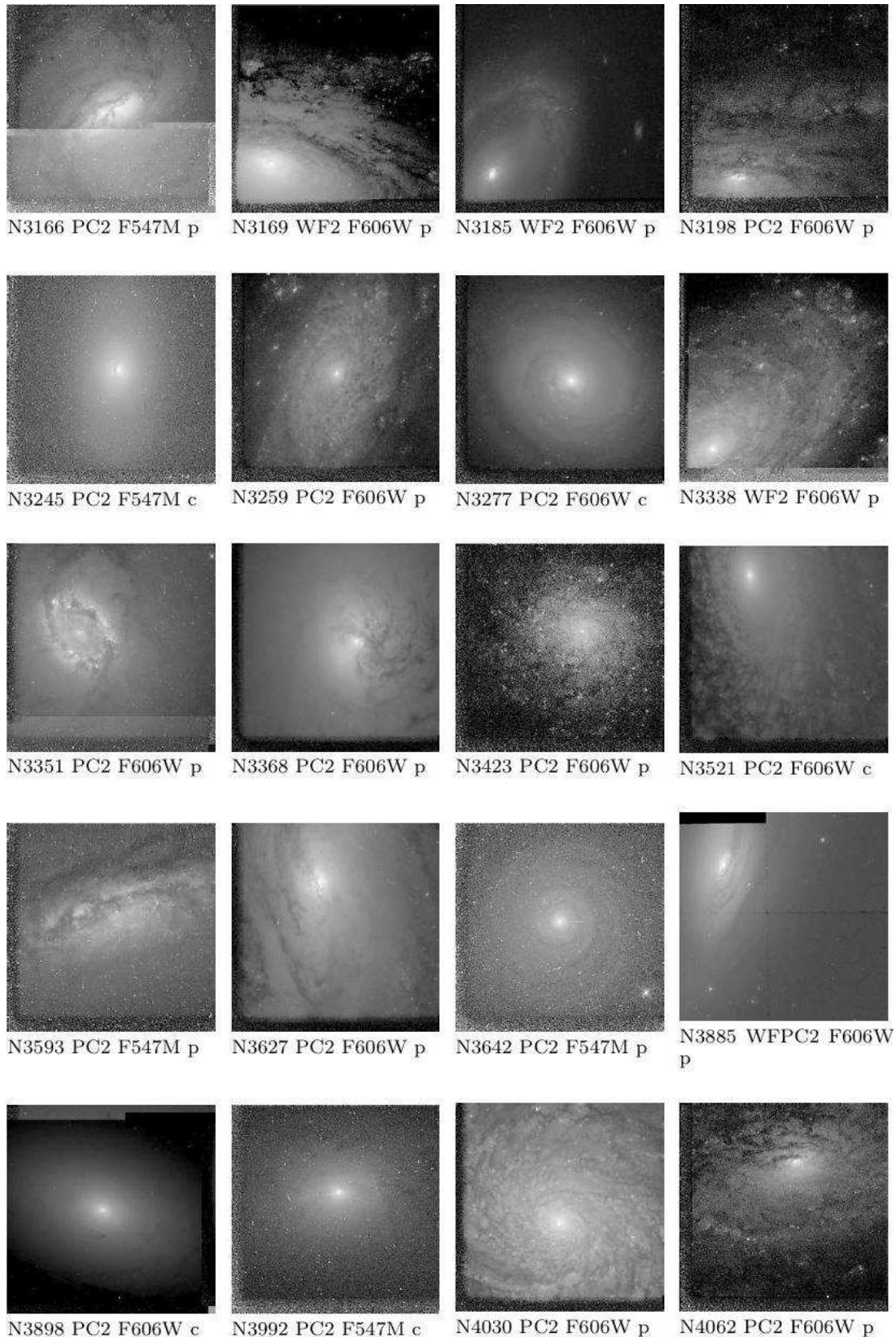


FIG. 2.— Cont.

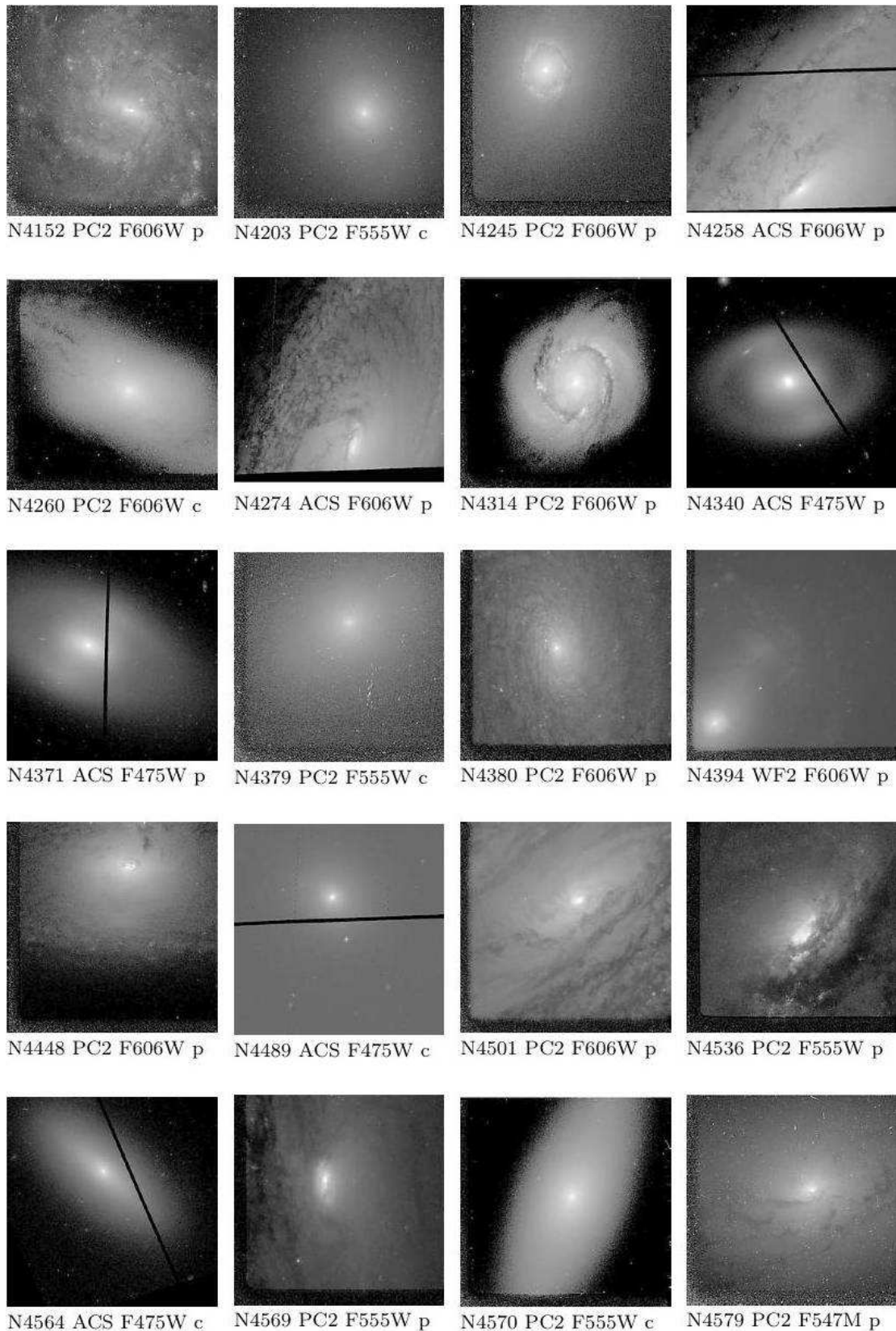


FIG. 2.— Cont.

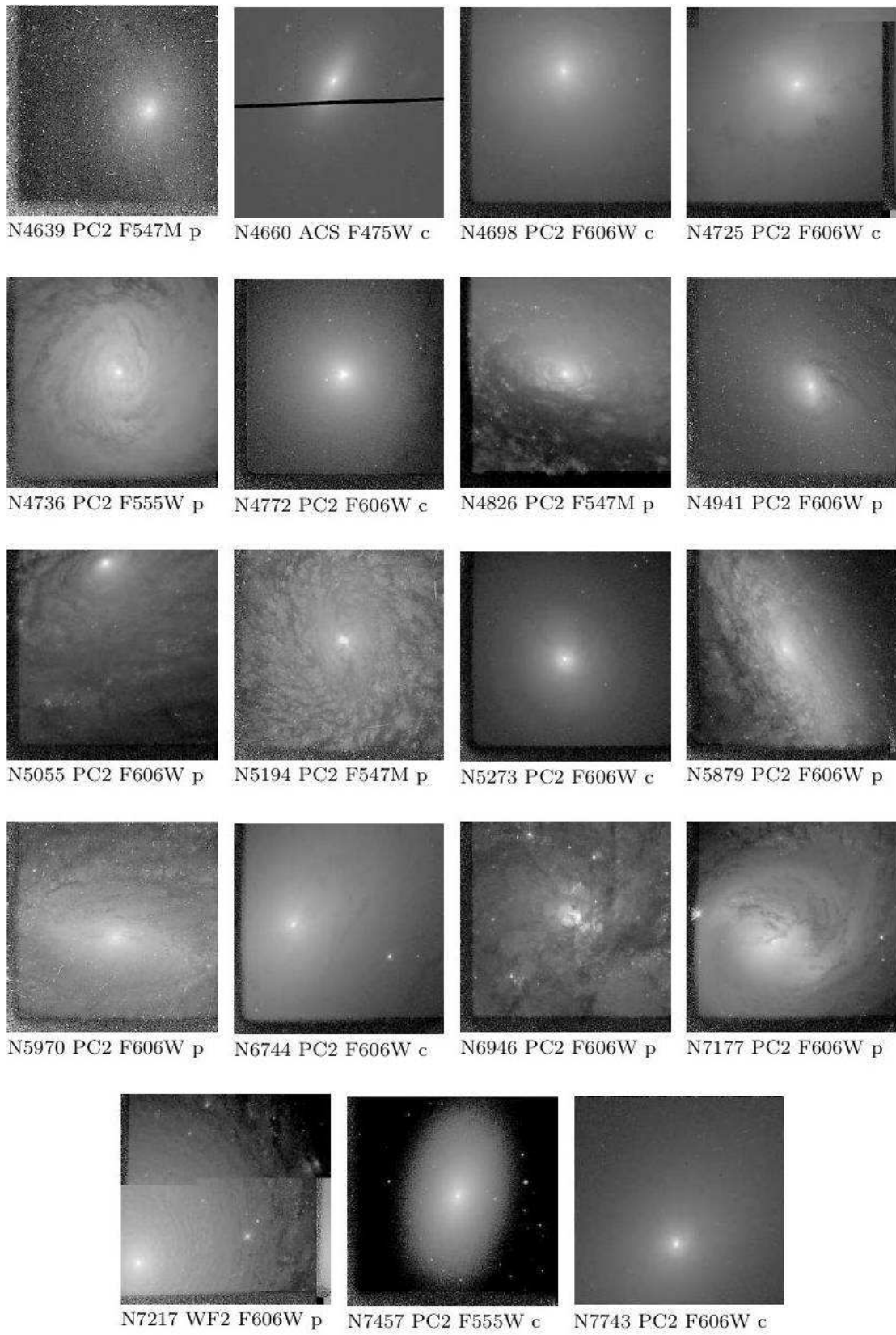


FIG. 2.— Cont.

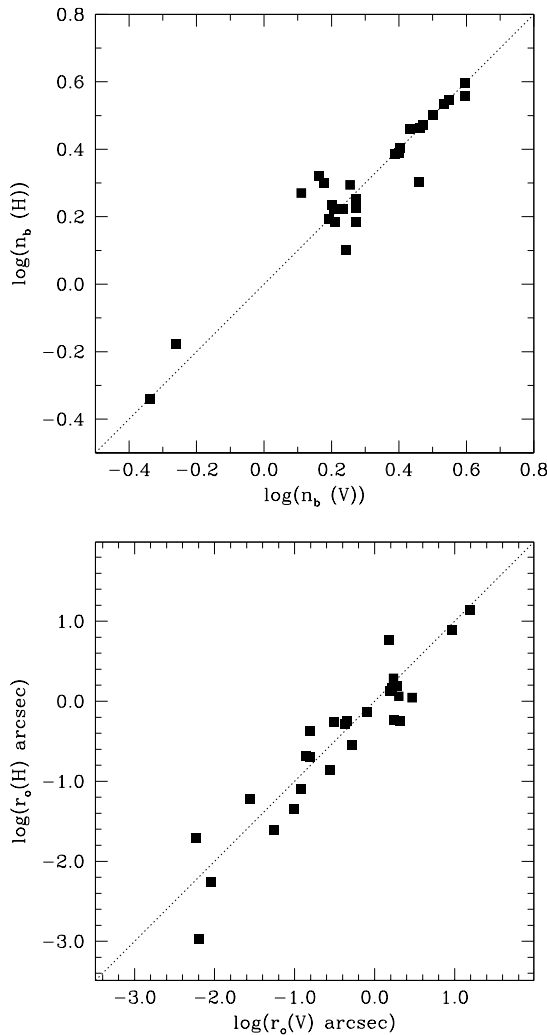


FIG. 3.— Comparison of structural parameters (r_0 & n_b) derived from bulge-disk decompositions in the H -band to those in the V -band. The identity relation is marked by the dashed line.

2.4. Bulge-Disk Decomposition

We carry out a bulge-disk decomposition on each galaxy in our sample by fitting Eq. 1 to the major axis surface brightness profiles. Our decomposition code is also used by Kormendy et al. (2006) to fit S0 and E-type galaxies with the disk component “turned off”. The average root-mean-square deviation is $\sim 0.09 \pm 0.03$ mag arcsec $^{-2}$. The largest deviation of any of the data from its fitted profile is 0.18 mag arcsec $^{-2}$.

The parameters determined in bulge-disk decomposition with a Sérsic model bulge are coupled. MacArthur et al. (2003) shows that if the bulge is sufficiently large and the resolution is sufficiently small, initial parameter estimates do not affect the final fit too much. For the most part, this is true. Yet, our experience is that initial parameter estimates may still affect the resulting fit. For each galaxy, we begin with a large parameter range that is symmetric about the initial guess. Then we re-fit the galaxy iteratively adjusting the range of allowed parameters to be narrower. This results in slight changes of best-fit values with lower χ^2 than without this iteration. The details of each profile are used to decide the width of available parameter space each parameter is given. Typically the available range for n_b is $\Delta n_b \sim 2 - 3$.

The decomposition is carried out on a major axis profile using the mean isophote brightness. It does not take ellipticity into account during the fitting. However, these galaxies are known to have varying ellipticity profiles (Kormendy 1993; Fathi & Peletier 2003). Thus, we take the mean ellipticity for each component and adjust the luminosity accordingly: $L = (1 - \bar{\epsilon})L_{\text{fit}}$. The radius of the component is defined as the radius range within which that component dominates the light of the profile. We also adjust all magnitude dependent quantities (luminosity and surface brightness) for Galactic reddening according to Schlegel et al. (1998). We use the distances of Tully & Fisher (1988). We do not make any corrections for extinction within the galaxies being studied.

We carry out the bulge-disk decompositions in the V band. This ensures that our results will remain applicable to large surveys commonly done in the optical bands (e.g. SDSS). However, the radial variation in age and metallicity that exists within galaxies may bias the parameters of bulge-disk decomposition. Carollo et al. (2002) shows that the centers of intermediate type galaxies contain significant structure in $V - I$ color maps, and this variation occurs on scales smaller than the bulge. Thus, there is doubt as to whether the parameters derived on profiles in the middle optical band passes truly reflect the properties of the stellar mass distribution.

It is beyond the scope of this paper to investigate the correlations of colors with Sérsic parameters. Yet, as a check of the stability of structural quantities compared to color gradients, we carry out bulge-disk decompositions on all galaxies in our sample that have archival NICMOS images in the filter $F160W$ (H band). We supplement those data with ground-based wide-field data. For this purpose we use mainly 2MASS data and any H -band data available in NED. We then compare the fit parameters in V to those in H . The results are shown in Fig. 4. In those parameters which do not depend on magnitude (r_0 and n_b) there is little difference. The average difference is $\Delta_{V-H} n_b \sim -0.03$, and $\Delta_{V-H} \log(r_0) \sim 0.07$. This is similar to the results of other papers that have done decompositions at multiple wavelengths (e.g. Graham 2001; MacArthur et al. 2003).

In Fig. 4 we show four examples of our photometry and the bulge-disk decompositions. For each galaxy we show an ellipticity profile, a residual profile, and a surface brightness profile along with the decomposition determined by fitting Eq. 1 to the galaxy’s surface brightness profile. These examples are selected to show the range in typical profiles in this paper. The entire sample of fits is shown in the appendix.

The top two panels of Fig. 4 shows two galaxies (NGC 3031, left panel; NGC 3169, right panel) that are well described by an inner Sérsic function and an outer exponential disk. In both profiles the fit covers a dynamic range of ~ 12 mag arcsec $^{-2}$. NGC 3031 is well fit (RMS=0.06 mag arcsec $^{-2}$) by Eq. 1 over $\Delta \log(r/\text{arcsec}) = 3.3$ and NGC 3169 for $\Delta \log(r/\text{arcsec}) = 2.51$. Deviations are small, and there is little-to-no substructure evident in these profiles. Note that each bulge has a nuclear excess of light over the inward extrapolation of the fit, and that this nucleus is excluded from the fit (vertical hatches indicate beginning and end of fit range and excluded data points are marked by open symbols).

Despite its successes, the Sérsic bulge plus outer exponential disk model of bulge-disk galaxies does not account for many features of galaxy surface brightness profiles. Disks of intermediate type galaxies commonly have features such as bars, rings, and lenses (see Kormendy 1982 for a description of these). Further, Carollo et al. (2002) shows that many

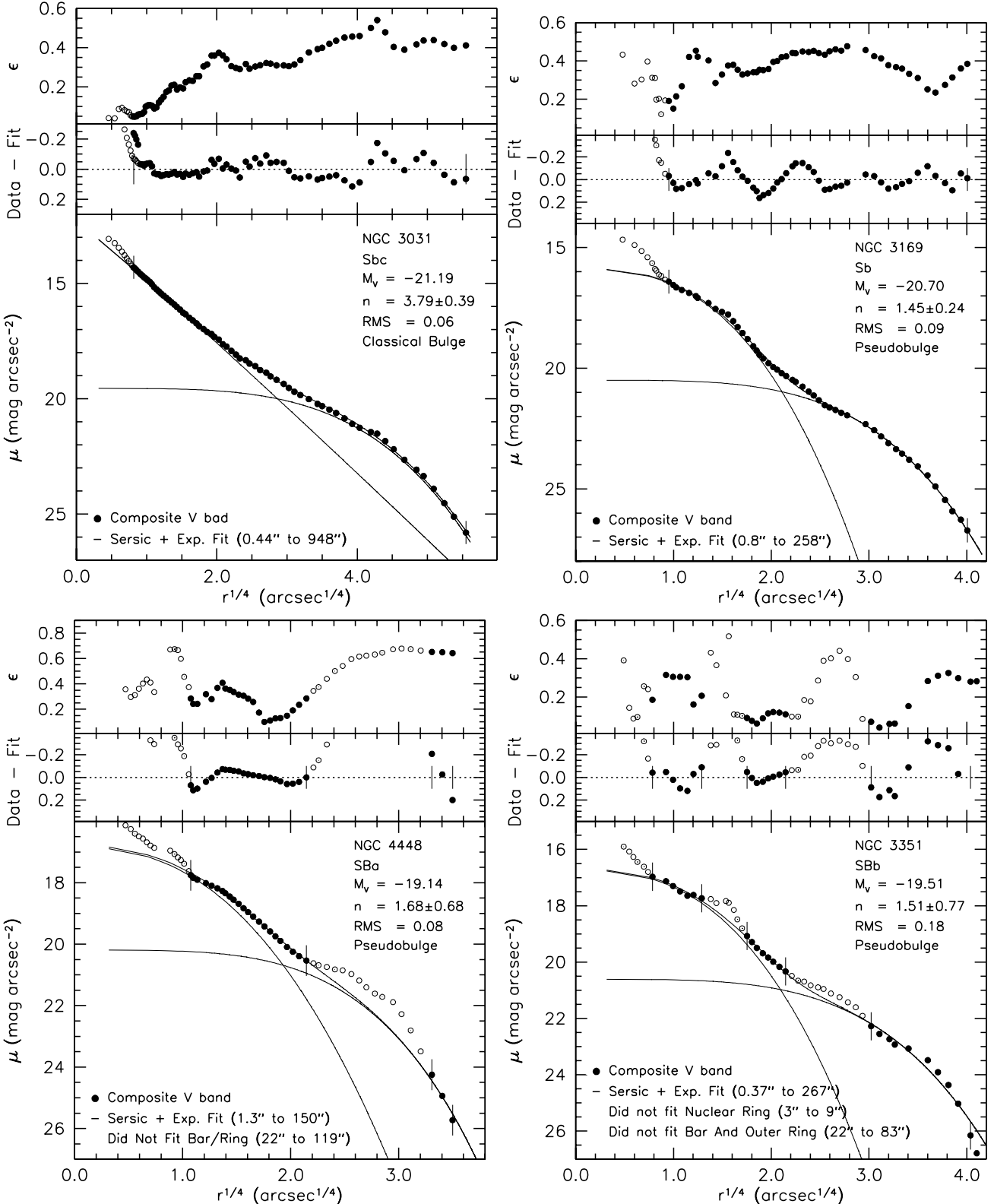


FIG. 4.— We show four example decompositions, spanning the range of the types of profiles that we find in the galaxies investigated in this paper. All data are plotted against $r^{1/4}$ as this projection emphasizes deviations from the fit better than $\log(r)$, and shows the central regions better than plotting against linear radius would. For each galaxy we show a profile (black dots) of (from bottom to top panel) V band surface brightness; residual profile of the data minus $-2.5 \log I(r)$, where $I(r)$ is the fit to Eq. 1; and ellipticity profile, where $\epsilon = 1 - b/a$, and b/a is the axial ratio of the galaxy. In the bottom panel we also show the decomposition: the inner Sérsic profile and the outer exponential profile as black lines. The vertical hatches on the profile indicate the boundaries of the regions included in the fit, the bottom caption also notes the total range of the fit. Excluded data regions are marked by open symbols, fitted regions by closed symbols. The caption gives the galaxy name, the Hubble type, the total absolute magnitude, the Sérsic index of the bulge and the root-mean-squared deviation of the fit to the fit region of the data.

bulges of early and intermediate type galaxies contain nuclei. The bottom panels of Fig. 4 shows two such examples of galaxy profiles with significant deviations from the fitted decompositions. NGC 4448 (bottom left) is an example of a barred galaxy in which the bar is an especially prominent perturbation to the outer exponential surface brightness profile. NGC 3351 (bottom right) is an example of a complicated surface brightness profile, with multiple substructures that are not well described by the smooth nature of the bulge-disk model used here. This galaxy contains a nuclear ring near ~ 4 arcsec, and a bar from about 20 to 80 arcsec. These galaxies are not well described by Eq. 1, yet we do our best to decompose as many galaxies as possible.

Bars, rings, lenses, and similar features do not conform to the smooth nature of Eq. 1, hence we carefully exclude regions of the profile perturbed by such structures from the fit. This is a risky procedure, as it requires selectively removing data from a galaxy's profile, and undoubtedly has an effect on the resulting parameters. We are often helped to identify bars by the structure of the ellipticity profile. Notice the peak in ellipticity near 50 arcsec in NGC 3351. We try to err on the side of removing the fewest points possible. For those galaxies in which a bar is present, it is our assumption that removing the bar from the fit provides the best estimation of the properties of the underlying bulge and disk. We test our method by removing a typical number of points from a few galaxies with smooth profiles (NGC 2841, NGC 1425, NGC 4203, & NGC 1325). The result is that Sérsic index can vary as much as $\Delta n_b \sim 0.5$, and characteristic radius by $\Delta \log(r_0) \sim 0.5$. The variance of these two parameters is tightly coupled and this is reflected by the uncertainty. Central surface brightness was mostly unaffected. If a region is not included in a fit we show that in the figure by using open symbols. A detailed discussion of the effects of bars and other features on the surface brightness profiles is given in the appendix.

3. STRUCTURAL PROPERTIES OF PSEUDOBULGES AND CLASSICAL BULGES

3.1. Bulge Prominence Of Classical & Pseudobulges Along The Hubble Sequence

The primary distinction between most previous studies and this one is that we do not treat bulges as an homogeneous set of objects. Here, we report on how morphologically identified pseudobulges and classical bulges, taken to be distinct entities, behave in the parameters obtained from bulge-disk decomposition. Further we wish to know if the Sérsic index is able to distinguish these two separate bulge types as has been suggested by many authors and not yet systematically tested.

Fig 5 shows how the bulge-to-total ratio (luminosity of the bulge, divided by total luminosity of the fit; hereafter B/T), and the ratio of the bulge half-light radius (r_e) to the scale-length of the outer disk (h) both correlate with Hubble type. We calculate the effective radius as

$$r_e = (b_n)^n r_0, \quad (2)$$

where b_n is a proportionality constant whose expansion given in MacArthur et al. (2003). In all figures red circles represent classical bulges and blue crosses represent pseudobulges. In fig 5, the connected black squares show the average for each Hubble type. There are only two S0/a (T=0) galaxies; thus the dip in the average of B/T could merely be small number

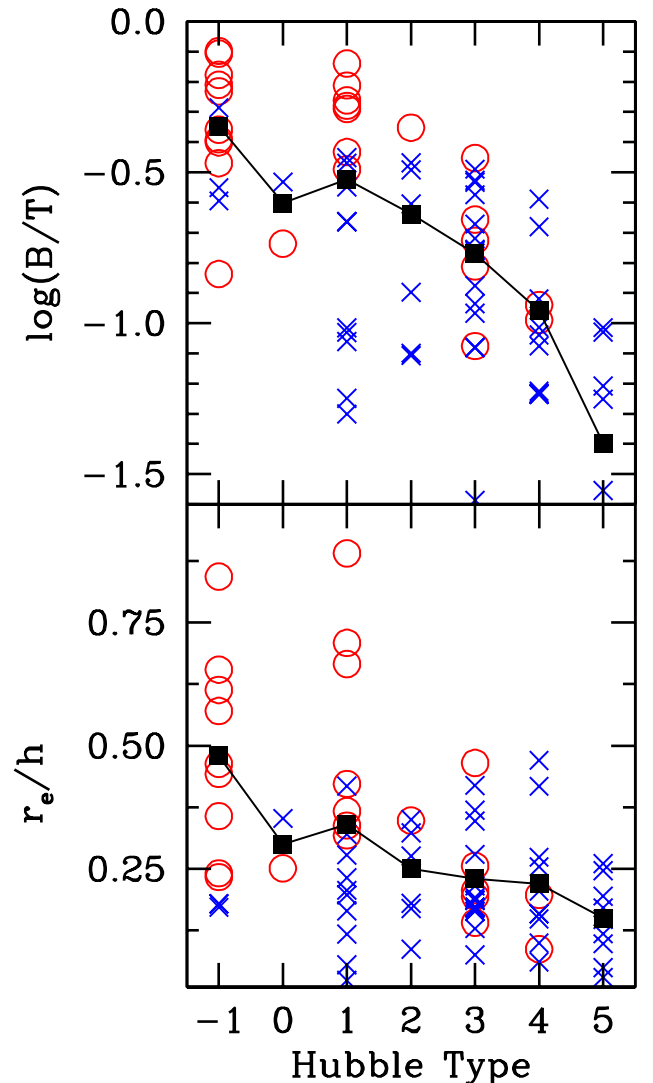


FIG. 5.— The bulge-to-total ratio, B/T , top, and the ratio of the effective radius to the disk scale length, r_e/h , bottom, of classical bulges (red circles) and pseudobulges (blue x's) plotted against Hubble types. The black squares, connected by the black line, represents the average for all bulges (both pseudo- and classical) in each type.

statistics. Also, a few of the Sc (T=5) galaxies are not shown due to their very small B/T .

As shown in the top panel of Fig. 5 bulge-to-total ratio is a decreasing function of Hubble type. This is not surprising as B/T is part of the original classification criteria. This behavior has been found by many authors, for a detailed study see Graham (2001). This at least confirms that our decomposition method is sound, and able to recover the well established correlation.

Pseudobulges and classical bulges overlap in range of bulge prominence, shown in the left panel of Fig. 6. The average classical bulge has $\langle B/T \rangle = 0.41$. The width of the distribution is 0.22. The average pseudobulge has $\langle B/T \rangle = 0.16$. The width of the distribution is 0.11. Pseudobulges are on average smaller fractions of the total luminosity of the galaxy in which they reside, yet there is significant overlap (see also Drory & Fisher 2007). This is no surprise, we would expect pseudobulges to be smaller as they are thought to be products

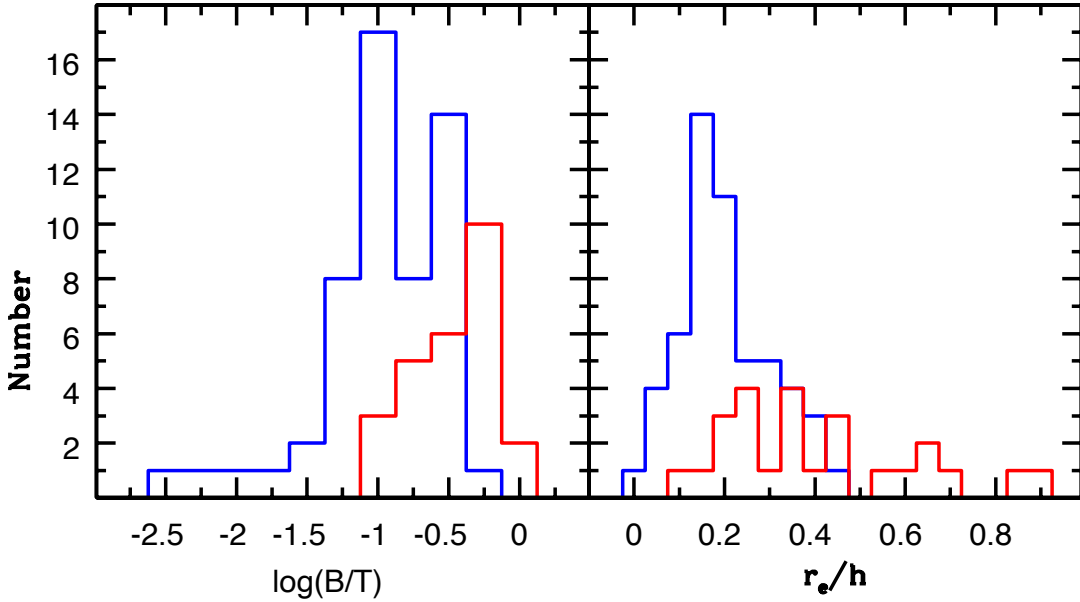


FIG. 6.— Histogram of $\log(B/T)$ (left) and r_e/h (right). Bin spacing is $\delta \log(B/T) = 0.25$ and $\delta(r_e/h) = 0.05$. Blue lines represent pseudobulges and red lines are for classical bulges.

of secular evolution of the disk; hence their luminosity is expected to be limited to some fraction of the luminosity of the disk. On the other hand, classical bulges form independently of their disk, presumably through major mergers. The full range values of B/T is therefore possible.

NGC 2950 is a pseudobulge with $B/T = 0.51$. It is hard to believe that secular evolution can drive half of the stellar mass into the central region of a galaxy. This galaxy is an SB0 with a prominent nuclear bar and nuclear ring, also noticed by Erwin & Sparks (2003). Thus, by our definition it is a good pseudobulge candidate. The next most prominent pseudobulge has $B/T = 0.35$; NGC 2950 is more than one standard deviation away in the distribution of pseudobulge B/T from the next most prominent pseudobulge. We feel that NGC 2950 is an exceptional case, and should not be taken as a normal pseudobulge. That it is an S0 galaxy strengthens this interpretation. The unusually large B/T may be a result of the processes which made the galaxy S0 (for example gas stripping by ram pressure and/or harassment; see Moore et al. 1996), rather than secular evolution. Also, our analysis may be an over simplification of the population of bulges, in that composite systems (“bulges” with both a pseudobulge and a classical bulge) may exist. This could artificially increase the B/T ratio.

Courteau et al. (1996) show that the ratio of scale lengths for galaxies when fitted with a double exponential (bulge and disk) is tightly coupled. MacArthur et al. (2003) find, with fits to Sérsic plus outer exponential profiles in galaxies spanning Hubble type Sab to Sd, that the coupling is $\langle r_e/h \rangle = 0.22 \pm 0.09$, and that the ratio becomes smaller toward later Hubble types (see also lower panel of Fig. 5). It appears that the correlation of r_e/h with Hubble type may be driven primarily by the number of classical bulges in each Hubble type; this statement is very uncertain due to small numbers in each Hubble type, though.

The right panel of Fig. 6 shows the distribution of r_e/h for the galaxies in our sample (red lines are for classical bulges and blue lines represent the distribution of pseudob-

ulges). We find that $\langle r_e/h \rangle = 0.28 \pm 0.28$ for all galaxies in our sample, and that r_e/h decreases toward later Hubble types. The average is higher and the scatter is larger than in MacArthur et al. (2003), most likely because our sample targets earlier-type galaxies. Considering bulge types separately, we find that for pseudobulges $\langle r_e/h \rangle = 0.21 \pm 0.10$, and for classical bulges $\langle r_e/h \rangle = 0.45 \pm 0.28$. The distribution of r_e/h for pseudobulges is clearly much narrower than that of the classical bulges. Furthermore, r_e and h do not appear to be correlated in classical bulges.

Our finding that the half-light radius of pseudobulges is well correlated with the scale length of the outer disk, while the scale length of classical bulges is not correlated with that of the disk is consistent with the interpretation that $r_e \propto h$ is due to a secular formation of pseudobulges. However, inspection of Fig. 6 shows that the range of r_e/h over which we find classical bulges is large and overlaps with the pseudobulges significantly. Thus, r_e/h may not be a good diagnostic tool for identifying pseudobulges and classical bulges; however the finding that the scale length of the disk is correlated with the size of its pseudobulge but not correlated with classical bulges is a strong indication that there indeed is a physical difference between the formation mechanisms of different bulge types.

3.2. The Sérsic Index In Bulges

Figure 7 shows the correlation of bulge properties with the shape of the surface brightness profile measured by the Sérsic index, n_b , of those bulges. We find that no classical bulge has Sérsic index less than two, and very few pseudobulges ($\sim 10\%$) have Sérsic index greater than 2. The correlations of Sérsic index with other structural properties (r_e , μ_e , and M_v) appear to be different for pseudobulges and classical bulges. This suggests that the Sérsic index may be used to distinguish pseudobulges from classical bulges.

The top panel of Fig. 7 shows the correlation of Sérsic index with absolute V -band bulge magnitude for pseudobulges, classical bulges, and elliptical galaxies. Classical bulges fit

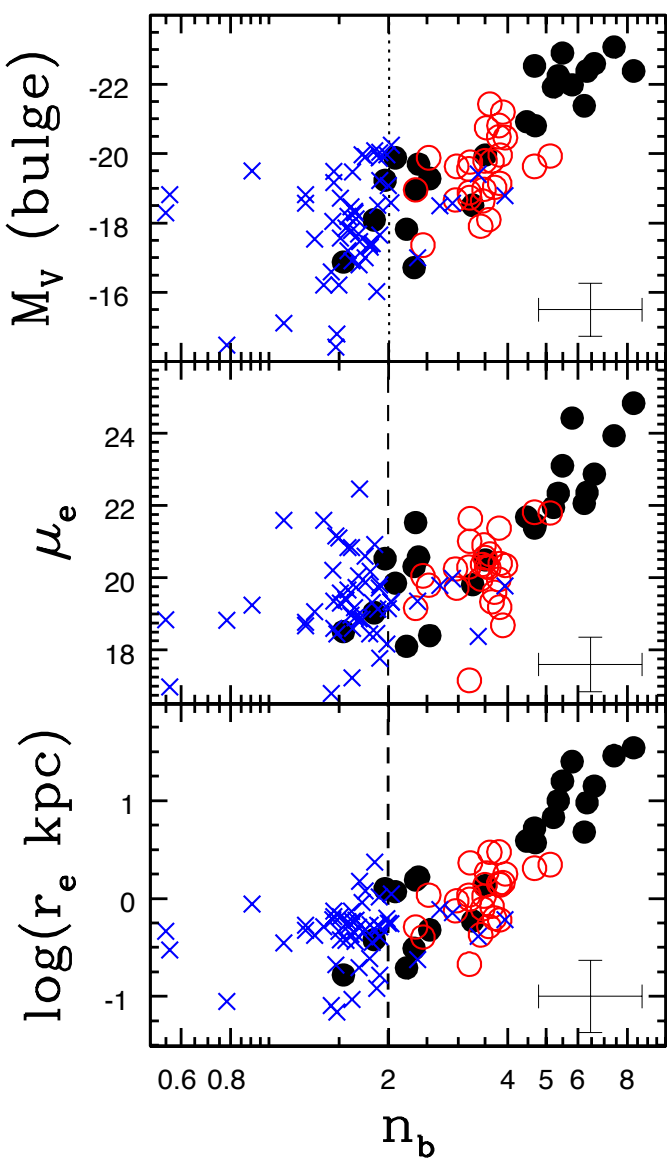


FIG. 7.— Correlation of the absolute magnitude (M_V), half-light radius (r_e), and surface brightness at the half-light radius (μ_e) of bulges with bulge Sérsic index. Pseudobulges are represented as blue crosses, classical bulges as red circles. We also show elliptical galaxies from Kormendy et al. (2006) for comparison, represented by black filled circles. The average uncertainty of the parameters of all bulges is represented by the error bars in the bottom right corner of each panel.

well within the correlation set by elliptical galaxies. They cover a range of Sérsic index from $n_b \sim 2 - 4.5$, and their absolute magnitude covers the range $M_V \sim -17.5$ to -21 . Notice that the Sérsic index of classical bulges is normally smaller than $n = 4$, suggesting their similarity to the low-luminosity ellipticals discussed by Kormendy et al. (2006). Classical bulges, yet again, resemble little elliptical galaxies that happen to be surrounded by a disk. The mean pseudobulge absolute magnitude is ~ 1.2 magnitudes fainter than the average classical bulge magnitude, and the faintest bulges are all pseudobulges. Yet, pseudobulges do no have to be faint: classical bulges are not much brighter than the brightest pseudobulges. Our data cannot show if the brightest pseudobulges are bright

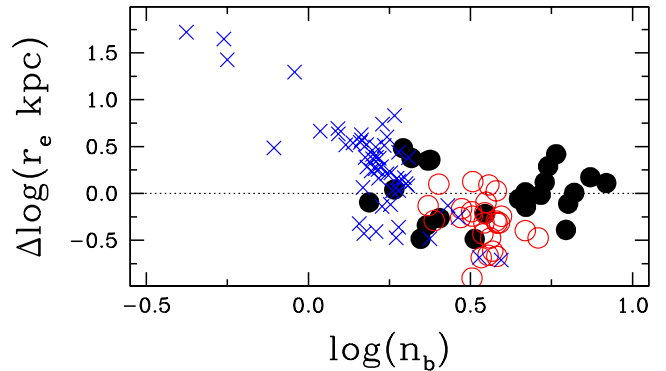


FIG. 8.— Residuals of pseudobulges (crosses), classical bulges (open circles), and elliptical galaxies (closed circles) from a fit to the elliptical galaxies given by $\log(r_e/\text{kpc}) = 2.9 \log(n_b) - 1.2$.

because of the nature of their stellar population, or because of greater stellar mass. Nonetheless, pseudobulges are not merely a change in observed properties at low magnitude. Finally, we note that the overall shape of the $M_V - n$ correlation for the super-set of systems represented in Fig. 7 is similar to those found in previous studies, (Graham 2001; Balcells et al. 2003; de Jong et al. 2004).

The bottom two panels of Fig. 7 show the correlation of Sérsic index with the half-light quantities (radius containing half the light, r_e , and surface brightness at that radius, μ_e) of pseudobulges, classical, bulges, and elliptical galaxies. The results are similar to those in the $M_V - n$ plane. Classical bulges exist within the bounds set by elliptical galaxies, more specifically by low-luminosity ellipticals. Pseudobulges, on the other hand, populate the small n extreme of this correlation. The smallest objects, in radius, are pseudobulges. Yet, pseudobulges in general are not that much smaller on average than classical bulges and low-luminosity ellipticals: the mean effective radius of pseudobulges lies within the range of effective radii spanned by the classical bulges and elliptical galaxies.

To more strongly emphasize the difference between pseudobulges from classical bulges and ellipticals (hot stellar systems), we show the residuals of all galaxies to the Caon et al. (1994) relation $r_e \propto \log(n_b)$ in Fig. 8. We fit this correlation to the elliptical galaxies only, and the resulting relation is $\log(r_e/\text{kpc}) = 2.9 \log(n_b) - 1.2$. E-type galaxies and classical bulges have similar amounts of scatter. Pseudobulges show a marked difference and systematically deviate further from the correlation as n_b gets smaller whereas the scatter among classical bulges is contained within the region occupied by ellipticals. Thus it appears that pseudobulges do not relate n_b to r_e in the same way as elliptical galaxies and classical bulges do. It is not clear from the bottom panel of Fig. 7 whether Sérsic index correlates at all with effective radius for pseudobulges.

Inspection of Fig. 7 shows that pseudobulges and classical bulges have separate distributions of bulge Sérsic index; the value that distinguishes the two types of bulges appears to be $n_b \sim 2$. Pseudobulges have Sérsic index smaller than $n_b \sim 2$; classical bulges have larger values than $n_b \sim 2$. We show this explicitly in Fig. 9 which shows the distributions of $\log(n_b)$ for pseudobulges (blue lines) and the superset of classical bulges and elliptical galaxies (red lines), both binned to $\delta \log(n_b) = 0.03$. We also show a histogram of all objects (pseudobulges, classical bulges, and elliptical galaxies) counted together. Each histogram is normalized by the num-

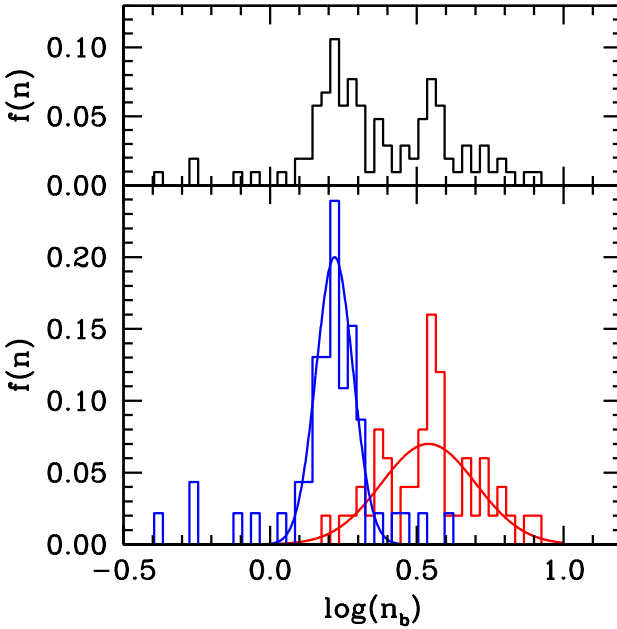


FIG. 9.— Histograms of bulge Sérsic index, $\log(n_b)$, by bulge type. The top panel shows the histogram of all objects. The bottom panel shows pseudobulges (blue lines with mode $\log(n_b) \sim 0.22$) and classical bulges + elliptical galaxies (red lines, mode $\log(n_b) \sim 0.54$). We also overplot Gaussian distributions that fit the histograms. Histograms are normalized by the total number of galaxies in each group, so that each bin reflects the frequency of Sérsic index within that object class.

ber of objects in that group, so that the counts reflect the frequency of Sérsic index within each class. Before discussing these distributions any further, we must strongly qualify this result. The sample studied in this paper is in no way complete. Thus, the relative abundance of pseudobulges and classical bulges cannot be determined from this distribution. However, we wish to study the distribution of Sérsic indices in different bulge types. We do the best we can with the data we have at present; when relevant, we attempt to point out how our sample selection may bias results. We note that distributions of bulge Sérsic indices in volume limited samples have been shown to be bimodal (Allen et al. 2006). We present any numbers derived from analysis of these distributions as preliminary.

The top panel of Fig. 9 shows that the distribution of Sérsic indices are clearly bimodal. This bimodality is completely coincident with the dichotomy in bulge morphology. The average values of bulges Sérsic index for pseudobulges and classical bulges are 1.69 ± 0.59 and 3.49 ± 0.60 , respectively, and the average of the superset of classical bulges and elliptical galaxies is 3.78 ± 1.5 . The range of Hubble types chosen for this sample (S0-Sc) certainly biases the distribution of Sérsic index to higher values since the Sérsic index has been found to get smaller at later Hubble types (Graham 2001; MacArthur et al. 2003). It is worth noting that the average uncertainty of a bulge (pseudo- or classical) is comparable to the standard deviation of either of these distributions, $\langle \Delta n_b \rangle = 0.60$. Inspection of Fig. 7 shows that neither $\log(r_e)$ nor μ_e show a bimodal distribution.

We fit a Gaussian to each histogram in Fig. 9 and solve for the Sérsic index where the frequencies are equal. Because our sample is not volume limited, we weight the distributions such that the number of galaxies earlier than Hubble type Sc with

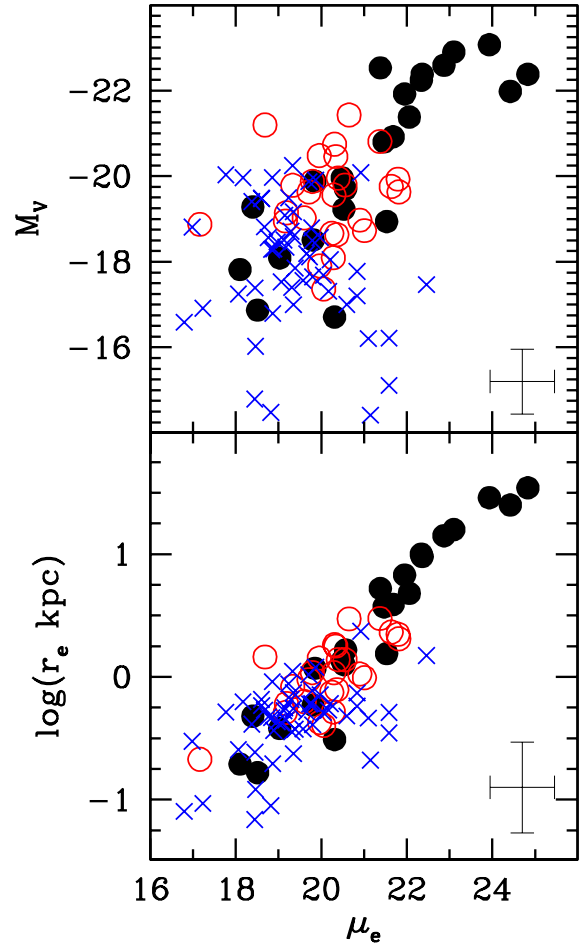


FIG. 10.— Two photometric projections of the fundamental plane. All symbols are the same as figure 7

pseudobulges is equal to the number of galaxies with classical bulges. We also solve for the case with 1/3 pseudobulges, and finally 2/3 pseudobulges. We find the critical Sérsic index to be $n_{crit} = 2.2 \pm 0.1$.

Of the 52 pseudobulges, 5 have Sérsic index significantly above two (two pseudobulges have $n_b \sim 2$). The interested reader can inspect their surface brightness profile in the appendix, which shows fits to all surface brightness profiles. We take a few lines to discuss these galaxies here. NGC 4314 is an SBa galaxy with $n_b = 2.37 \pm 0.78$; this fit appears good, although a significant amount of the profile is not included due to the outer bar and nuclear ring. NGC 4258 is an oval galaxy, with $n_b = 2.69 \pm 0.48$. The outer oval ring affects the surface brightness profile of the outer disk, and thus the fit covers a narrow range. However, this is unlikely to affect the fit of the bulge too much, especially given the relatively low uncertainty in Sérsic index in this fit. NGC 3627 is an Sb galaxy with $n_b = 2.90 \pm 0.83$. Its bar is not easily detectable, and thus not removed from the fit, as we try not to remove any unnecessary points. NGC 3642 is an Sb galaxy with $n_b = 3.37 \pm 0.61$, the profile does not go very deep, and may be allowing n_b to be artificially high. Finally, NGC 4826 has the largest Sérsic index of any bulge classified as a pseudobulge, and the fit appears quite good, unlike the others. We take these galaxies as exceptions rather than the rule, future studies comparing al-

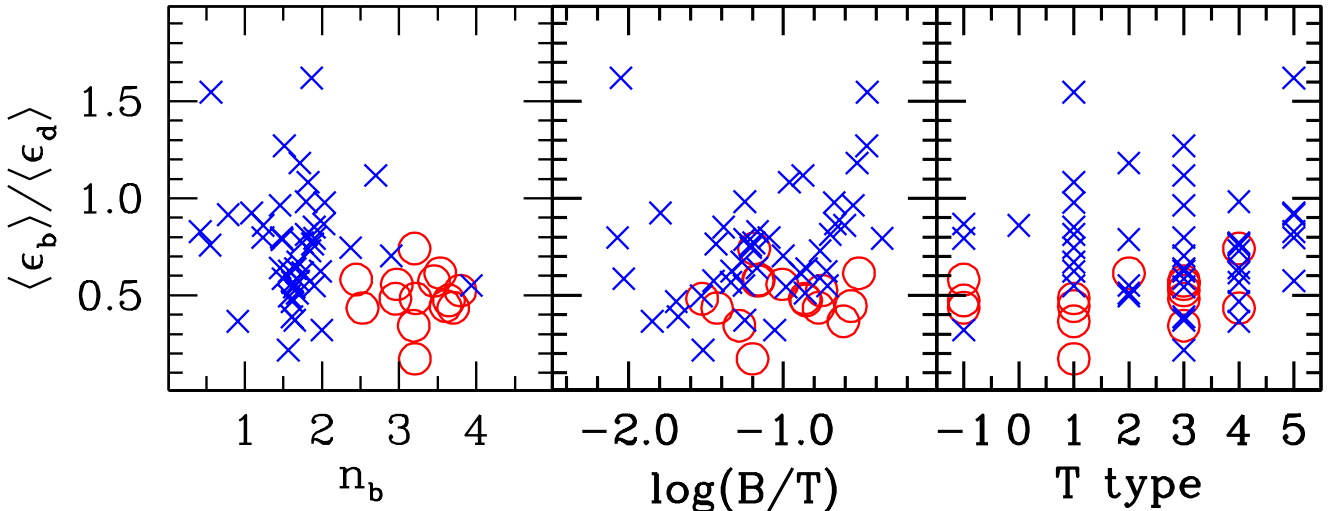


FIG. 11.— Ratio of average ellipticity of the bulge to that of the disk. As usual, pseudobulges are represented by blue crosses and classical bulges by open red circles. This ratio is plotted against Sérsic index of the bulge (left), bulge-to-total luminosity ratio (middle), and Hubble type (right).

ternative methods of pseudobulge detection (e.g. kinematics) will help shed light on their true nature. We remind the reader again that we are not classifying systems as composites, and these may have an effect. If for example a pseudobulge is embedded in a classical bulge (or vice versa), we might visually identify the pseudobulge even though the stellar light distribution is set by the classical bulge. Still, the dividing line of $n_b \sim 2$ is 90% successful at identifying pseudobulges, and thus is a good detector of pseudobulges.

3.3. Fundamental Plane Projections

Figure 10 shows the correlations of $\mu_e - r_e$ and $M_v - \mu_e$, two projections of the fundamental plane (Djorgovski & Davis 1987; Dressler et al. 1987; Faber et al. 1989). The top correlation shows the magnitude versus surface brightness plane, and the bottom panel shows the $\mu_e - r_e$ relation (Kormendy 1977). While the M_v versus μ_e plot has a lot of scatter, especially in the pseudobulges, the radius-surface brightness plane shows significantly less scatter. Yet in both of these fundamental plane projections, those bulges which are further from the correlations established by the elliptical galaxies are pseudobulges. For those pseudobulges that deviate from the fundamental plane correlation in Fig. 10 that deviation is towards lower densities.

This behavior has been noticed in the past. Carollo (1999) finds that exponential bulges are systematically lower in effective surface brightness than those better fit by an $r^{1/4}$ -profile. We note that this could be an effect of only fitting either $r^{1/4}$ or exponentials rather than a Sérsic function to the bulge profiles. If a bulge is not completely exponential then it may force other parameters to compensate for the more restrictive parameterization of the profile shape. Falcón-Barroso et al. (2002) find that bulges which deviate from the edge-on projection of the fundamental plane are found in late type (Sbc) galaxies. However, at least with the galaxies in our sample, we cannot say unambiguously that this is a function of differing bulge formation, because those bulges in Fig. 10 that deviate significantly from the correlations defined by the elliptical galaxies are also very low B/T . Thus, it could be that the potential of the bulge is more affected by the outer disk.

In fact, when looking at the pseudobulges in Fig. 10 alone, one would not infer the presence of a strong correlation of either magnitude or effective radius with surface brightness. This is another indication that pseudobulges and classical bulges are different classes of objects.

4. FLATTENING OF CLASSICAL BULGES AND PSEUDOBULGES

There has been very little work on the distribution of flattenings of bulges albeit the structures present in pseudobulges (e.g. nuclear spirals or nuclear bars) suggest that pseudobulges should have higher angular momentum and thus be flat stellar systems. However, the end products of secular evolution need not be flat (Kormendy 1993). Bar buckling and unstable disks can both drive stars higher above the plane of the disks (Pfenniger & Norman 1990; Friedli 1999), thus creating a pseudobulge that is less flat than its associated outer disk. Nonetheless, the data of Kent (1985) show that many bulges have median flattenings that are similar or greater than the median of the outer disk, and that flat bulges are more common in late-type galaxies. Fathi & Peletier (2003) find a similar result that $\epsilon_{bulge}/\epsilon_{disk} > 0.9$ in 36% of S0-Sb galaxies and 51% Sbc-Sm galaxies (where $\epsilon = 1 - b/a$). However, note that Möllenhoff & Heidt (2001) do not find this result, they find very few bulges are as flat as disks in ground based JHK imaging.

Kormendy & Kennicutt (2004) include the flattening of bulges (as manifest through the ratio of bulge ellipticity to that of the disk) in their list of preliminary criteria for identifying pseudobulges. We can test this hypothesis with our sample. Figure 11 shows the ratio of mean ellipticity of the bulge to that of the outer disk ($\langle \epsilon_b \rangle / \langle \epsilon_d \rangle$) for galaxies in this study. We do not include galaxies with average disk ellipticity less than 0.2, as face-on projections of galaxies do not allow the flattening to be determined. Also, galaxies with $B/T > 0.5$ are removed; if the bulge dominates the entire potential it may set the shape of the disk and therefore affect the disk's ellipticity making it more like its own. To calculate the average ellipticity of the profile we use only the data points that are also included in the fit (filled circles in Figs. 4 and in the Ap-

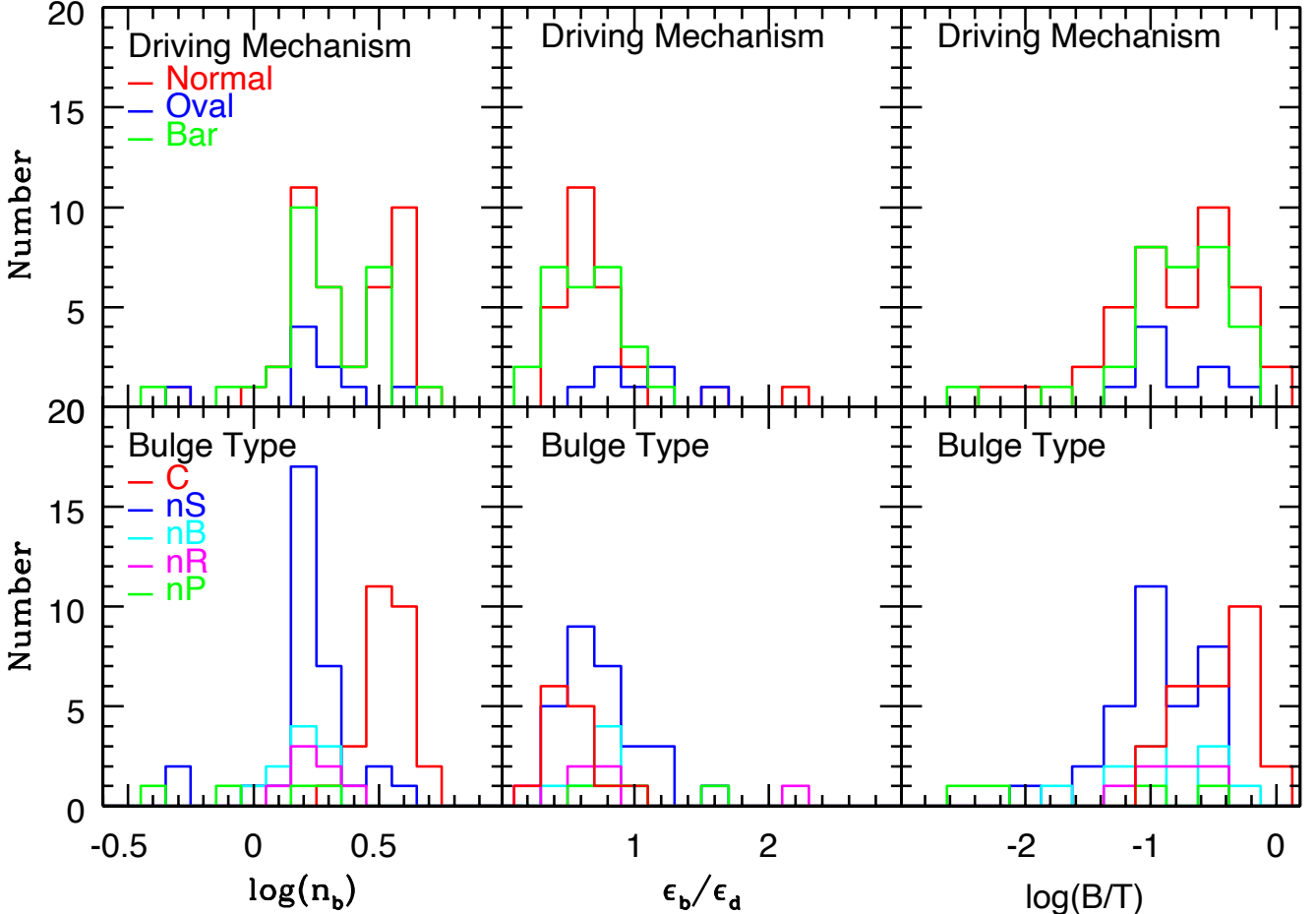


FIG. 12.— In the bottom panels, we show the distribution of o Sérsic index (bottom left), ratio of ellipticities (bottom middle), and B/T (bottom right) for different bulge morphologies. The bulge types are denoted by nS=nuclear spiral, nB=nuclear bar, nR=nuclear Ring, nP=nuclear patchiness, and C=classical bulge. We also show the comparison of the presence of driving mechanism (N=no driver, O=oval, and B=bar) to the Sérsic index (top left), ratio of ellipticities (top middle), and B/T (top right).

pendix). It is a matter of interpretation as to what features are a part of pseudobulges, especially in light of the fact that some nuclei may be formed secularly along with the pseudobulge. However, as a matter of consistency we choose to focus only on those isophotes we call the “bulge” from the bulge-disk decompositions. The boundary between the bulge and disk is chosen as the radius at which the surface brightness of the Sérsic function equals the surface brightness of the exponential disk in the decomposition. Yet, in many galaxies contamination from the disk artificially raises the average ellipticity of the bulge. This contamination is evident in the ellipticity profile. Thus, we choose to average the bulge over a region in which there is little contamination present. Those radii are given in Table 2.

The leftmost panel in Fig. 11 compares $\langle\epsilon_b\rangle/\langle\epsilon_d\rangle$ to bulge Sérsic index for pseudobulges and classical bulges. It is quite evident that classical bulges, in our sample, are not as flat as pseudobulges. The average ratio of ellipticities of pseudobulges is 0.79 ± 0.1 , whereas the average ratio for classical bulges is 0.49 ± 0.14 . In fact, the flattest classical bulge ($\langle\epsilon_b\rangle/\langle\epsilon_d\rangle = 0.75$) is less flat than the average pseudobulge.

The middle and rights panels of Fig. 11 compare this ratio to the bulge-to-total ratio and Hubble type, respectively. Classical bulges show no obvious trend of $\langle\epsilon_b\rangle/\langle\epsilon_d\rangle$ with B/T or

Hubble type. They are tightly clustered about the mean value $\sim 0.6 \pm 0.1$. Pseudobulges however show a slight correlation of $\langle\epsilon_b\rangle/\langle\epsilon_d\rangle$ with B/T . This correlation indicates that more prominent (in B/T) pseudobulges are slightly flatter. However, the trend is weak, and has large scatter. Finally, we find a similar result to Kormendy (1993) and Fathi & Peletier (2003), namely that flatter bulges are more frequent in later-type galaxies. Furthermore, this trend only exists for pseudobulges.

Invariably the flattest bulges are pseudobulges. However, we do not wish to overstate this result. It is possible that asymmetric dust extinction leads to higher apparent flattening in the V band. Future work at near-to-mid IR wavelengths is likely to provide less ambiguous results.

5. PSEUDOBULGES AS A CLASS OF OBJECTS

In this paper we identify pseudobulges as having any, but not necessarily all, of several structures (nuclear bars, rings, and ovals). We treat bulges with these structures as a group. The motivation for doing so is that all these phenomena are similar to properties that are commonly associated with high specific angular momentum systems. At least in the sense that they are the complement of classical bulges they can be treated as a group. However, here we have to ask the following question: do thusly identified pseudobulges act as a single

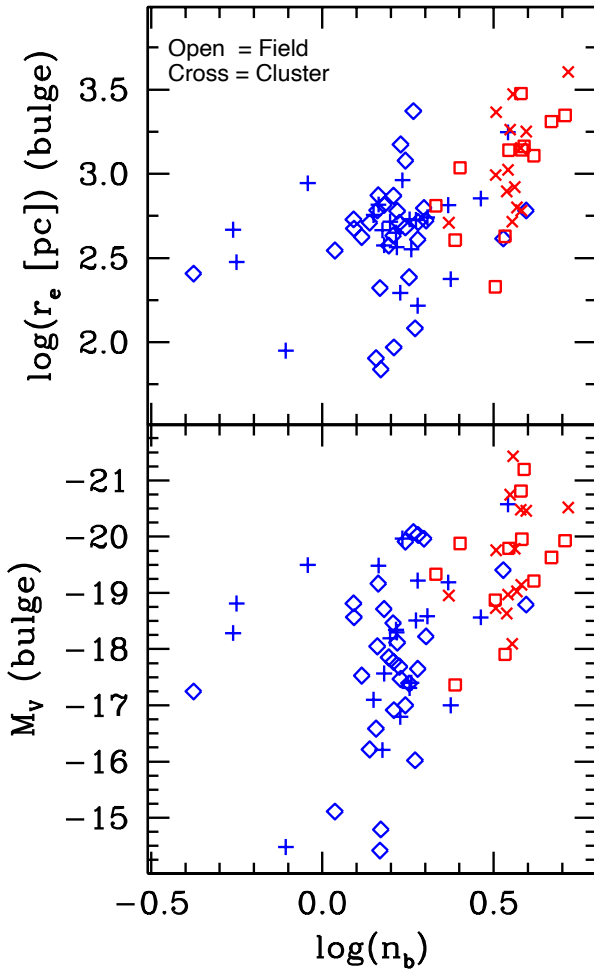


FIG. 13.— Structural parameters of bulges as a function of the environment. Field galaxies with classical bulges are marked by open squares, field pseudobulges with open diamonds. Cluster galaxies with classical bulges are marked by X's, cluster pseudobulge galaxies by crosses. All classical bulges are marked by red symbols, pseudobulges by blue symbols.

class of objects or do significant differences exist among the objects we are identifying as pseudobulges?

Figure 12 suggests an answer to this question. The left panels in the figure show the distribution of bulge properties for bulges that have smooth isophotes (C=classical), bulges with nuclear spirals (nS), bulges with nuclear bars (nB), bulges with nuclear rings (nR), and bulges with a chaotic nuclear patchiness that resembles late type galaxies (nP). See Fig. 2 for example images of each of these features. In Sérsic index, ellipticity ratio (bulge to disk), and bulge-to-total ratio there is no significant difference among the types of morphologies we call a pseudobulge.

Bulges with chaotic nuclear-disk-like patchiness (nP) seem to have smaller Sérsic index, and are more flat. It is unclear why this might be. This may be driven by them having smaller B/T and thus being more affected by the disk potential. We also note that pseudobulges with $n_b > 2$ are almost all in bulges with nuclear spirals. It is possible that these bulges are not truly a spiral, instead some other phenomenon, like contamination of the light by the outer disk, is causing us to identify them as pseudobulges. However, in each parameter the distinction appears to be between classical bulges and the rest of the objects, rather than among the objects we call pseu-

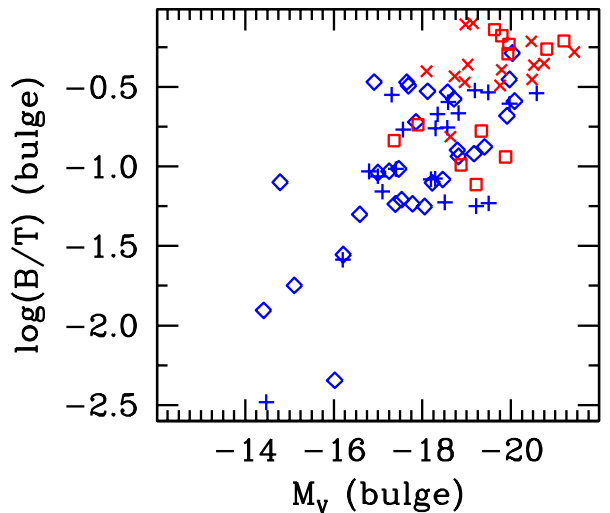


FIG. 14.— As in fig. 13, we distinguish those galaxies that exist in cluster (or group) environments (crossed symbols) from those that exist in the field (open symbols). Symbol color reflects bulge type, as before. Bulge-to-total ratio is plotted against absolute magnitude of the bulge.

dobulges.

We also show Sérsic index, ellipticity ratio (bulge to disk), and bulge-to-total ratio as a function of secular driving mechanism. We separate galaxies as having no driving mechanism, an oval disk, or a bar. Notice once again that we do not set grand design spiral as a class of object. There seems to be little differences in the averages, except ovoidal galaxies have smaller Sérsic index and flatter bulges. The phenomenon of flat bulges does not appear to require the presence of a bar. Thus it is not likely that all flat bulges are small bulges stretched by a bar potential making them flat. Also notice that the distributions of parameters for barred, oval, and normal spirals is roughly the same. Thus it does not seem likely that our method of removing the bar is artificially changing the bulge-disk decomposition parameters.

6. ENVIRONMENTAL EFFECTS

Secular evolution is not the only theory for building bulges that look like disks. Other possibilities such as extremely gas rich accretion events, distant gravitational encounters, or gravitational interactions with a cluster potential could all drive gas to the center of galaxies to increase B/T , as found by Mastropietro et al. (2005). Kannappan et al. (2004) find that blue bulges are statistically more likely to have companion galaxies within 100 kpc. Further, counter-rotating gas is frequently observed in spiral galaxies, and is taken as a sign of the galaxy having accreted galaxies in their past. Yet, pseudobulges are much more common in late-type galaxies, and the well known morphology-density relation (Dressler 1980) shows that late-type galaxies are not found in dense environments. Is it possible that pseudobulges in the field are formed through different mechanisms than those in cluster environments? We can not know the answer to this for certain, however we can look for signatures for such effects in our data.

In Fig. 13 we show our primary result again, namely that pseudobulges have a lower Sérsic index than classical bulges, but here we also mark environment. Field galaxies with classical bulges are marked by open squares, field pseudobulges with open diamonds. Cluster galaxies with classical bulges are marked by X's, cluster pseudobulge galaxies by crosses.

There seems to be no significant differences in the structure of the surface brightness profile between the pseudobulges that reside in the field galaxies and the ones in cluster galaxies. Cluster pseudobulges are not higher mass nor systematically different in radial size than field pseudobulges. Nor are their surface brightness profiles preferentially steeper in clusters.

The same holds for B/T : there is no substantial difference between pseudobulges in the field versus clustered environments. If pseudobulge formation was driven primarily by tidal encounters with distant galaxies, one would expect that this effect should be enhanced in cluster environments, where such encounters are more frequent. This would result in more massive pseudobulges existing in cluster environments. Our sample does not seem to indicate that pseudobulges are any more luminous in cluster environments than in the field. We feel that this supports the notion that externally driven disk evolution is not likely the dominant affect in driving pseudobulge formation.

Our results in no way rule out the possibility that pseudobulges are formed by gas-rich minor mergers. If we take an example of merging our Galaxy with one of the Magellanic clouds, and if this is done ~ 1 Gyr, when the gas fractions were much higher, it is entirely plausible that the result could look similar to what we call a pseudobulge. However, it is not certain if such a system would still be actively forming stars today, or if pseudobulge formation through minor mergers could only happen in extreme cases (e.g. prograde collisions at low inclination). Also, it is not clear how such accretion-driven formation of pseudobulges could maintain the bulge-disk correlations discussed in the previous sections.

7. SUMMARY & DISCUSSION

The main result of this paper is that bulge Sérsic index, n_b , is bimodally distributed in intermediate type galaxies where both classical bulges and pseudobulges exist. A value of $n_b \simeq 2$ marks the boundary for separating morphologically-identified pseudobulges from classical bulges. Below $n_b = 2$ no classical bulges are found, and above it very few pseudobulges are found. We also find that galaxies which are identified as pseudobulges, using either bulge morphology or bulge Sérsic index, are flatter than classical bulges. Thus suggesting that on average these systems are more disk-like in both their morphology and shape than are classical bulges. Pseudobulges exist that are as round as classical bulges, yet, invariably the flattest bulges are all pseudobulges. In both Sérsic index and flattening ratio, our results show a homogeneity in classical bulge properties, and a greater dispersion in pseudobulge properties. That is to say, classical bulges, in our sample, do not have Sérsic index less than two, nor do they have high ratios of bulge-to-disk ellipticity. Pseudobulges, on average, have lower B/T than classical bulges, however we find pseudobulges with B/T extending to ~ 0.35 .

We find that the half-light radius of pseudobulges is well correlated with the scale length of the outer disk, while the scale length of classical bulges is not correlated with that of the disk. This is consistent with the interpretation that $r_e \propto h$ is due to a secular formation of pseudobulges. Also, the fact that the scale length of the disk is correlated with the size of its pseudobulge but not correlated with the size of classical bulges is a strong indication that there indeed is a physical difference between the formation mechanisms of these different bulge types.

In photometric fundamental plane projections, pseudobulges populate and extend the low luminosity end of the range

occupied by classical bulges and elliptical galaxies. Pseudobulges deviate more from the relations set by the elliptical galaxies than classical bulges, and preferably towards lower density. In fact, it does not seem that on their own pseudobulges would establish any of these correlations, especially $M_V - \mu_e$.

In all correlations investigated in this work we find that the fundamental distinction is between classical bulges and pseudobulges. We do not find significant differences within the class of morphologies we identify as pseudobulges (nuclear spirals, nuclear bars, nuclear rings, and chaotic nuclear patchiness).

Is it possible that identifying pseudobulges visually using nuclear morphology is subject to an inherit flaw? That being that these systems are by definition bulge-disk systems, and thus is it possible that classical bulges coexist over large radius with the central parts of a disk. Pseudobulges in S0 galaxies exemplify this concern. In many ways elliptical galaxies and S0s are thought to be the extremes of a continuum of properties. Embedded disks are known to exist in elliptical galaxies (see, e.g. [Scorza & Bender 1995](#)). Would we call such a system where the embedded disk had a nuclear bar a pseudobulge? Most likely not. However, in S0s, which by definition have lower B/T , we are inclined to do so. Clearly, if there is no sharp change in properties along the E-S0 continuum, there should be some composite systems with secularly formed structure in the disk and a classical (i.e. kinematically hot) bulge. (Note, though, that many S0s resemble defunct later type disk galaxies much more than they do resemble elliptical galaxies as suggested by [van den Berg 1976](#)). This may be the case in NGC 2950, yet it does not appear to be the rule. [Erwin et al. \(2004\)](#) show that many bulges have more complicated dynamical profiles, with both hot and cold components. Yet, pseudobulges show a remarkable similarity to disk stellar populations, ISM, and star formation rates. These similarities have been shown in the flatness of stellar population gradients ([Peletier & Balcells 1996](#)), and the similarity of CO profiles to optical light ([Regan et al. 2001](#)). [Helfer et al. \(2003\)](#) show that many CO gas maps of bulge-disk galaxies have holes in their center, but also many CO profiles rise steeply to their center. A quick comparison of with our sample shows that those holes are found in classical bulges (e.g. NGC 2841). [Fisher \(2006\)](#) shows that the nuclear morphology of galaxies (as used here) predicts the shape of the 3.6–8.0 micron color profile: disk-like bulges have flat color profiles, and E-like bulges have holes in 8.0 micron emission. If we were merely mistakenly identifying disks superimposed on bulges as physically different pseudobulges, we'd expect to find larger B/T for such systems as compared to the bulges where we do not see evidence for the presence of a disk which we call classical in this work. This is because of the added light of the disk onto a fraction of bulges drawn from the same underlying distribution. However, we do not find this to be the case. Fig. 6 shows that pseudobulges are on average smaller than classical bulges.

It is not clear whether pseudobulges participate in the various correlations presented in this paper. If we look at the pseudobulges alone, they only show a convincing correlation in the Kormendy relation ($\mu_e - r_e$). Their distribution better resembles scatter diagrams in the $M_V - \mu_e$, $\mu_e - n$, and $r_e - n$ planes. However, it would seem to be an odd coincidence that in every parameter combination pseudobulges just happen to fall in the right location to extend the correlations set by the classical bulges and the elliptical galaxies. Putting all this

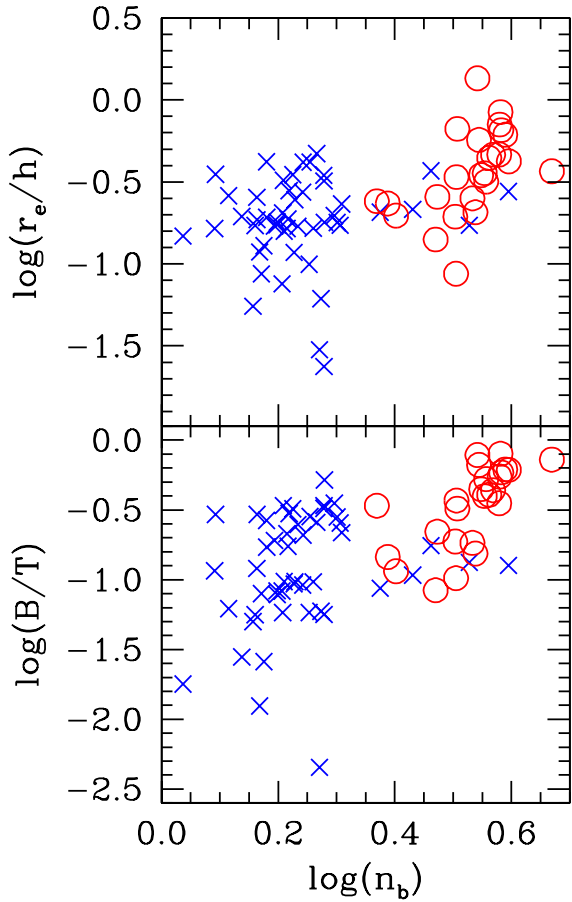


FIG. 15.— Bulge-to-total ratio (lower panel) and ratio of the bulge half-light radius to the scale length of the disk (top panel) plotted against the logarithm of the bulge Sérsic index. As before, classical bulges are represented by open red circles and pseudobulges by blue crosses.

together implies that we do not really understand the details of pseudobulge formation very well. It is also possible that the decomposition of pseudobulges may not be an appropriate procedure. Bulge-disk decomposition assumes that the structures are distinct (and that light extends to radius of infinity). If we accept that pseudobulges are formed through disk phenomena, then such a bulge-disk decomposition may not be an adequate description of those systems. In reality they might simply be a component of galactic disk. Also, parameters derived from the Sérsic function are coupled (Graham & Colless 1997). Thus, treating pseudobulges in the same way as classical bulges may artificially force them to extend some photometric correlations.

Concerning the six bulges with disk-like morphology near their centers that have $n_b > 2$, two have $\langle \epsilon_b \rangle / \langle \epsilon_d \rangle > 0.75$ (the maximum of classical bulges), and NGC 4314 has a very prominent star forming nuclear ring, making this bulge a strong candidate for being a pseudobulge. This galaxy might be an example for a composite system. Their existence certainly underscores the value of having as much information as possible when diagnosing bulge types. Future work may prove illuminating. For example, to what extent should we trust bulge morphology as an indicator of secular evolution? It is possible for the human eye to mistake merely the presence of dust for spiral structure?

We also find that the ratio of scale lengths, r_e/h , in pseu-

dobulges is more tightly correlated and closer to those values reported by other authors (e.g. MacArthur et al. 2003) than in classical bulges. However, the range in values of r_e/h for classical bulges and pseudobulges are similar; therefore this does not provide a good diagnostic tool for finding pseudobulges. Pseudobulges extend the parameter correlations of photometric quantities (r_e , μ_e , M_V , and n_b). However in many of these parameters it is unclear if pseudobulges actually show a correlation on their own.

We can compare the structural properties of the bulges in our sample the output of simulation. Unfortunately simulations of galaxies that resemble real galaxies including stars, dark matter, gas and star formation (and possibly feedback) are quite difficult. Thus there does not exist a statistically relevant set of simulations for full comparison. Nonetheless, we can compare our results to those that currently exist.

Debattista et al. (2004) provides a set of simulations that generate bulges from bar buckling in pure stellar (no gas) systems. The resulting bulges typically have $n_b \sim 1.5$, which is consistent with what we find. The bulges in our sample tend to be more round than their associated outer disk, and Debattista et al. (2004) separate their bulges based on flattening ratios. So we will only compare to those bulges that are less round than the outer disk. Their simulated galaxies have $B/D = 0.2 - 1.0$ (where B/D is bulge-to-disk light ratio). Where as our sample has a median $B/D = 0.12$ with a standard deviation of 0.20. Further, they are able to recover the coupling of r_e and h that we find in pseudobulges. Thus our pseudobulges tend to be a bit smaller. It may be that bar-buckling is one way to make a pseudobulge, as indicated by the fact that those simulated bulges from Debattista et al. (2004) are contained within the set of pseudobulges, but do not span the whole range in properties.

We reiterate a statement by Andredakis (1998), that is also discussed in Kormendy & Kennicutt (2004), namely that we do not really understand why pseudobulges should have a certain Sérsic index. It is understandable that mergers would drive up the Sérsic index, as discussed by van Albada (1982) and Kormendy et al. (2006), and thus classical bulges are found with higher Sérsic index. Aguerri et al. (2001) simulates minor mergers (accretion of satellites on the order of the mass of the bulge) in bulge-disk galaxies. They show that the Sérsic index grows as the amount of mass accreted becomes larger. Eliche-Moral et al. (2006) takes the study of satellite accretion to lower densities than those simulations of Aguerri et al. (2001). Their simulations do not include gas and star formation, and thus as with the Debattista et al. (2004) simulations they should be read with that caveat in mind. They find that low density satellite accretion does not necessarily drive Sérsic index above the critical value we find ($n_{crit} \sim 2$). Yet, they also find that satellite accretion leads to a simultaneous increase in B/T .

In Fig. 15, we therefore plot the bulge-to-total ratio, B/T , and the ratio of the bulge half-light radius to the scale length of the disk, r_e/h , against n_b . There is a tight correlation for classical bulges. However, pseudobulges do not follow this correlation. In fact, neither B/T nor r_e/h correlate with n_b in pseudobulges at all in the range of parameters shown, spanning an order of magnitude in B/T . The absence of correlation between n_b and B/T in pseudobulges seems to be pointing to a non-merger driven formation scenario for pseudobulges. Yet, these results are suggestive at best. There may be some underlying correlation that is destroyed by other factors (e.g. gas fraction or collision parameters). More work is

needed from both simulations and observations. That we do not see correlation of n_b and B/T for low-Sérsic index bulges (as found in Eliche-Moral et al. 2006) may be indicating that the classical bulges we observe today are the products of multiple mergers, and possibly at higher redshifts there is a population of low-Sérsic index classical bulges. Conversely it is entirely possible that a population of small classical bulges exists, yet they are embedded within pseudobulges. In this case the mass of a bulge, and hence the B/T within a specific galaxy would be coming from multiple mechanisms.

If pseudobulges are built by secular evolution, the simplest mechanism controlling the Sérsic index in bulges is that n_b grows with time as the bulge-to-total ratio increases. However, as discussed above, it appears that there is not a strong connection between B/T and Sérsic index. This would imply that Sérsic index in pseudobulges is not a time-dependent quantity. We wish to emphasize, though, that the error in the measurement of n_b is large, and might be masking an underlying weak correlation. Also, by focusing on intermediate-type galaxies, where both pseudobulges and classical bulges occur, we miss very low B/T systems. Expanding a sample to later types might reveal a weak correlation (Graham 2001). Since r_e correlates tightly with h for pseudobulges, it is no surprise that r_e/h does not correlate with n_b in pseudobulges. The linear coupling of r_e and h is well established in late type galaxies (Courteau et al. 1996).

It may be that the Sérsic index of pseudobulges is merely another manifestation of the dynamical state of the system. Stars in bulges with larger amounts of random motion often take on radial orbits, thus climbing higher out of the potential well. Thus there is more light at large radius, increasing n_b . However, stars in orbits with higher amounts of angular momentum would be less likely to take on radial orbits and thus bulge light would contribute less at large radius; driving n_b down. The observation that the distribution of Sérsic indices in bulges of galaxies from E to Sc is bimodal then strengthens the claim that what we are calling pseudobulges are not merely the low-mass counterparts of the same phenomena that form classical bulges and elliptical galaxies. This description fits well with the theory that secular evolution forms pseudobulges, and mergers, whether by a single event or succession of events, form classical bulges. The higher angular momentum (and thus low Sérsic index) systems have not had major mergers and thus have not experienced the violent processes that lower the ratio of rotational velocity to velocity dispersion. What is left unknown is why pseudobulges are not exponential, and also what keeps them from having larger Sérsic indices.

We conclude by returning to the results of Fig. 6, and the implications of the range of B/T for pseudobulges. It is now well known that the presence of many low- B/T systems presents a problem for current Λ CDM galaxy formation theories (D'Onghia & Burkert 2004). In our sample we find no classical bulge galaxies with $B/T < 0.1$. Recent studies which compare merger histories in Λ CDM simulations to the observed frequency of bulgeless galaxies suggest that either there are too many mergers in the simulations, or that disks must be much more robust to the merging process than previously thought (Stewart et al. 2007; Koda et al. 2007). Pseudobulges span a range of B/T from 0.35 to zero. If pseudobulges form through internal-disk processes then a galaxy with a pseudobulge can be thought of as a pure disk galaxy. Thus current estimates of the number of low- B/T systems could

only be thought of as lower-limits; the existence of pseudobulges would make the problem of forming bulgeless systems even more pressing.

We would like to thank Prof. John Kormendy & Dr. Mark Cornell for countless discussions on this work. Also, DBF would like to thank Prof. Alex Filippenko and University of California at Berkeley for providing him with a place to do much of this research.

DBF acknowledges support by the National Science Foundation under grant AST 06-07490. This work is based in part on observations made with the Spitzer Space Telescope, operated by the Jet Propulsion Laboratory, California Institute of Technology under a contract with NASA. Support for this work was provided by NASA through an award issued by JPL/Caltech.

This paper makes use of data obtained from the Isaac Newton Group Archive which is maintained as part of the CASU Astronomical Data Centre at the Institute of Astronomy, Cambridge. This research has made use of the NASA/IPAC Extragalactic Database (NED) which is operated by the Jet Propulsion Laboratory, California Institute of Technology, under contract with the National Aeronautics and Space Administration. This research has made use of the NASA/ IPAC Infrared Science Archive, which is operated by the Jet Propulsion Laboratory, California Institute of Technology, under contract with the National Aeronautics and Space Administration. Some of the data presented in this paper were obtained from the Multi-mission Archive at the Space Telescope Science Institute (MAST). STScI is operated by the Association of Universities for Research in Astronomy, Inc., under NASA contract NAS5-26555. Support for MAST for non-HST data is provided by the NASA Office of Space Science via grant NAG5-7584 and by other grants and contracts. Funding for the SDSS and SDSS-II has been provided by the Alfred P. Sloan Foundation, the Participating Institutions, the National Science Foundation, the U.S. Department of Energy, the National Aeronautics and Space Administration, the Japanese Monbukagakusho, the Max Planck Society, and the Higher Education Funding Council for England. The SDSS Web Site is <http://www.sdss.org/>. The SDSS is managed by the Astrophysical Research Consortium for the Participating Institutions. The Participating Institutions are the American Museum of Natural History, Astrophysical Institute Potsdam, University of Basel, Cambridge University, Case Western Reserve University, University of Chicago, Drexel University, Fermilab, the Institute for Advanced Study, the Japan Participation Group, Johns Hopkins University, the Joint Institute for Nuclear Astrophysics, the Kavli Institute for Particle Astrophysics and Cosmology, the Korean Scientist Group, the Chinese Academy of Sciences (LAMOST), Los Alamos National Laboratory, the Max-Planck-Institute for Astronomy (MPIA), the Max-Planck-Institute for Astrophysics (MPA), New Mexico State University, Ohio State University, University of Pittsburgh, University of Portsmouth, Princeton University, the United States Naval Observatory, and the University of Washington. This publication makes use of data products from the Two Micron All Sky Survey, which is a joint project of the University of Massachusetts and the Infrared Processing and Analysis Center/California Institute of Technology, funded by the National Aeronautics and Space Administration and the National Science Foundation.

REFERENCES

- Adelman-McCarthy, J. K., et al. 2006, *ApJS*, 162, 38
- Aguerri, J. A. L., Balcells, M., & Peletier, R. F. 2001, *A&A*, 367, 428
- Allen, P. D., Driver, S. P., Graham, A. W., Cameron, E., Liske, J., & de Propris, R. 2006, *MNRAS*, 371, 2
- Andredakis, Y. C. 1998, *MNRAS*, 295, 725
- Andredakis, Y. C., Peletier, R. F., & Balcells, M. 1995, *MNRAS*, 275, 874
- Andredakis, Y. C., & Sanders, R. H. 1994, *MNRAS*, 267, 283
- Balcells, M., Graham, A. W., Domínguez-Palmero, L., & Peletier, R. F. 2003, *ApJ*, 582, L79
- Bender, R., Burstein, D., & Faber, S. M. 1992, *ApJ*, 399, 462
- Bender, R., & Moellenhoff, C. 1987, *A&A*, 177, 71
- Böker, T., Laine, S., van der Marel, R. P., Sarzi, M., Rix, H.-W., Ho, L. C., & Shields, J. C. 2002, *AJ*, 123, 1389
- Caon, N., Capaccioli, M., & D'Onofrio, M. 1994, *A&AS*, 106, 199
- Carollo, C. M. 1999, *ApJ*, 523, 566
- Carollo, C. M., Stiavelli, M., de Zeeuw, P. T., & Mack, J. 1997, *AJ*, 114, 2366
- Carollo, C. M., Stiavelli, M., Seigar, M., de Zeeuw, P. T., & Dejonghe, H. 2002, *AJ*, 123, 159
- Cheng, K. P., Collins, N., Angione, R., Talbert, F., Hintzen, P., Smith, E. P., Stecher, T., & The UIT Team, ed. 1997, *Uv/visible Sky Gallery on CDROM*
- Courteau, S., de Jong, R. S., & Broeils, A. H. 1996, *ApJ*, 457, L73
- de Jong, R. S. 1996, *Journal of Astronomical Data*, 2, 1
- de Jong, R. S., Simard, L., Davies, R. L., Saglia, R. P., Burstein, D., Colless, M., McMahan, R., & Wegner, G. 2004, *MNRAS*, 355, 1155
- de Vaucouleurs, G., de Vaucouleurs, A., Corwin, H. G., Jr., Buta, R. J., Paturel, G., & Fouque, P. 1991, *Third Reference Catalogue of Bright Galaxies* (Volume 1-3, XII, 2069 pp. 7 figs.. Springer-Verlag Berlin Heidelberg New York)
- Debattista, V. P., Carollo, C. M., Mayer, L., & Moore, B. 2004, *ApJ*, 604, L93
- Djorgovski, S., & Davis, M. 1987, *ApJ*, 313, 59
- D'Onghia, E., & Burkert, A. 2004, *ApJ*, 612, L13
- Dressler, A. 1980, *ApJ*, 236, 351
- Dressler, A., Lynden-Bell, D., Burstein, D., Davies, R. L., Faber, S. M., Terlevich, R., & Wegner, G. 1987, *ApJ*, 313, 42
- Drory, N., & Fisher, D. B. 2007, *ApJ*, 664, 640
- Eliche-Moral, M. C., Balcells, M., Aguerri, J. A. L., & González-García, A. C. 2006, *A&A*, 457, 91
- Erwin, P., Beckman, J. E., & Vega-Beltran, J.-C. 2004, in *Astrophysics and Space Science Library*, Vol. 319, *Astrophysics and Space Science Library*, ed. D. L. Block, I. Puerari, K. C. Freeman, R. Groess, & E. K. Block, 775
- Erwin, P., & Sparke, L. S. 2002, *AJ*, 124, 65
- Erwin, P., & Sparke, L. S. 2003, *ApJS*, 146, 299
- Faber, S. M., Wegner, G., Burstein, D., Davies, R. L., Dressler, A., Lynden-Bell, D., & Terlevich, R. J. 1989, *ApJS*, 69, 763
- Falcón-Barroso, J., Peletier, R. F., & Balcells, M. 2002, *MNRAS*, 335, 741
- Fathi, K., & Peletier, R. F. 2003, *A&A*, 407, 61
- Fisher, D. B. 2006, *ApJ*, 642, L17
- Frei, Z., Guhathakurta, P., Gunn, J. E., & Tyson, J. A. 1996, *AJ*, 111, 174
- Friedli, D. 1999, in *Astronomical Society of the Pacific Conference Series*, Vol. 187, *The Evolution of Galaxies on Cosmological Timescales*, ed. J. E. Beckman & T. J. Mahoney, 88
- Graham, A., & Colless, M. 1997, *MNRAS*, 287, 221
- Graham, A., Lauer, T. R., Colless, M., & Postman, M. 1996, *ApJ*, 465, 534
- Graham, A. W. 2001, *AJ*, 121, 820
- Graham, A. W., & Driver, S. P. 2005, *Publications of the Astronomical Society of Australia*, 22, 118
- Helfer, T. T., Thornley, M. D., Regan, M. W., Wong, T., Sheth, K., Vogel, S. N., Blitz, L., & Bock, D. C.-J. 2003, *ApJS*, 145, 259
- Hohl, F. 1975, in *IAU Symp. 69: Dynamics of the Solar Systems*, ed. A. V. Oppenheim & R. W. Schafer, 349
- Holtzman, J. A., Burrows, C. J., Casertano, S., Hester, J. J., Trauger, J. T., Watson, A. M., & Worthey, G. 1995, *PASP*, 107, 1065
- Jogee, S., Scoville, N., & Kenney, J. D. P. 2005, *ApJ*, 630, 837
- Kannappan, S. J., Jansen, R. A., & Barton, E. J. 2004, *AJ*, 127, 1371
- Kennicutt, R. C., Jr., et al. 2003, *PASP*, 115, 928
- Kent, S. M. 1985, *ApJS*, 59, 115
- Khosroshahi, H. G., Wadadekar, Y., & Kembhavi, A. 2000, *ApJ*, 533, 162
- Knapen, J. H., Stedman, S., Bramich, D. M., Folkes, S. L., & Bradley, T. R. 2004, *A&A*, 426, 1135
- Koda, J., Milosavljevic, M., & Shapiro, P. R. 2007, *ArXiv e-prints*, 711
- Kormendy, J. 1977, *ApJ*, 218, 333
- Kormendy, J. 1982, in *Saas-Fee Advanced Course 12: Morphology and Dynamics of Galaxies* (Vol. 12: Morphology and Dynamics of Galaxies), 113
- Kormendy, J. 1993, in *IAU Symp. 153: Galactic Bulges*, 209
- Kormendy, J. 2007
- Kormendy, J., & Kennicutt, R. C. 2004, *ARA&A*, 42, 603
- Kormendy, J. K., Fisher, D. B., Cornell, M. E., & Bender, R. 2006, In Preparation
- Kuchinski, L. E., et al. 2000, *ApJS*, 131, 441
- Larsen, S. S., & Richtler, T. 1999, *A&A*, 345, 59
- Lauer, T. R., et al. 1995, *AJ*, 110, 2622
- Lauer, T. R., et al. 2005, *AJ*, 129, 2138
- MacArthur, L. A., Courteau, S., Bell, E., & Holtzman, J. A. 2004, *ApJS*, 152, 175
- MacArthur, L. A., Courteau, S., & Holtzman, J. A. 2003, *ApJ*, 582, 689
- Mastropietro, C., Moore, B., Mayer, L., Debattista, V. P., Piffaretti, R., & Stadel, J. 2005, *MNRAS*, 364, 607
- Moellenhoff, C., Matthias, M., & Gerhard, O. E. 1995, *A&A*, 301, 359
- Möllenhoff, C., & Heidt, J. 2001, *A&A*, 368, 16
- Moore, B., Katz, N., Lake, G., Dressler, A., & Oemler, A., Jr. 1996, *Nature*, 379, 613
- Noguchi, M. 1999, *ApJ*, 514, 77
- Peeples, M. S., & Martini, P. 2006, *ApJ*, 652, 1097
- Peletier, R. F., & Balcells, M. 1996, *AJ*, 111, 2238
- Pfenniger, D., & Friedli, D. 1991, *A&A*, 252, 75
- Pfenniger, D., & Norman, C. 1990, *ApJ*, 363, 391
- Regan, M. W., Thornley, M. D., Helfer, T. T., Sheth, K., Wong, T., Vogel, S. N., Blitz, L., & Bock, D. C.-J. 2001, *ApJ*, 561, 218
- Saglia, R. P., Bertschinger, E., Bagley, G., Burstein, D., Colless, M., Davies, R. L., McMahan, R. K., Jr., & Wegner, G. 1997, *ApJS*, 109, 79
- Sandage, A. 1961, *The Hubble atlas of galaxies* (Washington: Carnegie Institution, 1961)
- Sandage, A., & Bedke, J. 1994, *The Carnegie atlas of galaxies* (Washington, DC: Carnegie Institution of Washington with The Flintridge Foundation, 1994)
- Scarlata, C., et al. 2004, *AJ*, 128, 1124
- Schlegel, D. J., Finkbeiner, D. P., & Davis, M. 1998, *ApJ*, 500, 525
- Scorza, C., & Bender, R. 1995, *A&A*, 293, 20
- Sersic, J. L. 1968, *Atlas de galaxias australes* (Cordoba, Argentina: Observatorio Astronomico, 1968)
- Sheth, K., Vogel, S. N., Regan, M. W., Thornley, M. D., & Teuben, P. J. 2005, *ApJ*, 632, 217
- Simkin, S. M., Su, H. J., & Schwarz, M. P. 1980, *ApJ*, 237, 404
- Sirianni, M., et al. 2005, *PASP*, 117, 1049
- Skrutskie, M. F., et al. 2006, *AJ*, 131, 1163
- Smith, J. A., et al. 2002, *AJ*, 123, 2121
- Stewart, K. R., Bullock, J. S., Wechsler, R. H., Maller, A. H., & Zentner, A. R. 2007, *ArXiv e-prints*, 711
- Thomas, D., & Davies, R. L. 2006, *MNRAS*, 366, 510
- Tully, R. B., & Fisher, J. R. 1988, *Catalog of Nearby Galaxies* (Catalog of Nearby Galaxies, by R. Brent Tully and J. Richard Fisher, pp. 224. ISBN 0521352991. Cambridge, UK: Cambridge University Press, April 1988.)
- van Albada, T. S. 1982, *MNRAS*, 201, 939
- van den Bergh, S. 1976, *ApJ*, 206, 883